

University of Alberta

**Structural and Functional Insights into the Molecular Mechanisms of
Concentrative Nucleoside Transport Proteins**

by

Melissa Dawn Slugoski



A thesis submitted to the Faculty of Graduate Studies and Research
in partial fulfillment of the requirements for the degree of

Doctor of Philosophy

Department of Physiology

Edmonton, Alberta

Fall 2008



Library and
Archives Canada

Bibliothèque et
Archives Canada

Published Heritage
Branch

Direction du
Patrimoine de l'édition

395 Wellington Street
Ottawa ON K1A 0N4
Canada

395, rue Wellington
Ottawa ON K1A 0N4
Canada

Your file Votre référence
ISBN: 978-0-494-46425-0
Our file Notre référence
ISBN: 978-0-494-46425-0

NOTICE:

The author has granted a non-exclusive license allowing Library and Archives Canada to reproduce, publish, archive, preserve, conserve, communicate to the public by telecommunication or on the Internet, loan, distribute and sell theses worldwide, for commercial or non-commercial purposes, in microform, paper, electronic and/or any other formats.

The author retains copyright ownership and moral rights in this thesis. Neither the thesis nor substantial extracts from it may be printed or otherwise reproduced without the author's permission.

AVIS:

L'auteur a accordé une licence non exclusive permettant à la Bibliothèque et Archives Canada de reproduire, publier, archiver, sauvegarder, conserver, transmettre au public par télécommunication ou par l'Internet, prêter, distribuer et vendre des thèses partout dans le monde, à des fins commerciales ou autres, sur support microforme, papier, électronique et/ou autres formats.

L'auteur conserve la propriété du droit d'auteur et des droits moraux qui protègent cette thèse. Ni la thèse ni des extraits substantiels de celle-ci ne doivent être imprimés ou autrement reproduits sans son autorisation.

In compliance with the Canadian Privacy Act some supporting forms may have been removed from this thesis.

Conformément à la loi canadienne sur la protection de la vie privée, quelques formulaires secondaires ont été enlevés de cette thèse.

While these forms may be included in the document page count, their removal does not represent any loss of content from the thesis.

Bien que ces formulaires aient inclus dans la pagination, il n'y aura aucun contenu manquant.


Canada

Abstract

Concentrative nucleoside transporter (CNT) proteins mediate nucleoside transport using the electrochemical gradient of the coupling cation. The molecular mechanisms underlying interactions with both nucleosides and cations were investigated by heterologous expression of recombinant CNT family members in *Xenopus laevis* oocytes combined with radioisotope flux assays and electrophysiology studies. Structure-function investigations of chimeric and mutant CNTs revealed important roles for key regions and residues within the proteins.

In humans (h), the CNT protein family is represented by three members. hCNT1 and hCNT2 are pyrimidine nucleoside- and purine nucleoside-selective, respectively, while hCNT3 transports both pyrimidine and purine nucleosides. hCNT1 and hCNT2 function exclusively as Na⁺-coupled nucleoside transporters and share 1:1 Na⁺:nucleoside stoichiometry. Belonging to a CNT subfamily phylogenetically distinct from hCNT1/2, hCNT3 utilizes electrochemical gradients of Na⁺, Li⁺ or H⁺ to drive nucleoside transport and exhibits 2:1 Na⁺:nucleoside and 1:1 H⁺:nucleoside stoichiometries. Non-mammalian H⁺-coupled CNT family members also functionally characterized include NupC from the bacterium *Escherichia coli* and allelic isoforms of CaCNT from the pathogenic yeast *Candida albicans*. Both Na⁺ and H⁺ activate CNTs through mechanisms to increase nucleoside apparent binding affinity.

Multiple alignments of CNT family members reveal strong sequence similarities within the C-terminal halves of the proteins and hCNT1/3 chimeric studies demonstrated that this region determined nucleoside transport phenotype.

hCNT1/3 mutagenesis studies identified conserved serine, leucine and glutamate residues in transmembrane domains (TMs) 7 and 8 with roles in nucleoside selectivity and cation-coupling. In hCNT3, access of *p*-chloromercuribenzenesulfonate (PCMBS) to TM 12 Cys⁵⁶¹ reported a specific H⁺-activated state of the transporter and mutagenesis at this position revealed key roles in Na⁺/H⁺-coupling. Adjacent to this conformationally sensitive, mobile pore-lining region of TM 12, a conserved negatively charged residue (Glu⁵¹⁹) in TM 11A was established to be critical for CNT cation-coupling. Glu⁵¹⁹ is centrally positioned within the highly conserved CNT family motif (G/A)XKX₃NEFVA(Y/M/F) of TM 11A and substituted cysteine accessibility method analysis of the TM 11 - 13 region identified novel membrane-associated topology for this TM. These studies provide important structural and functional insights into the nature of the nucleoside/cation translocation pore and mechanism of nucleoside/cation cotransport by CNTs.

Acknowledgements

Primarily, I would like to acknowledge and thank my supervisor, Dr. James Young, for the opportunity to study in his laboratory and for his academic perspective, inspiration and mentorship. Additionally, I would like to sincerely thank Dr. Edward Karpinski for his invaluable and continual guidance and supervision. I am also grateful to the following individuals who have influenced my studies in numerous ways: Professor Stephen Baldwin for contributions to collaborative manuscripts and the opportunity to work on a project in his laboratory, Dr. Carol Cass for serving on my supervisory committee, supporting collaborative research and providing insightful discussion with respect to shared projects and publications, Dr. Chris Cheeseman for also serving on my supervisory committee and providing an inspiring environment for scientific discussion in the laboratory across the hallway, Dr. Marek Duszyk for serving on my candidacy examination committee, and to Drs. Susan Dunn and Jean-Yves Lapointe for serving on my thesis defense committee.

I wish to thank the members, past and present, of the Young laboratory, Amy Ng, Mabel Ritzel, Drs. Sylvia Yao, Kyla Smith and Shaun Loewen, Ras Mulinta, Nadira Mohibar, Kathy Labeledz, Queenie Lee, Ellen Morrison and Colin Lin, for sharing their expertise in and contributing to the research and discussion of my projects. I would especially like to acknowledge and express my sincere appreciation to Kyla for her collaborative work, insightful discussion and friendship. From across the hallway, I am also thankful to Debbie O'Neill for her support through the years. Last but not least, I am indebted and most thankful to my family and friends, and especially to Andrei, for endless love and support.

Table of Contents

	<u>Page</u>
Chapter 1: General Introduction	1
Nucleoside Transport	2
Physiological Importance	2
Pharmacological Importance	3
Nucleoside Transport Proteins	6
Equilibrative Nucleoside Transporter (ENT) Family	7
Mammalian ENT Family Members	8
ENT1	9
ENT2	13
ENT3	16
ENT4	18
ENT Physiological Implications	19
Non-Mammalian Eukaryotic ENT Family Members	21
Parasitic Protozoa	21
Nematodes	26
Insects	27
Plants	27
Fungi	28
Concentrative Nucleoside Transporter (CNT) Family	29
Mammalian CNT Family Members	29
CNT1	32
CNT2	35
CNT3	37
CNT Physiological Implications	40
Non-Mammalian Eukaryotic CNT Family Members	41
Lower Vertebrates	41

	<u>Page</u>
Nematodes	42
Fungi	43
Prokaryotic CNT Family Member	44
Bacteria	44
Organic Cation Transporter (OCT) Family	44
Organic Anion Transporter (OAT) Family	45
Nucleoside:H ⁺ Symporter (NHS) Family	46
Tsx Channel-Forming Protein Family	47
Uracil/Allantoin Permease Family	48
Nucleoside Permease (NUP) Family	48
Importance of Nucleoside Transporter Studies	48
Nucleoside Transport Protein Structure-Function Studies	53
Studies on ENT Family Members	54
Studies on CNT Family Members	57
ENT and CNT Mechanism(s) of Transport	61
Research Objectives	62
Bibliography	85
Chapter 2: Experimental Procedures	139
<i>Xenopus laevis</i> Oocyte Expression System	140
Molecular Biology	142
Constructs	142
Site-directed mutagenesis	142
Construction of chimeric hCNT3 and hCNT1 transporters	142
<i>In vitro</i> transcription and expression in <i>Xenopus</i> oocytes	143
Cell Surface Expression and Glycosylation	144
Chapter 4	144
Chapters 8 and 9	144
Immunoblotting	144
Transport Media	144

	<u>Page</u>
Radioisotope Flux Studies	145
Inhibition studies with thiol-reactive reagents	146
Electrophysiological Studies	146
Kinetic Parameters	148
Determination of Stoichiometry	149
Charge-to-nucleoside stoichiometry	149
Charge-to-Na ⁺ stoichiometry	150
Bibliography	151
Chapter 3: Allelic Isoforms of the H⁺/Nucleoside Cotransporter (CaCNT) from <i>Candida albicans</i> Reveal Separate High- and Low-Affinity Transport Systems for Nucleosides	155
Acknowledgements	156
Introduction	157
Results and Discussion	158
Construction of the CaCNT isoforms CaCNT/19-10196 and CaCNT/19-20196	158
Functional expression of recombinant CaCNT, CaCNT/19-10196 and CaCNT/19-20196 in <i>Xenopus</i> oocytes	159
Kinetic properties	160
Electrophysiological measurements	161
Conclusions	161
Endnotes	170
Bibliography	171
Chapter 4: Specific Mutations in Transmembrane Helix 8 of Human Concentrative Na⁺/Nucleoside Cotransporter hCNT1 Affect Permeant Selectivity and Cation Coupling	173
Acknowledgements	174

	<u>Page</u>
Introduction	175
Results and Discussion	176
Surface expression of hCNT1 TM 8 mutants	176
Nucleoside specificities of hCNT1 TM 8 mutants	176
Nucleoside inhibition of uridine uptake by hCNT1, S353T, L354V and S353T/L354V	177
Kinetic properties of hCNT1 TM 8 mutants	178
Additional mutants	179
Cation specificity of hCNT1 TM 8 mutants	180
Kinetics of Li ⁺ -dependent uridine transport by L354V	181
<i>p</i> -Chloromercuribenzenesulfonate (PCMBS) inhibition of S353C- and L354C-mediated uridine transport	182
Conclusions	183
Bibliography	198
Chapter 5: The Broadly Selective Human Na⁺/Nucleoside Cotransporter (hCNT3) Exhibits Novel Cation-Coupled Nucleoside Transport Characteristics	200
Acknowledgements	201
Introduction	202
Results	202
Cation-dependence of hCNT3	202
Cation-induced changes in hCNT3 permeant selectivity	203
Voltage-dependence of hCNT3 transport currents	204
Voltage-dependence of hCNT3 transport kinetics	205
Cation-dependence of uridine transport kinetics	206

	<u>Page</u>
Na ⁺ - and H ⁺ -activation kinetics	206
Na ⁺ :nucleoside and H ⁺ :nucleoside coupling ratios	207
Charge-to-Na ⁺ stoichiometry	208
Characterization of hCNT3/hCNT1 chimeras	208
Discussion	209
Bibliography	239
Chapter 6: Cation Coupling Properties of Human Concentrative Nucleoside Transporters hCNT1, hCNT2 and hCNT3	244
Acknowledgements	245
Introduction	246
Results	247
Cation specificity	247
Na ⁺ -activation kinetics	248
Na ⁺ :nucleoside coupling ratios	249
Charge-to-Na ⁺ stoichiometry	250
Discussion	250
Bibliography	266
Chapter 7: A Proton-Mediated Conformational Shift Identifies a Mobile Pore-Lining Cysteine Residue (Cys⁵⁶¹) in Human Concentrative Nucleoside Transporter 3 (hCNT3)	270
Acknowledgements	271
Introduction	272
Results	272

	<u>Page</u>
PCMBS inhibition of hCNT3	272
Concentration dependence and uridine protection of PCMBS inhibition	274
Electrophysiology of PCMBS inhibition	275
PCMBS inhibition of hCNT3 mutants	275
PCMBS inhibition of hCNT3C- mutants	276
PCMBS inhibition of mutant S561C(C-): concentration dependence and uridine protection	276
Effects of methanethiosulfonate (MTS) reagents	276
Substituted cysteine accessibility method (SCAM) analysis of TM 12	277
Discussion	278
Bibliography	304
Chapter 8: A Conformationally Mobile Cysteine Residue (Cys⁵⁶¹) Modulates Na⁺- and H⁺-Activation of Human Concentrative Nucleoside Transporter 3 (hCNT3)	307
Acknowledgements	308
Introduction	309
Results	310
Time course of radiolabeled uridine uptake by oocytes producing hCNT3C-	310
hCNT3C- nucleoside selectivity and cation dependence	310
Cell-surface expression and glycosylation of hCNT3C-	312
Kinetic characterization of hCNT3C-	312
Electrophysiological determination of hCNT3C- Na ⁺ -activation kinetics	314

	<u>Page</u>
Presteady-state electrophysiology of hCNT3C-	314
Na ⁺ :uridine and H ⁺ :uridine stoichiometry	315
Cation-activation of aglyco-hCNT3	315
Cation-activation of hCNT3C- mutants	316
Cation-activation of hCNT3 mutant C561S	317
Cation-activation of hCNT1 and hCNT1 mutant C540S	317
Other amino acid substitutions of hCNT3 residue Cys ⁵⁶¹	317
Discussion	318
Endnotes	343
Bibliography	344
Chapter 9: Conserved Glutamate Residues Glu³⁴³ and Glu⁵¹⁹ Provide Mechanistic and Structural Insights into Cation/Nucleoside Cotransport by Human Concentrative Nucleoside Transporter 3 (hCNT3)	347
Acknowledgements	348
Introduction	349
Results	349
Residues identified for mutagenesis	349
Transport activity of hCNT3 mutants	350
Additional hCNT3 mutants	351
Cell-surface expression of hCNT3 Glu ³⁴³ and Glu ⁵¹⁹ mutants	351
Nucleoside selectivity of hCNT3 Glu ³⁴³ and Glu ⁵¹⁹ mutants	352
Uridine transport kinetics of hCNT3 Glu ³⁴³ and Glu ⁵¹⁹ mutants	353
Guanosine inhibition kinetics of hCNT3 Glu ³⁴³ and Glu ⁵¹⁹ mutants	353

	<u>Page</u>
Na ⁺ -activation kinetics of hCNT3 Glu ³⁴³ and Glu ⁵¹⁹ mutants	354
H ⁺ -activation of hCNT3 Glu ³⁴³ and Glu ⁵¹⁹ mutants	355
Steady-state currents of hCNT3 Glu ³⁴³ and Glu ⁵¹⁹ mutants	355
Cation:nucleoside coupling ratios of hCNT3 Glu ³⁴³ and Glu ⁵¹⁹ mutants	356
Current-voltage (I-V) relationships of E343Q	357
Na ⁺ -activation kinetics of hCNT3 mutant E519C determined by electrophysiology	358
<i>p</i> -Chloromercuribenzenesulfonate (PCMBS) inhibition of hCNT3 E343C and E519C	358
Discussion	359
Bibliography	392
Chapter 10: Novel Topology of the TM 11A Region of Human Concentrative Nucleoside Transporter hCNT3 Revealed by Substituted Cysteine Accessibility Method (SCAM) Analysis	396
Acknowledgements	397
Introduction	398
Results	399
Functional activity of single cysteine mutants	399
PCMBS inhibition of single cysteine mutants	401
Uridine protection of PCMBS inhibition	402
Discussion	404
Bibliography	431
Chapter 11: General Discussion	433

	<u>Page</u>
Synopsis	434
Molecular Mechanisms of CNT Cation/Nucleoside Cotransport	441
TMs Involved in Interactions with Nucleosides	441
TMs Involved in Interactions with Cations	442
Putative Mechanisms of CNT Cation/Nucleoside Cotransport	443
Topology	449
Future Directions	451
Bibliography	454
Appendix 1: Identification and Functional Characterization of Variants in Human Concentrative Nucleoside Transporter 3, hCNT3 (SLC28A3), Arising from Single Nucleotide Polymorphisms in Coding Regions of the hCNT3 Gene	458
Appendix 2: Transport of Physiological Nucleosides and Anti-Viral and Anti-Neoplastic Nucleoside Drugs by Recombinant <i>Escherischia coli</i> Nucleoside-H⁺ Cotransporter (NupC) Produced in <i>Xenopus laevis</i> Oocytes	469
Appendix 3: Characterization of the Transport Mechanism and Permeant Binding Profile of the Uridine Permease Fui1p of <i>Saccharomyces cerevisiae</i>	480
Appendix 4: Conserved Glutamate Residues are Critically Involved in Na⁺/Nucleoside Cotransport by Human Concentrative Nucleoside Transporter 1 (hCNT1)	493

List of Tables

	<u>Page</u>
Table 1-1	Identified members of the equilibrative nucleoside transporter (ENT) family. 66
Table 1-2	Apparent K_m values for human ENT and CNT family members. 69
Table 1-3	Identified members of the concentrative nucleoside transporter (CNT) family. 70
Table 1-4	Identified members of the organic cation transporter (OCT) family. 71
Table 1-5	Identified members of the organic anion transporter (OAT) family. 73
Table 1-6	Identified members of the nucleoside:H ⁺ symporter (NHS) family. 76
Table 1-7	Identified members of the Tsx channel-forming protein family. 77
Table 1-8	Identified members of the uracil/allantoin permease family. 78
Table 1-9	Identified members of the nucleoside permease (NUP) family. 79
Table 3-1	CaCNT kinetic parameters. 163
Table 4-1	Kinetic parameters for uridine, thymidine and cytidine uptake by hCNT1 and hCNT1 mutants produced in <i>Xenopus</i> oocytes. 185
Table 5-1	Apparent K_m and V_{max} values for uridine transport by hCNT3. 215

	<u>Page</u>	
Table 5-2	Na ⁺ - and H ⁺ -activation kinetics of hCNT3.	216
Table 5-3	Stoichiometry of hCNT3.	217
Table 6-1	Na ⁺ -activation kinetics of uridine uptake by hCNT1, hCNT2 and hCNT3.	254
Table 6-2	Voltage-dependence of Na ⁺ -activation kinetics of hCNT1, hCNT2 and hCNT3.	255
Table 6-3	Stoichiometry of hCNT1, hCNT2 and hCNT3.	256
Table 7-1	Effects of PCMBs on uridine uptake in <i>Xenopus</i> oocytes expressing hCNT3C- and single-cysteine mutants.	285
Table 8-1	Uridine kinetic parameters for hCNT3 and hCNT3C-.	324
Table 8-2	Na ⁺ -activation kinetic parameters for hCNT3, hCNT3C- and mutants.	325
Table 8-3	H ⁺ -activation kinetic parameters for hCNT3, hCNT3C- and mutants.	326
Table 9-1	Mediated uptake of radiolabeled nucleosides by hCNT3 and mutants.	369
Table 9-2	Kinetic parameters for uridine uptake mediated by hCNT3 and mutants.	370
Table 9-3	Na ⁺ - and H ⁺ -activation kinetic parameters for hCNT3 and mutants.	371
Table 9-4	Na ⁺ :uridine and H ⁺ :uridine stoichiometry for hCNT3 and mutants.	372

	<u>Page</u>
Table 9-5 Comparison of hCNT1 and hCNT3 mutations.	373
Table 10-1 Na ⁺ - and H ⁺ -mediated uptake of uridine in <i>Xenopus</i> oocytes expressing hCNT3C- single cysteine mutants.	414
Table 10-2 Effect of PCMBS on uridine uptake in <i>Xenopus</i> oocytes expressing hCNT3C- single cysteine mutants.	420

List of Figures

		<u>Page</u>
Figure 1-1	Chemical structures of physiological pyrimidine and purine nucleosides and the purine nucleobase hypoxanthine.	80
Figure 1-2	Chemical structures of chemotherapeutic pyrimidine and purine nucleoside analogs.	81
Figure 1-3	Chemical structures of ENT inhibitors.	82
Figure 1-4	Putative ENT topology model.	83
Figure 1-5	Putative CNT topology model.	84
Figure 3-1	Differences in deduced amino acid sequences of CaCNT and those derived from Contigs 19-10196 and 19-20196 (Stanford Genome Technology Center database).	164
Figure 3-2	Transport of uridine by CaCNT-, CaCNT/19-10196- and CaCNT/19-20196-producing oocytes.	165
Figure 3-3	Permeant selectivity of CaCNT-, CaCNT/19-10196- and CaCNT/19-20196-producing oocytes.	166
Figure 3-4	Kinetic properties of CaCNT and CaCNT/19-20196.	167
Figure 3-5	Proton currents induced by exposure of recombinant CaCNT and CaCNT/19-20196 to uridine.	168
Figure 3-6	Stoichiometry of H ⁺ :uridine cotransport by recombinant CaCNT/19-20196.	169
Figure 4-1	hCNT1 topology model.	186

	<u>Page</u>
Figure 4-2	Functional activity and protein expression levels of hCNT1-, S353T-, L354V- and S353T/L354V-producing oocytes. 187
Figure 4-3	Nucleoside selectivity of hCNT1-, S353T-, L354V- and S353T/L354V-producing oocytes. 188
Figure 4-5	Inhibition of hCNT1-, S353T-, L354V- and S353T/L354V-mediated uridine uptake by physiological nucleosides. 189
Figure 4-5	Thymidine inhibition of uridine uptake by hCNT1- and S353T/L354V-producing oocytes. 190
Figure 4-6	Uridine, thymidine and cytidine uptake kinetics in oocytes producing hCNT1, S353T, L354V and S353T/L354V. 191
Figure 4-7	Na ⁺ - and Li ⁺ -dependent nucleoside transport by hCNT1 and L354V. 192
Figure 4-8	hCNT1 and L354V Na ⁺ - and Li ⁺ -activation kinetics. 193
Figure 4-9	Concentration dependence of Na ⁺ - and Li ⁺ -dependent uridine uptake by hCNT1 and L354V. 194
Figure 4-10	Uridine-evoked currents in hCNT1- and L354V-producing oocytes. 195
Figure 4-11	PCMBS inhibition of hCNT1-, S353C- and L354C-mediated uridine transport. 196
Figure 5-1	Effects of Na ⁺ , H ⁺ and Li ⁺ on the transport activities of oocytes expressing recombinant hCNT3. 218
Figure 5-2	Cation/nucleoside currents. 219

	<u>Page</u>
Figure 5-3	Permeant selectivity and pH-dependence of nucleoside transport by recombinant hCNT3. 221
Figure 5-4	Nucleoside drug-induced currents in hCNT3-producing <i>Xenopus</i> oocytes. 223
Figure 5-5	Voltage-dependence of hCNT3-mediated currents. 225
Figure 5-6	Voltage-dependence of the transport kinetics of hCNT3. 227
Figure 5-7	Kinetic properties of Na ⁺ - and H ⁺ -coupled hCNT3. 229
Figure 5-8	Na ⁺ - and H ⁺ -activation of hCNT3. 230
Figure 5-9	Stoichiometries of Na ⁺ :uridine and H ⁺ :uridine cotransport by recombinant hCNT3. 232
Figure 5-10	Charge-to-Na ⁺ stoichiometry of hCNT3. 234
Figure 5-11	Transport properties of chimera hCNT3/1. 235
Figure 6-1	Effects of Na ⁺ and H ⁺ on the transport activities of recombinant hCNT1, hCNT2 and hCNT3 produced in <i>Xenopus</i> oocytes. 257
Figure 6-2	Cation-activation kinetics of hCNT1, hCNT2 and hCNT3. 259
Figure 6-3	Voltage-dependence of hCNT1, hCNT2 and hCNT3 cation-activation kinetics. 261
Figure 6-4	Uridine coupling ratios of hCNT1, hCNT2 and hCNT3. 263
Figure 6-5	Adenosine coupling ratios of hCNT2 and hCNT3. 265

	<u>Page</u>
Figure 7-1	Cysteine residues in hCNT1, hCNT2 and hCNT3. 287
Figure 7-2	PCMBS inhibition of hCNT3. 289
Figure 7-3	PCMBS insensitivity of hCNT1 and hCNT2. 291
Figure 7-4	Reversal of PCMBS inhibition of hCNT3-mediated uridine uptake by DTT. 292
Figure 7-5	PCMBS inhibition of hCNT3: concentration dependence and uridine protection. 293
Figure 7-6	PCMBS inhibition of hCNT3: concentration dependence of uridine protection. 294
Figure 7-7	Time courses of presteady-state currents measured in a hCNT3-expressing oocyte elicited by voltage pulses before and after treatment with PCMBS. 295
Figure 7-8	Effects of PCMBS on hCNT3 and hCNT3C- mutants. 297
Figure 7-9	PCMBS inhibition of hCNT3C- mutant S561C(C-): concentration dependence and uridine protection. 299
Figure 7-10	Effects of MTS reagents on hCNT1, hCNT2, hCNT3 and mutants. 300
Figure 7-11	Molecular modeling of hCNT3 TM 12. 301
Figure 8-1	Topological model of hCNT3. 327
Figure 8-2	Time course of uridine uptake by hCNT3C- in <i>Xenopus</i> oocytes. 328

		<u>Page</u>
Figure 8-3	Nucleoside and cation selectivity of hCNT3C-.	329
Figure 8-4	Immunoblot analysis of hCNT3, hCNT3C- and aglyco-hCNT3.	330
Figure 8-5	Concentration dependence of Na ⁺ - and H ⁺ -coupled uridine uptake by oocytes producing hCNT3 and hCNT3C-.	331
Figure 8-6	Na ⁺ -and H ⁺ -activation kinetics of oocytes producing hCNT3 and hCNT3C-.	332
Figure 8-7	Na ⁺ -activation of hCNT3 and hCNT3C- determined by electrophysiology.	334
Figure 8-8	Presteady-state currents of hCNT3C-.	335
Figure 8-9	Na ⁺ :uridine and H ⁺ :uridine stoichiometry of hCNT3C-.	336
Figure 8-10	Na ⁺ -activation kinetics of oocytes producing hCNT3C- mutants S486C(C-), S561C(C-), S602C(C-) and S607C(C-).	338
Figure 8-11	Na ⁺ -and H ⁺ -activation kinetics of oocytes producing hCNT3 mutant C561S.	339
Figure 8-12	Na ⁺ -activation kinetics of oocytes producing hCNT1 and hCNT1 mutant C540S.	340
Figure 8-13	Cation selectivity of hCNT3 mutants.	341
Figure 8-14	Steady-state currents of hCNT3 mutants.	342
Figure 9-1	Putative hCNT3 topology model.	375

	<u>Page</u>
Figure 9-2	Cation selectivity of hCNT3 mutants. 376
Figure 9-3	Cell-surface expression levels of hCNT3 and mutants. 377
Figure 9-4	Nucleoside selectivity of hCNT3 and mutants. 378
Figure 9-5	Uridine kinetics of hCNT3 and mutants. 379
Figure 9-6	Guanosine inhibition of hCNT3 and mutants. 380
Figure 9-7	Na ⁺ -activation kinetics of hCNT3 and mutants. 381
Figure 9-8	H ⁺ -activation kinetics of hCNT3 and mutants. 382
Figure 9-9	Uridine-evoked steady-state currents of hCNT3 and mutants. 383
Figure 9-10	Na ⁺ :uridine stoichiometry of hCNT3 and mutants. 386
Figure 9-11	Current-voltage relationships of E343Q-mediated uridine transport. 388
Figure 9-12	Na ⁺ -activation kinetics of hCNT3 and E519C determined by electrophysiology. 390
Figure 9-13	PCMBS inhibition of hCNT3-, E343C- and E519C-mediated uridine transport. 391
Figure 10-1	Alternative models of hCNT3 topology. 422
Figure 10-2	hCNT3 TMs 11 - 13 depicting residues with altered Na ⁺ :H ⁺ uridine uptake ratios. 423

		<u>Page</u>
Figure 10-3	PCMBS inhibition of residues in hCNT3C- TMs 11, 12 and 13.	424
Figure 10-4	PCMBS inhibition of residues in hCNT3C- loop regions between TMs 11 and 12, and TMs 12 and 13.	425
Figure 10-5	hCNT3 TMs 11 - 13 depicting PCMBS-inhibited and uridine-protected residues.	426
Figure 10-6	Helical wheel projections of hCNT3 TMs 11, 12 and 13.	427
Figure 10-7	Revised hCNT3 TM 11 - 13 topology depicting TM 11A as membrane-spanning.	429

List of Nomenclature, Abbreviations and Symbols

2-CdA	cladribine
ACV	2-amino-9-[(2-hydroxyethoxy)methyl]-3,9-dihydro-6 <i>H</i> -purin-6-one; acyclic guanosine derivative; ACV
acyclovir	ACV
araA	adenine arabinoside
araC	cytarabine
At	<i>Arabidopsis thaliana</i>
AT	adenosine transporter
ATP	adenosine triphosphate
AV	atrioventricular
AZT	zidovudine
BLAST	basic local alignment search tool
BSA	bovine serum albumin
Ca	<i>Candida albicans</i>
cAMP	cyclic adenosine monophosphate
capecitabine	5'-deoxy-5- <i>N</i> -[(pentoxycarbonyl)]-cytidine

CCCP	carbonyl cyanide <i>m</i> -chlorophenylhydrazone
cDNA	complementary deoxyribonucleic acid
Ce	<i>Caenorhabditis elegans</i>
Cf	<i>Crithidia fasciculata</i>
cGMP	cyclic guanosine monophosphate
ChCl	choline chloride
Ci	curie
<i>cib</i>	concentrative, insensitive to NBMPR, broadly selective
<i>cif</i>	concentrative, insensitive to NBMPR, formycin B-transporting
<i>cit</i>	concentrative, insensitive to NBMPR, thymidine-transporting
cladribine	2'-chloro-2'-deoxyadenosine; 2-CdA
clofarabine	2-chloro-9-(2'-deoxy-2'-fluoro- β -D-arabinofuranosyl)adenine
CNT	concentrative nucleoside transporter
cordycepin	3'-deoxyadenosine
<i>cs</i>	concentrative, sensitive to NBMPR
CSF	colony stimulating factor

<i>csg</i>	concentrative, sensitive to NBMPR, guanosine-transporting
cytarabine	1- β -D-arabinofuranosyl cytosine; araC
ddC	zalcitabine
ddI	didanosine
deoxytubercidin	7-deazadeoxyadenosine
dFdC	gemcitabine
DHEA	dihydroepiandrosterone
didanosine	2', 3'-dideoxyinosine; ddI
Dm	<i>Drosophila melanogaster</i>
DMSO	dimethyl sulfoxide
DNA	deoxyribonucleic acid
DTT	dithiothreitol
<i>ei</i>	equilibrative insensitive
ENT	equilibrative nucleoside transporter
<i>es</i>	equilibrative sensitive
EST	expressed sequence tag
F-araA	fludarabine

fialuridine	1-(2-deoxy-2-fluoro- β -D-arabinofuranosyl)-5-iodouracil; FIAU
FIAU	fialuridine
fludarabine	9- β -D-arabinosyl-2-fluoroadenine; F-araA
FUN	function unknown now
g	gram
GABA	γ -aminobutyric acid
ganciclovir	2-amino-9-(1,3-dihydroxypropan-2-yloxymethyl)-3 <i>H</i> -purin-6-one; acyclic guanosine derivative; GCV
GCV	ganciclovir
gemcitabine	2', 2'-difluorodeoxycytidine; dFdC
GFP	green florescent protein
GTP	guanosine triphosphate
h	human
HEPES	4-(2-hydroxyethyl)-1-piperazineethanesulfonic acid
hf	hagfish
HIV	human immunodeficiency virus
HNP	hydrophobic nuclear protein

Hz	hertz
IC ₅₀	inhibitor concentration at half-maximal unidirectional flux; apparent inhibition constant
IFN	interferon
I _{max}	maximum current
I-V	current-voltage
K ₅₀	cation concentration at half-maximal unidirectional flux; apparent affinity for cation
K _m	permeant concentration at half-maximal unidirectional flux; apparent affinity for permeant
l	liter
lamivudine	2', 3'-dideoxy-3'-thiacytidine
Ld	<i>Leishmania donovani</i>
LPS	lipopolysaccharide
m	mouse
M	molar
MBSS	MES-buffered saline for silica
M-CSF	macrophage colony stimulating factor
MDCK	Madin-Darby canine kidney

MDR	multidrug resistance
MEK	MAP and ERK kinase; dual specificity protein kinase that phosphorylates tyrosine and serine residues
MES	2-(<i>N</i> -morpholino)ethanesulfonic acid
MFS	major facilitator superfamily
min	minute
mM	millimolar
mol	mole
MPP ⁺	1-methyl-4-phenylpyridinium
mRNA	messenger ribonucleic acid
mTOR	murine target of rapamycin
MTS	methanethiosulfonate
MTSEA	2-aminoethyl methanethiosulfonate hydrobromide
MTSES	sodium (2-sulfonatoethyl) methanethiosulfonate
MTSET	[(triethylammonium)ethyl] methanethiosulfonate bromide
mV	millivolts
NBMPR	nitrobenzylmercaptapurine ribonucleoside; 6-[(4-nitrobenzyl)thio]- 9-β-D-ribofuranosylpurine; nitrobenzylthioinosine

NBT	nucleobase transporter
nd	not determined
NHS	nucleoside:H ⁺ symporter
NLT	novel liver transporter
NO	nitric oxide
NT	nucleoside transporter
NUP	nucleoside permease
OAT	organic anion transporter
OAT-PG	organic anion transporter-prostaglandin-specific
OCT	organic cation transporter
OCTN	organic cation transporter-novel
Omp	outer membrane protein
Os	<i>Oryza sativa</i>
PAH	<i>p</i> -aminohippurate
PCMBS	<i>p</i> -chloromercuribenzenesulfonate
PCR	polymerase chain reaction
Pf	<i>Plasmodium falciparum</i>

PGE ₂	prostaglandin E ₂
PGF ₂	prostaglandin F ₂
pk	pig kidney
PKC	protein kinase C
PMA	phorbol 12-myristate 13-acetate
PMA-RE	phorbol myristate acetate response element
PMAT	plasma membrane monoamine transporter
r	rat
rb	rabbit
ribavirin	1-(β-D-ribofuranosyl)-1 <i>H</i> -1,2,4-triazole-3-carboxamide; guanosine analog with 1, 2, 4-triazole-3-carboxamide group at C-1' in place of pyrimidine group
RNA	ribonucleic acid
RT-PCR	reverse transcriptase polymerase chain reaction
SA	sinoatrial
SCAM	substituted cysteine accessibility method
SDS	sodium dodecyl sulphate
SE	standard error of the fitted estimate

sec	second
SEM	standard error of the mean
serotonin	5-hydroxytryptamine; 5-HT
SGLT	sodium glucose transporter
SLC	solute carrier
SNP	single nucleotide polymorphism
SNST	sodium-dependent nucleoside transporter
Sp1	specific protein 1
SPNT	sodium-dependent purine nucleoside transporter
stavudine	2', 3'-didehydro-3'-deoxythymidine
sulfo-NHS-LC-biotin	sulfosuccinimidyl-6-(biotinamido) hexanoate
TaraC	4'-thio- β -D-arabinofuranosyl cytosine
Tb	<i>Trypanosoma brucei brucei</i>
TEA	tetraethylammonium
Tg	<i>Toxoplasma gondii</i>
TM	transmembrane domain
TNF	tumor necrosis factor

trifluridine	2'-deoxy-5-(trifluoromethyl)uridine
Tsx	T6 (six) phage receptor
tubercidin	7-deazaadenosine
UTR	untranslated region
V	volt
V_h	holding potential
V_m	membrane potential
V_{max}	maximum transport rate
V_t	test potential
w/v	weight per volume
YFP	yellow florescent protein
zalcitabine	2', 3'-dideoxycytidine; ddC
zebularine	2-pyrimidine-1- β -D-ribose
zidovudine	3'-azido-3'-deoxythymidine; AZT
$^{\circ}\text{C}$	degrees Celsius
Ω	ohms
μ	micro; 10^{-6}

Chapter 1:
General Introduction

Nucleoside Transport

Physiological Importance

Nucleosides are important physiological molecules. Naturally occurring nucleosides include the purine nucleosides adenosine, guanosine and inosine and the pyrimidine nucleosides uridine, cytidine and thymidine (Fig. 1-1). Nucleosides serve as the metabolic precursors to nucleotides which are fundamental biological molecules involved in the formation of DNA, RNA and high-energy compounds, such as ATP. Adult pig erythrocytes, which lack glucose transporters, use inosine as an *in vivo* energy source (1, 2). Likewise, in the absence of glucose transporters, nucleosides are critical for sustaining metabolism in embryonic and adult chicken erythrocytes (3, 4). The purine nucleoside adenosine is also a ubiquitous signaling molecule that mediates numerous physiological processes by binding to cell-surface adenosine receptors (5, 6). For example, adenosine regulates myocardial O₂ supply-demand balance via coronary vasodilation and cardiac pacemaking and contractility, and functions as a cardioprotective agent in the ischemic/reperfused myocardium (5-14). Additionally, adenosine is involved in regulation of inflammation (15, 16), lipolysis (17), vascular tone (5, 14, 18), platelet aggregation (19, 20), renal function (21, 22), nociception (23, 24) and neurotransmission and neuromodulation in the central nervous system (25-28).

Nucleosides are hydrophilic molecules. As a result, passive diffusion of these molecules across biological membranes is limited, and therefore specialized nucleoside transport proteins are required for their passage across plasma membranes or between intracellular compartments (28-35). Thus, cellular uptake of both purine and pyrimidine nucleosides via nucleoside transport proteins is important for the synthesis of nucleic acid precursors by salvage pathways (28-35). Nucleoside salvage is energetically more favorable than *de novo* biosynthesis and plays an important role in nucleoside and nucleotide homeostasis (36-38). Additionally, some cell types are deficient in purine *de novo* biosynthetic pathways and thus, rely solely on imported nucleosides for purine nucleotide synthesis. In mammalian cells, for example, this

includes bone marrow cells (39), erythrocytes (40, 41), intestinal enterocytes (42), leukocytes and certain brain cells which lack purine *de novo* biosynthetic pathways (43). Nucleoside salvage pathways are also important for parasitic organisms, such as protozoan and helminth parasites, that lack purine *de novo* biosynthetic capability (44-49). Nucleosides are acquired from dietary sources, salvaged in the kidney and produced by tissues such as the liver (39, 50-54).

Once hydrophilic nucleosides are taken up into cells across the plasma membrane, nucleoside transport proteins are also involved in their movement from the cytosol into intracellular organelles (31). Nucleoside release from cells and intracellular organelles is also necessary for cell function, especially to prevent excess accumulation of nucleotide breakdown products. This is evident, for example, in fibroblast lysosomes which are responsible for the degradation of nucleic acids into nucleosides (55). Nucleoside transport proteins are also responsible for determining the levels of free nucleosides in the general circulation and are thus able to regulate the extracellular physiological effects of nucleosides. For example, nucleoside transporters regulate the concentration of adenosine available to cell surface purinoreceptors and therefore, play an important role in the many adenosine-regulated physiological processes (29, 32).

Pharmacological Importance

Exploitation of the importance of physiological nucleosides led to the development of nucleoside analogs as chemotherapeutic agents. This group of cytotoxic compounds has been used in the treatment of both neoplastic and viral disease, including hematological and solid malignancies, such as leukemias, lymphomas and gastrointestinal tract cancers, as well as human immunodeficiency virus (HIV) and herpes virus infections (28, 56-58). Upon entering the cell, nucleoside analogs exert cytotoxic actions by undergoing phosphorylation to their 5'-triphosphate derivatives by nucleoside kinases, such as deoxycytidine, deoxyguanosine and thymidine kinases, as well as by 5'-nucleoside monophosphate

and 5'-nucleoside diphosphate kinases (59). Deamination by adenosine or cytidine deaminase and interference by cytoplasmic 5'-nucleotidases will decrease the available concentration of active chemotherapeutic agent (59). Phosphorylated nucleoside analogs interfere with nucleotide metabolism and RNA and DNA replication events, resulting in antiproliferative effects and resistance to virus replication.

Antineoplastic chemotherapeutics include both purine nucleoside analogs, such as 2'-chloro-2'-deoxyadenosine (cladribine; 2-CdA) and 9- β -D-arabinosyl-2-fluoro-adenine (fludarabine; F-araA), and pyrimidine nucleoside analogs, such as 1- β -D-arabino-furanosyl cytosine (cytarabine; araC) and 2', 2'-difluorodeoxycytidine (gemcitabine; dFdC) (32, 56-59). The structures of these compounds are depicted in Fig. 1-2. F-araA is used clinically to treat chronic lymphocytic leukemia, low-grade lymphomas and other hematological malignancies (58, 59). Upon phosphorylation, F-araATP inhibits several enzymes involved in nucleoside synthesis and DNA replication including DNA polymerase, DNA primase, ribonucleotide reductase and DNA ligase I, and incorporation of F-araATP into DNA and RNA results in premature chain termination (58, 59). Differing in structure by a chlorine substitution of fluorine in the 2 position of the adenine moiety, 2-CdA in its active triphosphate form also inhibits DNA replication and repair, and ribonucleotide reductase (57, 58). Hematological malignancies, including low-grade lymphomas, chronic lymphocytic leukemia and hairy cell leukemia, are all treated clinically with 2-CdA (58, 59). The pyrimidine nucleoside analog, araC is also used clinically against haemotopoietic malignancies, such as acute myelogenous leukemia and non-Hodgkin's lymphoma (57-60). In its active phosphorylated form, araCTP inhibits DNA polymerase α and induces chain termination upon incorporation into DNA (57-59). The araC analog dFdC is used in the treatment of solid tumors, including pancreatic, breast, non-small cell lung, ovarian, bladder and head and neck cancers (58, 59). Unlike araC, but similar to 2-CdA, phosphorylated dFdCDP inhibits ribonucleotide reductase, thereby decreasing intracellular concentrations of natural deoxynucleotides (57-59, 61). Incorporation of dFdCTP into DNA is followed by the addition of a physiological deoxynucleotide, thereby causing masked chain termination and prevention of repair

by proof-reading exonucleases (57, 58, 61). In addition to their direct cytotoxic activity, fluoropyrimidines such as dFdC, also trigger sensitization to radiation by distributing cells into early S phase of the cell cycle, thereby taking advantage of the intrinsic differences in cell cycle progression between normal and tumor cells to confer relative specificity to the treatment (57, 62, 63).

Antiviral nucleoside analogs include 3'-deoxynucleosides such as 2', 3'-dideoxyinosine (didanosine; ddI), 2', 3'-dideoxycytidine (zalcitabine; ddC) and 3'-azido-3'-deoxythymidine (zidovudine; AZT) which are also depicted in Fig. 1-2 (57, 64). AZT, for example, is used clinically for the treatment of HIV (57, 65, 66). Similar to antineoplastic nucleoside analogs, these compounds are active in triphosphate form where incorporation into growing viral DNA results in chain termination through the inhibition of reverse transcription (57).

Similar to their physiological parent compounds, most synthetic nucleoside analogs are hydrophilic. Therefore, nucleoside transporters play a critical role in mediating the cellular uptake, and thus the subsequent metabolism and pharmacological action(s) of the nucleoside analog chemotherapeutic (29, 32, 35, 56, 57, 59). The efficient intracellular delivery of nucleoside analog chemotherapeutics is dependent upon the presence of functional nucleoside transporters in plasma membranes and is mechanistically linked to both drug toxicity and resistance (56).

The inability of parasitic protozoa to synthesize purines *de novo* results in dependence on scavenging mechanisms for the uptake of purine nucleosides to enable growth and survival, and provides an opportunity for pharmacologic intervention (67, 68). Parasitic disease presents a health problem worldwide. For example, the parasitic protozoa of the family *Trypanosomatidae* are responsible for Chagas' disease and African sleeping sickness, *Leishmania* are responsible for leishmaniasis and *Plasmodium* causes malaria (67, 69). The possible use of nucleoside analog drugs specific to nucleoside transport proteins in the parasite, or specific parasite purine nucleoside transporter inhibitors would be clinically beneficial in the treatment of parasitic disease.

The profound effects of adenosine as a signaling molecule have also made it a valuable pharmacological target. For example, adenosine is used for the treatment of supraventricular tachycardia, and adenosine agonists and antagonists have well defined clinical roles in the treatment of other human diseases including hypertension, renal failure and epilepsy (8, 53). Administration of adenosine to patients before coronary artery bypass surgery reduces myocardial injury (70, 71). Nucleoside transport across cellular membranes can profoundly influence local concentrations of adenosine, and nucleoside transporter inhibitors can potentiate the actions of adenosine (8, 53, 72, 73). In the heart for example, under normoxic conditions, the net flux of adenosine is into cardiomyocytes and endothelial cells (74); administration of nucleoside transport inhibitors, such as dipyridamole, dilazep or draflazine (Fig. 1-3), prevent influx of adenosine across the cell membrane, thereby increasing extracellular adenosine concentrations, potentiating the interaction with adenosine receptors and resulting in adenosine-mediated cardiovascular effects, such as vasodilation (8, 75, 76). In addition to vasodilatory effects, dipyridamole, for example, also potentiates the chronotropic and dromotropic effects of adenosine on the sinoatrial (SA) and atrioventricular (AV) nodes, respectively (77). Pharmacological manipulation of adenosine transport through the use of inhibitors may also provide an alternative strategy for exploiting the preconditioning abilities of adenosine to attenuate ischemic injury in patients undergoing heart surgery (76).

Nucleoside Transport Proteins

Nucleoside transport processes have been identified in both eukaryotic and prokaryotic cells. Molecular cloning strategies and functional expression of cDNAs, as well as genome sequencing projects and bioinformatic analysis, have resulted in the identification of a diverse array of structurally distinct nucleoside transport proteins. These nucleoside transport processes and corresponding proteins comprise members from eight different integral membrane protein families. In mammalian cells, this includes the equilibrative nucleoside transporter (ENT), concentrative

nucleoside transporter (CNT), organic cation transporter (OCT) and organic anion transporter (OAT) families. In lower eukaryotes and prokaryotes, this includes the nucleoside:H⁺ symporter (NHS), Tsx channel-forming protein, uracil/allantoin permease and nucleoside permease (NUP) families. Each protein family contains multiple members, the majority of which have been discovered only by virtue of their sequence similarity to previously cloned mammalian isoforms and remain functionally uncharacterized.

The research presented in this thesis focuses primarily on human CNTs, but also includes investigations of lower eukaryote and prokaryote CNTs and, as well, a fungal nucleoside transporter belonging to the uracil/allantoin permease family of proteins. To place this work in proper context, and to enable the progress made to be assessed relative to current knowledge of other eukaryote and prokaryote nucleoside transporters, information from all eight nucleoside transporter families has been incorporated. Tables 1-1 and 1-3 to 1-9 summarize the proteins from each family which have been identified at the molecular level by means other than or in addition to sequence similarity to previously known family members. Only those with defined nucleoside transport properties are discussed.

Equilibrative Nucleoside Transporter (ENT) Family

Passive nucleoside transport across biological membranes is mediated by members of the ENT family (reviewed in 28-33, 35, 54, 78-83). This family of integral membrane proteins enables the bidirectional movement of hydrophilic nucleosides and nucleoside analogs across cellular membranes down their concentration gradients. The ENT family is widely distributed in eukaryotes, including mammals, protozoa, nematodes, insects, plants and fungi. Despite the nomenclature, the ENT family also includes H⁺-coupled transporters, such as protozoan *Leishmania donovani* (Ld) nucleoside transporters (NT) 1.1, LdNT1.2 and LdNT2 (84) and *Trypanosoma brucei brucei* (Tb) NT2, TbNT2/927, TbNT5, TbNT6

and TbNT7 (48, 85-87), and plant *Arabidopsis thaliana* (At) ENT1 and AtENT3 (88, 89). ENT family members that have been identified are listed in Table 1-1.

Mammalian ENT Family Members

Facilitated diffusion of nucleosides mediated by equilibrative nucleoside transport systems was the first mammalian nucleoside transport mechanism to be studied and was initially characterized in erythrocytes (1, 90-93). Subsequent studies revealed that most mammalian cells exhibit low-affinity, passive equilibrative nucleoside transport. Equilibrative nucleoside transport processes were first distinguished and subsequently classified on the basis of their sensitivity to inhibition by the S⁶-substituted 6-thiol-purine nucleoside derivative nitrobenzylmercaptapurine ribonucleoside (NBMPR) (1, 30, 91, 94). The chemical structure of NBMPR is depicted in Fig. 1-3. Accordingly named, the equilibrative nucleoside transport system *es* was sensitive to inhibition by nanomolar concentrations of NBMPR, whereas the *ei* nucleoside transport system was insensitive to NBMPR concentrations of < 1 μM (32, 95-97). The *es* transporter was identified as a band 4.5 polypeptide in photolabeling experiments with NBMPR (98) and its identity later confirmed by functional reconstitution of the purified protein into phospholipid vesicles (99). In addition to NBMPR, most *es* and *ei* transport processes were also inhibited by the non-nucleoside coronary vasodilators dipyridamole, dilazep and draflazine (Fig. 1-3) (30). Initial characterization studies of *es* and *ei* transport systems revealed that both display broad permeant selectivity, transporting both physiological purine and pyrimidine nucleosides and synthetic nucleoside analogs (1, 29, 30, 32, 56). The *ei* process was also capable of transporting the purine nucleobase hypoxanthine (100, 101).

Molecular identification of the first ENT occurred in 1997 with the cloning of human (h) hENT1 (102). Subsequent to the purification and N-terminal sequencing of the archetypal *es* transporter from human erythrocytes, the cDNA encoding hENT1 was isolated from a human placental cDNA library (102). Soon after, cDNA

encoding the *ei*-type transporter hENT2 was identified in a human placental cDNA library using homology cloning techniques based on sequence similarity to hENT1 (103) and, independently, in a HeLa cell cDNA library by functional complementation studies (101). hENT1 and hENT2 belong to the human solute carrier (SLC) 29 gene family of proteins and are classified as SLC29A1 and SCL29A2, respectively. Together, ENT1 and ENT2, with *es* and *ei* transport function, respectively, account for the majority of equilibrative nucleoside transport activity in mammalian cells. Two additional ENT family members, ENT3 and ENT4, were originally identified by genome database analysis (78, 79) and have been confirmed to function as nucleoside transporters (54, 104).

ENT1

The *es* nucleoside transport process in humans corresponds to a 40 kDa protein of 456 residues identified as hENT1 (102). It is 78% identical in sequence to the 457 residue rat (r) homolog rENT1 isolated from rat jejunal cDNA library (105) and 78% identical to the 458 residue mouse (m) homolog mENT1 isolated from mouse brain (106). The chromosomal location of the hENT1 gene is 6p21.1-21.6 (107, 108). No splice variants of hENT1 have been reported to date, and cloning of hENT1 from different tissues has identified identical amino acid sequences (109). However, there are two isoforms of mENT1 designated mENT1.1 corresponding to a 460 residue protein and mENT1.2 corresponding to a 458 residue variant generated by alternative splicing at the end of exon 7 and lacking a potential casein kinase II phosphorylation site (110, 111). mENT1.2 is widely distributed and appears to be functionally identical to mENT1.1, except for altered NBMPR binding affinity (111, 112). Overall, hENT1 exhibits a low degree of mutability and a study involving 247 DNA samples identified only four synonymous and two non-synonymous variants with low allele frequencies (113). Single nucleotide polymorphisms (SNPs) which have been described in the promoter (114) and coding (115) regions of hENT1 have no effect on function. mENT1-null mice are viable and fertile (116, 117).

ENT1 exhibits broad permeant selectivity, transporting both purine and pyrimidine nucleosides (102, 105, 106, 118). Upon expression in *Xenopus laevis* oocytes, nucleoside transport by hENT1 was saturable and conformed to Michaelis-Menten kinetics with an apparent K_m value of 0.24 mM for uridine (102). Recombinant hENT1 in a nucleoside transporter-deficient pig kidney tubular epithelial cell line (PK15 cells) exhibited apparent K_m values for all physiological nucleosides ranging from 0.04 mM (adenosine) to 0.58 mM (cytidine) (118). Additionally, using the same expression system, a turnover number of 46 molecules/sec for uridine transport at room temperature was demonstrated (118). The corresponding turnover number in erythrocytes for native hENT1 and other mammalian ENT1 transporters was ~ 150 molecules/sec at 25°C (81). A comparison of apparent K_m values for hENT1-mediated transport obtained in different expression systems, as well as those of other hENT and hCNT family members, are given in Table 1-2. In addition to physiological nucleosides, hENT1 mediates the uptake of chemotherapeutic nucleoside analogs including dFdC (119, 120), araC (121, 122), 2-CdA (58, 123), F-araA (58, 124), 4'-thio- β -D-arabinofuranosyl cytosine (TaraC) (122) and 5'-deoxy-5-fluorouridine, an intermediate metabolite of 5'-deoxy-5-*N*-[(pentoxycarbonyl)-cytidine (capecitabine) (125). In contrast, the antiviral 2', 3'-dideoxynucleosides ddC and ddI are poorly transported and AZT is not transported by hENT1 (126). As indicated by the transport process name *es*, ENT1-mediated nucleoside uptake (and efflux) is inhibited by nanomolar concentrations of NBMPR (102, 105, 106, 111, 118). Additionally, hENT1 and mENT1 are sensitive to inhibition by dipyridamole and dilazep (102, 106, 127), as well as by draflazine (128). In contrast, the rat homolog rENT1 is relatively insensitive to both dipyridamole and dilazep, requiring concentrations in excess of 1 μ M to inhibit transport activity (105, 129).

Initial hydropathy plots predicted ENT1 to have 11 transmembrane domains (TMs) in which the N-terminus is cytoplasmic and the C-terminus is extracellular with a large cytoplasmic loop linking TMs 6 and 7 (102, 130). This putative topology was experimentally verified by glycosylation scanning mutagenesis and antibody studies (130). Based on sequence comparisons, ENT family members are all

predicted to share this 11 TM topology, and a representative topology model is depicted in Fig. 1-4 (78, 130). In agreement with biochemical studies of the native *es* protein in erythrocytes (131, 132), hENT1 is a glycoprotein (118) and mutagenesis studies have revealed a single site of glycosylation at Asn⁴⁸ between TMs 1 and 2 (127). Although conversion of asparagine to glutamine at position 48 in hENT1 decreased its affinity for NBMPR and increased its affinity for dilazep and dipyridamole, glycosylation was not essential for function (127).

Consistent with early demonstrations that nucleoside uptake in most cell types occurred via an *es* process, ENT1 appears to be ubiquitously distributed in human and rodent tissues at both the mRNA and protein levels, although its abundance varies between tissues (54, 110, 111, 133). For example, cDNA with > 90% identity to placental cDNA was identified in fetal brain, liver and spleen, and in adult adipose tissue, aortic endothelial cells, brain, breast, colon, heart, lung, ovary, placenta, prostate and uterus, as well as malignant cells (31, 78). In brain, ENT1 is most abundant in the frontal and parietal lobes of the cerebral cortex, with moderate abundance in the thalamus, midbrain and basal ganglia and lower levels in other brain regions (134-136). This pattern of hENT1 distribution correlates well with adenosine A₁ receptor abundance (135). In the rat hippocampus, A_{2A} adenosine receptors were demonstrated to regulate ENT activity (137). hENT1-mediated adenosine transport was reported in human fetal astrocytes (138). In the heart, plasma membrane-associated immunostaining of rENT1 is apparent in atrial and ventricular myocytes, as well as in the SA node (139). Polarized epithelial cells of the kidney primarily show basolateral expression of ENT1, as demonstrated by immunocytochemical studies in rat kidney cortex tubular epithelial cells (54) and yellow fluorescent protein (YFP) or green fluorescent protein (GFP) tagged constructs expressed in renal epithelial Madin-Darby canine kidney (MDCK) cells (140, 141). However, in human kidney, hENT1 has been demonstrated to be present in both apical and basolateral membranes in proximal tubules, loop of Henle and collecting ducts (142, 143). Basolateral expression was evident for hENT1 in T84 intestinal epithelial cells (144) and in human duodenum, hENT1 mRNA was present in crypt cells with protein localized to lateral membranes (143). hENT1 mRNA and cell surface-expressed

protein were also present in hepatocytes and placental trophoblasts (143). In addition to its predominant localization to the plasma membrane, hENT1 has also been reported in the mitochondrial membrane of MDCK cells, and a mitochondrial targeting motif, PEXN, in the extracellular loop between TMs 1 and 2 has been identified (145, 146). In contrast to hENT1, both mENT1 and rENT1 are not localized to mitochondrial membranes and exhibit PEXS in place of the hENT1 targeting motif (146). hENT1 has also been reported in the nuclear envelopes of cultured human choriocarcinoma BeWo cells (147).

Cell surface expression of hENT1 is coordinated with the cell cycle. Tumor tissues show higher levels of NBMPR-binding protein compared to normal tissues (148). It has been reported, in contrast, that induction of differentiation in HL-60 cells resulted in decreased NBMPR binding sites and hENT1 transport activity (149). However, protein levels have also been reported to double between G₁ and G₂-M phases of the cell cycle (150, 151). In a murine macrophage cell line, colony stimulating factor (CSF)-1 exerted a stimulatory effect on *es*-type activity (150) and the macrophage-CSF induced increase in ENT1 expression could be subsequently downregulated by interferon (IFN)- γ (152). Although the mechanism is unknown, experiments using nucleotide synthesis inhibitors suggest that hENT1 synthesis and/or cell surface expression is regulated in response to cellular deoxynucleotide levels (151). Protein kinase C (PKC) δ and/or ϵ isoforms have also been identified as responsible for the rapid activation of cell surface hENT1 in MCF-7 cultured cells in response to phorbol 12-myristate 13-acetate (PMA) treatment (153). However, in a human B-lymphocyte cell line, PMA and lipopolysaccharide (LPS) both downregulated expression of ENT1 through mechanisms involving tumor necrosis factor (TNF)- α and nitric oxide (NO), but not PKC (154, 155). Insulin up-regulated the *es* process in manner dependent on NO and cyclic guanosine monophosphate (cGMP) in human umbilical artery smooth muscle cells (156), but in rat cardiac fibroblasts (157) and T- and B-lymphocytes (158, 159), high levels of glucose decreased rENT1 mRNA levels and insulin exerted no effect. Similarly, exposure of human endothelial cells to D-glucose, which results in stimulation of adenosine purinoceptors, reduces both hENT1 protein and mRNA levels (160). This down-

regulation of hENT1 expression was demonstrated to be the result of increased specific protein 1 (Sp1) binding to the hENT1 promoter (161).

ENT2

At the molecular level, the *ei* nucleoside transport process corresponds to ENT2. Similar to hENT1, hENT2 is 456 residues in length (101, 103) and shares 46% amino acid identity to hENT1 and 88% identity to both rENT2 cloned from rat jejunal cDNA library (105) and mENT2 cloned from mouse brain (106). Both rENT2 and mENT2 are also 456 residues in length (105, 106). The gene corresponding to hENT2 protein is located on chromosome 11q12.1 (108) or 11q13 (58). An mRNA splice variant lacking part of exon 4 has been described as the product of a growth factor-induced delayed early-response gene (162) and results in a frameshift thereby producing a 326 residue truncated protein, human hydrophobic nuclear protein (hHNP) 36, that lacks the first three TMs of hENT2 and is non-functional as a nucleoside transporter (101). A second widely distributed splice variant with a 40 base pair deletion in exon 9 yields a 301 residue C-terminally truncated protein (hENT2A) that is retained intracellularly (141). A C-terminally truncated, but apparently functional variant of rabbit (rb) ENT2 (rbENT2A) has also been reported (163). Similar to hENT1, hENT2 is highly conserved and, in a study of 247 DNA samples, only 14 polymorphic sites were identified to occur at low frequencies of which 11 were in the coding regions and included three nonsynonymous variants and two deletions (113). Using site-directed mutagenesis of hENT2 and expression in *Xenopus* oocytes, all variants, except one deletion mutant resulting in premature truncation, displayed functional activity (164).

Similar to ENT1, ENT2 mediates the transport of a broad range of purine and pyrimidine nucleosides (101, 103, 105, 106, 118). Upon expression in *Xenopus* oocytes, an apparent K_m value for uridine of 0.2 mM was reported for hENT2 (103). With the exception of uridine and inosine, hENT2 mediates transport of other nucleosides with lower apparent affinities than hENT1 (118). For example,

recombinant hENT2 in PK15 cells exhibited apparent K_m values of 0.14, 0.71, 2.7 and 5.61 mM for adenosine, thymidine, guanosine and cytidine, respectively (118). Unlike ENT1, and consistent with previous reports of hypoxanthine induced inhibition of ENT2-mediated uridine uptake (101, 118), h/rENT2 transport both purine and pyrimidine nucleobases including hypoxanthine, adenine, guanine, uracil and thymine (165). hENT2, but not rENT2, also transports cytosine (165). The affinities for nucleobases are lower than those for nucleosides, but the turnover numbers for transport are higher such that, at physiological concentrations, the efficiencies of nucleoside and nucleobase transport are similar (165). Apparent K_m values for hENT2-mediated transport of nucleosides and hypoxanthine in various expression systems, as well as those of other hENT and hCNT family members, are listed in Table 1-2. Chemotherapeutic nucleoside analogs that are permeants of hENT2 include dFdC (119, 120), F-araA (124), araC (122), 2-CdA and 2-chloro-9-(2'-deoxy-2'-fluoro- β -D-arabinofuranosyl)adenine (clofarabine) (58, 123). h/rENT2 are capable of transporting antiviral 2', 3'-dideoxynucleosides, including AZT, and exhibit higher efficiency for the transport of ddC and ddI than ENT1 (126). As indicated by the transport process name *ei*, ENT2 is insensitive to low concentrations of NBMPR and is less sensitive to inhibition by dipyridamole, dilazep and draflazine than ENT1 (101, 103, 105, 106, 118, 128, 166).

hENT2 is predicted to exhibit an 11 TM membrane topology similar to that of hENT1 depicted in Fig. 1-4 (103). hENT2 migrated as 50 and 47 kDa on SDS-polyacrilamide gels and contains two glycosylation sites, Asn⁴⁸ and Asn⁵⁷, in the extracellular loop between TMs 1 and 2 (118, 167). Aglyco mutants are functionally comparable to wild-type hENT2, although *N*-glycosylation was required for efficient targeting of hENT2 to the plasma membrane (167). Changes in glycosylation status also increased IC₅₀ values for dipyridamole (hENT2 aglyco mutants N48D, N57D and N48D/N57D) and NBMPR (hENT2 aglyco mutants N57D and N48D/N57D), although these effects alone were not sufficient to account for the difference in inhibitor sensitivity between hENT2 and hENT1 (167).

Similar to ENT1, ENT2 mRNA is expressed in a wide range of tissues, including brain, heart, placenta, thymus, pancreas, prostate, lung and kidney and is particularly abundant in skeletal muscle (101, 103, 133, 143). The predominant distribution of hENT2 in skeletal muscle, in conjunction with a high affinity for the adenosine metabolites, inosine and hypoxanthine, suggests an important role in muscle physiology during and after strenuous exercise (101, 118). hENT2 protein expression in brain was found to be most abundant in the cerebellum and brainstem regions, particularly the pons (135). In contrast, rENT2 transcript was more widely distributed throughout the rat brain and found predominantly in hippocampus, cortex, striatum and cerebellum, which may indicate either a species differences or mRNA/protein level discrepancy (168). Human fetal astrocytes have been demonstrated to exhibit hENT2-mediated adenosine uptake (138). In the rat, the primary nucleoside transporter present in C6 glioma cells was rENT2 (169).

ENT2 is primarily targeted to the plasma membrane of cells. Immunocytochemistry studies show cell surface location of ENT2 in rat cardiomyocytes (54) and GFP fusions of hENT2 are targeted to the basolateral membrane when expressed in polarized renal epithelial MDCK cells (141). In human tissues, hENT2 was basolaterally localized in the duodenum and kidney and also found in the plasma membrane of hepatocytes and placental trophoblasts (143). The C-terminal dileucine motif in hENT2 is implicated in cell surface expression of the protein (141), and other studies have indicated that *N*-glycosylation is also required for efficient targeting to the plasma membrane (167). However, intracellular localization of ENT2 has also been reported. Antibodies raised against the central cytoplasmic loop of HNP36/hENT2 were reported to stain nucleolar structures in cultured cells (162) and, similar to hENT1, hENT2 was also found in the nuclear envelopes of cultured human choriocarcinoma BeWo cells (147).

In comparison to ENT1, less is known about the regulation of ENT2 and its role in the proliferative response. Quiescent murine fibroblasts can be induced to express mouse HNP36 splice variant upon stimulation with serum or growth factors as part of the delayed-early response (162). In contrast, regulation of hENT2 in a

similar manner was not detected (101). CSF-1 did not affect *ei*-type activity, despite stimulating *es*-type activity, in a murine macrophage cell line (150). However, hENT2 transport activity in human neuroblastoma cells increased upon differentiation (170). In rat hippocampus, there is evidence to support regulation of ENT activity by the adenosine A_{2A} receptor (137). rENT2 mRNA expression levels increased in T- and B-lymphocytes (158, 159) and cardiac fibroblasts (157) following insulin, but not glucose, exposure. This insulin-induced increase in rENT2 expression in cardiac fibroblasts occurred in a murine target of rapamycin (mTOR)- and protein synthesis-dependent manner (171).

ENT3

Database searching using the BLAST algorithm initially identified ENT3 cDNA sequences in human and mouse, which differed from ENT1 and ENT2 and were subsequently cloned from human placenta and mouse kidney, respectively (78). The hENT3 and mENT3 homologs are both 475 residues in length (78, 172). hENT3 is 31 - 33% identical in sequence to ENT1 and ENT2 family members from human, mouse and rat and 73% identical to mENT3 (78, 172). The hENT3 chromosomal location is 10q22.1 (108). Similar to other ENTs (Fig. 1-4), ENT3 is also predicted to have 11 TMs with a cytoplasmic N-terminus and a putative *N*-glycosylation site in the extracellular loop between TMs 1 and 2 (172). In contrast to ENT1/2, human and mouse ENT3 possess a long hydrophilic N-terminal region of 51 residues containing typical (DE)XXXL(LI) endosomal/lysosomal targeting motifs (172). In good agreement with this, GFP-tagged hENT3 was found to be a predominantly intracellular protein that partially co-localized with lysosomal markers in cultured human cells and truncation or mutation of the N-terminal dileucine motif to alanine caused the protein to be relocated to the plasma membrane (172). In agreement with initial predictions of an intracellular localization (78), these findings suggest that ENT3 may be primarily functioning in the transport of nucleosides across lysosomal membranes, such as that required for nucleoside release following nucleic acid

breakdown in the lysosomal interior (172). In this capacity, ENT3 is likely to equate to the equilibrative nucleoside transport process which was demonstrated in human lysosomes (173).

Replacement of the dileucine motif at positions 31 and 32 with alanine residues (hENT3AA) allowed expression in the plasma membrane of *Xenopus* oocytes at levels adequate for subsequent functional characterization (172). hENT3AA exhibited broadly selective, low affinity uptake of both purine and pyrimidine nucleosides (apparent K_m values for adenosine and uridine of 1.86 and 2.02 mM, respectively) and was also capable of mediating adenine, but not hypoxanthine transport (54, 172). The apparent K_m values for hENT3AA-mediated transport in comparison to those of the other hENT and hCNT family members are given in Table 1-2. This broadly-selective phenotype also extended to nucleoside analogs; 2-CdA, dFdC, F-araA, 3'-deoxyadenosine (cordycepin), 7-deazaadenosine (tubercidin), 2-pyrimidine-1- β -D-ribose (zebularine), ddi, ddC and AZT were all permeants (172). hENT3AA-mediated adenosine uptake was partially inhibited by the classic nucleoside transport inhibitors NBMPR, dipyrnidamole and dilazep, but only at high concentrations (172). Although hENT3AA-mediated transport was Na⁺-independent, dependency upon pH was evident with optimal transport rates occurring at pH 5.5 (172). This pH corresponds to that of late endosomes/lysosomes and may be an evolutionary adaptation to localization of the transporter in acidic, intracellular compartments (172).

Analysis of multiple tissue RNA arrays indicates that hENT3 is widely expressed in human adult and fetal tissues with particular abundance in placenta, from which tissue the hENT3 cDNA was originally cloned (54, 78, 172). More specifically, high levels of protein were detected in heart and liver and high levels of mRNA in placenta, uterus, ovary, spleen, lymph node and bone marrow (172).

ENT4

ENT4 is the most recent addition to the ENT family of transporters and hENT4 and mENT4 were originally identified by genome database analysis (79). hENT4, alternatively designated as a plasma membrane monoamine transporter (PMAT), is 55 kDa and 530 residues in length and shares only 18% identity with hENT1 (54, 174). The mouse homolog is 528 residues in length with 86% identity to hENT4 (54). hENT4 is more closely related to the products of the *Drosophila melanogaster* gene CG11010 (28% identity) and the *Anopheles gambiae* gene agCG56160 (30% identity), indicating an ancient and evolutionarily distinct divergence from the other members of the SLC29 family (54, 79). hENT4 is assigned to chromosome 7p22.1 (79).

Although preliminary studies reported hENT4 and mENT4 as low affinity adenosine-selective transporters (54), they were subsequently shown to function as multi-permeant transporters. As suggested by the alternate designation PMAT, other permeants included neurotransmitters such as 5-hydroxytryptamine (serotonin; 5-HT) and dopamine (apparent K_m values of 114 and 329 μM , respectively) and polyspecific organic cations such as 1-methyl-4-phenylpyridinium (MPP^+) (174, 175). In addition to adenosine, mENT4, but not hENT4, also mediates transport of the nucleobase adenine upon expression in *Xenopus* oocytes (104). Although transport by ENT4 is Na^+ - and Cl^- -independent, it is sensitive to membrane potential (174). H^+ -dependence of hENT4-mediated transport was demonstrated upon expression in *Xenopus* oocytes for adenosine, but not serotonin (104), and in MDCK cells for MPP^+ (176). The apparent K_m value for hENT4-mediated adenosine transport is compared to those of other hENT and hCNT family members in Table 1-2. Adenosine transport mediated by hENT4 was not inhibited by NBMPR, and only partially by dipryridamole and dilazep (104). hENT4-mediated serotonin uptake was also partially inhibited by dilazep (104).

Based on hydropathy plot predictions and multiple sequence alignments, ENT4 is predicted to have 11 TMs (79, 174). hENT4 and mENT4 are *N*-glycosylated

and the presence of putative glycosylation sites in the C-terminal tail, Asn⁵²³ and Asn⁵²¹, are consistent with the predicted extracellular location of C-terminus (104). A representative schematic of this topology is shown in Fig. 1-4.

Northern blot studies indicated abundant expression of hENT4 mRNA throughout the central nervous system and in skeletal muscle, as well as high levels in heart, kidney, liver, intestine, pancreas, bone marrow and lymph node (104, 174). Further analysis of protein levels largely confirmed these findings, identifying the highest levels of rENT4 in heart, including both cardiomyocytes and vascular endothelial cells, and in brain (104). hENT4 is primarily targeted to the apical membranes of renal epithelial cells when expressed in polarized MDCK cells (176). Present throughout the brain, rENT4 mRNA was expressed predominantly in cholinergic pathways, including brainstem motor nuclei, basal forebrain and striatum, corresponding with a suggested role in monoamine uptake in cholinergic neurons (177). Unlike ENT3, ENT4 is primarily present in plasma membranes, although ENT4 intracellular staining of vesicles suggests that ENT4 may be associated with a relocalization process (104).

ENT Physiological Implications

Bidirectional nucleoside transport mediated by ENTs has vast physiological implications. ENT1 and ENT2 share a widespread distribution, often coexisting, in most cell and tissue types. A key physiological role for ENT1 and ENT2, for example, is in the provision of nucleosides, derived from the diet or produced by the liver, for salvage pathways of nucleotide synthesis (30). Although both proteins exhibit similar nucleoside specificities, the enhanced ability of ENT2 to transport inosine and nucleobases, including hypoxanthine, may be indicative of a specific role in purine salvage (54). For example, bone marrow cells, which lack purine nucleoside *de novo* biosynthetic pathways, may be exposed to hypoxanthine concentrations as high as 30 μ M (178). The high affinity of ENT2 for both inosine and hypoxanthine, as well as its predominant distribution in skeletal muscle, suggests

a role in efflux or uptake during muscle exercise and recovery, respectively (101, 118, 165). A likely primary role for ENT3 is in the transport of nucleosides across lysosomal membranes, important for the release of nucleosides produced by nucleic acid breakdown in the lysosomal interior (172). This may be of particular importance for both basal and amino acid deprivation-induced cytoplasmic RNA degradation that occurs in the liver (179). The putative physiological roles of ENT4 are diverse. H^+ -dependent ENT4 may be a key player in regulation of extracellular adenosine levels in the heart, particularly under the acidotic conditions associated with ischemia (104). ENT4 may also be important for organic cation reabsorption in the kidney (176) and in monoamine uptake in the brain (177, 180).

ENTs have key roles in regulating the concentration of adenosine available to purinoceptors. This is of particular physiological importance in cardiac, as well as neural and pulmonary tissues, and is central to the use of adenosine, adenosine analogs and ENT inhibitors as pharmaceuticals. Both ENT1 (139) and adenosine-selective hENT4 (104) are abundant throughout heart tissue and are thus potential pharmaceutical targets of cardiac function, especially for ameliorating ischemic damage associated with coronary artery disease and during cardiac surgery. Inhibition of ENT-mediated transport in the heart, for example, potentiates the A_1 receptor-mediated chronotropic effects of adenosine in the SA node (77) and protects against ischemia-reperfusion injury (6, 181). In the brain, bidirectional ENT activity is important for maintaining adenosine concentrations (182). Although, ENT-mediated uptake of adenosine is usually favored due to inwardly-directed adenosine concentration gradients (27, 183), adenosine release has also been reported in experiments with rat brain synaptosomes (184). Studies with ENT1-null mice have established a link in the brain between ENT1-mediated adenosine uptake, decreased stimulation of A_1 receptors, and regulation of *in vivo* ethanol intoxication (116). The potential benefits of ENT inhibition on ischemia-reperfusion in the heart also extends to neuronal injury. For example, the ENT1 inhibitor NBMPR reduced the ischemia-induced loss of hippocampal CA1 neurons in the rat (185). Inhibition of nucleoside transport enhanced the opioid-mediated antinociception in the mouse (186) and increased antinociceptive presynaptic A_1 receptor-mediated inhibition of

glutamatergic synaptic transmission in the rat spinal cord (187). In human airway A549 epithelial cells, ENT1 and ENT2 regulation of adenosine concentrations influenced adenosine-activated A₁ receptor-mediated control of K⁺ channels (188).

Non-Mammalian Eukaryotic ENT Family Members

In addition to mammalian ENT proteins, ENT family members have been identified and functionally characterized in other eukaryotes, including parasitic protozoa, nematodes, insects, plants and fungi.

Parasitic Protozoa

Parasitic protozoa are unable to synthesize purine nucleotides *de novo* and thus rely on purine nucleoside salvage pathways (44-49). *Toxoplasma gondii* is the causative agent of toxoplasmic encephalitis in immunocompromised individuals (189) and congenital toxoplasmosis can result in neurological birth defects (190). *Plasmodium falciparum* is responsible for the majority of malaria caused deaths (191). Parasites of the *Leishmania* family result in leishmaniasis and, specifically, *Leishmania donovani* is responsible for visceral leishmaniasis (kala azar) (69). *Trypanosoma brucei* subspecies are responsible for sleeping sickness (African trypanosomiasis) and Chagas' disease (American trypanosomiasis) and, similar to the human diseases, *Trypanosoma brucei brucei* causes a wasting disease (nagana) in cattle (49, 69, 192). In order for survival, all parasites require purine transport across the parasite plasma membrane through nucleoside or nucleobase transport proteins. Transport and metabolic differences between pathogen and host purine salvage pathways offers the potential for rational design of new and more effective therapeutic strategies.

Two ENT family members from *Toxoplasma gondii* have been identified and characterized. *T. gondii* (Tg) adenosine transporter (AT) 1 is a 462 amino acid

protein identified through the use of insertional mutagenesis of *T. gondii* genomic DNA and selection of mutants resistant to the cytotoxic adenosine analog adenine arabinoside (araA) (193). TgAT1 is 22 and 26% identical to hENT1 and hENT2, respectively, and putatively shares a membrane topology similar to that of the 11 TM mammalian ENTs (193). Expression in *Xenopus* oocytes demonstrated saturable adenosine transport by TgAT1 with an apparent K_m value of 114 μ M that was inhibited by purine nucleosides, inosine analogs and the nucleobases hypoxanthine and guanine, but not pyrimidine nucleosides (193). Adenosine transport by TgAT1 was also inhibited by dipyridamole and partially inhibited by NBMPR (193). The protein largely responsible for adenosine transport in *T. gondii* was demonstrated to be TgAT1; disruption of the TgAT gene locus resulted in elimination of adenosine transport and high levels of araA resistance, but was not a fatal genetic lesion suggesting that additional purine nucleoside or nucleobase transport systems also exist (193). Indeed, other transporters were subsequently identified including a hypoxanthine-transporting nucleobase transporter TgNBT1 and a second nucleoside transporter TgAT2 (194). TgAT2 exhibited higher affinity permeant binding than TgAT1, with apparent K_m values ranging from 0.28 to 1.5 μ M for adenosine, inosine, guanosine, uridine and thymidine (194). TgAT2 nucleoside transport is also inhibited by cytidine (194).

Using sequence information obtained from the Malaria Genome Sequencing Project, a member of the ENT family was independently cloned from *Plasmodium falciparum* by two groups (195, 196). Designated as *P. falciparum* (Pf) ENT1 (196) or PfNT1 (195), this transport protein is 422 residues in length, contains 11 putative TMs and shares a sequence identity with hENT1 and hENT2 of 36 and 31%, respectively (195). Similar to mammalian ENTs, PfENT1/PfNT1 exhibited broad selectivity for both purine and pyrimidine nucleosides (195-197), although expression in *Xenopus* oocytes revealed different kinetic properties for the two transporters with apparent K_m values for adenosine of 0.32 and 1.86 mM for PfENT1 (196, 197), in contrast to 13.2 μ M for PfNT1 (195). Transport mediated by PfENT1 occurred in the absence of both Na^+ and H^+ gradients, suggesting that this transporter is unlikely to function as a symporter (196). PfENT1 was also capable of transporting the

nucleobases adenine and hypoxanthine, as well as the nucleoside analogs F-araA, 2-CdA, gemcitabine, AZT, ddC and ddi (196). PfENT1 was not sensitive to inhibition by NBMPR, dipyridamole, dilazep or draflazine (196, 197); however, inhibition of adenosine transport by 10 μ M dipyridamole was reported for PfNT1 (195). Using antibodies specific for PfENT1, immunoblot analysis revealed transporter localization to the parasite plasma membrane (198). Genetic disruption of PfNT1 in *P. falciparum* revealed the importance of hypoxanthine transport by PfNT1 in purine salvage and demonstrated that parasites lacking PfNT1 were still able to transport adenosine and inosine, suggesting the existence of other nucleoside transporters (199). Subsequent analysis of the *P. falciparum* genome identified three other putative ENT family members which are designated as PfNT2, PfNT3 and PfNT4 and remain to be functionally characterized (199).

Initial studies demonstrated that two nucleoside transport systems with nonoverlapping permeant specificities existed in *Leishmania donovani* (200) and the corresponding nucleoside transporters were cloned by functional rescue strategies (201, 202). In a cell line deficient in adenosine and pyrimidine nucleoside transport capabilities, LdNT1.1 and LdNT1.2 were identified as nucleoside transporters based on their capability to restore sensitivity to the cytotoxic adenosine analog tubercidin and mediate uptake of radiolabeled uridine and adenosine (201). LdNT1.1 and LdNT1.2 are each 491 amino acids in length, differing only by six amino acids, exhibit 33% identity to hENT1 and contain 11 putative TMs (201). Produced in *Xenopus* oocytes, LdNT1.1 exhibited apparent K_m values for adenosine and uridine transport (0.17 and 5.6 μ M, respectively) that were lower than those for LdNT1.2 (apparent K_m values for adenosine of 0.66 μ M and uridine of 40 μ M) (201). Likewise, in a cell line deficient in inosine and guanosine transport activity, the gene encoding LdNT2, which restored sensitivity to the inosine analog formycin B, was subsequently cloned (202). LdNT2 is 499 amino acids in length and shows sequence identity with hENT1, hENT2 and LdNT1.1 ranging from 25 to 44% (202). Upon expression in FBD5 cells, LdNT2 exhibited specificity for inosine and guanosine with apparent K_m values of 0.3 and 1.7 μ M, respectively, and was also capable of transporting cytotoxic inosine and guanosine analogs (202). Electrophysiological

characterization of LdNT1.1, LdNT1.2 and LdNT2 in *Xenopus* oocytes revealed that all three proteins function as H⁺ symporters (84).

Trypanosoma brucei brucei parasites have two high affinity purine nucleoside transport systems, designated P1 and P2. P1 transports adenosine and inosine and is detectable in both procyclic and bloodstream form trypanosomes, whereas the P2 system transports adenosine and adenine, as well as antitrypanosomal drugs including melaminophenyl arsenicals and diamidines and is detectable in only bloodstream form trypanosomes (203-205). A potent trypanocide, the adenosine analog cordycepin, was recently demonstrated to be transported by both the P1 and P2 systems (206). The first *T. b. brucei* nucleoside transporter, TbAT1, was cloned by functional complementation in a *S. cerevisiae* strain which was deficient in purine biogenesis and purine nucleoside uptake (207). Corresponding to the P2 type transport system, TbAT1 mediated transport of adenosine which was inhibited by adenine and melaminophenyl arsenicals, whereas other purine and pyrimidine nucleosides and nucleobases had no effect (207). TbAT1 is 463 amino acids in length and was present only in bloodstream form trypanosomes (207). TbNT2 corresponds to a P1 type nucleoside transporter and was cloned by PCR amplification of a *T. b. brucei* cDNA library using sequence information from LdNT1.1 of the related parasite *L. donovani* (85). TbNT2 exhibits 30, 22 and 25% sequence similarity to LdNT1.1, hENT1 and hENT2, respectively (85). TbNT2 is 464 residues in length and contains 11 putative TMs (85). Upon expression in *Xenopus* oocytes, TbNT2 mediated transport of purine nucleosides (adenosine, inosine and guanosine) with apparent K_m values of 0.99 and 1.18 μ M for adenosine and inosine, respectively (85). Protonophores, which uncouple proton gradients, partially inhibited adenosine transport mediated by TbNT2, thus suggesting that this protein may function as a proton symporter (85). This was also consistent with experiments in intact parasites in which nucleoside transport was dependent upon the proton motive force (205). TbNT2 mRNA is present only in bloodstream form trypanosomes (85). Subsequent to the molecular identification of TbNT2, BLAST searches of the *T. b. brucei* genome database identified additional P1 type TbNT family members, including TbNT2/927, TbNT3, TbNT4, TbNT5, TbNT6 and TbNT7 (87). Cloned from a different strain of

T. b. brucei, TbNT2/927 is 96% identical in sequence to TbNT2 (87). Functional expression in *Xenopus* oocytes revealed that TbNT2/927, TbNT5, TbNT6 and TbNT7 each mediated transport of purine nucleosides and that transporter-mediated adenosine uptake was dependent on the proton motive force and occurred with high affinity binding similar to that of inosine with apparent K_m values $< 5 \mu\text{M}$ (87). Additionally, TbNT5, TbNT6 and TbNT7 also mediated transport of hypoxanthine (87). While all six mRNAs are present in bloodstream stage of *T. b. brucei* life cycle, TbNT2/927 and TbNT5 are also expressed in procyclic form trypanosomes (87). Permeants for TbNT3 and TbNT4 could not be identified in *Xenopus* oocytes (87). Continued examination of the *T. b. brucei* genome database identified additional members. TbNT8 represents a family of clustered genes for which mRNAs are present in both bloodstream and procyclic form trypanosomes (48, 87). TbNT8.1, upon expression in both *Xenopus* oocytes and nucleoside-nucleobase deficient yeast, exhibited transport of purine nucleobases (208). Similarly, another TbNT8 family member, designated TbNBT1, also mediated transport of nucleobases, as well as guanosine, inosine and allopurinol (209). TbNT9 was originally identified by BLAST searches (87) and preliminarily identified as an ENT homolog transporting purine nucleosides and hypoxanthine (48). Recent characterization following expression in *S. cerevisiae* revealed that TbNT9 exhibited a high affinity for adenosine with an apparent K_m value of $0.068 \mu\text{M}$ and mediated the transport of other purine nucleosides (210). TbNT9-mediated transport was not inhibited by pyrimidine nucleosides or nucleobases (210). Functional expression in *S. cerevisiae* also revealed TbNT10, the main P1 transporter in procyclic trypanosomes, to be a high-affinity transporter of purine nucleosides with apparent K_m values of $\sim 1 \mu\text{M}$ (48, 210, 211). TbNT10 mRNA and protein are expressed primarily in the short-stumpy form of the parasite life cycle (48, 211). TbNT11.1 and TbNT11.2 have not yet been characterized functionally (48).

Three nucleoside transport systems mediating pyrimidine nucleoside uptake in *Trypanosoma brucei brucei* have also been identified, although only at the functional level. The C1 transport process has high affinity for cytosine (apparent K_m value of $0.048 \mu\text{M}$), U1 primarily transports uracil, but is also capable of transporting uridine

(apparent K_m value of 33 μM), and U2 represents a higher affinity uridine transport process (apparent K_m value of 4.1 μM) (212). Previous studies characterizing the U1 carrier showed that uracil uptake was inhibited by only uridine and 5-fluorouracil among a broad range of purine and pyrimidine nucleosides, nucleobases and uracil analogs that were tested (213). Additionally, a protonophore also inhibited uracil uptake suggesting that U1 may function as a H^+ -mediated symporter (213).

Two ENT family members from *Crithidia fasciculata* have been identified and are designated CfNT1 and CfNT2 (214, 215). CfNT1 is 497 residues in length and 72% identical to LdNT1 and CfNT2 is 502 residues in length and 73% identical to LdNT2 (215). Expression in *Xenopus* oocytes revealed CfNT1 functioned as a high-affinity adenosine transporter, also capable of mediating the uptake of inosine, uridine, cytidine and the nucleobase hypoxanthine (215). In contrast, inosine and guanosine, but not adenosine, pyrimidine nucleosides or nucleobases were identified as permeants for CfNT2 (214, 215).

Nematodes

The *Caenorhabditis elegans* genome contains six putative ENT family members designated *C. elegans* (Ce) ENT1-6, ranging in length from 434 (CeENT5) to 729 (CeENT3) amino acids (108, 216). Similar to hENT1 and hENT2, expression of CeENT1 and CeENT2 in *Xenopus* oocytes revealed H^+ -independent transport of both purine and pyrimidine nucleosides (35, 216). Additionally, CeENT1 mediated transport of 2', 3'-dideoxynucleosides, including AZT, ddC and ddI (35). NBMPR, dilazep and draflazine did not inhibit transport mediated by CeENT1 or CeENT2, but dipyrindamole did (35, 216). Using RNA interference to disrupt gene expression of CeENT1 and CeENT2 showed no effect when one gene was disrupted alone indicating functional redundancy, but the simultaneous disruption of both genes yielded developmental defects (216). Functional characterization of CeENT3-6 has not been undertaken.

Insects

Searches of *Drosophila melanogaster* genome database revealed three putative ENT sequences, designated *D. melanogaster* (Dm) ENT1, DmENT2 and DmENT3 respectively containing 476, 458 and 586 residues and 11 putative TMs (78, 108). Upon expression in *Xenopus* oocytes, no functional activity was identified for DmENT1 or DmENT3 (217). However, DmENT2 exhibited uridine uptake which was inhibited by purine and pyrimidine nucleosides and nucleobases, as well as 2'-deoxynucleosides, although not by the classic ENT inhibitors NBMPR, dipyridamole and dilazep (217).

Plants

In addition to similar requirements for formation of nucleic acids, nucleosides and nucleoside metabolism may also play a key role in cytokinin biogenesis in plants. Cytokinins are plant hormones involved in the regulation of plant cell proliferation and differentiation (218, 219).

Genome sequencing predicts eight potential ENT family members from *Arabidopsis thaliana* designated AtENT1-8 (78). Seven out of eight of these proteins have been functionally characterized, the exception being AtENT5 which could not be amplified from cDNA at full length (220, 221). AtENT1 was cloned using RT-PCR (222) and by functional complementation in *S. cerevisiae* strains unable to synthesize adenine (88). AtENT1 is 428 amino acids in length, 24% identical in sequence to hENT1 and predicted to have 11 TMs (88, 222). AtENT1 exhibited pH-dependent high-affinity adenosine transport (apparent K_m value of 3.6 μM) which was resistant to inhibition by NBMPR, dilazep and dipyridamole (88). AtENT1-mediated uptake of adenosine was also inhibited by inosine, guanosine and cytidine, but not by uridine or nucleobases (88). However, direct uptake experiments with recombinant AtENT1 expressed in yeast demonstrated pH-dependent uridine transport (223). Upon expression in yeast, AtENT3/4/6/7 exhibited broad permeant specificity

transport of adenosine, guanosine, cytidine and uridine with apparent K_m values ranging from 3 to 94 μM and which was inhibited by inosine, deoxynucleosides and, to a smaller extent, by nucleobases (220, 221). Thymidine was also a permeant for recombinant AtENT3/6/7, but not AtENT1/2/4/8, when expressed in yeast (223). AtENT8, expressed in yeast, did not mediate transport of adenosine, guanosine, cytidine, uridine or cytosine (221, 223). Partial sensitivity of AtENT3 to dilazep and dipyridamole was reported in the absence of sensitivity to NBMPR (220); however, AtENT4/6/7 exhibited no inhibition by dilazep or NMBPR (221). The H^+ -dependence of AtENT3 has been debated (220, 221, 223), although recent electrophysiological studies in AtENT3-expressing *Xenopus* oocytes verified H^+ -coupled adenosine transport (89). In contrast, pH-independent transport has been reported for AtENT4/6/7 (221, 223).

Four potential ENT family members have been identified in the rice *Oryza sativa* and are designated *O. sativa* (Os) ENT1-4 (224). OsENT1, OsENT2 and OsENT3 have 423, 418 and 418 residues respectively and contain 11 putative TMs, whereas OsENT4 contained only 276 amino acids and was assessed to be either a pseudogene or truncated ENT (224). OsENT1 exhibits 65% identity in sequence to AtENT1 (224). Upon expression in *S. cerevisiae*, only OsENT2 exhibited transport function whereas the other OsENTs did not (224). OsENT2 mediated high-affinity transport of adenosine and uridine (apparent K_m values of 3.0 and 0.7 μM , respectively) in a pH-dependent manner, and transport was inhibited by both purine and pyrimidine nucleosides and 2'-deoxynucleosides, although not by NMBPR, dilazep or dipyridamole (224). Additionally, OsENT2 mediated the uptake of the nucleoside cytokinins, isopentenyladenine riboside and trans-zeatin riboside (224).

Fungi

The single ENT family member from *Saccharomyces cerevisiae* with broadly selective transport of both purine and pyrimidine nucleosides is function unknown now (FUN) 26 (225). FUN26 has 517 amino acids and 11 putative TMs (225).

FUN26 shares ~ 18% sequence identity with hENT1 and hENT2 (225). Upon expression in *Xenopus* oocytes, FUN26 mediated the uptake of radiolabeled uridine, adenosine and cytidine in a pH-independent manner (225). This transport was not inhibited by dilazep, dipyridamole or NBMPR (225). Immunotagged recombinant FUN26 expressed in yeast primarily localized to intracellular membranes (225). FUN26 is not essential in *S. cerevisiae*, since gene disruption did not produce an altered phenotype (226).

Concentrative Nucleoside Transporter (CNT) Family

Active, cation-dependent nucleoside transport is mediated by members of the CNT family (reviewed in 28-33, 35, 80, 82, 227). This family of integral membrane proteins transports nucleosides across cellular membranes against their concentration gradients by coupling to cations moving down their electrochemical gradients. CNT family members have been identified and characterized in numerous eukaryotes, including mammals, lower vertebrates, nematodes and fungi, as well as in prokaryotic bacteria. Table 1-3 lists CNT family members that have been identified.

Mammalian CNT Family Members

In addition to the known equilibrative facilitated diffusion transport processes, a concentrative mechanism for nucleoside transport was also described in early studies of several mammalian tissues and cultured cell lines. This concentrative mechanism was known to be NBMPR-insensitive and Na⁺-dependent (228-234). Initial studies describing permeant specificity were ambiguous and provided key support for the existence of two distinct concentrative mechanisms. Using radiolabeled nucleosides to characterize nucleoside transport in mouse intestinal epithelial cells, uptake of formycin B, a non-metabolizable inosine analog, that was not inhibited by the presence of thymidine and corresponding uptake of thymidine that was not inhibited by the presence of formycin B was demonstrated (235). These

two transport processes were designated N1 or *cif* (concentrative, insensitive to NBMPR, formycin B-transporting) and N2 or *cit* (concentrative, insensitive to NBMPR, thymidine-transporting); additional permeants for *cif* included the purine nucleosides guanosine and inosine, and for *cit* included the pyrimidine nucleoside cytidine (235). These designations were given in contrast to, and to complement, those of the equilibrative, NBMPR-sensitive *es* and NBMPR-insensitive *ei* nucleoside transport processes. Concentrative nucleoside transport continued to be recognized in a number of different cells and tissues. The *cit* system was described, for example, in rabbit intestinal mucosa (236) and in guinea pig blood-brain and blood-CSF barrier (237). The *cif* system was described, for example, in murine splenocytes (238), murine and rat peritoneal macrophages (239), rat hepatocytes (240) and L1210 murine leukemia cells (241). Also, the *cit* and *cif* systems were found to coexist in some cells and tissues including rabbit (234), rat (242) and bovine (243) renal brush border membrane vesicles, rabbit intestinal brush border membrane vesicles (233) and guinea pig intestinal enterocytes (229). These concentrative nucleoside transport processes all displayed Na⁺-dependence and characteristically exhibited an apparent 1:1 Na⁺:nucleoside stoichiometry (30, 80, 232, 243).

Initial studies describing concentrative nucleoside transport also suggested the possible presence of a broadly selective concentrative nucleoside transport mechanism, referred to as the *cib* (concentrative, NBMPR-insensitive, broadly selective) or N3 nucleoside transport process. These early functional studies of *cib* included experiments in human fibroblast lysosomes (55), human (244), rat (245) and rabbit renal (234) and rabbit intestinal (233) brush border membrane vesicles, guinea pig intestinal epithelial cells (229) and mouse peritoneal macrophages (246). However, the possible coexistence of *cit* and *cif* transport processes in cells, and the relatively low *cib*-type activities that were encountered made characterization difficult (31). Several laboratories continued to pursue the possibility of a novel *cib* nucleoside transport system, including studies of differentiated (247) and undifferentiated (248) HL-60 leukemia cells and ATP-depleted rabbit choroid plexus (249-251), but the first direct demonstrations of *cib*-type transport activity occurred with isolated leukemic blasts (248), human colon cancer Caco-2 cells (252) and

Xenopus oocytes injected with rat jejunum mRNA (253). Since these initial descriptions, similar studies have been used to locate putative *cib* systems in other cells and tissues, such as in *Xenopus* oocytes expressing rabbit ileal mRNA (254) and rat MSL-9 microglia (255). In addition to differences in permeant selectivity, the *cib* system differed from the *cif* and *cit* systems in that an apparent Na⁺:nucleoside stoichiometry of 2:1 was reported both for rabbit choroid plexus and rat microglia (249, 255).

In addition to the *cif*, *cit* and *cib* nucleoside transport processes, three other functional concentrative mechanisms have been described. A separate putative subtype of the *cit* system in human renal brush border membrane vesicles, designated N4, was differentiated from other *cit* systems in counter-flux experiments which showed that the purine nucleoside guanosine, unlike inosine, was able to trans-stimulate radiolabeled thymidine uptake (244, 256, 257). However, uptake of radiolabeled guanosine by this *cit*-type process was not directly measured. The *cs* (concentrative, sensitive to NBMPR) or N5 transport process accepts adenosine analogs as permeants and has been observed in human leukemic cells (252, 258). Additionally, the guanosine selective *csg* (concentrative, sensitive to NMBPR, guanosine-transporting) transport process was observed in cultured human NB4 acute promyelocytic and murine L1210 leukemic cells (259, 260).

The *cit*, *cif* and *cib* nucleoside transport processes have been identified at the molecular level. The corresponding proteins are designated CNT1 (*cit*), CNT2 (*cif*) and CNT3 (*cib*). In humans, CNT1/2/3 belong to the SLC28 family of proteins. No further functional characterization of the other three systems, *cit*-type with specificity for guanosine, *cs* and *csg*, has been reported in the literature and the molecular identity of the corresponding proteins is not known.

CNT1

The first nucleoside transporter to be identified at the molecular level was that of a mammalian CNT cloned by expression screening of a rat jejunum cDNA library and designated rCNT1 (261). rCNT1 encodes a membrane protein containing 648 amino acids and mediated *cit*-type transport activity when produced in *Xenopus* oocytes (261). hCNT1, the first CNT cloned from human tissues, was later isolated from human kidney by hybridization/RT-PCR cloning and functional expression in *Xenopus* oocytes (262). Two closely related cDNAs were identified with minor differences between them which may result from genetic polymorphisms or PCR amplification errors; however, both cDNAs encoded proteins with *cit*-type functional activity (262). hCNT1 is 650 amino acids in length and 83% identical to the rat homolog rCNT1 (262). hCNT1 maps to chromosome 15q25-26 (262). Another mammalian homolog also identified by molecular cloning of its cDNA from renal tissue was pig kidney (pk) CNT1, a 647 amino acid protein (263). In contrast to highly conserved hENT1 and hENT2, a study of 247 DNA samples identified 56 SNPs in hCNT1, of which 26 were in the coding region including 13 that were nonsynonymous, one that contained an amino acid insertion and one that contained a base pair deletion (264). All variant transporters, except S546P and the base pair deletion mutation which resulted in a premature stop codon, were functional upon expression in *Xenopus* oocytes (264).

Upon expression in *Xenopus* oocytes and mammalian COS-1 cells, recombinant human, rat and pig kidney CNT1 expressed a *cit*/N2-type Na⁺-dependent pyrimidine nucleoside-selective transporter (261-263, 265). Electrophysiological studies using *Xenopus* oocytes also found h/rCNT1-mediated transport to be pyrimidine nucleoside-selective in a Na⁺- and voltage-dependent manner (266-268). The purine nucleoside adenosine was also demonstrated to be a permeant for both hCNT1 and rCNT1 (262, 265, 268, 269). Some studies have showed adenosine to be only an inhibitor of h/rCNT1 and not a permeant (266, 267); however, kinetic analysis of rCNT1-mediated adenosine transport demonstrated that adenosine binds with high affinity to the transporter, but was transported at low rates (269). Thus,

adenosine may regulate CNT1 activity *in vivo* by binding to the transporter and inhibiting the transport of pyrimidine nucleosides (56). Apparent K_m values for hCNT1-mediated transport in various expression systems are compared to those of other hENT and hCNT family members in Table 1-2. hCNT1 was partially inhibited by phloridzin (IC_{50} value of 0.2 mM) which putatively exerted its effect by binding after Na^+ to a site different from that of uridine (268).

The relationship between nucleoside flux and Na^+ concentration revealed hyperbolic curves for CNT1-mediated transport with apparent K_{50} values of ~ 10 mM and calculated Hill coefficients predicting a 1:1 Na^+ :nucleoside stoichiometry (263, 269). These results were in good agreement with those obtained by earlier functional studies of native *cit*-type transport activity (30, 243). Direct measurement of Na^+ :nucleoside coupling ratios for hCNT1 determined in *Xenopus* oocytes by simultaneous measurement of uridine-induced current and radiolabeled uridine uptake was reported independently by two groups to be 2:1 (267) and 1:1 (268).

Produced in *Xenopus* oocytes, human and rat CNT1 mediated uptake of the antiviral nucleoside analogs AZT and ddC, but not ddI (261, 262, 268, 270). Antineoplastic nucleoside chemotherapeutics that are permeants for hCNT1 include dFdC (119, 120, 267, 271) and the uridine analogs 5-fluorouridine, 2'-deoxyuridine, 5-fluoro-2'-deoxyuridine and 5-fluoro-5'-deoxyuridine (267, 268, 272). Although, 5'-deoxy-5-flourouridine is a hCNT1 permeant, the parent compound capecitabine and its metabolite 5'-fluorouracil are not (273). 2', 3'-Dideoxy-3'-thiacytidine (lamivudine) was shown to be a poor inhibitor of hCNT1-mediated uridine uptake (274). Although hCNT1 exhibits high-affinity adenosine transport that occurs at low rates, transport of the adenosine analogs 2-CdA and F-araA was not detected (271, 272); however, 2-CdA did induce inward currents in hCNT1-expressing *Xenopus* oocytes (268). Similarly, araC was demonstrated to be a poor permeant for hCNT1 in radiolabeled flux assays (274), but inward currents were apparent in electrophysiology experiments (268).

CNT1 is found in highly differentiated tissues such as epithelial cells of the kidney and intestine, as well as liver, placenta and brain (58, 143, 275). In rat, Northern blot analysis revealed rCNT1 transcripts in intestinal and renal tissues (261). In good agreement with the presence of a *cit*-type transport process in human intestinal brush border vesicles (276), CNT1 is localized to the apical membranes of epithelial cells. rCNT1 protein was present only in the brush border membrane of jejunum and renal cortical tubules (277), and similarly in human tissues, hCNT1 was apically localized in duodenum enterocytes and kidney proximal tubular cells (143). An apical localization in epithelial cells was also evident for both hCNT1-CFP (140) and rCNT1-GFP (278) expressed in renal MDCK cells. A wide variation in expression of hCNT1 mRNA was noted in kidney from different individuals, as well as particularly low levels in kidney tumor samples (133). The presence of rCNT1 was reported in bile canalicular membranes in rat liver (277) and of hCNT1 in human hepatocytes (143). mRNA for rCNT1 was identified throughout brain tissues, including cerebral cortex, cerebellum, hippocampus, striatum, brain stem, superior colliculus, posterior hypothalamus and choroid plexus (279).

rCNT1 was originally predicted by hydropathy plots to contain 14 TMs with intracellular N- and C-termini (261). However, experiments using endoglycosidase F treatment on rCNT1-expressing *Xenopus* oocytes revealed that the transporter was glycosylated (277). Since the only two potential sites of glycosylation in rCNT1 are located at the C-terminus, the 14 TM model was likely incorrect. Introduction of N-glycosylation sites at the N-terminus and in the loop between TMs 4 and 5 did not alter the glycosylation status of the protein and, together with studies using site-specific antibodies, led to a revised 13 TM topology model for CNT1 which is depicted in Fig. 1-5 (277).

In contrast to ENT1 and ENT2, little is known about the regulation of CNT1. rCNT1 mRNA levels decreased upon exposure to insulin, but not glucose in cardiac fibroblasts in a manner dependent upon the transcription/translation regulator protein mTOR (157, 171). IFN- γ , but not macrophage (M)-CSF, increased expression of CNT1 in murine bone marrow derived macrophages (152) and, in the same cells, LPS

was also demonstrated to upregulate CNT1 expression in a NO-independent manner (280).

CNT2

A second mammalian member of the CNT family was isolated from rat liver by expression cloning in *Xenopus* oocytes (281). This nucleoside transporter was first identified as sodium-dependent purine nucleoside transporter (SPNT), and later designated rCNT2 upon cloning from rat jejunum (269). SPNT/rCNT2 are both 659 amino acids in length and differ in two positions with alanine at residue 419 and isoleucine at residue 522 in SPNT (281) and glycine and valine at those positions, respectively, in rCNT2 (269). The human homolog hSPNT1, was later cloned from human kidney as a 658 amino acid protein and mapped to chromosome 15q13-14 (282). A second group also identified hCNT2 from intestine through the use of RT-PCR homology cloning strategies and functional expression in *Xenopus* oocytes and the gene was mapped to chromosome 15q15 (283). The human homologs are identical in sequence with the exception of residue 75 which is arginine in hCNT2 (283) and serine in hSPNT1 (282). hCNT2 shares 83% identity in sequence to rCNT2, with the greatest divergence at the N-terminal region, and 72% amino acid sequence identity with hCNT1 (282, 283). Subsequently, CNT2 homologs from mouse and rabbit were also cloned and designated mCNT2 (284) and SPNT/rbCNT2, respectively (285). In a study of 247 DNA samples, 10 coding region variants were identified of which six were nonsynonymous and all were functional upon expression in *Xenopus* oocytes (286).

The functional expression of h/r/rbCNT2 cDNAs in *Xenopus* oocytes, characterized the membrane transport protein as a *cif/N1*-type Na⁺-dependent nucleoside transporter selective for the purine nucleosides adenosine, inosine and guanosine, as well as the pyrimidine nucleoside uridine (269, 282, 283, 285, 287, 288). hCNT2-mediated transport of both inosine and uridine was saturable with apparent K_m values of 4.5 and 80 μ M, respectively (282). Apparent K_m values for

hCNT2-mediated transport in various expression systems are compared to those of other hENT and hCNT family members in Table 1-2. In addition to physiological nucleosides, hCNT2 also mediated uptake of uridine analogs, including 5-fluorouridine, 5-fluoro-2'-deoxyuridine and 2'-deoxyuridine (272, 289), as well as 2'-deoxyadenosine (282) and, at low levels, dIdI (283). Adenosine analogs such as 2-CdA and F-araA were poor permeants for hCNT2 (272, 289), and AZT and ddC were not transported (56). In contrast to hCNT2, rCNT2 transported the nucleoside analogs 2', 3'-dideoxyadenosine, araA, F-araA, 2-CdA and dIdI (287, 288, 290, 291).

Multiple transcripts of CNT2 were found not only in kidney, but also in other tissues such as intestine, liver, heart, skeletal muscle, pancreas, spleen, epididymis and brain, as well as in smaller quantities in prostate, cervix, placenta and lung (133, 281-283, 285, 292). Variability in transcript level was evident for different individuals (133). mRNA for rCNT2 was identified throughout brain tissues, including cerebral cortex, cerebellum, hippocampus, striatum, brain stem, superior colliculus, posterior hypothalamus and choroid plexus (136, 279). The distribution of hCNT2 correlates well with sites of action for purine nucleosides, primarily adenosine, especially in kidney and heart tissue (133, 282). Expression levels of hCNT2 decreased in tumors from kidney, stomach, rectum and small intestine, but increased in tumors from lung, ovary, uterus and prostate (133). GFP-tagged rCNT2 was localized primarily to the apical surface of MDCK cells (278), although significant expression on the basolateral side was also evident (293). In human tissues, hCNT2 was localized to the apical membrane of duodenum enterocytes and kidney proximal tubular cells (143). Cell surface expression of hCNT2 was reported in hepatocytes (143); furthermore, rCNT2 was demonstrated to be localized in the basolateral plasma membranes from rat liver (294).

Similar to hCNT1, hydropathy plots initially predicted CNT2 to have 14 TMs with intracellular N- and C-termini (281, 282) and this model was later revised to be similar to that of CNT1 as illustrated in the representative schematic shown in Fig. 1-5 (277). rCNT2 contains three putative glycosylation sites and only two, which are conserved across species (Asn⁶⁰⁶ and Asn⁶²⁵), were demonstrated to be glycosylated

(293). These glycosylation studies also demonstrated that *N*-linked glycosylation was not essential for the function or polarized trafficking of rCNT2 in stably transfected MDCK cells (293).

Similar to CNT1, little is known about the regulation of CNT2. A functional link between adenosine receptor A₁R activation, which stimulates rCNT2 activity in rat liver, and K_{ATP} channel function has been proposed (294). rCNT2 contains an N-terminal ATP/GTP binding motif which is absent from hCNT2 and may play a role in the regulation, targeting or activation of this particular protein (282). rCNT2 mRNA levels decreased upon exposure to insulin, but not glucose in T- and B-lymphocytes (158, 159) and cardiac fibroblasts (157). The insulin effect on rCNT2 in cardiac fibroblasts depended on activity of the kinase MEK and required protein synthesis (171). B-cell activators, PMA and LPS, upregulated expression of hCNT2 in a human B-lymphocyte cell line through mechanisms involving PKC and TNF- α (154), but not NO (155). Similar to CNT1, IFN- γ , but not M-CSF, increased expression of CNT2 in murine bone marrow derived macrophages (152) and, in the same cells, LPS was also demonstrated to upregulate CNT2 expression in a NO-independent manner (280).

CNT3

The molecular identification of hCNT3 resulted from BLAST searches of CNT sequences which identified overlapping human expressed sequence tags (ESTs) from mammary gland and colon adenocarcinoma (295). hCNT3, cloned by RT-PCR from mammary gland and differentiated HL-60 cells, is 691 amino acids in length with a molecular weight of 77 kDa and is 48 and 47% identical to hCNT1 and hCNT2, respectively (295). The molecular cloning of mCNT3 was accomplished in a similar manner with ESTs identified from mouse mammary gland and the corresponding full-length mouse cDNA obtained by RT-PCR from liver (295). hCNT3 was mapped to chromosome 9q22.2 (295, 296). The upstream promoter region of the gene expresses a eukaryotic phorbol myristate acetate (ester) response

element (PMA-RE) (295). In HL-60 cells, differentiation induced by phorbol ester resulted in the induction of *cib*-type functional activity and expression of hCNT3 mRNA (295). Human and rodent CNT3 and a related transporter from hagfish (hfCNT) form a phylogenetic subfamily of CNT family members distinct from that of CNT1 and CNT2 (295, 297, 298). In a study involving 270 DNA samples, 56 SNPs were identified, of which 16 were in the coding region (299). Ten variants were nonsynonymous and expression in *Xenopus* oocytes revealed hCNT3-like Na⁺-dependent uptake of radiolabeled thymidine and inosine for all variants except one (G367R), which exhibited only ~ 20% of the uptake seen with hCNT3 (299). In another study involving 96 DNA samples, 16 SNPs were identified and three of the five coding regions variants were nonsynonymous, but retained hCNT3-like nucleoside transport activity (300, Appendix 1). This suggests a high degree of conservation within the hCNT3 gene.

There is no sequence similarity between hCNT3 (295) and the sodium-dependent nucleoside transporter (SNST) 1 which was also proposed to be the *cib* transporter (301, 302). SNST1 was a chimeric protein constructed from a partial length cDNA identified in a rabbit renal cDNA library using the 5' untranslated region (UTR) and first 79 amino acids, including the start codon, 3' UTR and poly (A)⁺ tail, of the rabbit intestinal sodium-dependent glucose transporter (SGLT) 1 (301). Aside from the initial cloning and limited functional characterization in *Xenopus* oocytes, no further studies supporting the identity of SNST1 as a *cib*-type transporter or reporting the isolation of full-length SNST1 cDNA have been published.

Uptake of nucleosides by hCNT3-producing *Xenopus* oocytes was found to be concentrative, NBMPR-insensitive and Na⁺-dependent, as confirmed by studies involving the two-electrode voltage-clamp technique (295). Radiolabeled pyrimidine and purine nucleosides, but not the nucleobases uracil and hypoxanthine, were transported by hCNT3 and mCNT3 (295, 296). This permeant specificity was consistent with prior characterization of the *cib*/N3-type transport processes. hCNT3 transported both purine and pyrimidine nucleosides with similar kinetic efficiencies and apparent K_m values ranged between 15 and 53 μ M for all permeants tested (295).

Apparent K_m values for hCNT3-mediated transport in various expression systems are compared to those of other hENT and hCNT family members in Table 1-2. Mixed-type inhibition of hCNT3 transport activity by phloridzin was evident in Cos7L cells (296) and *Xenopus* oocytes (268) and IC_{50} values were 0.17 and 0.3 mM, respectively.

In contrast to hCNT1 (268), and in good agreement with 2:1 Na^+ :nucleoside coupling ratios reported for the *cib* transport processes in choroid plexus and microglia (251, 255), the relationship between uridine influx and Na^+ concentration revealed sigmoidal curves for both hCNT3 and mCNT3 (295). Apparent K_{50} values were 16 (hCNT3) and 7 mM (mCNT3) (295) and calculated Hill coefficients, from this and other studies, predicted 2:1 Na^+ :nucleoside stoichiometry for both transporters (295, 296, 303). Direct measurement of Na^+ :nucleoside coupling ratios for hCNT3 determined by comparison of uridine-induced currents and radiolabeled uridine uptake in the same oocyte revealed 2:1 stoichiometry (268, 295). In addition to Na^+ , initial studies suggested that nucleoside transport mediated by h/mCNT3 could also be coupled to H^+ gradients (268).

Assays of nucleoside drug transport revealed that the broadly selective CNT3 was also able to transport a broad range of both pyrimidine and purine antineoplastic and antiviral drugs (295). For example, hCNT3 was shown to transport the pyrimidine nucleoside analogs 5-fluorouridine, 5-fluoro-2'-deoxyuridine, 3-deazauridine, zebularine, dFdC, AZT and ddC and the purine nucleoside analogs 2-CdA, F-araA, ddI and ribavirin (119, 295, 303). Clofarabine was also transported well by hCNT3 (123). An antiviral nucleoside drug with an acyclic ribose moiety, 2-amino-9-(1,3-dihydroxypropan-2-ylloxymethyl)-3*H*-purin-6-one (ganciclovir), was not transported by hCNT3 (295).

High stringency hybridization studies found hCNT3 transcripts to be more ubiquitously expressed than hCNT1/2, with the greatest abundance in mammary gland, pancreas, bone marrow, trachea, duodenum and the lowest abundance in kidney, liver, lung, placenta, prostate, testis and other tissues including regions of the

brain and heart (295). Transcripts were present in fetal tissues and were also found in low amounts in cultured cell lines including K562, HeLa and undifferentiated HL-60 cells (295). Northern blot analysis supported these findings, revealing the presence of hCNT3 transcripts in pancreas, bone marrow and trachea (295). In human kidney, hCNT3 transcript and protein were detected in both cortex and medulla (142). hCNT3 immunostaining in human kidney was most evident on apical surfaces of proximal tubules and thick ascending loops of Henle, although cytoplasmic staining was also present (142). Cytoplasmic hCNT3 immunostaining has also been observed in polymorphocytic cells isolated from chronic lymphocytic leukemia patients (304).

h/mCNT3 contain multiple consensus sites for *N*-linked glycosylation (295) and treatment of hCNT3 membranes with PNGase F or Endo H shifted the electrophoretic mobility on SDS-polyacrylamide gels from 67 to 58 kDa, indicating that hCNT3 is a glycoprotein (296). Similar to hCNT1 and hCNT2, protein structure algorithms of hCNT3 predict a 13 TM model with large extramembraneous end termini regions similar to the membrane architecture depicted in Fig. 1-5 (295).

CNT Physiological Implications

The abundance of all three CNTs in specialized epithelial cells, such as intestine and kidney, as well as liver, suggests a role for these transporters in the systemic absorption, distribution and excretion of physiologic nucleosides and nucleoside analogs. The specific distribution of each CNT with respect to its cation selectivity and coupling stoichiometry may also be of physiological importance. For example, rCNT1 is present in jejunum in brush border membranes where it may function in absorption of dietary nucleosides (277). The presence of rCNT1 in brush border membranes of renal cortical tubules and canalicular membranes of liver parenchymal cells is consistent, respectively, with roles in reabsorption of nucleosides in the glomerular filtrate and retrieval from bile (277). Additionally, hCNT3 is also found in kidney, on the apical surfaces of proximal tubules and thick ascending loops of Henle (142). CNT3, with a 2:1 Na⁺:nucleoside stoichiometry, is better able than

CNT1 and CNT2 to concentrate nucleosides, while its ability to mediate H⁺-nucleoside cotransport may also be of particular physiological importance in the acidic environment of the kidney (142, 305).

CNT nucleoside transport activities differ depending on cell type and the stage of development of neoplastic transformation (58). Unlike hCNT1 and hCNT2, hCNT3 is transcriptionally regulated and changes in expression levels may be important in both physiological and pathophysiological conditions (295). A better understanding of the regulatory mechanisms of CNTs will facilitate our understanding of the functional importance of CNTs.

Additionally, all three mammalian CNTs transport adenosine and may thus play a role in the regulation of extracellular concentrations of adenosine available to purinergic receptors. Although not as ubiquitously expressed as ENTs, the ability of CNTs to concentrate nucleosides against a concentration gradient may play a key role in metabolism of adenosine and adenosine analogs. Interactions of adenosine, adenosine analogs and adenosine receptor ligands with CNTs are kinetically specific to each transporter and may be clinically relevant with respect to therapeutic manipulation of adenosine metabolism (272).

Non-Mammalian Eukaryotic CNT Family Members

In addition to mammalian CNT proteins, CNT family members have been identified and functionally characterized in other eukaryotes, including lower vertebrates, nematodes and fungi.

Lower Vertebrates

Through exploitation of sequence similarities between CNT family members, a CNT from the ancient marine prevertebrate the Pacific hagfish *Eptatretus stouti* was identified by molecular cloning of its cDNA (298). A PCR-acquired partial length

hagfish (hf) CNT cDNA was used as a probe to isolate a full length hfcCNT from a hagfish intestinal cDNA library (298). hfcCNT is 683 amino acids in length with 13 putative TMs (298). Although hagfish diverged from the main line of vertebrate evolution ~ 550 million years ago, hfcCNT shares 52, 50 and 57% sequence identity with hCNT1, hCNT2 and hCNT3, respectively, and this high degree of sequence conservation is most evident in TMs 4 to 13 (298). Sequence similarity is greater with hCNT3 than with hCNT1/2, identifying hfcCNT as a member of the CNT3 rather than CNT1/2 subfamily (298).

Consistent with its phylogenetic designation, recombinant hfcCNT exhibited *cib*-like transport activity upon expression in *Xenopus* oocytes and mediated Na⁺-dependent uptake of both purine and pyrimidine nucleosides as well as the nucleoside analogs AZT, ddC and dIdI (298). Electrogenic transport by hfcCNT was solely Na⁺-dependent as transport was not supported by H⁺ or Li⁺ gradients (298). Similar to the other CNT family members, the apparent K_m value for uridine uptake by hfcCNT expressed in *Xenopus* oocytes was 10.2 μ M (298). Electrophysiological current measurements combined with radiolabeled uridine uptake revealed a 2:1 Na⁺:uridine stoichiometry similar to hCNT3 (298). hfcCNT exhibited low-affinity binding of Na⁺ with an apparent K_{50} value > 100 mM, which is likely an adaptation to the high Na⁺ concentration of ~ 500 mM NaCl encountered by hagfish in sea water (298).

Nematodes

Two CNT family member homologs were identified by BLAST searches of the *Caenorhabditis elegans* genome encoded by F27E11.1 and F27E11.2 genes (306). Full-length cDNAs were cloned for both homologs, although F27E11.1 was not further characterized due to low expression in *Xenopus* oocytes (306). F27E11.2, expressed in *Xenopus* oocytes, exhibited broad selectivity for both purine (adenosine, inosine and guanosine) and pyrimidine (uridine and thymidine) nucleosides and was designated CeCNT3 to reflect its *cib*-like permeant selectivity (306). Surprisingly, cytidine was not a permeant for CeCNT3 (306). CeCNT exhibited high affinity for

inosine and thymidine with apparent K_m values of 15.2 and 11.0 μM respectively (306). CeCNT3 has 575 amino acids and exhibits $\sim 30\%$ sequence identity to mammalian CNTs (306). Transport mediated by CeCNT3 was Na^+ -independent, but pH-dependent, suggesting that it functions as a H^+ /nucleoside symporter (306).

Fungi

The *Saccharomyces cerevisiae* genome does not encode CNT family members; multiple CNTs, however, exist in pathogenic yeast genome sequence databases. A CNT family member from the pathogenic yeast *Candida albicans* was identified by BLAST searches of the genome sequence databank and cloned by PCR from a *C. albicans* cDNA library (307). *C. albicans* (Ca) CNT is 608 amino acids in length and putatively contains 13 TMs, but lacks the extended extracellular glycosylated C-terminus of mammalian CNTs (307). CaCNT exhibits 33, 34 and 38% sequence identity to hCNT1, hCNT2 and hCNT3, respectively (307). Upon expression in *Xenopus* oocytes, recombinant CaCNT exhibited transport of purine nucleosides (adenosine, inosine and guanosine) as well as uridine with apparent K_m values ranging from 16 to 64 μM (307). Chemotherapeutics that were permeants for CaCNT included the purine nucleoside analogs ddl, F-araA and 2-CdA and the uridine analogs, 5-fluorouridine, 5-fluoro-2'-deoxyuridine and zebularine (307). Low levels of transport of cordycepin, a purine nucleoside analog with anti-fungal activity, was also evident (307). In contrast to Na^+ -coupled CNTs, but similar to CeCNT3, CaCNT functioned as a H^+ symporter and charge/flux ratio experiments similar to CNT1-3 and hCNT revealed a 1:1 H^+ :uridine coupling ratio (307).

Prokaryotic CNT Family Member

Bacteria

Unlike ENTs, CNTs are also found in prokaryotes. A CNT family member from the inner membrane of *Escherichia coli* was isolated by functional rescue studies and designated NupC according to its gene name (308). Also cloned by PCR from an *E. coli* cDNA library (309, Appendix 2), NupC encodes a 400 residue protein and contains 10 predicted TMs corresponding to TMs 4 - 13 of eukaryote CNTs (308). NupC was functionally characterized following expression of its cDNA in *Xenopus* oocytes (309, Appendix 2).

Organic Cation Transporter (OCT) Family

Members of the OCT family are able to mediate the cellular uptake of a variety of compounds, including monoamines, organic cations, such as tetraethylammonium (TEA) and MPP⁺, as well as clinically relevant drugs, such as antihistamines and antivirals (310-315). The OCT family is comprised of two functionally distinct groups of transport proteins: OCTs are basolaterally-expressed electrogenic, potential-sensitive facilitative transporters also capable of electroneutral exchange, whereas organic cation transporters-novel (OCTNs) are apically-expressed and exhibit various energetic mechanisms, including electroneutral exchange (OCTN1), Na⁺-dependent cotransport (OCTN2) and electrogenic facilitated diffusion (OCTN2) (315). Members of the OCT family each have different permeant profiles and only OCT1, which primarily mediates the uptake of various cations in epithelial tissues, was demonstrated to transport nucleoside analogs (310-312, 314, 316, 317). OCT family members that have been identified are listed in Table 1-4.

Human, rat and mouse OCT1 are 554, 556 and 556 amino acids in length, respectively, and contain 12 predicted TMs (318-321). hOCT1 exhibits 78% sequence identity to rOCT1 (321). A second isoform cloned from rat kidney, rOCT1A, represents a functional, alternatively-spliced protein of 430 amino acids and

10 putative TMs (322). mRNA transcripts for hOCT1 were found primarily in the liver (321), whereas rOCT1 was found in kidney, liver, intestine and colon (318). Transport by hOCT1 was electrogenic, dependent on both pH and membrane potential and accepted permeants were multispecific and independent of charge (321). Upon expression in *Xenopus* oocytes, radiolabeled MPP⁺ uptake by hOCT1 was inhibited by the nucleosides thymidine and inosine, as well as by the organic anion taurocholate (321). Antiviral permeants for hOCT1 included acyclovir (ACV) and GCV, but not AZT (312). Also expressed in *Xenopus* oocytes, rOCT1 mediated transport of 7-deazadeoxyadenosine (deoxytubercidin), araC, 2-CdA and AZT (310). Deoxytubercin was later shown to be transported in its cationic form (317).

Organic Anion Transporter (OAT) Family

OATs belong to the same gene family as OCTs and are therefore structurally similar (323). Permeants for organic anion transporters include a wide variety of endogenous metabolites, xenobiotics and drugs, including vitamins, antihypertensive drugs, nucleoside analogs, anti-inflammatory drugs and the initially identified permeant, *p*-aminohippurate (PAH) (323). Organic anion transport is mediated by a family of proteins for which several members have been identified by molecular cloning and subsequent characterization: OAT1 (324-330), OAT2 (331, 332), OAT3 (333-335), OAT4 (336), OAT5 (337) and OAT6 (338). These proteins have diverse permeant selectivities and different tissue distributions, although all isoforms are present in kidney (323, 339). OAT family members that have been identified are listed in Table 1-5.

Among putative permeants for this diverse family of transporters, some studies have investigated nucleoside analogs. For example, transport of the antivirals ACV and GCV was apparent for only hOAT1, whereas AZT was transported by hOAT1, hOAT2, hOAT3 and hOAT4 (312). rOAT1, expressed in *Xenopus* oocytes, was also shown to transport ACV and AZT, as well as other nucleoside analogs including ddC, ddI, lamivudine, 2', 3'-didehydro-3'-deoxythymidine (stavudine) and

2'-deoxy-5-(trifluoromethyl)uridine (trifluridine) (340). Among many other structurally unrelated compounds, both hOAT2 (341) and mOAT3 (342) expressed in *Xenopus* oocytes mediated the uptake of 5-fluorouracil.

Nucleoside:H⁺ Symporter (NHS) Family

Two nucleoside transport systems, nupC and nupG, were initially characterized in *Escherichia coli* and differed in both permeant selectivity and resistance to the antibiotic nucleoside analog, showdomycin (308, 343). While the nupC system, corresponding to the NupC protein, belongs to the CNT family (308), nupG is a member of the nucleoside:H⁺ symporter family, which in turn is part of the larger major facilitator superfamily (MFS) of transporters (344). NupG, the membrane protein product of the nupG gene, is 418 amino acids in length (345). Recombinant expression of NupG in *E. coli* and *Xenopus* oocytes exhibited H⁺-dependent transport of both purine and pyrimidine nucleosides (346-348). Purification of over-expressed NupG in *E. coli* allowed application of Fourier transform infrared and circular dichroism spectroscopy analysis to indicate α -helical structure consistent with 12 putative TMs (347). The inhibition profile of recombinant NupG expressed in *Xenopus* oocytes by a series of 46 nucleosides and nucleoside analogs identified similar, but distinct recognition patterns in NupG and NupC, and allowed a homology model of the NupG binding site to be created based on the X-ray crystallographic structure of the MFS disaccharide transporter LacY from *E. coli*. (348).

Investigations of xanthine metabolism in *E. coli* identified the xapB gene which encodes a 418 amino acid protein with 12 putative TMs designated XapB that is 56% identical in sequence to NupG (346, 349). Expression in a transport-deficient *E. coli* strain and uptake experiments using radiolabeled permeants indicated that XapB transports all nucleosides, except guanosine, and, unlike NupG, also mediates transport of xanthine (346). Using an uncoupler of the proton motive force, xanthosine transport was shown to be H⁺-dependent (346). In addition to the *E. coli*

NupG and XapB proteins, one other NHS protein family member from *E. coli* was predicted to be a nucleoside transporter based on homology to NupG and XapB and was designated YegT, although this protein has yet to be functionally characterized (80). These NHS family members are listed in Table 1-6.

Tsx Channel-Forming Protein Family

Tsx channel-forming protein family members capable of nucleoside transport include the Tsx proteins found in the outer membrane of gram-negative bacteria such as *Escherichia coli* (Ec Tsx) (350) and *Salmonella typhimurium* (St Tsx), *Klebsiella pneumoniae* (Kp Tsx) and *Enterobacter aerogenes* (Ea Tsx) (351). Nucleoside transport by Tsx was first identified in *E. coli* tsx mutants in which adenosine and thymidine uptake were impaired (352). Later, Ec Tsx was identified as a 294 amino acid protein, in which the first 22 amino acids serve as the bacterial signal sequence peptide to target the protein across the cytoplasmic membrane, thus resulting in a mature form of Ec Tsx which is 272 amino acids long (350). St Tsx, Kp Tsx and Ea Tsx are 265, 272 and 272 residues in length in their mature form (351). More recently, a Tsx family member was also identified in *Salmonella enterica* (353). Tsx functions as a permeant-specific channel which transports nucleosides and deoxynucleosides (351, 354, 355). Although Tsx proteins are structurally unrelated to other nucleoside transporter families (356), one group has suggested, based on analysis of conserved sequence motifs, that Tsx proteins may be the evolutionary precursors to ENT proteins and thus be classified as prokaryote ENT family members (79).

Other members of the Tsx channel-forming protein family include distantly related outer membrane proteins (Omps). Similar to tsx proteins, Omps are also found in gram-negative bacteria, such as *Vibrio parahaemolyticus* and *Vibrio cholerae* (357-359). Tsx family members that have been identified are listed in Table 1-7.

Uracil/Allantoin Permease Family

The first member of the uracil/allantoin permease family to be identified was FUR4 from *Saccharomyces cerevisiae* (360). This protein, a uracil permease, is 633 amino acids in length (360). Also in *S. cerevisiae*, disruption of the *fui1* gene led to a mutant phenotype that was unable to grow on a medium containing uridine as nutrient, and was resistant to the cytotoxic effects of 5-fluorouridine (361, 362). The *fui1* gene product, also a uracil/allantoin permease family member, was designated FUI1 (225). FUI mediated transport of uridine and uridine analogs and was insensitive to inhibition by NBMPR, dilazep and dipyridamole (225). Further characterization of FUI1 in transport-deficient yeast and *Xenopus* oocytes revealed H⁺-dependence and identified key residues and permeant structures important for transport (363, Appendix 3). Other identified members of the uracil/allantoin family are listed in Table 1-8.

Nucleoside Permease (NUP) Family

Exploitation of the inability of *S. cerevisiae* to transport purine nucleosides allowed for the cloning of the nucleoside permease gene NUP from *Candida albicans* (364). The corresponding protein, NUP, is 407 amino acids in length, mediated transport of adenosine and guanosine, and was inhibited by NBMPR and dipyridamole (364). Another sequence related to *C. albicans* NUP was identified from *Giardia intestinalis*, but functional characterization remains as unpublished findings (80). These two NUP proteins are listed in Table 1-9.

Importance of Nucleoside Transporter Studies

Nucleoside transport in most tissues and cells studied thus far results from the presence of more than one nucleoside transport protein. The functional redundancy of nucleoside transporters with overlapping permeant selectivities (Table 1-2)

suggests that these proteins are highly regulated and indicates the importance of cellular and subcellular localizations. For example, both ENTs and CNTs are present in intestine (109, 143, 276, 365, 366). In intestinal epithelial cells, CNTs are present in brush border membranes, whereas ENTs are present in the basolateral membrane (143, 144, 277). Similarly, ENTs and CNTs are both present and have distinct membrane distributions in kidney tubular cells with CNTs apically expressed and ENTs primarily expressed basolaterally, although an apical localization for hENT1 has also been reported (54, 140-143, 277, 278, 305). This distribution of concentrative and equilibrative nucleoside transporters is important for their respective roles in intestinal absorption and renal reabsorption and secretion of nucleosides and nucleoside analogs (143, 305, 367). Also, the coexistence and distinct distribution of ENTs and CNTs in liver cells provides a method to deliver newly synthesized nucleosides into the blood, as well as salvage nucleosides when needed by the liver itself for regeneration (143, 275, 368). ENTs have been functionally implicated in regulation of adenosine metabolism, for example, in brain (116, 185) and heart (6, 77, 104, 139, 181). Although adenosine is a permeant for all three CNTs, and transcripts for all three CNTs have been identified in brain and heart tissue, a corresponding role is yet to be described. With the exception of ENT3 (172), human ENT and CNT family members are primarily found on the plasma membrane of cells, although there is also evidence to support intracellular localization of hENT1, hENT2 and hCNT3 (145, 147, 304). Nucleoside transporter activity varies with cell type and stage of differentiation; however, information on regulation of both protein expression and membrane targeting is limited (58, 368).

Nucleoside transporter studies are also critical to the application of nucleoside analog chemotherapy (reviewed in 32, 56-58, 369-372). Most nucleoside analog chemotherapeutics have been demonstrated to be permeants for nucleoside transporters and cellular uptake of these drugs is the prerequisite for intracellular metabolism and subsequent pharmacologic actions. Thus, the presence of appropriate nucleoside transporter(s) in the plasma membrane of diseased cells is important for both sensitivity and resistance to nucleoside chemotherapeutics and, thus, clinical outcome (54, 56-58, 371). For example, hENT1 abundance in plasma membranes has

been correlated with sensitivity to nucleoside analogs such as 5'-deoxy-5-fluorouridine in breast cancer cells (125), 2-CdA and F-araA in acute myelogenous and lymphoblastic leukemia cells (373) and dFdC in pancreatic cancer and non-small cell lung cancer cells (374, 375). An increasing number of studies, including those on treatment of infant acute lymphoblastic leukemia (376) and acute myelogenous and lymphoblastic leukemia in adults (373), have related hENT1 abundance to araC sensitivity and proposed hENT1 expression levels as a good prognostic determinant of araC cytotoxicity and resistance (59). For example, hENT1 deficiency was related to shorter disease-free survival times in araC-treated acute myeloid leukemia patients (121, 377). Similarly, in a retrospective study, the presence of hENT1 in pancreatic adenocarcinoma cells resulted in significantly longer patient survival times following dFdC chemotherapy than those patients for whom hENT1 was undetectable in a proportion of cells in tumor samples (375). The clinical outcome following dFdC treatment of pancreatic cancer was also significantly correlated to hENT1 expression levels (378). Sensitivity to 2-CdA was restored in araC-resistant CEM-ARAC leukemia cells upon *in vitro* stable transfer of hCNT2 cDNA (289). Sensitivity and resistance to dFdC also differed in cultured cell lines depending on the nucleoside transporters present (119).

While acquired resistance to cytotoxic nucleoside analogs may result from down-regulation of transporter expression and/or selection of transporter deficient cells, there are also many instances of increased abundance of nucleoside transporters in malignant cells compared to normal cells (133, 379). This accounts, at least in part, for the generally higher sensitivity of cancer cells to chemotherapeutic nucleoside drugs (133, 379). Ubiquitously expressed hENT1 is especially important in this regard and high proliferation rates of malignant cells are associated with elevated levels of *es*-type transport activity (54, 56). For example, increased hENT1 abundance was evident in breast cancer cells compared to normal breast epithelia (125). However, since ENTs are capable of mediating bidirectional transport, elevated expression of ENTs, especially in cells also expressing CNTs, may lead to drug efflux as a potential mechanism of resistance to nucleoside analogs. Intracellular localization of nucleoside transporters may also play a role in resistance

and/or toxicity. In a study of chronic lymphocytic leukemia patients, clinical resistance to F-araA was correlated with high levels of intracellular hCNT3 expression (304). In contrast, hENT1 present in mitochondrial membranes enhanced the mitochondrial toxicity of antiviral nucleoside analogs (145, 146). hENT3, which functions as an intracellularly targeted protein, may also be involved in intracellular sequestering of nucleoside analogs, particularly to the lysosome where degradation could occur (172).

Although little is known about regulation, nucleoside transporter gene expression is tissue-specific, dependent upon cell differentiation and growth and may be modulated by pharmaceuticals (56-58). Additionally, the presence of genetic variations within the patient population, such as SNPs, may account for some differences in therapeutic outcomes between individuals (58). Resistance to nucleoside analogs may also arise from gene redundancy because other protein families besides ENTs and CNTs, including OAT and OCT, as well as multidrug resistance (MDR) proteins are capable of mediating the transport of nucleoside analog chemotherapeutics and their metabolites and therefore may play key roles particularly in renal secretion of these compounds (58, 305). Although complex and the result of multiple interacting factors, resistance to nucleoside analog chemotherapy could be minimized through the development of predictive assays to determine the nucleoside transporter profiles of diseased cells and establish in advance their capacities to transport specific nucleoside analogs (59).

Nucleoside transporters play a role in nucleoside analog-induced toxicities and nucleoside transporter inhibitors may provide protection against these toxicities, as well as provide other alternative therapeutic options. Among other undesirable side-effects such as hematopoietic toxicity and nephrotoxicity, many nucleoside analog chemotherapeutics produce clinically significant dose-limiting mitochondrial toxicity resulting from their inhibitory action on mitochondrial DNA replication and repair (57, 305, 380). Mitochondrial toxicity may be linked to the presence of nucleoside transporters, particularly hENT1 (145, 146), on the mitochondrial membrane. In particular, energy-demanding tissues which consume high levels of ATP, such as

kidney, liver, muscle and pancreas, are susceptible to mitochondrial toxicity. For example, phase II clinical trial administration of 1-(2-deoxy-2-fluoro- β -D-arabinofuranosyl)-5-iodouracil (fialuridine), a uridine analog developed for the treatment of hepatitis B, caused severe widespread mitochondrial toxicity resulting in hepatotoxicity, pancreatitis, neuropathy and myopathy (381). In addition to fialuridine (382), other nucleoside drugs also cause mitochondrial toxicity including F-araA (383), ddI (384, 385), ddC and lamivudine (385, 386). A study using NBMPR, dilazep and dipyridamole demonstrated that these ENT inhibitors decreased toxicity of tubercidin against human hematopoietic cells (387). This strategy may provide pharmacologic resistance to normal tissues, thus minimizing dose-limiting toxicities and side-effects, while maintaining cytotoxic effects against target cells (57) and be of particular benefit with respect to the chemotherapy of malignant cells which tend to have increased abundance of nucleoside transport proteins (56). The same goal may be accomplished alternatively through the use of nucleoside transporter inhibitors administered in parallel with nucleoside analog chemotherapeutics in order to retain the nucleoside analog intracellularly and maximize cytotoxic actions (32, 56, 57). For example, exposure to NBMPR enhanced the cytotoxicity of 2-CdA in cultured human acute lymphocytic leukemia cells, suggesting that nucleoside transporter inhibition prevented drug efflux (388). For cells which have both ENTs and CNTs in their plasma membrane, the selective inhibition of ENTs may provide a means of increasing cytotoxicity when the nucleoside analog is also a permeant for CNTs (54). In addition to NBMPR and the coronary vasodilator drugs, such as dipyridamole, dilazep and draflazine, some protein kinase inhibitors, including rapamycin and inhibitors of tyrosine kinase, PKC and cyclin-dependent kinase, also inhibit nucleoside transport by ENTs (389). Further investigation of nucleoside transport inhibitors, including the development of new compounds, as well as studies of currently used compounds directed against other target proteins, is necessary to exploit these strategies and would be a valuable tool in mechanistic and physiological studies of nucleoside transport proteins. Especially valuable would be inhibitors specific to each individual transporter isoform. Currently no specific inhibitors of CNTs are known.

Similar to their handling of physiological nucleosides, nucleoside transport proteins also exhibit overlapping selectivities for nucleoside analogs (58, 59). Understanding the molecular determinants of permeant binding and translocation will aid in the development of improved nucleoside analogs for therapeutic purposes (59). Exploitation of these molecular determinants may facilitate development of nucleoside transporter inhibitors and ultimately contribute to a more detailed understanding of nucleoside transport mechanisms. In addition to improving the treatment of neoplastic and viral disease, the therapy of parasitic disease by nucleoside analogs will also benefit from the continued characterization of nucleoside transporters and the development of new chemotherapeutics (56, 390). Combining information on nucleoside transporter expression in diseased cells with detailed knowledge of nucleoside analog transportability may ultimately allow for individually tailored chemotherapy regimens.

Nucleoside Transport Protein Structure-Function Studies

Atomic resolution of three dimensional structure has been obtained for several bacterial membrane transport proteins, including the *E. coli* glycerol-3-phosphate transporter GlpT (391) and lac permease LacY (392), *Pyrococcus horikoshii* glutamate transporter Glt_{ph} (393) and *Aquifex aeolicus* Na⁺/Cl⁻-dependent leucine transporter LeuT_{Aa} (394). However, the current understanding of nucleoside transporter structures is limited to topological models derived from sequence homologies and hydropathy plot analysis combined with the use of molecular biology approaches in structure-function studies. Additionally, homology modeling based on solved crystal structures of distantly related proteins provides some additional insights. Studies to elucidate ENT and CNT molecular mechanisms have focused largely on structure-function studies involving protein-protein chimeras, amino acid mutations and chemical modification of permeants.

Studies on ENT Family Members

Substantial progress has been made in defining the structural basis of ENT protein function. Sequence alignments reveal TMs to be the most homologous regions of ENTs (54) and overall membrane topology is conserved amongst ENT family members (108). This common membrane architecture, as depicted in Fig. 1-4, consists of 11 TMs with cytoplasmic N-terminal and extracellular C-terminal regions, as well as large extracellular and cytoplasmic loops between TMs 1 and 2 and TMs 6 and 7, respectively (78, 130). Use of site-directed mutagenesis to construct glycosylation-defective mutants has revealed that both hENT1 (127, 130) and hENT2 (167) are glycosylated in the extracellular loop between TMs 1 and 2, although glycosylation is not required for function of either transporter. Extending this approach, glycosylation-scanning mutagenesis has confirmed the 11 TM topology of hENT1 (130).

Regions functionally important for ENT permeant and inhibitor interactions have been identified through the use of human and rat ENT chimeras. ENT interactions with inhibitors which compete with permeant for the nucleoside binding site, such as dipyridamole and dilazep (395), as well as NBMPR (396), involves the region encompassing TMs 3 to 6 and was identified using h/rENT1 and rENT1/2 chimeras, respectively. Additional domain swapping in rENT1/2 chimeras determined that the regions encompassing TMs 3 to 4 and TMs 5 to 6 contributed almost equally to NBMPR binding affinity (396). Also exploiting phenotype differences between transporters, rENT1/2 chimeras identified the regions encompassing TMs 1 to 6 to be responsible for the ability of ENT2 to efficiently transport the 3'-deoxynucleosides AZT, ddI and ddC (126) and TMs 5 to 6 for the ability of ENT2 to transport nucleobases (165).

Subsequent identification and characterization of the individual amino acid residues responsible for ENT permeant and inhibitor interactions has occurred through the use of point mutagenesis. Random mutagenesis of recombinant hENT1 produced in yeast identified Met³³ in TM 1 to be involved in dipyridamole and

dilazep binding, since hENT1 M33I mutants exhibited decreased sensitivity to both inhibitors in the absence of changes to NMBPR or uridine affinity (166). The role of this residue is conserved in hENT2; hENT2 I33M mutants exhibited increased sensitivity to dipyridamole and dilazep while retaining insensitivity to NBMPR (166, 397). Additionally, hENT2 I33M mutants displayed increased apparent affinity for uridine (166, 397). Mutation of hENT2 Ile³³ to cysteine rendered the protein sensitive to *p*-chloromercuribenzenesulfonate (PCMBS) in a nucleoside and inhibitor protectable manner, suggesting this residue is accessible from the extracellular medium and involved in permeant and inhibitor binding (397). Mutation of hENT1 Gly¹⁵⁴ in TM 4 to the corresponding residue in hENT2 (serine) resulted in decreased sensitivity to NBMPR, dilazep and dipyridamole, as well as decreased affinity for cytidine and adenosine (78, 398). The corresponding residue position in rENT2 is occupied by cysteine, Cys¹⁴⁰, which is both PCMBS-sensitive and nucleoside protectable, suggesting a key location within the inhibitor-nucleoside binding domain (399). Mutation of highly conserved residues Trp²⁹ (TM 1) and Gly¹⁷⁹ (TM 5) in hENT1 were both shown to inhibit transport activity and affect inhibitor binding (59, 400). Effects resulting from mutation of Gly¹⁷⁹ were consistent with a role for this residue in helix-helix packing (54). Additionally, TM 5 Gly¹⁸⁴ in hENT1 is important for targeting to the plasma membrane (400). Random mutagenesis and functional complementation also identified four additional residues, hENT1 Trp²⁹ (TM 1), Met⁸⁹ (TM 2), Leu⁹² (TM 2) and Ser¹⁶⁰ (TM 4), to be important for interactions with both inhibitors and nucleoside permeants (59, 401, 402) and, more recently, two TM 8 residues, Phe³³⁴ and Asn³³⁸, to be important for inhibitor interactions, protein folding and catalytic turnover (59, 403).

In addition to mutagenesis studies to identify functionally important residues in hENTs, other investigations have characterized hENT interactions with various nucleoside analogs containing base or ribose modifications. Using recombinant hENT1 and hENT2 produced in *S. cerevisiae*, inhibition profiles of uridine and cytidine analogs were used to identify key structural determinants responsible for transporter-permeant interactions (404, 405). With uridine for example, halogen modification at the 5 position of the base and the 2' and 5' positions of the ribose

moiety are tolerated by both hENT1 and hENT2, in contrast to the hydroxyl group at the 3' position of the ribose moiety, which is essential for recognition by both transporters (404). Both the 2'- and 3'-hydroxyl groups are important determinants for interaction of cytidine with hENT1, whereas hENT2 displayed an overall lower ability to interact with cytidine and cytidine analogs than hENT1 (404). hENT2 was shown to be more tolerant of sugar modifications than hENT1; strong interactions were apparent with the 3'-hydroxyl group for both hENT1 and hENT2, and moderate interactions were evident with the 2'- and 5'-hydroxyl groups for hENT1, whereas hENT2 showed weak interactions with the 5'-hydroxyl group only (405). Using pharmacophore models, nucleoside affinity was determined to be dependent largely on electrostatic and steric features for hENT1 (406).

In addition to mammalian ENT family members, insights toward transport mechanism have also been gained from non-mammalian homologs. Point mutations in *L. donovani* have identified residues influencing permeant recognition and transport in TM 5 (Gly¹⁸³) and TM 7 (Cys³³⁷) of LdNT1.1 (407), and in TM 4 - 5 loop (Asn¹⁷⁵) (408), TM 5 (Ser¹⁸⁹) (409) and TM 8 (Asp³⁸⁹) (410) of LdNT2. Investigation of *L. donovani* LdNT1.1 TM 5 using substituted cysteine accessibility method (SCAM) analysis strongly predicted involvement of this helix in the translocation pathway (48, 411). Site-directed mutagenesis of charged residues in *L. donovani* ENTs has also identified key residues in nucleoside binding and translocation, including LdNT1.1 Glu⁹⁴, Lys¹⁵³ and Asp³⁷⁴ in TMs 2, 4 and 8, respectively (412). *C. elegans* CeENT1 binds dipyridamole with high affinity similar to hENT1 (216) and random mutagenesis and functional screening of CeENT1 for reduced sensitivity to dipyridamole identified TM 11 residue Ile⁴²⁹ as a residue critical for high affinity interactions with dipyridamole (413). Mutagenesis studies of this residue, which corresponds to hENT1 Leu⁴⁴², and of the previously identified hENT1 TM 1 residue Met³³ (166, 397), in three different protein backgrounds (hENT1, hENT2 and CeENT1) confirmed the importance of these residues in both dipyridamole interactions and nucleoside transport and suggested close proximity integration of TMs 1 and 11 within the permeant translocation pore (413).

Thus, TMs 1, 2, 4, 5, 7, 8 and 11 have all been implicated in involvement in inhibitor interactions and/or nucleoside transport suggesting that they form part of the inhibitor and/or nucleoside binding domain(s). Combining these key regions with insights gained from studies identifying molecular determinants of permeant interactions allows for preliminary mapping of the putative ENT translocation pore. Assisting these efforts, a number of three dimensional homology models of ENTs (67, 408, 414) based upon distant similarities with MFS transporters have been generated from the crystal structures of *E. coli* GlpT (391) and lac permease LacY (392).

Studies on CNT Family Members

Although CNTs were identified at the molecular level prior to ENTs, structure-function studies addressing mechanisms of concentrative nucleoside transport lag behind those of their equilibrative counterparts. In part, this is largely a consequence of more complex molecular mechanisms, an inability of computer algorithms to unambiguously predict their membrane topology and an absence of even distantly related crystal structures. Studies of initially cloned CNTs predicted a 14 TM topology (261, 281, 282). However, *N*-glycosylation and immunocytochemical analysis revealed an extracellular C-terminus for rCNT1, leading to a revised 13 TM model of topology for CNTs as depicted in Fig. 1-5 (277). C-terminal glycosylation was also evident for rCNT2 (293) and hCNT3 (296). Although not strongly predicted by computer algorithms, two additional TMs (TMs 5A and 11A; Fig. 1-5) containing the highly conserved sequence motifs (G/A/S)XX(I/V)XXX(L/I)XYXXXGXXFVFG (rCNT1 residues 235 to 254) and (A/G)XXXGXKXXXNEFVAYXXLXXY (rCNT1 residues 486 to 507) were also postulated (277). Inclusion of TMs 5A and 11A would lead to an alternative 15 TM model of CNT membrane architecture (277).

In comparison to their prokaryote homologs, eukaryote CNTs are longer proteins which differ from the former by the possession of an extensive intracellular

N-terminal tail followed by three additional predicted TMs. For example, sequence comparisons align the 10 putative TMs of the CNT family member *E. coli* NupC with hCNT C-terminal TMs 4 to 13, thus suggesting that the N-terminal segment encompassing the first three putative TMs are not necessary for CNT function (308). This has been confirmed by truncation studies in which removal of the N-terminal region and first three TMs of rCNT1 and hCNT1 (residues 1 to 173, and 1 to 174 residues, respectively) led to truncated proteins, both of which retained functional activity (277). Furthermore, chimeric studies have revealed that the nucleoside specificity and cation coupling of CNT-mediated transport is determined by the C-terminal half of the protein. For example, a 50:50 chimera between hfCNT (TMs 1 - 6) and hCNT1 (TMs 7 - 13) generated a phenotype identical to that of hCNT1 with a hCNT1-like nucleoside selectivity (transport of uridine, thymidine, cytidine > adenosine, but not guanosine or inosine) and cation-dependence characterized by a high apparent K_{50} for Na^+ of 10 mM and Hill coefficient indicative of a 1:1 Na^+ :nucleoside coupling stoichiometry (298).

Chimeric and mutagenesis studies of rCNT1 and rCNT2 (415-417) and hCNT1 and hCNT2 (418) identified involvement of two central TMs (TMs 7 and 8) and associated residues in nucleoside binding and translocation. In the case of rCNT1/2, a chimeric protein consisting of rCNT1 with TM 7 replaced by that of rCNT2 was shown to display broad *cib*-like permeant selectivity (415) while maintaining a Hill coefficient for Na^+ -activation indicative of 1:1 Na^+ :nucleoside stoichiometry (416). Site-directed mutagenesis of Ser³¹⁸ in rCNT1 to the corresponding amino acid in rCNT2 (glycine) found this residue to be principally responsible for the phenotype (417). Another rCNT1 chimeric construct, in which TM 8 was replaced by that of rCNT2, showed compromised thymidine and inosine transport activity (415). In the case of hCNT1/2, introduction of an 85 residue segment of hCNT2 (corresponding to TMs 7 - 9) into hCNT1 changed the nucleoside selectivity of the transporter from *cit* to *cif* (418). By site-directed mutagenesis, two adjacent pairs of residues were identified in hCNT1 TMs 7 and 8 (Ser³¹⁹/Gln³²⁰ and Ser³⁵³/Leu³⁵⁴, respectively) that, when mutated to the corresponding residues in hCNT2 (Gly³¹³/Met³¹⁴ and Thr³⁴⁷/Val³⁴⁸), mediated the change. Mutation of the two

TM 7 residues alone resulted an intermediate *cib*-like phenotype, Ser³¹⁹ of hCNT1 being equivalent to Ser³¹⁸ of rCNT1 (418).

Additional studies in CNT family members using site-directed mutagenesis have also identified different key residues in TMs 7 and 8, as well as in other TMs. Mutation of highly conserved hCNT1 residues Phe³¹⁶ (TM 7) and Gly⁴⁷⁶ (TM 11) revealed roles in acquired guanosine sensitivity and membrane localization, respectively (419). Upon expression in MDCK cells, hCNT1 constructs F316A-GFP and F316Y-GFP were both found at the apical membrane similar to hCNT1, but in contrast to hCNT1 were sensitive to inhibition by guanosine (419). Additionally, a naturally occurring variant, F316H, was identified by analysis of hCNT1 SNPs and, upon expression in MDCK cells, also exhibited inhibition of transport by guanosine (419). This guanosine-sensitive phenotype was similar to the transport process *csg/N4* previously described in human kidney (259). Also in MDCK cells, GFP-tagged G476A and G476L hCNT1 mutants did not localize to the plasma membrane, thus suggesting a role for this TM 11 residue in membrane targeting and/or protein folding (419). Site-directed mutagenesis was used to investigate the role of conserved, negatively charged residues in hCNT1 structure and function and thereby identified important residues in TM 7 and the extracellular loop between TMs 11 and 12 (TM 11A) which influenced nucleoside and cation binding and/or translocation (420, Appendix 4). Mutation of Tyr³³² in CeCNT3 TM 8 to the corresponding residue in h/rCNT2 (phenylalanine) decreased apparent K_m and V_{max} values for thymidine and suggested a role for this residue in nucleoside recognition and translocation (306). Using SCAM methodology to probe a cysteine-less form of hCNT3 (hCNT3C-), residues in TMs 11, 12 and 13 were individually mutated to cysteine and tested for inhibition by methanethiosulfonate (MTS) reagents (421). This set of experiments provided evidence for participation of TMs 11 and 12, but not TM 13, in formation of the nucleoside translocation pathway (421).

Studies investigating SNPs have identified a greater degree of variability for hCNT1 than hCNT2, with a high degree of conservation evident for hCNT3 (59, 264, 286, 299). Characterization of 15 nonsynonymous variants in hCNT1 identified two,

S546P (TM 12) and the single base pair deletion variant CNT1-1153del, which were nonfunctional (264). All six nonsynonymous variants identified in hCNT2 were functional (286). The four most common of these variants showed similar apparent K_m values to that of hCNT2 for the nucleoside analog ribavirin (286); however, the F355S (TM 8) variant exhibited altered specificity for inosine and guanosine (286). Of 10 nonsynonymous variants identified in the coding region of hCNT3, only one, substitution of a highly conserved glycine (Gly³⁶⁷) in TM 8 with arginine, altered the nucleoside uptake profile of the transporter by exhibiting lower levels of thymidine and inosine uptake (299). A parallel study that identified and functionally characterized additional hCNT3 SNPs similarly revealed a high degree of conservation of function for this transporter (300, Appendix 1). Recently, a novel SNP in hCNT3 resulting in the mutation C602R in TM 13 was described in which the Hill coefficient for Na⁺-activation was shifted from 2 to 1, suggesting the possibility of an altered 1:1 Na⁺:nucleoside stoichiometry (422). The altered phenotype was attributed to the presence of arginine rather than the loss of cysteine at this position since hCNT3 mutant C602S retained wild-type transport properties (422).

Similar to ENTs, structure-function information on CNTs can be derived from studies investigating the effects of permeant modifications. For example, hCNT1 and hCNT2 exhibit different binding interactions with uridine and adenosine, permeants for both transporters, although the 6 position on uracil and the 8 position on adenine rings are critical for inhibition of both hCNT1 and hCNT2 (423). Similarly, rCNT1 did not transport pyrimidine nucleoside analogs with modifications at the 6 position of the base (266). Through the use of pharmacophore models, permeant interactions for hCNT1 were dominated by electrostatic and steric effects, whereas hydrogen bonding features were more critical for hCNT2 (406). In stably transfected cell lines, hCNT1 generally exhibited higher apparent affinity for uridine analogs in comparison to hCNT2, but unlike hCNT2 was unable to transport adenosine analogs (272). Inhibition of radiolabeled uridine uptake by hCNT3-expressing Cos7L cells determined that permeant recognition required the 3'-hydroxyl group and carbon at 6-position on the base of uridine (296). Similarly, a study measuring nucleoside analog-induced currents in hCNT3-producing *Xenopus* oocytes also identified the 3'-

hydroxyl group to be a critical determinant of hCNT3 transportability (303). A systematic series of experiments using uridine analogs to investigate the structural determinants in the sugar moiety important for interaction with hCNT1, hCNT2 and hCNT3 revealed that the uridine-binding profiles for each transporter were consistent with their respective transportability profiles (59, 424, 425). These experiments found that transport of uridine analogs mediated by hCNT1 was sensitive to modifications of the N-3, C-3' and C-5' positions, that hCNT2 was not tolerant of changes at C-3' or C-5' and only partially tolerant of modification at N-3, and that hCNT3 was sensitive to C-3' modifications only (59, 424, 425). Similarly, *E. coli* NupC produced in *Xenopus* oocytes was tested for inhibition by a series of 46 nucleosides and nucleoside analogs (348). These experiments revealed that binding to NupC required the C-3'-hydroxyl substituent as well as the natural α -configuration at C-3' and natural β -configuration at C-1' (348). The overall pattern of inhibition for NupC was similar to that of hCNTs (348).

ENT and CNT Mechanism(s) of Transport

Similar to members of the major facilitator superfamily, mechanisms of transport for ENT and CNT proteins have been based on the alternating access concept (426). Thus, the general model comprises two conformations in which permeant binding sites are only accessible to either the outward, extracellular-facing or inward, intracellular-facing orientation at any given time. Permeant binding to the transporter induces a conformational change which reorients the transporter thereby allowing release of permeant on the opposite side of the membrane. Mechanistically, little is known about the actual molecular process of transport for ENT and CNT family members. In facilitative diffusion mediated by ENTs, transitions between outward- and inward-facing conformations occur at a faster rate in the presence than in the absence of permeant (30). Some ENT family members in parasitic protozoa are similar to CNTs and couple nucleoside transport to a cation electrochemical across the cell membrane. In ENTs, this cation is H^+ , whereas in CNTs it is Na^+ and/or H^+ .

An in depth analysis of hCNT1 Na⁺/nucleoside cotransport has been carried out using electrophysiological techniques and hCNT1 expression in *Xenopus* oocytes (268). An ordered simultaneous transport model in which Na⁺ binds first followed by uridine was proposed based on kinetic analysis of steady-state uridine-induced Na⁺ currents (268). In these experiments the apparent affinity for uridine increased in the absence of changes to maximal currents as the concentration of extracellular sodium was increased (268). Additionally, analysis of hCNT1 presteady-state currents revealed that 61% of the membrane field was sensed by Na⁺ and the valency of the movable charge, -0.81, was consistent with 1:1 Na⁺:nucleoside stoichiometry (268). Presteady-state analysis was also used to calculate the average number of transporters, 6.8×10^{10} , in the oocyte plasma membrane to yield a turnover rate of 9.6 uridine molecules per hCNT1 protein per sec at -50 mV (268). Similar to hCNT1, hCNT2 is also Na⁺-dependent and, aside from Na⁺-activation curves which generate Hill plots predicting a 1:1 Na⁺:nucleoside stoichiometry, nothing is known about its mechanism of transport (30, 243). In contrast to hCNT1/2, but similar to CNT3 subfamily member hfCNT, a 2:1 Na⁺:nucleoside stoichiometry has been established for hCNT3 (268, 295, 298). As well, hCNT3 has as an ability to couple nucleoside transport to H⁺ electrochemical gradients (268, 295); however, little else is known about the mechanism(s) of hCNT3 cation/nucleoside cotransport.

Research Objectives

In contrast to ENTs, much less is known about CNTs with respect to the structure of the transporters and the function of specific residues within these structures. As mediators of concentrative nucleoside transport, the identification and characterization of regions and residues within the translocation pore, as well as those contributing to and participating in the nucleoside permeant and coupling cation binding sites, will be beneficial to the structural characterization and mechanistic understanding of CNTs. The objectives of this research, initiated at a time when only limited molecular information was available, was to undertake structure-function

investigations of representative eukaryotic and prokaryotic CNTs, with particular in depth focus on the human transporter hCNT3.

Xenopus oocytes lack endogenous nucleoside transport systems and have been used extensively in the kinetic characterization of nucleoside transport proteins. By recombinant expression in *Xenopus* oocytes, the mutagenesis and other molecular studies presented here characterized nucleoside transport using both radioisotope flux assays and electrophysiological techniques (Chapter 2). Upon expression in *Xenopus* oocytes, investigation of two allelic isoforms of *C. albicans* CaCNT identified a single amino acid substitution in TM 7 that altered the apparent affinity for uridine transport by this H⁺-coupled nucleoside transporter by ~ 10-fold (427, Chapter 3). Permeant binding and translocation were also influenced by mutation of two residues in TM 8 of hCNT1, one of which also influenced cation interactions and both of which are predicted to reside in a common cation/nucleoside translocation pore (428, Chapter 4). In contrast to H⁺-coupled CaCNT and Na⁺-coupled hCNT1, hCNT3 is capable of both H⁺- and Na⁺-mediated nucleoside transport, and is shown in Chapter 5 (429) to have novel cation-coupled nucleoside transport characteristics. Following the characterization of cation coupling in hCNT3 which revealed 2:1 Na⁺:uridine and 1:1 H⁺:uridine coupling ratios, a direct comparative analysis between all three hCNTs confirmed that, as members of a separate CNT subfamily, hCNT1 and hCNT2 exhibited a different Na⁺:nucleoside stoichiometry of 1:1 (430, Chapter 6). These experiments provided a fundamental understanding of cation coupling in CNT family members, and set the stage for structure-function studies to reveal additional insights into CNT mechanisms of transport.

Elucidation of transport mechanism(s) was pursued by site-directed mutagenesis of single residues in hCNT3 produced in *Xenopus* oocytes. The rationale for using hCNT3 as a template for these studies was based upon its phylogenetic background and unique transport properties. hCNT3 (and mCNT3) are more closely related to hagfish hfCNT than to the mammalian CNT1 and CNT2 proteins, despite approximately 550 million years of vertebrate evolution (295), suggesting that the physiological functions of *cib*-type nucleoside transporters have particular

importance. This is substantiated by the low frequency of hCNT3 SNPs. Mammalian CNT3 differs from CNT1/2 both with respect to nucleoside selectivity and cation coupling. While pyrimidine nucleoside-selective hCNT1 and purine nucleoside-selective hCNT2 couple exclusively with Na^+ , hCNT3 mediates the transport of both purine and pyrimidine nucleosides and nucleoside analogs, coupling transport to both Na^+ and H^+ electrochemical gradients (268, 295). Additionally, hCNT3 exhibits 2:1 Na^+ :nucleoside, but 1:1 H^+ :nucleoside stoichiometry whereas, in contrast, hCNT1 and hCNT2 share a common 1:1 Na^+ :nucleoside coupling ratio (295).

Despite having numerous endogenous cysteine residues common to all hCNTs, hCNT3 is the only transporter reactive to the hydrophilic thiol-reactive reagent PCMBS (431, Chapter 7). Studies to identify the residue responsible for this PCMBS reactivity revealed that a H^+ -mediated conformational shift was responsible for the unmasking of a pore-lining PCMBS-reactive cysteine residue in TM 12 (431, Chapter 7). The functional importance of this TM 12 residue in cation coupling was independently confirmed in a study characterizing a cysteine-less version of hCNT3 (hCNT3C-) as a prerequisite for continued hCNT3 SCAM analysis (Chapter 8). Additional insights on cation coupling in hCNT3 were revealed through exploitation of the unique multifunctional phenotype of hCNT3; key residues in TMs 7 and 11A involved in both Na^+ and H^+ interactions, as well as nucleoside binding and translocation were identified in Chapter 9 by site-directed mutagenesis of hCNT3 negatively charged residues. To verify the membrane-associated nature of TM 11A and further extend the study of Chapter 7 (431), SCAM analyses revealed important pore-lining residues in TMs 11, 11A and 13 and hence, provided key support for a new revised 15 TM model of CNT topology (Chapter 10). Additional studies presented here include the identification and analysis of three hCNT3 SNPs (300, Appendix 1) and the characterization of a bacterial H^+ -coupled CNT family member from *Escherichia coli*, NupC (309, Appendix 2) and a uridine permease, Fui1p, from *Saccharomyces cerevisiae* which is a member of the uracil/allantoin permease family (363, Appendix 3). The parallel study to that of Chapter 9 which investigated the role of negatively charged residues in hCNT1 is presented in Appendix 4 (420). Together, these studies contribute valuable insights into the molecular mechanisms of cation

coupling in concentrative nucleoside and nucleoside drug transport proteins (Chapter 11).

Table 1-1. Identified members of the equilibrative nucleoside transporter (ENT) family.

Species	Protein	GenBank™ Accession	Amino Acids	Permeant Selectivity	Transport Mode	Reference
<i>Homo sapiens</i>	hENT1	AAC51103	456	nucleosides	facilitative	102, 118
	hENT2	AAC39526	456	nucleosides; nucleobases	facilitative	103, 118, 165
	hENT3	AAK00958	475	nucleosides; adenine	H ⁺ - dependent	78, 172
	hENT4	DAA00308	530	adenosine; monoamines; MPP ⁺	H ⁺ - dependent; electrogenic	79, 104, 174
<i>Rattus norvegicus</i>	rENT1	AAB88049	457	nucleosides	facilitative	105
	rENT2	AAB88050	456	nucleosides, nucleobases	facilitative	105, 165
	rENT4	EDL89703	522	nd	nd	
<i>Mus musculus</i>	mENT1	AAF78452	458	nucleosides	facilitative	106
	mENT1.1	AAF76429	460	nucleosides	facilitative	110, 111
	mENT1.2	AAF64036	458	nucleosides	facilitative	111
	mENT2	AAF76431	456	nucleosides; nucleobases	facilitative	106, 111
	mENT3	AAK00957	475	nd	nd	78, 172
	mENT4	AAH25599	528	adenosine; adenine; monoamines	H ⁺ - dependent	79, 104
<i>Oryctolagus cuniculus</i>	rbENT2	AAK11605	456	nucleosides	facilitative	163
	rbENT2A	AAK11606	415	nucleosides	facilitative	163
<i>Toxoplasma gondii</i>	TgAT1	AAF03247	462	adenosine; inosine	nd	193, 194
	TgAT2			nucleosides	nd	194
<i>Plasmodium falciparum</i>	PfENT1	AAG09713	422	nucleosides; nucleobases	facilitative	196
	PfNT1	AAF67613	422	nucleosides	nd	195
	PfENT2			nd	nd	199
	PfENT3			nd	nd	199
	PfENT4			nd	nd	199
<i>Leishmania donovani</i>	LdNT1.1	AAC32597	491	adenosine; uridine	H ⁺ - dependent	84, 201
	LdNT1.2	AAC32315	491	adenosine; uridine	H ⁺ - dependent	84, 201
	LdNT2	AAF74264	499	inosine; guanosine	H ⁺ - dependent	84, 202

Table 1-1 (continued).

Species	Protein	GenBank™ Accession	Amino Acids	Permeant Selectivity	Transport Mode	Reference
<i>Trypanosoma brucei</i>	TbAT1	AAD45278	463	adenosine; adenine; mel- aminophenyl arsenicals	nd	207
	TbNT2	AAF04490	464	purine nucleosides	H ⁺ - dependent	85
	TbNT2/ 927			purine nucleosides	H ⁺ - dependent	87
	TbNT3			nd	nd	87
	TbNT4			nd	nd	87
	TbNT5			purine nucleosides; hypoxanthine	H ⁺ - dependent	87
	TbNT6			purine nucleosides; hypoxanthine	H ⁺ - dependent	87
	TbNT7			purine nucleosides; hypoxanthine	H ⁺ - dependent	87
	TbNT8.1			purine nucleobases	nd	87, 208
	TbNBT1			guanosine, inosine; nucleobases; allopurinol	nd	209
	TbNT9			purine nucleosides; hypoxanthine	nd	48, 87
	TbNT10			purine nucleosides	nd	210, 211
	TbNT11.1 TbNT11.2			nd nd	nd nd	48 48
	<i>Crithidia fasciculata</i>	CfNT1	AAF22610	497	nucleosides; hypoxanthine	nd
CfNT2		AAG22611	502	inosine; guanosine	nd	214, 215
<i>Trypanosoma equiperdum</i>	TeAT1	CAC41330	463	adenosine	nd	432
	(TeAT2)			adenosine; inosine	nd	432
<i>Caenorhabditis elegans</i>	CeENT1	AAM46663	445	nucleosides	facilitative	35, 108, 216
	CeENT2	CAB01882	450	nucleosides	facilitative	108, 216
	CeENT3	CAB01223	729	nd	nd	108
	CeENT4	CAB62793	451	nd	nd	108
	CeENT5	AAA98003	434	nd	nd	108
	CeENT6	CAB03075	441	nd	nd	108

Table 1-1 (continued).

Species	Protein	GenBank™ Accession	Amino Acids	Permeant Selectivity	Transport Mode	Reference
<i>Drosophila melanogaster</i>	DmENT1	AAF51506	467	nd	nd	78, 108
	DmENT2	AAF52405	458	uridine	nd	78, 108, 217
	DmENT3	AAF49871	668	nd	nd	108
<i>Arabidopsis thaliana</i>	AtENT1	AAC18807	428	nucleosides	H ⁺ - dependent (?)	88, 222, 223
	AtENT2	AAF04424	417	nd	nd	220, 221
	AtENT3	CAB81054	418	nucleosides	H ⁺ - dependent	89, 220, 221, 223
	AtENT4	CAB81055	418	adenosine, guanosine, cytidine, uridine	facilitative	221
	AtENT5	CAB81056	419	nd	nd	220, 221
	AtENT6	CAB81053	394	nucleosides	facilitative	221, 223
	AtENT7	AAD25545	382	nucleosides	facilitative	221, 223
	AtENT8	AAG10625	408	nd	nd	221, 223
<i>Oryza sativa</i>	OsENT1	AK059439	423	nd	nd	224
	OsENT2	BAD98465	418	nucleosides; nucleoside cytokinins	H ⁺ - dependent	224
	OsENT3	AK101098	418	nd	nd	224
	OsENT4	AK065096	276	nd	nd	224
<i>Saccharomyces cerevisiae</i>	FUN26	AAC04935	517	nucleosides	facilitative	225

nd, not determined.

Table 1-2. Apparent K_m values for human ENT and CNT family members.

Transporter	Nucleoside/ Nucleobase	Apparent K_m value (μM)					
		<i>Xenopus</i> oocytes	Reference	<i>S.</i> <i>cerevisiae</i>	Reference	Cultured cells	Reference
hENT1	uridine	240	102	44.1	397	260	118
	cytidine	600	83	234	397	580	118
	thymidine					300	118
	adenosine	50	83	17.8	397	40	118
	inosine			28.5	397	170	118
	guanosine			47.5	397	140	118
hENT2	uridine	200	103	195	397	250	118
						330	167
	cytidine					5610	118
						3900	167
	thymidine					710	118
	adenosine			106	397	140	118
	inosine			180	397	50	118
	guanosine hypoxanthine	700	165			2700	118
hENT3AA	uridine	1860	172				
	adenosine	2020	172				
hENT4	adenosine	780	104				
hCNT1	uridine	45	262	9.2	424	34	272
		22	268			59	274
	cytidine					140	274
hCNT2	uridine	80	282			46	289
		40	283			116	287
	adenosine	8	283	11.2	59		
	inosine	4.5	282			13.7	287
hCNT3	uridine	21.6	295	8.7	424	1.1	296
	cytidine	15.4	295			3.4	296
	thymidine	21.2	295			3.7	296
	adenosine	15.1	295			4.6	296
	inosine	52.5	295			4.3	296
	guanosine	43.0	295			5.1	296

Table 1-3. Identified members of the concentrative nucleoside transporter (CNT) family.

Species	Protein	GenBank™ Accession	Amino Acids	Permeant Selectivity	Transport Mode	Reference
<i>Homo sapiens</i>	hCNT1	AAB53839	649	pyrimidine nucleosides; adenosine	Na ⁺ -dependent	262
	hCNT2	AAC51930	658	purine nucleosides; uridine	Na ⁺ -dependent	282, 283
	hCNT3	AAG22551	691	nucleosides	Na ⁺ /H ⁺ -dependent	268, 295
<i>Rattus norvegicus</i>	rCNT1	AAB03626	648	pyrimidine nucleosides; adenosine	Na ⁺ -dependent	261
	rCNT2	AAA80640	659	purine nucleosides; uridine	Na ⁺ -dependent	269, 281
<i>Mus musculus</i>	mCNT1	AAH61230	648	nd	nd	284
	mCNT2	AAC28858	660	purine nucleosides; uridine	Na ⁺ -dependent	
	mCNT3	AAG22552	703	nucleosides	Na ⁺ /H ⁺ -dependent	268, 295
<i>Oryctolagus cuniculus</i>	rbCNT2	AAF80451	658	purine nucleosides; uridine	Na ⁺ -dependent	285
<i>Sus scrofa</i>	pkCNT1	AAC17947	647	pyrimidine nucleosides	Na ⁺ -dependent	263
<i>Eptatretus stouti</i>	hfCNT	AAD52151	683	nucleosides	Na ⁺ -dependent	298
<i>Caenorhabditis elegans</i>	CeCNT3	AAF80462	575	nucleosides except cytidine	H ⁺ -dependent	306
<i>Candida albicans</i>	CaCNT	AAO75038	608	purine nucleosides; uridine	H ⁺ -dependent	307
<i>Escherichia coli</i>	NupC	CAA52821	400	adenosine; uridine	H ⁺ -dependent	308, 309, Appendix 2
	YeiJ	AAC75222	416	nd	nd	
	YeiM	AAC75225	416	nd	nd	

nd, not determined.

Table 1-4. Identified members of the organic cation transporter (OCT) family.

Species	Protein	GenBank™ Accession	Amino Acids	Permeant Selectivity	Transport Mode	Reference
<i>Homo sapiens</i>	hOCT1	AAB67703	554	organic cations; MPP ⁺ ; TEA; ACV; GCV	electrogenic; H ⁺ -dependent	320, 321
	hOCT2	CAA66978	555	TEA; MPP ⁺	electrogenic	320
	hOCT2A	BAC02720	483	TEA	electrogenic	433
	hOCT3	BAA76350	551	MPP ⁺	nd	434
	hOCT4	BAA76351	594	nd	nd	434
	hOCTN1	BAA23356	551	TEA	electroneutral exchange	435
	hOCTN2	AAC24828	557	TEA; carnitine	Na ⁺ - and H ⁺ -dependent; electrogenic	436-438
<i>Rattus norvegicus</i>	rOCT1	CAA55411	556	TEA; dTub; nucleoside analogs	electrogenic	310, 318
	rOCT1A	AAB67702	430	TEA	nd	322
	rOCT2	BAA11754	593	TEA	nd	439
	rOCT3	AAC40150	551	TEA; guanidine	electrogenic	440
	rOCTN1	AAD46922	553	TEA	H ⁺ -dependent	441
	rOCTN2	AAD54059	557	TEA; carnitine; organic cations	Na ⁺ -dependent; electrogenic facilitative	442
<i>Mus musculus</i>	mOCT1	AAB19097	556	nd	nd	319
	mOCT2	CAA06827	553	nd	nd	443
	mOCT3	AAD20978	551	nd	nd	444
	mOCTN1	BAA36626	553	TEA; carnitine	Na ⁺ - and H ⁺ -dependent	445
	mOCTN2	AAD54060	557	TEA; carnitine	Na ⁺ - and H ⁺ -dependent	442, 445
	mOCTN3	BAA78343	564	carnitine	nd	445
<i>Oryctolagus cuniculus</i>	rbOCT1	AAC23661	554	MPP ⁺ ; TEA	nd	446, 447
	rbOCT2	AAM83256	554	TEA	nd	447
	rbOCT3	AAU05742	404	nd	nd	313
<i>Sus scrofa</i>	pOCT2	CAA70567	547	TEA	nd	448
<i>Caenorhabditis elegans</i>	CeOCT1	AAF21932	568	TEA	nd	449

Table 1-4 (continued).

Species	Protein	GenBank™ Accession	Amino Acids	Permeant Selectivity	Transport Mode	Reference
<i>Drosophila melanogaster</i>	Orct	CAA73031	548	nd	nd	450
<i>Phaseolus vulgaris</i>	PvOCT1	AAO83155	547	nd	nd	451

nd, not determined; MPP⁺, 1-methyl-4-phenylpyridinium; TEA, tetraethylammonium; ACV, acyclovir; GCV, ganciclovir; dTub, deoxytubercidin.

Table 1-5. Identified members of the organic anion transporter (OAT) family.

Species	Protein	GenBank™ Accession	Amino Acids	Permeant Selectivity	Transport Mode	Reference
<i>Homo sapiens</i>	hOAT1	AAD19356	550	ACV; GCV; AZT; PAH	exchanger	312, 334, 452
	hOAT1-1	BAA75072	563	PAH	nd	328
	hOAT2	AAD37091	548	AZT; estrone sulfate; 5-fluorouracil; organic anions	exchanger	312, 341
	hOAT3*	AAD19357	568	nd	nd	334
	hOAT3	BAB47393	543	PAH; esterone sulfate; methotrexate; cimetidine; AZT; urate	exchanger	312, 335, 453
	hOAT4	BAA95316	550	esterone sulfate; AZT; glutarate	exchanger	312, 336, 454
	hOAT5	DAA01503	531	nd	nd	455
	hOAT7	BAF51552	553	esterone sulfate; DHEA sulfate	exchanger	452
	URAT1	BAB96750	553	urate	exchanger	456
	<i>Rattus norvegicus</i>	rOAT1	AAC18772	551	PAH; ACV; AZT; nucleoside analogs; cAMP; cGMP; PGE ₂ ; glutarate; α-keto-glutarate; urate; folate; antibiotics; salicylate; methotrexate	exchanger

Table 1-5 (continued).

Species	Protein	GenBank™ Accession	Amino Acids	Permeant Selectivity	Transport Mode	Reference
<i>Rattus norvegicus</i>	rOAT2/ NLT	AAA57157	535	α-keto- glutarate; glutarate; salicylate; acetyl- salicylate; PGE ₂ ; metho- trexate; PAH	nd	331, 332
	rOAT3	BAA82552	536	PAH; estrone sulphate; ochratoxin A; cimetifine	exchanger	333, 339, 457
	rOAT5	XP_ 001072873	551	ochratoxin A, estrone sulfate; DHEA sulfate	exchanger	458
	rOAT8			esterone sulfate; DHEA sulfate	nd	452
<i>Mus musculus</i>	mOAT1/ NKT	AAC53112	545	PAH	exchanger	324, 329
	mOAT2	AAH13474	540			
	mOAT3	AAC61265	537	PAH; esterone sulfate; 5- fluorouracil; organic compounds	nd	342
	URAT1	NP_033229	553	urate	nd	459
	mOAT5	NP_659034	551	ochratoxin A	nd	337
	mOAT6	Q80UJ1	556	nd	nd	338
	mOAT9			nicotinic acid; salicylic acid; PGE ₂	nd	452
	mOAT-PG		PGE ₂ ; PGF ₂	nd	452	
<i>Oryctolagus cuniculus</i>	rbOAT1	CAB62587	551	nd	nd	
	rbOAT2	AAZ79452	542	nd	nd	
	rbOAT3	CAD34035	542	nd	nd	

Table 1-5 (continued).

Species	Protein	GenBank™ Accession	Amino Acids	Permeant Selectivity	Transport Mode	Reference
<i>Sus scrofa</i>	pOAT1	CAC87128	547	PAH	nd	460
	pOAT3	CAE53047	543	esterone sulfate	nd	461
<i>Pseudopleur- onectes americanus</i>	fROAT	CAB09724	562	PAH	exchanger	327
<i>Caenorhabditis elegans</i>	CeOAT1	AAF73198	526	PAH	exchanger	462

nd, not determined; ACV, acyclovir; GCV, ganciclovir; AZT, zidovudine; PAH, *p*-aminohippurate, DHEA, dehydroepiandrosterone; cAMP, cyclic adenosine monophosphate; cGMP, cyclic guanosine monophosphate; PGE₂, prostaglandin E₂; PGF₂, OAT-PG, organic anion transporter-prostaglandin-specific; prostaglandin F₂.

Table 1-6. Identified members of the nucleoside: H⁺ symporter (NHS) family.

Species	Protein	GenBank™ Accession	Amino Acids	Permeant Selectivity	Transport Mode	Reference
<i>Escherichia coli</i>	NupG	ABV07361	418	nucleosides	H ⁺ - dependent	308, 346
	XapB	AAC75459	418	nucleosides except guanosine; xanthine	H ⁺ - dependent	346

Table 1-7. Identified members of the Tsx channel-forming protein family.

Species	Protein	GenBank™ Accession	Amino Acids	Permeant Selectivity	Transport Mode	Reference
<i>Escherichia coli</i>	Ec Tsx	AAA24701	294	nucleosides; nucleoside analogs; serine; albicidin	channel	350, 354, 355
<i>Enterobacter aerogenes</i>	Ea Tsx	CAA81396	294	deoxyadenosine; albicidin	channel	351
<i>Klebsiella pneumoniae</i>	Kb Tsx	CAA81397	294	deoxyadenosine; albicidin	channel	351
<i>Salmonella typhimurium</i>	St Tsx	CAD08869	287	deoxyadenosine; albicidin	channel	351
<i>Salmonella enterica</i>	Se Tsx	CAD08869	287	adenosine; thymidine	channel	353, 463
<i>Vibrio parahaemolyticus</i>	OmpK	BAA09613	263	vibriophage KVP40	receptor	357, 358
	OmpK	AA Y44077	272	nd	nd	464
	OmpW	ABD83811	214	nd	nd	464
	OmpV	AA Y44076	258	nd	nd	464
	OmpU	AA Y23008	335	nd	nd	464
<i>Vibrio cholerae</i>	OmpK	AAF95449	296	nd	nd	
	OmpW	ABQ19175	217	nd	nd	359
	OmpU	AAB48973	341	nd	porin	465
	OmpT	AAC28105	344	nd	porin	466
	OmpV	ABQ19849	257	nd	nd	467
<i>Vibrio fischeri</i>	OmpU	AAL12480	321	nd	nd	468

nd, not determined.

Table 1-8. Identified members of the uracil/allantoin permease family.

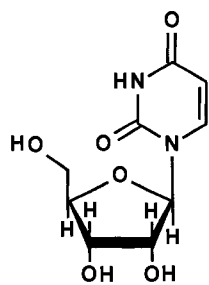
Species	Protein	GenBank™ Accession	Amino Acids	Permeant Selectivity	Transport Mode	Reference
<i>Saccharomyces cerevisiae</i>	FUR4	CAA53678	633	uracil	nd	360
	FUI1	CAA84862	639	uridine	H ⁺ - dependent	225, 361, 362
	DAL4	CAA78826	635	allantoin	nd	469
	THI10	BAA09504	598	thiamin	nd	470
	THI72	CAA99401	599	nd	nd	
	THI71	CAA99264	598	nd	nd	
	FCY2	AAB64592	533	adenine; guanine; cytosine; hypoxanthine	H ⁺ - dependent	471
<i>Schizosaccharomyces pombe</i>	SpFUR4	CAA67256	589	uracil	nd	472
<i>Escherichia coli</i>	codB	AAC73439	419	cytosine	nd	473
<i>Arabidopsis thaliana</i>	AtUPS1	NP_565303	390	allantoin; uracil; 5- fluorouracil	H ⁺ - dependent	474, 475
	AtUPS2	NP_178451	398	uracil; 5- fluorouracil	nd	475
<i>Phaseolus vulgaris</i>	PvUPS1	AAS19930	407	allantoin; xanthine; uric acid	nd	476

nd, not determined.

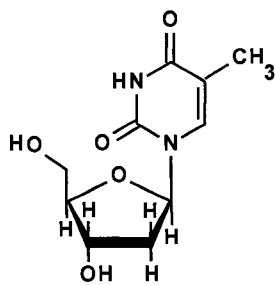
Table 1-9. Identified members of the nucleoside permease (NUP) family.

Species	Protein	GenBank™ Accession	Amino Acids	Permeant Selectivity	Transport Mode	Reference
<i>Candida albicans</i>	NUP	AF016246	407	adenosine; guanosine	nd	364
<i>Giardia intestinalis</i>	TPT1	AAA29158	377	nd	nd	80

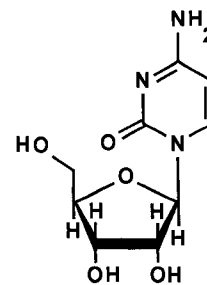
nd, not determined.



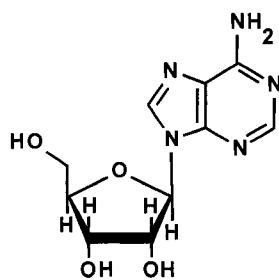
Uridine



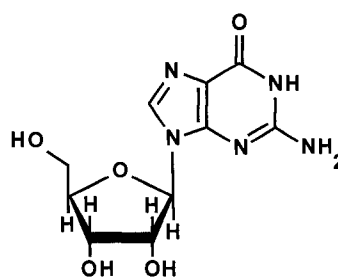
Thymidine



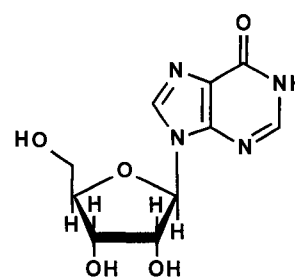
Cytidine



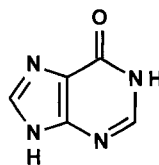
Adenosine



Guanosine

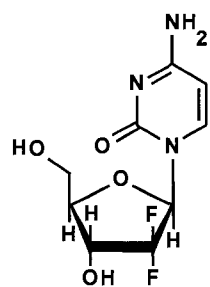


Inosine

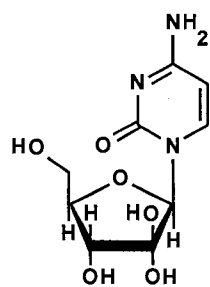


Hypoxanthine

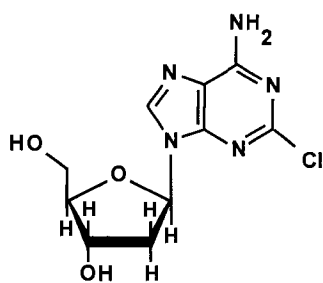
Figure 1-1. Chemical structures of physiological pyrimidine and purine nucleosides and the purine nucleobase hypoxanthine.



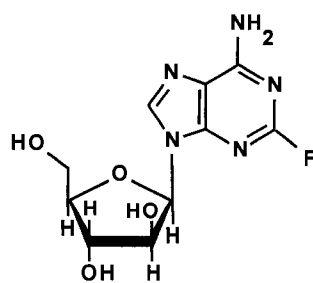
Gemcitabine (dFdC)



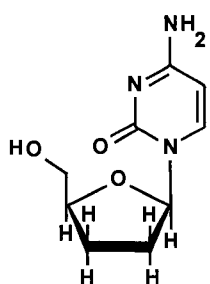
Cytarabine (araC)



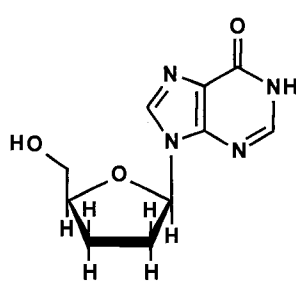
Cladribine (2-CdA)



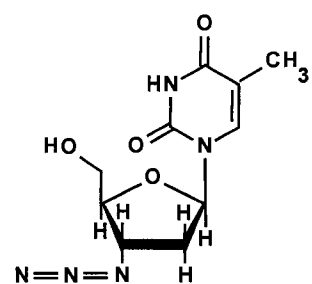
Fludarabine (F-araA)



Zalcitabine (ddC)

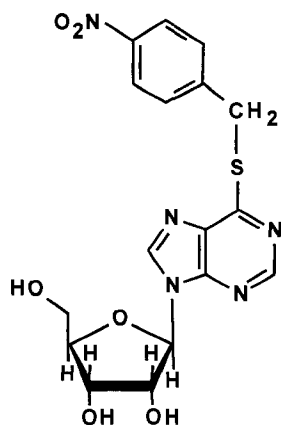


Didanosine (ddI)

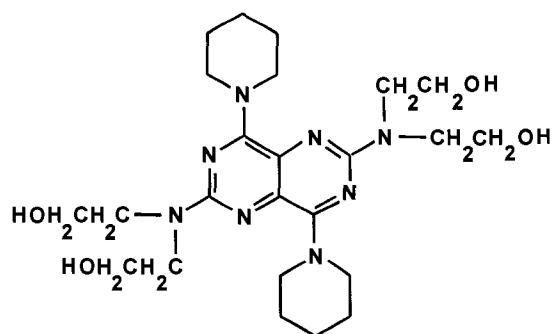


Zidovudine (AZT)

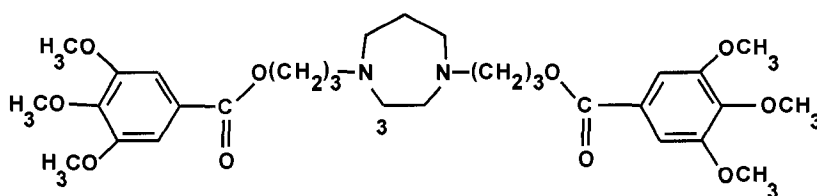
Figure 1-2. Chemical structures of chemotherapeutic pyrimidine and purine nucleoside analogs.



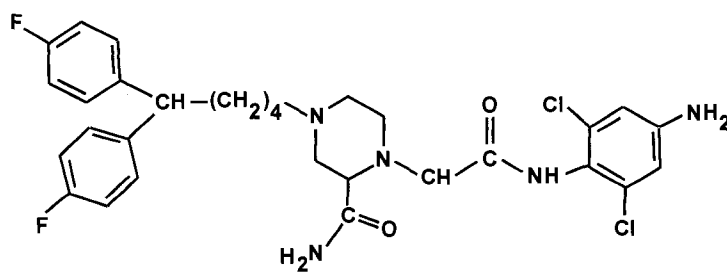
Nitrobenzylthioinosine



Dipyridamole



Dilazep



Draflazine

Figure 1-3. Chemical structures of ENT inhibitors.

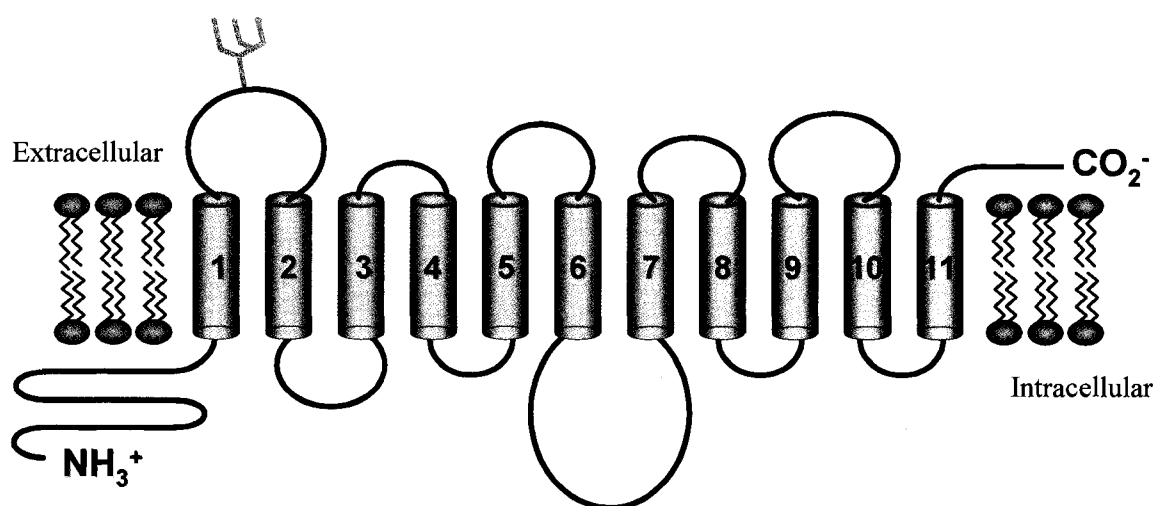


Figure 1-4. Putative ENT topology model. Potential transmembrane helices are numbered and the site of *N*-glycosylation in hENT1 (127) is indicated by ψ symbol.

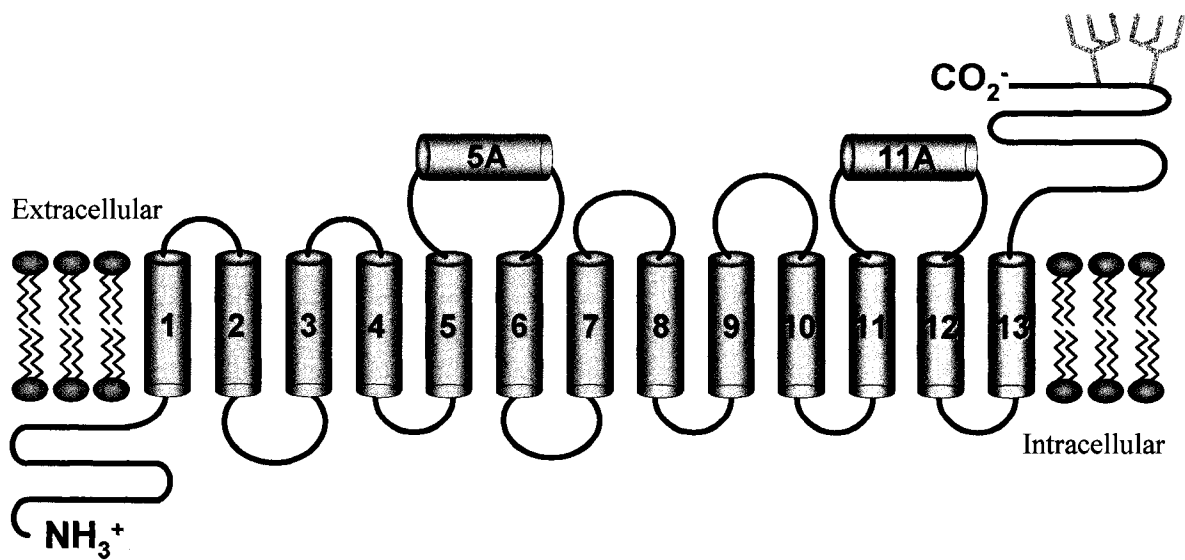


Figure 1-5. Putative CNT topology model. Potential transmembrane helices are numbered and the site of *N*-glycosylation in rCNT2 (293) is indicated by ψ symbol.

Bibliography

1. Young, J. D., and Jarvis, S. M. (1983) Nucleoside transport in animal cells. *Biosci. Rep.* **3**: 309-322.
2. Young, J. D., Paterson, A. R., and Henderson, J. F. (1985) Nucleoside transport and metabolism in erythrocytes from the Yucatan miniature pig. Evidence that inosine functions as an in vivo energy substrate. *Biochim. Biophys. Acta.* **842**: 214-224.
3. Mathew, A., Grdisa, M., and Johnstone, R. M. (1993) Nucleosides and glutamine are primary energy substrates for embryonic and adult chicken red cells. *Biochem. Cell Biol.* **71**: 288-295.
4. Mathew, A., Grdisa, M., Robbins, P. J., White, M. K., and Johnstone, R. M. (1994) Loss of glucose transporters is an early event in differentiation of HD3 cells. *Am. J. Physiol.* **266**: C1222-C1230.
5. Mubagwa, K., Mullane, K., and Flameng, W. (1996) Role of adenosine in the heart and circulation. *Cardiovasc. Res.* **32**: 797-813.
6. Mubagwa, K., and Flameng, W. (2001) Adenosine, adenosine receptors and myocardial protection: an updated overview. *Cardiovasc. Res.* **52**: 25-39.
7. West, G. A., and Belardinelli, L. (1985) Sinus slowing and pacemaker shift caused by adenosine in rabbit SA node. *Pflugers Arch.* **403**: 66-74.
8. Belardinelli, L., Linden, J., and Berne, R. M. (1989) The cardiac effects of adenosine. *Prog. Cardiovasc. Dis.* **32**: 73-97.
9. Zaza, A., Rocchetti, M., and DiFrancesco, D. (1996) Modulation of the hyperpolarization-activated current (I_f) by adenosine in rabbit sinoatrial myocytes. *Circulation* **94**: 734-741.
10. Shryock, J. C., and Belardinelli, L. (1997) Adenosine and adenosine receptors in the cardiovascular system: biochemistry, physiology, and pharmacology. *Am. J. Cardiol.* **79**: 2-10.

11. de Jong, J. W., de Jonge, R., Keijzer, E., and Bradamante, S. (2000) The role of adenosine in preconditioning. *Pharmacol. Ther.* **87**: 141-149.
12. Baxter, G. (2002) Role of adenosine in delayed preconditioning of myocardium. *Cardiovasc. Res.* **55**: 483-494.
13. Riksen, N. P., Smits, P., and Rongen, G. A. (2004) Ischaemic preconditioning: from molecular characterization to clinical application - part I. *Neth. J. Med.* **62**: 353-363.
14. Loffler, M., Morote-Garcia, J. C., Eltzschig, S. A., Coe, I. R., and Eltzschig, H. K. (2007) Physiological roles of vascular nucleoside transporters. *Arterioscler. Thromb. Vasc. Biol.* **27**: 1004-1013.
15. Cronstein, B. N. (1994) Adenosine, an endogenous anti-inflammatory agent. *J. Appl. Physiol.* **76**: 5-13.
16. Linden, J. (2001) Molecular approach to adenosine receptors: receptor-mediated mechanisms of tissue protection. *Annu. Rev. Pharmacol. Toxicol.* **41**: 775-787.
17. Fain, J. N., and Shepherd, R. E. (1979) Hormonal regulation of lipolysis: role of cyclic nucleotides, adenosine, and free fatty acids. *Adv. Exp. Med. Biol.* **111**: 43-77.
18. Koszalka, P., Ozúyaman, B., Huo, Y., Zerneck, A., Flögel, U., Braun, N., Buchheiser, A., Decking, U. K., Smith, M. L., Sévigny, J., Gear, A., Weber, A. A., Molojavyi, A., Ding, Z., Weber, C., Ley, K., Zimmermann, H., Gödecke, A., and Schrader, J. (2004) Targeted disruption of cd73/ecto-5'-nucleotidase alters thromboregulation and augments vascular inflammatory response. *Circ. Res.* **95**: 814-821.
19. Jennings, L. K., White, M. N., and Mandrell, T. D. (1995) Interspecies comparison of platelet aggregation, LIBS expression and clot retraction: observed differences in GPIIb-IIIa functional activity. *Thromb. Haemost.* **74**: 1551-1556.
20. Birk, A. V., Broekman, M. J., Gladek, E. M., Robertson, H. D., Drosopoulos, J. H., Marcus, A. J., and Szeto, H. H. (2002) Role of extracellular ATP metabolism in regulation of platelet reactivity. *J. Lab. Clin. Med.* **140**: 166-175.

21. Spielman, W. S., and Arend, L. J. (1991) Adenosine receptors and signaling in the kidney. *Hypertension* **17**: 117-130.
22. Navar, L. G., Inscho, E. W., Majid, D. S. A., Imig, J. D., Harrison-Bernard, L. M., and Mitchell, K. D. (1996) Paracrine regulation of the renal microcirculation. *Physiol. Rev.* **76**: 425-536.
23. Poon, A., and Sawynok, J. (1998) Antinociception by adenosine analogs and inhibitors of adenosine metabolism in an inflammatory thermal hyperalgesia model in the rat. *Pain* **74**: 235-245.
24. Sawynok, J. (1998) Adenosine receptor activation and nociception. *Eur. J. Pharmacol.* **347**: 1-11.
25. Fox, I. H., and Kelley, W. N. (1978) The role of adenosine and 2'-deoxyadenosine in mammalian cells. *Annu. Rev. Biochem.* **47**: 655-686.
26. Dunwiddie, T. V., and Masino, S. A. (2001) The role and regulation of adenosine in the central nervous system. *Annu. Rev. Neurosci.* **24**: 31-55.
27. Latini, S., and Pedata, F. (2001) Adenosine in the central nervous system: release mechanisms and extracellular concentrations. *J. Neurochem.* **79**: 463-484.
28. King, A. E., Ackley, M. A., Cass, C. E., Young, J. D., and Baldwin, S. A. (2006) Nucleoside transporters: from scavengers to novel therapeutic targets. *Trends Pharmacol. Sci.* **27**: 416-425.
29. Cass, C. E. (1995) Nucleoside transport, in *Drug Transport in Antimicrobial and Anticancer Chemotherapy* (Georgopapadakou, N. H., Ed.), pp 403-451, Marcel Dekker, New York.
30. Griffith, D. A., and Jarvis, S. M. (1996) Nucleoside and nucleobase transport systems of mammalian cells. *Biochim. Biophys. Acta* **1286**: 153-181.
31. Cass, C. E., Young, J. D., and Baldwin, S. A. (1998) Recent advances in the molecular biology of nucleoside transporters of mammalian cells. *Biochem. Cell Biol.* **76**: 761-770.

32. Baldwin, S. A., Mackey, J. R., Cass, C. E., and Young, J. D. (1999) Nucleoside transporters: molecular biology and implications for therapeutic development. *Mol. Med. Today* **5**: 216-224.
33. Cass, C. E., Young, J. D., Baldwin, S. A., Cabrita, M. A., Graham, K. A., Griffiths, M., Jennings, L. L., Mackey, J. R., Ng, A. M., Ritzel, M. W., Vickers, M. F., and Yao, S. Y. (1999) Nucleoside transporters of mammalian cells. *Pharm. Biotechnol.* **12**: 313-352.
34. Cheeseman, C. I., Mackey, J. R., Cass, C. E., Baldwin, S. A., and Young, J. D. (2000) Molecular mechanisms of nucleoside and nucleoside drug transport, in *A Volume of Current Topics in Membranes*, pp 330-379, Academic Press, San Diego.
35. Young, J. D., Cheeseman, C., Mackey, J. R., Cass, C. E., and Baldwin, S. A. (2000) In *Current Topics in Membranes*, 50 (Barrett, K. E., and Donowitz, M., eds.) pp 329-378, Academic Press, San Diego.
36. Moyer, J. D., Oliver, J. T., and Handschumacher, R. E. (1981) Salvage of circulating pyrimidine nucleosides in the rat. *Cancer Res.* **41**: 3010-3017.
37. Holstege, A., Manglitz, D., and Gerok, W. (1984) Depletion of blood plasma cytidine due to increased hepatocellular salvage in D-galactosamine-treated rats. *Eur. J. Biochem.* **141**: 339-344.
38. Karle, J. M., Anderson, L. W., and Cysyk, R. L. (1984) Effect of plasma concentrations of uridine on pyrimidine biosynthesis in cultured L1210 cells. *J. Biol. Chem.* **259**: 67-72.
39. Lajtha, L. G., and Vane, J. R. (1958) Dependence of bone marrow cells on the liver for purine supply. *Nature* **182**: 191-192.
40. Fontenelle, L. J., and Henderson, J. F. (1969) An enzymatic basis for the inability of erythrocytes to synthesize purine ribonucleotides *de novo*. *Biochim. Biophys. Acta.* **177**: 175-176.
41. Plagemann, P. G., Wohlheuter, R. M., and Kraupp, M. (1985) Adenine nucleotide metabolism and nucleoside transport in human erythrocytes under ATP depletion conditions. *Biochim. Biophys. Acta.* **817**: 51-60.

42. Mackinnon, A. M., and Deller, D. J. (1973) Purine nucleotide biosynthesis in gastrointestinal mucosa. *Biochem. Biophys. Acta.* **319**: 1-4.
43. Murray, A. W. (1971) The biological significance of purine salvage. *Annu. Rev. Biochem.* **40**: 811-826.
44. Marr, J. J., Berens, R. L., and Nelson, D. J. (1978) Purine metabolism in *Leishmania donovani* and *Leishmania braziliensis*. *Biochim. Biophys. Acta* **544**: 360-371.
45. Krug, E. C., Marr, J. J., and Berens, R. L. (1989) Purine metabolism in *Toxoplasma gondii*. *J. Biol. Chem.* **264**: 10601-10607.
46. Berens, R. L., Krug, E. C., and Marr, J. J. (1995) in *Biochemistry of Parasitic Organisms and Its Molecular Foundations* (Marr, J. J., and Muller, M., eds) pp. 89-117, Academic Press, London.
47. Landfear, S. M. (2001) Molecular genetics of nucleoside transporters in Leishmanian and African trypanosomes. *Biochemical Pharmacology* **63**: 149-155.
48. Landfear, S. M., Ullman, B., Carter, N. S., and Sanchez, M. A. (2004) Nucleoside and nucleobase transporters in parasitic protozoa. *Eukaryot. Cell* **3**: 245-254.
49. Bellofatto, V. (2007) Pyrimidine transport activities in trypanosomes. *Trends Parasitol.* **23**: 187-189.
50. Lerner, M. H., and Lowy, B. A. (1974) The formation of adenosine in rabbit liver and its possible role as a direct precursor of erythrocyte adenine nucleotides. *J. Biol. Chem.* **249**: 959-966.
51. Pritchard, J. B., O'Connor, N., Oliver, J. M., and Berlin, R. D. (1975) Uptake and supply of purine compounds by the liver. *Am. J. Physiol.* **229**: 967-972.
52. Monks, A., and Cysyk, R. L. (1982) Uridine regulation by the isolated rat liver: perfusion with an artificial oxygen carrier. *Am. J. Physiol.* **242**: R465-R470.

53. Thorn, J. A., and Jarvis, S. M. (1996) Adenosine transporters. *Gen. Pharmacol.* **27**: 613-620.
54. Baldwin, S. A., Beal, P. R., Yao, S. Y. M., King, A. E., Cass, C. E., and Young, J. D. (2004) The equilibrative nucleoside transporter family, SLC29. *Pflugers Arch.* **447**: 735-743.
55. Pisoni, R. L., and Thoene, J. G. (1989) Detection and characterization of a nucleoside transport system in human fibroblast lysosomes. *J. Biol. Chem.* **264**: 4850-4856.
56. Mackey, J. R., Baldwin, S. A., Young, J. D., and Cass, C. E. (1998) Nucleoside transport and its significance for anticancer drug resistance. *Drug Resist. Updat.* **1**: 310-324.
57. Pastor-Anglada, M., Felipe A., and Casado, F. J. (1998) Transport and mode of action of nucleoside derivatives used in chemical and antiviral therapies. *Trends Pharmacol. Sci.* **19**: 424-430.
58. Damaraju, V. L., Damaraju, S., Young, J. D., Baldwin, S. A., Mackey, J., Sawyer, M. B., and Cass, C. E. (2003) Nucleoside anticancer drugs: the role of nucleoside transporters in resistance to cancer chemotherapy. *Oncogene* **22**: 7524-7536.
59. Zhang, J., Visser, F., King, K. M., Baldwin, S. A., Young, J. D., and Cass, C. E. (2007) The role of nucleoside transporters in cancer chemotherapy with nucleoside drugs. *Cancer Metastasis Rev.* **26**: 85-110.
60. Grant, S. (1998) Ara-C: cellular and molecular pharmacology. *Adv. Cancer Res.* **72**: 197-233.
61. Plunkett, W., Huang, P., and Gandhi, V. (1995) Preclinical characteristics of gemcitabine. *Anticancer Drugs* **6**: 7-13.
62. McGinn, C. J., Miller, E. M., Lindstrom, M. J., Kunugi, K. A., Johnston, P. G., and Kinsella, T. J. (1994) The role of cell cycle redistribution in radiosensitization: implications regarding the mechanism of fluorodeoxyuridine radiosensitization. *Int. J. Radiat. Oncol. Biol. Phys.* **30**: 851-859.

63. McGinn, C. J., Shewach, D. S., and Lawrence, T. S. (1996) Radiosensitizing nucleosides. *J. Natl. Cancer Inst.* **88**: 1193-1203.
64. Rosenblum, L. L., Patton, G., Grigg, A. R., Frater, A. J., Cain, D., Erlwein, O., Hill, C. L., Clarke, J. R., and McClure, M. O. (2001) Differential susceptibility of retroviruses to nucleoside analogues. *Antivir. Chem. Chemother.* **12**: 91-97.
65. Giaquinto, C., Rampon, O., Penazzato, M., Fregonese, F., de Rossi, A., and D'Elia, R. (2007) Nucleoside and nucleotide reverse transcriptase inhibitors in children. *Clin. Drug Investig.* **27**: 509-531.
66. Sturmer, M., Staszewski, S., and Doerr, H. W. (2007) Quadruple nucleoside therapy with zidovudine, lamivudine, adacavir and tenofovir in the treatment of HIV. *Antivir. Ther.* **12**: 695-703.
67. Baldwin, S. A., McConkey, G. A., Cass, C. E., and Young, J. D. (2007) Nucleoside transport as a potential target for chemotherapy in malaria. *Curr. Pharm. Des.* **13**: 569-580.
68. el Kouni, M. H. (2007) Adenosine metabolism in *Toxoplasma gondii*: potential targets for chemotherapy. *Curr. Pharm. Des.* **13**: 581-597.
69. Heby, O., Persson, L., and Rentala, M. (2007) Targeting the polyamine biosynthetic enzymes: a promising approach to therapy of African sleeping sickness, Chaga' disease, and leishmaniasis. *Amino Acids* **33**: 359-366.
70. Lee, H. T., LaFaro, R. J., and Reed, G. E. (1995) Pretreatment of human myocardium with adenosine during open heart surgery. *J. Card. Surg.* **10**: 665-676.
71. Wasir, H., Bhan, A., Choudhary, S. K., Sharma, R., Chauhan, S., and Venugopal, P. (2001) Pretreatment of human myocardium with adenosine. *Eur. J. Cardiothorac. Surg.* **19**: 41-46.
72. Dennis, D. M., Raatikainen, P., Martens, J. R., and Belardinelli, L. (1996) Modulation of atrioventricular nodal function by metabolic and allosteric regulators of endogenous adenosine in guinea-pig heart. *Circulation* **94**: 2551-2559.

73. Deussen, A. (2000) Metabolic flux rates of adenosine in the heart. *Naunyn-Schmiedebergs Arch. Pharmacol.* **362**: 351-363.
74. Deussen, A., Stappert, M., Schäfer, S., and Kelm, M. (1999) Quantification of extracellular and intracellular adenosine production: understanding the transmembranous concentration gradient. *Circulation* **99**: 2041-2047.
75. Zhang, Y., Legare, D. J., Geiger, J. D., and Lautt, W. W. (1991) Dilazep potentiation of adenosine-mediated superior mesenteric arterial vasodilation. *J. Pharmacol. Exp. Ther.* **258**: 767-771.
76. Rongen, G. A., Smits, P., Ver Donck, K., Willemsen, J. J., De Abreu, R. A., Van Belle, H., and Thien, T. (1995) Hemodynamic and neurohumoral effects of various grades of selective adenosine transport inhibition in humans. Implications for its future role in cardioprotection. *J. Clin. Invest.* **95**: 658-668.
77. Meester, B. J., Shankley, N. P., Welsh, N. J., Meijler, F. L., and Black, J. W. (1998) Pharmacological analysis of the activity of the adenosine uptake inhibitor, dipyridamole, on the sinoatrial and atrioventricular nodes of the guinea-pig. *Br. J. Pharmacol.* **124**: 729-741.
78. Hyde, R. J., Cass, C. E., Young, J. D., and Baldwin, S. A. (2001) The ENT family of eukaryote nucleoside and nucleobase transporters: recent advances in the investigation of structure/function relationships and the identification of novel isoforms. *Mol. Membr. Biol.* **18**: 53-63.
79. Acimovic, Y., and Coe, I. R. (2002) Molecular evolution of the equilibrative nucleoside transporter family: identification of novel family members in prokaryotes and eukaryotes. *Mol. Biol. Evol.* **19**: 2199-2210.
80. Cabrita, M. A., Baldwin, S. A., Young, J. D., and Cass, C. E. (2002) Molecular biology and regulation of nucleoside and nucleobase transporter proteins in eukaryotes and prokaryotes. *Biochem. Cell Biol.* **80**: 623-638.
81. Young, J. D., Yao, S. Y. M., Cass, C. E., and Baldwin, S. A. (2003) Equilibrative nucleoside transport proteins. In *Red Cell Transport in Health and Disease* pp 321-337. Springer Verlag, Berlin.
82. Kong, W., Engel, K., and Wang, J. (2004) Mammalian nucleoside transporters. *Current Drug Metabolism* **5**: 63-84.

83. Young, J. D., Yao, S. Y. M., Sun, L., Cass, C. E., and Baldwin, S. A. (2008) The ENT family of nucleoside and nucleobase transporter proteins. *Xenobiotica* (epub ahead of print).
84. Stein, A., Vaseduvan, G., Carter, N. S., Ullman, B., Landfear, S. M., and Kavanaugh, M. P. (2003) Equilibrative nucleoside transporter family members from *Leishmania donovani* are electrogenic proton symporters. *J. Biol. Chem.* **278**: 35127 - 35134.
85. Sanchez, M. A., Ullman, B., Landfear, S. M., and Carter, N. S. (1999) Cloning and functional expression of a gene encoding a P1 type nucleoside transporter from *Trypanosoma brucei*. *J. Biol. Chem.* **274**: 30244-30249.
86. Carter, N. S., Landfear, S. M., and Ullman, B. (2001) Nucleoside transporters of parasitic protozoa. *Trends Parasitol.* **17**: 142-145.
87. Sanchez, M. A., Tryon, R., Green, J., Boor, I., and Landfear, S. M. (2002) Six related nucleoside/nucleobase transporters from *Trypanosoma brucei* exhibit distinct biochemical functions. *J. Biol. Chem.* **277**: 21499-21504.
88. Mohlmann, T., Mezher, Z., Schwerdtfeger, G., and Neuhaus, H. E. (2001) Characterization of a concentrative type of adenosine transporter from *Arabidopsis thaliana* (ENT1, At). *FEBS Lett.* **509**: 370-374.
89. Traub, M., Florchinger, M., Piecuch, J., Kunz, H. H., Weise-Steinmetz, A., Deitmer, J. W., Ekkehard Neuhaus, H., and Mohlmann, T. (2007) The fluorouridine insensitive 1 (fur1) mutant is defective in equilibrative nucleoside transporter 3 (ENT3), and thus represents an important pyrimidine nucleoside uptake system in *Arabidopsis thaliana*. *Plant J.* **49**: 855-864.
90. Oliver, J. M., and Paterson, A. R. (1971) Nucleoside transport. I. A mediated process in human erythrocytes. *Can. J. Biochem.* **49**: 262-270.
91. Paterson, A. R., and Oliver, J. M. (1971) Nucleoside transport. II. Inhibition by *p*-nitrobenzylthioguanosine and related compounds. *Can. J. Biochem.* **49**: 271-274.
92. Cass, C. E., and Paterson, A. R. (1972) Mediated transport of nucleosides in human erythrocytes. Accelerative exchange diffusion of uridine and thymidine

- and specificity toward pyrimidine nucleosides as permeants. *J. Biol. Chem.* **247**: 3314-3320.
93. Cass, C. E., and Paterson, A. R. (1973) Mediated transport of nucleosides by human erythrocytes. Specificity toward purine nucleosides as permeants. *Biochim. Biophys. Acta* **291**: 734-746.
 94. Cass, C. E., Gaudette, L. A., and Paterson, A. R. (1974) Mediated transport of nucleosides in human erythrocytes. Specific binding of the inhibitor nitrobenzylthioinosine to nucleoside transport sites in the erythrocyte membrane. *Biochim. Biophys. Acta* **345**: 1-10.
 95. Dahlig-Harley, E., Eilam, Y., Paterson, A. R., and Cass, C. E. (1981) Binding of nitrobenzylthioinosine to high-affinity sites on the nucleoside-transport mechanism of HeLa cells. *Biochem. J.* **200**: 295-305.
 96. Belt, J. A. (1983) Heterogeneity of nucleoside transport in mammalian cells. Two types of transport activity in L1210 and other cultured neoplastic cells. *Mol. Pharmacol.* **24**: 479-484.
 97. Jarvis, S. M., and Young, J. D. (1986) Nucleoside transport in rat erythrocytes: two components with differences in sensitivity to inhibition by nitrobenzylthioinosine and *p*-chloromercuriphenyl sulfonate. *J. Membr. Biol.* **93**: 1-10.
 98. Wu, J.-S. R., Kwong, F. Y. P., Jarvis, S. M., and Young, J. D. (1983) Identification of the erythrocyte nucleoside transporter as a band 4.5 polypeptide. *J. Biol. Chem.* **258**: 13745-13751.
 99. Kwong, F. Y., Davies, A., Tse, C. M., Young, J. D., Henderson, P. J., and Baldwin, S. A. (1988) Purification of the human erythrocyte nucleoside transporter by immunoaffinity chromatography. *Biochem. J.* **255**: 243-249.
 100. Osses, N., Pearson, J. D., Yudilevich, D. L., and Jarvis, S. M. (1996) Hypoxanthine enters human vascular endothelial cells (ECV 304) via the nitrobenzylthioinosine-insensitive equilibrative nucleoside transporter. *Biochem. J.* **317**: 843-848.
 101. Crawford, C. R., Patel, D. H., Naeve, C., and Belt, J. A. (1998) Cloning of the human equilibrative, nitrobenzylmercaptapurine riboside (NBMPR)-insensitive

- nucleoside transporter *ei* by functional expression in a transport-deficient cell line. *J. Biol. Chem.* **273**: 5288-5293.
102. Griffiths, M., Beaumont, N., Yao, S. Y. M., Sundaram, M., Bouman, C. E., Davies, A., Kwong, F. Y. P., Coe, I. R., Cass, C. E., Young, J. D., and Baldwin, S. A. (1997) Cloning of a human nucleoside transporter implicated in the cellular uptake of adenosine and chemotherapeutic drugs. *Nat. Med.* **3**: 89-93.
 103. Griffiths, M., Yao, S. Y. M., Abidi, F., Phillips, S. E. V., Cass, C. E., Young, J. D., and Baldwin, S. A. (1997) Molecular cloning and characterization of a nitrobenzylthioinosine-insensitive (*ei*) equilibrative nucleoside transporter from human placenta. *Biochem. J.* **328**: 739-743.
 104. Barnes, K., Dobrzynski, H., Foppolo, S., Beal, P. R., Ismat, F., Scullion, E. R., Sun, L., Tellez, J., Ritzel, M. W. L., Claycomb, W. C., Cass, C. E., Young, J. D., Billeter-Clark, R., Boyett, M. R., and Baldwin, S. A. (2006) Distribution and functional characterization of equilibrative nucleoside transporter-4, a novel cardiac adenosine transporter activated at acidic pH. *Circ. Res.* **99**: 510-519.
 105. Yao, S. Y. M., Ng, A. M. L., Muzyka, W. R., Griffiths, M., Cass, C. E., Baldwin, S. A., and Young, J. D. (1997) Molecular cloning and functional characterization of nitrobenzylthioinosine (NBMPR)-sensitive (*es*) and NBMPR-insensitive (*ei*) equilibrative nucleoside transporter proteins (rENT1 and rENT2) from rat tissues. *J. Biol. Chem.* **272**: 28423-28430.
 106. Kiss, A., Farah, K., Kim, J., Garriock, R. J., Drysdale, T. A., and Hammond, J. R. (2000) Molecular cloning and functional characterization of inhibitor-sensitive (mENT1) and inhibitor-resistant (mENT2) equilibrative nucleoside transporters from mouse brain. *Biochem. J.* **352**: 363-372.
 107. Coe, I. R., Griffiths, M., Young, J. D., Baldwin, S. A., and Cass, C. E. (1997) Assignment of the human equilibrative nucleoside transporter (hENT1) to 6p21.1-p21.2. *Genomics* **45**: 459-460.
 108. Sankar, N., Machado, J., Abdulla, P., Hilliker, A. J., and Coe, I. R. (2002) Comparative genomic analysis of equilibrative nucleoside transporters suggests conserved protein structure despite limited sequence identity. *Nucleic Acids Res.* **30**: 433904350.

109. Lum, P. Y., Ngo, L. K., Bakken, A. H., and Unadkat, J. D. (2000) Human intestinal *es* nucleoside transporter: molecular characterization and nucleoside inhibitory profiles. *Cancer Chemother. Pharmacol.* **45**: 273-278.
110. Choi, D. S., Handa, M., Young, H., Gordon, A. S., Diamond, I., and Messing, R. O. (2000) Genomic organization and expression of the mouse equilibrative, nitrobenzylthioinosine-sensitive nucleoside transporter 1 (ENT1) gene. *Biochem. Biophys. Res. Commun.* **277**: 200-208.
111. Handa, M., Choi, D. S., Caldeiro, R. M., Messing, R. O., Gordon, A. S., and Diamond, I. (2001) Cloning of a novel isoform of the mouse NBMPR-sensitive equilibrative nucleoside transporter (ENT1) lacking a putative phosphorylation site. *Gene* **262**: 301-307.
112. Bone, D. B., Robillard, K. R., Stolk, M., and Hammond, J. R. (2007) Differential regulation of mouse equilibrative nucleoside transporter 1 (mENT1) splice variants by protein kinase CK2. *Mol. Membr. Biol.* **24**: 294-303.
113. Leabman, M. K., Huang, C. C., DeYoung, J., Carlson, E. J., Taylor, T. R., de la Cruz, M., Johns, S. J., Stryke, D., Kawamoto, M., Urban, T. J., Kroetz, D. L., Ferrin, T. E., Clark, A. G., Risch, N., Herskowitz, I., Giacomini, K. M., and Pharmacogenetics of Membrane Transporters Investigators (2003) Natural variation in human membrane transporter genes reveals evolutionary and functional constraints. *Proc. Natl. Acad. Sci. U.S.A.* **100**: 5896-5901.
114. Myers, S. N., Goyal, R. K., Roy, J. D., Fairfull, L. D., Wilson, J. W., and Ferrell, R. E. (2006) Functional single nucleotide polymorphism haplotypes in the human equilibrative nucleoside transporter 1. *Pharmac. Genomics* **16**: 315-320.
115. Osato, D. H., Huang, C. C., Kawamoto, M., Johns, S. J., Stryke, D., Wang, J., Ferrin, T. E., Herskowitz, I., and Giacomini, K. M. (2003) Functional characterization in yeast of genetic variants in the human equilibrative nucleoside transporter, ENT1. *Pharmacogenetics* **13**: 297-301.
116. Choi, D. S., Cascini, M. G., Mailliard, W., Young, H., Paredes, P., McMahon, T., Diamond, I., Bonci, A., and Messing, R. O. (2004) The type 1 equilibrative nucleoside transporter regulates ethanol intoxication and preference. *Nat. Neurosci.* **7**: 855-861.

117. Chen, J., Rinaldo, L., Lim, S. J., Young, H., Messing, R. O., and Choi, D. S. (2007) The type 1 equilibrative nucleoside transporter regulates anxiety-like behavior in mice. *Genes Brain Behav.* **6**: 776-793.
118. Ward, J. L., Sherali, A., Mo, Z.-P, and Tse, C.-M. (2000) Kinetic and pharmacological properties of cloned human equilibrative nucleoside transporters, ENT1 and ENT2, stably expressed in nucleoside transporter-deficient PK 15 cells. ENT2 exhibits a low affinity for guanosine and cytidine but a high affinity for inosine. *J. Biol. Chem.* **275**: 8375-8381.
119. Mackey, J. R., Mani, R. S., Selner, M., Mowles, D., Young, J. D., Belt, J. A., Crawford, C. R., and Cass, C. E. (1998) Functional nucleoside transporters are required for gemcitabine influx and manifestation of toxicity in cancer cell lines. *Cancer Res.* **58**: 4349-4357.
120. Mackey, J. R., Yao, S. Y., Smith, K. M., Karpinski, E., Baldwin, S. A., Cass, C. E., and Young, J. D. (1999) Gemcitabine transport in *Xenopus* oocytes expressing recombinant plasma membrane mammalian nucleoside transporters. *J. Natl. Canc. Institute* **91**: 1876-1881.
121. Galmarini, C. M., Thomas, X., Calvo, F., Rousselot, P., El Jafaari, A., Cros, E., and Dumontet, C. (2002) Potential mechanisms of resistance to cytarabine in AML patients. *Leuk. Res.* **26**: 621-629.
122. Clarke, M. L., Damaraju, V. L., Zhang, J., Mowles, D., Tackaberry, T., Lang, T., Smith, K. M., Young, J. D., Tomkinson, B., and Cass, C. E. (2006) The role of human nucleoside transporters in cellular uptake of 4'-thio- β -D-arabinofuranosylcytosine and β -D-arabinosylcytosine. *Mol. Pharm.* **70**: 301-310.
123. King, K. M., Damaraju, V. L., Vickers, M. F., Yao, S. Y., Lang, T., Tackaberry, T. W., Mowles, D. A., Ng, A. M., Young, J. D., and Cass, C. E. (2006) A comparison of the transportability, and its role in cytotoxicity, of clofarabine, cladribine, and fludarabine by recombinant human nucleoside transporters produced in three model expression systems. *Mol. Pharmacol.* **69**: 346-353.
124. Molina-Arcas, M., Bellosillo, B., Casado, F. J., Montserrat, E., Gil, J., Colomer, D., and Pastor-Anglada, M. (2003) Fludarabine uptake mechanisms in B-cell chronic lymphocytic leukemia. *Blood* **101**: 2328-2334.

125. Mackey, J. R., Jennings, L. L., Clarke, M. L., Santos, C. L., Dabbagh, L., Vsianska, M., Koski, S. L., Coupland, R. W., Baldwin, S. A., Young, J. D., and Cass, C. E. (2002) Immunohistochemical variation of human equilibrative nucleoside transporter 1 protein in primary breast cancers. *Clin. Cancer Res.* **8**: 110-116.
126. Yao, S. Y., Ng, A. M., Sundaram, M., Cass, C. E., Baldwin, S. A., and Young, J. D. (2001) Transport of antiviral 3'-deoxy-nucleoside drugs by recombinant human and rat equilibrative, nitrobenzylthioinosine (NBMPR)-insensitive (ENT2) nucleoside transporter proteins produced in *Xenopus* oocytes. *Mol. Membr. Biol.* **18**: 161-167.
127. Vickers, M. F., Mani, R. S., Sundaram, M., Hogue, D. L., Young, J. D., Baldwin, S. A., and Cass, C. E. (1999) Functional production and reconstitution of the human equilibrative nucleoside transporter (hENT1) in *Saccharomyces cerevisiae*. Interaction of inhibitors of nucleoside transport with recombinant hENT1 and a glycosylation-defective derivative (hENT1/N48Q). *Biochem. J.* **339**: 21-32.
128. Hammond, J. R. (2000) Interaction of a series of draflazine analogues with equilibrative nucleoside transporters: species differences and transporter subtype selectivity. *Naunyn Schmiedebergs Arch Pharmacol.* **361**: 373-382.
129. Kwong, F. Y., Fincham, H. E., Davies, A., Beaumont, N., Henderson, P. J., Young, J. D., and Baldwin, S. A. (1992) Mammalian nitrobenzylthioinosine-sensitive nucleoside transport proteins. Immunological evidence that transporters differing in size and inhibitor specificity share sequence homology. *J. Biol. Chem.* **267**: 21954-21960.
130. Sundaram, M., Yao, S. Y., Ingram, J. C., Berry, Z. A., Abidi, F., Cass, C. E., Baldwin, S. A., and Young, J. D. (2001) Topology of a human equilibrative, nitrobenzylthioinosine (NBMPR)-sensitive nucleoside transporter (hENT1) implicated in the cellular uptake of adenosine and anti-cancer drugs. *J. Biol. Chem.* **276**: 45270-45275.
131. Kwong, F. Y. P., Baldwin, S. A., Scudder, P. R., Jarvis, S. M., Choy, M. Y. M., and Young, J. D. (1986) Erythrocyte nucleoside and sugar transport. Endo- β -galactosidase and endoglycosidase-F digestion of partially purified human and pig transporter proteins. *Biochem. J.* **240**: 349-356.

132. Kwong, F. Y., Wu, J. S., Shi, M. M., Fincham, H. E., Davies, A., Henderson, P. J., Baldwin, S. A., and Young, J. D. (1993) Enzymatic cleavage as a probe of the molecular structures of mammalian equilibrative nucleoside transporters. *J. Biol. Chem.* **268**: 22127-22134.
133. Pennycooke, M., Chaudary, N., Shuralyova, I., Zhang, Y., and Coe, I. R. (2001) Differential expression of human nucleoside transporters in normal and tumor tissue. *Biochem. Biophys. Res. Commun.* **280**: 951-959.
134. Anderson, C. M., Xiong, W., Geiger, J. D., Young, J. D., Cass, C. E., Baldwin, S. A., and Parkinson, F. E. (1999) Distribution of equilibrative, nitrobenzylthioinosine-sensitive nucleoside transporters (ENT1) in brain. *J. Neurochem.* **73**: 867-873.
135. Jennings, L. L., Hao, C. H., Cabrita, M. A., Vickers, M. F., Baldwin, S. A., Young, J. D., and Cass, C. E. (2001) Distinct regional distribution of human equilibrative nucleoside transporter proteins 1 and 2 (hENT1 and hENT2) in the central nervous system. *Neuropharmacology* **40**: 722-731.
136. Guillen-Gomez, E., Calbet, M., Casado, J., de Lecea, L., Soriano, E., Pastor-Anglada, M., and Burgaya, F. (2004) Distribution of CNT2 and ENT1 transcripts in rat brain: selective decrease of CNT2 mRNA in the cerebral cortex of sleep-deprived rats. *J. Neurochem.* **90**: 883-893.
137. Pinto-Duarte, A., Coelho, J. E., Cunha, R. A., Ribeiro, J. A., and Sebastiao, A. M. (2005) Adenosine A_{2A} receptors control the extracellular levels of adenosine through modulation of nucleoside transporters activity in the rat hippocampus. *J. Neurochem.* **93**: 595-604.
138. Gu, J. G., Nath, A., and Geiger, J. D. (1996) Characterization of inhibitor-sensitive and -resistant adenosine transporters in cultured human fetal astrocytes. *J. Neurochem.* **67**: 972-977.
139. Musa, H., Dobrzynski, H., Berry, F., Abidi, F., Cass, C. E., Young, J. D., Baldwin, S. A., and Boyett, M. R. (2002) Immunocytochemical demonstration of the equilibrative nucleoside transporter rENT1 in rat sinoatrial node. *J. Histochem. Cytochem.* **50**: 305-309.
140. Lai, Y. R., Bakken, A. H., and Unadkat, J. D. (2002) Simultaneous expression of hCNT1-CFP and hENT1-YFP in Madin-Darby canine kidney cells - localization and vectorial transport studies. *J. Biol. Chem.* **277**: 37711-37717.

141. Mangravite, L. M., Xiao, G., Giacomini, K. M. (2003) Localization of human equilibrative nucleoside transporters, hENT1 and hENT2, in renal epithelial cells. *Am. J. Physiol.* **284**: F902-910.
142. Damaraju, V. L., Elwi, A. N., Hunter, C., Carpenter, P., Santos, C., Barron, G. M., Sun, X., Baldwin, S. A., Young, J. D., Mackey, J. R., Sawyer, M. B., and Cass, C. E. (2007) Localization of broadly selective equilibrative and concentrative nucleoside transporters, hENT1 and hCNT3, in human kidney. *Am. J. Physiol. Renal Physiol.* **293**: F200-F211.
143. Govindarajan, R., Bakken, A. H., Hudkins, K. L., Lai, Y., Casado, F. J., Pastor-Anglada, M., Tse, C. M., Hayashi, J., and Unadkat, J. D. (2007) *In situ* hybridization and immunolocalization of concentrative and equilibrative nucleoside transporters in the human intestine, liver, kidneys and placenta. *Am. J. Physiol. Regul. Integr. Comp. Physiol.* **293**: R1809-1822.
144. Mun, E. C., Tally, K. J., and Matthews, J. B. (1998) Characterization and regulation of adenosine transport in T84 intestinal epithelial cells. *Am. J. Physiol.* **274**: G261-G269.
145. Lai, Y., Tse, C.-M., and Unadkat, J. D. (2004) Mitochondrial expression of the human equilibrative nucleoside transporter 1 (hENT1) results in enhanced mitochondrial toxicity of antiviral drugs. *J. Biol. Chem.* **279**: 4490-4497.
146. Lee, E. W., Lai, Y., Zhang, H., and Unadkat, J. D. (2006) Identification of the mitochondrial targeting signal of the human equilibrative nucleoside transporter 1 (hENT1): implications for interspecies differences in mitochondrial toxicity of fialuridine. *J. Biol. Chem.* **281**: 16700-16706.
147. Mani, R. S., Hammond, J. R., Marjan, J. M. J., Graham, K. A., Young, J. D., Baldwin, S. A., and Cass, C. E. (1998) Demonstration of equilibrative nucleoside transporters (hENT1 and hENT2) in nuclear envelopes of cultured human choriocarcinoma (BeWo) cells by functional reconstitution in proteoliposomes. *J. Biol. Chem.* **273**: 30818-30825.
148. Goh, L. B., Mack, P., and Lee, C. W. (1995) Nitrobenzylthioinosine-binding protein overexpression in human breast, liver, stomach and colorectal tumor tissues. *Anticancer Res.* **15**: 2575-2579.
149. Chen, S. F., Cleaveland, J. S., Hollmann, A. B., Wiemann, M. C., Parks, R. E. Jr., and Stoeckler, J. D. (1986) Changes in nucleoside transport of HL-60

- human promyelocytic cells during N, N-dimethylformamide induced differentiation. *Cancer Res.* **46**: 3449-3455.
150. Meckling-Gill, K. A., Guilbert, L., and Cass, C. E. (1993) CSF-1 stimulates nucleoside transport in S1 macrophages. *J. Cell Physiol.* **155**: 530-538.
 151. Pressacco, J., Wiley, J. S., Jamieson, G. P., Erlichman, C., and Hedley, D. W. (1995) Modulation of the equilibrative nucleoside transporter by inhibitors of DNA synthesis. *Br. J. Cancer* **72**: 939-942.
 152. Soler, C., Garcia-Manteiga, J., Valdes, R., Xaus, J., Comalada, M., Casado, F. J., Pastor-Anglada, M., Celada, A., and Felipe, A. (2001) Macrophages require different nucleoside transport systems for proliferation and activation. *FASEB J.* **15**: 1979-1988.
 153. Coe, I., Zhang, Y., McKenzie, T., and Naydenova, Z. (2002) PKC regulation of the human equilibrative nucleoside transporter, hENT1. *FEBS Lett.* **517**: 201-205.
 154. Soler, C., Felipe, A., Mata, J. F., Casado, F. J., Celada, A., and Pastor-Anglada, M. (1998) Regulation of nucleoside transport by lipopolysaccharide, phorbol esters, and tumor necrosis factor-alpha in human B-lymphocytes. *J. Biol Chem.* **273**: 26939-26945.
 155. Soler, C., Felipe, A., Casado, F. J., Celada, A., and Pastor-Anglada, M. (2000) Nitric oxide regulates nucleoside transport in activated B lymphocytes. *J. Leukoc. Biol.* **67**: 345-349.
 156. Aguayo, C., Flores, C., Parodi, J., Rojas, R., Mann, G. E., Pearson, J. D., and Sobrevia, L. (2001) Modulation of adenosine transport by insulin in human umbilical artery smooth muscle cells from normal or gestational diabetic pregnancies. *J. Physiol.* **534**: 243-254.
 157. Podgorska, M., Kocbuch, K., Grden, M., Szutowicz, A., and Pawelczyk, T. (2006) Reduced ability to release adenosine by diabetic rat cardiac fibroblasts due to altered expression of nucleoside transporters. *J. Physiol.* **576**: 179-189.
 158. Sakowicz, M., Szutowicz, A., and Pawelczyk, T. (2004) Insulin and glucose induced changes in expression level of nucleoside transporters and adenosine transport in rat T lymphocytes. *Biochem. Pharmacol.* **68**: 1309-1320.

159. Sakowicz, M., Szutowicz, A., and Pawelczyk, T. (2005) Differential effect of insulin and elevated glucose level on adenosine transport in rat B lymphocytes. *Int. Immunol.* **17**: 145-154.
160. Parodi, J., Flores, C., Aguayo, C., Rudolph, M. I., Casanello, P., and Sobrevia, L. (2002) Inhibition of nitrobenzylthioinosine-sensitive adenosine transport by elevated D-glucose involves activation of P2Y2 purinoceptors in human umbilical vein endothelial cells. *Circ. Res.* **90**: 570-577.
161. Puebla, C., Farias, M., Gonzalez, M., Vecchiola, A., Aguayo, C., Krause, B., Pastor-Anglada, M., Casanello, P., and Sobrevia, L. (2007) High D-glucose reduces SLC29A1 promoter activity and adenosine transport involving specific protein 1 in human umbilical vein endothelium. *J. Cell. Physiol.* (epub ahead of print).
162. Williams, J. B., and Lanahan, A. A. (1995) A mammalian delayed-early response gene encodes HNP36, a novel, conserved nucleolar protein. *Biochem Biophys. Res. Commun.* **213**: 325-333.
163. Wu, S. K., Ann, D. K., Kim, K. J., and Lee, V. H. (2005) Fine tuning of rabbit equilibrative nucleoside transporter activity by an alternatively spliced variant. *J. Drug Target.* **13**: 521-533.
164. Owen, R. P., Lagpacan, L. L., Taylor, T. R., de la Cruz, M., Huang, C. C., Kawamoto, M., Johns, S. J., Stryke, D., Ferrin, T. E., and Giacomini, K. M. (2006) Functional characterization and haplotype analysis of polymorphisms in the human equilibrative nucleoside transporter, ENT2. *Drug Metab. Dispos.* **34**: 12-15.
165. Yao, S. Y. M., Ng, A. M. L., Vickers, M. F., Sundaram, M., Cass, C. E., Baldwin, S. A., and Young, J. D. (2002) Functional and molecular characterization of nucleobase transport by recombinant human and rat equilibrative nucleoside transporters 1 and 2 - Chimeric constructs reveal a role for the ENT2 helix 5-6 region in nucleobase translocation. *J. Biol. Chem.* **277**: 24938-24948.
166. Visser, F., Vickers, M. F., Ng, A. L., Baldwin, S. A., Young, J. D., and Cass, C. E. (2002) Mutation of residue 33 of human equilibrative nucleoside transporters 1 and 2 alters sensitivity to inhibition of transport by dilazep and dipyridamole. *J. Biol. Chem.* **277**: 395-401.

167. Ward, J. L., Leung, G. P., Toan, S. V., and Tse, C. M. (2003) Functional analysis of site-directed glycosylation mutants of the human equilibrative nucleoside transporter-2. *Arch. Biochem. Biophys.* **411**: 19-26.
168. Anderson, C. M., Baldwin, S. A., Young, J. D., Cass, C. E., and Parkinson, F. E. (1999) Distribution of mRNA encoding a nitrobenzylthioinosine-insensitive nucleoside transporter (ENT2) in rat brain. *Mol. Brain Res.* **70**: 293-297.
169. Sinclair, C. J., LaRiviere, C. G., Young, J. D., Cass, C. E., Baldwin, S. A., and Parkinson, F. E. (2000) Purine uptake and release in rat C6 glioma cells: nucleoside transport and purine metabolism under ATP-depleting conditions. *J. Neurochem.* **75**: 1528-1538.
170. Jones, K. W., Rylett, R. J., and Hammond, J. R. (1994) Effect of cellular differentiation on nucleoside transport in human neuroblastoma cells. *Brain Res.* **660**: 104-112.
171. Podgorska, M., Kocbuck, K., Grden, M., Szulc, A., Szutowicz, A., and Pawelczyk, T. (2007) Different signaling pathways utilized by insulin to regulate the expression of ENT2, CNT1, CNT2 nucleoside transporters in rat cardiac fibroblasts. *Arch. Biochem. Biophys.* **464**: 344-349.
172. Baldwin, S. A., Yao, S. Y. M., Hyde, R. J., Ng, A. M. L., Foppolo, S., Barnes, K., Ritzel, M. W. L., Cass, C. E., and Young, J. D. (2005) Functional characterization of novel human and mouse equilibrative nucleoside transporters (hENT3 and mENT3) located in intracellular membranes. *J. Biol. Chem.* **280**: 15880-15887.
173. Pisoni, R. L., and Thoene, J. G. (1991) The transport systems of mammalian lysosomes. *Biochim. Biophys. Acta* **1071**: 351-373.
174. Engel, K., Zhou, M., and Wang, J. (2004) Identification and characterization of a novel monomamine transporter in the human brain. *J. Biol. Chem.* **279**: 50042-50049.
175. Engel, K., and Wang, J. (2005) Interaction of organic cations with a newly identified plasma membrane monoamine transporter. *Mol. Pharmacol.* **68**: 1397-1407.

176. Xia, L., Engel, K., Zhou, M., and Wang, J. (2006) Membrane localization and pH-dependent transport of a newly cloned organic cation transporter (PMAT) in kidney cells. *Am. J. Physiol. Renl Physiol.* **292**: F682-F690.
177. Vialou, V., Balasse, L., Dumas, S., Giros, B., and Gautron, S. (2007) Neurochemical characterization of pathways expressing plasma membrane monoamine transporter in the rat brain. *Neuro.* **144**: 616-622.
178. Tattersall, M. H. N., Slowiaczek, P., and De Fazio, A. (1983) Regional variation in human extracellular purine levels. *J. Lab. Clin. Med.* **102**: 411-420.
179. Heydrick, S. J., Lardeux, B. R., and Mortimore, G. E. (1991) Uptake and degradation of cytoplasmic RNA by hepatic lysosomes. Quantitative relationship to RNA turnover. *J. Biol. Chem.* **266**: 87890-8796.
180. Zhou, M., Engel, K., and Wang, J. (2007) Evidence for significant contribution of a newly identified monomamine transporter (PMAT) to serotonin uptake in the human brain. *Biochem. Pharm.* **73**: 147-154.
181. Martin, B. J., Lasley, R. S., and Mentzer, R. M. (1997) Infarct size reduction with the nucleoside transport inhibitor R-75231 in swine. *Am. J. Physiol.* **41**: J1857-J1865.
182. Gu, J. G., Foga, I. O., Parkinson, F. E., and Geiger, J. D. (1995) Involvement of bidirectional adenosine transporters in the release of L-[³H]adenosine from rat brain synaptosomal preparations. *J. Neurochem.* **54**: 2105-2110.
183. Zimmermann, H. (2000) Extracellular metabolism of ATP and other nucleosides. *Naunyn. Schmiedebergs Arch. Pharmacol.* **362**: 299-309.
184. MacDonald, W. F., and White, T. D. (1985) Nature of extrasynaptosomal accumulation of endogenous adenosine evoked by K⁺ and veratridine. *J. Neurochem.* **45**: 791-797.
185. Parkinson, F. E., Zhang, Y. W., Shepel, P. N., Greenway, S. C., Peeling, J., and Geiger, J. D. (2000) Effects of nitrobenylthioinosine on adenosine levels and neuronal injury in rat forebrain ischemia. *J. Neurochem.* **75**: 795-802.

186. Keil, G. J., and DeLander, G. E. (1995) Time-dependent antinociceptive interactions between opioids and nucleoside transport inhibitors. *J. Pharmacol. Exp. Ther.* **274**: 1387-1392.
187. Ackley, M. A., Governo, R. J., Cass, C. E., Young, J. D., Baldwin, S. A., and King, A. (2003) Control of glutamatergic neurotransmission in the rat spinal dorsal horn by the nucleoside transporter ENT1. *J. Physiol. (Lond)* **548**: 507-517.
188. Szkotak, A. J., Ng, A. L., Sawicka, J., Baldwin, S. A., Man, S. P., Cass, C. E., Young, J. D., and Duszyk, M. (2001) Regulation of K⁺ current in human airway epithelial cells by exogenous and autocrine adenosine. *Am. J. Physiol.* **281**: C1991-C2002.
189. Luft, B. J., and Remington, J. S. (1992) Toxoplasmic encephalitis in AIDS. *Clin. Infect. Dis.* **15**: 211-222.
190. Roizen, N., Swisher, C. N., Stein, M. A., Hopkins, J., Boyer, K. M., Holfels, E., Mets, M. B., Stein, L., Patel, D., Meier, P., *et al.* (1995) Neurologic and developmental outcome in treated congenital toxoplasmosis. *Pediatrics* **95**: 11-20.
191. Tuteja, R. (2007) Malaria - an overview. *FEBS J.* **274**: 4670-4679.
192. Masocha, W., Rottenberg, M. E., and Kristensson, K. (2007) Migration of African trypanosomes across the blood-brain barrier. *Physiol. Behav.* **192**: 110-114.
193. Chiang, C.-W., Carter, N., Sullivan, W. J. Jr., Donald, R. G. K., Roos, D. S., Naguib, F. N. M., el Kouni, M. H., Ullman, B., and Wilson, C. M. (1999) The adenosine transporter of *Toxoplasma gondii*. Identification by insertional mutagenesis, cloning, and recombinant expression. *J. Biol. Chem.* **274**: 35255-35261.
194. de Koning, H. P., Ao-Salabi, M. I., Cohen, A. M., Coombs, G. H., and Wasling, J. M. (2003) Identification and characterization of high affinity nucleoside and nucleobase transporters in *Toxoplasma gondii*. *Int. J. Parasitol.* **33**: 821-831.

195. Carter, N. S., Ben Mamoun, C., Liu, W., Silva, E. O., Landfear, S. M., Goldberg, D. E., and Ullman, B. (2000) Isolation and functional characterization of the PfNT1 nucleoside transporter gene from *Plasmodium falciparum*. *J. Biol. Chem.* **275**: 10683-10691.
196. Parker, M. D., Hyde, R. J., Yao, S. Y. M., McRobert, L., Cass, C. E., Young, J. D., McConkey, G. A., and Baldwin, S. A. (2000) Identification of a nucleoside/nucleobase transporter from *Plasmodium falciparum*, a novel target for anti-malarial chemotherapy. *Biochem. J.* **349**: 67-75.
197. Downie, M. J., Saliba, K. J., Howitt, S. M., Broer, S., and Krik, K. (2006) Transport of nucleosides across the *Plasmodium falciparum* parasite plasma membrane has characteristics of PfENT1. *Mol. Microbiol.* **60**: 738-748.
198. Rager, N., Momoun, C. B., Carter, N. S., Goldberg, D. E., and Ullman, B. (2001) Localization of the *Plasmodium falciparum* PfNT1 nucleoside transporter to the parasite plasma membrane. *J. Biol. Chem.* **276**: 41095-41099.
199. El Bissati, K., Zufferey, R., Witola, W. H., Carter, N. S., Ullman, B., and Ben Mamoun, C. (2006) The plasma membrane permease PfNT1 is essential for purine salvage in the human malaria parasite *Plasmodium falciparum*. *Proc. Natl. Acad. Sci. U.S.A.* **103**: 9286-9291.
200. Aronow, B., Kaur, K., McCartan, K., and Ullman, B. (1987) Two high affinity nucleoside transporters in *Leishmania donovani*. *Mol. Biochem. Parasitol.* **22**: 29-37.
201. Vasudevan, G., Carter, N. S., Drew, M. E., Beverley, S. M., Sanchez, M. A., Seyfang, A., Ullman, B., and Landfear, S. M. (1998) Cloning of *Leishmania* nucleoside transporter genes by rescue of a transport-deficient mutant. *Proc. Natl. Acad. Sci. U.S.A.* **95**: 9873-9878.
202. Carter, N. S., Drew, M. E., Sanchez, M., Vasudeven, G., Landfear, S. M., and Ullman, B. (2000) Cloning of a novel inosine-guanosine transporter gene from *Leishmania donovani* by functional rescue of a transport-deficient mutant. *J. Biol. Chem.* **275**: 20935-20941.
203. Carter, N. S., and Fairlamb, A. H. (1993) Arsenical-resistant trypanosomes lack an unusual adenosine transporter. *Nature* **361**: 173-176.

204. Carter, N. S., Berger, B. J., and Fairlamb, A. H. (1995) Uptake of diamidine drugs by the P2 nucleoside transporter in melarsen-sensitive and -resistant *Trypanosoma brucei brucei*. *J. Biol. Chem.* **270**: 28153-28157.
205. de Koning, H. P., Watson, C. J., and Jarvis, S. M. (1998) Characterization of a nucleoside/proton symporter in procyclic *Trypanosoma brucei brucei*. *J. Biol. Chem.* **273**: 9486-9494.
206. Geiser, F., Luscher, A., de Koning, H. P., Seebeck, T., and Maser, P. (2005) Molecular pharmacology of adenosine transport in *Trypanosoma brucei*: P1/P2 revisited. *Mol. Pharmacol.* **68**: 589-595.
207. Mäser, P., Sütterlin, C., Kralli, A., and Kaminsky, R. (1999) A nucleoside transporter from *Trypanosoma brucei* involved in drug resistance. *Science* **285**: 242-244.
208. Henriques, C., Sanchez, M. A., Tyron, R., and Landfear, S. M. (2003) Molecular and functional characterization of the first nucleobase transporter gene from African trypanosomes. *Mol. Biochem. Parasitol.* **130**: 101-110.
209. Burchmore, R. J., Wallace, L. J., Candlish, D., Al-Salabi, M. I., Beal, P. R., Barrett, M. P., Baldwin, S. A., and de Koning, H. P. (2003) Cloning, heterologous expression, and *in situ* characterization of the first high affinity nucleobase transporter from a protozoan. *J. Biol. Chem.* **278**: 23502-23507.
210. Al-Salabi, M. I., Wallace, L. J., Luscher, A., Maser, P., Candlish, D., Rodenko, B., Gould, M. K., Jabeen, I., Ajith, S. N., and de Koning, H. P. (2007) Molecular interactions underlying the unusually high adenosine affinity of a novel *Trypanosoma brucei* nucleoside transporter. *Mol. Pharmacol.* **71**: 921-929.
211. Sanchez, M. A., Drutman, S., van Ampting, M., Matthews, K., and Landfear, S. M. (2004) A novel purine nucleoside transporter whose expression is up-regulated in the short stumpy form of the *Trypanosoma brucei* life cycle. *Mol. Biochem. Parasitol.* **136**: 265-272.
212. Gudín, S., Quashie, N. B., Candlish, D., Al-Salabi, M. I., Jarvis, S. M., Ranford-Cartwright, L. C., and de Koning, H. P. (2006) *Trypanosoma brucei*: a survey of pyrimidine transport activities. *Exp. Parasitol.* **114**: 118-125.

213. de Koning, H. P., and Jarvis, S. M. (1998) A highly selective, high-affinity transporter for uracil in *Trypanosoma brucei brucei*: evidence for proton-dependent transport. *Biochem. Cell. Biol* **76**: 853-858.
214. de Koning, H. P., Watson, C. J., Sutcliffe, J., and Jarvis, S. M. (2000) Differential regulation of nucleoside and nucleobase transporters in *Crithidia fasciculata* and *Trypanosoma brucei brucei*. *Mol. Biochem. Parasitol.* **106**: 93-107.
215. Liu, W., Arendt, C. S., Gessford, S. K., Ntaba, D., Carter, N. S., and Ullman, B. (2005) Identification and characterization of purine nucleoside transporters from *Crithidia fasciculata*. *Mol. Biochem. Parasitol.* **140**: 1-12.
216. Appleford, P. J., Griffiths, M., Yao, S. Y. M., Ng, A. M., Chomey, E. G., Isaac, R. E., Coates, D., Hope, I. A., Cass, C. E., Young, J. D., and Baldwin, S. A. (2004) Functional redundancy of two nucleoside transporters of the ENT family (CeENT1, CeENT2) required for development of *Caenorhabditis elegans*. *Mol. Membr. Biol.* **21**: 247-259.
217. Machado, J., Abdulla, P., Hanna, W. J., Hilliker, A. J., and Coe, I. R. (2007) Genomic analysis of nucleoside transporters in *Deoptera* and functional characterization of DmENT2, a *Drosophila* equilibrative nucleoside transporter. *Physiol. Genomics* **28**: 337-347.
218. Mok, D. W., and Mok, M. C. (2001) Cytokinin metabolism and action. *Annu. Rev. Plant Physiol. Plant Mol. Biol.* **52**: 89-118.
219. Sakakibara, H., Takei, K., and Hirose, N. (2006) Interactions between nitrogen and cytokinin in the regulation of metabolism and development. *Trends Plant Sci.* **11**: 440-448.
220. Li, G., Liu, K., Baldwin, S. A., and Wang, D. (2003) Equilibrative nucleoside transporters of *Arabidopsis thaliana*. cDNA cloning, expression pattern, and analysis of transport activities. *J. Biol. Chem.* **278**: 35732-35742.
221. Wormit, A., Traub, M., Florchinger, M., Neuhaus, H. E., and Mohlmann, T. (2004) Characterization of three novel members of the *Arabidopsis thaliana* equilibrative nucleoside transporter (ENT) family. *Biochem. J.* **383**: 19-26.

222. Li, J., and Wang, D. (2000) Cloning and in vitro expression of the cDNA encoding a putative nucleoside transporter from *Arabidopsis thaliana*. *Plant Sci.* **157**: 23-32.
223. Chen, K. L., Xu, M. X., Li, G. Y., Liang, H., Xia, Z. L., Liu, X., Zhang, J. S., Zhang, A. M., and Wang, D. W. (2006) Identification of AtENT3 as the main transporter for uridine uptake in Arabidopsis roots. *Cell Res.* **16**: 377-388.
224. Hirose, N., Makita, N., Yamaya, T., and Sakakibara, H. (2005) Functional characterization and expression analysis of a gene, OsENT2, encoding an equilibrative nucleoside transporter in rice suggest a function in cytokinin transport. *Plant Physiol.* **138**: 196-206.
225. Vickers, M. F., Yao, S. Y., Baldwin, S. A., Young, J. D., and Cass, C. E. (2000) Nucleoside transporter proteins of *Saccharomyces cerevisiae*: demonstration of a transporter (FUI1) with high uridine selectivity in plasma membranes and a transporter (FUN26) with broad nucleoside selectivity in intracellular membranes. *J. Biol. Chem.* **275**: 25931-25938.
226. Barton, A. B., and Kaback, D. B. (1994) Molecular cloning of chromosome I DNA from *Saccharomyces cerevisiae*: analysis of the genes in the FUN38-MAK16-SPO7 region. *J. Bacteriol.* **176**: 1872-1880.
227. Gray, J. H., Owen, R. P., and Giacomini, K. M. (2004) The concentrative nucleoside transporter family, SLC28. *Pflugers Arch.* **447**: 728-734.
228. Le Hir, M., and Duback, U. C. (1984) Sodium gradient-energized concentrative transport of adenosine in renal brush border vesicles. *Pflugers Arch.* **401**: 58-63.
229. Schwenk, M., Hegazy, E., and del Pino, V. L. (1984) Uridine uptake by isolated intestinal epithelial cells of guinea pig. *Biochim. Biophys. Acta* **805**: 370-374.
230. Le Hir, M., and Duback, U. C. (1985) Concentrative transport of purine nucleosides in brush border vesicles of the rat kidney. *Eur. J. Clin. Invest.* **15**: 121-127.
231. Le Hir, M., and Duback, U. C. (1985) Uphill concentrative transport of pyrimidine nucleosides in renal brush border vesicles. *Pflugers Arch.* **404**: 238-243.

232. Lee, C. W., Cheeseman, C. I., and Jarvis, S. M. (1988) Na⁺- and K⁺-dependent uridine transport in rat renal brush-border membrane vesicles. *Biochim. Biophys. Acta.* **942**: 139-149.
233. Jarvis, S. M. (1989) Characterization of sodium-dependent nucleoside transport in rabbit intestinal brush-border membrane vesicles. *Biochem. Biophys. Acta.* **979**: 132-138.
234. Williams, T. C., Doherty, A. J., Griffith, D. A., and Jarvis, S. M. (1989) Characterization of sodium-dependent and sodium-independent nucleoside transport systems in rabbit brush-border and basolateral plasma-membrane vesicles from the renal outer cortex. *Biochem. J.* **264**: 223-231.
235. Vijayalakshmi, D., and Belt, J. A. (1988) Sodium-dependent nucleoside transport in mouse intestinal epithelial cells. *J. Biol. Chem.* **263**: 19419-19423.
236. Jarvis, S. M., and Griffith, D. A. (1991) Expression of the rabbit intestinal N2 Na⁺/nucleoside transporter in *Xenopus laevis* oocytes. *Biochem. J.* **278**: 605-607.
237. Thomas, S. A., and Segal, M. B. (1997) Saturation kinetics, specificity and NBMPR sensitivity of thymidine entry into the central nervous system. *Brain Res.*, **760**: 59-67.
238. Plagemann, P. G. W., and Woffendin, C. (1989) Na⁺-dependent and -independent transport of uridine and its phosphorylation in mouse spleen cells. *Biochim. Biophys. Acta* **981**: 315-325.
239. Plagemann, P. G. W., and Aran, J. M. (1990) Characterization of Na⁺-dependent, active nucleoside transport in rat and mouse peritoneal macrophages, a mouse macrophage cell line and normal rat kidney cells. *Biochim. Biophys. Acta* **1028**: 289-298.
240. Che, M., Nishida, T., Gatmaitan, Z., and Arias, I. M. (1992) A nucleoside transporter is functionally linked to ectonucleotidases in rat liver canalicular membrane. *J. Biol. Chem.* **267**: 9684-9688.
241. Crawford, C. R., Ng, C. Y. C., Noel, L. D., and Belt, J. A. (1990) Nucleoside transport in L1210 murine leukemia cells. Evidence for three transporters. *J. Biol. Chem.* **265**: 9732-9736.

242. Le Hir, M. (1990) Evidence for separate carriers for purine nucleosides and for pyrimidine nucleosides in the renal brush border membrane. *Ren. Physiol. Biochem.* **13**: 154-161.
243. Williams, T. C., and Jarvis, S. M. (1991) Multiple sodium-dependent nucleoside transport systems in bovine renal brush-border membrane vesicles. *Biochem. J.* **274**: 27-33.
244. Gutierrez, M. M., Brett, C. M., Ott, R. J., Hui, A. C., and Giacomini, K. M. (1992) Nucleoside transport in brush border membrane vesicles from human kidney. *Biochim. Biophys. Acta* **1105**: 1-9.
245. Franco, R., Centelles, J. J., and Kinne, R. K. H. (1990) Further characterization of adenosine transport in renal brush-border membranes. *Biochim. Biophys. Acta* **1024**: 241-248.
246. Baer, H. P., and Moorji, A. (1990) Sodium-dependent and inhibitor-insensitive uptake of adenosine by mouse peritoneal exudate cells. *Biochim. Biophys. Acta* **1026**: 241-247.
247. Lee, C. W., Sokoloski, J. A., Sartorelli, A. C., and Handschumacher, R. E. (1991) Induction of the differentiation of HL-60 cells by phorbol 12-myristate 13-acetate activates a Na⁺-dependent uridine-transport system. *Biochem. J.* **27**, 85-90.
248. Belt, J. A., Harper, E. H., Byl, J. A., and Noel, L. D. (1992) Na⁺-dependent nucleoside transport in human myeloid leukemic cell lines and freshly isolated myeloblasts. *Proc. Am. Assoc. Cancer Res.* **33**: 20.
249. Wu, X., Yuan, G., Brett, C. M., Hui, A. C., and Giacomini, K. M. (1992) Sodium-dependent nucleoside transport in choroid plexus from rabbit. Evidence for a single transporter for purine and pyrimidine nucleosides. *J. Biol. Chem.* **267**: 8813-8818.
250. Wu, X., and Giacomini, K. (1994) Expression of the choroid plexus sodium-nucleoside cotransporter (N3) in *Xenopus laevis* oocytes. *Biochem. Pharmacol.* **48**: 432-434.

251. Wu, X., Gutierrez, M. M., and Giacomini, K. M. (1994) Further characterization of the sodium-dependent nucleoside transporter (N3) in choroid plexus from rabbit. *Biochim. Biophys. Acta* **1191**: 190-196.
252. Belt, J. A., Marina, N. M., Phelps, D. A., and Crawford, C. R. (1993) Nucleoside transport in normal and neoplastic cells. *Adv. Enzyme Regul.* **33**: 235-252.
253. Huang, Q., Harvey, C. M., Paterson, A. R. P., Cass, C. E., and Young, J. D. (1993) Functional expression of Na⁺-dependent nucleoside transport systems of rat intestine in isolated oocytes of *Xenopus laevis*. Demonstration that rat jejunum expresses the purine-selective system N1 (*cif*) and a second, novel system N3 having broad specificity for purine and pyrimidine nucleosides. *J. Biol. Chem.* **268**: 20613-20619.
254. Redlak, M. J., Zehner, Z. E., and Betcher, S. L. (1996) Expression of rabbit ileal N3 Na⁺/nucleoside cotransport activity in *Xenopus laevis* oocytes. *Biochem. Biophys. Res. Commun.* **225**: 106-111.
255. Hong, M., Schlichter, L., and Bendayan, R. (2000) A Na⁺-dependent nucleoside transporter in microglia. *J. Pharmacol. Exp. Ther.* **292**: 366-374.
256. Gutierrez, M. M., and Giacomini, K. M. (1993) Substrate selectivity, potential sensitivity and stoichiometry of Na⁺-nucleoside transport in brush border membrane vesicles from human kidney. *Biochim. Biophys. Acta* **1149**: 202-208.
257. Gutierrez, M. M., and Giacomini, K. M. (1994) Expression of a human renal nucleoside transporter in *Xenopus laevis* oocytes. *Biochem. Pharmacol.* **48**: 2251-2253.
258. Paterson, A. R., Gati, W. P., Vijayalakshmi, D., Cass, C. E., Mant, M. J., Young, J. D., and Belch, A. R. (1993) Inhibitor-sensitive, Na⁺-linked transport of nucleoside analogs in leukemic cells from patients. *Proc. Am. Assoc. Cancer Res.* **34**: A84.
259. Flanagan, S. A. and Meckling-Gill, K. A. (1997) Characterization of a novel Na⁺-dependent, guanosine-specific, nitrobenzylthiolinosine-sensitive transporter in acute promyelocytic leukemia cells. *J. Biol. Chem.* **272**: 18026-18032.

260. Flanagan, S. A., Gandhi, V., Secrist, J. A. 3rd, and Meckling, K. A. (2003) The novel nucleoside transport system exhibited by NB4 cells, *csg*, transports deoxyguanosine analogues, including ara-G. *Biochem. Pharmacol.* **66**: 733-737.
261. Huang, Q. Q., Yao, S. Y. M., Ritzel, M. W. L., Paterson, A. R. P., Cass, C. E., and Young, J. D. (1994) Cloning and functional expression of a complementary DNA encoding a mammalian nucleoside transport protein. *J. Biol. Chem.* **269**: 17757-17760.
262. Ritzel, M. W. L., Yao, S. Y. M., Huang, M. Y., Elliot, J. F., Cass, C. E., and Young, J. D. (1997) Molecular cloning and functional expression of cDNAs encoding a human Na⁺-nucleoside cotransporter (hCNT1). *Am. J. Physiol.* **272**: C707-C714.
263. Pajor, A. M. (1998) Sequence of a pyrimidine-selective Na⁺-nucleoside cotransporter from pig kidney, pKCNT1. *Biochim. Biophys. Acta.* **1415**: 266-269.
264. Gray, J. H., Mangravite, L. M., Owen, R. P., Urban, T. J., Chan, W., Carlson, E. J., Huang, C. C., Kawamoto, M., Johns, S. J., Stryke, D., Ferrin, T. E., and Giacomini, K. M. (2004) Functional and genetic diversity in the concentrative nucleoside transporter, CNT1, in human populations. *Mol. Pharmacol.* **65**: 512-519.
265. Fang, X., Parkinson, F. E., Mowles, D. A., Young, J. D., and Cass, C. E. (1996) Functional characterization of a recombinant sodium-dependent nucleoside transporter with selectivity for pyrimidine nucleosides (cNT1rat) by transient expression in cultured mammalian cells. *Biochem. J.* **317**: 457-465.
266. Dresser, M. J., Gerstin, K. M., Gray, A. T., Loo, D. D., and Giacomini, K. M. (2000) Electrophysiological analysis of the substrate selectivity of a sodium-coupled nucleoside transporter (rCNT1) expressed in *Xenopus laevis* oocytes. *Drug Metab. Dispos.* **28**: 1135-1140.
267. Larráyoz, I. M., Casado, F. J., Pastor-Anglada, M., and Lostao, M. P. (2004) Electrophysiological characterization of the human Na⁺/nucleoside cotransporter 1 (hCNT1) and role of adenosine on hCNT1 function. *J. Biol. Chem.* **279**: 8999-9007.

268. Smith, K. M., Ng, A. M., Yao, S. Y. M., Labedz, K. A., Knauss, E. E., Wiebe, L. I., Cass, C. E., Baldwin, S. A., Chen, X.-Z., Karpinski, E., and Young, J. D. (2004) Electrophysiological characterization of a recombinant human Na⁺-coupled nucleoside transporter (hCNT1) produced in *Xenopus* oocytes. *J. Physiol.* **558**: 807-823.
269. Yao, S. Y. M., Ng, A. M. L., Ritzel, M. W. L., Gati, W. P., Cass, C. E., and Young, J. D. (1996) Transport of adenosine by recombinant purine- and pyrimidine-selective sodium/nucleoside cotransporters from rat jejunum expressed in *Xenopus laevis* oocytes. *Mol. Pharmacol.* **50**: 1529-1535.
270. Yao, S. Y. M., Cass, C. E., and Young, J. D. (1996) Transport of the antiviral nucleoside analogs 3'-azido-3'-deoxythymidine and 2',3'-dideoxycytidine by a recombinant nucleoside transporter (rCNT1) expressed in *Xenopus laevis* oocytes. *Mol. Pharmacol.* **50**: 388-393.
271. Lostao, M. P., Mata, J. F., Larrayoz, I. M., Inzillo, S. M., Casado, F. J., and Pastor-Anglada, M. (2000) Electrogenic uptake of nucleosides and nucleoside-derived drugs by the human nucleoside transporter 1 (hCNT1) expressed in *Xenopus laevis* oocytes. *FEBS Lett.* **481**: 137-140.
272. Lang, T. T., Young, J. D., and Cass, C. E. (2004) Interactions of nucleoside analogs, caffeine, and nicotine with human concentrative nucleoside transporters 1 and 2 stably produced in a transport-defective human cell line. *Mol. Pharm.* **65**: 925-933.
273. Mata, J. F., Garcia-Manteiga, J. M., Lostao, M. P., Fernández-Veledo, S., Guillén-Gómez, E., Larrayoz, I. M., Lloberas, J., Casado, F. J., and Pastor-Anglada, M. (2001) Role of the human concentrative nucleoside transporter (hCNT1) in the cytotoxic action of 5'-deoxy-5-fluorouridine, an active intermediate metabolite of capecitabine, a novel oral anticancer drug. *Mol. Pharm.* **59**: 1542-1548.
274. Graham, K. A., Leithoff, J., Coe, I. R., Mowles, D., Mackey, J., R., Young, J. D., and Cass, C. E. (2000) Differential transport of cytosine-containing nucleosides by recombinant human concentrative nucleoside transporter protein hCNT1. *Nucleosides Nucleotides Nucleic Acids* **19**: 415-434.
275. Felipe, A., Valdes, R., Santo, B., Lloberas, J., Casado, J., and Pastor-Anglada, M. (1998) Na⁺-dependent nucleoside transport in liver: Two different isoforms

- from the same gene family are expressed in liver cells. *Biochem. J.* **330**: 997-1001.
276. Patil, S. D., and Unadkat, J. D. (1997) Sodium-dependent nucleoside transport in the human intestinal brush-border membrane. *Am. J. Physiol.* **272**: G1314-G1320.
277. Hamilton, S. R., Yao, S. Y., Ingram, J. C., Hadden, D. A., Ritzel, M. W., Gallagher, M. P., Henderson, P. J., Cass, C. E., Young, J. D., and Baldwin, S. A. (2001) Subcellular distribution and membrane topology of the mammalian concentrative Na⁺-nucleoside cotransporter, rCNT1. *J. Biol. Chem.* **276**: 27981-27988.
278. Mangravite, L. M., Lipschutz, J. H., Mostov, K. E., and Giacomini, K. M. (2001) Localization of GFP-tagged concentrative nucleoside transporters in a renal polarized epithelial cell line. *Am. J. Physiol. Renal Physiol.* **280**: F879-F885.
279. Anderson, C. M., Xiong, W., Young, J. D., Cass, C. E., and Parkinson, F. E. (1996) Demonstration of the existence of mRNAs encoding N1/*cif* and N2/*cit* sodium/nucleoside cotransporters in rat brain. *Mol. Brain Res.* **42**: 358-361.
280. Soler, C., Valdes, R., Garcia-Manteiga, J., Xaus, J., Comalada, M., Casado, E. J., Modolell, M., Nicholson, B., MacLeod, C., Felipe, A., Celada, A., and Pastor-Anglada, M. (2001) Lipopolysaccharide-induced apoptosis of macrophages determines the up-regulation of concentrative nucleoside transporters Cnt1 and Cnt2 through tumor necrosis factor-alpha-dependent and -independent mechanisms. *J. Biol. Chem.* **276**: 30043-30049.
281. Che, M., Ortiz, D. F., and Arias, I. M. (1995) Primary structure and functional expression of a cDNA encoding the bile canalicular, purine-specific Na⁺-nucleoside cotransporter. *J. Biol. Chem.* **270**: 13596-13599.
282. Wang, J., Su, S. F., Dresser, M. J., Schaner, M. E., Washington, C. B., and Giacomini, K. M. (1997) Na⁺-dependent purine nucleoside transporter from human kidney: cloning and functional characterization. *Am. J. Physiol.* **273**: F1058-F1065.
283. Ritzel, M. W. L., Yao, S. Y. M., Ng, A. M. L., Mackey, J. R., Cass, C. E., and Young, J. D. (1998) Molecular cloning, functional expression and chromosomal localization of a cDNA encoding a human Na⁺/nucleoside cotransporter

- (hCNT2) selective for purine nucleosides and uridine. *Mol. Membr. Biol.* **15**: 203-211.
284. Patel, D., Crawford, C., Naeve, C., and Belt, J. (1997) Molecular cloning and characterization of a mouse purine-selective concentrative nucleoside transporter. *Proc. Am. Assoc. Cancer Res.* **38**: 60.
285. Gerstin, K. M., Dresser, M. J., Wang, J., and Giacomini, K. M. (2000) Molecular cloning of a Na⁺-dependent nucleoside transporter from rabbit intestine. *Pharm. Res.* **17**: 906-910.
286. Owen, R. P., Gray, J. H., Taylor, T. R., Carlson, E. J., Huang, C. C., Kawamoto, M., Johns, S. J., Stryke, D., Ferrin, T. E., and Giacomini, K. M. (2005) Genetic analysis and functional characterization of polymorphisms in the human concentrative nucleoside transporter, CNT2. *Pharmacogenet. Genomics* **15**: 83-90.
287. Schaner, M. E., Wang, J., Zhang, L., Su, S. F., Gerstin, K. M., and Giacomini, K. M. (1999) Functional characterization of a human purine-selective, Na⁺-dependent nucleoside transporter (hSPNT1) in a mammalian expression system. *J. Pharm. Exp. Ther.* **289**: 1487-1491.
288. Gerstin, K., M., Dresser, M. J., and Giacomini, K. M. (2002) Specificity of human and rat orthologs of the concentrative nucleoside transporter, SPNT. *Am. J. Phys. Renal Phys.* **283**: F344-F349.
289. Lang, T. T., Selner, M., Young, J. D., and Cass, C. E. (2001) Acquisition of human concentrative nucleoside transporter 2 (hcnt2) activity by gene transfer confers sensitivity to fluoropyrimidine nucleosides in drug-resistance leukemia cells. *Mol. Pharmacol.* **60**: 1143-1152.
290. Li, J. Y., Boado, R. J., and Pardridge, W. M. (2001) Differential kinetics of transport of 2', 3'-dideoxyinosine and adenosine via concentrative Na⁺ nucleoside transporter CNT2 cloned from rat blood-brain barrier. *J. Pharm. Exp. Ther.* **299**: 735-740.
291. Larráyoz, I. M., Fernández-Nistal, A., Garcés, A. Gorraitz, E., and Lostao, M. P. (2006) Characterization of the rat Na⁺/nucleoside cotransporter 2 and transport of nucleoside-derived drugs using electrophysiological methods. *Am. J. Physiol. Cell Physiol.* **291**: C1395-C1404.

292. Leung, G. P., Ward, J. L., Wong, P. Y., and Tse, C. T. (2001) Characterization of nucleoside transport systems in cultured rat epididymal epithelium. *Am. J. Physiol. Cell. Physiol.* **280**: C1076-C1082.
293. Mangravite, L. M., and Giacomini, K. M. (2003) Sorting of rat SPNT in renal epithelium is independent of N-glycosylation. *Pharm. Res.* **20**: 319-323.
294. Duflot, S., Riera, B., Fernandez-Veledo, S., Casado, V., Norman, R. I., Casado, F. J., Lluís, C., Franco, R., and Pastor-Anglada, M. (2004) ATP-sensitive K⁺ channels regulate the concentrative adenosine transporter CNT2 following activation by A₁ adenosine receptors. *Mol. Cell Biol.* **24**: 2710-2719.
295. Ritzel, M. W. L., Ng, A. M. L., Yao, S. Y. M., Graham, K., Loewen, S. K., Smith, K. M., Ritzel, R. G., Mowles, D. A., Carpenter, P., Chen, X.-Z., Karpinski, E., Hyde, R. J., Baldwin, S. A., Cass, C. E., and Young, J. D. (2001) Molecular identification and characterization of novel human and mouse concentrative Na⁺-nucleoside cotransporter proteins (hCNT3 and mCNT3) broadly selective for purine and pyrimidine nucleosides (system *cib*). *J. Biol. Chem.* **276**: 2914-2927.
296. Toan, S. V., To, K. K., Leung, G. P., de Souza, M. O., Ward, J. L., and Tse, C. M. (2003) Genomic organization and functional characterization of the human concentrative nucleoside transporter-3 isoform (hCNT3) expressed in mammalian cells. *Pflugers Archiv.* **447**: 195-204.
297. Ritzel, M. W., Ng, A. M., Yao, S. Y., Graham, K., Loewen, S. K., Smith, K. M., Hyde, R. J., Karpinski, E., Cass, C. E., Baldwin, S. A., and Young, J. D. (2001) Recent molecular advances in studies of the concentrative Na⁺-dependent nucleoside transporter (CNT) family: identification and characterization of novel human and mouse proteins (hCNT3 and mCNT3) broadly selective for purine and pyrimidine nucleosides (system *cib*). *Mol. Memb. Biol.* **18**: 65-72.
298. Yao, S. Y., Ng, A. M., Loewen, S. K., Cass, C. E., Baldwin, S. A., and Young, J. D. (2002) An ancient prevertebrate Na⁺-nucleoside cotransporter (hfCNT) from the Pacific hagfish (*Eptatretus stouti*). *Am. J. Phys. Cell Phys.* **283**: C155-C168.
299. Badagnani, I., Chan, W., Castro, R. A., Brett, C. M., Huang, C. C., Stryke, D., Kawamoto, M., Johns, S. J., Ferrin, T. E., Carlson, E. J., Burchard, E. G., and Giacomini, K. M. (2005) Functional analysis of genetic variants in the human

- concentrative nucleoside transporter 3 (CNT3; SLC28A3). *Pharmacogenomics J.* **5**: 157-165.
300. Damaraju, V. L., Zhang, J., Visser, F., Tackaberry, T., Dufour, J., Smith, K. M., Slugoski, M. D., Ritzel, M. W., Baldwin, S. A., Young, J. D., and Cass, C. E. (2005) Identification and functional characterization of variants in human concentrative nucleoside transporter 3, hCNT3 (SLC28A3), arising from single nucleotide polymorphisms in coding regions of the hCNT3 gene. *Pharmacogenet. Genomics* **15**: 173-182.
301. Pajor, A. M., and Wright, E. M. (1992) Cloning and functional expression of a mammalian Na⁺/nucleoside cotransporter. A member of the SGLT family. *J. Biol. Chem.* **267**: 3557-3566.
302. Pajor, A. M. (1994) Molecular cloning and expression of SNST1, a renal sodium/nucleoside cotransporter. *Drug Dev. Res.* **31**: 305.
303. Hu, H., Endres, C. J., Chang, C., Umpathy, N. S., Lee, E. W., Fei, Y. J., Itagaki, S., Swann, P. W., Ganapathy, V., and Unadkat, J. D. (2006) Electrophysiological characterization and modeling of the structure activity relationship of the human concentrative nucleoside transporter 3 (hCNT3). *Mol. Pharmacol.* **69**: 1542-1553.
304. Mackey, J. R., Galmarini, C. M., Graham, K. A., Joy, A. A., Delmer, A., Dabbagh, L., Glubrecht, D., Jewell, L. D., Lai, R., Lang, T., Hanson, J., Young, J. D., Merle-Béral, H., Binet, J. L., Cass, C. E., and Dumontet, C. (2005) Quantitative analysis of nucleoside transporter and metabolism gene expression in chronic lymphocytic leukemia (CLL): identification of fludarabine-sensitive and -insensitive populations. *Blood* **105**: 767-774.
305. Elwi, A. N., Damaraju, V. L., Baldwin, S. A., Young, J. D., Sawyer, M. B., and Cass, C. E. (2006) Renal nucleoside transporters: physiological and clinical implications. *Biochem. Cell. Biol.* **84**: 844-858.
306. Xiao, G., Wang, J., Tangen, T., and Giacomini, K. M. (2001) A novel proton-dependent nucleoside transporter, CeCNT3, from *Caenorhabditis elegans*. *Mol. Pharmacol.* **59**: 339-348.
307. Loewen, S. K., Ng, A. M. L., Mohabir, N. M., Baldwin, S. A., Cass, C. E., and Young, J. D. (2003) Functional characterization of a H⁺/nucleoside cotransporter (CaCNT) from *Candida albicans*, a fungal member of the

concentrative nucleoside transporter (CNT) family of membrane proteins. *Yeast* **20**: 661-675.

308. Craig, J. E., Zhange, Y., and Gallagher, M. P. (1994) Cloning of the nupC gene of *Escherichia coli* encoding a nucleoside transport system, and identification of an adjacent insertion element, IS 186. *Mol. Micr.* **11**: 1159-1168.
309. Loewen, S. K., Yao, S. Y., Slugoski, M. D., Mohabir, N. N., Turner, R. J., Mackey, J. R., Gallagher, M. P., Henderson, P. J., Baldwin, S. A., Cass, C. E., and Young, J. D. (2004) Transport of physiological nucleosides and anti-viral and anti-neoplastic nucleoside drugs by recombinant *Escherichia coli* nucleoside-H⁺ cotransporter (NupC) produced in *Xenopus laevis* oocytes. *Mol. Membr. Biol.* **21**: 1-10.
310. Chen, R., and Nelson, A. J. (2000) Role of organic cation transporters in renal secretion of nucleosides. *Biochem. Pharmacol.* **60**: 215-219.
311. Hayer-Zillgen, M., Bruss, M., and Bonisch, H. (2002) Expression and pharmacological profile of the human organic cation transporters hOCT1, hOCT2, and hOCT3. *Brit. J. Pharmacol.* **136**: 829-836.
312. Takeda, M., Khamdang, S., Narikawa, S., Kimura, H., Kobayashi, Y., Yamamoto, T., Ho Cha, S., Sekine, T., and Endou, H. (2002) Human organic anion transporters and human organic cation transporters mediated renal antiviral transport. *J. Pharmacol. Exp. Ther.* **300**: 918-924.
313. Wright, S. H., Evans, K. K., Zhang, X., Cherrington, N. J., Sitar, D. S., and Dantzler, W. H. (2004) Functional map of TEA transport activity in isolated rabbit renal proximal tubules. *Am. J. Physiol. Renal Physiol.* **287**: F442-F451.
314. Bourdet, D. L., Pritchard, J. B., and Thakker, D. R. (2005) Differential substrate and inhibitory activities of rantidine and famotidine toward human organic cation transporter 1 (hOCT1; SLC22A1), hOCT2 (SLC22A2), and hOCT3 (SLC22A3). *J. Pharmacol. Exp. Ther.* **315**: 1288-1297.
315. Wright, S. H. (2005) Role of organic cation transporters in the renal handling of therapeutic agents and xenobiotics. *Toxicol. Appl. Pharmacol.* **204**: 309-319.

316. Zhang, L., Brett, C. M., and Giacomini, K. M. (1998) Role of organic cation transporters in drug absorption and elimination. *Annu. Rev. Pharmacol. Toxicol.* **38**: 431-460.
317. Chen, R., Jonker, J. W., and Nelson, J. A. (2002) Renal organic cation and nucleoside transport. *Biochem. Pharmacol.* **64**: 185-190.
318. Grudemann, D., Gorboulev, V., Gambaryan, S., Veyhl, M., and Koepsell, H. (1994) Drug excretion mediated by a new prototype of polyspecific transporter. *Nature* **372**: 549-552.
319. Schweifer, N., and Barlow, D. P. (1996) The Lx1 gene maps to mouse chromosome 17 and codes for a protein that is homologous to glucose and polyspecific transmembrane transporters. *Mamm. Genome* **7**: 735-740.
320. Gorboulev, V., Ulzheimer, J. C., Akhoundova, A., Ulzheimer-Teuber, I., Karbach, U., Quester, S., Baumann, C., Lang, F., Busch, A. E., and Koepsell, H. (1997) Cloning and characterization of two human polyspecific organic cation transporters. *DNA Cell Biol.* **16**: 871-881.
321. Zhang, L., Dresser, M. J., Gray, A. T., Yost, S. C., Terashita, S., and Giacomini, K. M. (1997) Cloning and functional expression of a human liver organic cation transporter. *Mol. Pharmacol.* **51**: 913-921.
322. Zhang, L., Dresser, M. J., Chun, J. K., Babbitt, P. C., and Giacomini, K. M. (1997) Cloning and functional characterization of a rat renal organic cation transporter isoform (rOCT1A). *J. Biol. Chem.* **272**: 16548-16554.
323. Sekine, T., Mihazaki, H., and Endou, H. (2006) Molecular physiology of renal organic anion transporters. *Am. J. Physiol. Renal Physiol.* **290**: F251-F261.
324. Lopez-Nieto, C. E., You, G., Bush, K. T., Barros, E. J., Beier, D. R., and Nigam, S. K. (1997) Molecular cloning and characterization of NKT, a gene product related to the organic cation transporter family that is almost exclusively expressed in the kidney. *J. Biol. Chem.* **272**: 6471-6478.
325. Sekine, T., Watanabe, N., Hosoyamada, M., Kanai, Y., and Endou, H. (1997) Expression cloning and characterization of a novel multispecific organic anion transporter. *J. Biol. Chem.* **272**: 18526-18529.

326. Sweet, D. H., Wolff, N. A., and Pritchard, J. B. (1997) Expression cloning and characterization of ROAT1. The basolateral organic anion transporter in rat kidney. *J. Biol. Chem.* **272**: 30088-30095.
327. Wolff, N. A., Werner, A., Burkhardt, S., and Burchhardt, G. (1997) Expression cloning and characterization of a renal organic anion transporter from winter flounder. *FEBS Lett.* **417**: 287-291.
328. Hosoyamada, M., Sekine, Y., Kanai, Y., and Endou, H. (1999) Molecular cloning and functional expression of a multispecific organic anion transporter from human kidney. *Am. J. Physiol.* **276**: F122-F128.
329. Kuze, K., Graves, P., Leahy, A., Wilson, P., Stuhlmann, H., and You, G. (1999) Heterologous expression and functional characterization of a mouse renal organic anion transporter in mammalian cells. *J. Biol. Chem.* **274**: 1519-1524.
330. Lu, R., Chan, B. S., and Schuster, V. L. (1999) Cloning of the human kidney PAH transporter: narrow substrate specificity and regulation by protein kinase C. *Am. J. Physiol.* **276**: F295-F303.
331. Simonson, G. D., Vincent, A. C., Roberg, K. J., Huang, Y., and Iwanij, V. (1994) Molecular cloning and characterization of a novel liver-specific transport protein. *J. Cell. Sci.* **107**: 1065-1072.
332. Sekine, T., Cha, S. H., Tsuda, M., Apiwattanakul, N., Nakajima, N., Kanai, Y., and Endou, H. (1998) Identification of multispecific organic anion transporter 2 expressed predominantly in the liver. *FEBS Lett.* **429**: 179-182.
333. Kusuhara, H., Sekine, T., Utsunomiya-Tate, N., Tsuda, M., Kojima, R., Cha, S. H., Sugiyama, Y., Kanai, Y., and Endou, H. (1999) Molecular cloning and characterization of a new multispecific organic anion transporter from rat brain. *J. Biol. Chem.* **274**: 13675-13680.
334. Race, J. E., Grassi, S. M., Williams, W. J., and Holtzman, E. J. (1999) Molecular cloning and characterization of two novel human renal organic anion transporters (hOAT1 and hOAT3). *Biochem. Biophys. Res. Commun.* **255**: 508-514.
335. Cha, S. H., Sekine, T., Fukushima, J. I., Kanai, Y., Kobayashi, Y., Goya, T., and Endou, H. (2001) Identification and characterization of human organic

- anion transporter 3 expressing predominantly in the kidney. *Mol. Pharmacol.* **59**: 1277-1286.
336. Cha, S. H., Sekine, T., Kusuhara, H., Yu, E., Kim, J. Y., Kim, D. K., Sugiyama, Y., Kanai, Y., and Endou, H. (2000) Molecular cloning and characterization of multispecific organic anion transporter 4 expressed in the placenta. *J. Biol. Chem.* **275**: 4507-4512.
337. Youngblood, G. L., and Sweet, D. H. (2004) Identification and functional assessment of the novel murine organic anion transporter Oat5 (Slc22a19) expressed in kidney. *Am. J. Physiol. Renal Physiol.* **287**: F236-F244.
338. Monte, J. C., Nagle, M. A., Eraly, S. A., and Nigam, S. K. (2004) Identification of a novel murine organic anion transporter family member, OAT6, expressed in olfactory mucosa. *Biochem. Biophys. Res. Commun.* **323**: 429-436.
339. Sekine, T., Cha, S. J., and Endou, H. (2000) The multispecific organic anion transporter (OAT) family. *Pflugers Arch.* **89**: 337-344.
340. Wada, S., Tsuda, M., Sekine, T., Cha, S. H., Kimura, M., Kanai, Y., and Endou, H. (2000) Rat multispecific organic anion transporter 1 (rOAT1) transports zidovudine, acyclovir, and other antiviral nucleoside analogs. *J. Pharmacol. Exp. Ther.* **294**: 844-849.
341. Kobayashi, Y., Ohshiro, N., Sakai, R., Ohbayashi, M., Kohyama, N., and Yamamoto, T. (2005) Transport mechanism and substrate specificity of human organic anion transporter 2 (hOat2 [SLC22A7]). *J. Pharm. Pharmacol.* **57**: 573-578.
342. Kobayashi, Y., Ohshiro, N., Tsuchiya, A., Kohyama, N., Ohbayashi, M., and Yamamoto, T. (2004) Renal transport of organic compounds mediated by mouse organic anion transporter 3 (mOat3): further substrate specificity of mOat3. *Drug Metab. Dispos.* **32**: 479-483.
343. Munch-Petersen, A., Mygind, B., Nicolaisen, A., and Pihl, N. J. (1979) Nucleoside transport in cells and membrane vesicles from *Escherichia coli* K12. *J. Biol. Chem.* **254**: 3730-3737.
344. Pao, S. S., Paulsen, I. T., and Saier, M. H., Jr. (1998) Major facilitator superfamily. *Microbiol. Mol. Biol. Rev.* **62**: 1-34.

345. West Hansen, S. E., Jensen, N., and Munch-Petersen, A. (1987) Studies on the sequence and structure of the *Escherichia coli* K-12 nupG gene, encoding a nucleoside-transport system. *Eur. J. Biochem.* **168**: 385-391.
346. Norholm, M. H., and Dandanell, G. (2001) Specificity and topology of the *Escherichia coli* xanthosine permease, a representative of the NHS subfamily of the major facilitator superfamily. *J. Bacteriol.* **183**: 4900-4904.
347. Xie, H., Patching, S. G., Gallagher, M. P., Litherland, G. J., Brough, A. R., Venter, H., Yao, S. Y., Ng, A. M., Young, J. D., Herbert, R. B., Henderson, P. J., and Baldwin, S. A. (2004) Purification and properties of the *Escherichia coli* nucleoside transporter NupG, a paradigm for a major facilitator transporter sub-family. *Mol. Membr. Biol.* **21**: 323-336.
348. Patching, S. G., Baldwin, S. A., Baldwin, A. D., Young, J. D., Gallagher, M. P., Henderson, P. J., and Herbert, R. B. (2005) The nucleoside transport proteins, NupC and NupG, from *Escherichia coli*: specific structural motifs necessary for the binding of ligands. *Org. Biomol. Chem.* **3**: 462-470.
349. Seeger, C., Poulsen, C., and Dandanell, G. (1995) Identification and characterization of genes (xapA, xapB, and xapR) involved in xanthosine catabolism in *Escherichia coli*. *J. Bacteriol.* **177**: 5506-5516.
350. Bremer, E., Middendorf, A., Martinussen, J., and Valentin-Hansen, P. (1990) Analysis of the tsx gene, which encodes a nucleoside-specific channel-forming protein (Tsx) in the outer membrane of *Escherichia coli*. *Gene* **96**: 59-65.
351. Nieweg, A., and Bremer, E. (1997) The nucleoside-specific Tsx channel from the outer membrane of *Salmonella typhimurium*, *Klebsiella pneumoniae* and *Enterobacter aerogenes*: functional characterization and DNA sequence analysis of the tsx genes. *Microbiol.* **143**: 603-615.
352. Hantke, K. (1976) Phage T6--colicin K receptor and nucleoside transport in *Escherichia coli*. *FEBS Lett.* **70**: 109-112.
353. Bucarey, S. A., Villagra, N. A., Marinic, M. P., Trombert, A. N., Santiviago, C. A., Maulen, N. P., Youderian, P., and Mora, G. C. (2005) The *Salmonella enterica* serovar Typhi tsx gene, encoding a nucleoside-specific porin, is essential for prototrophic growth in the absence of nucleosides. *Infect. Immun.* **73**: 6210-6219.

354. Maier, C., Bremer, E., Schmid, A., and Benz, R. (1988) Pore-forming activity of the Tsx protein from the outer membrane of *Escherichia coli*. Demonstration of a nucleoside-specific binding site. *J. Biol. Chem.* **263**: 2493-2499.
355. Fsihi, H., Kottwitz, B., and Bremer, E. (1993) Single amino acid substitutions affecting the substrate specificity of the *Escherichia coli* K-12 nucleoside-specific Tsx channel. *J. Biol. Chem.* **268**: 17495-17503.
356. Nikaido, H. (2003) Molecular basis of bacterial outer membrane permeability revisited. *Microbiol. Mol. Biol. Rev.* **67**: 593-656.
357. Inoue, T., Matsuzaki, S., and Tanaka, S. (1995) A 26-kDa outer membrane protein, OmpK, common to *Vibrio* species is the receptor for a broad-host-range vibriophage, KVP40. *FEMS Microbiol. Lett.* **125**: 101-105.
358. Inoue, T., Matsuzaki, S., and Tanaka, S. (1995) Cloning and sequence analysis of *Vibrio parahaemolyticus* ompK gene encoding a 26-kDa outer membrane protein, OmpK, that serves as receptor for a broad-host-range vibriophage, KVP40. *FEMS Microbiol. Lett.* **134**: 245-249.
359. Nandi, B., Nandy, R. K., Sarkar, A., and Ghose, A. C. (2005) Structural features, properties and regulation of the outer-membrane protein W (OmpW) of *Vibrio cholerae*. *Microbiology* **151**: 2975-2986.
360. Jund, R., Weber, E., and Chevallier, M. R. (1988) Primary structure of the uracil transport protein of *Saccharomyces cerevisiae*. *Eur. J. Biochem.* **171**: 417-424.
361. Jund, R., and Lacroute, F. (1970) Genetic and physiological aspects of resistance to 5-fluoropyrimidines in *Saccharomyces cerevisiae*. *J. Bacteriol.* **102**: 607-615.
362. Wagner, R., deMonigny, J., de Wergifosse, P., Souciet, J. L., and Potier, S. (1998) The ORF YBL042 of *Saccharomyces cerevisiae* encodes a uridine permease. *FEMS Microbiol. Lett.* **159**: 69-75.
363. Zhang, J., Smith, K. M., Tackaberry, T., Sun, X., Carpenter, P., Slugoski, M. D., Robins, M. J., Nielsen, L. P., Nowak, I., Baldwin, S. A., Young, J. D., and Cass, C. E. (2006) Characterization of the transport mechanism and permeant

binding profile of the uridine permease Fui1p of *Saccharomyces cerevisiae*. **281**: 28210-28221.

364. Detke, S. (1998) Cloning of the *Candida albicans* nucleoside transporter by complementation of nucleoside transport-deficient *Saccharomyces*. *Yeast* **14**: 1257-1265.
365. Chandrasena, G., Giltay, R., Patil, S. D., Bakken, A., and Unadkat, J. D. (1997) Functional expression of human intestinal Na⁺-dependent and Na⁺-independent nucleoside transporters in *Xenopus laevis* oocytes. *Biochem. Pharmacol.* **53**: 1909-1918.
366. Ngo, L. Y., Patil, S. D., and Unadkat, J. D. (2001) Ontogenic and longitudinal activity of Na⁺-nucleoside transporters in the human intestine. *Am. J. Physiol. Gastrointest. Liver Physiol.* **280**: G475-G481.
367. Pastor-Anglada, M., Errasti-Murugarren, E., Aymerich, I., and Casado, F. J. (2007) Concentrative nucleoside transporters (CNTs) in epithelia: from absorption to cell signaling. *J. Physiol. Biochem.* **63**: 97-110.
368. Pastor-Anglada, M., Casado, F. J., Valdes, R., Mata, J., Garcia-Manteiga, J., and Molina, M. (2001) Complex regulation of nucleoside transporter expression in epithelial and immune system cells. *Mol. Memb. Biol.* **18**: 81-85.
369. Vickers, M. F., Young, J. D., Baldwin, S. A., Mackey, J. R., and Cass, C. E. (2000) Nucleoside transporter proteins: emerging targets for drug discovery. *Emerg. Ther. Targets* **4**, 515-539.
370. Clarke, M. L., Mackey, J. R., Baldwin, S. A., Young, J. D., and Cass, C. E. (2002) The role of membrane transporters in cellular resistance to anticancer nucleoside drugs. *Cancer Treat. Res.* **112**: 27-47.
371. Galmarini, C. M., Mackey, J. R., and Dumontet, C. (2002) Nucleoside analogues and nucleobases in cancer treatment. *Lancet Oncol.* **3**: 415-424.
372. Pastor-Anglada, M., Cano-Soldado, R., Molina-Arcas, M., Lostao, M. P., Larrayoz, I., Martinez-Picado, J., and Casado, F. J. (2005) Cell entry and export of nucleoside analogues. *Virus Research* **107**: 151-164.

373. Gati, W. P., Paterson, A. R., Belch, A. R., Chlumecky, V., Larratt, L., M., Mant, M. J., and Turner, A. R. (1998) *Es* nucleoside transporter content of acute leukemia cells: role in cell sensitivity to cytarabine (araC). *Leuk. Lymph.* **32**: 45-54.
374. Achiwa, H., Oguri, T., Sato, S., Maeda, H., Niimi, T., and Ueda, R. (2004) Determinants of sensitivity and resistance to gemcitabine: the roles of human equilibrative nucleoside transporter 1 and deoxycytidine kinase in non-small cell lung cancer. *Cancer Sci.* **95**: 753-757.
375. Spratlin, J., Sangha, R., Glubrecht, D., Dabbagh, L., Young, J. D., Dumontet, C., Cass, C. E., Lai, R., and Mackey, J. R. (2004) The absence of human equilibrative nucleoside transporter 1 is associated with reduced survival in patients with gemcitabine-treated pancreas adenocarcinoma. *Clin. Cancer Res.* **10**: 6956-6961.
376. Stam, R. W., den Boer, M. L., Meijerink, J. P., Ebus, M. E., Peters, G. J., Noordhuis, P., Janka-Schaub, G. E., Armstrong, S. A., Korsmeyer, S. J., and Pieters, R. (2003) Differential mRNA expression of Ara-C-metabolizing enzymes explains Ara-C sensitivity in MLL gene-rearranged infant acute lymphoblastic leukemia. *Blood* **101**: 1271-1276.
377. Galmarini, C. M., Thomas, X., Calvo, F., Rousselot, P., Rabilloud, M., El Jaffari, A., Cros, E., and Dumontet, C. (2002) *In vivo* mechanisms of resistance to cytarabine in acute myeloid leukaemia. *Br. J. Haematol.* **117**: 860-868.
378. Giovannetti, E., del Tacca, M., Mey, V., Funel, N., Nannizzi, S., Ricci, S., Orlandini, C., Boggi, U., Campani, D., del Chiaro, M., Iannopollo, M., Bevelacqua, G., Mosca, F., and Danesi, R. (2006) Transcription analysis of human equilibrative nucleoside transporter-1 predicts survival in pancreas cancer patients treated with gemcitabine. *Cancer Res.* **66**: 3928-3935.
379. Reiman, T., Clarke, M. L., Dabbagh, L., Vsianska, M., Coupland, R. W., Belch, A. R., Baldwin, S. A., Young, J. D., Cass, C., E., and Mackey, J. R. (2002) Differential expression of human equilibrative nucleoside transporter 1 (hENT1) protein in the Reed-Sternberg cells of Hodgkins' disease. *Leuk. Lymph.* **43**: 1435-1440.
380. Agarwal, R. P., and Olivero, O. A. (1997) Genotoxicity and mitochondrial damage in human lymphocytic cells chronically exposed to 3'-azido-2', 3'-dideoxythymidine. *Mutat. Res.* **390**: 223-231.

381. McKenzie, R., Fried, M. W., Sallie, R., Conjeevaram, H., Di Bisceglie, A. M., Park, Y., Savarese, B., Kleiner, D., Tsokos, M., Luciano, C., Pruett, T., Stotka, J. L., Straus, S. E., and Hoofnagle, J. H. (1995) Hepatic failure and lactic acidosis due to fialuridine (FIAU), an investigational nucleoside analogue for chronic hepatitis B. *N. Engl. J. Med.* **333**: 1099-1105.
382. Horn, D. M., Neeb, L. A., Colacino, J. M., and Richardson, F. C. (1997) Fialuridine is phosphorylated and inhibits DNA synthesis in isolated rat hepatic mitochondria. *Antiviral Res.* **34**: 71-74.
383. Genini, D., Adachi, S., Chao, Q., Rose, D. W., Carrera, C. J., Cottam, H. B., Carson, D. A., and Leoni, L. M. (2000) Deoxyadenosine analogs induce programmed cell death in chronic lymphocytic leukemia cells by damaging the DNA and by directly affecting the mitochondria. *Blood* **96**: 3537-3543.
384. Walker, U. A., Setzer, B., and Volksbeck, S. I. (2000) Toxicity of nucleoside-analogue reverse-transcriptase inhibitors. *Lancet.* **355**: 1096.
385. White, A. J. (2001) Mitochondrial toxicity and HIV therapy. *Sex. Transm. Infect.* **77**: 158-173.
386. Feng, J. Y., Johnson, A. A., Johnson, K. A., and Anderson, K. S. (2001) Insights into the molecular mechanism of mitochondrial toxicity by AIDS drugs. *J. Biol. Chem.* **276**: 23832-23837.
387. Cass, C. E., King, K. M., Montano, J. T., and Janowska-Wieczorek, A. (1992) A comparison of the abilities of nitrobenzylthioinosine, dilazep, and dipyridamole to protect human hematopoietic cells from 7-deazaadenosine (tubercidin). *Cancer Res.* **52**: 5879-5886.
388. Wright, A. M., Gati, W. P., and Paterson, A. R. (2000) Enhancement of retention and cytotoxicity of 2-chlorodeoxyadenosine in cultured human leukemic lymphoblasts by nitrobenzylthioinosine, an inhibitor of equilibrative nucleoside transport. *Leukemia* **14**: 52-60.
389. Huang, M., Wang, Y., Cogut, S. B., Mitchell, B. S., and Graves, L. M. (2003) Inhibition of nucleoside transport by protein kinase inhibitors. *J. Pharmacol. Exp. Ther.* **304**: 753-760.

390. de Koning, H. P., Bridges, D. J., and Burchmore, R. J. (2005) Purine and pyrimidine transport in pathogenic protozoa: From biology to therapy. *FEMS Microbiology Reviews* **29**: 987-1020.
391. Huang, Y., Lemieux, M. J., Song, J., Auer, M., and Wang, D. N. (2003) Structure and mechanism of the glycerol-3-phosphate transporter from *Escherichia coli*. *Science* **301**: 616-620.
392. Abramson, J., Smirnova, I., Kasho, V., Verner, G., Kaback, H. R., and Iwata, S. (2003) Structure and mechanism of the lactose permease of *Escherichia coli*. *Science* **301**: 610-605.
393. Yernool, D., Boudker, O., Jin, Y., and Gouaux, E. (2004) Structure of a glutamate transporter homologue from *Pyrococcus horikoshii*. *Nature* **431**: 811-818.
394. Yamashita, A., Singh, S. K., Kawate, T., Jin, Y., and Gouaux, E. (2005) Crystal structure of a bacterial homologue of Na⁺/Cl⁻-dependent neurotransmitter transporters. *Nature* **437**: 215-223.
395. Sundaram, M., Yao, S. Y., Ng, A. M., Griffiths, M., Cass, C. E., Baldwin, S. A., and Young, J. D. (1998) Chimeric constructs between human and rat equilibrative nucleoside transporters (hENT1 and rENT1) reveal hENT1 structural domains interacting with coronary vasoactive drugs. *J. Biol. Chem.* **273**: 21519-21525.
396. Sundaram, M., Yao, S. Y., Ng, A. M., Cass, C. E., Baldwin, S. A., and Young, J. D. (2001) Equilibrative nucleoside transporters: mapping regions of interaction for the substrate analogue nitrobenzylthioinosine (NBMPR) using rat chimeric proteins. *Biochemistry* **40**: 8146-8151.
397. Visser, F., Zhang, J., Raborn, R. T., Baldwin, S. A., Young, J. D., and Cass, C. E. (2005) Residue 33 of human equilibrative nucleoside transporter 2 is a functionally important component of both the dipyridamole and nucleoside binding sites. *Mol. Pharmacol.* **67**: 1291-1298.
398. SenGupta, D. J., and Unadkat, J. D. (2004) Glycine 154 of the equilibrative nucleoside transporter, hENT1, is important for nucleoside transport and for conferring sensitivity to the inhibitors nitrobenzylthioinosine, dipyridamole, and dilazep. *Biochem. Pharmacol.* **67**: 453-458.

399. Yao, S. Y. M., Sundaram, M., Chomey, E. G., Cass, C. E., Baldwin, S. A., and Young, J. D. (2001) Identification of Cys₁₄₀ in helix 4 as an exofacial cysteine residue within the substrate-translocation channel of rat equilibrative nitrobenzylthionosine (NBMPR)-insensitive (ENT2) nucleoside transporter rENT2. *Biochem. J.* **353**: 387-393.
400. SenGupta, D. J., Lum, P. Y., Lai, Y. R., Shubochkina, E., Bakken, A. H., Schneider, G., and Unadkat, J. D. (2002) A single glycine mutation in the equilibrative nucleoside transporter gene, hENT1, alters nucleoside transport activity and sensitivity to nitrobenzylthioinosine. *Biochemistry* **41**: 1512-1519.
401. Endres, C. J., SenGupta, D. J., and Unadkat, J. D. (2004) Mutation of leucine-92 selectively reduces the apparent affinity of inosine, guanosine, NBMPR [*S*⁶-(4-nitrobenzyl)-mercaptapurine riboside] and dilazep for the human equilibrative nucleoside transporter, hENT1. *Biochem. J.* **380**: 131-137.
402. Endres, C. J., and Unadkat, J. D. (2005) Residues Met89 and Ser160 in the human equilibrative nucleoside transporter 1 affect its affinity for adenosine, guanosine, *S*⁶-(4-Nitrobenzyl)-mercaptapurine riboside, and dipyridamole. *Mol. Pharm.* **67**: 837-844.
403. Visser, F., Sun, L., Damaraju, V., Tackaberry, T., Peng, Y., Robins, M. J., Baldwin, S. A., Young, J. D., and Cass, C. E. (2007) Residues 334 and 338 in transmembrane segment 8 of human equilibrative nucleoside transporter 1 are important determinants of inhibitor sensitivity, protein folding, and catalytic turnover. *J. Biol. Chem.* **282**: 14148-14157.
404. Vickers, M. F., Kumar, R., Visser, F., Zhang, J., Charania, J., Raborn, R. T., Baldwin, S. A., Young, J. D., and Cass, C. E. (2002) Comparison of the interaction of uridine, cytidine, and other pyrimidine nucleoside analogues with recombinant human equilibrative nucleoside transporter 2 (hENT2) produced in *Saccharomyces cerevisiae*. *Biochem. Cell Biol.* **80**: 639-644.
405. Vickers, M. F., Zhang, J., Visser, F., Tackaberry, T., Robins, M. J., Nielsen, L. P., Nowak, I., Baldwin, S. A., Young, J. D., and Cass, C. E. (2004) Uridine recognition motifs of human equilibrative nucleoside transporters 1 and 2 produced in *Saccharomyces cerevisiae*. *Nucleosides Nucleotides Nucleic Acids* **23**: 361-373.

406. Chang, C., Swaan, P. W., Ngo, L. Y., Lum, P. Y., Patil, S. D., and Unadkat, J. D. (2004) Molecular requirements of the human nucleoside transporters hCNT1, hCNT2, and hENT1. *Mol. Pharmacol.* **65**: 558-570.
407. Vasudeven, G., Ullman, B., and Landfear, S. M. (2001) Point mutations in a nucleoside transporter gene from *Leishmania donovani* confer drug resistance and alter substrate selectivity. *Proc. Natl. Acad. Sci. USA* **98**: 6092-6097.
408. Arastu-Kapur, S., Arendt, C. S., Purnat, T., Carter, N. S., and Ullman, B. (2005) Second-site suppression of a nonfunctional mutation within the *Leishmania donovani* inosine-guanosine transporter. *J. Biol. Chem.* **280**: 2213-2219.
409. Galazka, J., Carter, N. S., Bekhouche, S., Arastu-Kapur, S., and Ullman, B. (2006) Point mutations within the LdNT2 nucleoside transporter gene from *Leishmania donovani* confer drug resistance and transport deficiency. *Int. J. Biochem. Cell. Biol.* **38**: 1221-1229.
410. Arastu-Kapur, S., Ford, E., Ullman, B., and Carter, N. S. (2003) Functional analysis of an inosine-guanosine transporter from *Leishmania donovani*. The role of conserved residues, aspartate 389 and arginine 393. *J. Biol. Chem.* **278**: 33327-33333.
411. Valdes, R., Vasudevan, G., Conklin, D., and Landfear, S. M. (2004) Transmembrane domain 5 of the LdNT1.1 nucleoside transporter is an amphipathic helix that forms part of the nucleoside translocation pathway. *Biochemistry* **43**: 6793-6802.
412. Valdes, R., Liu, W., Ullman, B., and Landfear, S. M. (2006) Comprehensive examination of charged intramembrane residues in a nucleoside transporter. *J. Biol. Chem.* **281**: 22647-22655.
413. Visser, F., Baldwin, S. A., Isaac, R. E., Young, J. D., and Cass, C. E. (2005) Identification and mutational analysis of amino acid residues involved in dipyridamole interactions with human and *Caenorhabditis elegans* equilibrative nucleoside transporters. *J. Biol. Chem.* **280**: 11025-11034.
414. Papageorgiou, I., de Koning, H. P., Soteriadou, K., and Diallinas, G. (2007) Kinetic and mutational analysis of the *Trypanosoma brucei* NBT1 nucleobase transporter expressed in *Saccharomyces cerevisiae* reveals structural similarities between ENT and MFS transporters. *Int. J. Parasitol.* (epub ahead of print).

415. Wang, J., and Giacomini, K. M. (1997) Molecular determinants of substrate selectivity in Na⁺-dependent nucleoside transporters. *J. Biol. Chem.* **272**: 18026-18032.
416. Wang, J., and Giacomini, K. M. (1999) Characterization of a bioengineered chimeric Na⁺-nucleoside transporter. *Mol. Pharmacol.* **55**: 234-240.
417. Wang, J., and Giacomini, K. M. (1999) Serine 318 is essential for the pyrimidine selectivity of the N2 Na⁺-nucleoside transporter. *J. Biol. Chem.* **274**: 2298-2302.
418. Loewen, S. K., Ng, A. M., Yao, S. Y., Cass, C. E., Baldwin, S. A., and Young, J. D. (1999) Identification of amino acid residues responsible for the pyrimidine and purine nucleoside specificities of human concentrative Na⁺ nucleoside cotransporters hCNT1 and hCNT2. *J. Biol. Chem.* **274**: 24475-24484.
419. Lai, Y., Lee, E. W., Ton, C. C., Vijay, S., Zhang, H., and Unadkat, J. D. (2005) Conserved residues F316 and G476 in the concentrative nucleoside transporter 1 (hCNT1) affect guanosine sensitivity and membrane expression, respectively. *Am. J. Physiol. Cell Physiol.* **288**: C39-C45.
420. Yao, S. Y. M., Ng, A. M., Slugoski, M. D., Smith, K. M., Mulinta, R., Karpinski, E., Cass, C. E., Baldwin, S. A., and Young, J. D. (2007) Conserved glutamate residues are critically involved in Na⁺/nucleoside cotransport by human concentrative nucleoside transporter 1 (hCNT1). *J. Biol. Chem.* **282**: 30607-30617.
421. Zhang, J., Tackaberry, T., Ritzel, M. W., Raborn, T., Barron, G., Baldwin, S. A., Young, J. D., and Cass, C. E. (2006) Cysteine-accessibility analysis of transmembrane domains 11-13 of human concentrative nucleoside transporter 3. *Biochem. J.* **394**: 389-398.
422. Errasti-Murugarren, E., Cano-Soldado, P., Pastor-Anglada, M., and Casado, F. J. (2008) Functional characterization of a nucleoside-derived drug transporter variant (hCNT3C602R) showing altered sodium-binding capacity. *Mol. Pharmacol.* **73**: 379-386.
423. Patil, S. D., Ngo, L. Y., and Undadkat, J. D. (2000) Structure-inhibitory profiles of nucleosides for the human intestinal N1 and N2 Na⁺-nucleoside transporters. *Cancer Chemother. Pharmacol.* **46**: 394-402.

424. Zhang, J., Visser, F., Vickers, M. F., Lang, T., Robins, M. J., Nielsen, L. P., Nowak, I., Baldwin, S. A., Young, J. D., and Cass, C. E. (2003) Uridine binding motifs of human concentrative nucleoside transporters 1 and 3 produced in *Saccharomyces cerevisiae*. *Mol. Pharmacol.* **64**: 1512-1520.
425. Zhang, J., Smith, K. M., Tackaberry, T., Visser, F., Robins, M. J., Nielsen, L. P., Nowak, I., Karpinski, E., Baldwin, S. A., Young, J. D., and Cass, C. E. (2005) Uridine binding and transportability determinants of human concentrative nucleoside transporters. *Mol. Pharmacol.* **68**: 830-839.
426. Widdas, W. F. (1952) Inability of diffusion to account for placental glucose transfer in the sheep and consideration of the kinetics of a possible carrier transfer. *J. Physiol.* **118**: 23-39.
427. Slugoski, M. D., Loewen, S. K., Ng, A. M., Baldwin, S. A., Cass, C. E., and Young, J. D. (2004) Allelic isoforms of the H⁺/nucleoside co-transporter (CaCNT) from *Candida albicans* reveal separate high- and low-affinity transport systems for nucleosides. *Yeast* **21**: 1269-1277.
428. Slugoski, M. D., Loewen, S. K., Ng, A. M., Smith, K. M., Yao, S. Y., Karpinski, E., Cass, C. E., Baldwin, S. A., and Young, J. D. (2007) Specific mutations in transmembrane helix 8 of human concentrative Na⁺/nucleoside cotransporter hCNT1 affect permeant selectivity and cation coupling. *Biochemistry* **46**: 1684-1693.
429. Smith, K. M., Slugoski, M. D., Loewen, S. K., Ng, A. M., Yao, S. Y., Chen, X.-Z., Karpinski, E., Cass, C. E., Baldwin, S. A., and Young, J. D. (2005) The broadly selective human Na⁺/nucleoside cotransporter (hCNT3) exhibits novel cation-coupled nucleoside transport characteristics. *J. Biol. Chem.* **280**: 25436-25449.
430. Smith, K. M., Slugoski, M. D., Cass, C. E., Baldwin, S. A., Karpinski, E., and Young, J. D. (2007) Cation coupling properties of human concentrative nucleoside transporters hCNT1, hCNT2 and hCNT3. *Mol. Membr. Biol.* **24**: 53-64.
431. Slugoski, M. D., Ng, A. M., Yao, S. Y., Smith, K. M., Lin, C. C., Zhang, J., Karpinski, E., Cass, C. E., and Baldwin, S. A., and Young, J. D. (2008) A proton-mediated conformational shift identifies a mobile pore-lining cysteine residue (Cys-561) in human concentrative nucleoside transporter 3. *J. Biol. Chem.* (epub ahead of print).

432. Barrett, M. P., Zhang, Z. Q., Denise, H., Giroud, C., and Baltz, T. (1995) A diamidine-resistant *Trypanosoma equiperdum* clone contains a P2 purine transporter with reduced substrate affinity. *Mol. Biochem. Parasitol.* **73**: 223-229.
433. Urakami, Y., Akazawa, M., Saito, H., Okuda, M., and Inui, K. (2002) cDNA cloning, functional expression, and tissue distribution of an alternatively spliced variant of organic cation transporter hOCT2 predominantly expressed in the human kidney. *J. Am. Soc. Nephrol.* **13**: 1703-1710.
434. Nishiwaki, T., Daigo, Y., Tamari, M., Fujii, Y., and Nakamura, Y. (1998) Molecular cloning, mapping, and characterization of two novel human genes, ORCTL3 and ORCTL4, bearing homology to organic-cation transporters. *Cytogenet. Cell Genet.* **83**: 251-255.
435. Tamai, I., Yabuuchi, H., Nezu, J., Sai, Y., Oku, A., Shimane, M., and Tsuji, A. (1997) Cloning and characterization of a novel human pH-dependent organic cation transporter, OCTN1. *FEBS Lett.* **419**: 107-111.
436. Tamai, I., Ohashi, R., Nezu, J.-I., Yabuuchi, H., Oku, A., Shimane, M., Sai, Y., and Tsuji, A. (1998) Molecular and functional identification of sodium ion-dependent, high affinity human carnitine transporter OCTN2. *J. Biol. Chem.* **273**: 20378-20382.
437. Wu, X., Prasad, P. D., Leibach, J. H., and Ganapathy, V. (1998) cDNA sequence, transport function, and genomic organization of human OCTN2, a new member of the organic cation transporter family. *Biochem. Biophys. Res. Commun.* **246**: 589-595.
438. Wagner, C. A., Lukewille, U., Kaltenbach, S., Moschen, I., Broer, A., Risler, T., Broer, S., and Lang, F. (2000) Functional and pharmacological characterization of human Na⁺-carnitine cotransporter hOCTN2. *Am. J. Physiol. Renal Physiol.* **279**: F584-F591.
439. Okuda, M., Saito, H., Urakami, Y., Takano, M., and Inui, K. (1996) cDNA cloning and functional expression of a novel rat kidney organic cation transporter, OCT2. *Biochem. Biophys. Res. Commun.* **224**: 500-507.
440. Kekuda, R., Prasad, P. D., Wu, X., Wang, H., Fei, Y. J., Leibach, F. H., and Ganapathy, V. (1998) Cloning and functional characterization of a potential-

sensitive, polyspecific organic cation transporter (OCT3) most abundantly expressed in placenta. *J. Biol. Chem.* **273**: 15971-15979.

441. Wu, X., George, R. L., Huang, W., Wang, H., Conway, S. J., Leibach, F. H., and Ganapathy, V. (2000) Structural and functional characteristics and tissue distribution pattern of rat OCTN1, an organic cation transporter, cloned from placenta. *Biochim. Biophys. Acta.* **1466**: 315-327.
442. Wu, X., Huang, W., Prasad, P. D., Seth, P., Rajan, D. P., Leibach, F. H., Chen, J., Conway, S. J., and Ganapathy, V. (1999) Functional characteristics and tissue distribution pattern of organic cation transporter 2 (OCTN2), an organic cation/carnitine transporter. *J. Pharmacol. Exp. Ther.* **290**: 1482-1492.
443. Mooslehner, K. A., and Allen, N. D. (1999) Cloning of the mouse organic cation transporter 2 gene, Slc22a2, from an enhancer-trap transgene integration locus. *Mamm. Genome* **10**: 218-224.
444. Verhaagh, S., Schweifer, N., Barlow, D. P., and Zwart, R. (1999) Cloning of the mouse and human solute carrier 22a3 (Slc22a3/SLC22A3) identifies a conserved cluster of three organic cation transporters on mouse chromosome 17 and human 6q26-q27. *Genomics* **55**: 209-218.
445. Tamai, I., Ohashi, R., Nezu, J. I., Sai, Y., Kobayashi, D., Oku, A., Shimane, M., and Tsuji, A. (2000) Molecular and functional characterization of organic cation/carnitine transporter family in mice. *J. Biol. Chem.* **275**: 40064-40072.
446. Terashita, S., Dresser, M. J., Zhang, L., Gray, A. T., Yost, S. C., and Giacomini, K. M. (1998) Molecular cloning and functional expression of a rabbit renal organic cation transporter. *Biochim. Biophys. Acta* **1369**: 1-6.
447. Zhang, X., Evans, K. K., and Wright, S. H. (2002) Molecular cloning of rabbit organic cation transporter rbOCT2 and functional comparisons with rbOCT1. *Am. J. Physiol. Renal Physiol.* **283**: F124-F133.
448. Grundemann, D., Babin-Ebell, J., Martel, F., Ording, N., Schmidt, A., and Schomig, E. (1997) Primary structure and functional expression of the apical organic cation transporter from kidney epithelial LLC-PK1 cells. *J. Biol. Chem.* **272**: 10408-10413.

449. Wu, X., Fei, Y. J., Huang, W., Chancy, C., Leibach, F. H., and Ganapathy, V. (1999) Identity of the F52F12.1 gene product in *Caenorhabditis elegans* as an organic cation transporter. *Biochim. Biophys. Acta* **1418**: 239-244.
450. Taylor, C. A., Stanley, K. N., and Shirras, A. D. (1997) The Orct gene of *Drosophila melanogaster* codes for a putative organic cation transporter with six or 12 transmembrane domains. *Gene* **201**: 69-74.
451. Torres, G. A., Lelandais-Briere, C., Besin, E., Jubier, M. F., Roche, O., Mazubert, C., Corre-Menguy, F., and Hartmann, C. (2003) Characterization of the expression of *Phaseolus vulgaris* OCT1, a dehydration-regulated gene that encodes a new type of phloem transporter. *Plant Mol. Biol.* **51**: 341-349.
452. Anzai, N., Kanai, Y., and Endou, H. (2006) Organic anion transporter family: current knowledge. *J. Pharmacol. Sci.* **100**: 411-426.
453. Bakhiya, A., Bahn, A., Burckhardt, G., and Wolff, N. (2003) Human organic anion transporter 3 (hOAT3) can operate as an exchanger and mediate secretory urate flux. *Cell Physiol. Biochem.* **13**: 249-256.
454. Ekaratanawong, S., Anzai, N., Jutabha, P., Miyazaki, H., Noshiro, R., Takeda, M., Kanai, Y., Sophasan, S., and Endou, H. (2004) Human organic anion transporter 4 is a renal apical organic anion/dicarboxylate exchanger in the proximal tubules. *J. Pharmacol. Sci.* **94**: 297-304.
455. Sun, W., Wu, R. R., van Poelje, P. D., and Erion, M. D. (2001) Isolation of a family of organic anion transporters from human liver and kidney. *Biochem. Biophys. Res. Commun.* **283**: 417-422.
456. Enomoto, A., Kimura, H., Chairoungdua, A., Shigeta, Y., Jutabha, P., Cha, S. H., Hosoyamada, M., Takeda, M., Sekine, T., Igarashi, T., Matsuo, H., Kikuchi, Y., Oda, T., Ichida, K., Hosoya, T., Shimokata, K., Niwa, T., Kanai, Y., and Endou, H. (2002) Molecular identification of a renal urate anion exchanger that regulates blood urate levels. *Nature* **417**: 447-452.
457. Sweet, D. H., Chan, L. M., Walden, R., Yang, X. P., Miller, D. S., and Pritchard, J. B. (2003) Organic anion transporter 3 (Slc22a8) is a dicarboxylate exchanger indirectly coupled to the Na⁺ gradient. *Am. J. Physiol. Renal Physiol.* **284**: F763-F769.

458. Anzai, N., Jutabha, P., Enomoto, A., Yokoyama, H., Nonoguchi, H., Hirata, T., Shiraya, K., He, X., Cha, S. H., Takeda, M., Miyazaki, H., Sakata, T., Tomita, K., Igarashi, T., Kanai, Y., and Endou, H. (2005) Functional characterization of rat organic anion transporter 5 (Slc22a19) at the apical membrane of renal proximal tubules. *J. Pharmacol. Exp. Ther.* **315**: 534-544.
459. Hosoyamada, M., Ichida, K., Enomoto, A., Hosoya, T., and Endou, H. (2004) Function and localization of urate transporter 1 in mouse kidney. *J. Am. Soc. Nephrol.* **15**: 261-268.
460. Hagos, Y., Bahn, A., Asif, A. R., Krick, W., Sandler, M., and Burckhardt, G. (2002) Cloning of the pig renal organic anion transporter 1 (pOAT1). *Biochimie.* **84**: 1221-1224.
461. Hagos, Y., Braun, I. M., Krick, W., Burckhardt, G., and Bahn, A. (2005) Functional expression of pig renal organic anion transporter 3 (pOAT3). *Biochimie.* **87**: 421-424.
462. George, R. L., Wu, X., Huang, W., Fei, Y. J., Leibach, F. H., and Ganapathy, V. (1999) Molecular cloning and functional characterization of a polyspecific organic anion transporter from *Caenorhabditis elegans*. *J. Pharmacol. Exp. Ther.* **291**: 596-603.
463. Bucarey, S. A., Villagra, N. A., Fuentes, J. A., and Mora, G. C. (2006) The cotranscribed *Salmonella enterica* sv. Typhi tsx and impX genes encode opposing nucleoside-specific import and export proteins. *Genetics* **173**: 25-34.
464. Mao, Z., Yu, L., You, Z., Wei, Y., and Liu, Y. (2007) Cloning, expression and immunogenicity analysis of five outer membrane proteins of *Vibrio parahaemolyticus* zj2003. *Fish Shellfish Immunol.* **23**: 567-575.
465. Sperandio, V., Bailey, C., Giron, J. A., DiRita, V. J., Silveira, W. D., Vettore, A. L., and Kaper, J. B. (1996) Cloning and characterization of the gene encoding the OmpU outer membrane protein of *Vibrio cholerae*. *Infect. Immun.* **64**: 5406-5409.
466. Li, C. C., Crawford, J. A., DiRita, V. J., and Kaper, J. B. (2000) Molecular cloning and transcriptional regulation of ompT, a ToxR-repressed gene in *Vibrio cholerae*. *Mol. Microbiol.* **35**: 189-203.

467. Stevenson, G., Leavesley, D. I., Lagnado, C. A., Heuzenroeder, M. W., and Manning, P. S. (1985) Purification of the 25-kDa *Vibrio cholerae* major outer-membrane protein and the molecular cloning of its gene: ompV. *Eur. J. Biochem.* **148**: 385-390.
468. Aeckersberg, F., Lupp, C., Feliciano, B., and Ruby, E. G. (2001) *Vibrio fischeri* outer membrane protein OmpU plays a role in normal symbiotic colonization. *J. Bacteriol.* **183**: 6590-6597.
469. Yoo, H. S., Cunningham, T. S., and Cooper, T. G. (1992) The allantoin and uracil permease gene sequences of *Saccharomyces cerevisiae* are nearly identical. *Yeast* **8**: 997-1006.
470. Enjo, F., Nosaka, K., Ogata, M., Iwashima, A., and Nishimura, H. (1997) Isolation and characterization of a thiamin transport gene, THI10, from *Saccharomyces cerevisiae*. *J. Biol. Chem.* **272**: 19165-19170.
471. Weber, E., Rodriguez, C., Chevallier, M. R., and Jund, R. (1990) The purine-cytosine permease gene of *Saccharomyces cerevisiae*: primary structure and deduced protein sequence of the FCY2 gene product. *Mol. Microbiol.* **4**: 585-596.
472. de Montigny, J., Straub, M. L., Wagner, R., Bach, M. L., and Chevallier, M. R. (1998) The uracil permease of *Schizosaccharomyces pombe*: a representative of a family of 10 transmembrane helix transporter proteins of yeast. *Yeast* **14**: 1051-1059.
473. Danielsen, S., Kilstrup, M., Barilla, K., Jochimsen, B., and Neuhard, J. (1992) Characterization of the *Escherichia coli* codBA operon encoding cytosine permease and cytosine deaminase. *Mol Microbiol.* **6**: 1335-1344.
474. Desimone, M., Catoni, E., Ludewig, U., Hilpert, M., Schneider, A., Kunze, R., Tegeder, M., Frommer, W. B., and Schumacher, K. (2002) A novel superfamily of transporters for allantoin and other oxo derivatives of nitrogen heterocyclic compounds in *Arabidopsis*. *Plant Cell* **14**: 847-856.
475. Schmidt, A., Su, Y. H., Kunze, R., Warner, S., Hewitt, M., Slocum, R. D., Ludewig, U., Frommer, W. B., and Desimone, M. (2004) UPS1 and UPS2 from *Arabidopsis* mediate high affinity transport of uracil and 5-fluorouracil. *J. Biol. Chem.* **279**: 44817-44824.

476. Pelissier, H. C., Frerich, A., Desimone, M., Schumacher, K., and Tegeder, M. (2004) PvUPS1, an allantoin transporter in nodulated roots of French bean. *Plant Physiol.* **134**: 664-675.

Chapter 2:
Experimental Procedures

***Xenopus laevis* Oocyte Expression System**

The *Xenopus laevis* oocyte heterologous expression system was fundamental to the initial cloning and characterization of both human and other mammalian ENT and CNT nucleoside transport proteins and is the expression system used in all of the experiments described in this thesis. The key advantage of *Xenopus* oocytes over other heterologous expression systems is that they lack, or have insignificant, endogenous nucleoside transport activity (1-3). For example, a putative *Xenopus* CNT protein of 645 amino acids (GenBank™ accession number NP_001086782) has been identified by genomic sequencing (4), but is not functionally expressed in oocytes. Oocytes therefore provide a powerful experimental vehicle to produce and functionally characterize recombinant nucleoside transport proteins in the absence of other competing transport processes with potentially overlapping permeant preferences (5). In radiolabeled flux experiments, the slow non-mediated uptake of nucleosides that occurs in oocytes by simple diffusion across the lipid bilayer is readily identified by measuring uptake in control water-injected oocytes. The cDNA encoding human and rodent CNT1, CNT2 and CNT3 were all initially cloned and characterized in *Xenopus* oocytes (2, 6-11).

Xenopus oocytes robustly translate injected exogenous mRNA and are capable of post-translational protein modifications (12). Disadvantages of the *Xenopus* oocyte system include the requirement for *in vitro* cDNA transcription to produce mRNAs for the cloned transport proteins, although direct injection of cDNA into the oocyte nucleus is also possible, but less frequently employed. Therefore, there is the possibility of RNA degradation and resultant variability of expression. Also, there is the possibility of species differences arising from the use of amphibian oocytes to study mammalian proteins, particularly with respect to post-translational processing of membrane proteins (3). However, despite these potential drawbacks, characterization of nucleoside transport proteins in *Xenopus* oocytes has, to date, accurately reflected the phenotypes of these proteins characterized in native cell types and tissues.

The characterization of membrane transport mechanisms by radioisotope flux measurements in *Xenopus* oocytes may possibly be complicated, and even prevented, by the intracellular metabolism of permeant (3, 13). With respect to nucleosides, both thymidine (1) and uridine (14) have been shown to have slow and insignificant metabolism in mRNA-injected *Xenopus* oocytes. The use of short uptake intervals is beneficial in minimizing the possible effects of nucleoside metabolism on nucleoside transport kinetics (2, 3, 5, 14). Due to their large size, equilibrium is reached more slowly in *Xenopus* oocyte than in smaller cells, thereby extending the time period before which nucleoside or nucleoside metabolite backflux would occur (5).

An additional advantage of *Xenopus* oocytes when studying electrogenic transport processes such as those of CNT family members is that electrophysiological experiments using the two microelectrode voltage-clamp, for example, are readily performed. Electrophysiology techniques enable characterization of the movement of charge across the membrane (steady-state currents), as well as charge movements within the membrane (presteady-state or transient currents) (15, 16). Unlike radioisotope flux experiments, electrophysiology permits the voltage-dependence of transport to be studied and is also capable of resolving time-dependent changes in the transport system of less than one second (15).

Therefore, by exploiting the innate ability of *Xenopus* oocytes to effectively translate injected exogenous mRNA and produce post-translationally modified proteins at the oocyte plasma membrane, the studies presented here utilized *Xenopus* oocytes as an expression system for CNTs. Using molecular biology, mRNA was transcribed from wild-type and mutant cDNAs by *in vitro* techniques. Upon expression in *Xenopus* oocytes, the presence of these proteins at the cell surface, as well as their glycosylation status, an example of post-translational processing, was verified by immunoblotting. Subsequent functional characterization of the proteins occurred through both radioisotope flux assays and electrophysiology studies.

Molecular Biology

Constructs – The molecular cloning of CaCNT (17), hCNT1 (9), hCNT2 (10) and hCNT3 (11) has been previously described. cDNAs (GenBank™ accession numbers AY235425, U62968, AF036109 and AF305210, respectively) were subcloned into the enhanced *Xenopus* plasmid expression vector pGEM-HE (18) as previously described (11). By providing 5'- and 3'-untranslated regions from the *Xenopus* β -globin gene flanking the multiple cloning site, pGEM-HE gave greater functional activity than the pBluescript II KS(+) (Stratagene, USA) vector used in earlier studies (9, 10, 19).

The CaCNT cDNA provided the template for construction of both the CaCNT/19-10196 and CaCNT/19-20196 cDNAs (corresponding to Contigs 19-10196 and 19-20196, respectively, of the Stanford *Candida albicans* genome sequence database: Stanford Genome Technology Center website <http://www-sequence.stanford.edu/group/candida>) (Chapter 3). The hCNT1 and hCNT3 cDNAs provided the template for construction of the corresponding hCNT1 (Chapter 4) and hCNT3 mutants (Chapters 7 - 9). hCNT3 cDNA also provided the template for the construction of a cysteine-less version of hCNT3 (hCNT3C-) with all 14 endogenous cysteine residues converted to serine (20). hCNT3C- was transferred from the yeast *Escherichia coli* shuttle vector pYPGE15 (20) into the *Xenopus* oocyte expression vector pGEM-HE. In pGEM-HE, hCNT3C- was then used as template for the construction of hCNT3C- mutants (Chapters 7, 8 and 10).

Site-directed mutagenesis – Individual residue changes were introduced into CNT cDNA templates by the oligonucleotide-directed technique (21) using reagents from the QuikChange™ multi site-directed mutagenesis kit (Stratagene, USA). All constructs were sequenced in both directions by Taq dyedeoxy-terminator cycle sequencing to ensure that only the correct mutation(s) had been introduced.

Construction of chimeric hCNT3 and hCNT1 transporters – Two sets of overlap primers were designed at a splice site between Lys³¹⁴ and Val³¹⁵ of hCNT3 and the corresponding residues in hCNT1 (Lys²⁹³ and Ile²⁹⁴) in the putative loop

linking transmembrane domain (TM) 6 and TM 7 (*arrow* in Fig. 5-11A) to create reciprocal 50:50 chimeras by a two step overlap extension polymerase chain reaction (PCR) method (22, 23). Chimeric constructs containing the restriction site *KpnI* downstream of the M13 forward primer and the restriction site *SphI* upstream of the M13 reverse primer were subcloned into the respective restriction sites of the pGEM-HE vector. The chimeras were sequenced in both directions to verify the splice sites and ensure that no mutations had been introduced.

In vitro transcription and expression in *Xenopus* oocytes – Plasmid cDNAs were linearized with *NheI* with the exception of hCNT2 which was linearized with *SphI*. Following linearization, cDNA was transcribed with T7 polymerase using the mMESSAGE mMACHINE™ (Ambion, USA) *in vitro* transcription system. Remaining template was removed by digestion with RNase-free DNase1. Healthy stage V - VI oocytes were isolated by collagenase treatment (2 mg/ml for 2 hours) of ovarian lobes from female *Xenopus laevis* (Biological Sciences Vivarium, University of Alberta, Canada) that had been anaesthetized by immersion in 0.3% (w/v) tricaine methanesulfonate (pH 7.4). Frogs were humanely killed following collection of oocytes in compliance with guidelines approved by the Canadian Council on Animal Care. The remaining follicular layers were removed by phosphate treatment (100 mM K₂PO₄) and manual defolliculation. Twenty-four hours after defolliculation, oocytes were injected with either 10 - 20 nl of water containing 1 ng/nl of capped RNA transcript or the same volume of water alone. Injected oocytes were then incubated for either 4 days (radioisotope flux studies) or 4 - 7 days (electrophysiology) at 18°C in modified Barth's solution (changed daily) (88 mM NaCl, 1 mM KCl, 0.33 mM Ca(NO₃)₂, 0.41 mM CaCl₂, 0.82 mM MgSO₄, 2.4 mM NaHCO₃, 10 mM Hepes, 2.5 mM sodium pyruvate, 0.1 mg/ml penicillin and 0.05 mg/ml gentamycin sulfate, pH 7.5) prior to the assay of nucleoside transport activity. In some specified instances, oocytes were microinjected with twice the amount of transcript and incubated in Barth's medium for 5 - 7 days in efforts to increase the expression level of catalytically-impaired mutants (Chapter 9). These techniques have been established in previous studies (2, 5, 9-11).

Cell Surface Expression and Glycosylation

Chapter 4 – Purified plasma membranes were prepared from groups of 100 oocytes using silica beads as described by Kamsteeg and Deen (24). Protein concentrations were determined by the bicinchoninic acid protein assay (Pierce, USA) using bovine serum albumin (BSA) as a standard.

Chapters 8 and 9 – Production of recombinant protein at the oocyte cell surface was determined by labeling of intact oocytes with EZ-Link sulfosuccinimidyl-6-(biotinamido) hexanoate (sulfo-NHS-LC-biotin) (Pierce, USA) followed by isolation of the resultant biotinylated plasma membrane proteins using immobilized streptavidin resin (Pierce, USA) according to the manufacturer's instructions. Glycosylation status was established by digestion with *N*-Glycosidase-F (Roche Molecular Biochemicals, USA). Identically treated samples omitting enzyme were used as controls.

Immunoblotting – For immunoblotting, one μg aliquots of plasma membrane proteins (Chapter 4) or solubilized proteins from 2 oocytes/lane (Chapters 8 and 9) were resolved on 12% sodium dodecyl sulphate (SDS)-polyacrylamide gels (25). The electrophoresed proteins were transferred to polyvinylidene difluoride membranes and probed with affinity-purified rabbit anti-hCNT1₃₁₋₅₅ (Chapter 4) or anti-hCNT3₄₅₋₆₉ (Chapters 8 and 9) polyclonal antibodies (26). Blots were then incubated with horseradish peroxidase-conjugated anti-rabbit antibodies (GE Healthcare Biosciences Inc. (formerly Amersham Pharmacia Biotech), Canada) and developed with enhanced chemiluminescence reagents (GE Healthcare Biosciences Inc., Canada).

Transport Media

Na^+ -containing transport medium was composed of 100 mM NaCl, 2 mM KCl, 1 mM CaCl_2 , 1 mM MgCl_2 and 10 mM HEPES (for pH values > 6.5) or 10 mM MES (for pH values \leq 6.5). In Na^+ -free, choline-containing transport medium, 100

mM NaCl was replaced with 100 mM choline chloride (ChCl) and in Li⁺-containing transport medium, 100 mM NaCl was replaced with 100 mM LiCl. In cation-activation experiments where the indicated Na⁺ or Li⁺ concentration was less than 100 mM, Na⁺ or Li⁺ in the transport medium was replaced by equimolar Ch⁺ to maintain isomolarity. Unless otherwise indicated, Na⁺- and Li⁺-activation experiments were performed in transport medium at pH 8.5 to minimize the H⁺ concentration. In experiments examining the H⁺-dependence of transport, Na⁺-free choline-containing transport medium (100 mM ChCl) was used with pH values ranging from 4.5 to 8.5. Experiments replacing NaCl with equimolar ChCl or LiCl included a 10 min pre-incubation period and several washes with ChCl- or LiCl-containing transport medium, respectively, to ensure complete removal of extracellular Na⁺ prior to addition of nucleoside-containing transport medium.

Radioisotope Flux Studies

Radioisotope transport assays were performed as described previously (2, 5, 9-11, 17, 19) on groups of 10 - 12 oocytes at room temperature (20°C) using ¹⁴C- or ³H-labeled nucleosides (1 or 2 - 4 µCi/ml, respectively) in 200 µl of the appropriate transport medium. Unless otherwise indicated, nucleoside uptake was determined at a concentration of 20 µM (Chapters 3 - 7 and 9) or 10 µM (Chapters 8 and 10). Nucleosides were obtained from Moravsek Biochemicals (USA), Sigma (Canada) or GE Healthcare Biosciences Inc. (Canada). Transport medium for adenosine uptake experiments also contained 1 µM deoxycoformycin to inhibit adenosine deaminase activity. All uptake values, at both high and low permeant concentrations, represent initial rates of transport (*e.g.* 2, 8, 9, 17, 19) determined using an incubation period of 5 - 30 min (Chapter 3) or 1 - 10 min (Chapters 4 - 10), depending upon the construct and coupling cation used in the experiment. In Chapters 4 to 10, data in all experiments are presented as pmol/oocyte.min⁻¹ for ease of comparison.

At the end of the incubation period, the oocytes were rapidly washed seven times with ice-cold Na⁺-free 100 mM ChCl transport medium (pH 7.5) to remove

extracellular radioactivity and then transferred individually into scintillation vials containing 0.3 - 0.5 ml of 1% (w/v) SDS. Oocyte-associated radioactivity was determined by liquid scintillation counting (LS 6000 IC, Beckman Canada Inc., Canada). The flux values shown are the means \pm SEM (standard error of the mean) of 10 - 12 oocytes from representative experiments and individual experiments were performed on cells from single batches of oocytes used on the same day. Values for the transporter-mediated component of uptake were calculated as uptake in RNA transcript-injected oocytes *minus* uptake in oocytes injected with water alone. Each experiment was performed at least twice using oocytes from different frogs. Flux values varied in different batches of oocytes by up to 3-fold between experiments.

Inhibition studies with thiol-reactive reagents – Oocytes were pretreated with *p*-chloromercuribenzenesulfonate (PCMBS) on ice for 10 min in 200 μ l of the appropriate transport medium and then washed five times with ice-cold transport medium to remove excess organomercurial before the assay of transport activity. Control experiments established that 10 min exposure to PCMBS resulted in maximum inhibition of hCNT3 transport activity. Corresponding pretreatment with the methanethiosulfonate (MTS) reagents 2-aminoethyl methanethiosulfonate hydrobromide (MTSEA), sodium (2-sulfonatoethyl) methanethiosulfonate (MTSES) and [(triethylammonium)ethyl] methanethiosulfonate bromide (MTSET) was performed at room temperature (20°C) for 5 min. In permeant protection experiments, unlabeled uridine (20 mM, unless otherwise indicated) was included along with PCMBS (27). To demonstrate reversal of inhibition, PCMBS-treated oocytes were subjected to a second preincubation with 5 mM dithiothreitol (DTT) at room temperature for 1 min (27). PCMBS and MTS reagents were obtained from Toronto Research Chemicals (Canada) and Sigma (Canada), respectively.

Electrophysiological Studies

Steady-state and presteady-state membrane currents were measured in oocytes at room temperature (20°C) using the whole-cell, two-electrode voltage clamp

technique (GeneClamp 500B, Molecular Devices Corp. (formerly Axon Instruments Inc.), USA) as previously described (16). The GeneClamp 500B was interfaced to a dedicated IBM-compatible computer *via* a Digidata 1200 (Chapters 3 and 5) or Digidata 1322A (Chapters 4 and 6 - 9) A/D converter and controlled by Axoscope or pCLAMP software (Molecular Devices Corp., USA). The microelectrodes were filled with 3 M KCl and had resistances ranging from 0.5 to 2.5 M Ω (megaohms). Following microelectrode penetration, resting membrane potential was measured over a 10 - 15 min period prior to the start of the experiment. Oocytes exhibiting an unstable membrane potential or a potential more positive than -30 mV were discarded. Unless otherwise indicated, the oocyte membrane potential was clamped at a holding potential (V_h) of -50 mV in the appropriate transport medium. To initiate transport, the transport medium perfusing the oocyte was changed to one containing 1 mM uridine (Chapters 3 and 4) or 100 μ M nucleoside (Chapters 5 and 7) for the desired length of time and then exchanged with fresh medium lacking the nucleoside permeant. Current signals were filtered at 0.02 - 2 kHz (four-pole Bessel filter) at a sampling interval of 20 (Chapters 3 and 6) or 50 (Chapters 4, 5 and 9) msec. For data presentation, the signals were further filtered at 0.5 - 0.75 Hz by use of pCLAMP software (Version 9.0, Molecular Devices Corp., USA).

Presteady-state (transient) currents were studied using a voltage pulse protocol, as described previously (16). Membrane voltage was stepped from the holding potential (V_h) of -50 mV to a range of test potentials (V_t) from -130 to +30 mV in 20 mV increments (Chapter 7) or from -150 to +75 mV in 25 mV increments (Chapter 8) or from -110 to +60 mV in 10 mV increments (Chapter 9). The voltage rise time of the clamp was adjusted by use of an oscilloscope such that it varied between 200 and 500 μ sec. In experiments examining the effect of PCMBBS (Chapter 7), current measurements were sampled before and after incubation with 500 μ M PCMBBS (100 mM NaCl, pH 5.5; 10 min) in the appropriate transport medium. Current signals were filtered at 2 kHz (four-pole Bessel filter) at a sampling interval of 200 μ sec/point (corresponding to a sampling frequency of 5 kHz). For data presentation, the current at each test potential was averaged from 5 sweeps and

further filtered at 0.75 kHz by pCLAMP software (Version 9.0, Molecular Devices Corp., USA).

In protonophore studies, carbonyl cyanide *m*-chlorophenylhydrazone (CCCP) (100 μ M) was preincubated with oocytes for 15 min prior to measuring uridine-evoked currents (100 μ M) in Na⁺-free 100 mM ChCl, pH 5.5 transport medium. CCCP was obtained from Sigma (Canada), and stock solutions of CCCP were dissolved in dimethyl sulfoxide (DMSO). Control experiments confirmed that oocytes were unaffected by DMSO at its final concentration of 0.5% (w/v).

Current-voltage (I-V) curves were determined from differences in steady-state currents generated in the presence and absence of permeant during 300 msec voltage pulses to potentials between +60 and -110 mV (10 mV steps). For I-V relations, currents were filtered at 2 kHz (four-pole Bessel filter) and sampled at a rate of 200 μ sec/point (corresponding to a sampling frequency of 5 kHz).

Data from individual electrophysiology experiments are presented as nucleoside-evoked currents from single representative cells or as mean values (\pm SEM) from 4 or more oocytes from the same batch used on the same day. Each experiment was repeated at least twice on oocytes from different frogs. No nucleoside-evoked currents were detected in oocytes injected with water alone, demonstrating that currents in transcript-injected oocytes were transporter specific.

Kinetic Parameters

Kinetic parameters (K_m , K_{50} , V_{max} , IC_{50} , Hill coefficient) derived from radioisotope flux and electrophysiological experiments were calculated using SigmaPlot software (Jandel Scientific Software, USA). Those from radioisotope experiments were derived from curve fits to averaged mediated fluxes from 10 - 12 oocytes, and are presented as means \pm SE (standard error of the fitted estimate). Mediated fluxes were determined as uptake in RNA-injected oocytes *minus* uptake in water-injected control oocytes. Kinetic parameters derived from electrophysiological experiments were

determined from fits to data from individual oocytes normalized to the I_{\max} value obtained for that oocyte, and are presented as values \pm SE for single representative oocytes or as means \pm SEM of 4 or more cells.

Determination of Stoichiometry

Charge-to-nucleoside stoichiometry – Na^+ :nucleoside and H^+ :nucleoside coupling ratios were determined by simultaneously measuring radiotracer transport-induced current measurements under voltage clamp conditions in transport medium containing 100 mM NaCl, pH 8.5 or 100 mM ChCl, pH 5.5, respectively, unless otherwise indicated. Radioisotopes and respective nucleoside concentrations varied depending on the construct and experiment. Stoichiometry was determined for CaCNT/19-20196 (Chapter 3) using 1 mM ^3H -uridine (2 $\mu\text{Ci/ml}$), for hCNT3 (Chapter 5) using 200 μM ^{14}C -uridine (1 $\mu\text{Ci/ml}$), for hCNT1/2/3 (Chapter 6) using 200 μM ^{14}C -uridine and ^{14}C -adenosine (1 $\mu\text{Ci/ml}$), for hCNT3C- (Chapter 8) using 100 μM ^3H -uridine (2 $\mu\text{Ci/ml}$) and for hCNT3 and hCNT3 mutants (Chapter 9) using 200 μM ^3H -uridine (2 $\mu\text{Ci/ml}$). Individual oocytes were placed in a perfusion chamber and voltage-clamped at V_h of -30, -50 or -90 mV, as indicated, in the appropriate nucleoside-free medium for a 5 - 10 min period to monitor baseline currents. When the baseline was stable, the perfusion was stopped and medium of the same composition containing unlabeled and radiolabeled nucleoside was manually added to the perfusion chamber. Current was measured for 0.5 - 3 min, and uptake of nucleoside was terminated by washing the oocyte with nucleoside-free medium until the current returned to baseline (< 15 sec). The oocyte was then immediately transferred to a scintillation vial and solubilized with 1% (w/v) SDS for quantitation of oocyte-associated radioactivity. Nucleoside-induced current was obtained as the difference between baseline current and the inward nucleoside-induced current. The total charge translocated into the oocyte during the uptake period was calculated from the current-time integral and correlated with the measured radiolabeled flux for each oocyte to determine the charge:uptake ratio. Basal radiolabeled nucleoside uptake

was determined in control water-injected oocytes (from the same donor frog) under equivalent conditions and used to correct for endogenous non-mediated uridine uptake over the same incubation period. Coupling ratios (\pm SE) were calculated from slopes of least-squares fits of uridine-dependent charge *versus* uridine accumulation for five or more oocytes.

Charge-to- Na^+ stoichiometry – hCNT-mediated uptake of $^{22}\text{Na}^+$ was optimized for specific activity and transport rate by using a saturating concentration of uridine (200 μM) and a $^{22}\text{Na}^+$ concentration of 1 mM, a value close to the -90 mV Na^+ apparent K_{50} for hCNTs. Individual CNT-producing oocytes were voltage clamped at -90 mV and perfused with Na^+ -free medium (100 mM ChCl, pH 8.5) for a period of 5 min. A stable baseline current was recorded, perfusion was stopped and the bath solution was manually changed to one containing 200 μM uridine, 1 mM $^{22}\text{Na}^+$ (1 $\mu\text{Ci/ml}$) and 99 mM ChCl (pH 8.5) for a period of 2 - 3 min. The solution was rapidly changed back to uridine- and Na^+ -free medium until the current returned to baseline (< 15 sec). The oocyte was then immediately transferred to a scintillation vial and solubilized with 1% (w/v) SDS for quantitation of oocyte-associated radioactivity. Testing of each individual CNT-producing oocyte prior to addition of uridine and $^{22}\text{Na}^+$ showed no shift in the baseline current when the composition of the bath solution was changed from 100 mM ChCl to 1 mM NaCl + 99 mM ChCl, indicating an absence of detectable hCNT3 Na^+ slippage under the experimental conditions used. Similarly, basal $^{22}\text{Na}^+$ uptake in control water-injected oocytes (from the same donor frog) was determined under equivalent conditions over the same incubation period and used to correct for endogenous non-mediated Na^+ uptake. For each CNT-producing oocyte, the total charge translocated during the uptake period was calculated from the current-time integral and correlated with the measured $^{22}\text{Na}^+$ flux to determine charge:uptake ratio. The charge-to- Na^+ stoichiometry (\pm SE) was calculated from the slope of a least-squares fit of uridine-dependent charge *versus* $^{22}\text{Na}^+$ accumulation for 5 oocytes. $^{22}\text{Na}^+$ was obtained from GE Healthcare Biosciences Inc. (Canada).

Bibliography

1. Jarvis, S. M., and Griffith, D. A. (1991) Expression of the rabbit intestinal N2 Na⁺/nucleoside transporter in *Xenopus laevis* oocytes. *Biochem. J.* **278**: 605-607.
2. Huang, Q. Q., Yao, S. Y. M., Ritzel, M. W., Paterson, A. R., Cass, C. E., and Young, J. D. (1994) Cloning and functional expression of a complementary DNA encoding a mammalian nucleoside transport protein. *J. Biol. Chem.* **269**: 17757-17760.
3. Wang, J., Schaner, M. E., Thomassen, S., Su, S., Piquette-Miller, M., and Giacomini, K. M. (1997) Functional and molecular characteristics of Na⁺-dependent nucleoside transporters. *Pharm. Res.* **14**: 1524-1532.
4. Klein, S. L., Strausberg, R. L., Wagner, L., Pontius, J., Clifton, S. W., and Richardson, P. (2002) Genetic and genomic tools for *Xenopus* research: The NIH *Xenopus* initiative. *Dev. Dyn.* **225**: 384-391.
5. Yao, S. Y. M., Cass, C. E., and Young, J. D. (2000) The *Xenopus* oocyte expression system for the cDNA cloning and characterization of plasma membrane transport proteins. In *Membrane Transport. A Practical Approach*. (Baldwin, S. A., ed.) Oxford: Oxford University Press; 47-78.
6. Che, M., Ortiz, D. F., and Arias, I. M. (1995) Primary structure and functional expression of a cDNA encoding the bile canalicular, purine-specific Na⁺-nucleoside cotransporter. *J. Biol. Chem.* **270**: 13596-13599.
7. Yao, S. Y. M., Cass, C. E., and Young, J. D. (1996) Transport of the antiviral nucleoside analogs 3'-azido-3'-deoxythymidine and 2', 3'-dideoxycytidine by a recombinant nucleoside transporter (rCNT1) expressed in *Xenopus laevis* oocytes. *Mol. Pharmacol.* **50**: 388-393.
8. Yao, S. Y. M., Ng, A. M. L., Ritzel, M. W. L., Gati, W. P., Cass, C. E., and Young, J. D. (1996) Transport of adenosine by recombinant purine- and pyrimidine-selective sodium/nucleoside cotransporters from rat jejunum expressed in *Xenopus laevis* oocytes. *Mol. Pharmacol.* **50**: 1529-1535.
9. Ritzel, M. W. L., Yao, S. Y. M., Huang, M. Y., Elliot, J. F., Cass, C. E., and Young, J. D. (1997) Molecular cloning and functional expression of cDNAs

- encoding a human Na⁺-nucleoside cotransporter hCNT1. *Am. J. Physiol.* **272**: C707-C714.
10. Ritzel, M. W. L., Yao, S. Y. M., Ng, A. M. L., Mackey, J. R., Cass, C. E., and Young, J. D. (1998) Molecular cloning, functional expression and chromosomal localization of a cDNA encoding a human Na⁺/nucleoside cotransporter (hCNT2) selective for purine nucleosides and uridine. *Mol. Membr. Biol.* **15**: 203-211.
 11. Ritzel, M. W. L., Ng, A. M. L., Yao, S. Y. M., Graham, K., Loewen, S. K., Smith, K. M., Ritzel, R. G., Mowles, D. A., Carpenter, P., Chen, X.-Z., Karpinski, E., Hyde, R. J., Baldwin, S. A., Cass, C. E., and Young, J. D. (2001) Molecular identification and characterization of novel human and mouse concentrative Na⁺-nucleoside cotransporter proteins (hCNT3 and mCNT3) broadly selective for purine and pyrimidine nucleosides (system *cib*). *J. Biol. Chem.* **276**: 2914-2927.
 12. Wang, H. C., Beer, B., Sassano, D., Blume, A. J., and Ziai, M. R. (1991) Gene expression in *Xenopus* oocytes. *Int. J. Biochem.* **23**: 271-276.
 13. Hong, M., Schlichter, L., and Bendayan, R. (2000) A Na⁺-dependent nucleoside transporter in microglia. *J. Pharmacol. Exp. Ther.* **292**: 366-374.
 14. Huang, Q., Harvey, C. M., Paterson, A. R. P., Cass, C. E., and Young, J. D. (1993) Functional expression of Na⁺-dependent nucleoside transport systems of rat intestine in isolated oocytes of *Xenopus laevis*. Demonstration that rat jejunum expresses the purine-selective system N1 (*cif*) and a second, novel system N3 having broad specificity for purine and pyrimidine nucleosides. *J. Biol. Chem.* **268**: 20613-20619.
 15. Mager, S., Cao, Y., and Lester, H. A. (1998) Measurement of transient currents from neurotransmitter transporters expressed in *Xenopus* oocytes. *Methods Enzymol.* **296**: 551-566.
 16. Smith, K. M., Ng, A. M. L., Yao, S. Y. M., Labeledz, K. A., Knaus, E. E., Wiebe, L. I., Cass, C. E., Baldwin, S. A., Chen, X.-Z., Karpinski, E., and Young, J. D. (2004) Electrophysiological characterization of a recombinant human Na⁺-coupled nucleoside transporter (hCNT1) produced in *Xenopus* oocytes. *J. Physiol.* **558**: 807-823.

17. Loewen, S. K., Ng, A. M. L., Mohabir, N. N., Baldwin, S. A., Cass, C. E., and Young, J. D. (2003) Functional characterization of a H⁺/nucleoside co-transporter (CaCNT) from *Candida albicans*, a fungal member of the concentrative nucleoside transporter (CNT) family of membrane proteins. *Yeast* **20**: 661-675.
18. Liman, E. R., Tytgat, J., and Hess, P. (1992) Subunit stoichiometry of a mammalian K⁺ channel determined by construction of multimeric cDNAs. *Neuron* **9**: 861-871.
19. Loewen, S. K., Ng, A. M., Yao, S. Y., Cass, C. E., Baldwin, S. A., and Young, J. D. (1999) Identification of amino acid residues responsible for the pyrimidine and purine nucleoside specificities of human concentrative Na⁺ nucleoside cotransporters hCNT1 and hCNT2. *J. Biol. Chem.* **274**: 24475-24484.
20. Zhang, J., Tackaberry, T., Ritzel, M. W., Raborn, T., Barron, G., Baldwin, S. A., Young, J. D., and Cass, C. E. (2006) Cysteine-accessibility analysis of transmembrane domains 11-13 of human concentrative nucleoside transporter 3. *Biochem. J.* **394**: 389-398.
21. Kirsch, R. D., and Joly, E. (1998) An improved PCR-mutagenesis strategy for two-site mutagenesis of sequence swapping between related genes. *Nucleic Acid Res.* **26**: 1848-1850.
22. Yao, S. Y., Ng, A. M., Loewen, S. K., Cass, C. E., Baldwin, S. A., and Young, J. D. (2002) An ancient prevertebrate Na⁺-nucleoside cotransporter (hfCNT) from the Pacific hagfish (*Eptatretus stouti*). *Am. J. Phys. Cell Phys.* **283**: C155-C168.
23. Horton, R. M., Hunt, H. D., Ho, S. N., Pullen, J. K., and Pease, L. R. (1989) Engineering hybrid genes without the use of restriction enzymes: gene splicing by overlap extension. *Gene* **77**: 61-68.
24. Kamsteeg, E.-J., and Deen, P. M. (2001) Detection of aquaporin-2 in the plasma membranes of oocytes: a novel isolation method with improved yield and purity. *Biochim. Biophys. Res. Comm.* **282**: 683-690.
25. Laemmli, U. K. (1970) Cleavage of structural proteins during the assembly of the head of bacteriophage T4. *Nature* **227**: 680-685.

26. Damaraju, V. L., Elwi, A. N., Hunter, C., Carpenter, P., Santos, C., Barron, G. M., Sun, X., Baldwin, S. A., Young, J. D., Mackey, J., Sawyer, M. B., and Cass, C. E. (2007) Localization of broadly selective equilibrative and concentrative nucleoside transporters, hENT1 and hCNT3, in human kidney. *Am. J. Physiol. Renal Physiol.* **293**: F200-F211.

27. Yao, S. Y. M., Sundaram, M., Chomey, E. G., Cass, C. E., Baldwin, S. A., and Young, J. D. (2001) Identification of Cys¹⁴⁰ in helix 4 as an exofacial cysteine residue within the substrate-translocation channel of rat equilibrative nitrobenzylthioinosine (NBMPR)-insensitive nucleoside transporters rENT2. *Biochem. J.* **353**: 387-393.

Chapter 3:

Allelic Isoforms of the H⁺/Nucleoside Cotransporter (CaCNT) from *Candida albicans* Reveal Separate High- and Low-Affinity Transport Systems for Nucleosides*

* A version of this chapter has been published.

Slugoski, M. D., Loewen, S. K., Ng, A. M. L., Baldwin, S. A., Cass, C. E., and Young, J. D. (2004) Allelic isoforms of the H⁺/nucleoside cotransporter (CaCNT) from *Candida albicans* reveal separate high- and low-affinity transport systems for nucleosides. *Yeast* **21**: 1269-1277.

Acknowledgements

Dr. Shaun K. Loewen and Mrs. Amy M. L. Ng provided technical assistance with this project. Drs. Stephen A. Baldwin and Carol E. Cass are collaborative principal investigators who assisted with research funding and manuscript preparation. This research was funded by the National Cancer Institute of Canada, Medical Research Council of the United Kingdom, Alberta Cancer Board and Alberta Heritage Foundation for Medical Research. *Candida albicans* Contig 19-10196 and Contig 19-20196 sequences were obtained from the Stanford Genome Technology Center website at <http://www-sequence.stanford.edu/group/candida>.

Introduction

Yeasts display diverse nucleoside transport profiles. *Saccharomyces cerevisiae*, for instance, transports only uridine and uridine analogs (1, 2), whereas the opportunistic pathogen *Candida albicans* transports both pyrimidine and purine nucleosides (3, 4). At the molecular level, two *S. cerevisiae* nucleoside transporter (NT) proteins have been identified: a uridine-selective cell surface NT (FUI1), and a broadly-selective intracellular membrane NT (FUN26) with a probable role in the vacuolar release of nucleosides following nucleic acid catabolism (2). FUI1 is a member of the uracil/allantoin permease family, whereas FUN26 belongs to the equilibrative nucleoside transporter (ENT) protein family. There are no concentrative nucleoside transporters (CNTs) encoded by the *S. cerevisiae* genome. In *C. albicans*, nucleoside transport is more complex. The Stanford *C. albicans* genome sequence database contains genes for at least five putative NT proteins, including orthologs of FUI1 and FUN26, as well as a member of the NUP protein family (NUP). Characterized functionally in transformed *S. cerevisiae*, the *C. albicans* NUP protein transports purine nucleosides and perhaps thymidine, but not uridine (5). In addition, the Stanford *C. albicans* genome database contains two allelic Contigs (19-10196 and 19-20196)¹ encoding almost identical versions of a protein belonging to the CNT transporter family. Both Contigs contain full-length open reading frames of 608 amino acid residues and 13 predicted transmembrane domains (TMs). Using primers flanking the open reading frame of Contig 19-20196, a *C. albicans* CNT cDNA was previously amplified by PCR from logarithmically growing cells (6). When produced in oocytes of *Xenopus laevis*, the encoded 608 amino acid residue protein (designated CaCNT) mediated H⁺-coupled transport of uridine, adenosine, inosine and guanosine, but not thymidine or cytidine (6).

Although almost identical in amino acid sequence, the open reading frames of Contigs 19-10196 and 19-20196 differed from CaCNT by four and one amino acid residues, respectively. In this study, an extended characterization of *C. albicans* CNT proteins was performed by using site-directed mutagenesis of recombinant CaCNT to recreate and functionally characterize the proteins encoded by these two Contigs. The

results provide evidence of multiple CaCNT allelic isoforms that exhibit functional as well as structural heterogeneity.

Results and Discussion

The proteins encoded by Contigs 19-10196 and 19-20196 of the Stanford *C. albicans* genomic database and the cDNA isolated previously by PCR from a *C. albicans* cDNA library (6) have very similar, but not identical, predicted amino acid sequences. According to the Stanford diploid database (assembly 19, May 2002), Contigs 19-10196 and 19-20196 originate from separate alleles and encode two separate allelic proteins that are polymorphic in origin. Fig. 3-1 outlines the 10 single nucleotide differences between the open reading frames of the two Contigs, resulting in five single residue differences in predicted amino acid sequence at residue positions 328, 416, 418, 483 and 506. Of the two, Contig 19-20196 most closely resembles CaCNT and differs by only one amino acid at position 328 where glycine in CaCNT is replaced by serine. Contig 19-10196 resembles CaCNT in this regard and shares glycine at this position. Multiple sequence alignments placed CaCNT residue 328 at a position in TM 7 equivalent to a previously studied serine/glycine difference between human (h) and rat (r) CNT1/2 that is responsible, in part, for the contrasting pyrimidine and purine nucleoside selectivities of the two transporters (7, 8). Therefore, the sequence differences at this position in *C. albicans* CNTs were hypothesized to also have functional consequences.

Construction of the CaCNT isoforms CaCNT/19-10196 and CaCNT/19-20196

– The amino acid sequences encoded by Contigs 19-10196 and 19-20196 differ from CaCNT by four and one residues, respectively (Fig. 3-1). Repeat PCR amplifications of the cDNA library used to generate the original CaCNT clone (6) confirmed that differences in predicted amino acid sequence between CaCNT and Contigs 19-10196 and 19-20196 were not a consequence of PCR-induced errors. Therefore, although the CaCNT allele has yet to be identified in a *C. albicans* genome, it is unlikely to be an artificial sequence generated during the cloning process. The residue differences

identified in Fig. 3-1 were incorporated into CaCNT by site-directed mutagenesis to generate the constructs CaCNT/19-10196 and CaCNT/19-20196. Both cDNAs were sequenced in each direction to eliminate the possibility of introducing unwanted sequence errors.

Functional expression of recombinant CaCNT, CaCNT/19-10196 and CaCNT/19-20196 in Xenopus oocytes – Fig. 3-2 depicts a representative experiment showing uptake of the radiolabeled pyrimidine nucleoside uridine (20 μ M, 20°C) by oocytes producing either CaCNT, CaCNT/19-10196 or CaCNT/19-20196. Since CaCNT is H⁺-coupled (6), uptake was measured in acidified medium at pH 5.5. Initial rates of transport (influx) in this and subsequent nucleoside selectivity studies were determined using an extended 30 min flux to maximize detection of weakly transported permeants. Basal non-mediated uptake (< 5% of the total flux) was measured in control oocytes injected with water alone. As shown in Fig. 3-2, all three recombinant proteins were functional, with CaCNT and CaCNT/19-10196 exhibiting greater transport activity than CaCNT/19-20196.

Previously, two sets of adjacent residues in TMs 7 and 8 of hCNT1 (Ser³¹⁹/Gln³²⁰ and Ser³⁵³/Leu³⁵⁴) were identified that, when converted to the corresponding residues in hCNT2 (Gly³¹³/Met³¹⁴ and Thr³⁴⁷/Val³⁴⁸), changed the specificity of the transporter from pyrimidine nucleoside-selective to purine nucleoside-selective (*ie.*, hCNT2-like) (7). On its own, mutation of hCNT1 Ser³¹⁹ in TM 7 to glycine enabled transport of purine nucleosides, a result also obtained by mutation of the corresponding residue in rCNT1 (7, 8). Since hCNT1 Ser³¹⁹ and hCNT2 Gly³¹³ correspond in position to CaCNT/19-20196 Ser³²⁸ and CaCNT and CaCNT/19-10196 Gly³²⁸, respectively, the abilities of CaCNT, CaCNT/19-10196 and CaCNT/19-20196 to transport a panel of physiological pyrimidine and purine nucleosides were compared (Fig. 3-3). Uptake of the nucleobase hypoxanthine was also tested, and values were corrected for non-mediated uptake in control water-injected oocytes. In contrast to mutagenesis studies of h/rCNT1, each of the three *C. albicans* constructs displayed a nucleoside selectivity profile similar to CaCNT, as previously reported by Loewen *et al.* (6). In addition to uridine, all three proteins

transported the purine nucleosides adenosine, inosine and guanosine, with minimal fluxes of cytidine and no detectable transport of thymidine or the nucleobase hypoxanthine.

Kinetic properties – The kinetic properties of both uridine and inosine transport by CaCNT- and CaCNT/19-20196-producing oocytes in transport medium at pH 5.5 were determined by concentration dependence experiments, as shown in Fig. 3-4. Apparent K_m and V_{max} values derived from these data are presented in Table 3-1. CaCNT-mediated transport was consistent with simple Michaelis-Menten kinetics, with apparent K_m values of 35 and 43 μM for uridine and inosine, respectively (Figs. 3-4A and 3-4C, respectively). V_{max} values for the two permeants were 38 pmol/oocyte.5min⁻¹ for uridine and 30 pmol/oocyte.5min⁻¹ for inosine, giving calculated $V_{max}:K_m$ ratios of 1.1 (uridine) and 0.7 (inosine). These values are in good agreement with the previous kinetic characterization of CaCNT (apparent K_m values of 33 μM for uridine and 57 μM for inosine, with $V_{max}:K_m$ ratios of 1.3 and 0.7, respectively) (6). In marked contrast, however, CaCNT/19-20196 exhibited substantially higher apparent K_m values of 416 μM for uridine (Fig. 3-4B) and 421 μM for inosine (Fig. 3-4D). V_{max} values of 36 and 38 pmol/oocyte.5min⁻¹ for uridine and inosine, respectively, were similar to those of CaCNT (Figs. 3-4A and 3-4C), suggesting similar levels of transporter protein at the cell surface and giving a calculated CaCNT/19-20196 $V_{max}:K_m$ ratio of 0.09 for both nucleosides. This large (10 - 12 fold) reduction in apparent affinity and consequent decrease in transporter efficiency for CaCNT/19-20196 relative to CaCNT explains the relatively low transport of 20 μM uridine and other nucleosides by CaCNT/19-20196 seen in Figs. 3-2 and 3-3. Since the single residue difference between CaCNT and CaCNT/19-20196 at position 328 is CaCNT-like in CaCNT/19-10196, the uridine transport kinetics for this transporter was also determined. Consistent with sequence predictions and the uptake data in Figs. 3-2 and 3-3, CaCNT/19-10196 exhibited uridine apparent K_m and V_{max} values comparable to those of CaCNT (47 μM and 36 pmol/oocyte.5min⁻¹, respectively) (Table 3-1).

Electrophysiological measurements – Recombinant CaCNT is an electrogenic H⁺/nucleoside symporter and generates inward currents in *Xenopus* oocytes following application of external uridine and purine nucleosides (6). Therefore, the possibility that low-affinity CaCNT/19-20196 might represent a nonenergized, uncoupled form of the transporter was investigated. To test this, individual voltage-clamped *Xenopus* oocytes producing either CaCNT or CaCNT/19-20196 were perfused with pH 5.5 transport medium containing 1 mM uridine. As demonstrated in the representative current traces shown in Fig. 3-5, and consistent with their similar V_{\max} values for radiolabeled uridine influx (Table 3-1), the two recombinant proteins generated comparable inward currents in the range of 45 - 50 nA. Under similar conditions, no currents were evident with control water-injected oocytes. Thus, CaCNT and CaCNT/19-20196 are both capable of H⁺-coupled transport. The H⁺:nucleoside coupling ratio of CaCNT/19-20196 was directly determined by simultaneous measurement of H⁺ currents and radiolabeled uridine influx (1 mM) under voltage clamp conditions, as described previously for CaCNT (6). The experiments presented in Fig. 3-6 demonstrate that CaCNT/19-20196, like CaCNT, has a H⁺:nucleoside coupling ratio of 1:1 (the slope of the regression line \pm SE for data from 9 individual oocytes is 1.00 ± 0.09). Therefore, CaCNT/19-20196 is fully H⁺-coupled.

Conclusions

CaCNT, CaCNT/19-10196 and CaCNT/19-20196 correspond to functional allelic isoforms of the *C. albicans* CNT nucleoside transporter. CaCNT/19-20196 differs from previously characterized CaCNT by a single amino acid substitution of serine for glycine at position 328 in putative TM 7 (Fig. 3-1). CaCNT/19-10196 retains glycine at this position, but has four other amino acid substitutions located in TM 11 (residue 483) and in the loops linking TMs 9/10 (residue 416 and 418) and TMs 11/12 (residue 506). Serine/glycine residue 328 is located at a position in TM 7 where there is a corresponding serine/glycine substitution in h/rCNT1/2 that is involved in the different permeant selectivities of the two mammalian CNT isoforms

(7, 8). Helix modeling studies of hCNT1 have placed this amino acid within the permeant translocation channel of the transporter (7). In contrast to h/rCNT1/2, all three *C. albicans* CNTs exhibited similar permeant selectivities for purine nucleosides and uridine, but differed instead in permeant apparent affinities (CaCNT and CaCNT/19-10196 >> CaCNT/19-20196). The high CaCNT/19-20196 apparent K_m value and associated low $V_{max}:K_m$ ratio, a measure of transporter efficiency, were not secondary to altered cation coupling. Therefore, the *C. albicans* CNT allelic transporters exist in both high-affinity (CaCNT, CaCNT/19-10196) and low-affinity (CaCNT/19-20196) forms. CaCNT/19-20196 is the first example of a CNT protein that displays a low apparent affinity for uridine, and the G328S substitution in *C. albicans* CNTs is the first example of a single amino acid substitution altering a CNT protein's overall affinity for nucleosides. The marked, but contrasting effects of mutating this residue in *C. albicans* and mammalian CNTs demonstrates the functional and/or structural importance of this amino acid position. The results also suggest that permeant selectivity is determined by different amino acid residues in the two CNT subfamilies.

The existence of multiple CaCNT isoforms that exhibit kinetic as well as structural heterogeneity may confer adaptive advantage to *C. albicans*, a dimorphic fungus which functions as an opportunistic human pathogen and exists in both yeast and hyphal forms (9). The existence of high-affinity and low-affinity isoforms may therefore impact pathogen virulence and is also likely to influence sensitivity to antifungal nucleoside analog drugs such as cordycepin (6). It will thus be of interest to examine the distribution of the three allelic forms of CaCNT amongst different clinical *C. albicans* isolates. Consistent with an important role for nucleoside transport in this organism, the *C. albicans* genome also encodes NTs (FUN26, FUI1 and NUP) from three other protein families, and it is likely that the pattern of NT expression changes in response to developmental and environmental factors. In the initial cDNA cloning of CaCNT, for example, a PCR-amplified product corresponding to CaCNT was obtained from logarithmically growing, but not stationary phase, cells (6). In *S. cerevisiae*, FUN26 expression is most abundant during M phase and may be linked to nucleoside release from vacuoles prior to cell division (2, 10).

Table 3-1. CaCNT kinetic parameters.

Permeant	Protein	Apparent K_m^a (μM)	V_{max}^a ($\text{pmol}/\text{oocyte} \cdot 5\text{min}^{-1}$)	$V_{\text{max}}:K_m$ Ratio
Uridine	CaCNT	35.0 ± 4.7	38.6 ± 1.2	1.10
	CaCNT/19-10196	47.3 ± 7.0	36.0 ± 1.4	0.76
	CaCNT/19-20196	416 ± 78	36.4 ± 2.9^b	0.09
Inosine	CaCNT	43.0 ± 2.9	29.8 ± 0.5	0.69
	CaCNT/19-20196	421 ± 69	37.6 ± 2.6^b	0.09

^a, From Fig. 3-4; ^b, Values corrected to $\text{pmol}/\text{oocyte} \cdot 5\text{min}^{-1}$.

	<i>Residue number</i>									
	188	203	283	328	416	417	418	441	483	506
pCaCNT-HE	A (GCT)	V (GTT)	T (TTT)	G (GGT)	S (TCT)	E (GAG)	A (GCA)	G (GGA)	I (ATA)	N (AAT)
Contig19-10196	A (GCC)	V (GTC)	T (TTC)	G (GGT)	P (CCT)	E (GAA)	E (GAA)	G (GGG)	M (ATG)	S (AGT)
Contig19-20196	A (GCT)	V (GTC)	T (TTT)	S (AGT)	S (TCT)	E (GAA)	A (GCA)	G (GGA)	I (ATA)	N (AAT)

Figure 3-1. Differences in deduced amino acid sequences of CaCNT and those derived from Contigs 19-10196 and 19-20196 (Stanford Genome Technology Center database). Nucleotide sequences encoding each amino acid residue are provided in *parentheses*.

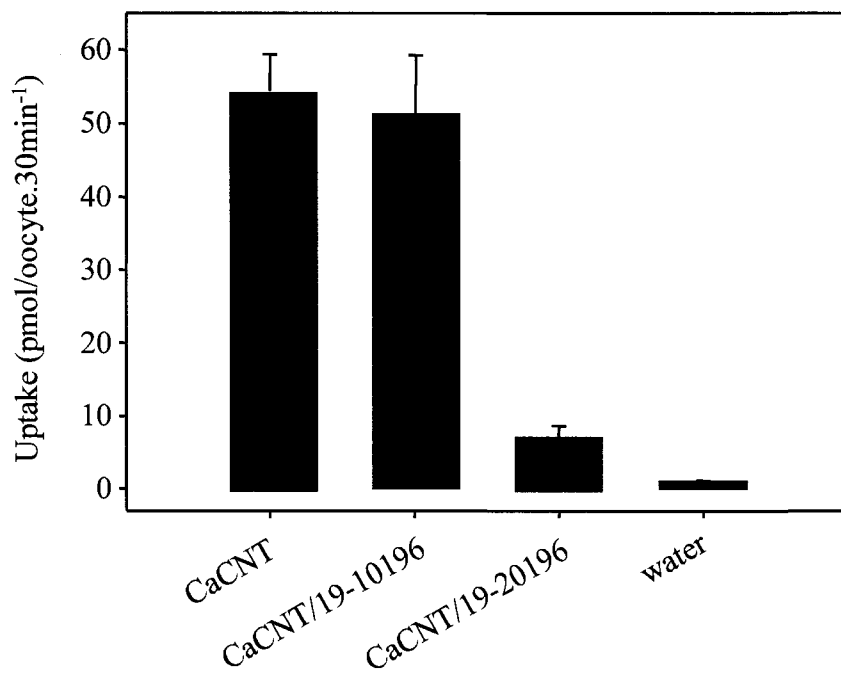


Figure 3-2. Transport of uridine by CaCNT-, CaCNT/19-10196- and CaCNT/19-20196-producing oocytes. Uptake of the ¹⁴C-labeled uridine (20 μM, 20°C, 30 min) was measured in transport medium at pH 5.5. Each value is the mean ± SEM of 10 - 12 oocytes.

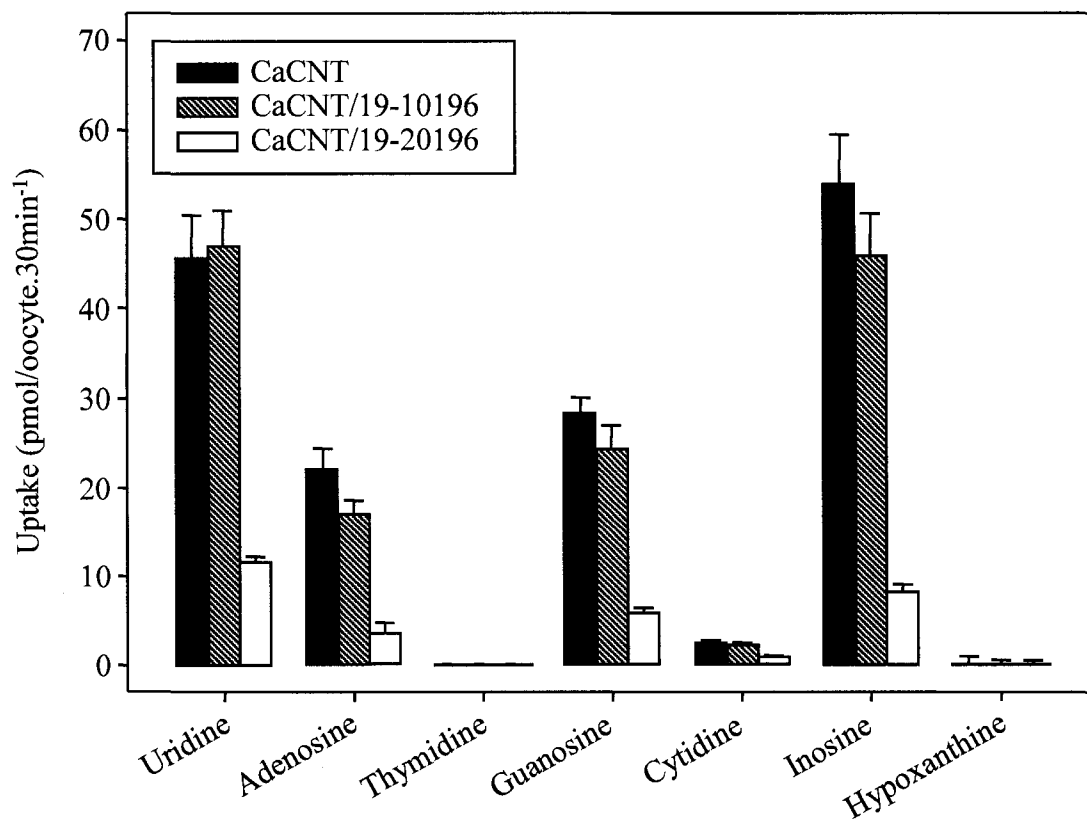


Figure 3-3. Permeant selectivity of CaCNT-, CaCNT/19-10196- and CaCNT/19-20196-producing oocytes. Uptake of the ¹⁴C-labeled nucleosides uridine, adenosine, thymidine, guanosine, cytidine and inosine and nucleobase hypoxanthine (20 μM, 20°C, 30 min) by CaCNT- (*solid bars*), CaCNT/19-10196- (*open bars*) and CaCNT/19-20196-producing oocytes (*grey bars*) was measured in transport medium at pH 5.5. Each value is the mean ± SEM of 10 - 12 oocytes.

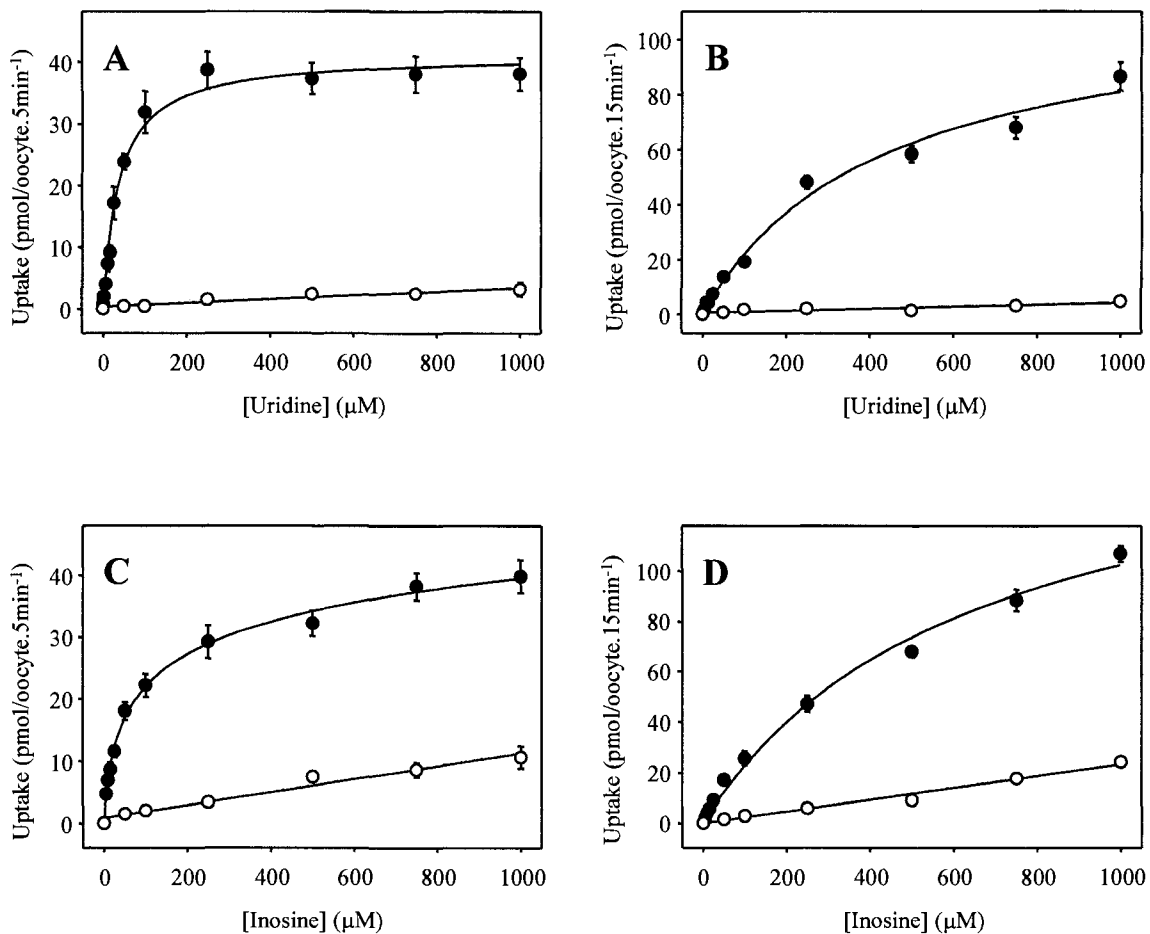


Figure 3-4. Kinetic properties of CaCNT and CaCNT/19-20196. Initial rates of uridine (*A, B*) and inosine (*C, D*) uptake in CaCNT- (*A, C*) (5 min fluxes, 20°C) and CaCNT/19-20196-producing oocytes (*B, D*) (15 min fluxes, 20°C) (*solid circles*) or control water-injected oocytes (*open circles*) were measured in transport medium at pH 5.5. Each value is the mean \pm SEM of 10 - 12 oocytes. Calculated kinetic parameters from these data are presented in Table 3-1.

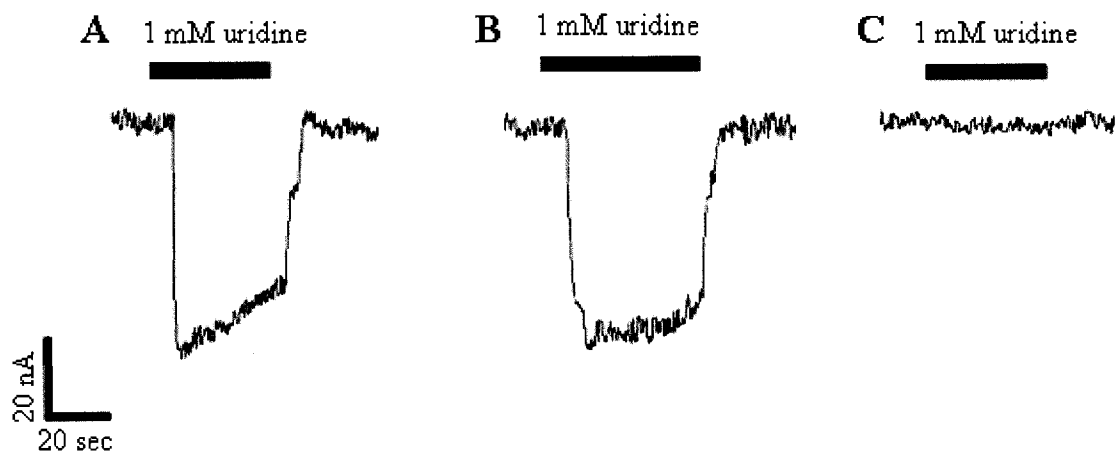


Figure 3-5. Proton currents induced by exposure of recombinant CaCNT and CaCNT/19-20196 to uridine. Current traces of a representative voltage-clamped CaCNT-producing oocyte (*A*), CaCNT/19-20196-producing oocyte (*B*) or control water-injected oocyte (*C*) perfused with transport medium at pH 5.5 and 1 mM uridine. The downward deflection of the current trace is indicative of the inward movement of positively-charged molecules.

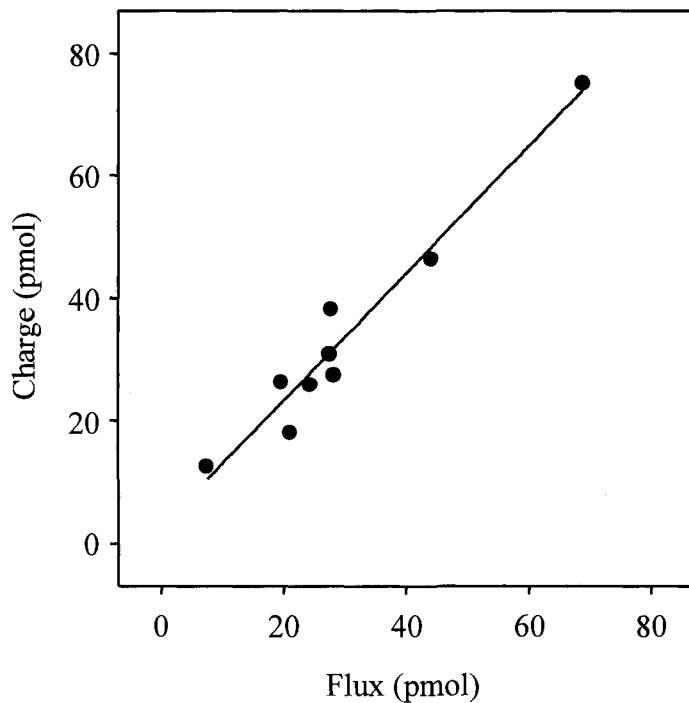


Figure 3-6. Stoichiometry of H^+ :uridine cotransport by recombinant CaCNT/19-20196. Uridine-dependent charge and 3H -uridine uptake were simultaneously determined at a membrane potential of -50 mV in the presence of a proton gradient for 3 min. Integration of the uridine-evoked inward current with time was used to calculate the net cation influx by converting picocoulombs to picomoles using the Faraday constant. Mediated 3H -uridine uptake was calculated as uptake in CaCNT/19-20196-producing oocytes minus uptake in water-injected oocytes. Each data point represents a single oocyte.

Endnotes

¹ Assembly 19 Contigs 19-10196 and 19-20196 correspond to former assembly 6 Contigs 6-2474 and 6-1709, respectively.

Bibliography

1. Horak, J. (1997) Yeast nutrient transporters. *Biochim. Biophys. Acta* **1331**: 41-79.
2. Vickers, M. F., Yao, S. Y. M., Baldwin, S. A., Young, J. D., and Cass, C. E. (2000) Nucleoside transporter proteins of *Saccharomyces cerevisiae*. Demonstration of a transporter (FUI1) with high uridine selectivity in plasma membranes and a transporter (FUN26) with broad nucleoside selectivity in intracellular membranes. *J. Biol. Chem.* **275**: 25931-25938.
3. Rao, T. V., Verma, R. S., and Prasad, R. (1983) Transport of purine, pyrimidine bases and nucleosides in *Candida albicans*, a pathogenic yeast. *Biochem. Int.* **6**: 409-417.
4. Fasoli, M. O., Kerridge, D. (1990) Uptake of pyrimidines and their derivatives into *Candida glabrata* and *Candida albicans*. *J. Gen. Microbiol.* **136**: 1475-1481.
5. Detke, S. (1998) Cloning of the *Candida albicans* nucleoside transporter by complementation of nucleoside transport-deficient *Saccharomyces*. *Yeast* **14**: 1257-1265.
6. Loewen, S. K., Ng, A. M. L., Mohabir, N. N., Baldwin, S. A., Cass, C. E., and Young, J. D. (2003) Functional characterization of a H⁺/nucleoside co-transporter (CaCNT) from *Candida albicans*, a fungal member of the concentrative nucleoside transporter (CNT) family of membrane proteins. *Yeast* **20**: 661-675.
7. Loewen, S. K., Ng, A. M., Yao, S. Y., Cass, C. E., Baldwin, S. A., and Young, J. D. (1999) Identification of amino acid residues responsible for the pyrimidine and purine nucleoside specificities of human concentrative Na⁺ nucleoside co-transporters hCNT1 and hCNT2. *J. Biol. Chem.* **274**: 24475-24484.
8. Wang, J., and Giacomini, K. M. (1999) Serine 318 is essential for the pyrimidine selectivity of the N2 Na⁺-nucleoside transporter. *J. Biol. Chem.* **274**: 2298-2302.
9. Liu, H. (2001) Transcriptional control of dimorphism in *Candida albicans*. *Curr. Opin. Microbiol.* **4**: 728-735.

10. Spellman, P. T., Sherlock, G., Zhang, M. Q., Iyer, V. R., Anders, K., Eisen, M. B., Brown, P. O., Botstein, D., and Futcher, B. (1998) Comprehensive identification of cell cycle-regulated genes of the yeast *Saccharomyces cerevisiae* by microarray hybridization. *Mol. Biol. Cell* **9**: 3273-3297.

Chapter 4:

Specific Mutations in Transmembrane Helix 8 of Human Concentrative Na⁺/Nucleoside Cotransporter hCNT1 Affect Permeant Selectivity and Cation Coupling*

* A version of this chapter has been published. Reproduced in part with permission from

Slugoski, M. D., Loewen, S. K., Ng, A. M. L., Smith, K. M., Yao, S. Y. M., Karpinski, E., Cass, C. E., Baldwin, S. A., and Young, J. D. (2007) Specific mutations in transmembrane helix 8 of human concentrative Na⁺/nucleoside cotransporter hCNT1 affect permeant selectivity and cation coupling. *Biochemistry* **46**: 1684-1693.

Copyright 2007 American Chemical Society.

Acknowledgements

Dr. Shaun K. Loewen shares first author on this publication as he provided the rationale for initiating this project. Mrs. Amy M. L. Ng provided technical assistance with construction of the mutant proteins, cell surface and glycosylation experiments and radioisotope flux assays. Dr. Kyla M. Smith provided technical assistance with the electrophysiology experiments. Dr. Sylvia Y. M. Yao contributed to the discussion of results. Drs. Edward Karpinski, Carol E. Cass and Dr. Stephen A. Baldwin are collaborative principal investigators who assisted with research funding and manuscript preparation. This research was funded by the National Cancer Institute of Canada with funds from the Canadian Cancer Society, Alberta Cancer Board, Heart and Stroke Foundation of Canada and Medical Research Council of the United Kingdom.

Introduction

Human concentrative nucleoside transporters (hCNTs) and other eukaryote CNT family members have a predicted 13 transmembrane domain (TM) architecture, and multiple alignments reveal strong sequence similarities within the carboxyl-terminal half of the proteins, particularly within putative TM regions. Previously, hCNT1/2 sequence comparisons, chimeric constructs and site-directed mutagenesis were used in combination with heterologous expression in *Xenopus laevis* oocytes to identify key residues involved in hCNT1 permeant selectivity (1). Two pairs of residues in TMs 7 and 8 of hCNT1 (Ser³¹⁹/Gln³²⁰ and Ser³⁵³/Leu³⁵⁴) were identified that, when converted together to the corresponding residues in hCNT2 (Gly/Met and Thr/Val, respectively), changed the permeant selectivity of the transporter from pyrimidine nucleoside-selective (*cit*) to purine nucleoside-selective, or *cif*-type. Mutation of Ser³¹⁹ in TM 7 of hCNT1 to glycine enabled transport of purine nucleosides, and concurrent mutation of Gln³²⁰ to methionine augmented this transport. The additional mutation of Ser³⁵³ in TM 8 of hCNT1 to threonine converted S319G/Q320M from broadly selective (*cib*-type) to purine nucleoside-selective (*cif*-type), but with relatively low adenosine transport activity. Further mutation of Leu³⁵⁴ to valine increased the adenosine transport capability of S319G/Q320M/S353T, producing a full *cif*-type phenotype. Residues in both TMs 7 and 8 therefore play key roles in determining hCNT1/2 nucleoside selectivity.

To further explore the structural and functional significance of hCNT1 TM 8 residues, a follow-up series of experiments in which TM 8 residues Ser³⁵³ and Leu³⁵⁴ were subjected to site-directed mutagenesis in the absence of changes to TM 7 was performed. The results reveal dual effects on both nucleoside specificity and cation coupling and, combined with findings from cysteine-directed protein chemistry studies, suggest that the two adjacent TM 8 residues face a common water-accessible cation/nucleoside translocation pathway.

Results and Discussion

In humans, hCNT1/2/3 are functionally distinguished on the basis of nucleoside selectivity. All three proteins transport uridine and adenosine, but are otherwise pyrimidine nucleoside-selective (hCNT1), purine nucleoside-selective (hCNT2), or broadly selective for both pyrimidine and purine nucleosides (hCNT3). Previously, we identified two pairs of isoform-specific residues in the central regions of TMs 7 and 8 of hCNT1 (Ser³¹⁹/Gln³²⁰ and Ser³⁵³/Leu³⁵⁴, respectively) that, when converted to the corresponding residues in hCNT2 (Gly³¹³/Met³¹⁴ and Thr³⁴⁷/Val³⁴⁸) (Fig. 4-1), changed the nucleoside specificity of the protein to that of a hCNT2-like transporter (1). The goal of the present study was to examine the role of the two hCNT1 TM 8 residues (Ser³⁵³/Leu³⁵⁴) independent of those in TM 7.

Surface expression of hCNT1 TM 8 mutants – Wild-type hCNT1, the two individual hCNT1 mutants S353T and L354V, and the double hCNT1 mutant S353T/L354V all exhibited uptake of radiolabeled uridine (20 μ M) in 100 mM NaCl transport medium (pH 7.5) when produced in *Xenopus* oocytes (Fig. 4-2A). In contrast, only basal non-mediated uptake of uridine was evident in control water-injected oocytes under the same conditions. Immunoblots of purified oocyte plasma membranes revealed similar levels of surface expression for each of the constructs and wild-type and mutant hCNT1 proteins migrated with an apparent molecular weight of \sim 70 kDa (Fig. 4-2B). Antibody specificity for hCNT1 was evident from the lack of immunoreactivity in control water-injected oocytes. Thus, the introduced mutations did not affect cell-surface processing of the recombinant proteins.

Nucleoside specificities of hCNT1 TM 8 mutants – As an extension of our previous study (1) and to assess the effects of TM 8 mutations on permeant selectivity, initial experiments compared wild-type hCNT1 uptake of a panel of radiolabeled pyrimidine and purine nucleosides to that of S353T, L354V and S353T/L354V (Fig. 4-3). Mediated transport, defined as the difference in uptake between RNA transcript-injected and control water-injected oocytes, was measured at nucleoside concentrations of 20 μ M in 100 mM NaCl transport medium (pH 7.5).

Uptake in water-injected oocytes was < 0.08 pmol/oocyte.min⁻¹ for all nucleosides tested (thymidine $>$ inosine $>$ cytidine $>$ guanosine $>$ uridine $>$ adenosine) (data not shown). In agreement with previous studies (1, 2-6), the fluxes in Fig. 4-3A show hCNT1 to be selective for pyrimidine nucleosides (uridine $>$ thymidine $>$ cytidine), with no measurable uptake of inosine and guanosine. Previous studies have established that adenosine is a high-affinity, low-capacity permeant of human and rat CNT1 (3, 7). The apparent lack of adenosine transport shown by hCNT1 in Fig. 4-3A reflects the very low $V_{max}:K_m$ ratio exhibited by this permeant. Similar to hCNT1, pyrimidine nucleoside-selective uptake was evident for both S353T (Fig. 4-3B) and L354V (Fig. 4-3C), although relative to uridine uptake, transport of cytidine by S353T was significantly reduced. Additionally, L354V (Fig. 4-3C) showed modestly elevated transport of purine nucleosides (adenosine $>$ inosine $>$ guanosine). This is in good agreement with our previous finding that the L354V mutation augmented adenosine transport by the double TM 7 mutant S319G/Q320M, an effect that occurred through an increase in adenosine V_{max} , with no change in apparent K_m (1). In contrast to the individual mutations, the double mutant S353T/L354V (Fig. 4-3D) showed a unique uridine-selective phenotype with only low levels of uptake for other pyrimidine and purine nucleosides (uridine \gg inosine, thymidine and cytidine $>$ adenosine and guanosine). Similar to L354V, a corresponding small elevation in inosine transport was also apparent for S353T/L354V (Fig. 4-3D).

Nucleoside inhibition of uridine uptake by hCNT1, S353T, L354V and S353T/L354V – To determine if mutation-induced changes in hCNT1 permeant selectivity resulted from modifications to the nucleoside binding pocket and/or changes in nucleoside translocation, uptake of 20 μ M radiolabeled uridine (100 mM NaCl, pH 7.5) by wild-type hCNT1, S353T, L354V and S353T/L354V was measured in the presence of excess (1 mM) non-radioactive nucleosides (Fig. 4-4). In agreement with the nucleoside uptake profile shown in Fig. 4-3A, uridine uptake by wild-type hCNT1 was inhibited $> 91\%$ in the presence of adenosine, uridine, thymidine and cytidine, with lower levels of inhibition evident for inosine (20%) and guanosine (27%) (Fig. 4-4A). Inhibition profiles similar to that of hCNT1 were seen for S353T (Fig. 4-4B), L354V (Fig. 4-4C) and S353T/L354V (Fig. 4-4D), except that L354V

and S353T/L354V showed modestly increased inhibition by inosine and guanosine (L354V) and inosine (S353T/L354V), which reflects the slightly elevated uptake of these nucleosides seen in Figs. 4-3C and D, respectively. The marked inhibition of hCNT1-mediated uridine uptake by adenosine (Fig. 4A), but apparent lack of adenosine transport in Fig. 4-3A, reflected previous demonstrations of this nucleoside's role as a high-affinity, low-capacity hCNT1 permeant (3, 7) and was shared by all three mutant proteins (Figs. 4-3B - D and 4-4B - D). Potentially similar behavior was also apparent for cytidine interactions with mutant S353T (Figs. 4-3B and 4-4B), and for both cytidine and thymidine interactions with mutant S353T/L354V (Figs. 4-3D and 4-4D). Thus, despite exhibiting altered nucleoside transport profiles, the hCNT1 mutant proteins maintained relatively unaltered nucleoside binding pockets in that they retained thymidine and cytidine binding activities. This was confirmed for the uridine-selective S353T/L354V mutant in the experiments of Fig. 4-5 which examined the concentration dependence of thymidine inhibition of uridine uptake (20 μ M). Thymidine effectively inhibited both wild-type hCNT1 and S353T/L354V with broadly similar IC_{50} values of $55 \pm 9 \mu$ M (hCNT1) and $26 \pm 4 \mu$ M (S353T/L354V).

Kinetic properties of hCNT1 TM 8 mutants – To further characterize the differences in pyrimidine nucleoside uptake evident in Figs. 4-3 and 4-4, we determined kinetic parameters of radiolabeled uridine, thymidine and cytidine influx in *Xenopus* oocytes producing wild-type hCNT1 and mutants S353T, L354V and S353T/L354V. Representative concentration dependence curves in 100 mM NaCl transport medium (pH 7.5) for transporter-mediated influx corrected for basal non-mediated uptake measured in control water-injected oocytes are presented in Fig. 4-6. The corresponding kinetic parameters derived from the data are given in Table 4-1. Control fluxes in water-injected oocytes were linear with respect to nucleoside concentration and $< 3.0 \text{ pmol/oocyte.min}^{-1}$ at 1 mM extracellular nucleoside (thymidine \gg cytidine $>$ uridine) (data not shown). In all cases, mediated transport was saturable and conformed to simple Michaelis-Menten kinetics. For wild-type hCNT1 (Fig. 4-6A), lower V_{max} values for transport of thymidine and cytidine relative to that of uridine were partly compensated by lower apparent K_m values, such that $V_{max}:K_m$

ratios, a measure of transport efficiency, were broadly similar for all three nucleosides (1.24 ± 0.05 for uridine, 0.70 ± 0.06 for thymidine and 0.57 ± 0.07 for cytidine) (Table 4-1). Apparent K_m values and the $V_{max}:K_m$ trend of uridine > thymidine > cytidine were consistent with those of previous studies (1, 4-6) and are in good agreement with uptake values presented in Fig. 4-3A.

Similarly, results for mutants S353T, L354V and S353T/L354V (Figs. 4-6B - D) confirmed the findings for uridine, thymidine and cytidine uptake presented in Fig. 4-3, and established the kinetic basis for the unique uridine-selective phenotype of the double mutant S353T/L354V. Mutant L354V (Fig. 4-6C, Table 4-1) exhibited an overall decrease in both apparent K_m and V_{max} values and, as a result, $V_{max}:K_m$ ratios (1.36 ± 0.12 for uridine, 1.06 ± 0.13 for thymidine and 0.46 ± 0.03 for cytidine), were similar to those of wild-type hCNT1. In marked contrast, mutant S353T (Fig. 4-6B, Table 4-1) exhibited substantially reduced $V_{max}:K_m$ ratios (0.35 ± 0.02 for uridine, 0.17 ± 0.02 for thymidine and 0.02 ± 0.01 for cytidine), with cytidine transport being especially compromised as a consequence of a large drop in V_{max} (22-fold decrease relative to uridine). The combination mutant S353T/L354V (Fig. 4-6D, Table 4-1) demonstrated efficient transport of uridine similar to that of wild-type hCNT1 ($V_{max}:K_m$ ratios 1.35 ± 0.10 and 1.24 ± 0.05 , respectively), but was severely compromised with respect to transport of both thymidine and cytidine. As was the case with S353T, low $V_{max}:K_m$ ratios of 0.03 ± 0.01 for thymidine and cytidine transport by S353T/L354V were the result of large decreases in V_{max} with only moderately increased thymidine and cytidine K_m values in comparison to wild-type hCNT1. Overall, the kinetic data confirmed that mutations S353T and S353T/L354V primarily altered pyrimidine nucleoside translocation rather than binding affinities.

Additional mutants – To investigate the relationship between side chain structure and function, the role of hCNT1 TM 8 residue positions 353 and 354 in determining nucleoside selectivity were further studied through additional mutations changing Ser³⁵³ to alanine, cysteine and valine and Leu³⁵⁴ to alanine, cysteine, isoleucine and methionine. Mutant proteins were produced in oocytes and assayed for uridine, thymidine, cytidine and inosine uptake under the same conditions used in

Fig. 4-3. Conversion of hCNT1 Ser³⁵³ to alanine (S353A), cysteine (S353C) or valine (S353V) resulted in proteins with hCNT1-like nucleoside uptake phenotypes, with transport of uridine > thymidine > cytidine and only basal levels of inosine uptake (< 0.1 pmol/oocyte.min⁻¹) (data not shown). Therefore, hydrogen bonding at hCNT1 residue position 353 was not critical for maintaining pyrimidine nucleoside selectivity of the transporter. Conversion of Leu³⁵⁴ to alanine (L354A), cysteine (L354C), isoleucine (L354I) or methionine (L354M) also resulted in proteins with hCNT1-like nucleoside selectivity profiles, with none of the amino acid substitutions mimicking the small L354V increase in inosine uptake (data not shown).

Cation specificity of hCNT1 TM 8 mutants – Mammalian CNTs function predominantly as Na⁺-coupled nucleoside transporters. For hCNT3, H⁺ and Li⁺ have been shown to substitute for Na⁺ (8, 9, Chapter 5), a phenomenon also observed with other Na⁺-coupled membrane cotransport proteins, including the bacterial MelB melibiose transporter, and the mammalian SGLT Na⁺-glucose and SDCT1/NaDC-1 Na⁺/dicarboxylate cotransporters (10-14). To investigate whether changes in nucleoside specificity of hCNT1 TM 8 mutants were accompanied by corresponding alterations in cation selectivities, wild-type hCNT1 and mutant S353T, L354V and S353T/L354V proteins were assayed for radiolabeled uridine uptake (20 μM) in the presence of Na⁺ (100 mM NaCl, pH 7.5), H⁺ (100 mM ChCl, pH 5.5) and Li⁺ (100 mM LiCl, pH 7.5) and in the absence of cation (100 mM ChCl, pH 7.5) (data not shown). Similar to previous studies (6, Chapter 6), Na⁺ was confirmed to be the primary hCNT1 coupling cation with robust uridine uptake in the presence of Na⁺ (7.2 ± 0.7 pmol/oocyte.min⁻¹) and only basal levels of uridine uptake in Na⁺-free H⁺-containing or cation-free medium. Very low, but significant, hCNT1-mediated uptake of uridine was seen in Na⁺-free Li⁺-containing medium (0.16 ± 0.03 pmol/oocyte.min⁻¹). A similar cation selectivity profile was seen for S353T. In contrast, L354V, and to a lesser extent S353T/L354V, showed elevated Li⁺-mediated uridine transport activity (1.2 ± 0.1 (Li⁺) and 5.3 ± 0.4 (Na⁺) pmol/oocyte.min⁻¹ for L354V and 0.6 ± 0.1 (Li⁺) and 3.8 ± 0.1 (Na⁺) pmol/oocyte.min⁻¹ for S353T/L354V). Similar to hCNT1 however, L354V and S353T/L354V showed only basal uridine uptake in Na⁺-free H⁺-containing or cation-

free medium. L354V Li⁺-dependence was most marked for uridine, but was also apparent for other nucleosides (adenosine, thymidine, cytidine) (Fig. 4-7). All of the other residue mutations that were constructed (S353A, S353C, S353V, L354A, L354C, L354I and L354M) maintained hCNT1-like cation selectivity and were not able to mimic the L354V increase in Li⁺-dependence of uridine uptake (data not shown).

Kinetics of Li⁺-dependent uridine transport by L354V – Fig. 4-8 compares Na⁺- and Li⁺-activation curves for wild-type hCNT1 and L354V (20 μM radiolabeled uridine, pH 7.5). Both L354V cation-activation curves indicated that the Li⁺-dependence of L354V reflects a generalized increase in apparent affinities of the mutant transporter for both Na⁺ and Li⁺. Apparent K_{50} values for Na⁺-activation of hCNT1 and L354V were 12 ± 1 and 3.8 ± 0.4 mM, respectively (Fig. 4-8A), compared to > 100 and 71 ± 17 mM, respectively, for Li⁺ (Fig. 4-8B). As expected from previous studies (3, 4, 7, Chapter 6), Hill coefficients for Na⁺-activation of hCNT1 and L354V (0.99 ± 0.04 and 0.91 ± 0.08 , respectively) were consistent with Na⁺:nucleoside coupling stoichiometries of 1:1. Similarly, the Hill coefficient for Li⁺-activation of L354V (0.61 ± 0.05) was also consistent with a 1:1 coupling ratio. A Hill coefficient for Li⁺-mediated transport by hCNT1 could not be determined because of the low apparent affinity of the wild-type transporter for Li⁺.

Previously, we have established that hCNT1 mediates Na⁺-coupled nucleoside transport by a sequential ordered binding mechanism in which cation binds to the transporter first, increasing its affinity for the nucleoside, which then binds second (6). It was predicted, therefore, that the low apparent affinity of hCNT1 for Li⁺ would be matched by a correspondingly low apparent affinity for Li⁺-mediated uridine influx, and that the Li⁺ K_{50} difference between L354V and hCNT1 would be mirrored by a corresponding downward shift in nucleoside apparent K_m value. The experiments of Fig. 4-9, which confirmed these predictions, compared the concentration dependence of hCNT1- and L354V-mediated radiolabeled uridine influx in Na⁺- and Li⁺-containing transport medium (100 mM NaCl and LiCl, pH 7.5). In agreement with Figs. 4-6A and 4-6C and Table 4-1, the apparent K_m values for Na⁺-mediated uridine transport were 24 ± 2 (hCNT1) and 15 ± 2 μM (L354V). Li⁺-

mediated uridine uptake was non-saturable for hCNT1 (Fig. 4-9A), but exhibited an apparent K_m value of $210 \pm 20 \mu\text{M}$ for L354V (Fig. 4-9B). No such K_m shift was apparent for Na^+ -mediated uridine uptake (Figs. 4-6A and 4-6C and Table 4-1), because these transport assays were performed at a Na^+ concentration of 100 mM which was sufficient to fully saturate both the mutant and wild-type transporters. The V_{max} value for Li^+ -mediated uridine uptake by L354V was similar to that in the presence of Na^+ (9.9 ± 0.3 and $10 \pm 1 \text{ pmol/oocyte.min}^{-1}$, respectively).

The electrogenic nature of the Li^+ -dependent uridine transport by wild-type hCNT1 and L354V is demonstrated in Fig. 4-10, which shows results of experiments that used the two-electrode, voltage clamp method to compare representative whole-cell currents induced by 1 mM uridine measured in medium containing either Na^+ (100 mM NaCl, pH 7.5) or Li^+ (100 mM LiCl, pH 7.5). Since the Leu³⁵⁴ mutation affected Na^+ and hence uridine apparent binding affinity, the transport difference between L354V and hCNT1 in Li^+ medium was minimized at the high uridine concentration used in this experiment. Thus, the electrophysiology recordings demonstrated uridine-induced Li^+ currents for both L354V and hCNT1. These representative electrophysiology current recordings are consistent with the radioisotope flux data shown in Fig. 4-9.

p-Chloromercuribenzenesulfonate (PCMBS) inhibition of S353C- and L354C-mediated uridine transport – Residues lining the translocation pore can be identified through the use of water-soluble thiol-reactive reagents such as membrane-impermeant PCMBS (15). Although wild-type hCNT1 contains 20 endogenous cysteine residues, there was no change in hCNT1-mediated uptake of 20 μM radiolabeled uridine (100 mM NaCl, pH 7.5) following preincubation with PCMBS at concentrations up to 1 mM (Fig. 4-11A). However, uridine uptake by both S353C and L354C was strongly inhibited by low μM concentrations of PCMBS and the presence of extracellular uridine (20 mM) significantly protected both mutants against this inhibition (Figs. 4-11B and 4-11C). While previous helix modeling of hCNT1 TM 8 predicted that Ser³⁵³ faces the translocation pore and Leu³⁵⁴ is involved in helix-helix interactions (1), the present results suggested that both residues are

accessible from the extracellular medium, pore-lining and in close proximity to the uridine-binding pocket. Additional evidence supporting this conclusion is found in a cysteine-less version of hCNT3 in which the corresponding residues, when individually mutated to cysteine, also show inhibition of uridine uptake by PCMBBS (unpublished observations).

Conclusions

Mutational analysis of hCNT1 TM 8 Ser³⁵³ and Leu³⁵⁴ has revealed a dual role for these adjacent residues in both nucleoside selectivity and cation coupling. Mutation of these residue positions to the corresponding residues in hCNT2 resulted in (i) decreased cytidine transport (S353T), (ii) a unique uridine-selective phenotype (S353T/L354V), (iii) a modest increase in inosine transport (L354V) and (iv) increased apparent affinities for Na⁺ and Li⁺ (L354V). In all cases, the alterations in hCNT1 functional phenotype were amino acid-specific. A possible role for Ser³⁵³ in forming hydrogen bonds with the nucleoside permeant was discounted by substitution of other amino acids at this position. Competition studies revealed that the double mutant S353T/L354V retained an apparently normal nucleoside binding pocket, its novel uridine-selective transport phenotype resulting instead from changes in the subsequent nucleoside translocation phase of the transport cycle. The present results also revealed that wild-type hCNT1 exhibited a low, but significant, affinity for Li⁺ as the coupling cation, an interaction that was markedly enhanced in mutant L354V and, to a lesser extent, in S353T/L354V. This is similar to hCNT3, which can utilize Na⁺ and Li⁺ (and H⁺) electrochemical gradients to drive transport (10). The L354V and S353T/L354V mutations did not lead to H⁺-dependence, indicating different structural requirements for CNT H⁺- and Na⁺/Li⁺-coupling. Mutation of both TM 8 residue positions to cysteine resulted in uridine-protected inhibition by PCMBBS. Structurally, this places each of these residues in an orientation facing the translocation pore and in the vicinity of the uridine binding pocket. This proposed topology, as well as the influence of both hCNT1 TM 8 residues Ser³⁵³ and Leu³⁵⁴,

either alone or in combination, on permeant and cation interactions, therefore suggest closely adjacent interactions of nucleosides and cations within a common hCNT1 translocation pore. The recently reported crystal structure of *Aquifex aeolicus* Leu_{Aa}, a homolog of mammalian Na⁺/Cl⁻-dependent neurotransmitter transporters, depicts a similar structural model for transport whereby bound leucine and Na⁺ ions are located in close association within the protein core halfway across the membrane with both binding sites being defined by partially unwound transmembrane helices (16).

Table 4-1. Kinetic parameters for uridine, thymidine and cytidine uptake by hCNT1 and hCNT1 mutants produced in *Xenopus* oocytes^a.

Transporter	Nucleoside	Apparent K_m (μM)	V_{max} (pmol/oocyte.min ⁻¹)	$V_{max} \cdot K_m$ ratio
hCNT1	Uridine	33 \pm 2	41 \pm 1	1.24 \pm 0.05
	Thymidine	27 \pm 2	19 \pm 1	0.70 \pm 0.06
	Cytidine	23 \pm 2	13 \pm 1	0.57 \pm 0.07
S353T	Uridine	19 \pm 1	6.7 \pm 0.1	0.35 \pm 0.02
	Thymidine	12 \pm 1	2.0 \pm 0.1	0.17 \pm 0.02
	Cytidine	16 \pm 2	0.3 \pm 0.1	0.02 \pm 0.01
L354V	Uridine	14 \pm 1	19 \pm 1	1.36 \pm 0.12
	Thymidine	7.2 \pm 0.9	7.6 \pm 0.2	1.06 \pm 0.13
	Cytidine	14 \pm 1	6.4 \pm 0.1	0.46 \pm 0.03
S353T/L354V	Uridine	5.7 \pm 0.4	7.7 \pm 0.1	1.35 \pm 0.10
	Thymidine	46 \pm 9	1.2 \pm 0.1	0.03 \pm 0.01
	Cytidine	41 \pm 3	1.1 \pm 0.1	0.03 \pm 0.01

^a, values (\pm SE) taken from Fig. 4-6.

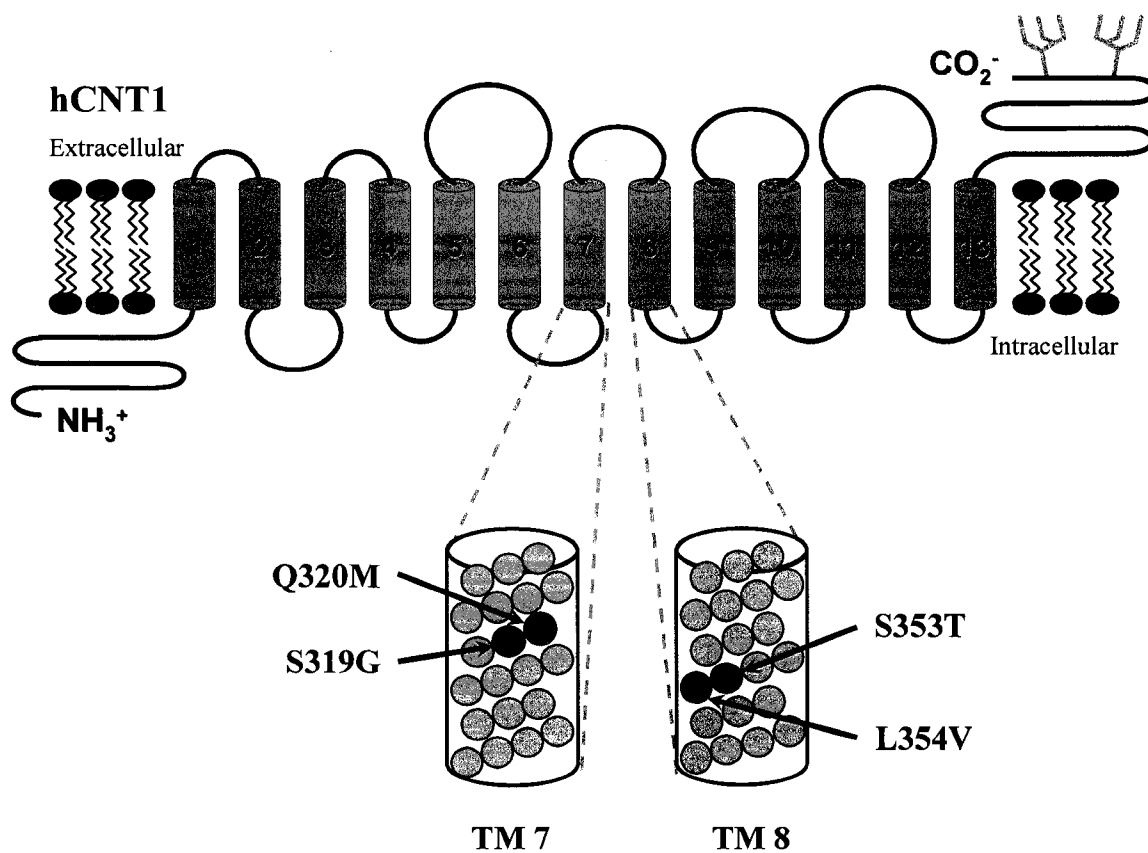


Figure 4-1. hCNT1 topology model. Putative membrane-spanning α -helices are *numbered* and glycosylation sites are indicated by the ψ -like symbol in the extracellular C-terminal tail. Residues identified in hCNT1 to be important for nucleoside selectivity are shown in the expanded TMs 7 and 8 by *solid circles*.

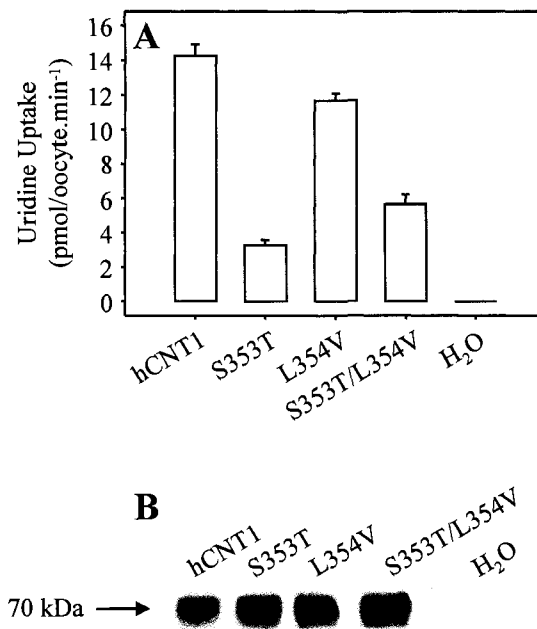


Figure 4-2. Functional activity and protein expression levels of hCNT1-, S353T-, L354V- and S353T/L354V-producing oocytes. *Xenopus* oocytes injected with RNA transcripts encoding hCNT1, S353T, L354V or S353T/L354V and control water-injected oocytes were assayed for functional activity by uptake of 20 μ M radiolabeled-uridine in 100 mM NaCl transport medium (pH 7.5) (A) and plasma membrane recombinant protein expression by immunoblotting (B). Flux assay values are the means \pm SEM of 10 - 12 oocytes. Flux values that are less than the thickness of the line appear as zero.

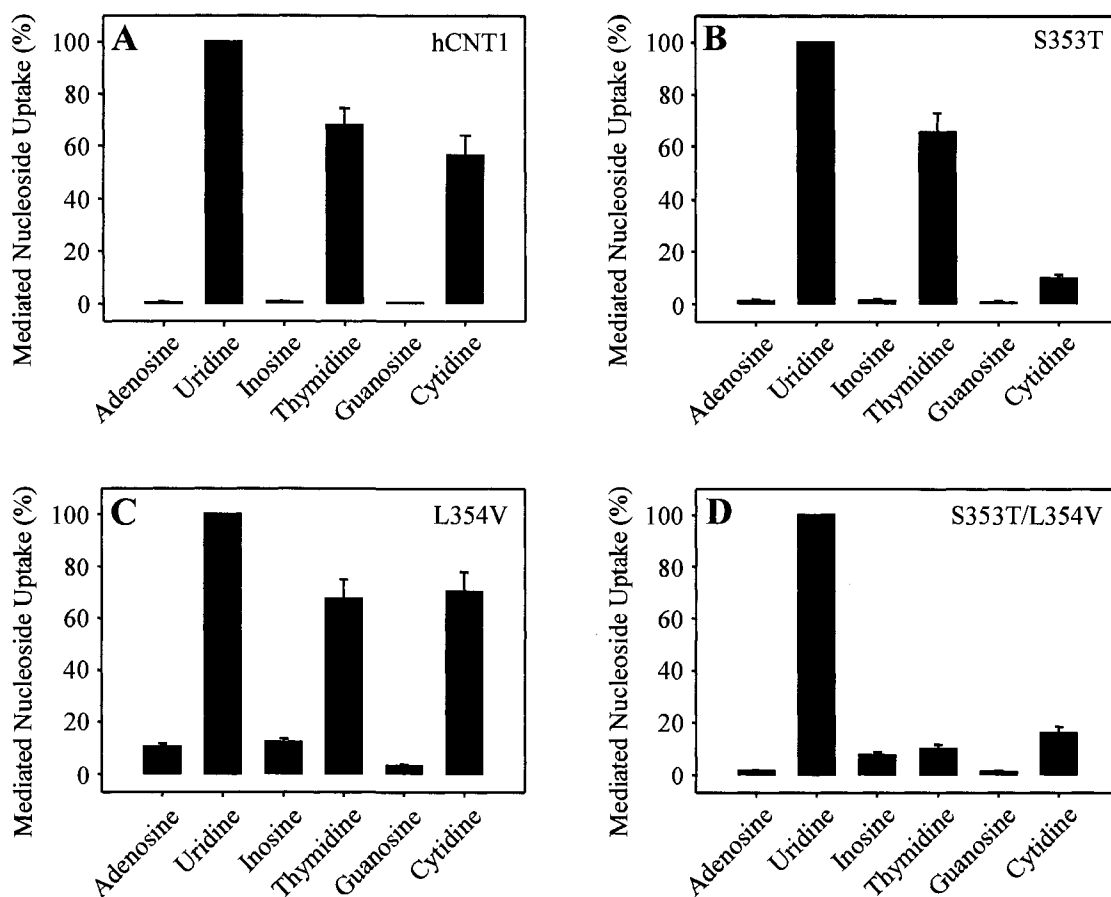


Figure 4-3. Nucleoside selectivity of hCNT1-, S353T-, L354V- and S353T/L354V-producing oocytes. *Xenopus* oocytes were injected with RNA transcripts encoding hCNT1 (A), S353T (B), L354V (C) or S353T/L354V (D). Uptake of a panel of radiolabeled physiological nucleosides (adenosine, uridine, inosine, thymidine, guanosine, cytidine) at a concentration of 20 μ M was measured in transport medium containing 100 mM NaCl, pH 7.5. Data are presented as mediated transport, calculated as uptake in RNA-injected oocytes *minus* uptake in oocytes injected with water alone, and normalized to the mediated uridine uptake for each transport protein. Mediated uridine fluxes were 6.1 ± 0.4 (hCNT1), 1.3 ± 0.1 (S353T), 3.8 ± 0.3 (L354V) and 2.7 ± 0.3 (S353T/L354V) pmol/oocyte.min⁻¹. Each value represents the mean \pm SEM of 10 - 12 oocytes. Mediated uptake values that are less than the thickness of the line appear as zero. Experiments were performed on the same batch of oocytes used on the same day.

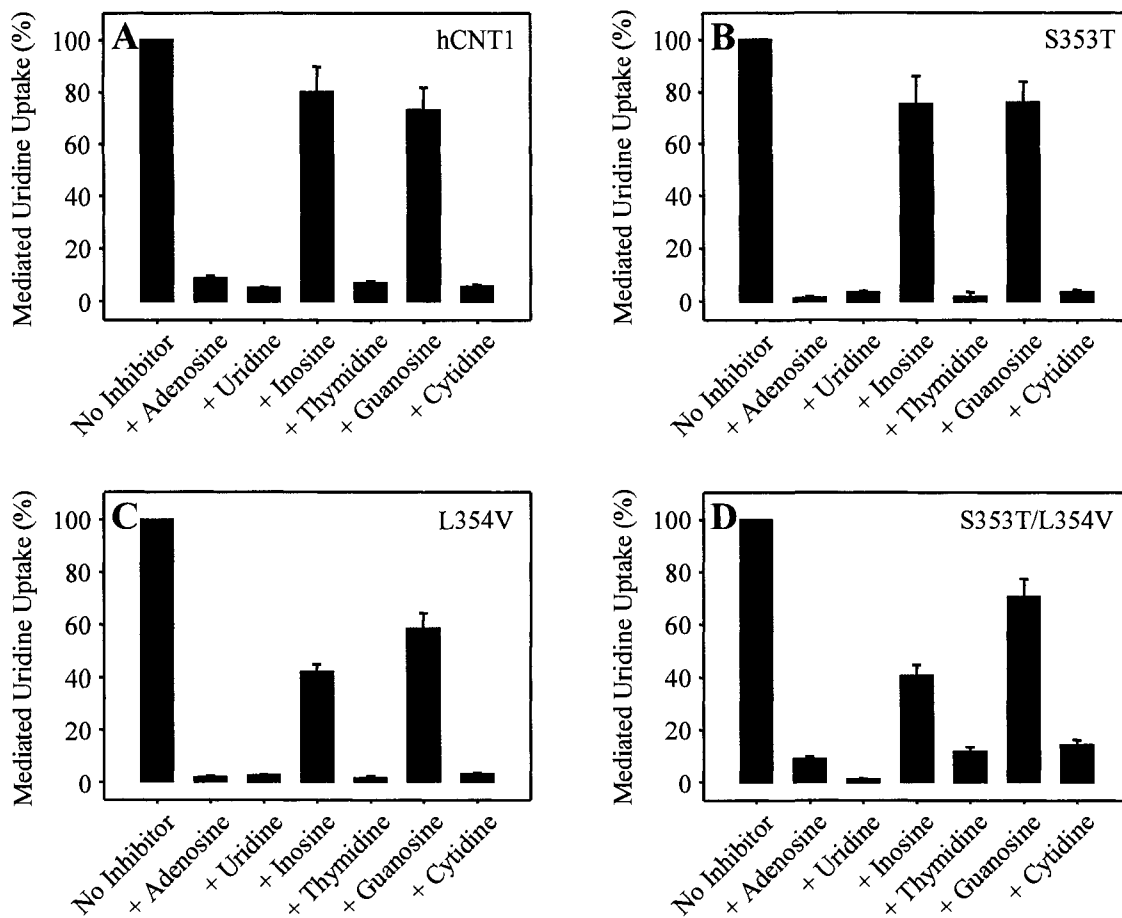


Figure 4-4. Inhibition of hCNT1-, S353T-, L354V- and S353T/L354V-mediated uridine uptake by physiological nucleosides. hCNT1- (A), S353T- (B), L354V- (C) and S353T/L354V-mediated (D) uptake of 20 μ M radiolabeled uridine was measured in the presence and absence of a panel of physiological nucleosides (adenosine, uridine, inosine, thymidine, guanosine, cytidine) at a concentration of 1 mM in transport medium containing 100 mM NaCl, pH 7.5. Data are presented as mediated transport, calculated as uptake in RNA-injected oocytes *minus* uptake in oocytes injected with water alone, and normalized to uptake in the absence of inhibitor for each transport protein. Mediated uridine fluxes were 7.1 ± 0.6 (hCNT1), 1.7 ± 0.2 (S353T), 3.9 ± 0.2 (L354V) and 2.3 ± 0.2 (S353T/L354V) pmol/oocyte.min⁻¹. Each value represents the mean \pm SEM of 10 - 12 oocytes. Mediated uptake values that are less than the thickness of the line appear as zero. Experiments were performed on the same batch of oocytes used on the same day.

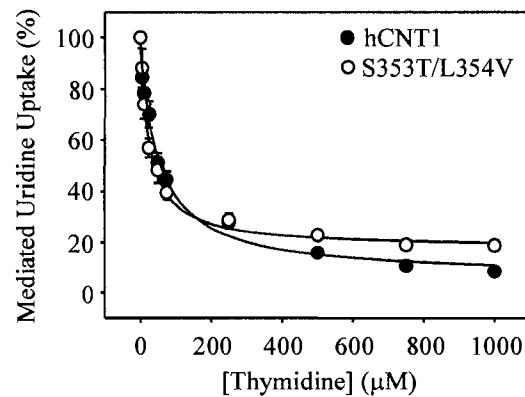


Figure 4-5. Thymidine inhibition of uridine uptake by hCNT1- and S353T/L354V-producing oocytes. Uptake of 20 μM radiolabeled uridine in the presence of increasing concentrations of thymidine was measured in hCNT1- (*solid circles*) and S353T/L354V-producing oocytes (*open circles*) in 100 mM NaCl transport medium, pH 7.5. Data are presented as mediated transport, calculated as uptake in RNA-injected oocytes *minus* uptake in water-injected oocytes, and normalized to mediated uridine uptake in the absence of extracellular thymidine. Mediated uridine fluxes in the absence of thymidine were 20 ± 1 (hCNT1) and 8.2 ± 0.5 (S353T/L354V) $\text{pmol}/\text{oocyte}\cdot\text{min}^{-1}$. Each value represents the mean \pm SEM of 10 - 12 oocytes. Error bars are not shown where values were smaller than that represented by the symbols. Experiments were performed on the same batch of oocytes used on the same day.

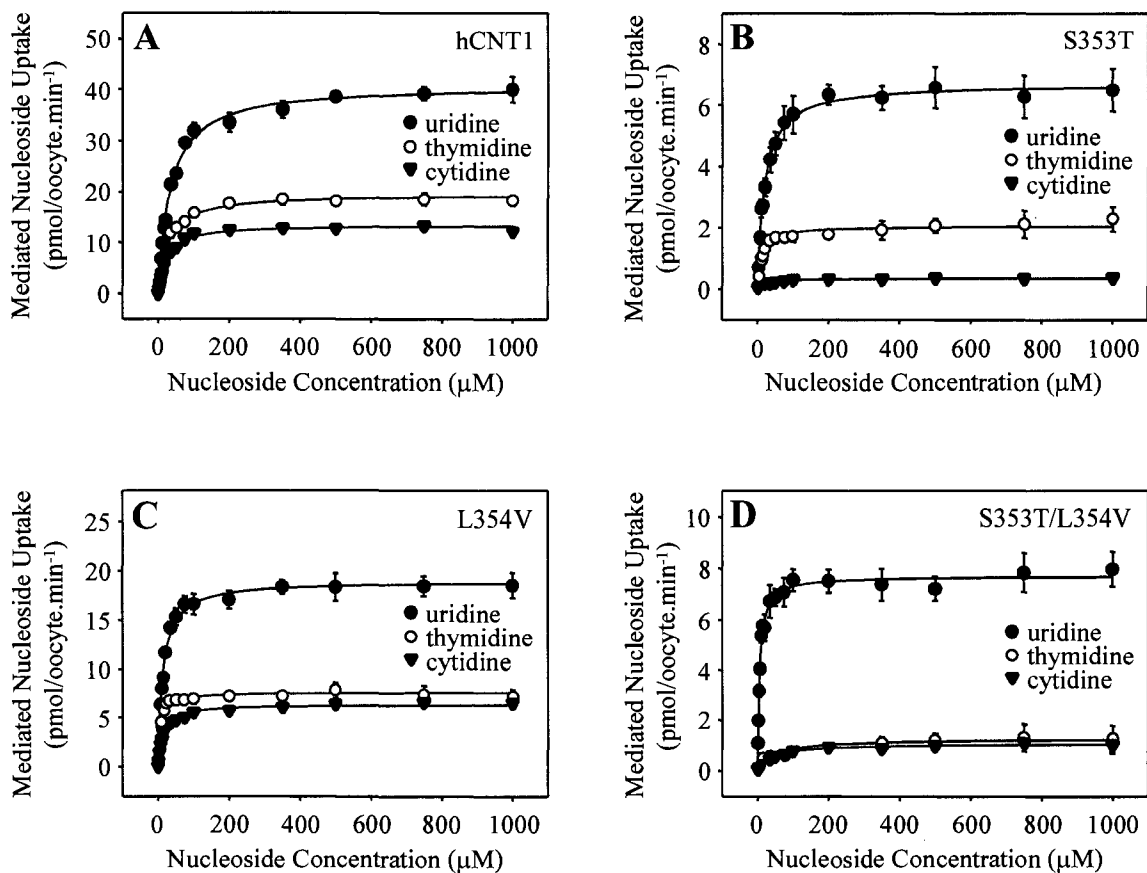


Figure 4-6. Uridine, thymidine and cytidine uptake kinetics in oocytes producing hCNT1, S353T, L354V and S353T/L354V. Uptake of radiolabeled uridine (*solid circles*), thymidine (*open circles*) and cytidine (*solid triangles*) in 100 mM NaCl transport medium (pH 7.5) were measured in hCNT1- (*A*), S353T- (*B*), L354V- (*C*) or S353T/L354V-producing (*D*) *Xenopus* oocytes. Data are presented as mediated transport, calculated as uptake in RNA-injected oocytes *minus* uptake in oocytes injected with water alone. Each value represents the mean \pm SEM of 10 - 12 oocytes. Error bars are not shown where values were smaller than that represented by the symbols. Experiments were performed on the same batch of oocytes used on the same day.

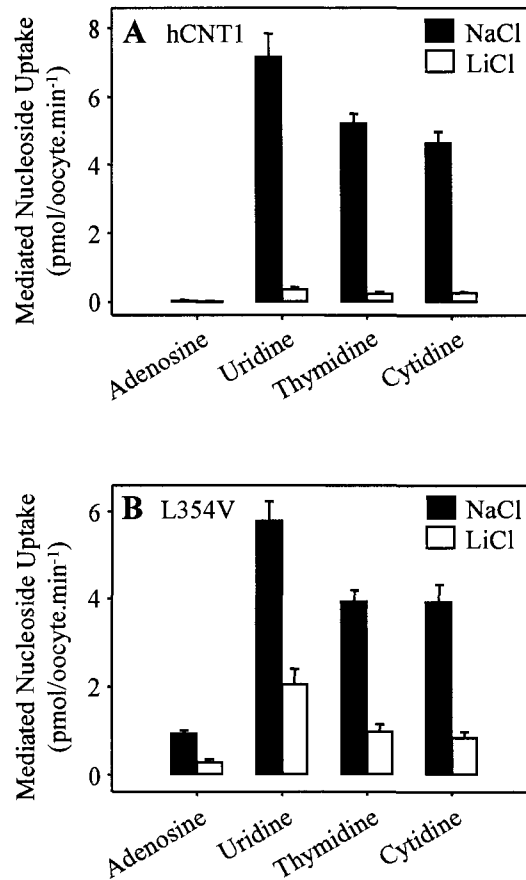


Figure 4-7. Na⁺- and Li⁺-dependent nucleoside transport by hCNT1 and L354V. Uptake of 20 μ M radiolabeled physiological nucleosides (adenosine, uridine, thymidine, cytidine) in oocytes producing hCNT1 (A) or L354V (B) was measured in transport medium containing 100 mM NaCl (*solid bars*) or LiCl (*open bars*) (pH 7.5). Data are presented as mediated transport, calculated as uptake in RNA-injected oocytes *minus* uptake in water-injected oocytes. Each value represents the mean \pm SEM of 10 - 12 oocytes. Mediated uptake values that are less than the thickness of the line appear as zero. Experiments were performed on the same batch of oocytes used on the same day.

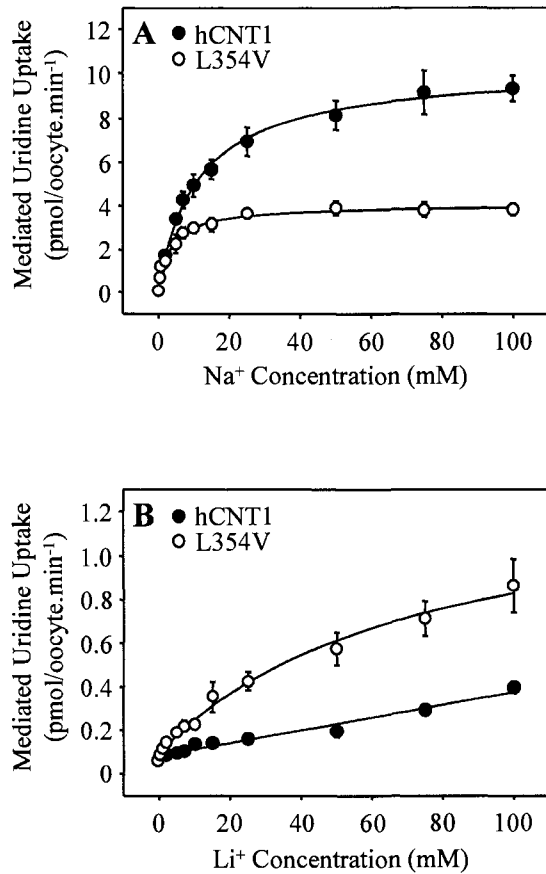


Figure 4-8. hCNT1 and L354V Na⁺- and Li⁺-activation kinetics. Uptake of 20 μ M radiolabeled uridine by hCNT1 (*solid circles*) and L354V (*open circles*) was measured as a function of Na⁺ (*A*) and Li⁺ concentration (*B*), using choline⁺ as an isosmotic Na⁺ substitute (pH 7.5). Data are presented as mediated transport, calculated as uptake in RNA-injected oocytes *minus* uptake in water-injected oocytes. Each value represents the mean \pm SEM of 10 - 12 oocytes. Error bars are not shown where values were smaller than that represented by the symbols. Experiments were performed on the same batch of oocytes used on the same day.

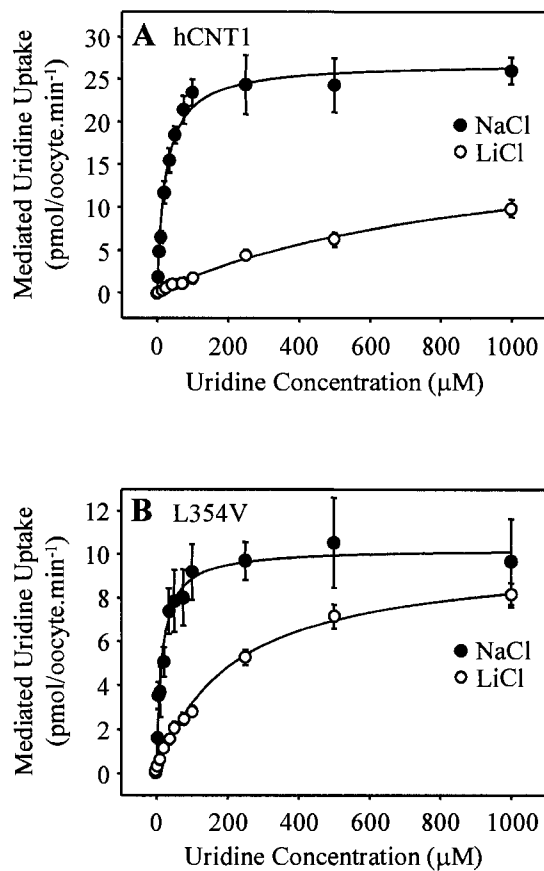


Figure 4-9. Concentration dependence of Na⁺- and Li⁺-dependent uridine uptake by hCNT1 and L354V. Radiolabeled uridine uptake in Na⁺- (*solid circles*) and Li⁺-containing transport medium (*open circles*) was determined in oocytes expressing hCNT1 (*A*) and L354V (*B*) (100 mM NaCl or LiCl, pH 7.5). Data are presented as mediated transport, calculated as uptake in RNA-injected oocytes *minus* uptake in water-injected oocytes. Each value represents the mean \pm SEM of 10 - 12 oocytes. Error bars are not shown where values were smaller than that represented by the symbols. Experiments were performed on the same batch of oocytes used on the same day.

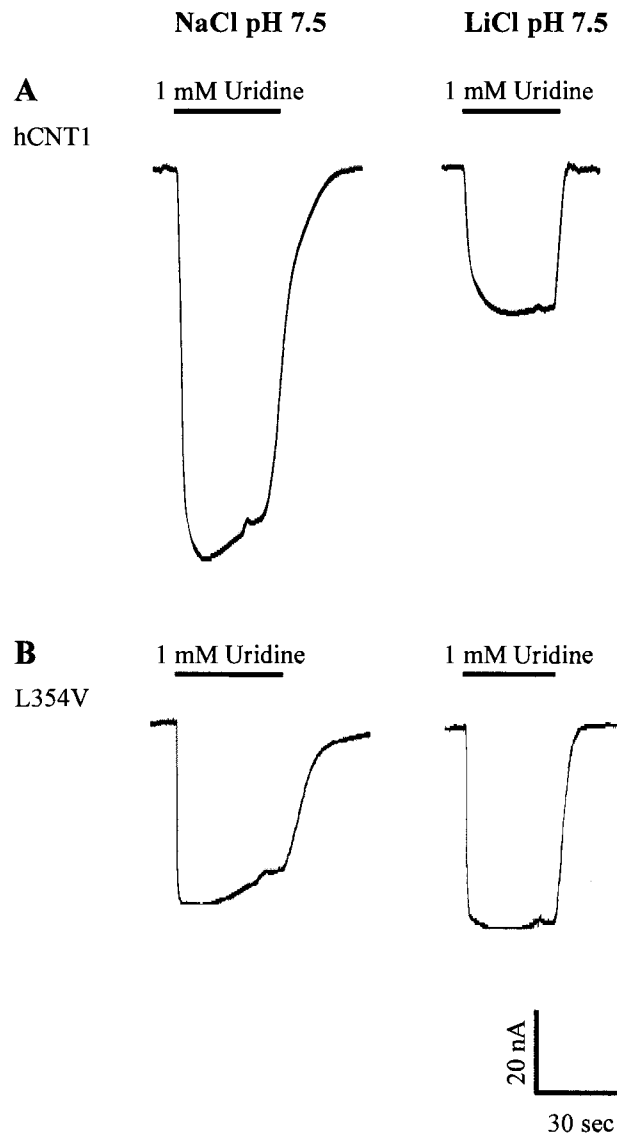


Figure 4-10. Uridine-evoked currents in hCNT1- and L354V-producing oocytes. Uridine-evoked currents in 100 mM NaCl and LiCl transport medium at pH 7.5 (right and left columns, respectively) are shown for representative oocytes producing hCNT1 (A) or L354V (B). No current was detected in control water-injected oocytes (data not shown). Bars indicate the duration of exposure to 1 mM uridine. Currents were recorded in the same batch of oocytes used on the same day.

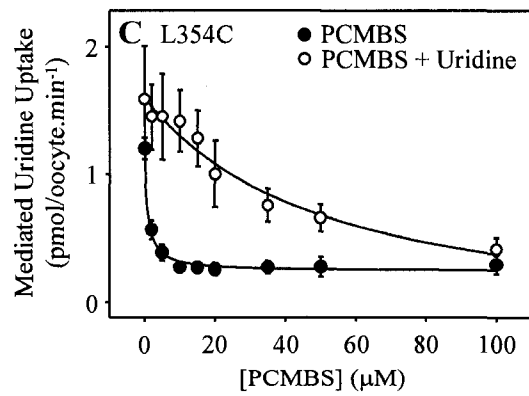
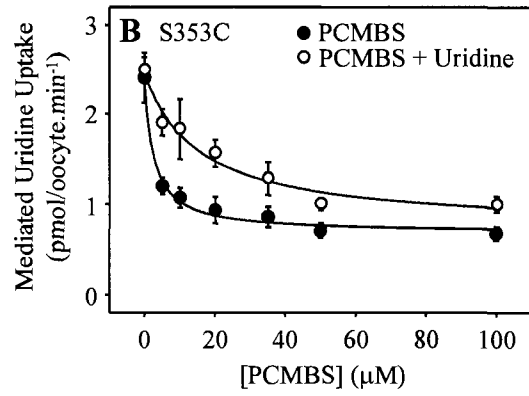
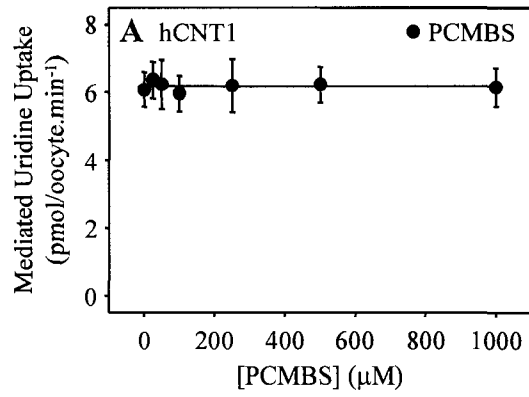


Figure 4-11.

Figure 4-11. PCMBS inhibition of hCNT1-, S353C- and L354C-mediated uridine transport. Radiolabeled uridine uptake (20 μ M) was measured in oocytes producing hCNT1 (A), S353C (B) or L354C (C) that had been preincubated in the presence of PCMBS (*solid circles*) or in the presence of PCMBS and 20 mM uridine (*open circles*) (100 mM NaCl, pH 7.5). Data are presented as mediated transport, calculated as uptake in RNA-injected oocytes *minus* uptake in water-injected oocytes. Each value represents the mean \pm SEM of 10 - 12 oocytes. Error bars are not shown where values were smaller than that represented by the symbols. Experiments were performed on the same batch of oocytes used on the same day.

Bibliography

1. Loewen, S. K., Ng, A. M., Yao, S. Y., Cass, C. E., Baldwin, S. A., and Young, J. D. (1999) Identification of amino acid residues responsible for the pyrimidine and purine nucleoside specificities of human concentrative Na⁺ nucleoside cotransporters hCNT1 and hCNT2. *J. Biol. Chem.* **274**: 24475-24484.
2. Huang, Q. Q., Yao, S. Y. M., Ritzel, M. W. L., Paterson, A. R. P., Cass, C. E., and Young, J. D. (1994) Cloning and functional expression of a complementary DNA encoding a mammalian nucleoside transport protein. *J. Biol. Chem.* **269**: 17757-17760.
3. Ritzel, M. W. L., Yao, S. Y. M., Huang, M. Y., Elliot, J. F., Cass, C. E., and Young, J. D. (1997) Molecular cloning and functional expression of cDNAs encoding a human Na⁺-nucleoside cotransporter (hCNT1). *Am. J. Physiol.* **272**: C707-C714.
4. Dresser, M. J., Gerstin, K. M., Gray, A. T., Loo, D. D. F., and Giacomini, K. M. (2000) Electrophysiological analysis of the substrate selectivity of a sodium-coupled nucleoside transporter (rCNT1) expressed in *Xenopus laevis* oocytes. *Drug Metab. Dispos.* **28**: 1135-1140.
5. Lostao, M. P., Mata, J. F., Larrayoz, I. M., Inzillo, S. M., Casado, F. J., and Pastor-Anglada, M. (2000) Electrogenic uptake of nucleosides and nucleoside-derived drugs by the human nucleoside transporter 1 (hCNT1) expressed in *Xenopus laevis* oocytes. *FEBS Lett.* **481**: 137-140.
6. Smith, K. M., Ng, A. M. L., Yao, S. Y. M., Labedz, K. A., Knaus, E. E., Wiebe, L. I., Cass, C. E., Baldwin, S. A., Chen, X-Z., Karpinski, E., and Young, J. D. (2004) Electrophysiological characterization of a recombinant human Na⁺-coupled nucleoside transporter (hCNT1) produced in *Xenopus oocytes*. *J. Physiol.* **558**: 807-823.
7. Yao, S. Y. M., Ng, A. M. L., Ritzel, M. W. L., Gati, W. P., Cass, C. E., and Young, J. D. (1996) Transport of adenosine by recombinant purine- and pyrimidine-selective sodium/nucleoside cotransporters from rat jejunum expressed in *Xenopus laevis* oocytes. *Mol. Pharmacol.* **50**: 1529-1535.
8. Ritzel, M. W. L., Yao, S. Y. M., Ng, A. M. L., Mackey, J. R., Cass, C. E., and Young, J. D. (1998) Molecular cloning, functional expression and chromosomal localization of a cDNA encoding a human Na⁺/nucleoside cotransporter

- (hCNT2) selective for purine nucleosides and uridine. *Mol. Membr. Biol.* **15**: 203-211.
9. Ritzel, M. W. L., Ng, A. M. L., Yao, S. Y. M., Graham, K., Loewen, S. K., Smith, K. M., Ritzel, R. G., Mowles, D. A., Carpenter, P., Chen, X-Z., Karpinski, E., Hyde, R. J., Baldwin, S. A., Cass, C. E., and Young, J. D. (2001) Molecular identification and characterization of novel human and mouse concentrative Na⁺-nucleoside cotransporter proteins (hCNT3 and mCNT3) broadly selective for purine and pyrimidine nucleosides (system *cib*). *J. Biol. Chem.* **276**: 2914-2927.
 10. Pourcher, T., Bassilana, M., Sarkar, H. K., Kaback, R., and Leblanc, G. (1990) The melibiose/Na⁺ symporter of *Escherichia coli*: kinetic and molecular properties. *Philos. Trans. R. Soc. Lond. Ser. B. Biol. Sci.* **326**: 411-423.
 11. Hirayama, B. A., Loo, D. D. F., and Wright, E. M. (1994) Protons drive sugar transport through the Na⁺/glucose cotransporter (SGLT1). *J. Biol. Chem.* **269**: 21407-21410.
 12. Hirayama, B. A., Loo, D. D. F., and Wright, E. M. (1997) Cation effects on protein conformation and transport in the Na⁺/glucose cotransporter. *J. Biol. Chem.* **272**: 2110-2115.
 13. Pajor, A. M., Hirayama, B. A., and Loo, D. D. F. (1998) Sodium and lithium interactions with the Na⁺/dicarboxylate cotransporter. *J. Biol. Chem.* **273**: 18923-18929.
 14. Chen, X.-Z., Shayakul, C., Berger, U. V., Tian, W., and Hediager, M. A. (1998) Characterization of a rat Na⁺-dicarboxylate cotransporter. *J. Biol. Chem.* **273**: 20972-20981.
 15. Yao, S. Y. M., Sundaram, M., Chomey, E. G., Cass, C. E., Baldwin, S. A., and Young, J. D. (2001) Identification of Cys140 in helix 4 as an exofacial cysteine residue within the substrate-translocation channel of rat equilibrative nitrobenzylthioinosine (NBMPR)-insensitive nucleoside transporter rENT2. *Biochem. J.* **353**: 387-393.
 16. Yamashita, A., Singh, S. K., Kawate, T., Jin, Y., and Gouaux, E. (2005) Crystal structure of a bacterial homologue of Na⁺/Cl⁻-dependent neurotransmitter transporters. *Nature* **437**: 215-223.

Chapter 5:
**The Broadly Selective Human Na⁺/Nucleoside Cotransporter
(hCNT3) Exhibits Novel Cation-Coupled Nucleoside Transport
Characteristics***

* A version of this chapter has been published.

Smith, K., M., Slugoski, M. D., Loewen, S. K., Ng, A. M. L., Yao, S. Y. M., Chen, X.-Z., Karpinski, E., Cass, C. E., Baldwin, S. A., and Young, J. D. (2005) The broadly selective human Na⁺/nucleoside cotransporter (hCNT3) exhibits novel cation-coupled nucleoside transport characteristics. *J. Biol. Chem.* **280**: 25436-25449.

Acknowledgements

Sharing first author on this publication, Dr. Kyla M. Smith completed the electrophysiology experiments in this project and Dr. Shaun K. Loewen completed the preliminarily corresponding work on mCNT3. Mrs. Amy M. L. Ng and Dr. Sylvia Y. M. Yao provided technical assistance with this project. Dr. Xing-Zhen Chen assisted with interpretation and discussion of the electrophysiology experiments. Drs. Edward Karpinski, Carol E. Cass and Stephen A. Baldwin are collaborative principal investigators who assisted with research funding and manuscript preparation. This research was funded by the National Cancer Institute of Canada with funds from the Canadian Cancer Society, Alberta Cancer Board, Heart and Stroke Foundation of Canada and Medical Research Council of the United Kingdom.

Introduction

Human and mouse concentrative nucleoside transporters (hCNT3 and mCNT3, respectively) are the most recent mammalian CNT family members to be identified (1) and, together with *cib*-type hagfish CNT (hfCNT) (2), form a phylogenetic CNT subfamily separate from the mammalian CNT1/2 subfamily (1). In addition to differences in nucleoside selectivities (3-5), members of the two subfamilies also differ in the stoichiometry of Na⁺:nucleoside coupling. For example, hCNT1 has a Na⁺:nucleoside coupling ratio of 1:1 (6), whereas the coupling ratio of hfCNT is 2:1 (2). This study further extends these investigations and presents a mechanistic and chimeric analysis of cation coupling in hCNT3. The results validate previously reported differences in cation-coupling between the CNT3/hfCNT and CNT1/2 subfamilies and reveal additional novel features of CNT3/cation interactions.

Results

Cation-dependence of hCNT3 – In a previous study, heterologous expression in *Xenopus laevis* oocytes was used in combination with radioisotope flux assays and the two-microelectrode voltage-clamp to demonstrate that recombinant hCNT3 functions as a broad specificity *cib*-type electrogenic Na⁺/nucleoside symporter (1). The experiment of Fig. 5-1 extended these findings and demonstrated the effect of an imposed H⁺ gradient on the initial rate of hCNT3-mediated uptake (influx) of ¹⁴C-uridine (20 μM) measured at extracellular pH values ranging from 5.5 to 8.5 under Na⁺-free conditions. Choline (Ch⁺) was substituted for Na⁺, and values were corrected for basal non-mediated uptake in control water-injected oocytes (< 0.03 pmol/oocyte.min⁻¹ under all conditions tested). A marked pH-dependence of uridine influx was apparent. In 100 mM ChCl at pH 5.5, for example, hCNT3-mediated uridine influx was 26-fold higher than at pH 8.5, and was ~ 60% of that obtained in the presence of 100 mM NaCl at pH 7.5. In the absence of either H⁺ or Na⁺, hCNT3 also exhibited Li⁺-dependent uridine influx (100 mM LiCl, pH 8.5 *versus* 100 mM ChCl, pH 8.5). In marked contrast, hCNT1 and hCNT2, the two other human CNT

isoforms, showed no pH-dependent uridine uptake and exhibited very small Li^+ -mediated uridine influx ($\leq 2\%$ of the corresponding Na^+ -mediated uridine flux; data not shown). As illustrated in Fig. 5-2, the novel H^+ - and Li^+ -dependence of hCNT3 was further investigated by electrophysiology. External application of $100 \mu\text{M}$ uridine to a representative hCNT3-producing oocyte clamped at -50 mV under Na^+ -free conditions elicited inward H^+ and Li^+ currents that returned to baseline upon removal of nucleoside (Fig. 5-2A). As demonstrated by the mean current data in Fig. 5-2B, H^+ currents were markedly inhibited by pre-treatment of oocytes with the protonophore carbonyl cyanide *m*-chlorophenylhydrazone (CCCP). No currents were observed in control water-injected oocytes (data not shown). Thus, in addition to being Na^+ -dependent, hCNT3 functioned as an electrogenic H^+ /nucleoside and Li^+ /nucleoside symporter. These findings were also confirmed in parallel studies of mCNT3 (data not shown). Subsequent experiments focused on the mechanism(s) of Na^+ - and H^+ -coupling of hCNT3.

Cation-induced changes in hCNT3 permeant selectivity – In Na^+ -containing medium at physiologic pH 7.5, hCNT3 transports different radiolabeled physiologic pyrimidine and purine nucleosides with similar apparent K_m values and $V_{\text{max}}:K_m$ ratios (1). As illustrated by the mean current data in Fig. 5-3A, a panel of pyrimidine (uridine, thymidine and cytidine) and purine (adenosine, inosine and guanosine) nucleosides elicited similar large inward Na^+ currents when applied at $100 \mu\text{M}$ to hCNT3-producing oocytes in NaCl transport medium at pH 7.5. The corresponding inward currents generated by the same panel of nucleosides under Na^+ -free conditions were measured in ChCl transport medium of increasing acidity (pH 8.5, 7.5, 6.5 and 5.5). For clarity of presentation, only values obtained at pH 5.5 and 8.5 are shown in Fig. 5-3B. Similar to the trend seen for uridine in Fig. 5-1, inward pH-dependent nucleoside-evoked currents were evident for uridine, thymidine and adenosine, were less marked for cytidine and inosine, and were absent for guanosine. A corresponding selectivity profile for hCNT3 H^+ /nucleoside cotransport was obtained in radioisotope nucleoside influx assays (Fig. 5-3C). Those nucleosides in Figs. 5-3B and C that exhibited the lowest transport activity in Na^+ -free acidified medium (cytidine, inosine and guanosine) were also tested by electrophysiology at a higher

nucleoside concentration of 1 mM (Fig. 5-3D). Permeant-induced H⁺ currents were confirmed for cytidine and inosine, while guanosine-evoked currents remained low and pH-independent. For all nucleosides and conditions tested, no currents were evident (data not shown) and basal non-mediated radioisotope fluxes were < 0.07 pmol/oocyte.min⁻¹ in control water-injected oocytes. Na⁺- and H⁺-coupled hCNT3 therefore exhibited markedly different selectivity profiles for physiologic nucleosides.

This difference in nucleoside selectivity between Na⁺- and H⁺-coupled hCNT3 extended to interactions with therapeutic nucleoside analogs. In Na⁺-containing medium at physiologic pH 7.5, hCNT3 efficiently transports the anticancer nucleoside drug gemcitabine (dFdC), and mediates lower, but still significant, fluxes of the antiviral nucleoside drugs zidovudine (AZT), zalcitabine (ddC) and didanosine (ddI) (1). As shown by the traces from a single representative oocyte in Fig. 5-4A and by the mean current data in Fig. 5-4B, dFdC (100 μM) elicited inward Na⁺ and H⁺ currents that returned to baseline upon removal of permeant, whereas ddC and AZT (1 mM) produced inward currents only in the presence of Na⁺. No currents were detected in control water-injected oocytes (data not shown). The inability of H⁺-coupled hCNT3 to support ddC and AZT transport was confirmed in parallel radioisotope flux experiments (data not shown).

Voltage-dependence of hCNT3 transport currents – Fig. 5-5A shows representative current traces in a hCNT3-producing oocyte in Na⁺-containing medium (pH 8.5) before and after perfusion with 100 μM uridine in an experiment undertaken to examine the effects of membrane potential on uridine-induced steady-state currents. Currents evoked by uridine at potentials between +60 and -110 mV were voltage-dependent and increased as the membrane potential became more negative (Fig. 5-5B). Uridine-induced Na⁺ currents approached zero, but did not reverse polarity at potentials up to +60 mV. Measured in the same oocyte, uridine-induced H⁺ currents (ChCl, pH 5.5) were approximately half those in Na⁺-containing medium and exhibited a similar voltage-dependence. In other experiments performed over a wider V_h range, uridine-induced Na⁺ and H⁺ currents did not saturate at negative potentials up to -150 mV (data not shown).

Voltage-dependence of hCNT3 transport kinetics – The effects of membrane potential on hCNT3 transport kinetics in the presence of external Na^+ were examined in detail by measuring the apparent affinities for uridine (K_m) and Na^+ (K_{50}) and the uridine-evoked maximum current (I_{\max}) at four different holding potentials ($V_h = -10, -30, -50$ and -70 mV) (Fig. 5-6). K_m was determined in transport medium containing either 10 or 100 mM NaCl (pH 8.5), and mean values plotted as a function of V_h are summarized in Fig. 5-6C. As representative examples of the kinetic data used to generate K_m values, Figs. 5-6A and B show uridine concentration dependence curves recorded from individual oocytes at a membrane potential of -10 mV and external Na^+ concentrations of 10 and 100 mM, respectively. K_{50} was determined at an external uridine concentration of 100 μM (pH 8.5), and mean values plotted as a function of V_h summarized in Fig. 5-6E. The representative single oocyte Na^+ -activation curve shown in Fig. 5-6D was measured at a holding potential of -10 mV. I_{\max} values were determined independently at a saturating external uridine concentration of 100 μM and a Na^+ concentration of 100 mM (pH 8.5) (Fig. 5-6F).

As demonstrated in Fig. 5-6C, K_m was unaffected by membrane potential at 100 mM external Na^+ , but was voltage-dependent at 10 mM Na^+ , decreasing from 24 to 7.3 μM as the membrane potential was made more negative. At high negative potentials, the K_m value at 10 mM NaCl approached that observed at 100 mM external Na^+ , suggesting that the effect of membrane potential on K_m was predominantly the result of voltage-dependence of Na^+ binding (7, 8). Consistent with this, the Na^+ K_{50} value decreased from 5.3 mM at -10 mV to 2.1 mM at -70 mV (Fig. 5-6E). As shown in Fig. 5-6F, I_{\max} also increased as the membrane potential was made more negative. At a holding potential of -10 mV (100 mM NaCl), the mean uridine-evoked inward current was 37 nA. This increased to 97 nA at -70 mV, a trend that was similar to the current-voltage (I-V) relationship shown in Fig. 5-5B. Calculated over the same limited V_h range (-10 to -70 mV), I-V curves for 5 oocytes gave an e -fold change (\pm SE) in current per 77 ± 4 mV, compared to 67 ± 11 mV for the data in Fig. 5-6F. I_{\max} reflects movement of the loaded and empty carrier (8). Therefore, similar to the Na^+ /glucose cotransporter SGLT1, membrane potential

influenced the electrogenic rate-limiting step of ion-binding and/or carrier translocation (7, 8).

Cation-dependence of uridine transport kinetics – Fig. 5-7 shows the concentration dependence of ^{14}C -uridine influx in Na^+ - and choline-containing transport media at pH 5.5 and 7.5 measured in both hCNT3-producing and control water-injected oocytes. Kinetic parameters (K_m and V_{\max}) derived from these data for the hCNT3-mediated component of influx (uptake in RNA transcript-injected oocytes *minus* uptake in water-injected oocytes) are presented in Table 5-1. Removal of extracellular Na^+ at pH 7.5 led to a greater than 30-fold increase in the K_m value for uridine influx from 17 to 580 μM that was partially offset by a small (1.6-fold) increase in V_{\max} (Figs. 5-7A and B). As shown in Fig. 5-7D, the decrease in uridine apparent affinity was substantially reversed by acidification of the transport medium to pH 5.5 (uridine K_m 110 μM). In contrast, acidification of the transport medium in the presence of Na^+ had only modest effects on uridine transport kinetics (Figs. 5-7A and C). $V_{\max}:K_m$ ratios, a measure of transporter efficiency, were: 2.0 in the presence of Na^+ (NaCl, pH 7.5), 0.09 in the absence of Na^+ (ChCl, pH 7.5), 0.58 in the presence of H^+ (ChCl, pH 5.5) and 1.7 with both cations ($\text{Na}^+ + \text{H}^+$) present (NaCl, pH 5.5). Therefore, Na^+ and H^+ activated hCNT3 through mechanisms resulting in increased uridine apparent binding affinity. Relative to Na^+ alone, $\text{Na}^+ + \text{H}^+$ elicited no further shift in uridine K_m , suggesting that the two cations exert their effects by binding to a common or overlapping site(s).

Na^+ - and H^+ -activation kinetics – The relationship between hCNT3-mediated uridine-evoked current and Na^+ concentration (pH 8.5) was measured in oocytes clamped at -50 mV at three different uridine concentrations (5, 25 and 100 μM). Kinetic parameters derived from these experiments are presented in Table 5-2. As reported previously for hCNT3 (and mCNT3) based on ^{14}C -uridine influx experiments (1), and as illustrated in Fig. 5-8A for a single representative oocyte measured at a uridine concentration of 5 μM , the Na^+ -activation curve was sigmoidal with a Hill coefficient (n) consistent with an apparent $\text{Na}^+:\text{nucleoside}$ coupling stoichiometry of 2:1 (see also Fig. 5-6D). Both the apparent affinity for Na^+ (K_{50}) and

the maximal current (I_{\max}) increased as the external concentration of uridine was raised (Table 5-2). This pattern resembled that found for hCNT1 (6) and was consistent with a sequential mechanism of transport in which Na^+ binds to the transporter first, increasing its affinity for nucleoside, which then binds second (9-12). Parallel experiments with ^{14}C -uridine produced similar findings (data not shown).

The relationship between hCNT3 current evoked by 100 μM uridine and external pH in the absence of Na^+ (ChCl, pH 8.5 - 4.5) was also investigated (Table 5-2). As illustrated for the representative oocyte in Fig. 5-8B, and in contrast to the sigmoidal activation curve observed for Na^+ , a plot of current *versus* H^+ concentration was hyperbolic with a Hill coefficient (n) consistent with a H^+ :nucleoside coupling stoichiometry of 1:1. Parallel ^{14}C -uridine influx experiments revealed similar hyperbolic H^+ -activation kinetics (data not shown). Apparent K_{50} values for H^+ and Na^+ differed by four orders of magnitude (480 nM and 2.4 - 5.9 mM, respectively) (Table 5-2).

Na⁺:nucleoside and H⁺:nucleoside coupling ratios – The Na^+ :uridine and H^+ :uridine stoichiometries of hCNT3 were directly determined by simultaneously measuring uridine-evoked currents and ^{14}C -uridine uptake under voltage-clamp conditions, as described previously for SGLT1 (13), the rat kidney dicarboxylate transporter SDCT1 (14) and, most recently, for hCNT1 (6), hfCNT (2) and CaCNT (15). Each data point in Figs. 5-9A - F represents a single oocyte, and the Na^+ :nucleoside or H^+ :nucleoside coupling ratio is given by the slope of the linear fit of charge (pmol) *versus* uptake (pmol) (Table 5-3).

The first series of experiments was performed in Na^+ -containing transport medium at pH 8.5, and at holding potentials of -30, -50 and -90 mV to determine the Na^+ :nucleoside coupling ratio and its voltage-dependence. At a holding potential of -30 mV, the linear correlation between uridine-dependent charge and uridine accumulation gave a stoichiometry of 1.4 (Fig. 5-9A) (Table 5-3). This increased to 1.6 at -50 mV and 1.9 at -90 mV (Figs. 5-9B and C) (Table 5-3). In marked contrast, parallel experiments performed in Na^+ -free ChCl transport medium at pH 5.5 to

determine the H^+ :nucleoside coupling ratio at V_h -30, -50 and -90 mV found voltage-independent stoichiometries in the range 0.92 - 1.1 (Figs. 5-9D -F) (Table 5-3). The same analysis was also performed in the presence of Na^+ and H^+ (NaCl, pH 5.5). As summarized in Table 5-3, coupling ratios were voltage-independent and in the range 1.9 - 2.0.

Charge-to- Na^+ stoichiometry – The relationship between uridine-evoked charge influx (pmol) and $^{22}Na^+$ uptake (pmol) was measured in 5 oocytes clamped at -90 mV (Fig. 5-10). A linear fit of the data gave a regression line with a slope of 0.97, indicating that 1 net inward positive charge was transported for every Na^+ ion cotransported with uridine into the cell (Table 5-3).

Characterization of hCNT3/hCNT1 chimeras – hCNT3 and hCNT1 are 48% identical and 57% similar in predicted amino acid sequence, with the strongest residue conservation in transmembrane domains (TMs) of the C-terminal halves of the proteins (Fig. 5-11A). The major differences lie in the putative N- and C-terminal tails and in the first three TMs. To localize domains involved in cation recognition, a chimera, (hCNT3/1) in which the C-terminal half of hCNT3 (incorporating TMs 7 - 13) was replaced with that of hCNT1, was constructed. The splice site between the two proteins following hCNT3 residue Lys³¹⁴ was engineered at the beginning of the putative extramembraneous loop prior to TM 7 to divide the proteins into two approximately equal halves and to minimize disruption of native TMs and loops. The resulting hCNT3/1 chimeric protein was functional when produced in *Xenopus* oocytes, and exhibited hCNT1-like permeant selectivity for influx of 20 μ M radiolabeled pyrimidine and purine nucleosides (NaCl, pH 7.5): uridine, thymidine, cytidine \gg adenosine, and no detectable transport of guanosine or inosine (Fig. 5-11B). The reciprocal chimera (hCNT1/3), representing a 50:50 construct incorporating the N-terminal half of hCNT1 and the C-terminal half of hCNT3, was non-functional and not studied further. As shown in Fig. 5-11C, hCNT3/1 was Na^+ -dependent, but H^+ -independent, demonstrating that the structural features determining H^+ -coupling reside in the C-terminal half of the protein. Similar to hCNT1 (6, 16), the relationship between hCNT3/1-mediated ^{14}C -uridine influx and Na^+ concentration

at pH 7.5 was hyperbolic with a Hill coefficient (n) of 1.0 ± 0.1 (Fig. 5-11D), a value consistent with a Na^+ :nucleoside coupling stoichiometry of 1:1.

Discussion

The CNT protein family in humans is represented by three members, hCNT1, hCNT2 and hCNT3, corresponding to concentrative nucleoside transport processes *cit*, *cif* and *cib*, respectively. hCNT3 is a transcriptionally-regulated electrogenic transport protein that, unlike hCNT1 and hCNT2, transports a broad range of pyrimidine and purine nucleosides and nucleoside drugs (1). hCNT3 and its mouse ortholog mCNT3 are more closely related in sequence to the prevertebrate hagfish transporter hfCNT (2) than to mammalian CNT1/2, and thus form a separate CNT subfamily. The present study utilized heterologous expression in *Xenopus* oocytes in combination with electrophysiological, radioisotope flux and chimeric experiments to characterize the selectivity, mechanism, energetics and structural basis of hCNT3 cation coupling. Parallel experiments with mCNT3 confirmed the general applicability of the reported findings.

Unlike hCNT1 and hCNT2, which are largely Na^+ -specific, hCNT3 exhibited Na^+ -, H^+ - and Li^+ -dependence, all three cations supporting electrogenic uridine influx. In this regard, hCNT3 resembles the mammalian concentrative glucose transporters SGLT1 and SGLT3, the bacterial MelB melibiose transporter and the mammalian Na^+ /dicarboxylate cotransporter SDCT1/NaDC-1, all of which can also utilize Na^+ , H^+ or Li^+ to drive cellular accumulation of permeant (14, 17-20). Consistent with an intracellular oocyte pH of 7.3 - 7.6 (21), nucleoside-evoked H^+ currents were minimal at external pH values of 7.5 or higher. Use of CCCP to dissipate the imposed H^+ electrochemical gradient across the cell membrane (22, 23) decreased the uridine-evoked current in acidified Na^+ -free medium by $\sim 60\%$, confirming that hCNT3 is coupled to the proton-motive force. H^+ - and Li^+ -coupling within the CNT3/hfCNT subfamily is unique to h/mCNT3 and is not shared by hfCNT (2). In contrast, some other CNTs function exclusively as H^+ /nucleoside symporters, including NupC from

Escherichia coli, CeCNT3 from *Caenorhabditis elegans* and CaCNT from *Candida albicans* (15, 24, Appendix 2).

Na⁺/nucleoside and H⁺/nucleoside symport by hCNT3 exhibited markedly different selectivity characteristics for physiologic nucleosides and therapeutic nucleoside drugs, suggesting that Na⁺ and H⁺ binding induce cation-specific conformational changes in the hCNT3 nucleoside-binding pocket and/or translocation channel. For H⁺-coupled hCNT3, this was reflected in markedly reduced transport activity for thymidine, cytidine, adenosine and inosine, and inability to transport guanosine, AZT and ddC. In a possibly related phenomenon, functional studies with microglia have shown that an inwardly-directed H⁺ gradient can inhibit AZT uptake (25). Microglia have *cib*-type activity as a major component of their nucleoside transport machinery (26).

Consistent with results of recent studies of hCNT1 (6), the proton/myo-inositol cotransporter (10) and SGLT1 (11), hCNT3 kinetic experiments revealed an ordered binding mechanism. Na⁺ removal increased the transporter's K_m for uridine by more than 30-fold, this being accompanied by a smaller (1.6-fold) increase in V_{max} . Limiting the concentration of Na⁺ can therefore be overcome by increasing the concentration of uridine to reach similar maximal rates of transport (9-12). In contrast, limiting the concentration of uridine reduced both the apparent affinity of hCNT3 for Na⁺ and the maximal current. Na⁺ therefore binds to hCNT3 first, followed by nucleoside. Like SGLT1 (18), the apparent affinity of hCNT3 for H⁺ was four orders of magnitude higher than for Na⁺. H⁺ and Na⁺ binding to SGLT1 also lead to cation-specific conformational changes which, like hCNT3, were reflected in a decrease in sugar-binding affinity and transport efficiency of the H⁺-coupled transporter (19). In the case of hCNT3, substitution of H⁺ for Na⁺ resulted in a six-fold change in uridine apparent affinity, and an ~ 70% decrease in $V_{max} \cdot K_m$ ratio (Table 5-1). Unlike hCNT3, however, H⁺-coupled SGLT1 exhibited only modest changes in sugar specificity compared to the Na⁺-coupled transporter (19). Similar to SGLT1, hCNT3-mediated Na⁺/nucleoside and H⁺/nucleoside symport were voltage-dependent (7, 8). The apparent affinity of hCNT3 for uridine was voltage insensitive

at high external Na^+ concentrations, but voltage dependent when the concentration of Na^+ was reduced, suggesting that the voltage dependence of the transporter's apparent affinity for uridine may be due to the voltage dependence of Na^+ binding (7, 8). This was supported by experiments showing a similar voltage dependence of the apparent affinity of hCNT3 for Na^+ . As in the case of SGLT1, these results are indicative of the presence of an ion-well effect (7, 8), with presteady-state electrophysiological studies suggesting that Na^+ binds to hCNT3 $\sim 40\%$ within the membrane electric field (27). Na^+ /nucleoside and H^+ /nucleoside I-V curves and the effect of membrane potential on I_{max} values suggest that membrane potential also influences carrier translocation. This is consistent with the fact that the driving force for an electrogenic transporter is dependent upon not only the gradients of nucleoside and cotransported ion, but also upon the membrane potential.

Based on indirect Hill-type analyses of the relationship between nucleoside influx and Na^+ concentration, Na^+ :nucleoside stoichiometries of 1:1 have been described for *cit* and *cif* transport activities in different mammalian cells and tissues (3-5), and for recombinant rCNT1 and hCNT1 produced in *Xenopus* oocytes (6, 28). Although Larráyoz *et al.* (29) have reported a hCNT1 Na^+ :nucleoside coupling ratio of 2:1 based on results of direct charge *versus* ^3H -uridine and $^{22}\text{Na}^+$ uptake studies, the stoichiometry of hCNT1 has also been reported as 1:1 (6). H^+ -dependent CaCNT also exhibits a coupling ratio of 1:1 (15). In marked contrast, there is evidence from Na^+ -activation studies of mammalian *cib* transporters (1, 16, 30) and from charge *versus* uridine uptake experiments with hagfish hfcNT (2) that members of the CNT3/hfcNT subfamily have a coupling ratio of 2:1. The charge *versus* uridine and charge *versus* Na^+ uptake experiments reported here for hCNT3 confirmed this stoichiometry. The Hill coefficient for Na^+ -activation of hCNT3 is close to 2, implying strong cooperativity between the two Na^+ -binding sites (31, 32).

Similar to SGLT1 (11, 33, 34), but unique amongst the other CNTs that have been examined to date (hCNT1, hfcNT and CaCNT) (2, 6, 15), the experimentally determined Na^+ :nucleoside coupling ratio of hCNT3 was voltage-dependent, increasing progressively to its maximum value of 2:1 as the membrane potential

became more negative. As in the case of SGLT1 (34), this may reflect an effect of membrane potential on Na^+ dissociation from the cytoplasmic face of the transporter, with a consequent reduction in Na^+ recycling back to the external surface of the membrane. Other transporter families also have individual members with different cation-coupling ratios. For example, members of the SGLT family have been described with 1:1 and 2:1 Na^+ :glucose coupling ratios (1:1 for SGLT2 and 2:1 for SGLT1/3) (11, 33-35). Similarly, the PepT1 and PepT2 proton-linked peptide transporters have 1:1 and 2:1 H^+ :peptide coupling ratios, respectively (36). Mechanistically, the cation-to-nucleoside coupling ratio determines the energetic cost of transport, and sets the thermodynamic limit to the transmembrane nucleoside gradients that can be achieved. The concentrative capacity of hCNT3 is therefore greater than that of either hCNT1 or hCNT2.

In marked contrast to SGLT1, where both Na^+ and H^+ have the same 2:1 cation:sugar stoichiometries (18, 34, 37), charge/uptake analyses revealed a hCNT3 Na^+ :nucleoside coupling ratio of 2:1 *versus* 1:1 for H^+ . Unlike Na^+ , the H^+ coupling ratio was membrane potential-independent. Charge/uptake experiments with both Na^+ and H^+ present together (Na^+ -containing transport medium at pH 5.5) revealed features intermediate between Na^+ or H^+ alone (2:1 coupling ratio and voltage-independent), suggesting that both cations contributed to the driving force under these conditions. The 2:1 charge:uptake coupling ratio under these conditions implies that one of the two Na^+ binding sites is shared by H^+ . Since proton-activation experiments gave a Hill coefficient consistent with a 1:1 H^+ :nucleoside coupling ratio, it is unlikely that there exists a second (recycled) H^+ bound to hCNT3. The hCNT3 cation binding site shared by Na^+ and H^+ is likely to be the same as that responsible for single-site cation coupling in CNTs that are either exclusively H^+ -dependent (CaCNT, NupC) (15, Appendix 2) or Na^+ -dependent (hCNT1/2) (3-6, 28).

The results for cation coupling of hCNT3 can be interpreted in terms of the conformational equilibrium model of secondary active transport developed by Krupka (38, 39). This modified ordered binding model of secondary active transport alleviates the stringent sequential carrier states of earlier models and instead allows

for flexible cation interactions such as those observed for Na⁺- and H⁺-coupling of hCNT3. Because the transporter can accept two different solutes, cation (A) and nucleoside (S), it is proposed to exist in two inwardly-facing or outwardly-facing conformational states: one that binds cation only (T_i' and T_o') and one that binds both cation and nucleoside (T_i'' and T_o''). Normally, the equilibrium between the two outwardly-facing carrier states overwhelmingly favours the T_o' form, and requires the addition of cation (two Na⁺ ions or one H⁺ in the case of hCNT3) to “unlock” or open the nucleoside binding site (T_o'A ↔ T_o''A), thereby promoting active transport. Both T_o''S and T_o''AS are considered mobile. The finding that binding of a H⁺ to one of the two Na⁺-binding sites is sufficient to activate nucleoside transport presents an experimental paradigm to enable mutagenic dissection of amino acid residues contributing to each of the sites. The 50:50 hCNT3/1 chimera demonstrated that the structural determinants of cation/nucleoside stoichiometry and H⁺-dependence reside in the C-terminal half of the protein. Hill-type analysis of Na⁺:nucleoside coupling in a corresponding 50:50 chimera between hCNT and hCNT1 yielded similar results (2). The present finding that determinants of hCNT1 *versus* hCNT3 nucleoside selectivity also reside in the C-terminal half of the protein is consistent with previous mutagenesis experiments that identified residues in TMs 7 and 8 of hCNT1 that, when sequentially mutated to the corresponding residues in hCNT2, progressively changed the selectivity of the transporter from *cit* to *cib* to *cif* (40).

In conclusion, hCNT3 exhibited unique cation interactions with Na⁺, H⁺ and Li⁺ that are not shared by other members of the CNT protein family. Both indirect and direct methods indicated 2:1 and 1:1 cation/nucleoside stoichiometries for Na⁺ and H⁺, respectively, and Na⁺- and H⁺-coupled hCNT3 exhibited markedly different selectivities for nucleoside and nucleoside drug transport. Location of hCNT3-specific cation interactions to the C-terminal half of the protein sets the stage for site-directed mutagenesis experiments to identify the residues involved. The ability of hCNT3 to couple nucleoside and nucleoside drug accumulation to H⁺ as well as Na⁺ cotransport may have physiological and pharmacological relevance in the duodenum and proximal jejunum where the pH of luminal contents can be relatively acidic. As

well, there is a reported acidic microenvironment present on the surface of the intestinal epithelium (41).

Table 5-1. Apparent K_m and V_{max} values for uridine transport by hCNT3.

		Apparent K_m^a (μM)	V_{max}^a ($\text{pmol}/\text{oocyte}\cdot\text{min}^{-1}$)	$V_{max}\cdot K_m$
pH 7.5	NaCl ^b	17 ± 1	34 ± 1	2.0
	ChCl ^b	580 ± 70	53 ± 3	0.09
pH 5.5	NaCl ^b	25 ± 3	43 ± 1	1.7
	ChCl ^b	110 ± 10	64 ± 1	0.58

^a, from Fig. 5-7A - D; ^b, in transport media containing either 100 mM NaCl or 100 mM ChCl.

Table 5-2. Na⁺- and H⁺-activation kinetics of hCNT3. Hill coefficients (*n*) and apparent affinities (*K*₅₀) for Na⁺ were determined from Na⁺ concentration response curves (0 - 100 mM NaCl, pH 8.5) in hCNT3-producing oocytes measured at uridine concentrations of 5, 25 and 100 μM (see Fig. 5-8A for a representative experiment at 5 μM uridine). Those for H⁺ were determined from H⁺ concentration response curves (pH 8.5 - 4.5) measured in Na⁺-free transport medium (100 mM ChCl) at a uridine concentration of 100 μM (see Fig. 5-8B for a representative experiment). Values were obtained from fits to data from individual oocytes normalized to the fitted *I*_{max} value obtained for that cell, and are presented as means ± SEM. *I*_{max} values (nA) (± SEM) in the presence of Na⁺ were determined separately at a saturating concentration of uridine (100 μM) with 100 mM external Na⁺ (pH 8.5) in oocytes from a single batch of cells used on the same day. The numbers in parentheses denote the number of oocytes. The membrane potential was -50 mV.

	Uridine Concentration (μM)	<i>n</i>	Apparent <i>K</i> ₅₀ ^a	<i>I</i> _{max} (nA)
Na ⁺	5	1.7 ± 0.1(5)	5.9 ± 0.3 (5)	22 ± 2 (6)
	25	1.8 ± 0.1(4)	3.1 ± 0.1 (4)	43 ± 2 (6)
	100	1.7 ± 0.1(5)	2.4 ± 0.4 (5)	56 ± 4 (6)
H ⁺	100	0.66 ± 0.02 (6)	480 ± 70 (6)	-----

^a, The apparent *K*₅₀ for Na⁺ is in mM, while that for H⁺ is in nM.

Table 5-3. Stoichiometry of hCNT3.

V_h (mV)	Charge: ^{14}C -uridine Stoichiometry			Charge: $^{22}\text{Na}^+$ Stoichiometry
	Na^{+a} (100 mM NaCl, pH 8.5)	$\text{Na}^+ + \text{H}^+$ (100 mM NaCl, pH 5.5)	H^{+a} (100 mM ChCl, pH 5.5)	Na^{+b} (1 mM NaCl, pH 8.5)
-30	1.4 ± 0.1 (9)	2.0 ± 0.1 (9)	0.92 ± 0.05 (9)	
-50	1.6 ± 0.1 (9)	1.9 ± 0.1 (8)	1.1 ± 0.1 (9)	
-90	1.9 ± 0.1 (10)	2.0 ± 0.1 (10)	0.94 ± 0.04 (9)	0.97 ± 0.04 (5)

^a, from Fig. 5-9; ^b, from Fig. 5-10. The numbers in parentheses denote the number of oocytes.

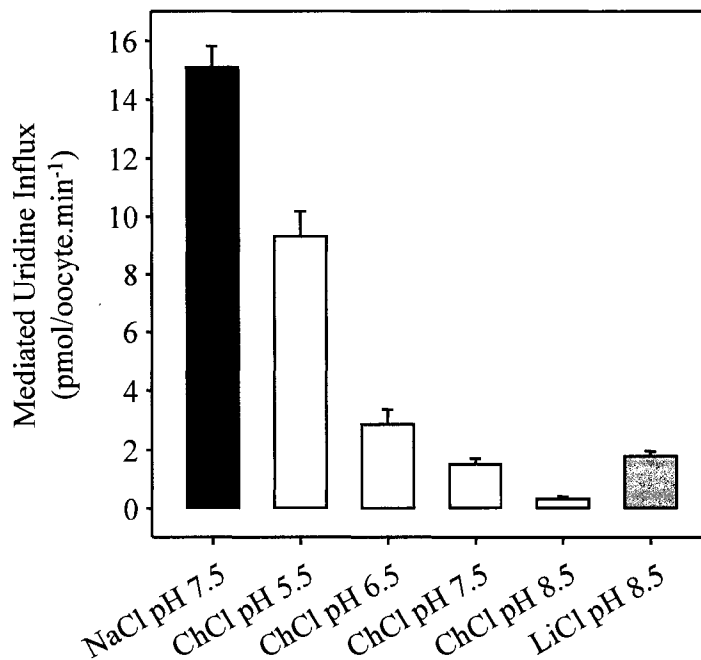


Figure 5-1. Effects of Na⁺, H⁺ and Li⁺ on the transport activities of oocytes expressing recombinant hCNT3. Radiolabeled fluxes of uridine (20 μM, 20°C, 1 min flux) in hCNT3-producing oocytes were measured in transport media containing Na⁺ (*black bar*; 100 mM NaCl, pH 7.5), choline (*open bars*; 100 mM ChCl, pH 5.5 - 8.5) or Li⁺ (*gray bar*; 100 mM LiCl, pH 8.5). Values were corrected for basal non-mediated uptake in control water-injected oocytes and are means ± SEM of 10 - 12 oocytes. The experiment was performed on a single batch of oocytes used on the same day.

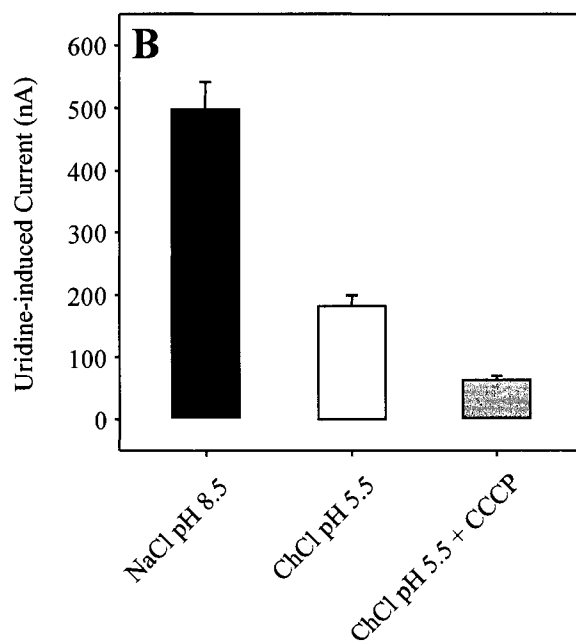
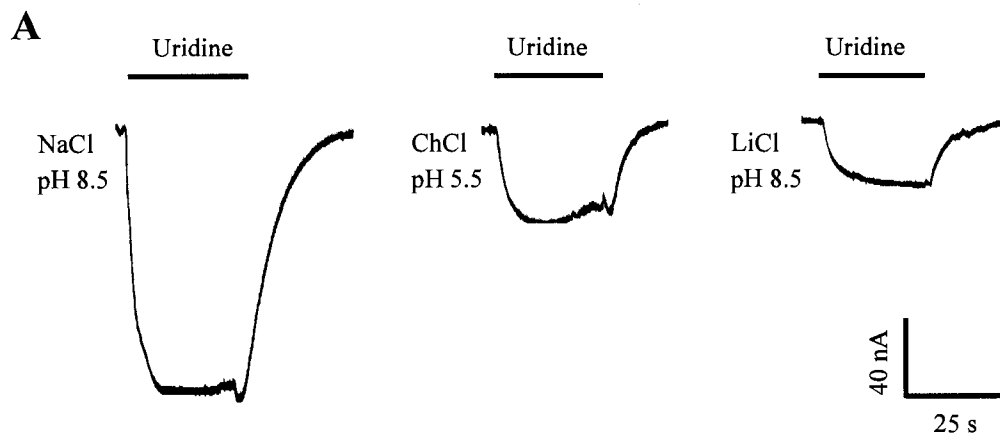


Figure 5-2.

Figure 5-2. Cation/nucleoside currents. (A) Representative cation/nucleoside current traces in a single hCNT3-producing oocyte clamped at -50 mV in transport medium containing either Na⁺ (100 mM NaCl, pH 8.5), choline (100 mM ChCl, pH 5.5) or Li⁺ (100 mM LiCl, pH 8.5). The *bar* denotes addition of uridine (100 μM) to the bath. No currents were observed in control water-injected oocytes. (B) Averaged inward currents in hCNT3-producing oocytes perfused sequentially with 100 μM uridine in (i) Na⁺-containing transport medium (*black bar*; 100 mM NaCl, pH 8.5), (ii) Na⁺-free transport medium (*open bar*; 100 mM ChCl, pH 5.5) and (iii) Na⁺-free transport medium containing 100 μM CCCP (*gray bar*; 100 mM ChCl, pH 5.5). Currents are means ± SEM of 5 different oocytes from the same batch of cells used on the same day.

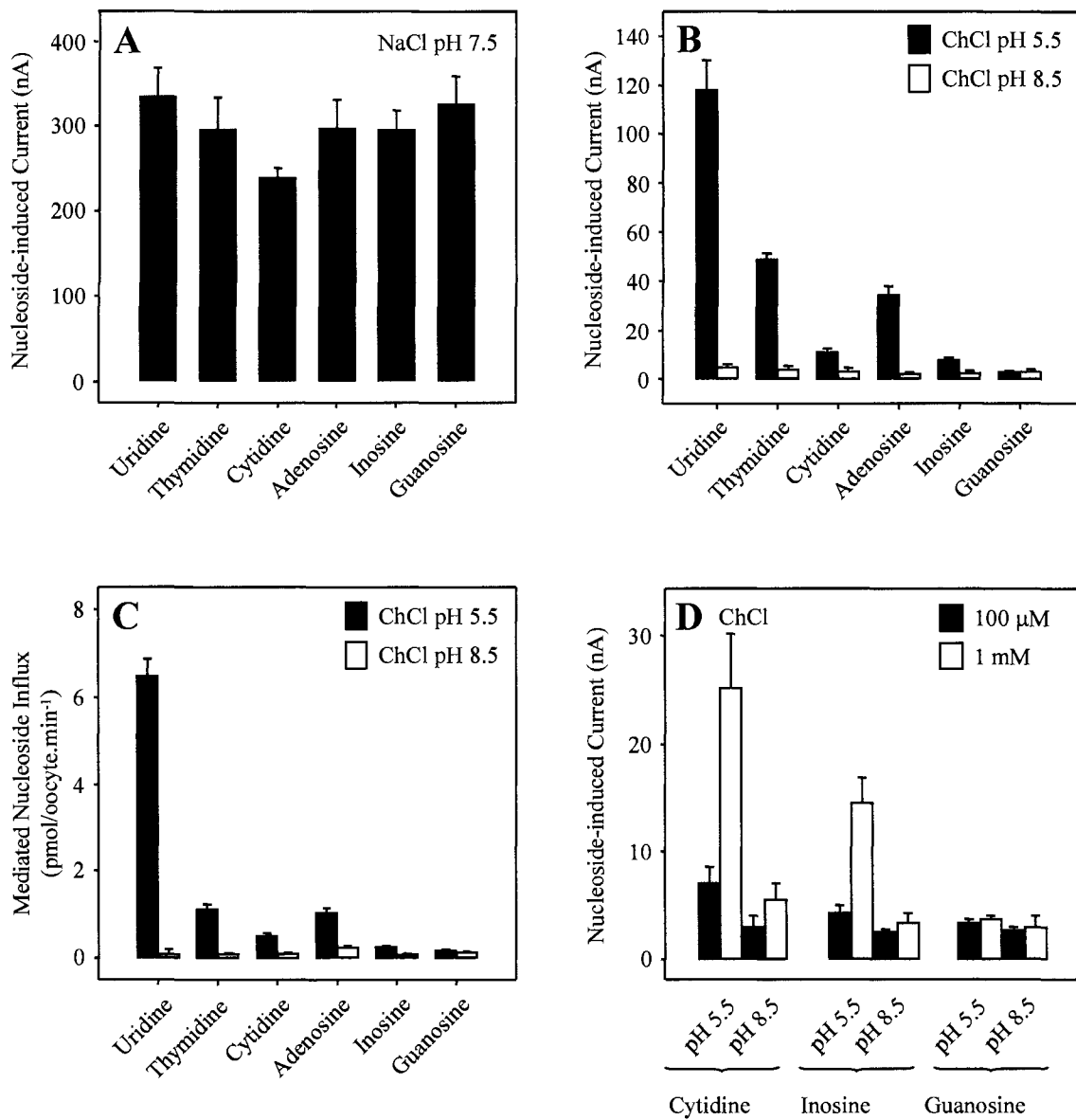


Figure 5-3.

Figure 5-3. Permeant selectivity and pH-dependence of nucleoside transport by recombinant hCNT3. Oocytes were injected with either water alone or water containing hCNT3 RNA transcripts. (A) Averaged nucleoside-induced inward currents measured by perfusing hCNT3-producing oocytes with 100 μ M pyrimidine (uridine, thymidine, cytidine) or purine (adenosine, inosine, guanosine) nucleosides in Na⁺-containing transport medium (100 mM NaCl, pH 7.5). Currents are means \pm SEM of 5 - 6 different oocytes from the same batch of cells used on the same day. (B) Mean nucleoside-induced inward currents measured by perfusing hCNT3-producing oocytes with 100 μ M pyrimidine and purine nucleosides in Na⁺-free transport medium (100 mM ChCl, pH 5.5 and 8.5). Currents are means \pm SEM of 5 - 6 oocytes from the same batch of cells used on the same day. (C) Mediated radiolabeled fluxes of pyrimidine and purine nucleosides (20 μ M, 20°C, 1 min flux) in oocytes injected with hCNT3 RNA transcripts measured in Na⁺-free transport media (100 mM ChCl, pH 5.5 and 8.5). Mediated transport was calculated as uptake in RNA-injected oocytes *minus* uptake in control water-injected oocytes. Each value represents the mean \pm SEM of 10 - 12 oocytes obtained from the same batch of cells and used on the same day. (D) Mean nucleoside-induced inward currents measured by perfusing hCNT3-producing oocytes with cytidine, inosine or guanosine (100 μ M and 1 mM) in Na⁺-free transport medium (100 mM ChCl, pH 5.5 and 8.5). Currents are means \pm SEM of 5 - 6 oocytes from the same batch of cells used on the same day. In (A), (B) and (D), no currents were observed in control water-injected oocytes.

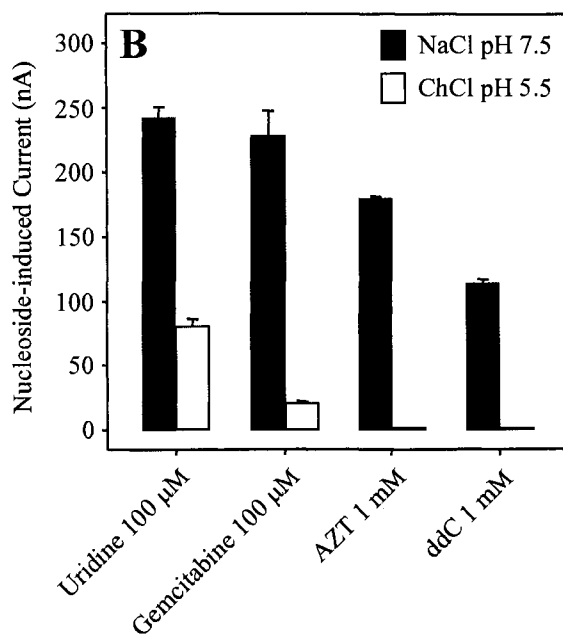
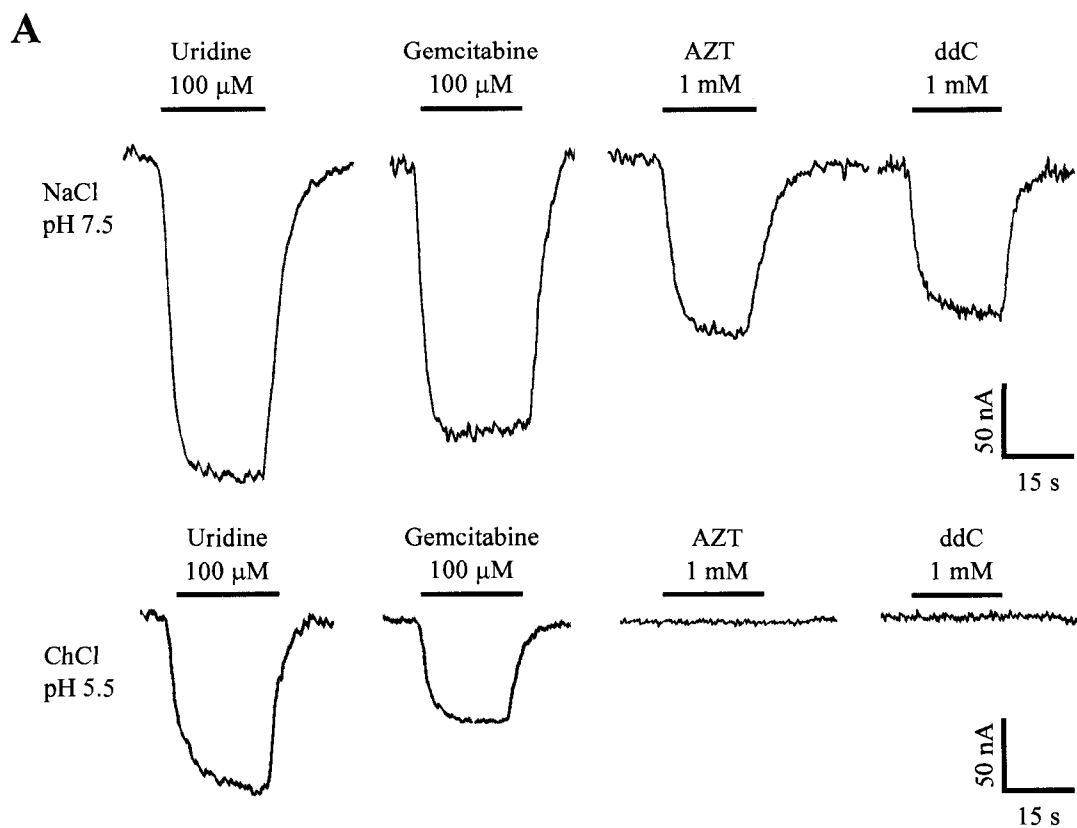


Figure 5-4.

Figure 5-4. Nucleoside drug-induced currents in hCNT3-producing *Xenopus* oocytes. (A) Representative inward currents induced by dFdC (100 μ M), AZT (1 mM) or ddC (1 mM) in a hCNT3-producing oocyte in transport medium containing either Na⁺ (100 mM NaCl, pH 7.5) or choline (100 mM ChCl, pH 5.5). Uridine-evoked currents in the same hCNT3-producing oocyte were 210 and 90 nA in Na⁺-containing and choline-containing transport media, respectively. (B) A comparison of hCNT3-mediated inward currents following sequential addition of uridine (100 μ M), dFdC (100 μ M), AZT (1 mM) or ddC (1 mM) to transport media containing either Na⁺ (100 mM NaCl, pH 7.5) or choline (100 mM ChCl, pH 5.5). Currents are means \pm SEM for 3 different oocytes from the same batch of cells used on the same day. No currents were observed in control water-injected oocytes.

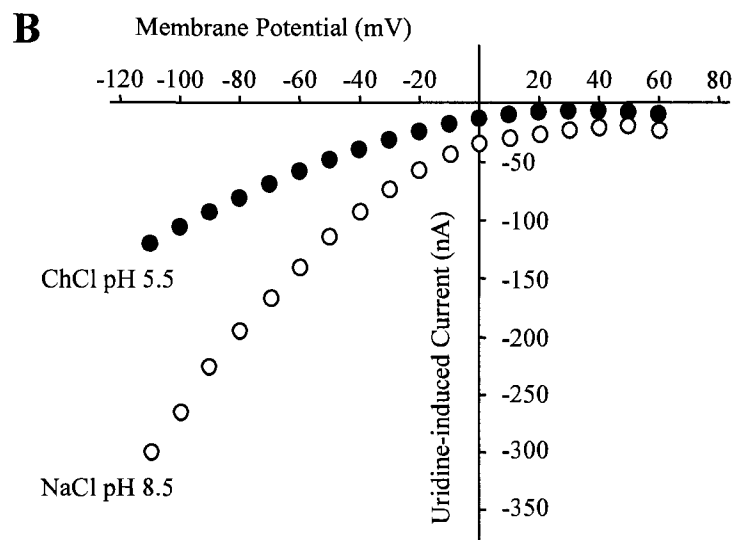
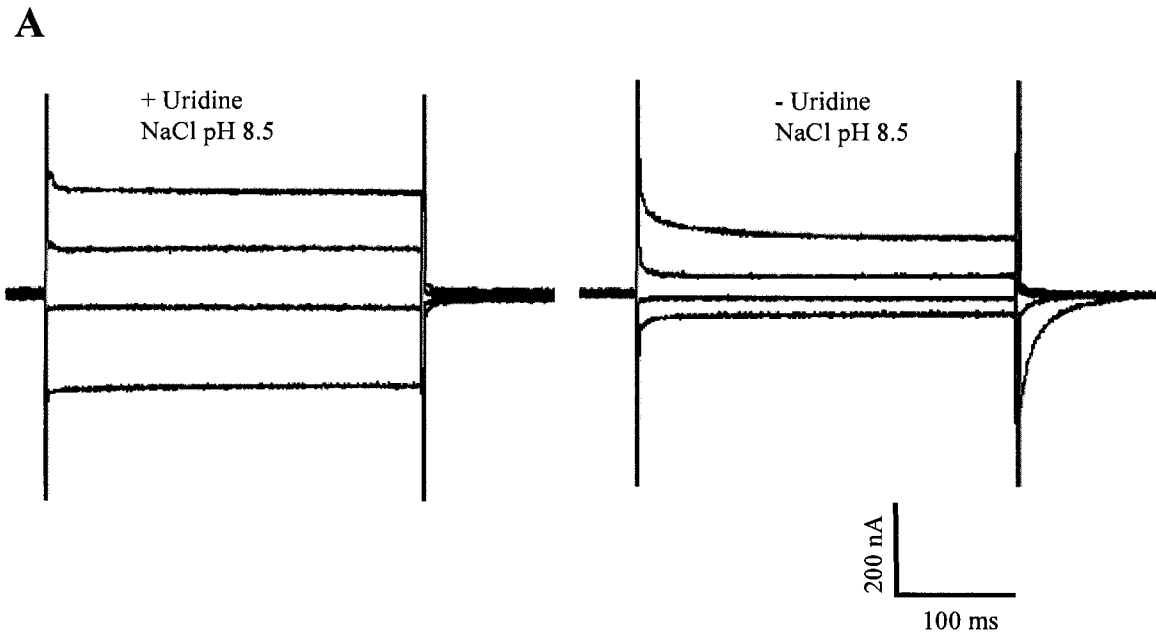


Figure 5-5.

Figure 5-5. Voltage-dependence of hCNT3-mediated currents. (A) Time course of transmembrane currents recorded from a representative hCNT3-producing oocyte in the presence of 100 μ M external uridine (100 mM NaCl, pH 8.5) in response to 300 ms voltage pulses from a holding potential of -50 mV (*left trace*). Currents are shown at four different test potentials only ($V_t = +50, -10, -60$ and -110 mV). The capacitive transients have been truncated to clearly demonstrate the steady-state currents. The *right trace* shows corresponding currents from the same oocyte recorded in the same transport medium in the absence of uridine. The records are offset to zero. (B) The current-voltage (I-V) curves for hCNT3 were generated from the difference between steady-state currents recorded in the presence and absence of 100 μ M uridine in Na^+ -containing (*open circles*; 100 mM NaCl, pH 8.5) or choline-containing (*solid circles*; 100 mM ChCl, pH 5.5) transport media upon voltage pulses from V_h of -50 mV to final potentials ranging between +60 and -110 mV, in 10 mV steps. The data are from the same oocyte as in (A). No uridine-induced currents were observed in control water-injected oocytes.

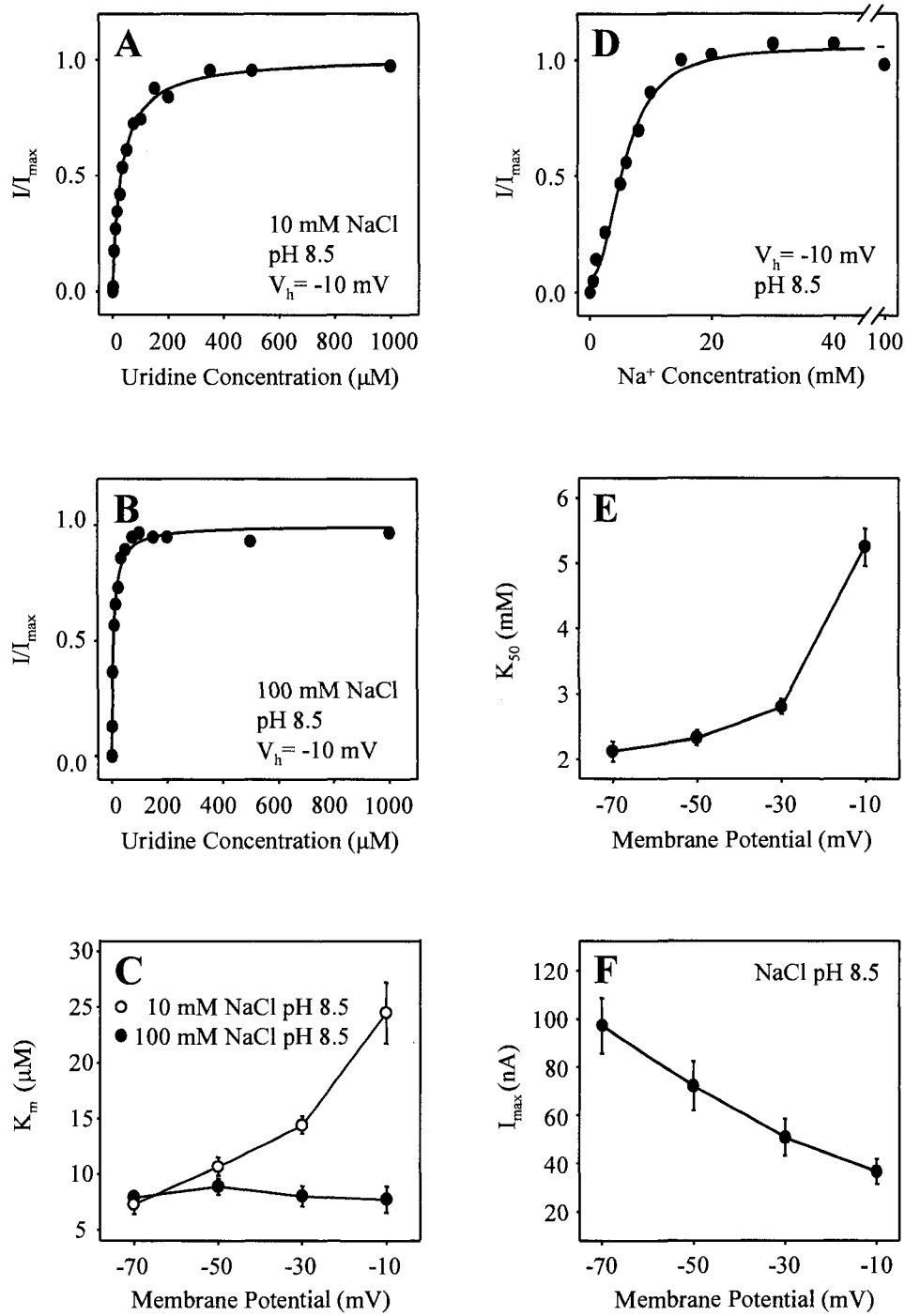


Figure 5-6.

Figure 5-6. Voltage-dependence of the transport kinetics of hCNT3. (A) Uridine concentration-response curve measured in a single representative hCNT3-producing oocyte at an external Na^+ concentration of 10 mM (pH 8.5) and a membrane potential of -10 mV. Currents at each uridine concentration were normalized to the fitted I_{max} value for that oocyte (\pm SE) of 52 ± 1 nA. The K_m value was 32 ± 3 μM . (B) Recordings from a single representative hCNT3-producing oocyte demonstrating a corresponding experiment at the same membrane potential (-10 mV) in the presence of 100 mM external Na^+ (pH 8.5). Currents were normalized to the fitted I_{max} of 55 ± 3 nA. The K_m was 7.6 ± 1.1 μM . (C) The effect of membrane potential on uridine K_m was determined at external Na^+ concentrations of 10 mM (*open circles*) and 100 mM (*solid circles*) (pH 8.5), and holding potentials of -10, -30, -50 and -70 mV. K_m values at each membrane potential were obtained from fits to data from individual oocytes normalized to the I_{max} value obtained for that cell, and are presented as means \pm SEM of 4 - 8 oocytes. (D) Na^+ concentration-response curve (pH 8.5) measured in a single representative hCNT3-producing oocyte at a membrane potential of -10 mV (100 μM uridine). Currents at each Na^+ concentration were normalized to the fitted I_{max} value of 43 ± 2 nA. The Na^+ K_{50} was 5.5 ± 0.5 mM. (E) The effect of membrane potential on Na^+ K_{50} was determined at holding potentials of -10, -30, -50 and -70 mV (100 μM uridine, pH 8.5). K_{50} values at each membrane potential were obtained from fits to data from individual oocytes normalized to the I_{max} value obtained for that cell and are presented as means \pm SEM of 5 - 7 oocytes. (F) The effect of membrane potential on maximum current (I_{max}) was determined at holding potentials of -10, -30, -50 and -70 mV in the presence of 100 mM external Na^+ (pH 8.5) and a saturating concentration of uridine (100 μM). Each value is the mean \pm SEM of 3 - 4 oocytes from the same batch of cells used on the same day. No currents were observed in control water-injected oocytes. *Note:* to more accurately determine K_m and K_{50} values (*panels A - E*), kinetic experiments at low membrane potentials were performed on preselected oocytes with maximal currents ≥ 40 nA. The effect of membrane potential on I_{max} (*panel F*) was measured independently in a separate experiment.

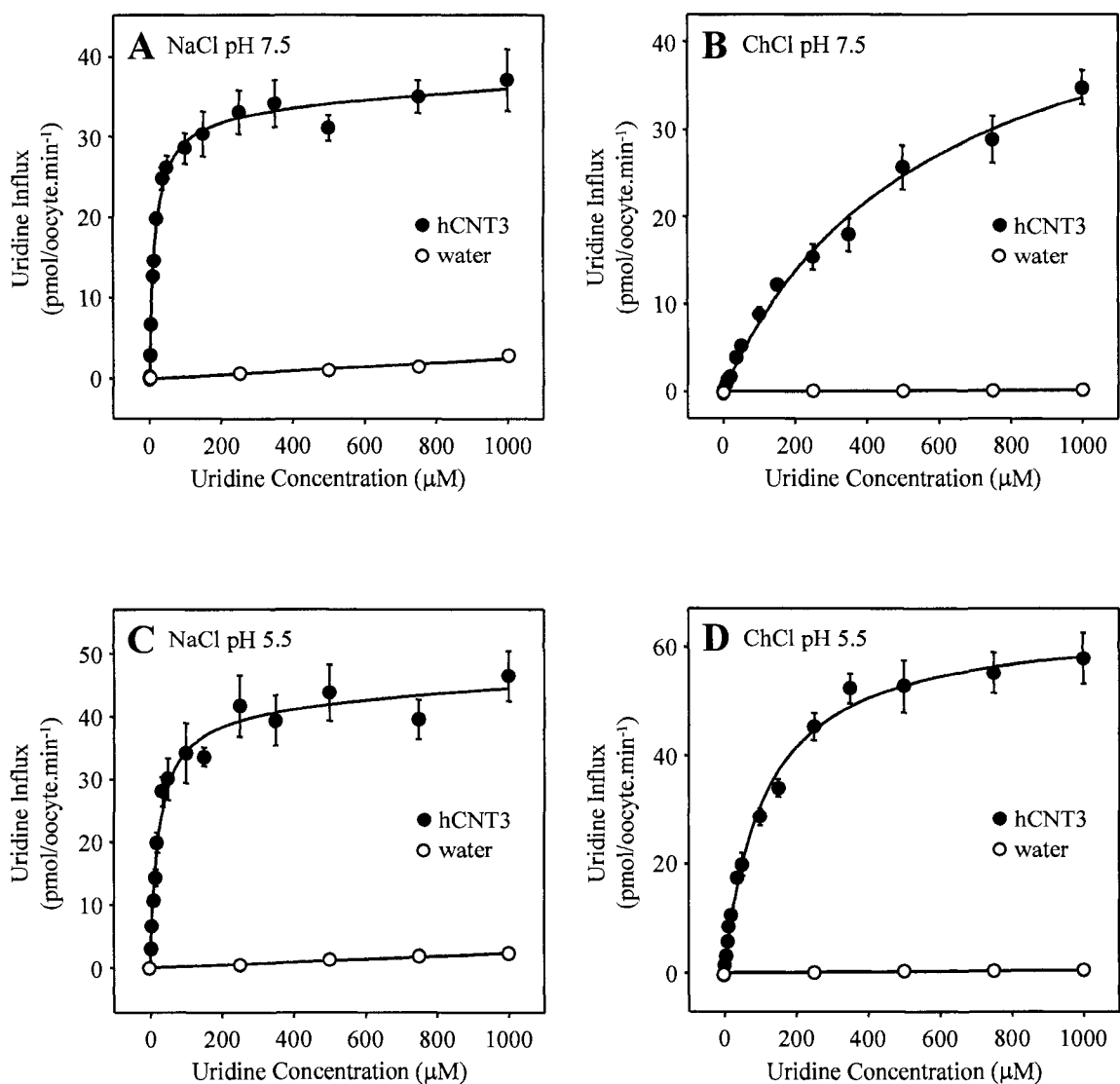


Figure 5-7. Kinetic properties of Na⁺- and H⁺-coupled hCNT3. Initial rates of ¹⁴C-uridine uptake (20°C, 1 min flux) were measured in Na⁺-containing (100 mM NaCl) and choline-containing (100 mM ChCl) transport media at either pH 7.5 (A and B, respectively) or pH 5.5 (C and D, respectively) in oocytes injected either with water alone (*open circles*) or with water containing hCNT3 RNA transcripts (*solid circles*). All of the fluxes were performed on the same batch of oocytes used on the same day. Kinetic parameters derived from these data for the hCNT3-mediated component of transport (uptake in RNA transcript-injected oocytes *minus* uptake in water-injected oocytes) are presented in Table 5-1.

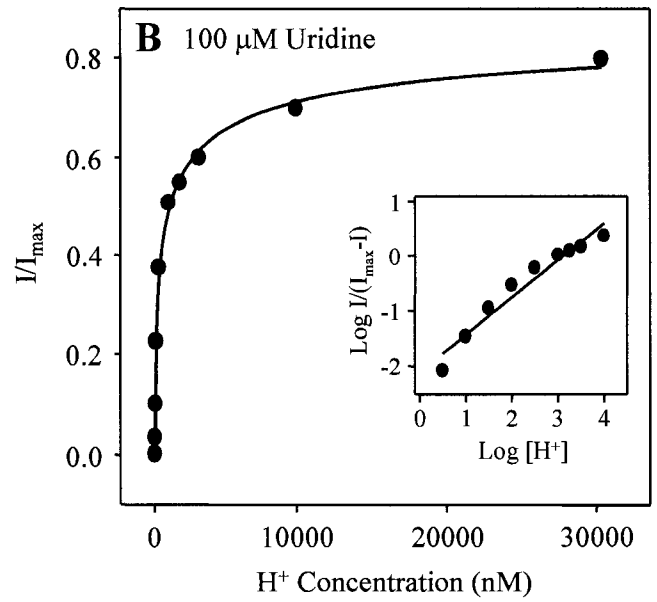
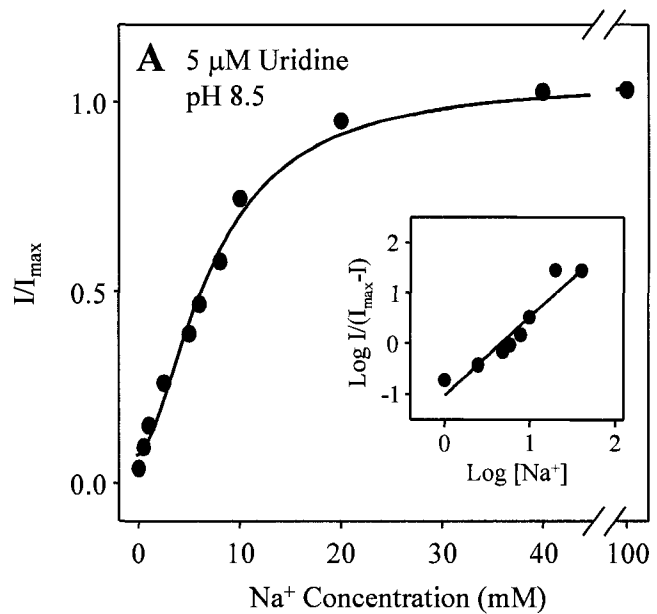


Figure 5-8.

Figure 5-8. Na⁺- and H⁺-activation of hCNT3. (A) Na⁺-activation curve in a single representative hCNT3-producing oocyte measured in transport medium containing 0 - 100 mM NaCl (pH 8.5) at a uridine concentration of 5 μM and a membrane potential of -50 mV. Currents were normalized to the fitted I_{\max} (\pm SE) of 53 ± 3 nA. The *inset* in A is a Hill plot of the data. The K_{50} was 7.0 ± 0.6 mM and the Hill coefficient was 1.6 ± 0.2 . No currents were observed in control water-injected oocytes. Results from mean Na⁺-activation experiments performed at different uridine concentrations are presented in Table 5-2. (B) H⁺-activation curve in a single representative hCNT3-producing oocyte measured in Na⁺-free transport medium (100 mM ChCl) at pH 8.5 - 4.5 and a membrane potential of -50 mV. Currents were normalized to the fitted I_{\max} of 120 ± 11 nA. The *inset* in B is a Hill plot for the data. The K_{50} was 470 ± 99 nM and the Hill coefficient was 0.68 ± 0.06 . No currents were observed in control water-injected oocytes. Mean H⁺-activation data from 6 individual oocytes are summarized in Table 5-2.

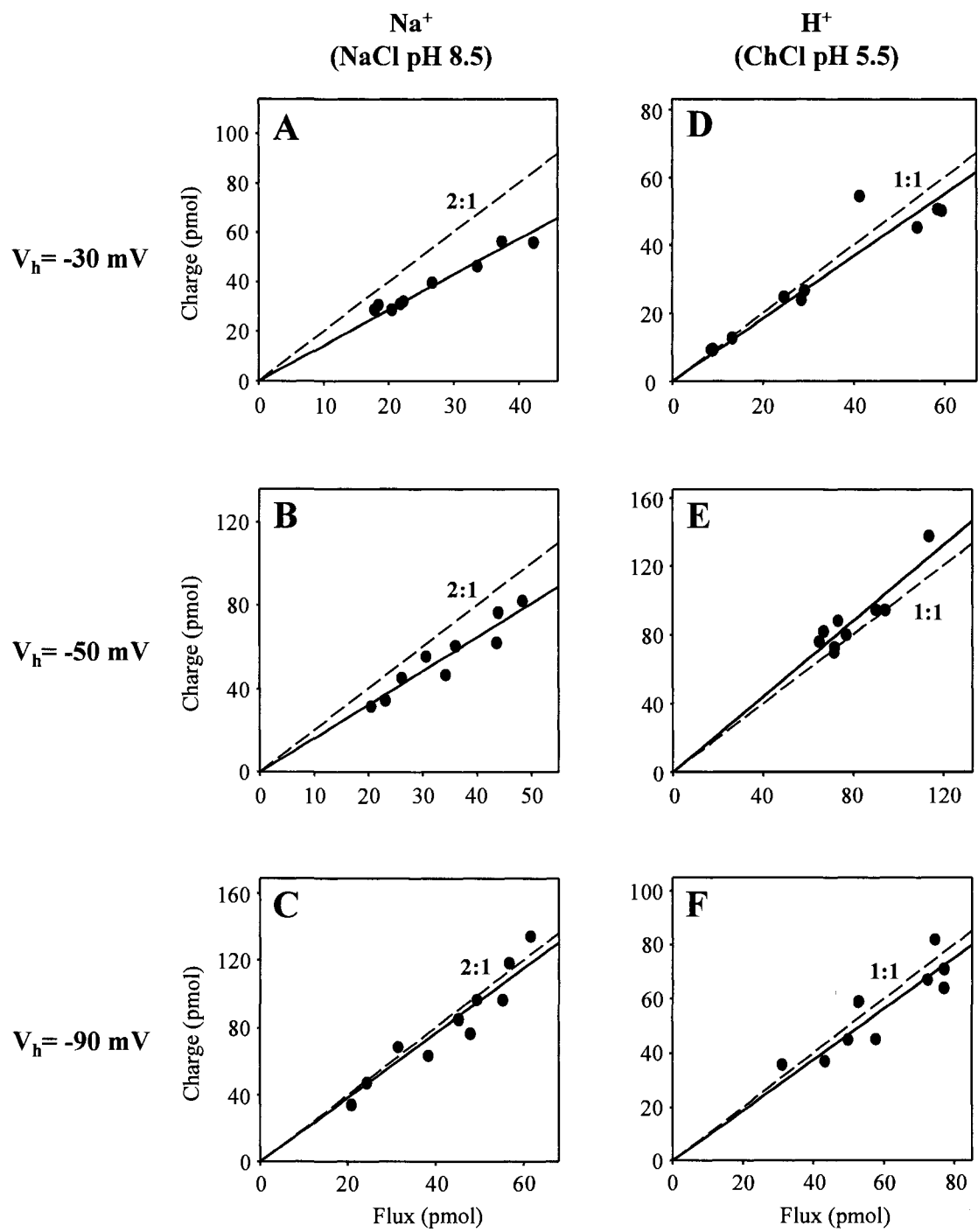


Figure 5-9.

Figure 5-9. Stoichiometries of Na⁺:uridine and H⁺:uridine cotransport by recombinant hCNT3. Charge to ¹⁴C-uridine uptake ratio plots were generated with 9 to 10 different hCNT3-producing oocytes in Na⁺-containing transport media (100 mM NaCl, pH 8.5) at membrane holding potentials V_h= -30 mV (A), V_h= -50 mV (B) and V_h= -90 mV (C). Similar conditions were used for D - F (n = 9) except that Na⁺ in the transport buffer was replaced by choline (100 mM ChCl) and the medium was acidified to pH 5.5. Integration of the uridine-evoked current was used to calculate the net cation influx (charge) and was correlated to the net ¹⁴C-uridine influx (flux). Linear regression analysis of the data for each plot is indicated by the *solid line*. The *dashed line* indicates a theoretical 2:1 charge:uptake ratio in A - C (presence of Na⁺) and a 1:1 charge:uptake ratio in D - F (presence of H⁺). Linear fits passed through the origin. Stoichiometries (± SE) obtained from these data and from corresponding experiments performed in Na⁺-containing transport media (100 mM NaCl) at pH 5.5 (*ie.* in the presence of both Na⁺ and H⁺) are summarized in Table 5-3.

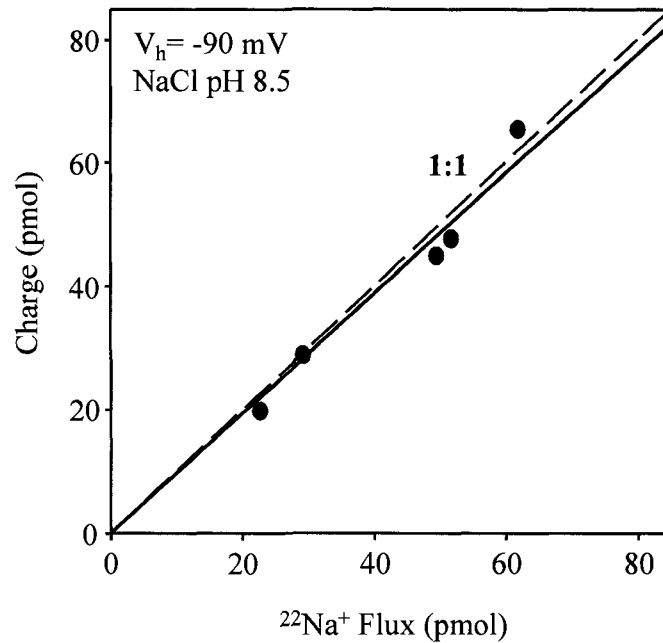


Figure 5-10. Charge-to- Na^+ stoichiometry of hCNT3. The charge to $^{22}\text{Na}^+$ uptake plot was generated from 5 different hCNT3-producing oocytes at a membrane potential of -90 mV. The sodium and uridine concentrations were 1 mM (pH 8.5) and 200 μM , respectively. Linear regression analysis of the data is indicated by the *solid line* (please see Table 5-3 for the fitted slope). The *dashed line* indicates a theoretical charge:uptake ratio of 1:1. The linear fit passed through the origin.

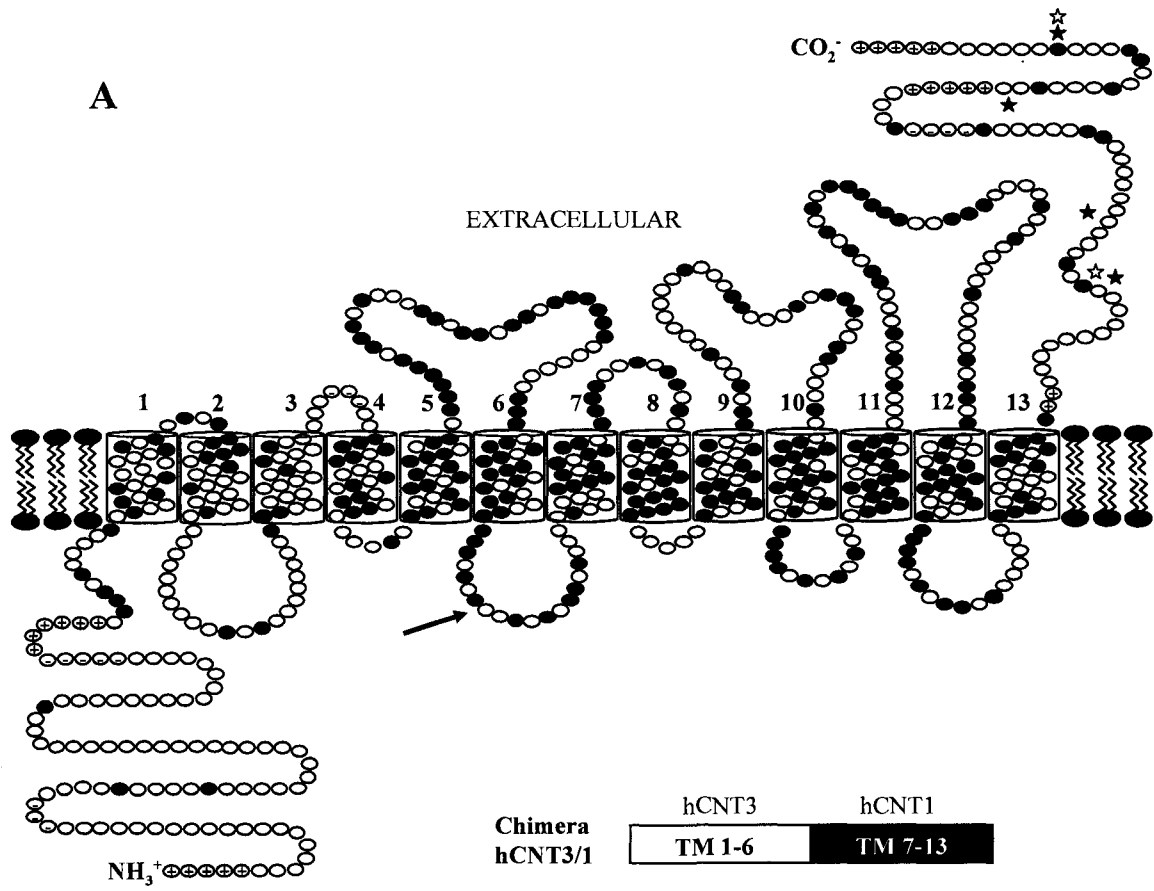


Figure 5-11.

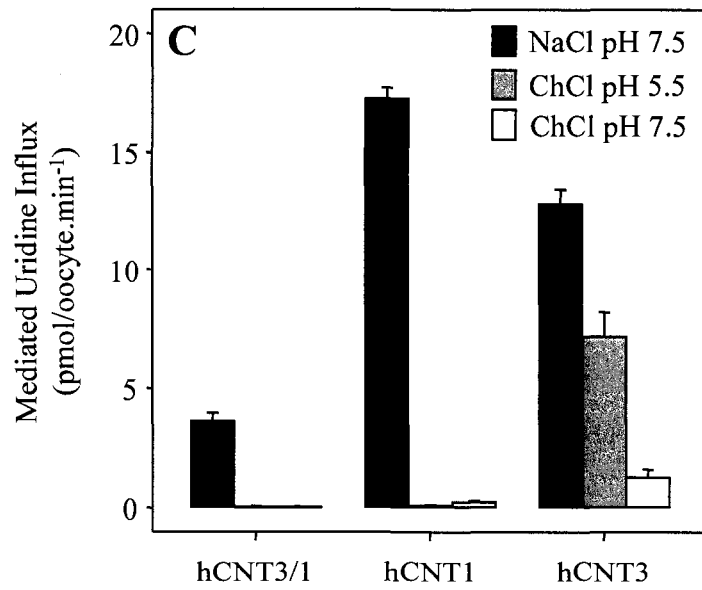
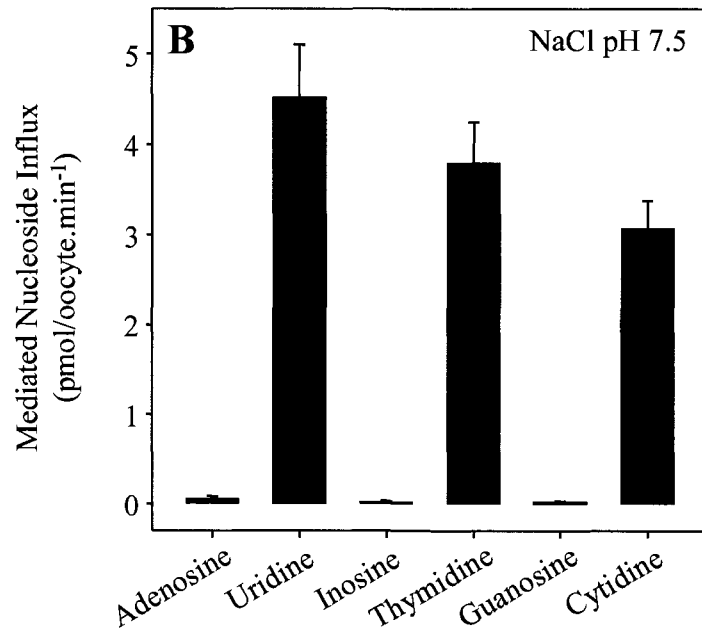


Figure 5-11.

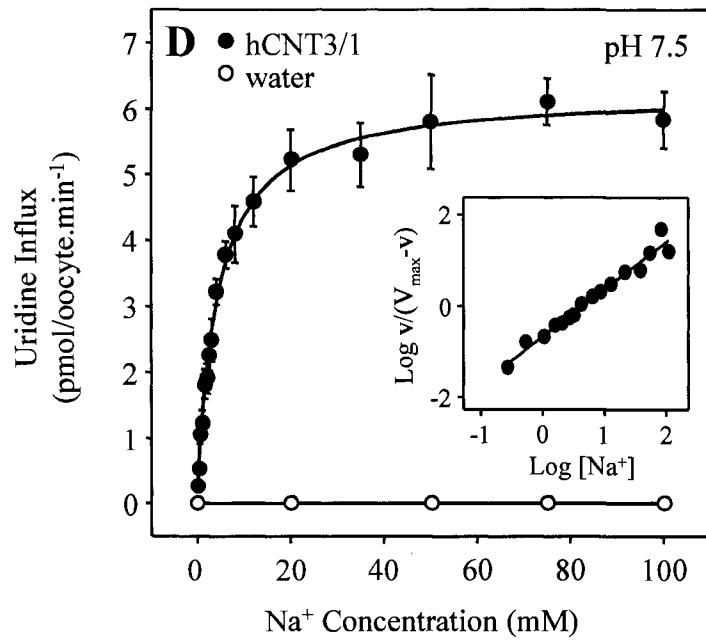


Figure 5-11.

Figure 5-11. Transport properties of chimera hCNT3/1. (A) Topographical model of hCNT3 and hCNT1. Potential membrane-spanning α -helices are *numbered*, and putative glycosylation sites in predicted extracellular domains in hCNT3 and hCNT1 are indicated by *solid* and *open stars*, respectively. Residues identical in the two proteins are shown as *solid circles*. Residues corresponding to insertions in the sequence of hCNT3 or hCNT1 are indicated by *circles* containing “+” and “-” signs, respectively. The *arrow* represents the splice site used for construction of the chimera. (B) Uptake of radiolabeled nucleosides by chimera hCNT3/1. Nucleoside influx (20 μ M, 20°C, 1 min flux) was measured in transport medium containing 100 mM NaCl at pH 7.5. Mediated transport was calculated as uptake in RNA transcript-injected oocytes *minus* uptake in control water-injected oocytes. (C) Radiolabeled uridine influx (20 μ M, 20°C, 1 min flux) by hCNT1, hCNT3 and hCNT3/1 was measured in transport medium containing 100 mM NaCl at pH 7.5 (*black bars*) or in Na⁺-free transport medium (100 mM ChCl) at both pH 5.5 (*gray bars*) and 7.5 (*open bars*). Mediated transport was calculated as uptake in RNA-injected oocytes *minus* uptake in control water-injected oocytes. (D) Influx of ¹⁴C-uridine (20 μ M, 20°C, 1 min flux) measured as a function of Na⁺ concentration at pH 7.5 using choline as Na⁺ substitute in oocytes injected with water alone (*open circles*) or with water containing hCNT3 RNA transcripts (*solid circles*). The *inset* in B is a Hill plot of the mediated data (Hill coefficient (*n*) and Na⁺ apparent affinity (*K*₅₀) presented in the text). Values in B - D are means \pm SEM of 10 - 12 oocytes. Each experiment in B - D was performed on cells from single batches of oocytes used on the same day.

Bibliography

1. Ritzel, M. W. L., Ng, A. M. L., Yao, S. Y. M., Graham, K., Loewen, S. K., Smith, K. M., Ritzel, R. G., Mowles, D. A., Carpenter, P., Chen, X.-Z., Karpinski, E., Hyde, R. J., Baldwin, S. A., Cass, C. E., and Young, J. D. (2001) Molecular identification and characterization of novel human and mouse concentrative Na⁺-nucleoside cotransporter proteins (hCNT3 and mCNT3) broadly selective for purine and pyrimidine nucleosides (system *cib*). *J. Biol. Chem.* **276**: 2914-2927.
2. Yao, S. Y., Ng, A. M., Loewen, S. K., Cass, C. E., Baldwin, S. A., and Young, J. D. (2002) An ancient prevertebrate Na⁺-nucleoside cotransporter (hfCNT) from the Pacific hagfish (*Eptatretus stouti*). *Am. J. Phys. Cell Phys.* **283**: C155-C168.
3. Cass, C. E. (1995) Nucleoside transport, in *Drug Transport in Antimicrobial and Anticancer Chemotherapy* (Georgopapadakou, N. H., ed.), pp 403-451, Marcel Dekker, New York, USA.
4. Griffith, D. A., and Jarvis, S. M. (1996) Nucleoside and nucleobase transport systems of mammalian cells. *Biochim. Biophys. Acta* **1286**: 153-181.
5. Young, J. D., Cheeseman, C., Mackey, J. R., Cass, C. E., and Baldwin, S. A. (2000) in *Current Topics in Membranes*, 50 (Barrett, K. E., and Donowitz, M., eds.) pp 329-378, Academic Press, San Diego, USA.
6. Smith, K. M., Ng, A. M., Yao, S. Y. M., Labedz, K. A., Knauss, E. E., Wiebe, L. I., Cass, C. E., Baldwin, S. A., Chen, X. Z., Karpinski, E., and Young, J. D. (2004) Electrophysiological characterization of a recombinant human Na⁺-coupled nucleoside transporter (hCNT1) produced in *Xenopus* oocytes. *J. Physiol.* **558**: 807-823.
7. Birnir, B., Loo, D. D. F., and Wright, E. M. (1991) Voltage-clamp studies of the Na⁺/glucose cotransporter cloned from rabbit small intestine. *Pflügers Arch.* **418**: 79-85.
8. Parent, L., Supplisson, S., Loo, D. D., and Wright, E. M. (1992) Electrogenic properties of the cloned Na⁺/glucose cotransporter: I. Voltage-clamp studies. *J. Membr. Biol.* **125**: 49-62.

9. Jauch, P., and Lauger, P. (1986) Electrogenic properties of the sodium-alanine cotransporter in pancreatic acinar cells: II. Comparison with transport models. *J. Membr. Biol.* **94**: 117-127.
10. Klamo, E. M., Drew, M. E., Landfear, S. M., and Kavanaugh, M. P. (1996) Kinetics and stoichiometry of a proton/myo-inositol cotransporter. *J. Biol. Chem.* **271**: 14937-14943.
11. Mackenzie, B., Loo, D. D. F., Panayotova-Heiermann, M., and Wright, E. M. (1996) Biophysical characteristics of the pig kidney Na⁺/glucose cotransporter SGLT2 reveal a common mechanism for SGLT1 and SGLT2. *J. Biol. Chem.* **271**: 32678-32683.
12. Stein, W. D. (1990) *Channels, Carriers, and Pumps: An Introduction to Membrane Transport*, p 173, Academic Press Inc., San Diego, USA.
13. Wright, E. M., Loo, D. D. F., Panayotova-Heiermann, M., Lostao, M. P., Hirayama, B. H., Mackenzie, B., Boorer, K., and Zampighi, G. (1994) 'Active' sugar transport in eukaryotes. *J. Exp. Biol.* **196**: 197-212.
14. Chen, X.-Z., Shayakul, C., Berger, U. V., Tian, W., and Hediger, M. A. (1998) Characterization of a rat Na⁺-dicarboxylate cotransporter. *J. Biol. Chem.* **273**: 20972-20981.
15. Loewen, S. K., Ng, A. M. L., Mohabir, N. M., Baldwin, S. A., Cass, C. E., and Young, J. D. (2003) Functional characterization of a H⁺/nucleoside cotransporter (CaCNT) from *Candida albicans*, a fungal member of the concentrative nucleoside transporter (CNT) family of membrane proteins. *Yeast* **20**: 661-675.
16. Ritzel, M. W. L., Yao, S. Y. M., Huang, M. Y., Elliot, J. F., Cass, C. E., and Young, J. D. (1997) Molecular cloning and functional expression of cDNAs encoding a human Na⁺-nucleoside cotransporter (hCNT1). *Am. J. Physiol.* **272**: C707-C714.
17. Pourcher, T., Bassilana, M., Sarkar, H. K., Kaback, H. R., and Leblanc, G. (1990) The melibiose/Na⁺ symporter of *Escherichia coli*: kinetic and molecular properties. *Philos. Trans. R. Soc. Lond. B. Biol. Sci.* **326**: 411-423.

18. Hirayama, B. A., Loo, D. D. F., and Wright, E. M. (1994) Protons drive sugar transport through the Na⁺/glucose cotransporter (SGLT1). *J. Biol. Chem.* **269**: 21407-21410.
19. Hirayama, B. A., Loo, D. D. F., and Wright, E. M. (1997) Cation effects on protein conformation and transport in the Na⁺/glucose cotransporter. *J. Biol. Chem.* **272**: 2110-2115
20. Pajor, A. M., Hirayama, B. A., and Loo, D. D. F. (1998) Sodium and lithium interactions with the Na⁺/dicarboxylate cotransporter. *J. Biol. Chem.* **273**: 18923-18929.
21. Burckhardt, B.-C., Kroll, B., and Frömter, E. (1992) Proton transport mechanism in the cell membrane of *Xenopus laevis* oocytes. *Pflügers Arch.* **420**: 78-82.
22. Seyfang, A., Kavanaugh, M. P., and Landfear, S. M. (1997) Aspartate 19 and glutamate 121 are critical for transport function of the myo-inositol/H⁺ symporter from *Leishmania donovani*. *J. Biol. Chem.* **272**: 24210-24215.
23. de Koning, H. P., Watson, C. J., and Jarvis, S. M. (1998) Characterization of a nucleoside/proton symporter in procyclic *Trypanosoma brucei brucei*. *J. Biol. Chem.* **273**: 9486-9494.
24. Xiao, G., Wang, J., Tangen, T., and Giacomini, K. M. (2001) A novel proton-dependent nucleoside transporter, CeCNT3, from *Caenorhabditis elegans*. *Mol. Pharmacol.* **59**: 339-348.
25. Hong, M., Schlichter, L., and Bendayan, R. (2001) A novel zidovudine uptake system in microglia. *J. Pharmacol. Exp. Ther.* **296**: 141-149.
26. Hong, M., Schlichter, L., and Bendayan, R. (2000) A Na⁺-dependent nucleoside transporter in microglia. *J. Pharmacol. Exp. Ther.* **292**: 366-374.
27. Smith, K. M., Chen, X.-Z., Cass, C. E., Baldwin S. A., Karpinski, E., and Young, J. D. (2004) Voltage clamp analysis of the presteady-state currents mediated by the human concentrative Na⁺-nucleoside cotransporter hCNT3. *Biophys. J. Supplement* **86**: 262a.

28. Yao, S. Y. M., Cass, C. E., and Young, J. D. (1996) Transport of the antiviral nucleoside analogs 3'-azido-3'-deoxythymidine and 2', 3'-dideoxycytidine by a recombinant nucleoside transporter (rCNT1) expressed in *Xenopus laevis* oocytes. *Mol. Pharmacol.* **50**: 388-393.
29. Larrayoz, I. M., Casado, F. J., Pastor-Anglada, M., and Lostao, M. P. (2004) Electrophysiological characterization of the human Na⁺/nucleoside cotransporter 1 (hCNT1) and role of adenosine on hCNT1 function. *J. Biol. Chem.* **279**: 8999-9007.
30. Wu, X., Yuan, G., Brett, C. M., Hui, A. C., and Giacomini, K. M. (1992) Sodium-dependent nucleoside transport in choroid plexus from rabbit. Evidence for a single transporter for purine and pyrimidine nucleosides. *J. Biol. Chem.* **267**: 8813-8818.
31. Segel, I. H. (1975) *Enzyme Kinetics*, pp 346-464, Wiley Interscience, New York, USA.
32. Weiss, J. N. (1997) The Hill equation revisited: uses and misuses. *FASEB J.* **11**: 835-841.
33. Chen, X.-Z., Coady, M. J., Jackson, F., Berteloot, A., and Lapointe, J.-Y. (1995) Thermodynamic determination of the Na⁺:glucose coupling ratio for the human SGLT cotransporter. *Biophys. J.* **69**: 2405-2414.
34. Mackenzie, B., Loo, D. D., and Wright, E. M. (1998) Relationships between Na⁺/glucose cotransporter (SGLT1) currents and fluxes. *J. Membr. Biol.* **162**: 101-106.
35. Diez-Sampedro, A., Eskandari, S., Wright, E. M., and Hirayama, B. A. (2001) Na⁺-to-sugar stoichiometry of SGLT3. *Am. J. Physiol. Renal Physiol.* **280**: F278-F282.
36. Chen, X.-Z., Zhu, T., Smith, D. E., and Hediger, M. A. (1999) Stoichiometry and kinetics of the high-affinity H⁺-coupled peptide transporter PepT2. *J. Biol. Chem.* **274**: 2773-2779.
37. Diez-Sampedro, A., Hirayama, B. A., Osswald, C., Gorboulev, V., Baumgarten, K., Volk, C., Wright, E. M., and Koepsell, H. (2003) A glucose

- sensor hiding in a family of transporters. *Proc. Natl. Acad. Sci. USA.* **100**: 11753-11758.
38. Krupka, R. M. (1993) Coupling mechanisms in active transport. *Biochim. Biophys. Acta.* **1183**: 105-113.
39. Krupka, R. M. (1994) Interpreting the effects of site-directed mutagenesis on active transport systems. *Biochim. Biophys. Acta.* **1193**: 165-178.
40. Loewen, S. K., Ng, A. M., Yao, S. Y., Cass, C. E., Baldwin, S. A., and Young, J. D. (1999) Identification of amino acid residues responsible for the pyrimidine and purine nucleoside specificities of human concentrative Na⁺ nucleoside cotransporters hCNT1 and hCNT2. *J. Biol. Chem.* **274**: 24475-24484.
41. McEwan, G. T. A., Daniel, H., Fett, C., Burgess, M. N., and Lucas, M. L. (1988) The effect of *Escherichia coli* STA enterotoxin and other secretagogues on mucosal surface pH of rat small intestine *in vivo*. *Proc. R. Soc. Lond. B. Biol. Sci.* **234**: 219-237.

Chapter 6:

**Cation Coupling Properties of Human Concentrative Nucleoside
Transporters hCNT1, hCNT2 and hCNT3***

* A version of this chapter has been published.

Smith, K., M., Slugoski, M. D., Cass, C. E., Baldwin, S. A., Karpinski, E., and Young, J. D. (2007) Cation coupling properties of human concentrative nucleoside transporters hCNT1, hCNT2 and hCNT3. *Mol. Membr. Biol.* **24**: 53-64.

Acknowledgements

Dr. Kyla M. Smith completed the electrophysiology experiments in this project and shares equal contribution as first author on this publication. Drs. Carol E. Cass, Stephen A. Baldwin and Edward Karpinski are collaborative principal investigators who assisted with research funding and manuscript preparation. This research was funded by the National Cancer Institute of Canada with funds from the Canadian Cancer Society, Alberta Cancer Board, Heart and Stroke Foundation of Canada and Medical Research Council of the United Kingdom.

Introduction

In human (h) cells, three concentrative nucleoside transporter (CNT) isoforms (hCNT1-3) have been identified. Although both hCNT1 and hCNT2 transport uridine and adenosine, hCNT1 is otherwise pyrimidine nucleoside-selective and corresponds to functional nucleoside transport system *cit* (concentrative, insensitive to nitrobenzylthioinosine (NBMPR), thymidine-transporting) while hCNT2 is purine nucleoside-selective and corresponds to functional nucleoside transport system *cif* (concentrative, insensitive to NBMPR, formycin B-transporting) (1-3). hCNT1 and hCNT2 mediate inwardly-directed Na^+ /nucleoside cotransport, and are present primarily in intestinal and renal epithelia and other specialized cells. hCNT3 corresponds to functional nucleoside transport system *cib* (concentrative, insensitive to NBMPR, broadly selective), mediates Na^+ /nucleoside cotransport of both purine and pyrimidine nucleosides, and appears to have a wider tissue and cellular distribution than either hCNT1 or hCNT2 (4). Tissues containing hCNT3 transcripts include pancreas, bone marrow, trachea, mammary gland, liver, prostate, and regions of intestine, brain and heart (4). Mammalian hCNT1/2 and hCNT3 belong to two distinct CNT phylogenetic subfamilies; the CNT3 subfamily also contains a second broad specificity *cib*-type CNT (hfCNT) from an ancient pre-vertebrate, the Pacific hagfish (5).

In addition to their well established differences in nucleoside preference, there is evidence that hCNT1, hCNT2 and hCNT3 may also differ with respect to cation interactions. For example, indirect Hill-type analyses of the relationship between nucleoside influx and Na^+ concentration suggest Na^+ :nucleoside stoichiometries of 1:1 for *cit* (CNT1) and *cif* (CNT2) transport activities in different mammalian cells and tissues, compared to 2:1 for *cib* (CNT3) (6, 7). A Na^+ :nucleoside coupling ratio of 2:1 has been confirmed for recombinant hCNT3 and hagfish hfCNT produced in *Xenopus laevis* oocytes based upon direct charge *versus* radiolabeled uridine uptake measurements (5, Chapter 5). hCNT3 has also been shown to be H^+ -dependent, with a H^+ :nucleoside coupling ratio of 1:1 (Chapter 5). In the case of recombinant hCNT1, however, corresponding analyses of oocyte charge *versus* radiolabeled uridine uptake

has provided conflicting Na^+ :nucleoside stoichiometries of either 1:1 (8) or 2:1 (9). No corresponding data exists in the literature for recombinant hCNT2. To fill in this important gap with respect to hCNT2, and to address whether the Na^+ :nucleoside coupling ratio of hCNT1 is indeed different from that of hCNT3, heterologous expression in *Xenopus* oocytes was used in combination with both radioisotope flux and electrophysiological techniques to undertake a systematic side-by-side comparison of cation interactions with all three human CNTs.

Results

Cation specificity – The experiment of Fig. 6-1 directly compared the Na^+ - and H^+ -dependence of nucleoside transport mediated by hCNT1, hCNT2 and hCNT3. CNT-mediated uptake (influx) of ^{14}C -uridine (20 μM) in the presence of Na^+ was measured in oocytes expressing hCNT1 (A), hCNT2 (B) or hCNT3 (C) in transport media containing 100 mM NaCl (pH 8.5). To examine CNT-mediated uptake of uridine in the presence of H^+ , Na^+ in the transport medium was replaced by equimolar choline, and the pH varied from 5.5 to 8.5. Values were corrected for basal non-mediated uptake in control water-injected oocytes (< 0.03 pmol/oocyte.min $^{-1}$ under all conditions tested). All three recombinant transporters mediated similar levels of uridine influx in the presence of external Na^+ , but only hCNT3 demonstrated pH-dependent uridine influx. Previous studies have established that pH has minimal effect on hCNT3 Na^+ -mediated uridine binding affinity (Chapter 5). The intracellular oocyte pH has been shown to be 7.3 - 7.6 (10) and consistent with this, and in agreement with previous findings (Chapter 5), H^+ -coupled uptake of uridine by hCNT3 was minimal at pH values of 7.5 or higher, but increased markedly as the external medium was acidified. In 100 mM ChCl at pH 5.5, hCNT3 mediated uridine influx was ~ 60% of that obtained in the presence of 100 mM NaCl at pH 8.5. As the pH was raised from 5.5 to 8.5, uridine influx was reduced by 96%. Influx of uridine by hCNT2 and hCNT1 under the same conditions also exhibited marked Na^+ -dependence, but showed no indication of H^+ -coupling. This was confirmed by

electrophysiology: all three transporters generated large inward Na^+ currents in the presence of uridine, but only hCNT3 exhibited uridine-evoked H^+ currents (Fig. 6-1D - F). Subsequent experiments focused on the kinetics of Na^+ -activation and the determination of Na^+ :nucleoside coupling ratios.

Na⁺-activation kinetics – Na^+ -activation curves measured by radioisotope nucleoside flux assays are presented in Fig. 6-2 for oocytes producing either hCNT1, hCNT2 or hCNT3. Uptake was compared to that in control water-injected oocytes, and the kinetic parameters derived from these experiments for the CNT-mediated component of influx (uptake in RNA-injected oocytes *minus* uptake in water-injected oocytes) are presented in Table 6-1. For both hCNT1 and hCNT2, the relationship between uridine influx and Na^+ concentration (0 - 100 mM NaCl, pH 8.5) was hyperbolic, with Hill coefficients consistent with an apparent Na^+ :nucleoside coupling stoichiometry of 1:1 (Figs. 6-2A and B). In marked contrast, the Na^+ -activation curve for hCNT3 was sigmoidal, with a Hill coefficient consistent with an apparent Na^+ :nucleoside coupling ratio of 2:1 (Fig. 6-2C). The three transporters (hCNT1/2/3) exhibited similar millimolar apparent affinities for Na^+ and similar V_{max} values (Table 6-1).

The effects of membrane potential on CNT cation-activation kinetics were examined electrophysiologically by measuring hCNT1/2/3 apparent affinities (K_{50} values) for Na^+ and corresponding Hill coefficients (n) at two different holding potentials ($V_h = -30$ and -90 mV). The kinetic parameters for Na^+ -activation were determined at the same external uridine concentration used in the radioisotope studies (20 μM). The relationship between CNT-mediated uridine-evoked currents and Na^+ concentration (pH 8.5) is illustrated in Fig. 6-3 for single representative oocytes measured at -30 and -90 mV. Mean kinetic parameters for hCNT1, hCNT2 and hCNT3 calculated from four or more individual oocytes are presented in Table 6-2. In agreement with the ^{14}C -uridine influx experiments (Fig. 6-2B), hCNT2 Na^+ -activation curves were hyperbolic, with Hill coefficients consistent with an apparent Na^+ :nucleoside coupling stoichiometry of 1:1. The Hill coefficient was independent of membrane potential, while the Na^+ apparent K_{50} value decreased from 16 to 2.8

mM as the membrane potential was made more negative. Similar to hCNT2, the Hill coefficient for hCNT1 was ~ 1 and independent of membrane potential; the Na^+ apparent K_{50} value decreased from 11 to 1.9 mM as the membrane potential was changed from -30 to -90 mV (Table 6-2). In marked contrast to hCNT1/2, but again in agreement with the ^{14}C -radioisotope flux experiments (Fig. 6-2C), hCNT3 Na^+ -activation curves were sigmoidal, with Hill coefficients of ~ 2 , suggesting an apparent Na^+ :nucleoside coupling stoichiometry of 2:1 (Table 6-2). Similar to hCNT1/2, however, the Hill coefficient was independent of membrane potential, while the Na^+ apparent K_{50} value decreased from 4.7 to 1.7 mM as the membrane potential was made more negative.

Na⁺:nucleoside coupling ratios – The Na^+ :nucleoside stoichiometries of hCNT1, hCNT2 and hCNT3 were directly determined by simultaneously measuring nucleoside-evoked currents and ^{14}C -nucleoside uptake under voltage-clamp conditions. Data for the Na^+ :uridine stoichiometry of hCNT2 is compared with those of hCNT1 and hCNT3 in Fig. 6-4. To further characterize the stoichiometries of human CNTs, the coupling ratios for hCNT2 and hCNT3 were also measured with adenosine as permeant (Fig. 6-5) in transport medium containing 1 μM deoxycoformycin to inhibit adenosine deaminase activity (11). Due to the small magnitudes (≤ 3 nA) of adenosine-evoked hCNT1 Na^+ currents (8), a corresponding hCNT1 Na^+ :adenosine coupling ratio could not be measured. Each data point in Figs. 6-4 and 6-5 represents a single oocyte and the Na^+ :nucleoside coupling ratio is given by the slope of the linear fit of charge (pmol) *versus* uptake (pmol) (Table 6-3).

Stoichiometries were measured at a nucleoside concentration of 200 μM in Na^+ -containing transport medium (100 mM) at pH 8.5 and at a holding potential of -90 mV. Fig. 6-4A is a representative uridine-dependent current recording in a hCNT2-producing oocyte. As previously observed for several other cotransporters, including hCNT1 (8) and hCNT3 (Chapter 5), current reached an initial maximal value and then progressively decreased, returning to baseline upon removal of nucleoside. The linear correlations between integrated uridine-dependent charge and ^{14}C -uridine accumulation measured in Na^+ -containing transport medium (100 mM) gave

calculated stoichiometries of 0.89 for hCNT2 (Fig. 6-4C) *versus* 0.89 for hCNT1 (Fig. 6-4B) and 2.1 for hCNT3 (Fig. 6-4D) (Table 6-3). Similarly, the linear correlation between adenosine-dependent charge and adenosine accumulation (100 mM NaCl, pH 8.5) gave calculated stoichiometries of 0.93 for hCNT2 (Fig. 6-5A) and 1.9 for hCNT3 (Fig. 6-5B) (Table 6-3).

Charge-to-Na⁺ stoichiometry – The relationship between uridine-evoked charge influx (pmol) and ²²Na⁺ uptake (pmol) was measured in oocytes producing hCNT1, hCNT2 or hCNT3 at a holding potential of -90 mV. A linear fit of the data gave regression lines with slopes of 0.93 for hCNT2 *versus* 0.90 for hCNT1 and 0.90 for hCNT3, indicating that for all three transporters 1 net inward positive charge was transported for every Na⁺ ion cotransported with uridine into the cell (Table 6-3).

Discussion

The cation-coupled concentrative nucleoside transport processes *cit*, *cif* and *cib* are mediated by isoforms of the CNT (SLC28) transporter family, designated in humans as hCNT1, hCNT2 and hCNT3, respectively. All three proteins transport uridine and adenosine (although hCNT1-mediated adenosine transport activity is low), but are otherwise pyrimidine nucleoside-selective (hCNT1), purine nucleoside-selective (hCNT2), or broadly selective for both pyrimidine and purine nucleosides (hCNT3). Conducted under identical experimental conditions, the present study utilized heterologous expression in *Xenopus* oocytes in combination with radioisotope flux experiments and electrophysiological measurements to demonstrate that hCNT2 has cation coupling characteristics similar to those of subfamily member hCNT1, and markedly different from those of hCNT3.

Like hCNT1, hCNT2 was Na⁺-specific, while hCNT3 was able to utilize both Na⁺ and H⁺ to drive permeant uptake into cells. Dual Na⁺/H⁺-coupling is not, however, a general characteristic of the CNT3/hfCNT subfamily: hagfish hfCNT has been shown to be Na⁺-dependent, but not H⁺-dependent (5). CNTs from other species

that exclusively use H^+ as the coupling cation include CeCNT3 from *Caenorhabditis elegans* (12), CaCNT from *Candida albicans* (13) and NupC from *Escherichia coli* (14, Appendix 2). hCNT3 is closer evolutionarily to these proteins than hCNT1/2 (4). H^+ -coupling of hCNT3 may be physiologically and pharmacologically important in tissues such as the duodenum, proximal jejunum and kidney proximal tubule where apical contents can be relatively acidic. The CNT protein family is therefore similar to other cotransporter families in which members are able to utilize Na^+ and/or H^+ to drive permeant uptake into cells (15-17). Since hCNT2 was not H^+ -coupled, subsequent analyses focused on a comparison of hCNT2 and hCNT1/3 interactions with Na^+ .

Na^+ -concentration dependence experiments directly compared the apparent affinities (K_{50}) of all three hCNTs for Na^+ . ^{14}C -Uridine influx studies revealed that hCNT1/2/3 exhibited apparent K_{50} values for Na^+ -activation in the range of 10 - 12 mM, and similar results were seen by electrophysiology (apparent K_{50} values ranging from 5 - 16 mM at $V_h = -30$ mV). Similar to hCNT1 and hCNT3, and in agreement with results reported previously for hCNT3 (Chapter 5), the Na^+ binding affinity of hCNT2 increased as the membrane potential was made more negative.

Previously published studies suggest that differences in Na^+/H^+ specificity between hCNT1/2 and hCNT3 may also extend to differences in cation-coupling ratios. Hill-type analyses of the relationships between nucleoside influx and Na^+ concentration, for example, suggest a 1:1 Na^+ :nucleoside coupling stoichiometry for (i) various *cit* (CNT1) and *cif* (CNT2) transport activities in different mammalian cells and tissues (6, 18-22), (ii) recombinant rCNT1 transport of both adenosine and uridine (11), and (iii) recombinant rCNT2 transport of adenosine and 2', 3'-dideoxyinosine (23, 24). In marked contrast, Hill coefficients consistent with a 2:1 Na^+ :nucleoside coupling stoichiometry have been reported for system *cib* in choroid plexus (25) and microglia (26), and for recombinant mouse CNT3 (mCNT3), hCNT3 and hfCNT transport of uridine (4, 5). Direct determination of coupling stoichiometries by simultaneous measurement of radiolabeled nucleoside influx and cation current has yielded Na^+ :uridine coupling ratios of either 1:1 (8) or 2:1 (9) for

hCNT1, and 2:1 for hCNT3 (Chapter 5). The equivalent H⁺:uridine coupling ratio for hCNT3 was 1:1 (Chapter 5). No corresponding published data are available for recombinant hCNT2.

In the present study, both Hill analyses of Na⁺-activation curves and charge:flux studies were used to determine the Na⁺:nucleoside coupling ratio of hCNT2, and to compare results for this transporter with those for hCNT1 and hCNT3 determined under identical experimental conditions and in the same batches of oocytes. Na⁺-activation curves derived from radioisotope flux experiments for both hCNT1 and hCNT2 were hyperbolic, with Hill coefficients consistent with a Na⁺:nucleoside coupling ratio of 1:1. In contrast, there was a sigmoidal relationship between nucleoside flux and Na⁺ concentration for hCNT3, with a Hill coefficient consistent with a Na⁺:nucleoside coupling ratio of 2:1. Parallel electrophysiology experiments measuring the relationship between uridine-evoked inward current and Na⁺ concentration confirmed these results. Similar to members of the SGLT protein family (27), Hill coefficients for hCNT2 and the other hCNTs were independent of membrane potential.

Hill coefficients reflect the number of ions interacting with the transporter rather than the actual number of ions entering the cell as a result of transport activity, and therefore provide only indirect estimates of transporter coupling ratios (28). Therefore, charge *versus* nucleoside and charge *versus* Na⁺ uptake experiments under voltage-clamp conditions were also used to determine hCNT2 stoichiometry directly and to compare that stoichiometry with hCNT1 and hCNT3. The ratio of charge to uridine uptake determined for both hCNT2 and hCNT1 yielded a Na⁺:uridine coupling ratio of 1:1. In contrast, the Na⁺:uridine coupling ratio of hCNT3 was 2:1. Na⁺:nucleoside coupling ratios for hCNT2 and hCNT3 were also determined with the purine nucleoside adenosine as permeant and yielded results identical to those seen with the pyrimidine nucleoside uridine. Contrary to a report by Larráyoz *et al.* (9), adenosine is also transported by the CNT1 isoform (1, 8, 11, 29-32). Kinetically, adenosine functions as a high-affinity, but low-capacity CNT1 permeant, precluding studies of hCNT1 Na⁺:adenosine coupling stoichiometry. Measurements correlating

$^{22}\text{Na}^+$ uptake to the translocated charge indicated that 1 net positive charge was transported for every Na^+ ion cotransported, verifying that, like hCNT1 and hCNT3, hCNT2 nucleoside-dependent currents are carried by Na^+ ions.

Both direct and indirect methods therefore give Na^+ :nucleoside coupling ratios of 1:1 for hCNT1 and hCNT2, and 2:1 for hCNT3. The Na^+ :nucleoside stoichiometry determined for hCNT1 agrees with previously published results (8), and contradicts the 2:1 coupling ratio reported by Larráyoz *et al.* (9). The corresponding 1:1 stoichiometry for recombinant hCNT2 is the first report of this transporter's Na^+ :nucleoside coupling ratio, while the contrasting characteristics of hCNT3 (2:1 coupling ratio) also confirm previous findings (Chapter 5). A 2:1 Na^+ :nucleoside stoichiometry for hCNT3 also mirrors that for hCNT (5). CNTs therefore resemble other transporter families in which individual members have different cation-coupling ratios. For example, members of the SGLT family have been described with 1:1 and 2:1 Na^+ :glucose coupling ratios (1:1 for SGLT2 and 2:1 for SGLT1/3) (16, 27, 33, 34). Similarly, the PepT1 and PepT2 proton-linked peptide transporters have 1:1 and 2:1 H^+ :peptide coupling ratios, respectively (35). Energetically, a 2:1 Na^+ :nucleoside coupling stoichiometry for hCNT3 *versus* a 1:1 coupling ratio for hCNT1/2 implies a greater ability of hCNT3 to transport permeants (including nucleoside drugs) against their concentration gradient and, hence, achieve higher levels within the cell.

In conclusion, the cation coupling characteristics of hCNT2 are similar to those of subfamily member hCNT1, and different from those of hCNT3. These results therefore validate and expand upon previously reported differences in cation coupling between human members of the CNT1/2 and CNT3/hCNT subfamilies of CNT proteins. These observed functional differences in Na^+/H^+ specificity and Na^+ coupling, in addition to being of potential physiologic and therapeutic importance, will facilitate future structure/function analyses to identify protein structural domains and specific amino acid residues responsible for CNT cation recognition and coupling.

Table 6-1. Na⁺-activation kinetics of uridine uptake by hCNT1, hCNT2 and hCNT3. Apparent affinities (K_{50}), predicted maximum flux values (V_{max}) and Hill coefficients (n) were determined from Na⁺ concentration response curves (0 - 100 mM NaCl, pH 8.5) in oocytes producing hCNT1, hCNT2 or hCNT3 measured at a ¹⁴C-uridine concentration of 20 μM (Figs. 6-2A - C). Values were obtained from curve fits to mediated averaged data from 10 - 12 oocytes, and are presented as means ± SE.

	Apparent K_{50} (mM)	V_{max} (pmol/oocyte.min ⁻¹)	Hill Coefficient
hCNT1	11 ± 1	11 ± 1	1.0 ± 0.1
hCNT2	10 ± 1	11 ± 1	1.0 ± 0.1
hCNT3	12 ± 1	13 ± 1	1.5 ± 0.1

Table 6-2. Voltage-dependence of Na⁺-activation kinetics of hCNT1, hCNT2 and hCNT3. Apparent affinities (K_{50}) and Hill coefficients (n) for Na⁺ were determined from Na⁺ concentration response curves (0 - 100 mM NaCl, pH 8.5) in oocytes producing hCNT1, hCNT2 or hCNT3 measured at a uridine concentration of 20 μ M and membrane potentials of -30 and -90 mV (see Fig. 6-3 for representative hCNT1-, hCNT2-, or hCNT3-producing oocytes). Values were obtained from fits to data from individual oocytes normalized to the fitted I_{max} value obtained for that cell, and are presented as means \pm SEM. The numbers in parentheses denote the number of oocytes.

	Apparent K_{50} (mM)		Hill Coefficient	
	$V_h = -30$ mV	$V_h = -90$ mV	$V_h = -30$ mV	$V_h = -90$ mV
hCNT1	11 \pm 1 (4)	1.9 \pm 0.1 (4)	1.0 \pm 0.1 (4)	0.99 \pm 0.02 (4)
hCNT2	16 \pm 2 (4)	2.8 \pm 0.3 (4)	0.95 \pm 0.02 (4)	0.90 \pm 0.02 (4)
hCNT3	4.7 \pm 0.4 (4)	1.7 \pm 0.1 (5)	1.8 \pm 0.1 (4)	1.8 \pm 0.1 (5)

Table 6-3. Stoichiometry of hCNT1, hCNT2 and hCNT3. Charge to ^{14}C -nucleoside (Figs. 6-4 and 6-5; 100 mM NaCl, pH 8.5) and charge to $^{22}\text{Na}^+$ (data not shown; 1 mM NaCl, pH 8.5) uptake ratio plots were generated at a membrane potential of -90 mV in hCNT1-, hCNT2- and hCNT3-producing oocytes. The numbers in parentheses denote the number of oocytes.

	Charge: ^{14}C -Uridine Stoichiometry	Charge: ^{14}C -Adenosine Stoichiometry	Charge: $^{22}\text{Na}^+$ Stoichiometry
hCNT1	0.89 ± 0.02 (11)	-----	0.90 ± 0.02 (5)
hCNT2	0.89 ± 0.02 (12)	0.93 ± 0.08 (8)	0.93 ± 0.02 (5)
hCNT3	2.1 ± 0.1 (12)	1.9 ± 0.1 (10)	0.90 ± 0.05 (6)

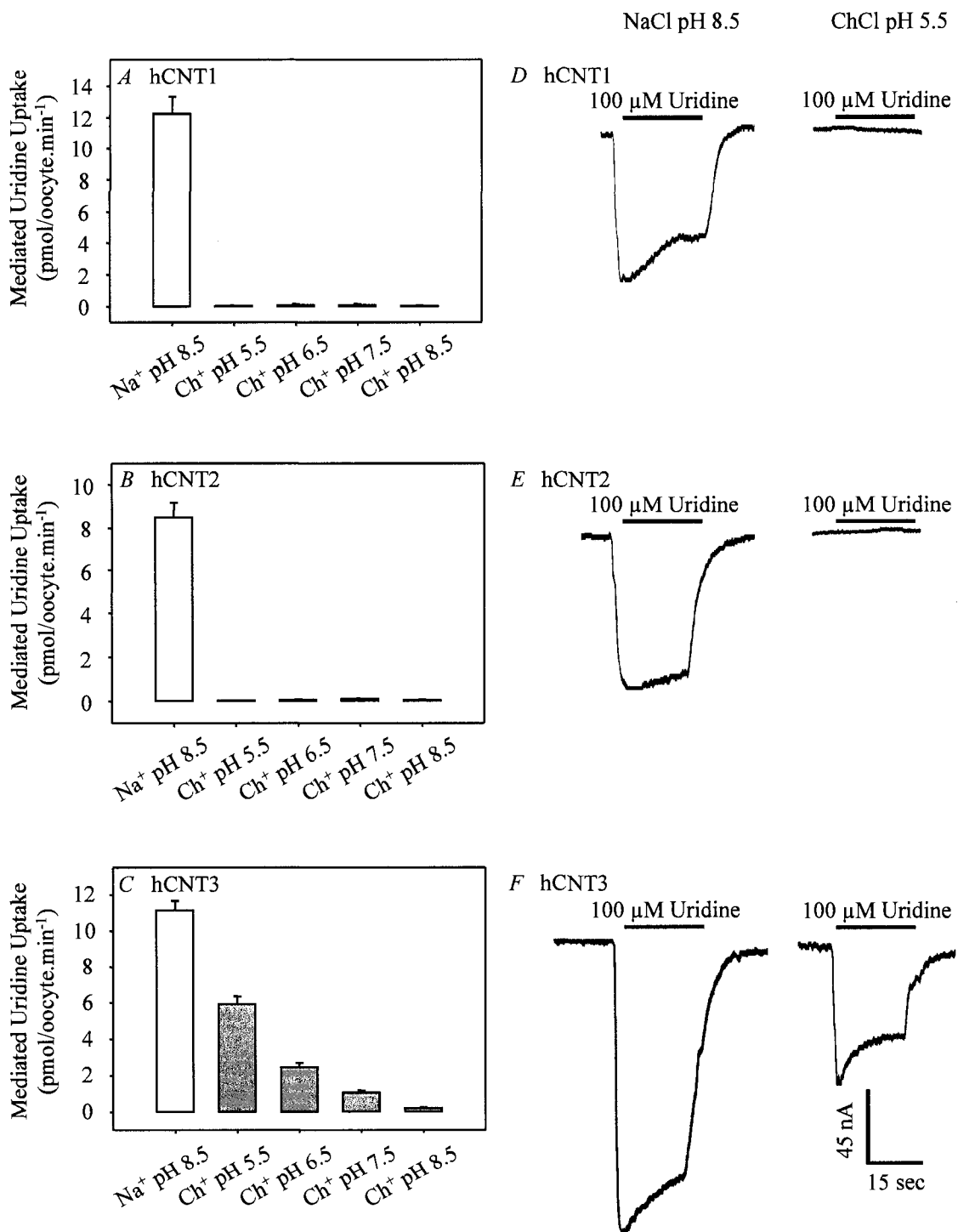


Figure 6-1.

Figure 6-1. Effects of Na⁺ and H⁺ on the transport activities of recombinant hCNT1, hCNT2 and hCNT3 produced in *Xenopus* oocytes. Radiolabeled fluxes of uridine (20 μM, 20°C, 1 min flux) in oocytes injected with RNA transcripts encoding hCNT1 (*A*), hCNT2 (*B*), or hCNT3 (*C*) were measured in transport media containing Na⁺ (*open bar*; 100 mM NaCl, pH 8.5) or choline (*gray bars*; 100 mM ChCl, pH 5.5 - 8.5). Values were corrected for basal non-mediated uptake in control water-injected oocytes and are means ± SEM of 10 - 12 oocytes. The experiment was performed on a single batch of oocytes used on the same day. Representative cation/nucleoside current traces in single hCNT1- (*D*), hCNT2- (*E*), or hCNT3-producing oocytes (*F*) clamped at -50 mV in transport medium containing Na⁺ (100 mM NaCl, pH 8.5) or choline (100 mM ChCl, pH 5.5). The bar denotes addition of uridine (100 μM) to the bath. No currents were observed in control water-injected oocytes (traces not shown).

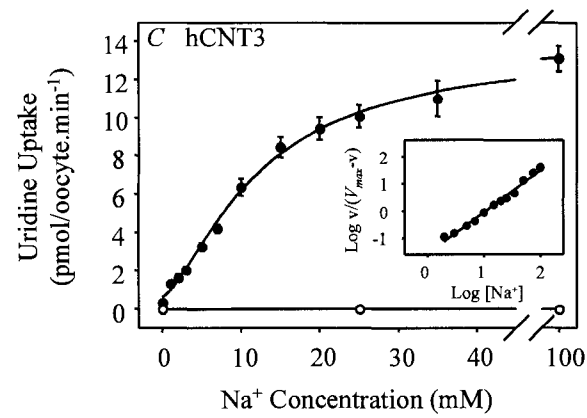
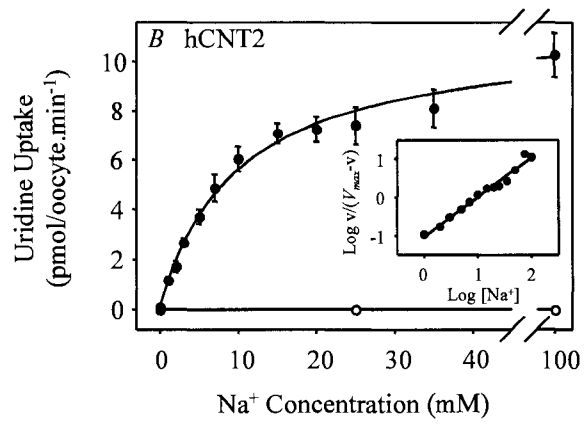
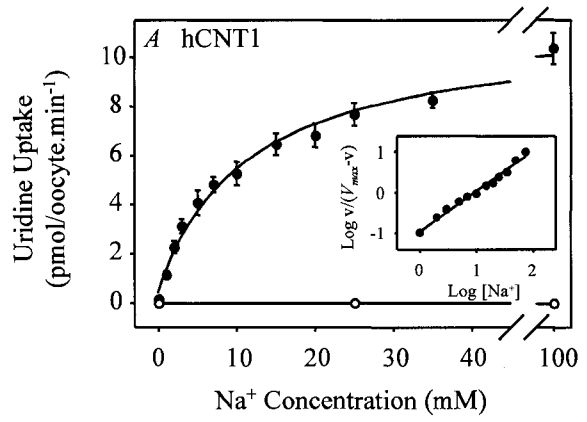


Figure 6-2.

Figure 6-2. Cation-activation kinetics of hCNT1, hCNT2 and hCNT3. Initial rates of ^{14}C -uridine uptake ($20\ \mu\text{M}$, 20°C , 1 min flux) were measured in Na^+ -containing (0 - 100 mM NaCl) transport media at pH 8.5 in oocytes injected either with water alone (*open circles*) or with water containing RNA transcripts encoding hCNT1 (*A*), hCNT2 (*B*) or hCNT3 (*C*) (*solid circles*). All of the fluxes were performed on the same batch of oocytes used on the same day. Kinetic parameters derived from these data for the hCNT-mediated component of transport (uptake in RNA transcript-injected oocytes *minus* uptake in water-injected oocytes) are presented in Table 6-1. The *inset* in each graph shows the Hill plot for the data.

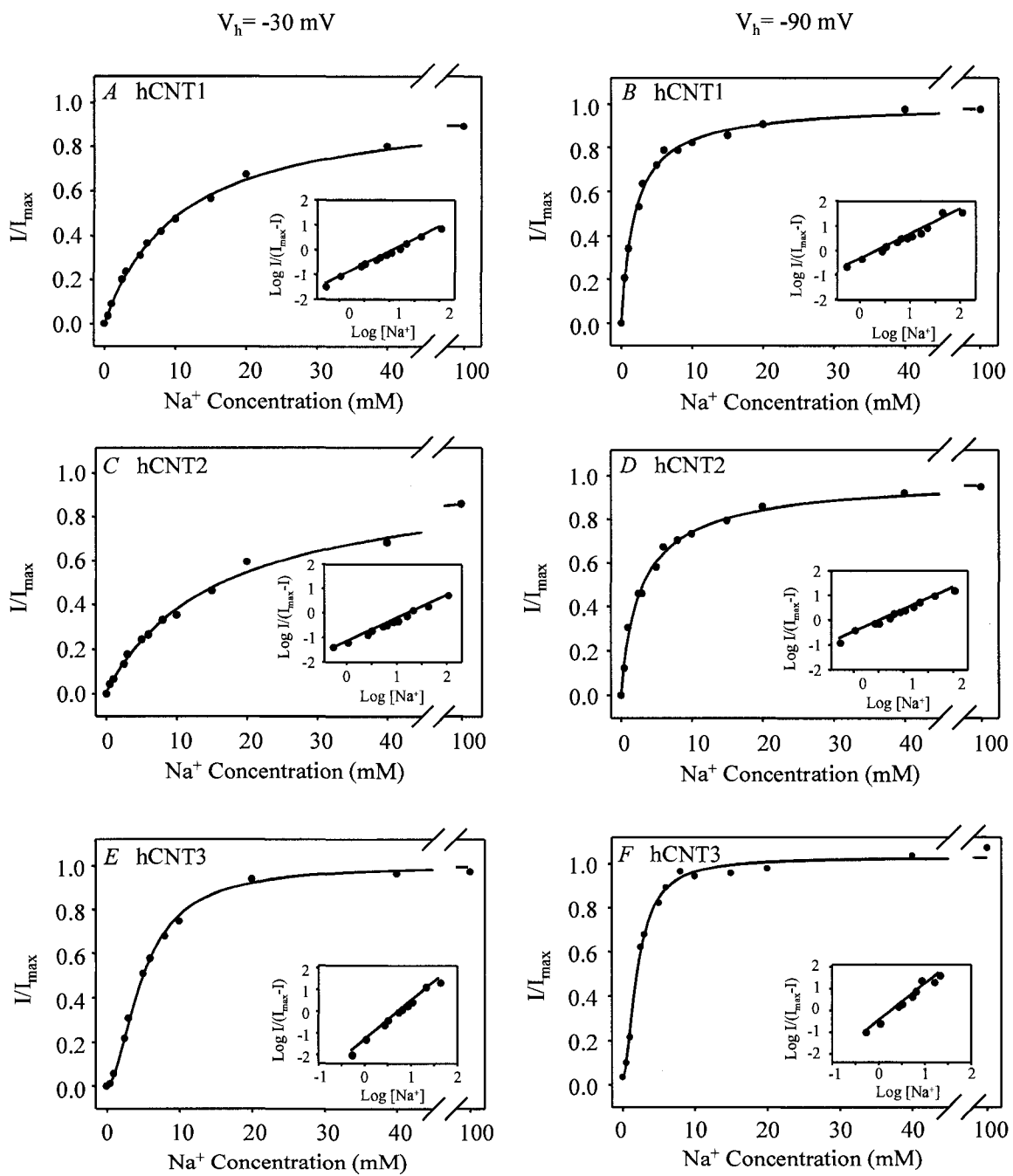


Figure 6-3.

Figure 6-3. Voltage-dependence of hCNT1, hCNT2 and hCNT3 cation-activation kinetics. Na⁺ concentration-response curves (pH 8.5) measured in single representative hCNT1- (*A, B*), hCNT2- (*C, D*) and hCNT3-producing oocytes (*E, F*) at membrane potentials of -30 (*A, C, E*) and -90 (*B, D, F*) mV (20 μM uridine). Currents at each Na⁺ concentration were normalized to the fitted I_{\max} value for that oocyte. I_{\max} values ranged from 45 to 101 nA. No currents were observed in control water-injected oocytes. Mean Na⁺-activation data for hCNT1, hCNT2, and hCNT3 is summarized in Table 6-2. The *insets* are Hill plots of the data.

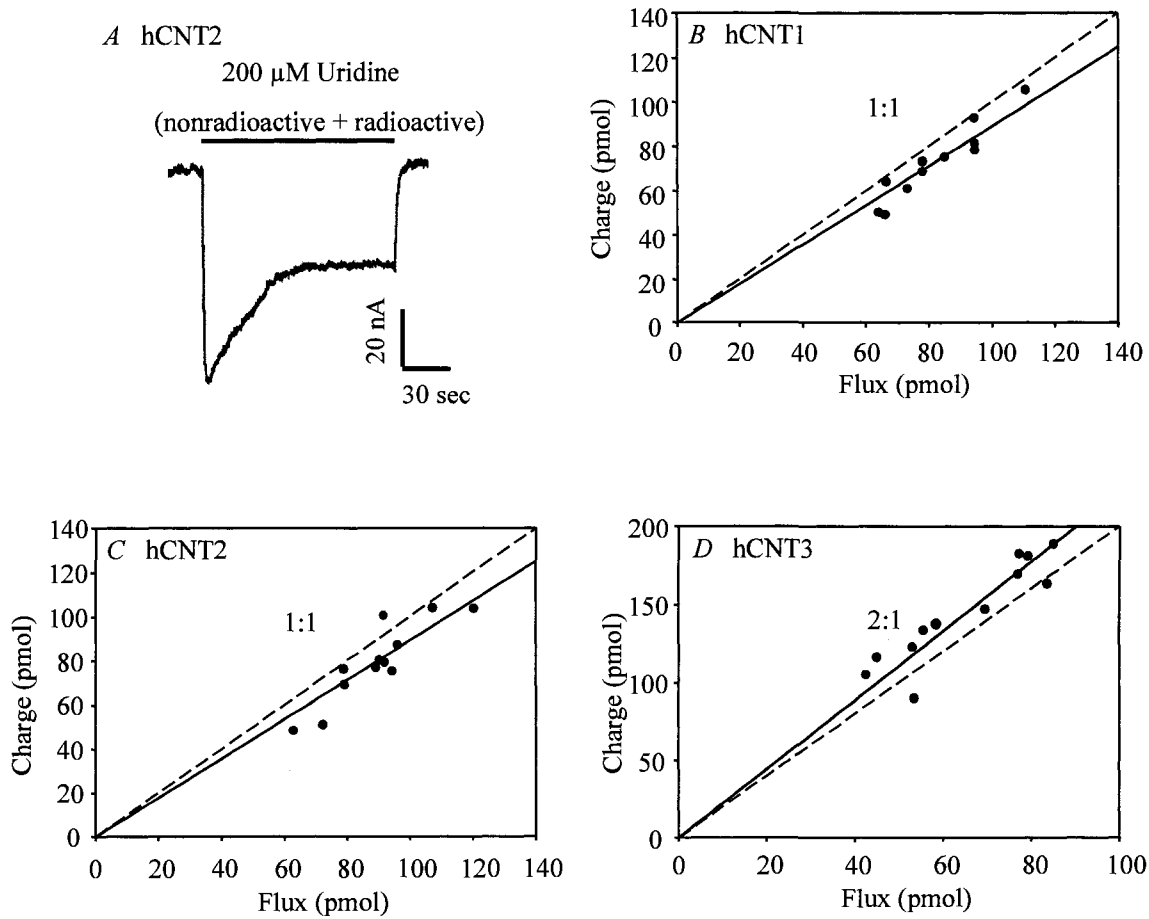


Figure 6-4.

Figure 6-4. Uridine coupling ratios of hCNT1, hCNT2 and hCNT3. (A) Representative example of the current generated during application of 200 μM ^{14}C -uridine to a hCNT2-producing oocyte in Na^+ -containing transport medium (100 mM NaCl, pH 8.5) at a membrane potential of -90 mV. Integration of the uridine-evoked current over the uptake period (2 min) yielded the charge moved which was converted to pmol and plotted against radiolabeled uridine uptake (pmol) in the same oocyte. The experiment was repeated in 12 different hCNT2-producing oocytes (C). Corresponding charge-to- ^{14}C -uridine uptake ratio plots are also shown for hCNT1 (B, n = 11) and hCNT3 (D, n = 12) (100 mM NaCl, pH 8.5; $V_h = -90$ mV). Linear regression analysis of the data for each plot is indicated by the *solid line*. The *dashed line* indicates a theoretical 1:1 charge:flux ratio in (B) and (C) and a 2:1 charge:flux ratio in (D). Lines were fitted through the origin. Stoichiometries (\pm SE) obtained from these data are given in Table 6-3.

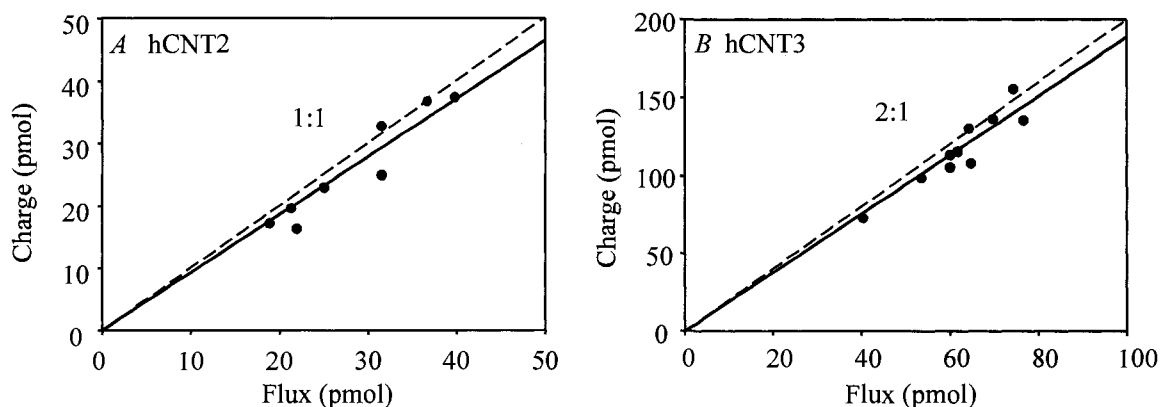


Figure 6-5. Adenosine coupling ratios of hCNT2 and hCNT3. Charge to ^{14}C -adenosine uptake ratio plots were generated at a membrane potential of -90 mV in Na^+ -containing transport media (100 mM NaCl , $\text{pH } 8.5$) in hCNT2- (*A*, $n = 8$) and hCNT3-producing oocytes (*B*, $n = 10$). The time of exposure of oocytes to ^{14}C -adenosine ($200\text{ }\mu\text{M}$) was 2 min . Integration of the adenosine-evoked current was used to calculate the net cation influx (charge) and was correlated to the net ^{14}C -adenosine influx (flux). Linear regression analysis of the data for each plot is indicated by the *solid line*. The *dashed line* indicates a theoretical 1:1 charge:flux ratio in (*A*) and a 2:1 charge:flux ratio in (*B*). Lines were fitted through the origin. Stoichiometries ($\pm\text{ SE}$) obtained from these data are indicated in Table 6-3.

Bibliography

1. Ritzel, M. W., Yao, S. Y., Huang, M.-Y., Elliot, J. F., Cass, C. E., and Young, J. D. (1997) Molecular cloning and functional expression of cDNAs encoding a human Na⁺-nucleoside cotransporter (hCNT1). *Am. J. Physiol. Cell Physiol.* **272**: C707-C714.
2. Wang, J., Su, S.-F., Dresser, M. J., Schaner, M. E., Washington, C. B., and Giacomini, K. M. (1997) Na⁺-dependent purine nucleoside transporter from human kidney: cloning and functional characterization. *Am. J. Physiol. Renal Physiol.* **273**: F1058-F1065.
3. Ritzel, M. W., Yao, S. Y., Ng, A. M., Mackey, J. R., Cass, C. E., and Young, J. D. (1998) Molecular cloning, functional expression and chromosomal localization of a cDNA encoding a human Na⁺/nucleoside cotransporter (hCNT2) selective for purine nucleosides and uridine. *Mol. Membr. Biol.* **15**: 203-211.
4. Ritzel, M. W., Ng, A. M., Yao, S. Y., Graham, K., Loewen, S. K., Smith, K. M., Ritzel, R. G., Mowles, D. A., Carpenter, P., Chen, X.-Z., Karpinski, E., Hyde, R. J., Baldwin, S. A., Cass, C. E., and Young, J. D. (2001) Molecular identification and characterization of novel human and mouse concentrative Na⁺-nucleoside cotransporter proteins (hCNT3 and mCNT3) broadly selective for purine and pyrimidine nucleosides (system *cib*). *J. Biol. Chem.* **276**: 2914-2927.
5. Yao, S. Y. M., Ng, A. M. L., Loewen, S. K., Cass, C. E., Baldwin, S. A., and Young, J. D. (2002) An ancient prevertebrate Na⁺-nucleoside cotransporter (hfCNT) from the Pacific hagfish (*Eptatretus stouti*). *Am. J. Physiol. Cell Physiol.* **283**: C155-C168.
6. Griffith, D. A., and Jarvis, S. M. (1996) Nucleoside and nucleobase transport systems of mammalian cells. *Biochem. Biophys. Acta* **1286**: 153-181.
7. Cass, C. E. (1995) Nucleoside transport, in *Drug Transport in Antimicrobial and Anticancer Chemotherapy* (Georgopapadakou, N. H., ed.), pp 403-451, Marcel Dekker, New York, USA.
8. Smith, K. M., Ng, A. M. L., Yao, S. Y., Labeledz, K. A., Knaus, E. E., Wiebe, L. I., Cass, C. E., Baldwin, S. A., Chen, X.-Z., Karpinski, E., and Young, J. D. (2004) Electrophysiological characterization of a recombinant human Na⁺-

- coupled nucleoside transporter (hCNT1) produced in *Xenopus* oocytes. *J. Physiol.* **558**: 807-823.
9. Larráyoz, I. M., Casado, F. J., Pastor-Anglada, M., and Lostao, M. P. (2004) Electrophysiological characterization of the human Na⁺/nucleoside cotransporter 1 (hCNT1) and role of adenosine on hCNT1 function. *J. Biol. Chem.* **279**: 8999-9007.
 10. Burckhardt, B. C., Kroll, B., and Frömter, E. (1992) Proton transport mechanism in the cell membrane of *Xenopus laevis* oocytes. *Pflugers Archiv.* **420**: 78-82.
 11. Yao, S. Y., Ng, A. M., Ritzel, M. W., Gati, W. P., Cass, C. E., and Young, J. D. (1996) Transport of adenosine by recombinant purine- and pyrimidine-selective sodium/nucleoside cotransporters from rat jejunum expressed in *Xenopus laevis* oocytes. *Mol. Pharmacol.* **50**: 1529-1535.
 12. Xiao, G., Wang, J., Tangen, T., and Giacomini, K. M. (2001) A novel proton-dependent nucleoside transporter, CeCNT3, from *Caenorhabditis elegans*. *Mol. Pharmacol.* **59**: 339-348.
 13. Loewen, S. K., Ng, A. M. L., Mohabir, N. N., Baldwin, S. A., Cass, C. E., and Young, J. D. (2003) Functional characterization of a H⁺/nucleoside cotransporter (CaCNT) from *Candida albicans*, a fungal member of the concentrative nucleoside transporter (CNT) family of membrane proteins. *Yeast* **20**: 661-675.
 14. Craig, J. E., Zhang, Y., and Gallagher, M. P. (1994) Cloning of the *nupC* gene of *Escherichia coli* encoding a nucleoside transport system, and identification of an adjacent insertion element, IS 186. *Mol. Microbiol.* **11**: 1159-1168.
 15. Pourcher, T., Bassilana, M., Sarkar, H. K., Kaback, H. R., and Leblanc, G. (1990) The melibiose/Na⁺ symporter of *Escherichia coli*: kinetic and molecular properties. *Philos. Trans. R. Soc. Lond. B. Biol. Sci.* **326**: 411-423.
 16. Mackenzie, B. M., Loo, D. D. F., Panayotova-Heiermann, M., and Wright, E. M. (1996) Biophysical characteristics of the pig kidney Na⁺/glucose cotransporter SGLT2 reveal a common mechanism for SGLT1 and SGLT2. *J. Biol. Chem.* **271**: 32678-32683.

17. Wright, E. M., Loo, D. D., Hirayama, B. A., and Turk, E. (2004) Surprising versatility of Na⁺-glucose cotransporters: SLC5. *Physiology* **19**: 370-376.
18. Plagemann, P. G., Aran, J. M., and Woffendin, C. (1990) Na⁺-dependent, active and Na⁺-independent, facilitated transport of formycin B in mouse spleen lymphocytes. *Biochem. Biophys. Acta* **1022**: 93-102.
19. Dagnino, L., Bennett, L. L. Jr., and Paterson, A. R. (1991) Substrate specificity, kinetics, and stoichiometry of sodium-dependent adenosine transport in L1210/AM mouse leukemia cells. *J. Biol. Chem.* **266**: 6312-6317.
20. Plagemann, P. G. (1991) Na⁺-dependent, concentrative nucleoside transport in rat macrophages. Specificity for natural nucleosides and nucleoside analogs, including dideoxynucleosides, and comparison of nucleoside transport in rat, mouse and human macrophages. *Biochem. Pharmacol.* **42**: 247-252.
21. Williams, T. C., and Jarvis, S. M. (1991) Multiple sodium-dependent nucleoside transport systems in bovine renal brush-border membrane vesicles. *Biochem. J.* **274**: 27-33.
22. Che, M., Nishida, T., Gatmaitan, Z., and Arias, I. M. (1992) A nucleoside transporter is functionally linked to ectonucleotidases in rat liver canalicular membrane. *J. Biol. Chem.* **267**: 9684-9688.
23. Li, J. Y., Boado, R. J., and Pardridge, W. M. (2001) Differential kinetics of transport of 2', 3'-dideoxyinosine and adenosine *via* concentrative Na⁺ nucleoside transporter CNT2 cloned from rat blood-brain barrier. *J. Pharmacol. Exp. Ther.* **299**: 735-740.
24. Li, J. Y., Boado, R. J., and Pardridge, W. M. (2001) Cloned blood-brain barrier adenosine transporter is identical to the rat concentrative Na⁺ nucleoside cotransporter CNT2. *J. Cereb. Blood Flow Metab.* **21**: 929-936.
25. Wu, X., Yuan, G., Brett, C. M., Hui, A. C., and Giacomini, K. M. (1992) Sodium-dependent nucleoside transport in choroid plexus from rabbit. Evidence for a single transporter for purine and pyrimidine nucleosides. *J. Biol. Chem.* **267**: 8813-8818.
26. Hong, M., Schlichter, L., and Bendayan, R. (2000) A Na⁺-dependent nucleoside transporter in microglia. *J. Pharmacol. Exp. Ther.* **292**: 366-374.

27. Díez-Sampedro, A., Eskandari, S., Wright, E. M., and Hirayama, B. A. (2001) Na⁺-to-sugar stoichiometry of SGLT3. *Am. J. Physiol. Renal Physiol.* **280**: F278-F282.
28. Weiss, J. N. (1997) The Hill equation revisited: uses and misuses. *FASEB J.* **11**: 835-841.
29. Huang, Q.-Q., Yao, S. Y. M., Ritzel, M. W. L., Paterson, A. R. P., Cass, C. E., and Young, J. D. (1994) Cloning and functional expression of a complementary DNA encoding a mammalian nucleoside transport protein. *J. Biol. Chem.* **269**: 17757-17760.
30. Fang, X., Parkinson, F. E., Mowles, D. A., Young, J. D., and Cass, C. E. (1996) Functional characterization of a recombinant sodium-dependent nucleoside transporter with selectivity for pyrimidine nucleosides (cNT1_{rat}) by transient expression in cultured mammalian cells. *Biochem. J.* **317**: 457-465.
31. Loewen, S. K., Ng, A. M., Yao, S. Y., Cass, C. E., Baldwin, S. A., and Young, J. D. (1999) Identification of amino acid residues responsible for the pyrimidine and purine nucleoside specificities of human concentrative Na⁺ nucleoside cotransporters hCNT1 and hCNT2. *J. Biol. Chem.* **274**: 24475-24484.
32. Gray, J. H., Owen, R. P., and Giacomini, K. S. (2004) The concentrative nucleoside family, SLC28. *Pflugers Archiv.* **447**: 728-734.
33. Chen, X.-Z., Coady, M. J., Jackson, F., Berteloot, A., and Lapointe, J.-Y. (1995) Thermodynamic determination of the Na⁺:glucose coupling ratio for the human SGLT1 cotransporter. *Biophys. J.* **69**: 2405-2414.
34. Mackenzie, B., Loo, D. D., and Wright, E. M. (1998) Relationships between Na⁺/glucose cotransporter (SGLT1) currents and fluxes. *J. Membr. Biol.* **162**: 101-106.
35. Chen, X.-Z., Zhu, T., Smith, D. E., and Hediger, M. A. (1999) Stoichiometry and kinetics of the high-affinity H⁺-coupled peptide transporter PepT2. *J. Biol. Chem.* **274**: 2773-2779.

Chapter 7:

A Proton-Mediated Conformational Shift Identifies A Mobile Pore-Lining Cysteine Residue (Cys⁵⁶¹) in Human Concentrative Nucleoside Transporter 3 (hCNT3)*

* A version of this chapter has been published.

Slugoski, M. D., Ng, A. M. L., Yao, S. Y. M., Smith, K. M., Lin, C. C., Zhang, J., Karpinski, E., Cass, C. E., Baldwin, S. A., and Young, J. D. (2008) A proton-mediated conformational shift identifies a mobile pore-lining cysteine residue (Cys-561) in human concentrative nucleoside transporter 3. *J. Biol. Chem.* **283**: 8496-8507.

Acknowledgements

Mrs. Amy M. L. Ng was involved in construction of the mutants and, together with Dr. Sylvia Y. M. Yao, completed the SCAM analysis of TM 12. Dr. Kyla M. Smith completed the electrophysiology experiments in this project. Mr. Colin C. Lin assisted with this project by confirming the pattern of uridine protection for the SCAM analysis of TM 12. Dr. Jing Zhang constructed the hCNT3C- construct for use in yeast experiments. Drs. Edward Karpinski, Carol E. Cass and Stephen A. Baldwin are collaborative principal investigators who assisted with research funding and manuscript preparation. This research was funded by the National Cancer Institute of Canada with funds from the Canadian Cancer Society and Alberta Cancer Board.

Introduction

In humans (h), the concentrative nucleoside transporter (CNT) protein family is represented by three members, hCNT1, hCNT2 and hCNT3. Similar to their orthologs in other mammalian species, hCNT1 and hCNT2 are pyrimidine nucleoside-selective and purine nucleoside-selective, respectively, while hCNT3 transports both pyrimidine and purine nucleosides (1-3). hCNT1 and hCNT2 function exclusively as Na⁺-coupled nucleoside transporters, whereas hCNT3 can utilize electrochemical gradients of either Na⁺ or H⁺ to accumulate nucleosides within cells (4, Chapters 5 and 6). Whereas Na⁺-coupled hCNT3 transports a broad range of physiological purine and pyrimidine nucleosides, as well as anticancer and antiviral nucleoside drugs, H⁺-coupled hCNT3 is unable to transport guanosine, 3'-azido-3'-deoxythymidine (zidovudine; AZT) or 2', 3'-dideoxycytidine (zalcitabine; ddC) (3, Chapter 5). This suggests that Na⁺- and H⁺-bound versions of hCNT3 have significantly different conformations of the nucleoside binding pocket and/or translocation channel. Through the use of site-directed mutagenesis and heterologous expression of hCNT1-3 in *Xenopus laevis* oocytes, this study reveals a conformationally-sensitive pore-lining cysteine residue in transmembrane domain (TM) 12 of hCNT3 whose accessibility to the hydrophilic membrane-impermeant thiol reagent *p*-chloromercuribenzenesulfonate (PCMBS) reports a specific H⁺-activated state of the transporter.

Results

PCMBS inhibition of hCNT3 – hCNT3 has 14 endogenous cysteine residues, compared to 20 each for hCNT1 and hCNT2, of which 10 are common to all three hCNTs (Fig. 7-1). Five of the hCNT3 cysteine residues are located in putative TMs (TMs 1, 11, 12 and 13) and the remainder reside within the extramembraneous N- and C-terminal regions of the protein. Despite having multiple endogenous cysteine residues, it was previously established that wild-type hCNT1 is not inhibited by PCMBS (Chapter 4). Fig. 7-2 depicts the effects of PCMBS (500 μM) on wild-type hCNT3.

Since hCNT3 is both Na⁺- and H⁺-coupled (3, 4, Chapters 5 and 6), the protein was exposed to PCMBS either in the presence of Na⁺ or H⁺ (100 mM NaCl, pH 8.5 and 100 mM ChCl, pH 5.5, respectively). By employing Na⁺-containing medium buffered at pH 8.5, the small, but significant, amount of hCNT3 H⁺-activation that occurs at pH 7.5 was avoided (Chapters 5 and 6). Control experiments have been undertaken to verify that Na⁺-coupled uridine transport by hCNT3 at pH 8.5 is kinetically indistinguishable from that at pH 7.5 (Chapter 8). Following treatment with PCMBS, the same two media were used in assays of uridine transport activity.

Similar to the previous findings with hCNT1 (Chapter 4), and independent of whether uridine transport activity was subsequently determined in Na⁺- or H⁺-containing medium (Figs. 7-2A and B, respectively), hCNT3-mediated uridine influx was unaffected by PCMBS when exposed to H⁺-reduced medium containing Na⁺ (100 mM NaCl, pH 8.5). In contrast however, Figs. 7-2A and B also reveal marked inhibition (80 - 90%) of both Na⁺- and H⁺-coupled uridine influx when hCNT3 was reacted with PCMBS under acidified, Na⁺-free conditions (100 mM ChCl, pH 5.5). The flux values shown in Figs. 7-2A and B depict mediated transport activity, defined as the difference in uptake between RNA transcript-injected and control water-injected oocytes. In this and subsequent experiments, uridine uptake in water-injected oocytes was < 0.02 pmol/oocyte.min⁻¹ under all conditions tested (data not shown).

As demonstrated in Fig. 7-2C, hCNT3-mediated uridine influx was unaffected by PCMBS (500 μM) when incubated in H⁺-reduced medium also lacking Na⁺ (100 mM ChCl, pH 8.5). Inhibition was evident, however, when exposure to PCMBS (500 μM) occurred in acidified, Na⁺-containing medium (100 mM NaCl, pH 5.5) (Fig. 7-2C). These findings eliminate the possibility that Na⁺ exerts a protective effect against PCMBS binding and suggest instead that inhibition of hCNT3 by PCMBS results from a specific H⁺-dependent exofacial conformational shift which exposes PCMBS-sensitive residue(s) to the extracellular medium. The H⁺-dependent effect of PCMBS on hCNT3 was not secondary to enhanced chemical reactivity of PCMBS with cysteinyl sulfhydryl groups under acidic conditions or to non-specific pH-induced changes in protein conformation, because control experiments confirmed that uridine transport by Na⁺-

specific hCNT1 was unchanged by exposure to PCMBS (500 μM) either in the presence of Na^+ or H^+ (100 mM NaCl, pH 8.5 and 100 mM ChCl, pH 5.5, respectively) (Fig. 7-3A). Fig. 7-3B extends this finding of PCMBS-insensitivity to Na^+ -specific hCNT2.

H^+ -induced PCMBS inhibition of hCNT3 was also evident in influx assays employing other physiological nucleosides. In a representative experiment measuring Na^+ -coupled influx of a panel of 20 μM ^{14}C -labeled nucleosides following incubation in the presence and absence of 500 μM PCMBS (100 mM ChCl, pH 5.5), the percentage inhibition of influx of uridine, thymidine, cytidine, adenosine, inosine and guanosine was 89 ± 1 , 91 ± 2 , 90 ± 1 , 87 ± 1 , 89 ± 1 and $89 \pm 1\%$, respectively. Therefore, PCMBS binding interferes with translocation of both purine and pyrimidine nucleosides. PCMBS-inhibited hCNT3 nucleoside transport activity was restored by incubation with 5 mM DTT, verifying a specific and reversible interaction of PCMBS with hCNT3 cysteine residue(s) (Fig. 7-4). Since PCMBS is both hydrophilic and membrane impermeant (5, 6), the targeted residue(s) must be accessible from the external medium and is most likely located within an outward-facing conformation of the hCNT3 translocation pore.

Concentration dependence and uridine protection of PCMBS inhibition – Dose-response curves for PCMBS inhibition of hCNT3 in the concentration range 25 μM to 1 mM are presented in Fig. 7-5. Quantitatively, both Na^+ - and H^+ -mediated modes of uridine influx were equally affected, with IC_{50} values of $130 \pm 20 \mu\text{M}$ (Fig. 7-5A) and $93 \pm 18 \mu\text{M}$ (Fig. 7-5B), respectively. Figs. 7-5A and B also demonstrate the ability of extracellular uridine (20 mM) to fully protect the transporter against this inhibition. As shown in Figs. 7-6A and B, the uridine concentration required for half-maximal protection against PCMBS was $12 \pm 2 \mu\text{M}$. This compares favourably with a previously determined apparent K_m value of 110 μM for H^+ -coupled uridine influx (Chapter 5), especially if an anticipated increase in permeant apparent affinity at low temperature is taken into consideration (the uridine protection was performed on ice). Therefore, the PCMBS-binding residue(s) is likely located in a position within or closely adjacent to the nucleoside binding pocket.

Electrophysiology of PCMBS inhibition – Steady-state electrophysiological experiments confirmed (i) that PCMBS inhibition of wild-type hCNT3 required exposure under acidified conditions, and (ii) that uridine-induced Na⁺ and H⁺ inward currents were equally affected by bound PCMBS (data not shown).

In parallel electrophysiological experiments performed under presteady-state conditions and in the absence of uridine (4, Chapter 6), hCNT3-producing oocytes were voltage clamped at a holding potential (V_h) of -50 mV and presteady-state currents were activated by voltage steps to the series of test potentials (V_t) outlined in the voltage pulse protocol shown in Fig. 7-7A. Current recordings in a representative hCNT3-producing oocyte are shown in Fig. 7-7B in both the presence (*left*) and absence (*right*) of Na⁺ (100 mM NaCl and ChCl, pH 8.5, respectively). As reported previously for both hCNT1 (4, Appendix 4) and hCNT3 (7), current relaxations persisting for tens of ms after the time required to charge the membrane capacitance were apparent in both the ON response (when V_h was stepped to V_t) and in the OFF response (when V_t was returned to V_h). These presteady-state currents were reduced, but not eliminated, upon removal of external Na⁺. Representing both Na⁺- and carrier-associated charge movements within the membrane, these presteady-state currents were absent in control water-injected oocytes (data not shown). As demonstrated in Fig. 7-7C for the same oocyte, exposure to 500 μ M PCMBS in H⁺-containing medium (100 mM NaCl, pH 5.5) abolished presteady-state currents in both the presence and absence of Na⁺ (Fig. 7-7C *left* and *right*, respectively). Confirming the specificity of PCMBS for hCNT3, and as anticipated from the lack of effect on transport seen in Fig. 7-3A, hCNT1 presteady-state currents were unaffected by incubation with PCMBS (data not shown).

PCMBS inhibition of hCNT3 mutants – hCNT3 contains 14 endogenous cysteine residues, of which five lie within predicated TMs (TMs 1, 11, 12 and 13) (Fig. 7-1). Since TMs 1-3 of mammalian CNTs are not required for transport activity (8) and because the C-terminal half of CNTs comprises the functional domain for cation-coupling (9, Chapter 5), cysteine residues 486 (TM 11), 561 (TM 12), 602 (TM 13) and 607 (TM 13) were identified as potential candidate residues responsible for H⁺-induced PCMBS binding. Of these, Cys⁴⁸⁶, Cys⁵⁶¹ and Cys⁶⁰⁷ are conserved in all three human

CNTs (Fig. 7-1). Using site-directed mutagenesis, the four hCNT3 cysteine residues were individually mutated to serine, generating hCNT3 mutants C486S, C561S, C602S and C607S. All four constructs were functional when produced in *Xenopus* oocytes (Fig. 7-8A). Similar to wild-type hCNT3 (Fig. 7-2B), inhibition of uridine transport following incubation with 500 μ M PCMBS in H⁺-containing medium was evident for C486S, C602S and C607S, but there was no effect on mutant C561S (Fig. 7-8A). None of the mutants were affected by exposure to PCMBS in medium containing 100 mM NaCl, pH 8.5 (data not shown).

PCMBS inhibition of hCNT3C- mutants – In subsequent experiments, site-directed mutagenesis was also used to generate revertant mutants in the cysteine-less background of hCNT3C- (10). As shown in Fig. 7-8B, each of the four revertant mutants (S486C(C-), S561C(C-), S602C(C-) and S607C(C-)) were functional when produced in oocytes. Complementary to the results presented for the corresponding hCNT3 mutants (Fig. 7-8A), only S561C(C-) showed inhibition of uridine influx following incubation with 500 μ M PCMBS in H⁺-containing medium (Fig. 7-8B). The extent of inhibition was similar to that observed with wild-type hCNT3 (Fig. 7-2B). None of the mutants were affected by exposure to PCMBS in medium containing 100 mM NaCl, pH 8.5 (data not shown).

PCMBS inhibition of mutant S561C(C-): concentration dependence and uridine protection – Dose-response and uridine protection experiments were undertaken to confirm the identity of Cys⁵⁶¹ in TM 12 as the residue responsible for PCMBS binding. Similar to wild-type hCNT3 (Fig. 7-5), exposure of S561C(C-) to PCMBS in H⁺-containing medium produced inhibition of uridine transport activity with an IC₅₀ value of 190 \pm 60 μ M (Fig. 7-9). Furthermore, extracellular uridine (20 mM) protected the mutant transporter against this inhibition (Fig. 7-9).

Effects of methanethiosulfonate (MTS) reagents – In addition to PCMBS, the inhibitory effects of three MTS derivatives, MTSEA, MTSES and MTSET were also tested. Included in the analysis were wild-type hCNT1, hCNT2 and hCNT3, hCNT3 mutant C561S, cysteine-less hCNT3C- and hCNT3C- mutant S561C(C-). Reflecting

their different reactivities towards thiol groups, 2-aminoethyl methanethiosulfonate hydrobromide (MTSEA), sodium (2-sulfonatoethyl) methanethiosulfonate (MTSES) and [(triethylammonium)ethyl] methanethiosulfonate bromide (MTSET) were used at concentrations of 2.5, 10 and 1 mM, respectively. Similar to PCMBBS, oocytes producing each of the constructs were exposed to MTS reagents in acidified 100 mM ChCl transport medium (pH 5.5), then assayed for radiolabeled uridine transport activity, either in 100 mM NaCl, pH 7.5 (hCNT1 and hCNT2) or 100 mM ChCl, pH 5.5 (hCNT3, C561S, hCNT3C- and S561C(C-)). In no case was transport activity affected (Fig. 7-10). Similarly, and in agreement with previously published studies for hCNT1 (Appendix 4) and hCNT3C- mutant S561C(C-) (10) under non-acidified conditions, there was also no inhibition of uridine uptake when constructs were incubated with the three MTS reagents in Na⁺-containing medium at pH 8.5 (data not shown).

To eliminate the possibility that MTS reagents bind to hCNT3 Cys⁵⁶¹ without affecting transport, oocytes producing wild-type hCNT3 or revertant hCNT3C- mutant S561C(C-) were incubated first in acidified medium (100 mM ChCl, pH 5.5) containing 2.5 mM MTSEA, followed by a subsequent incubation under the same conditions with 500 μM PCMBBS (Fig. 7-10, *inset*). Oocytes producing hCNT3 or S561C(C-) both showed the expected degree of uridine transport inhibition when treated with PCMBBS alone (compare with Figs. 7-2B and 7-7B, respectively), and the extent of this inhibition was unaffected by pre-exposure to MTSEA. Therefore, MTSEA, the smallest of the MTS reagents examined, was unable to access Cys⁵⁶¹.

Substituted cysteine accessibility method (SCAM) analysis of TM 12 – To explore the relationship between Cys⁵⁶¹ and other TM 12 residues, the cysteine-less background of hCNT3C- was used in conjunction with SCAM to systematically screen all 21 putative positions in the helix for PCMBBS sensitivity. In this analysis, a series of hCNT3C- mutants with individual TM 12 residues mutated to cysteine were produced in *Xenopus* oocytes. Functional mutants, together with hCNT3C- as control, were investigated for inhibition by 200 μM PCMBBS both in the presence of Na⁺ or H⁺ and, where inhibition was obtained, uridine protection (Table 7-1).

Of the 21 mutants investigated, only two (F563C(C-) and S568C(C-)) had functional activity too low to characterize further ($10 \mu\text{M}$ uridine influx $< 0.1 \text{ pmol/oocyte.min}^{-1}$). F563C(C-) is also nonfunctional when produced in yeast, while S568C(C-) exhibits very low transport activity (25). Since both mutant proteins are localized to the yeast plasma membrane in amounts similar to hCNT3 and hCNT3C-(10), it is likely that residues Phe⁵⁶³ and Ser⁵⁶⁸ are structurally and/or functionally important for hCNT3 transport activity. Both residues are highly conserved within the CNT protein family (Fig. 7-11). Of the remaining 19 cysteine substitutions, seven resulted in substantial ($> 40\%$) inhibition by $200 \mu\text{M}$ PCMBS (I554C(C-), T557C(C-), Y558C(C-), S561C(C-), N565C(C-), G567C(C-) and I571C(C-)). Of these, two resembled S561C(C-) and were selectively inhibited by PCMBS in the presence of H^+ , but not Na^+ (I554C(C-) and Y558C(C-)), while four were approximately equally PCMBS-sensitive in either Na^+ - or H^+ -containing media (T557C(C-), N565C(C-), G567C(C-) and I571C(C-)). The presence of uridine (20 mM) during exposure to PCMBS resulted in partial protection of Y558C(C-) and essentially complete protection of S561C(C-), N565C(C-), G567C(C-) and I571C(C-). No uridine protection was seen for I554C(C-) or T557C(C-). Two additional mutants that were more weakly inhibited by PCMBS (I555C(C-) and I566C(C-)) in both Na^+ - and H^+ -containing media were not tested for uridine protection.

Discussion

As shown in Fig. 7-1, current models of hCNT topology have 13 putative TMs (8). Computer algorithms also weakly predict two additional potential transmembrane regions, designated in Fig. 7-1 as 5A and 11A (8). Consistent with both a 13 and 15 TM membrane architecture, the loop linking TMs 4 and 5 has been shown to be cytoplasmic, while the N-terminus and glycosylated C-terminus are intracellular and extracellular, respectively (8). Initial SCAM analyses of TMs 11, 12 and 13 of hCNT3C- using MTS reagents (10), as well as other previously published structure/function studies (*e.g.* 11,

Chapter 4), are also consistent with both models. Recent investigations of hCNT1 glutamate residues (Appendix 4), however, favour a 15 TM membrane architecture.

Previously, TMs 7 and 8 (Fig. 7-1) were identified to contain residues of functional importance and are predicted to be pore-lining (11, Chapter 4, Appendix 4). The presently revealed H⁺-activated reactivity of wild-type hCNT3 Cys⁵⁶¹ to PCMBS, as determined by inhibition of uridine transport activity, now establishes that TM 12 is also pore-lining. Pore-lining status has also been ascribed to this TM on the basis of an initial series of SCAM analyses of cysteine-less hCNT3C- (10). Performed at neutral pH, this study found partial sensitivity of TM 12 mutants T557C(C-), N565C(C-), G567C(C-) and I571C(C-) to MTS reagents, and variable protection against that inhibition by uridine (10). S561C(C-) was unreactive to MTS reagents in that analysis, a finding confirmed here in experiments performed with MTSEA, MTSES and MTSET under both acidified and H⁺-reduced conditions and with Cys⁵⁶¹ present in either a cysteine-less (hCNT3C-) or wild-type (hCNT3) background.

PCMBS (12, 13) and MTS (14, 15) reagents both react preferentially with the ionized thiolate form of cysteine (-S⁻) rather than with the uncharged thiol form (-SH) (16). PCMBS and the MTS derivatives MTSEA, MTSES and MTSET differ, however, in charge (PCMBS and MTSES are negatively-charged, MTSEA and MTSET are positively-charged) and membrane permeability (PCMBS, MTSES and MTSET are membrane-impermeable, MTSEA is membrane-permeable). They also differ in size (PCMBS < MTSEA < MTSES < MTSET). It is possible, therefore, that steric and/or electrostatic factors contributed to the specificity of the interaction of Cys⁵⁶¹ with PCMBS. MTSEA, the smallest of the MTS reagents tested, failed to block addition of PCMBS to hCNT3 Cys⁵⁶¹, confirming the inability of MTS reagents to react with this residue.

hCNT3 Cys⁵⁶¹ is, at least transiently, pore-lining because (i) only cysteines on the water-accessible surface of the protein will ionize to a significant extent, and (ii) hydrophilic negatively charged PCMBS is unlikely to enter hydrophobic regions in the lipid bilayer or protein interior. Since PCMBS was added extracellularly, the aqueous

pathway that it traverses to reach Cys⁵⁶¹ must be contiguous with the external medium and, therefore, part of the outward-facing aspect of the hCNT3 translocation pore. The exofacial pore-lining status of Cys⁵⁶¹ is confirmed by the ability of micromolar concentrations of uridine in the extracellular medium to protect the transporter against PCMBs inhibition. Opposite to the predicted effect of pH on thiol group chemical reactivity towards PCMBs, inhibition of hCNT3 only occurred under acidified conditions. Na⁺ had no influence on PCMBs inhibition of the transporter.

Conserved in all three human CNTs, accessibility of Cys⁵⁶¹ to PCMBs was unique to hCNT3. hCNT3 differs from Na⁺-specific hCNT1 and hCNT2 by being able to couple uphill nucleoside transport to both Na⁺ and H⁺ electrochemical gradients (1-4, Chapters 5 and 6). It is proposed, therefore, that PCMBs reactivity with hCNT3 Cys⁵⁶¹ reports a specific H⁺-activated conformational state of the protein. Since exofacial uridine occludes this residue and blocks access to PCMBs, hCNT3 Cys⁵⁶¹ is likely located within, or closely adjacent to, the nucleoside binding pocket of the transporter. H⁺-induced changes in hCNT3 nucleoside and nucleoside drug selectivity (3, Chapter 5) are also strongly indicative of a H⁺-specific conformation of the nucleoside binding pocket and/or translocation pore. H⁺-coupled hCNT3 is also distinguished by a cation:nucleoside stoichiometry of 1:1, compared to 2:1 for Na⁺ (Chapters 5 and 6). In acidified Na⁺-containing transport medium, when both cations are present together, charge/uptake experiments suggest that the transporter binds one Na⁺ ion and one H⁺ (Chapter 5).

hCNT1-3 kinetics and cation coupling can be interpreted in terms of a conformational equilibrium model of secondary active transport (17, 18). Developed by Krupka, this modified ordered binding model of secondary active transport alleviates the stringent sequential carrier states of earlier models and instead allows for flexible cation interactions such as those observed for Na⁺- and H⁺-coupling of hCNT3. In the model, binding of cation (Na⁺ and/or H⁺ in the case of hCNT3) shifts the equilibrium between two carrier states to “unlock” or open the nucleoside binding site, thereby promoting active transport. The reactivity of hCNT3 Cys⁵⁶¹ to PCMBs senses unique characteristics of the H⁺-bound transporter.

As part of a larger, more comprehensive analysis encompassing the entire C-terminal half of hCNT3C- (19, Chapter 10), SCAM experiments have been undertaken utilizing PCMBS to investigate the molecular and functional properties of all 21 putative residues of TM 12 (Table 7-1). In addition to S561C(C-), these studies have identified two further cysteine-substituted constructs in TM 12, I554C(C-) and Y558C(C-), which also exhibit H⁺-activated inhibition by PCMBS. Consistent with their anticipated relative depth within the membrane (and likely proximity to the nucleoside binding pocket) and as demonstrated in Fig. 7-9 for S561C(C-), the constructs exhibited no protection (I554C(C-)), partial protection (Y558C(C-)) and full protection by extracellular uridine (S561C(C-)). More than Cys⁵⁶¹ alone, therefore, three adjacent pore-lining residues of hCNT3 (Ile⁵⁵⁴, Tyr⁵⁵⁸ and Cys⁵⁶¹) combine to delineate a conformationally-sensitive exofacial pore-lining region of TM 12 specifically responsive to H⁺ binding. In addition, each of the four residue positions in TM 12 previously shown to be sensitive to MTS reagents at neutral pH (Thr⁵⁵⁷, Asn⁵⁶⁵, Gly⁵⁶⁷ and Ile⁵⁷¹) were also found to display inhibition by PCMBS in the presence of both Na⁺ and H⁺. All, except Thr⁵⁵⁷ (the most exofacial), were uridine protectable. None of the remaining 14 residue positions in TM 12 were strongly PCMBS-sensitive.

H⁺-activation therefore distinguishes two discrete classes of PCMBS-sensitive residues within TM 12 of hCNT3. To provide additional information on these residues and the possible nature of the H⁺-induced conformational shift, Fig. 7-11 presents α -helical wheel projections (Fig. 7-11A) and space-filling models of hCNT3 TM 12 (Fig. 7-11B), although it is appreciated that the true structure of this region of the protein may differ appreciably from the perfect α -helix illustrated. Based on the aligned sequences of 126 eukaryote and prokaryote CNT family members, individual residues are colour-coded to indicate patterns of residue conservation and polarity within the helix. Residues Ile⁵⁵⁴, Ser⁵⁵⁸ and Cys⁵⁶¹, and Thr⁵⁵⁷, Asn⁵⁶⁵, Gly⁵⁶⁷ and Ile⁵⁷¹ are highlighted. TM 12 has the membrane orientation shown in Fig. 7-11 irrespective of whether hCNT3 has a 13 or 15 TM membrane architecture (Fig. 7-1).

All 21 residue positions in TM 12 exhibited restricted variability, showing a high degree of conservation among CNT family members (Fig. 7-11A). This suggests

involvement either in maintaining the structures of the transporters or in cation and nucleoside binding and translocation, these being features of CNT family members that are held in common. Thus, TM 12 residues are likely either to face another helix or to line the translocation pore.

The helical wheel projections in Fig. 7-11*A* establish that residues insensitive to PCMBBS (and MTS reagent) inhibition are localized to one half of the helix surface. Consistent with a role in helix-helix packing, this half of TM 12 contains six residue positions exhibiting the highest level of sequence conservation (Ile⁵⁵⁵, Ala⁵⁵⁹, Gly⁵⁶², Phe⁵⁶³, Gly⁵⁷⁰ and Gly⁵⁷⁴). In contrast, the other side of TM 12 is mostly PCMBBS/MTS-reactive and likely, therefore, to be pore-lining. The uridine protection observed with many of these residues and the demonstration that polar residues localize predominantly to this face of the helix support this conclusion. The four residue positions (Thr⁵⁵⁷, Asn⁵⁶⁵, Gly⁵⁶⁷ and Ile⁵⁷¹) which show inhibition by PCMBBS in the presence of both Na⁺ and H⁺ are distributed throughout the PCMBBS-sensitive face of the helix, whereas Ser⁵⁶¹ and the two adjacent residue positions (Ile⁵⁵⁴ and Tyr⁵⁵⁸) which exhibit H⁺-activated PCMBBS inhibition come together in one quadrant of that surface.

Fig. 7-11*B* spatially differentiates within the plane of the membrane the H⁺-dependent class of PCMBBS-sensitive residues from those which are inhibited in the presence of both Na⁺ and H⁺. Residues which are inhibited by PCMBBS only in the presence of H⁺ cluster together in a small exofacial aspect of the helix specific to the H⁺-bound conformation of hCNT3, whereas those which exhibit inhibition by PCMBBS in the presence of both Na⁺ and H⁺ have more endofacial locations. Additionally, Fig. 7-11*B* reveals that the five TM 12 residue positions that are both PCMBBS-sensitive and uridine-protectable (Tyr⁵⁵⁸, Cys⁵⁶¹, Asn⁵⁶⁵, Gly⁵⁶⁷ and Ile⁵⁷¹) are grouped centrally within the putative pore-lining face of TM 12 in a position that likely delineates the location of the uridine binding pocket. Presteady-state current measurements of hCNT1 (4) and hCNT3 (20) reveal that the site(s) of Na⁺ binding also reside approximately half way across the membrane.

Within the plane of the membrane, uridine-protectable Cys⁵⁶¹, the residue identified and characterized in the present study, is located at the interface between those residues sensitive to inhibition by PCMBS in H⁺-containing medium only and those where inhibition occurs in the presence of both Na⁺ and H⁺. Amongst other possibilities, the surface domain of hCNT3 TM 12 represented by residues Ile⁵⁵⁴, Tyr⁵⁵⁸ and Cys⁵⁶¹ may be masked to PCMBS in the H⁺-unbound state and upon H⁺-binding, movement of the helix occurs such that these residues now become accessible to the aqueous translocation pore. hCNT3, unlike hCNT1/2, has two cation binding sites, one of which is Na⁺-specific and the second of which may functionally interact with both H⁺ and Na⁺. Thus, hCNT3 Cys⁵⁶¹ likely senses conformational changes associated with H⁺-binding to the second of these sites.

hCNT3 presteady-state currents have components contributed by carrier-associated charge movements as well as by Na⁺ binding. PCMBS addition to Cys⁵⁶¹ will contribute a negative charge to the modified transporter. The total abolition of hCNT3 presteady-state currents that is seen following treatment with PCMBS is consistent with blockade of hCNT3 function by a mechanism involving loss of cation binding and locking of the transporter in a conformationally-restricted state.

In addition to the pore-lining residues present in TMs 7 and 8 of hCNT1 (11, Chapter 4, Appendix 4), the present study identifies a conformationally-sensitive pore-lining residue in TM 12 of hCNT3. A glutamate residue in hCNT1 and hCNT3 with a critical role in cation binding has also been identified within the conserved motif (G/A)XKX₃NEFVA(Y/M/F) of TM 11A (Appendix 4). In the 15 TM model of hCNT membrane architecture TMs 7/8 and 11A/12 are separated by a large and likely flexible cytoplasmic loop, evident in Fig. 7-1 as the 37 residue linker region between TMs 9 and 10. It is possible that this loop enables TMs 7/8 and 11A/12 to come together in the translocation pore in a manner that facilitates conformational transitions within the cation/nucleoside translocation cycle.

An emerging theme of recently solved high resolution molecular structures of cation-transporters such as LeuT_{Aa} (21) and Glt_{Ph} (22) is close-proximity integration

of cation/solute binding and transport within a common cation/permeant translocation pore. The present results for hCNT3 Cys⁵⁶¹ mirror this principle and reveal a residue centrally positioned within a mobile region of the cation/nucleoside translocation machinery. Further investigation of this conformationally-sensitive residue is likely to provide mechanistic and structural insights into differences between hCNT3 and hCNT1/2.

Table 7-1. Effects of PCMBS on uridine uptake in *Xenopus* oocytes expressing hCNT3C- and single-cysteine mutants. Influx of 10 μM ^3H -uridine was measured in both Na^+ - and H^+ -containing medium (100 mM NaCl, pH 8.5 or 100 mM ChCl, pH 5.5, respectively; 1 min; 20°C) following 10 min incubation on ice in the absence or presence of 200 μM PCMBS or 200 μM PCMBS + 20 mM uridine in media of the same composition (*i.e.* Na^+ - or H^+ -containing, as indicated). Values are corrected for basal non-mediated uptake in control water-injected oocytes and are presented as a percentage of mediated uridine influx in the absence of inhibitor for each individual mutant. Each value is the mean \pm SEM of 10 - 12 oocytes. nd, not determined because of low functional activity.

	Na^+ (100 mM NaCl, pH 8.5) ^a		H^+ (100 mM ChCl, pH 5.5) ^b	
	+ PCMBS	+ PCMBS and uridine	+ PCMBS	+ PCMBS and uridine
hCNT3C-	109 \pm 9	-	103 \pm 13	-
I554C(C-)	98 \pm 16	-	52 \pm 6	67 \pm 9
I555C(C-)	73 \pm 8	-	66 \pm 7	-
A556C(C-)	97 \pm 13	-	114 \pm 21	-
T557C(C-)	7 \pm 1	16 \pm 2	22 \pm 2	33 \pm 2
Y558C(C-)	92 \pm 15	-	19 \pm 3	71 \pm 11
A559C(C-)	106 \pm 13	-	117 \pm 14	-
L560C(C-)	101 \pm 14	-	106 \pm 14	-
S561C(C-)	102 \pm 19	-	54 \pm 5	94 \pm 8
G562C(C-)	104 \pm 17	-	92 \pm 18	-
F563C(C-)	nd	-	nd	-
A564C(C-)	110 \pm 31	-	88 \pm 13	-
N565C(C-)	37 \pm 5	109 \pm 8	46 \pm 9	106 \pm 16
I566C(C-)	85 \pm 19	-	71 \pm 6	-
G567C(C-)	17 \pm 4	97 \pm 19	14 \pm 5	94 \pm 15
S568C(C-)	nd	-	nd	-
L569C(C-)	112 \pm 17	-	113 \pm 12	-
G570C(C-)	107 \pm 15	-	93 \pm 12	-
I571C(C-)	44 \pm 8	85 \pm 9	30 \pm 3	90 \pm 8
V572C(C-)	89 \pm 11	-	104 \pm 9	-
I573C(C-)	92 \pm 11	-	109 \pm 15	-
G574C(C-)	92 \pm 23	-	95 \pm 16	-

^aValues for mediated uridine influx in 100 mM NaCl, pH 8.5 (pmol/oocyte.min⁻¹) in the absence of inhibitor are: hCNT3C- (1.5 ± 0.2); I554C(C-) (2.0 ± 0.3); I555C(C-) (1.9 ± 0.2); A556C(C-) (1.5 ± 0.3); T557C(C-) (2.7 ± 0.3); Y558C(C-) (0.11 ± 0.01); A559C(C-) (0.78 ± 0.05); L560C(C-) (2.1 ± 0.3); S561C(C-) (2.4 ± 0.4); G562C(C-) (0.75 ± 0.2); A564C(C-) (0.50 ± 0.1); N565C(C-) (2.6 ± 0.4); I566C(C-) (0.91 ± 0.2); G567C(C-) (1.4 ± 0.3); L569C(C-) (1.8 ± 0.3); G570C(C-) (1.1 ± 0.2); I571C(C-) (3.2 ± 0.4); V572C(C-) (3.3 ± 0.3); I573C(C-) (3.8 ± 0.5); G574C(C-) (0.18 ± 0.04).

^bValues for mediated uridine influx in 100 mM ChCl, pH 5.5 (pmol/oocyte.min⁻¹) in the absence of inhibitor are: hCNT3C- (1.5 ± 0.3); I554C(C-) (1.5 ± 0.2); I555C(C-) (2.1 ± 0.2); A556C(C-) (1.5 ± 0.1); T557C(C-) (1.9 ± 0.1); Y558C(C-) (0.50 ± 0.04); A559C(C-) (1.0 ± 0.1); L560C(C-) (2.1 ± 0.3); S561C(C-) (3.6 ± 0.2); G562C(C-) (0.51 ± 0.1); A564C(C-) (0.10 ± 0.01); N565C(C-) (0.79 ± 0.1); I566C(C-) (0.35 ± 0.1); G567C(C-) (0.9 ± 0.1); L569C(C-) (1.5 ± 0.2); G570C(C-) (0.69 ± 0.1); I571C(C-) (1.4 ± 0.1); V572C(C-) (2.0 ± 0.2); I573C(C-) (1.8 ± 0.2); G574C(C-) (0.13 ± 0.03).

hCNT1 MENDPSRRRESISLTPVAK - - - GLENMGADFLLESLEEGQLPRSDL
hCNT2 MEKASGR - - QSIALSTVET - - - GTVNPGLLEME - - KEVEPEGSKR
hCNT3 MELRSTAAAPRAEGYSNVGFQNEENFLENENTSGNNSIRSRAVQSREHTNT 50

hCNT1 SPAEIRSSWSEAAKPPFSRWRNLQPALRAR - - - - - SF CREHMQL
hCNT2 TDAQGHS LGDGLGPSTYQR - RSRWPFASKAR - - - - - SF CKTHASL
hCNT3 KQDEEQVTVEQDSPRNREHMEDDDEEMQKGCLEERRYDTVCGFCRKHKTT 100

TM1 **TM2**
hCNT1 FRWIGTGLLCTGLSAFLLVACLDFQRALALFVLTGVVLTFLGHRLLKRL
hCNT2 FKKILLGLLCLAYAAAYLLAACILNFQRALALFVITGLVIFVLVHVSFLKKL
hCNT3 LRHIIWGILLLAGYLVMVISA CVLNFHRALPLFVITVAAIFFVVDHLMK 150

TM3
hCNT1 LGPKLRRFLKPPQG - - HPRLLLWFKRGLALAAFLGLVLWLSLDTISQR - PEQ
hCNT2 LGKKLTRCLKPF - - NSRRLRWTKWVFAGVSLVGLILWLALDTAQR - PEQ
hCNT3 YEHRIDEMLS PGRLLNSHWFWLKWVIWSSLVLA VIFWLA FDTAKLGGQQ 200

TM4 **TM5**
hCNT1 LVSFAGICVFIALLFACSKHHC AVSWRAVSWGLGLQFVLGLLVIRT EPGF
hCNT2 LIPFAGICMFIILILFACSKHHS AVSWRTVFSGLGLQFVFGILVIRT D LGY
hCNT3 LVSFGGIMYI VLLFLFSKY PTRVYWRPVLWGIGLQFLLGLLILRT DPGF 250

TM5A **TM6**
hCNT1 IAFEWLGEQIRIFLSYTKAGSSSFVFG EALVKDVFQAFQVLP IIVFFS CVIS
hCNT2 TVFQWLGEQVQIFLNYTVAGSSSFVFG DTLVKDVFQAFQALP IIVFFG CVVS
hCNT3 IAFDWLGRQVQTFLEYTDAGASSFVFG EKYKDHFFAFKVLPIVVFSTVMS 300

TM7
hCNT1 VLYHVGLMQVWVILKIAWLMQVTMGTTA TETLSVAGNIFVVSQTEAPLLIRP
hCNT2 ILYYLVGLVQWV VQKVAWFLQITMGTTA TETLAVAGNIFVGMTEAPLLIRP
hCNT3 MLYYLVGLMQWIIRKVGWIMLVTTGSSP IESVVASGNIFVVGQTESPLLVRP 350

TM8 **TM9**
hCNT1 YLADMTLSEVHVVM TGGYATIAGSLLGAYISFGIDATSLIAASVMAAPCA
hCNT2 YLGDMT LSEIHAVMTGGFATISGTVLGAFI AFGVDASSLISASVMAAPCA
hCNT3 YLPYITKSE LHAIMTAGFSTIAGSVLGAYISFGVPS SHLLTASVMSAPAS 400

hCNT1 LALS KLVYPEVEESKFRREEGVKLTYGDAQNLIEAASTGAAISVKVVANI
hCNT2 LASSKLAYPEVEESKFKSEEGVKLPRGKERNVLEAASNGAVDAIGLATNV
hCNT3 LAAAKLFWPETEKPKITLKNAMKMESGDSGNLLEAATQGASSISLVANI 450

TM10 **TM11**
hCNT1 AANLIAFLAVLDFINA ALSWLGDMVDIQGLSFQLICSYILRPVAFMLMGVA
hCNT2 AANLIAFLAVLAFINA ALSWLGELVDIQGLTFQVICSYLLRPMVFM MGVE
hCNT3 AVNLIAFLALLSFMNS ALSWFGNMFDPQLSFELICSYIFMPFSFMMGVE 500

TM11A
hCNT1 WEDCPVVAELLGIKLFLNEFVAYQDLSKYKQRRLAGAEWVGNRKQWISV
hCNT2 WTDGPMVAEMVGIKFFINEFVAYQQLSIQYKNKRLSGMEEWIEGKQWISV
hCNT3 WQDSFMVARLLIGYKTFEFNEFVAYEHL SKWIHLRKEGGPKFVNGVQQYISI 550

TM12
hCNT1 RAEVLTTFALCGFANFSSIGIMLGLTSMVPQRKSDFSQIVLRALFTGAC
hCNT2 RAEIITTFSLCGFANLSSIGITLGLT SIVPHRKS DLSKVVVRALFTGAC
hCNT3 RSELIATYALCGFANIGSLGIVIGLTSMAPSRKRDIASGAVRALIAGTV 600

TM13
hCNT1 VSLVNA CMAGILYMPRGA EVDMSLLN - - - - T LSSSSSFEIYQCCREAFQ
hCNT2 VSLISA CMAGILYVPRGA EADCVSFPN - - - - TSFTNRTYETMCCRGLFQ
hCNT3 ACFMTACIAGILSSTP - VDINGHHVLENAFNSTFPNGTTKVIA C C Q S L L S 649

hCNT1 S - - - - VNP - - - - - EFSPEALDNCCRFYNHTICAQ - - - - -
hCNT2 STSLNGTNPPSFSGPWEDKEFSAMALTNCCGFYNNTVCA - - - - -
hCNT3 STVAKGPPGEVIPGG - - - - - N H S L Y S L K G C C T L L N P S T F N C N G I S N T F 691

Figure 7-1.

Figure 7-1. Cysteine residues in hCNT1, hCNT2 and hCNT3. An alignment of the amino acid sequences of hCNT1, hCNT2 and hCNT3 (GenBank™ accession numbers AAB53839, AAB88539 and AAG22551, respectively). The positions of 13 putative TMs are indicated by *solid* boxes. Two additional TMs present in an alternative 15 TM model of hCNT membrane architecture are indicated by *dashed* boxes. Cysteine residues are shown on *black* squares. Numbers refer to hCNT3 residue positions.

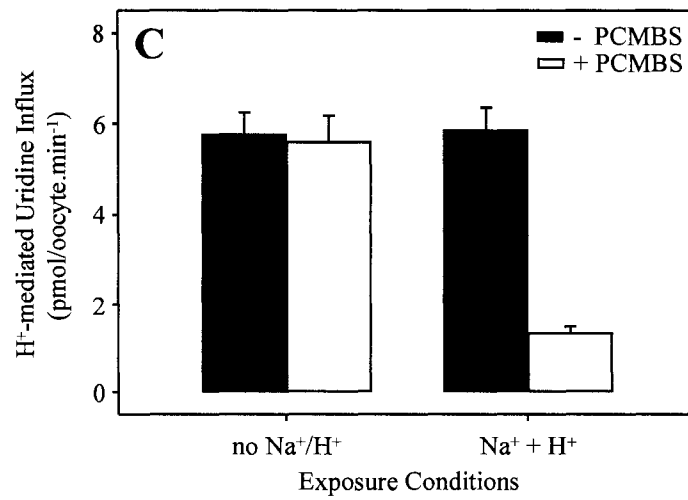
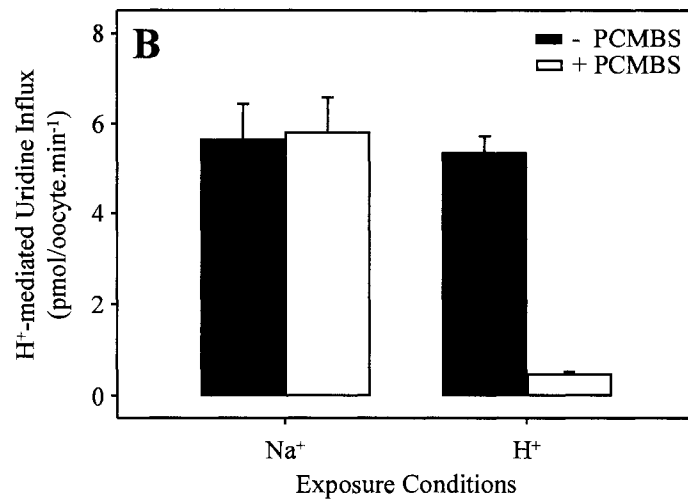
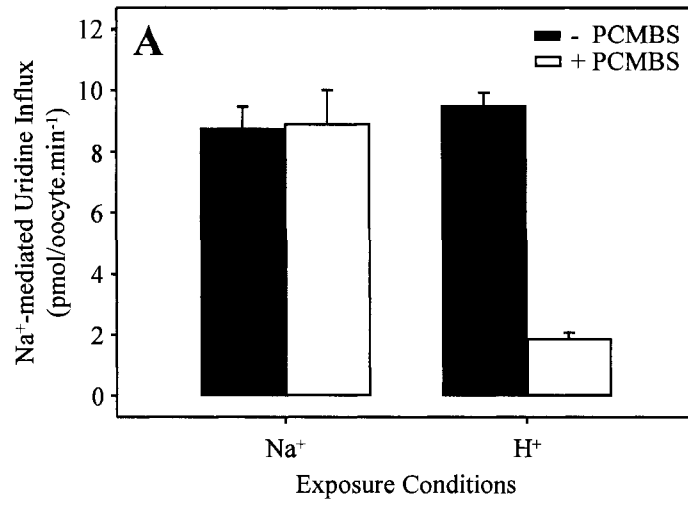


Figure 7-2.

Figure 7-2. PCMBS inhibition of hCNT3. hCNT3-mediated influx of 20 μM ^{14}C -uridine in Na^+ -containing (A) or H^+ -containing (B, C) medium (100 mM NaCl, pH 8.5 or 100 mM ChCl, pH 5.5, respectively; 1 min at 20°C) was measured following 10 min incubation on ice in the absence (*solid* bars) or presence (*open* bars) of 500 μM PCMBS in the following media: Na^+ -containing H^+ -reduced (100 mM NaCl, pH 8.5), acidified Na^+ -free (100 mM ChCl, pH 5.5), Na^+ -free H^+ -reduced (100 mM ChCl, pH 8.5) or acidified Na^+ -containing (100 mM NaCl, pH 5.5), as indicated by the x-axis labels Na^+ , H^+ , no Na^+/H^+ or $\text{Na}^+ + \text{H}^+$, respectively. Values are corrected for basal non-mediated uptake in control water-injected oocytes and are means \pm SEM of 10 - 12 oocytes.

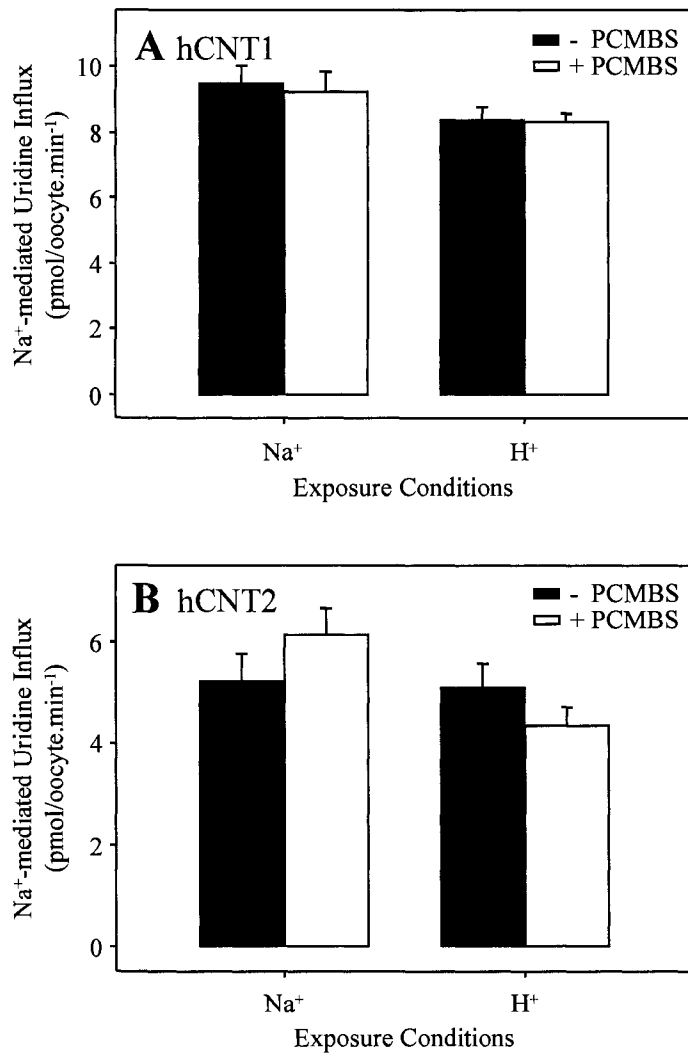


Figure 7-3. PCMBs insensitivity of hCNT1 and hCNT2. Influx of 20 μM ^{14}C -uridine in the presence of Na^+ (100 mM NaCl, pH 7.5; 1 min at 20°C) was measured in oocytes producing hCNT1 (A) or hCNT2 (B) following 10 min incubation on ice in the absence (solid bars) or presence (open bars) of 500 μM PCMBs in media containing either Na^+ , but not H^+ (100 mM NaCl, pH 8.5) or H^+ , but not Na^+ (100 mM ChCl, pH 5.5), as indicated. Values are corrected for basal non-mediated uptake in control water-injected oocytes and are means \pm SEM of 10 - 12 oocytes.

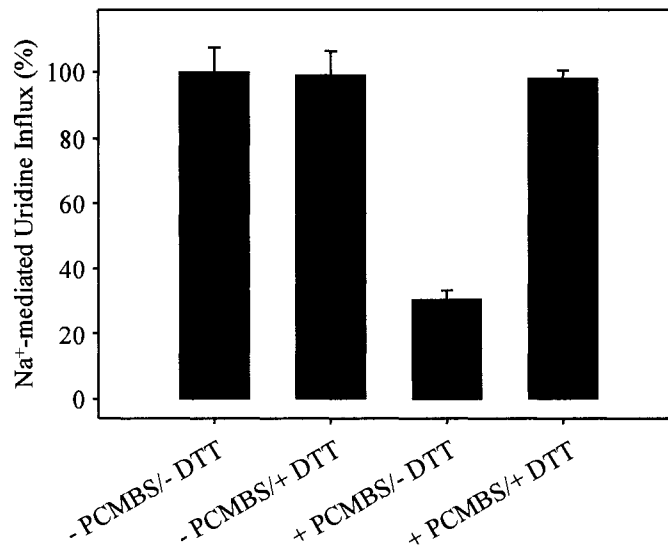


Figure 7-4. Reversal of PCMBS inhibition of hCNT3-mediated uridine uptake by DTT. hCNT3-expressing oocytes were incubated in the absence or presence of 500 μ M PCMBS (100 mM ChCl, pH 5.5; 10 min on ice) followed by a second incubation in the absence or presence of 5 mM DTT (100 mM ChCl, pH 7.5; 1 min at 20°C) prior to measuring uptake of 20 μ M ¹⁴C-uridine in Na⁺-containing transport medium (100 mM NaCl, pH 7.5; 1 min at 20°C). Data are presented as mediated transport, calculated as uptake in RNA-injected oocytes *minus* uptake in water-injected oocytes, and are normalized to the respective influx of uridine in the absence of PCMBS and DTT (12.8 ± 1.0 pmol/oocyte.min⁻¹). Each value is the mean \pm SEM of 10 - 12 oocytes.

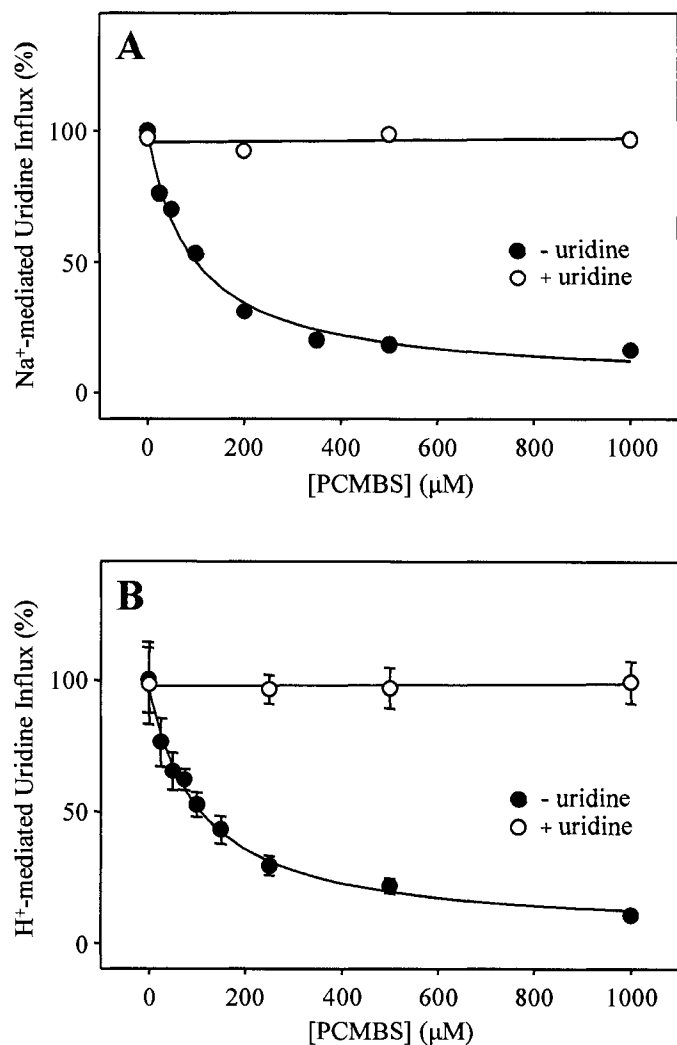


Figure 7-5. PCMBBS inhibition of hCNT3: concentration dependence and uridine protection. Influx of 20 μM ^{14}C -uridine in both Na^+ - and H^+ -containing media (A and B, respectively) was measured after hCNT3-producing oocytes were incubated with various concentrations of PCMBBS under acidic conditions either in the absence (*solid* circles) or in the presence (*open* circles) of 20 mM extracellular uridine as described in Fig. 7-2. Data are presented as mediated transport, calculated as uptake in RNA-injected oocytes *minus* uptake in water-injected oocytes, and are normalized to the respective influx of uridine in the absence of inhibitor (8.7 ± 0.5 (A) and 5.3 ± 0.7 (B) pmol/oocyte.min⁻¹). Each value is the mean \pm SEM of 10 - 12 oocytes. Error bars are not shown where values were smaller than that represented by the symbols.

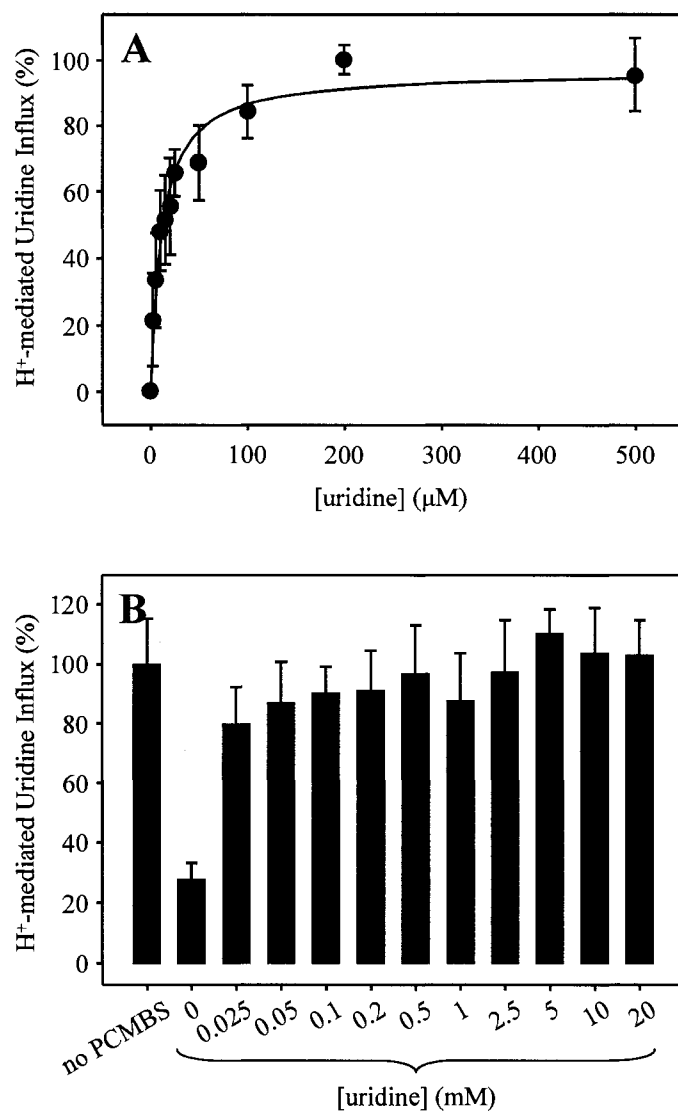


Figure 7-6. PCMBMS inhibition of hCNT3: concentration dependence of uridine protection. Influx of 20 μM ^3H -uridine in H^+ -containing medium was measured in oocytes producing hCNT3 following incubation with 500 μM PCMBMS under acidic conditions in the presence of 0 - 500 μM (A) or 0 - 20 mM (B) extracellular uridine as described in Fig. 7-2. Data are presented as mediated transport, calculated as uptake in RNA-injected oocytes *minus* uptake in water-injected oocytes, and are normalized to the respective influx of uridine in the absence of inhibitor (8.3 ± 1.3 (A) and 7.3 ± 0.6 (B) pmol/oocyte.min⁻¹). Each value is the mean \pm SEM of 10 - 12 oocytes. Error bars are not shown where values were smaller than that represented by the symbols (A).

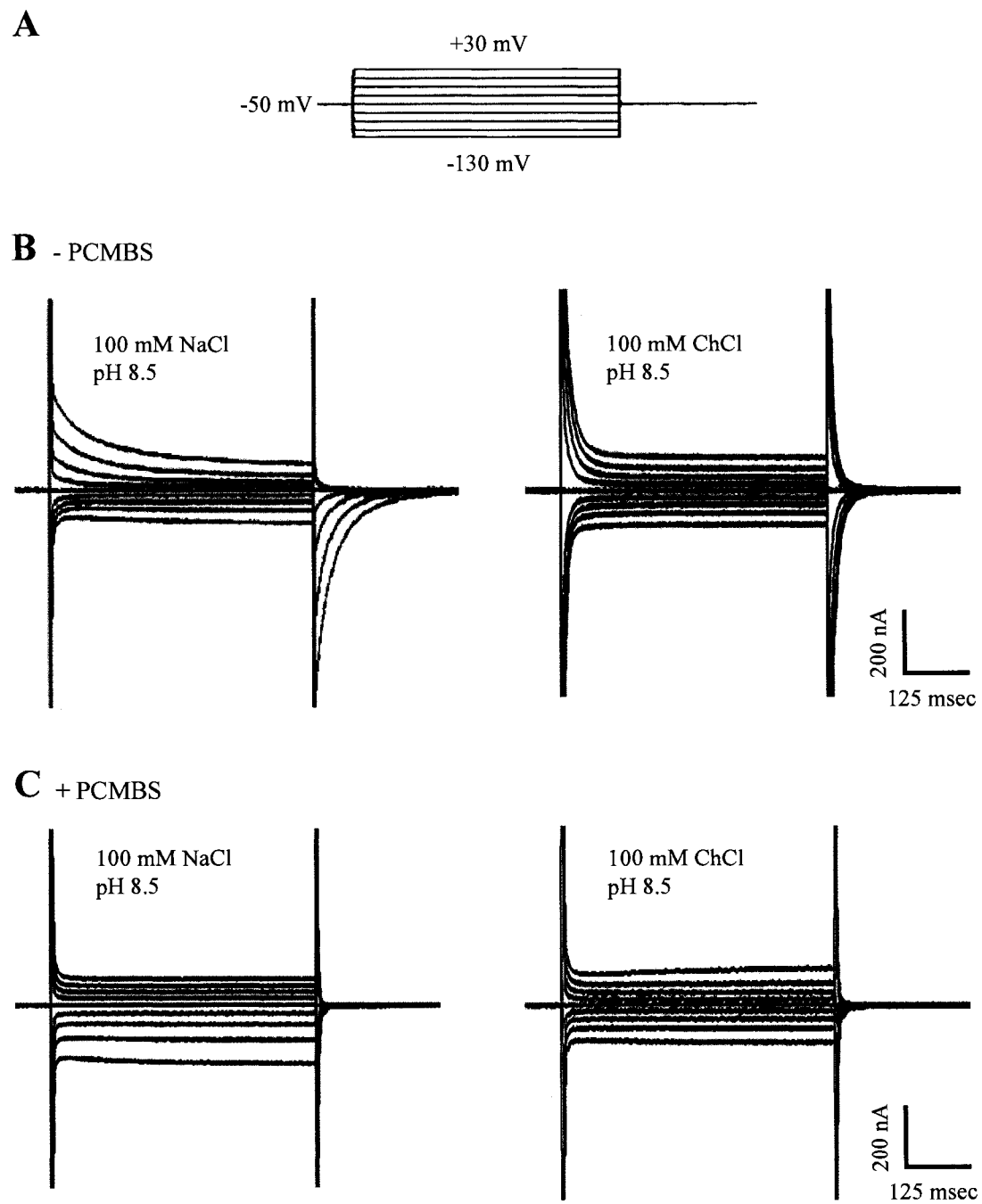


Figure 7-7.

Figure 7-7. Time courses of presteady-state currents measured in a hCNT3-expressing oocyte elicited by voltage pulses before and after treatment with PCMBS. (A) Voltage pulse protocol: the oocyte membrane was held at a holding potential (V_h) of -50 mV and stepped to a range of test potentials (V_t). Shown are V_t from -130 to +30 mV (20 mV increments). (B) Representative total membrane current records. A hCNT3-producing oocyte displays slow current relaxations in the presence (100 mM NaCl, pH 8.5; *left* current record) and absence (100 mM ChCl, pH 8.5; *right* current record) of Na^+ in response to voltage pulses prior to incubation with PCMBS (-PCMBS). (C) Presteady-state currents were measured in the same hCNT3-expressing oocyte following incubation with PCMBS (500 μM ; 10 min). Currents were measured in the presence (100 mM NaCl, pH 8.5; *left* current record) and absence (100 mM ChCl, pH 8.5; *right* current record) of Na^+ .

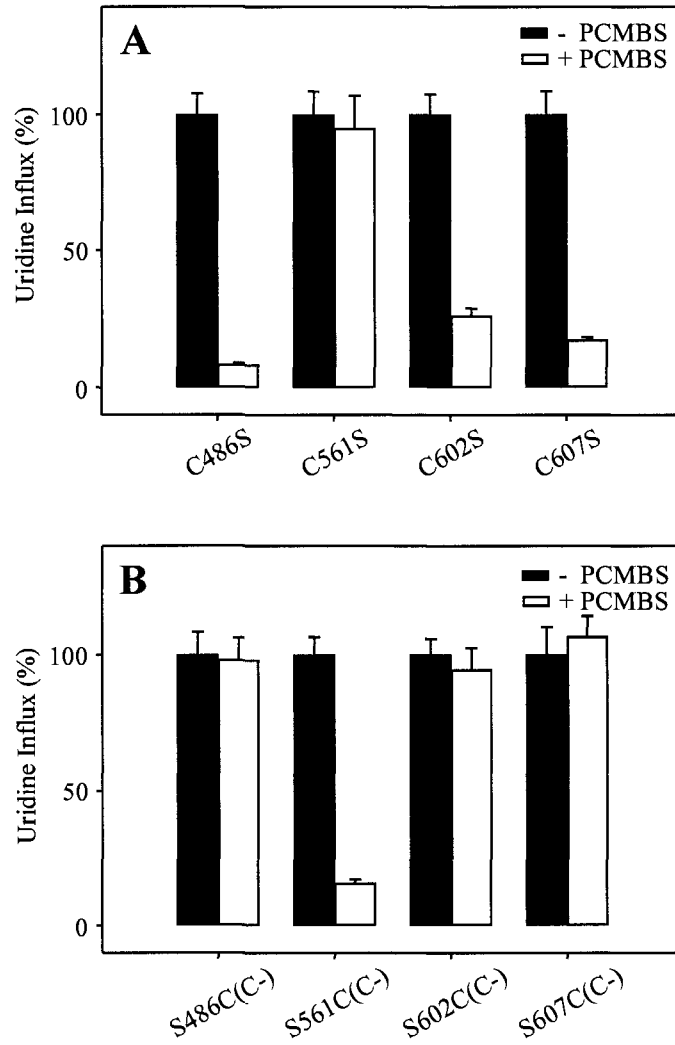


Figure 7-8.

Figure 7-8. Effects of PCMBS on hCNT3 and hCNT3C- mutants. Influx of 20 μM ^{14}C -uridine in H^+ -containing medium was measured after oocytes producing hCNT3 mutants C486S, C561S, C602S and C607S (A) and hCNT3C- mutants S486C(C-), S561C(C-), S602C(C-) and S607C(C-) (B) were incubated with or without 500 μM PCMBS (*open* and *solid* bars, respectively) under acidic conditions as described for wild-type hCNT3 in Fig. 7-2. Data are presented as mediated transport, calculated as uptake in RNA-injected oocytes *minus* uptake in water-injected oocytes, and are normalized to the respective values of mediated uridine influx in the absence of inhibitor (7.4 ± 0.6 , 3.7 ± 0.3 , 7.2 ± 0.5 and 6.7 ± 0.6 $\text{pmol/oocyte}\cdot\text{min}^{-1}$ for hCNT3 mutants C486S, C561S, C602S and C607S, respectively, and 5.1 ± 0.4 , 7.9 ± 0.5 , 4.2 ± 0.2 and 6.3 ± 0.6 $\text{pmol/oocyte}\cdot\text{min}^{-1}$ for hCNT3C- mutants S486C(C-), S561C(C-), S602C(C-) and S607C(C-), respectively). Each value is the mean \pm SEM of 10 - 12 oocytes.

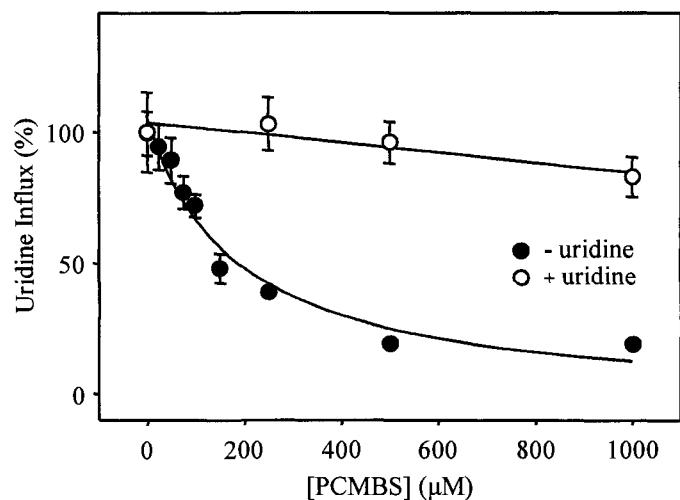


Figure 7-9. PCMBS inhibition of hCNT3C- mutant S561C(C-): concentration dependence and uridine protection. Influx of 20 μM ^{14}C -uridine in H^+ -containing medium was measured after S561C(C-)-producing oocytes were incubated with various concentrations of PCMBS under acidic conditions either in the absence (*solid circles*) or in the presence (*open circles*) of 20 mM extracellular uridine as described in Fig. 7-2. Data are presented as mediated transport, calculated as uptake in RNA-injected oocytes *minus* uptake in water-injected oocytes, and are normalized to the influx of uridine in the absence of inhibitor ($7.5 \pm 1.1 \text{ pmol/oocyte}\cdot\text{min}^{-1}$). Each value is the mean \pm SEM of 10 - 12 oocytes. Error bars are not shown where values were smaller than that represented by the symbols.

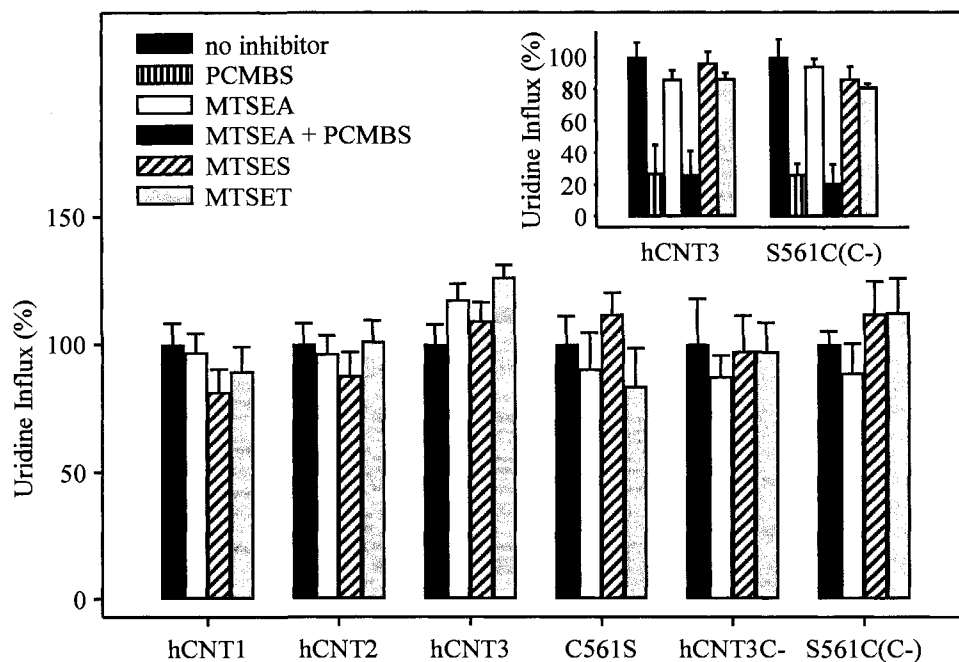
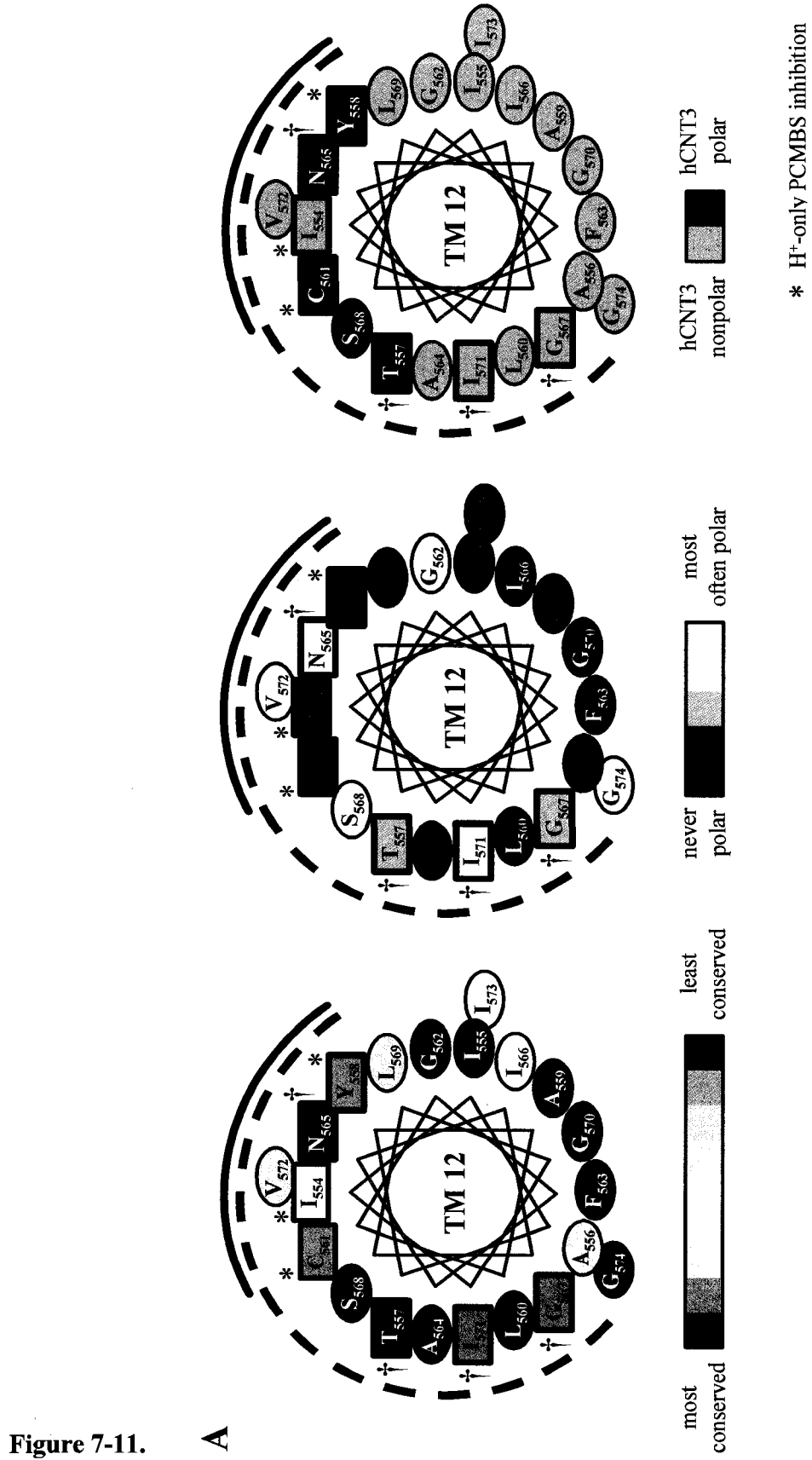


Figure 7-10. Effects of MTS reagents on hCNT1, hCNT2, hCNT3 and mutants. Oocytes producing hCNT1, hCNT2, hCNT3, C561S, hCNT3C- or S561C(C-) were incubated under acidic conditions in the absence of inhibitor or in the presence of 500 μ M PCMB5 (*inset* only), 2.5 mM MTSEA, 2.5 mM MTSEA followed by 500 μ M PCMB5 (*inset* only), 10 mM MTSES or 1 mM MTSET. Following incubation, 20 μ M 3 H-uridine influx was measured in the presence of 100 mM NaCl, pH 7.5 (hCNT1 and hCNT2) or 100 mM ChCl, pH 5.5 (hCNT3, C561S, hCNT3C- and S561C(C-)) as described in Fig. 7-2. Data are presented as mediated transport, calculated as uptake in RNA-injected oocytes minus uptake in water-injected oocytes, and are normalized to the influx of uridine in the absence of inhibitor (7.0 ± 0.6 , 6.5 ± 0.5 , 6.6 ± 0.5 , 3.6 ± 0.4 , 1.0 ± 0.2 and 4.1 ± 0.2 pmol/oocyte.min $^{-1}$ for hCNT1, hCNT2, hCNT3, C561S, hCNT3C- and S561C(C-), respectively (large panel), and 8.2 ± 0.8 and 7.0 ± 0.8 pmol/oocyte.min $^{-1}$ for hCNT3 and S561C(C-), respectively (*inset*). Each value is the mean \pm SEM of 10 - 12 oocytes.



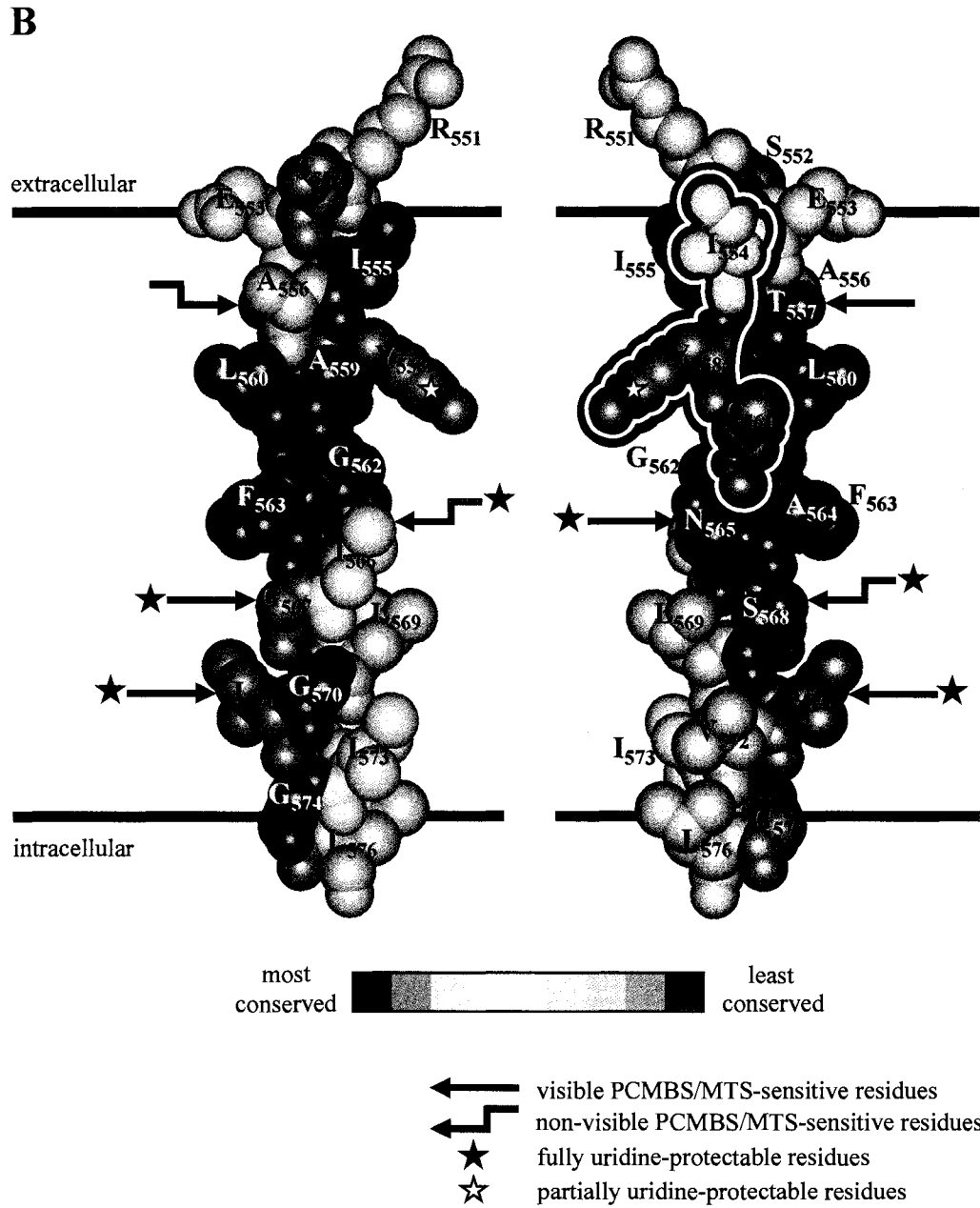


Figure 7-11.

Figure 7-11. Molecular modeling of hCNT3 TM 12. Analysis of residue conservation in the region corresponding to residues 551 - 576 of hCNT3 and its homologs was performed by the ConSeq method (23) on the aligned sequences of 126 eukaryote and prokaryote CNT family members. Fig. 7-11A presents three identical α -helical wheel projections of hCNT3 TM 12 viewed from the extracellular side of the membrane and coloured either to indicate degrees of residue conservation (*left*), polarity based on analysis of the multiple sequence alignment (*middle*) or polarity of hCNT3 residues (*right*). Residue positions in hCNT3 sensitive to inhibition by PCMBs are *boxed*. Those reactive with PCMBs in H⁺-containing medium only are indicated by an *asterisk* (*). Four residue positions previously shown to be reactive towards MTS reagents (10) are indicated by a *sword* symbol (†). The same four residues are also characterized by PCMBs inhibition in the presence of both Na⁺ and H⁺. Fig. 7-11B shows corresponding views of an α -helical space-filling model of the region. The view on the *left* differs from that on the *right* by a 180° rotation. To permit comparison with the left-hand helical wheel projection in Fig. 7-11A, the views are coloured to indicate degrees of residue conservation. The conformationally mobile cluster of three residues specifically reactive with PCMBs only in H⁺-containing medium are outlined in the schematic on the *right*. Other PCMBs/MTS-sensitive residues are indicated by *black straight arrows* where visible or *grey elbow arrows* where present on the non-visible, opposite face of the helix. PCMBs/MTS-sensitive positions that are fully and partially uridine-protected and therefore likely to be within or closely adjacent to the nucleoside binding pocket are indicated by *black* and *white stars*, respectively.

Bibliography

1. Ritzel, M. W. L., Yao, S. Y. M., Huang, M. Y., Elliott, J. F., Cass, C. E., and Young, J. D. (1997) Molecular cloning and functional expression of cDNAs encoding a human Na⁺-nucleoside cotransporter (hCNT1). *Am. J. Physiol.* **272**: C707-C714.
2. Ritzel, M. W. L., Yao, S. Y. M., Ng, A. M. L., Mackey, J. R., Cass, C. E., and Young, J. D. (1998) Molecular cloning, functional expression and chromosomal localization of a cDNA encoding a human Na⁺/nucleoside cotransporter (hCNT2) selective for purine nucleosides and uridine. *Mol. Membr. Biol.* **15**: 203-211.
3. Ritzel, M. W. L., Ng, A. M. L., Yao, S. Y. M., Graham, K., Loewen, S. K., Smith, K. M., Ritzel, R. G., Mowles, D. A., Carpenter, P., Chen, X.-Z., Karpinski, E., Hyde, R. J., Baldwin, S. A., Cass, C. E., and Young, J. D. (2001) Molecular identification and characterization of novel human and mouse concentrative Na⁺-nucleoside cotransporter proteins (hCNT3 and mCNT3) broadly selective for purine and pyrimidine nucleosides (system *cib*). *J. Biol. Chem.* **276**: 2914-2927.
4. Smith, K. M., Ng, A. M. L., Yao, S. Y. M., Labeledz, K. A., Knaus, E. E., Wiebe, L. I., Cass, C. E., Baldwin, S. A., Chen, X.-Z., Karpinski, E., and Young, J. D. (2004) Electrophysiological characterization of a recombinant human Na⁺-coupled nucleoside transporter (hCNT1) produced in *Xenopus* oocytes. *J. Physiol.* **558**: 807-823.
5. Yao, S. Y. M., Sundaram, M., Chomey, E. G., Cass, C. E., Baldwin, S. A., and Young, J. D. (2001) Identification of Cys₁₄₀ in helix 4 as an exofacial cysteine residue within the substrate-translocation channel of rat equilibrative nitrobenzylthionosine (NBMPR)-insensitive (ENT2) nucleoside transporter rENT2. *Biochem. J.* **353**: 387-393.
6. Rothstein, A. (1970) Sulfhydryl groups in membrane structure and function. In *Current Topics in Membranes and Transport*, **1** (Bronner, F., and Kleinzeller, A., eds.) pp 135-176, Academic Press Inc., New York.
7. Hu, H., Endres, C. J., Chang, C., Umapathy, N. S., Lee, E.-W., Fei, Y.-J., Itagaki, S., Swaan, P. W., Ganapathy, V., and Unadkat, J. D. (2006) Electrophysiological characterization and modeling of the structure activity relationship of the human concentrative nucleoside transporter 3 (hCNT3). *Mol. Pharmacol.* **69**: 1542-1553.

8. Hamilton, S. R., Yao, S. Y. M., Ingram, J. C., Hadden, D. A., Ritzel, M. W. L., Gallagher, M. P., Henderson, P. J. F., Cass, C. E., Young, J. D., and Baldwin, S. A. (2001) Subcellular distribution and membrane topology of the mammalian concentrative nucleoside transporter rCNT1. *J. Biol. Chem.* **276**: 27981-27988.
9. Yao, S. Y. M., Ng, A. M. L., Loewen, S. K., Cass, C. E., Baldwin, S. A., and Young, J. D. (2002) An ancient prevertebrate Na⁺-nucleoside cotransporter (hfCNT) from the Pacific hagfish (*Eptatretus stouti*). *Am. J. Physiol. Cell Physiol.* **283**: C155-C168.
10. Zhang, J., Tackaberry, T., Ritzel, M. W., Raborn, T., Barron, G., Baldwin, S. A., Young, J. D., and Cass, C. E. (2006) Cysteine-accessibility analysis of transmembrane domains 11-13 of human concentrative nucleoside transporter 3. *Biochem. J.* **394**: 389-398.
11. Loewen, S. K., Ng, A. M. L., Yao, S. Y. M., Cass, C. E., Baldwin, S. A., and Young, J. D. (1999) Identification of amino acid residues responsible for the pyrimidine and purine nucleoside specificities of human concentrative Na⁺ nucleoside cotransporters hCNT1 and hCNT2. *J. Biol. Chem.* **274**: 24475-24484.
12. Yan, R. T., and Maloney, P. C. (1993) Identification of a residue in the translocation pathway of a membrane carrier. *Cell* **75**: 37-44.
13. Yan, R. T., and Maloney, P. C. (1995) Residues in the pathway through a membrane transporter. *Proc. Natl. Acad. Sci. U.S.A.* **92**: 5973-5976.
14. Akabas, M. H., Stauffer, D. A., Xu, M., and Karlin, A. (1992) Acetylcholine receptor channel structure probed in cysteine-substitution mutants. *Science* **258**: 307-310.
15. Stauffer, D. A., and Karlin, A. (1994) Electrostatic potential of the acetylcholine binding sites in the nicotinic receptor probed by reactions of binding-site cysteines with charged methanethiosulfonates. *Biochemistry* **33**: 6840-6849.
16. Williams, D. B., and Akabas, M. H. (1999) γ -Aminobutyric acid increases the water accessibility of M3 membrane-spanning segment residues in γ -aminobutyric acid type A receptors. *Biophys. J.* **77**: 2563-2574.

17. Krupta, R. M. (1993) Coupling mechanisms in active transport. *Biochim. Biophys. Acta* **1183**: 105-113.
18. Krupta, R. M. (1994) Interpreting the effects of site-directed mutagenesis on active transport systems. *Biochim. Biophys. Acta*. **1193**: 165-178.
19. Mulinta, R., Ng, A. M. L., Yao, S. Y. M., Slugoski, M. D., Smith, K. M., Cass, C. E., Baldwin, S. A., and Young, J. D. (2008) Substituted cysteine accessibility method analysis of transmembrane domains 7 and 8 of human concentrative nucleoside transporter 3 (hCNT3) reveal novel discontinuous regions within helices. *J. Biol. Chem.* (submission pending).
20. Smith, K. M., Cass, C. E., Baldwin, S. A., Karpinski, E., and Young, J. D. (2008) Presteady-state currents of human concentrative nucleoside transporter 3 (hCNT3). *J. Physiol.* (submission pending).
21. Yamashita, A., Singh, S. K., Kawate, T., Jin, Y., and Gouaux, E. (2005) Crystal structure of a bacterial homologue of Na⁺/Cl⁻-dependent neurotransmitter transporter. *Nature* **437**: 215-223.
22. Boudker, O., Ryan, R. M., Yernool, D., Shimamoto, K., and Gouaux, E. (2007) Coupling substrate and ion binding to extracellular gate of a sodium-dependent aspartate transporter. *Nature* **445**: 387-393.
23. Berezin, C., Glaser, F., Rosenberg, J., Paz, I., Pupko, T., Fariselli, P., Casadio, R., and Ben-Tal, N. (1994) ConSeq: the identification of functionally and structurally important residues in protein sequences. *Bioinformatics* **20**: 1322-1324.

Chapter 8:

A Conformationally Mobile Cysteine Residue (Cys⁵⁶¹) Modulates Na⁺ - and H⁺-Activation of Human Concentrative Nucleoside Transporter 3 (hCNT3)*

* A version of this chapter has been published.

Slugoski, M. D., Smith, K. M., Mulinta, R., Ng, A. M. L., Yao, S. Y. M., Morrison, E. L., Lee, Q. O. T., Zhang, J., Karpinski, E., Cass, C. E., Baldwin, S. A., and Young, J. D. (2008) A conformationally mobile cysteine residue (C561) modulates Na⁺ - and H⁺-activation of human concentrative nucleoside transporter 3 (hCNT3). *J. Biol. Chem.* (accepted, pending final editorial review).

Acknowledgements

Dr. Kyla M. Smith assisted with the electrophysiology experiments. Ms. Ras Mulinta provided the Na⁺-activation curves of the aglyco mutants. Mrs. Amy M. L. Ng constructed the mutants and, together with Dr. Sylvia Y. M. Yao completed the Na⁺-activation curves of hCNT1 and the hCNT1 mutant. Ms. Ellen L. Morrison and Ms. Queenie O. T. Lee were involved with the characterization of the Cys⁵⁶¹ mutants. Dr. Jing Zhang constructed the hCNT3C- construct for use in yeast experiments. Drs. Edward Karpinski, Carol E. Cass and Stephen A. Baldwin are collaborative principal investigators who assisted with research funding and manuscript preparation. This research was funded by the National Cancer Institute of Canada with funds from the Canadian Cancer Society and Alberta Cancer Board.

Introduction

In the absence of a crystal structure, molecular strategies employing substituted cysteine accessibility method (SCAM) analysis provides a powerful approach to systematically investigate membrane protein architecture and structure/function relationships (1). Pioneered by studies of *E. coli* LacY lactose permease (2), human transporters investigated by this methodology include the equilibrative glucose transporter GLUT1 (3, 4), the Cl⁻/HCO₃⁻ exchanger AE1 (5-7), the Na⁺/H⁺ exchanger NHE1 (8) and, most recently, human nucleoside transporter hCNT3 (9, Chapter 7).

To avoid confounding background reactivity with endogenous cysteine residues, SCAM analysis requires construction of a functional cysteine-less version of the transporter to serve as a template for subsequent cysteine reinsertion at defined positions. In the case of hCNT3, the protein was engineered by mutation of all 14 endogenous cysteine residues to serine, resulting in the cysteine-less construct hCNT3C- (9). Expressed in yeast, hCNT3C- was used to assess residues in TMs 11-13 for accessibility to methanethiosulfonate (MTS) reagents (9). More recently, hCNT3C-, expressed in *Xenopus laevis* oocytes, was used to identify a H⁺-mediated conformational shift that allows access of *p*-chloromercuribenzenesulfonate (PCMBS) to specific residues in TM 12 under acidified conditions (Chapter 7). One of these conformationally mobile amino acids, native cysteine residue 561, was fully protected against PCMBS inhibition by micromolar concentrations of extracellular uridine, suggesting likely proximity to the nucleoside binding pocket. In the present study, heterologous expression in *Xenopus* oocytes, cell-surface biotinylation and site-directed mutagenesis were used in combination with radioisotope flux and presteady- and steady-state electrophysiological kinetic experiments to undertake an in depth functional comparison between wild-type and cysteine-less hCNT3. The present investigation, which validates hCNT3C- as a template for SCAM analyses of CNTs, reveals that Cys⁵⁶¹ modulates Na⁺- as well as H⁺-coupled modes of hCNT3 nucleoside transport.

Results

As depicted in Fig. 8-1, hCNT3 contains 14 endogenous cysteine residues. Nine of these are located within either the extramembraneous N-terminal (Cys⁸², Cys⁹¹ and Cys⁹⁴) or C-terminal (Cys⁶²¹, Cys⁶⁴³, Cys⁶⁴⁴, Cys⁶⁷³, Cys⁶⁷⁴ and Cys⁶⁸⁴) regions of the transporter. Five are positioned in predicted TMs (Cys¹²¹ in TM 1, Cys⁴⁸⁶ in TM 11, Cys⁵⁶¹ in TM 12, and Cys⁶⁰² and Cys⁶⁰⁷ in TM 13). To enable transmembrane protein topology mapping and structure/function analysis of hCNT3 by SCAM, all 14 cysteine residues of hCNT3 were mutated to serine. The resulting cysteine-less version of hCNT3 (hCNT3C-) was capable of Na⁺-dependent nucleoside transport when produced in yeast and has been used as template in an initial series of SCAM analyses of hCNT3 TMs 11 - 13 (9, Chapter 7). The current work extended these studies by using the dual radioisotope flux and electrophysiological capabilities of the *Xenopus* oocyte heterologous expression system to undertake a detailed functional characterization of hCNT3C-.

Time course of radiolabeled uridine uptake by oocytes producing hCNT3C- – Fig. 8-2 depicts time courses for uptake of 10 μM ¹⁴C-labeled uridine in Na⁺-containing transport medium (100 mM NaCl, pH 7.5) by control water-injected oocytes and oocytes producing recombinant hCNT3C-. Uridine uptake by hCNT3C- was rapid and approximately linear with time for the first 3 min. Transport was also concentrative with the 10 min uptake value exceeding the initial extracellular uridine concentration by ~ 2.5-fold, assuming an intracellular water volume of 1 μl (10, 11). Only basal uptake of uridine was evident in control water-injected oocytes under the same conditions. In all subsequent experiments, an uptake interval of 1 min was used to determine initial rates of transport.

hCNT3C- nucleoside selectivity and cation dependence – The experiment of Fig. 8-3A investigated the ability of hCNT3C- to transport a panel of radiolabeled physiological pyrimidine and purine nucleosides. Since wild-type hCNT3 is both Na⁺- and H⁺-coupled (12, Chapters 5 and 6) and since Na⁺- and H⁺-coupled hCNT3 exhibit different nucleoside selectivity profiles (Chapter 5), the experiment was performed both

in the presence of Na^+ and H^+ (100 mM NaCl, pH 7.5 and 100 mM ChCl, pH 5.5, respectively). The flux values shown in this and subsequent experiments depict mediated transport activity, defined as the difference in uptake between RNA transcript-injected and control water-injected oocytes. Nucleoside uptake in water-injected oocytes was $< 0.1 \text{ pmol/oocyte.min}^{-1}$ under all conditions tested (data not shown).

Similar to wild-type hCNT3 (12, Chapter 5), hCNT3C- in Na^+ -containing medium transported uridine, adenosine, thymidine, cytidine, guanosine and inosine at equivalent rates (4.8 - 7.0 $\text{pmol/oocyte.min}^{-1}$). Also similar to the wild-type protein (Chapter 5), this broad selectivity profile was markedly altered in H^+ -containing medium (uridine \gg adenosine, thymidine $>$ cytidine $>$ guanosine, inosine) with only uridine showing similar rates of transport in the two media. The different nucleoside selectivity profiles of Na^+ - and H^+ -coupled hCNT3 and hCNT3C- suggest that Na^+ - and H^+ -bound versions of the transporters have significantly different conformations of the nucleoside binding pocket and/or translocation channel (Chapter 5). Only the H^+ -coupled form of hCNT3 is susceptible to inhibition by the hydrophilic thiol-reactive agent PCMBBS (Chapter 7).

Fig. 8-3B compares the cation-dependence of hCNT3 and hCNT3C- influx of 10 μM ^{14}C -labeled uridine in the presence of Na^+ and/or H^+ (100 mM NaCl or ChCl, pH 7.5 or 5.5, as indicated). Like hCNT3, hCNT3C- displayed high levels of uridine uptake in the presence of Na^+ (NaCl, pH 7.5), H^+ (ChCl, pH 5.5) and both Na^+ and H^+ (NaCl, pH 5.5). Relative to hCNT3, hCNT3C- exhibited an equivalent rate of uridine transport in the presence of H^+ (ChCl, pH 5.5), but did not show the wild-type increase in uridine influx in the presence of Na^+ (NaCl, pH 7.5) or Na^+ plus H^+ (NaCl, pH 5.5). As a result, the ratio of uridine influx in the presence of Na^+ (NaCl, pH 7.5) to that in the presence of H^+ (ChCl, pH 5.5) decreased from 1.60 for wild-type protein to 0.98 for hCNT3C-. These uridine uptake ratios are in good agreement with that reported previously for hCNT3 (Chapter 5) and with the other results for hCNT3C- shown in Fig. 8-3A. The residual uridine fluxes evident in the absence of Na^+ and at a low H^+ concentration (ChCl, pH 7.5) can be attributed to the small, but significant amount of H^+ -activation that occurs under these conditions (Chapter 5).

Cell-surface expression and glycosylation of hCNT3C- – The equivalent levels of transport activity shown in Fig. 8-3B suggest that hCNT3 and hCNT3C- were present in oocyte plasma membranes in similar quantities. This was investigated directly by cell-surface labeling with sulfo-NHS-LC-biotin using immobilized streptavidin resin to separate cell-surface protein (Fig. 8-4A) from that associated with total (plasma + intracellular) membranes (Fig. 8-4B). Immunoblots of the fractions were probed with hCNT3 polyclonal antibodies (13) directed against amino acid residues 45 - 69 of the extramembraneous N-terminal region of the protein (Fig. 8-1). To evaluate the glycosylation status of hCNT3 and hCNT3C-, the immunoblots in Figs. 8-4A and B also include aglyco-hCNT3, a construct produced by mutating all four potential N-terminal glycosylation acceptor sites, asparagine residues 630, 636, 664 and 678, to aspartate (Fig. 8-1). For comparison with the electrophoretic mobility of aglyco-hCNT3, Fig. 8-4B also shows the same streptavidin fractions of total hCNT3 and hCNT3C- membranes before and after digestion with *N*-glycosidase-F. Antibody specificity was evaluated in membrane fractions prepared from control water-injected oocytes.

Consistent with the presence of multiple possible sites of *N*-linked glycosylation, cell surface hCNT3 and hCNT3C- exhibited three discreet immunobands at 100, 86 and 75 kDa (Fig. 8-4A). Total cell surface immunoreactivity was similar for the two transporters, the majority of hCNT3 and hCNT3C- staining being associated with the highest and intermediate molecular weight forms, respectively (Fig. 8-4A). Corresponding patterns of immunoreactivity were apparent in total membranes (Fig. 8-4B). Indicative of proper protein folding, therefore, hCNT3C- was processed to the oocyte plasma membrane in amounts similar to wild-type hCNT3. Digestion with *N*-glycosidase-F shifted hCNT3 and hCNT3C- immunoreactivity to the lower molecular weight band at 75 kDa, an electrophoretic mobility identical to that of aglyco-hCNT3 and in good agreement with the molecular weight of hCNT3 calculated from its amino acid sequence (77 kDa). Confirming antibody specificity for hCNT3/hCNT3C-, no immunoreactivity was detected in blots from control water-injected oocytes.

Kinetic characterization of hCNT3C- – To further investigate hCNT3C- function, Fig. 8-5 compares the concentration dependence of radiolabeled uridine (0 - 1

mM) influx by hCNT3 and hCNT3C- measured either in the presence of Na⁺ (100 mM NaCl, pH 7.5) or in the presence of H⁺ (100 mM ChCl, pH 5.5). The corresponding kinetic parameters are given in Table 8-1. The results demonstrate robust high-affinity transport of uridine by hCNT3C-. Similar to hCNT3, and in agreement with previous kinetic data for the wild-type transporter (Chapter 5), the apparent K_m value of hCNT3C- for uridine in Na⁺-containing transport medium was lower than that in the presence of H⁺ (15 and 62 μ M, respectively, for hCNT3 compared to 18 and 63 μ M, respectively, for hCNT3C-). Calculated uridine $V_{max}:K_m$ ratios, an indicator of transporter efficiency and a kinetic predictor of relative transport rates at permeant concentrations less than K_m values, were consistent with the 10 μ M influx data shown in Fig. 8-3B (hCNT3(Na⁺) > hCNT3(H⁺), hCNT3C-(Na⁺), hCNT3C-(H⁺)).

Cation-activation curves were also determined for both transporters using a radiolabeled uridine concentration of 10 μ M. Na⁺-activation was measured over the concentration range 0 - 100 mM NaCl in transport medium at pH 7.5 and 8.5 (Figs. 8-6A and B, respectively), the latter to eliminate the small amount of H⁺-activation that occurs at neutral pH (Chapter 5). Isosmolarity was maintained with ChCl. H⁺-activation was measured in 100 mM ChCl transport medium at pH values ranging from 4.5 - 8.5 (Fig. 8-6C). Kinetic parameters derived from these data are presented in Tables 8-2 and 8-3 (Na⁺ and H⁺, respectively). Reflecting previously reported differences in Na⁺ and H⁺ coupling by hCNT3 (Chapters 5 and 6), the wild-type protein exhibited saturable Na⁺- and H⁺-activation curves that were sigmoidal and hyperbolic in nature, respectively, with apparent K_{50} values of 12 (pH 7.5) and 11 mM (pH 8.5) for Na⁺ and 690 nM for H⁺. Calculated Hill coefficients were consistent with 2:1 (Na⁺) and 1:1 (H⁺) cation:nucleoside coupling ratios. Validating the subsequent use of pH 8.5 to study Na⁺ coupling of hCNT3/hCNT3C- without interference from H⁺, there was no difference in hCNT3 Na⁺-activation kinetics at pH 7.5 and 8.5.

In marked contrast to wild-type hCNT3, and consistent with the relative decrease in Na⁺- versus H⁺-coupled uridine transport activity noted for the cysteine-less transporter in Fig. 8-3B and Table 8-1, the corresponding cation-activation curves for hCNT3C- revealed a marked and specific decrease in apparent affinity for Na⁺ (apparent

$K_{50} > 40$ mM). This shift in Na^+ affinity did not extend to H^+ , since kinetic parameters for hCNT3C- H^+ -activation were comparable to those of hCNT3 (apparent K_{50} value of 550 nM). Similarly, the corresponding Hill coefficient was consistent with a H^+ :nucleoside coupling ratio of 1:1. That for Na^+ could not be determined, although the curve appeared sigmoidal (Figs. 8-6A and B), and therefore potentially consistent with the wild-type Na^+ :nucleoside coupling ratio of 2:1. Similar to the wild-type protein, there was no difference in hCNT3C- Na^+ -activation kinetics at pH 7.5 and 8.5. All subsequent hCNT3/hCNT3C- Na^+ -activation and Na^+ -coupling experiments were performed at pH 8.5.

Electrophysiological determination of hCNT3C- Na^+ -activation kinetics – Since hCNT3 is electrogenic, the Na^+ -activation kinetic parameters of hCNT3C- were also determined by electrophysiology. Fig. 8-7 depicts the relationship between Na^+ concentration and 100 μM uridine-evoked current for oocytes expressing wild-type hCNT3 or hCNT3C- clamped at a membrane holding potential of -90 mV. Oocytes were individually normalized to their predicted I_{max} values and subsequently averaged to produce mean kinetic parameters. In agreement with previous studies (Chapters 5 and 6), the apparent K_{50} value for Na^+ -coupled uridine uptake by hCNT3 under these conditions was 2.2 ± 0.1 mM. Similar to the radioisotope flux data in Figs. 8-6A and B, hCNT3C- exhibited a marked decrease (~ 11 -fold) in the apparent affinity for Na^+ in comparison to that of the wild-type protein, with an increased apparent K_{50} value of 24.7 ± 0.8 mM. The corresponding Hill coefficients for hCNT3C- and hCNT3 were ≥ 1.5 , suggesting that the wild-type Na^+ :uridine stoichiometry of 2:1 was maintained by hCNT3C-. The apparent K_{50} values for hCNT3 and hCNT3C- as determined by electrophysiology were lower than those derived from radioisotope flux data because of (i) the different uridine concentrations used in the two studies (100 and 10 μM , respectively), and (ii) the difference in membrane potential in the two situations (-90 mV for the voltage-clamped oocytes *versus* ~ -40 mV under radioisotope flux conditions) (Chapter 5).

Presteady-state electrophysiology of hCNT3C- – Presteady-state electrophysiological experiments were performed on oocytes producing hCNT3C-

voltage-clamped at a holding potential (V_h) of -50 mV. Presteady-state currents were activated by voltage steps to a series of test potentials (V_t) in the presence of varying concentrations of Na^+ (0 - 100 mM NaCl, pH 8.5; Figs. 8-8A-E) and in the presence of both Na^+ and extracellular uridine (100 mM NaCl, pH 8.5 + 500 μM uridine; Fig. 8-8F). hCNT3C- exhibited presteady-state currents similar to those previously described for wild-type hCNT3 (Chapter 5) and wild-type hCNT1 (14), which increased in magnitude upon exposure to extracellular Na^+ and were largely eliminated upon addition of uridine. However, consistent with a reduced binding affinity for Na^+ , and different from the wild-type protein, presteady-state currents approached maximum values only at Na^+ concentrations > 50 mM, a behavior also observed for hCNT, another CNT with low apparent affinity for Na^+ .¹ Presteady-state currents were absent from control water-injected oocytes (data not shown) (14, Appendix 4).

Na⁺:uridine and H⁺:uridine stoichiometry – The Na^+ :uridine and H^+ :uridine stoichiometries of hCNT3C- were determined directly by simultaneous measurement of uridine evoked currents and 100 μM radiolabeled uridine uptake under voltage clamp conditions, as described previously (14, Chapters 5 and 6). A representative current trace is depicted in Fig. 8-9A for an oocyte expressing hCNT3C-exposed to 100 μM radiolabeled uridine in 100 mM NaCl transport medium, pH 8.5. Presented in Fig. 8-9B and C, each data point represents a single oocyte, and the coupling ratio is given by the slope of the linear fit of charge (pmol) *versus* uptake (pmol). In 100 mM NaCl transport medium (pH 8.5) and at a holding potential of -90 mV, the linear correlation between uridine-dependent charge and uridine accumulation gave a Na^+ :uridine coupling ratio of 2.08 ± 0.11 (Fig. 8-9B). The corresponding H^+ :uridine stoichiometry was determined in acidified 100 mM ChCl transport medium (pH 5.5) and resulted in a coupling ratio of 1.11 ± 0.06 (Fig. 8-9C). Both hCNT3C- stoichiometries agree with previously published values for hCNT3 (Chapters 5 and 6), and with the Hill coefficients derived from hCNT3 and hCNT3C- from Figs. 8-6 and 8-7 (Tables 8-2 and 8-3).

Cation-activation of aglyco-hCNT3 – The experiment of Fig. 8-4 demonstrated that wild-type hCNT3 and hCNT3C- have different patterns of *N*-linked glycosylation.

To exclude the possibility that the shift in hCNT3C- Na⁺ affinity was secondary to the altered glycosylation status of the protein, the apparent K_{50} and V_{\max} values for Na⁺- and H⁺-activation of aglyco-hCNT3 were determined under conditions identical to those used in Fig. 8-6B for hCNT3C-. Kinetic parameters for both cations were not significantly different from those of the wild-type protein measured in parallel in the same experiment (aglyco-hCNT3 and hCNT3 apparent K_{50} and V_{\max} values of 10.5 ± 1.1 and 8.8 ± 1.2 mM and 6.8 ± 0.4 and 7.4 ± 0.5 pmol/oocyte.min⁻¹, respectively, for Na⁺, and 399 ± 98 and 506 ± 182 nM and 4.7 ± 0.2 and 5.3 ± 0.4 pmol/oocyte.min⁻¹, respectively, for H⁺) (cation-activation curves not shown).

Cation-activation of hCNT3C- mutants – The hCNT3C- construct differs from wild-type hCNT3 by the replacement of all 14 endogenous cysteine residues with serine. Five of these substitutions lie within predicted TM regions of the protein (Fig. 8-1). Of these, four reside in the C-terminal half of the protein which corresponds to the region that chimeric studies between hCNT1 and hCNT3 (Chapter 5) and between hCNT1 and hfCNT (15) have demonstrated to be responsible for Na⁺ coupling. Site-directed mutagenesis experiments to identify the residue(s) responsible for the shift in hCNT3C- Na⁺-affinity therefore focused on the four C-terminal intramembraneous cysteine residues: Cys⁴⁸⁶ (TM 11), Cys⁵⁶¹ (TM 12), Cys⁶⁰² (TM 13) and Cys⁶⁰⁷ (TM 13). In the hCNT3C- background, cysteine residues were individually reintroduced at each of these positions, yielding constructs S486C(C-), S561C(C-), S602C(C-) and S607C(C-). Measured under conditions identical to those used in Fig. 8-6B, Fig. 8-10 shows oocyte Na⁺-activation curves for each mutant. Corresponding kinetic parameters are given in Table 8-2. S486C(C-), S602C(C-) and S607C(C-) (Figs. 8-10A, C, D) each retained Na⁺-activation curves similar to that of hCNT3C- (Fig. 8-6B), with apparent K_{50} values > 40 mM. In contrast, the Na⁺-activation curve for S561C(C-) (Fig. 8-10B) closely resembled that of wild-type hCNT3 (Fig. 8-6B) with an apparent K_{50} value of 7.2 ± 0.6 mM. H⁺-activation kinetics were also determined for S561C(C-) yielding apparent K_{50} and V_{\max} values that were similar to those of both hCNT3C- and hCNT3 (cation-activation curve not shown; Table 8-3).

Cation-activation of hCNT3 mutant C561S – To confirm the role of Cys⁵⁶¹ in the shift in Na⁺-affinity of hCNT3C-, serine was substituted for cysteine in wild-type hCNT3, creating the mutant protein C561S. Na⁺- and H⁺-activation kinetics for oocytes producing C561S were determined under identical experimental conditions to those described above for other hCNT3/hCNT3C- constructs and are depicted in Fig. 8-11. Kinetic parameters derived from the curves are presented in Tables 8-2 and 8-3. Similar to hCNT3C- (Figs. 8-6B and C), C561S exhibited a decreased apparent affinity for Na⁺ (> 40 mM) in the absence of a parallel shift in H⁺ apparent binding affinity.

Cation-activation of hCNT1 and hCNT1 mutant C540S – In contrast to hCNT3, which is both H⁺- and Na⁺-coupled and exhibits H⁺:nucleoside and Na⁺:nucleoside stoichiometries of 1:1 and 2:1, respectively, hCNT1 and hCNT2 are Na⁺-specific and have a Na⁺:nucleoside stoichiometry of 1:1 (12, 14, 16, Chapters 5 and 6). All three proteins share similar high affinities for Na⁺ binding with apparent K_{50} values of ~ 10 mM (14, 16, Chapters 5 and 6). The residue corresponding to hCNT3 Cys⁵⁶¹ in hCNT1 is Cys⁵⁴⁰. To investigate the effects of a cysteine to serine mutation at this position in another CNT family member, the same change was made in hCNT1 to create the mutant protein C540S. Mutant C540S and wild-type hCNT1 were then produced in oocytes, and their Na⁺-activation kinetics investigated under experimental conditions identical to those described above for hCNT3/hCNT3C- and mutants (Fig. 8-12). In agreement with previous studies (16, Chapter 4), hCNT1 displayed a hyperbolic Na⁺-activation curve with an apparent affinity for Na⁺ of 6.6 ± 1.0 mM and a V_{\max} of 4.5 ± 0.2 pmol/oocyte.min⁻¹ (Fig. 8-12B). Similarly, Na⁺-activation of C540S was also hyperbolic with apparent K_m and V_{\max} values of 8.4 ± 1.1 mM and 4.3 ± 0.1 pmol/oocyte.min⁻¹, respectively (Fig. 8-12A). Corresponding Hill coefficients were both 1.0 ± 0.1 .

Other amino acid substitutions of hCNT3 residue Cys⁵⁶¹ – Sequence comparisons of 126 eukaryotic and prokaryotic CNT family members revealed that the residue corresponding to hCNT3 Cys⁵⁶¹ is highly conserved. However, in addition to cysteine (90 family members), the amino acids alanine, valine, threonine and isoleucine were also represented at this position (4, 21, 6 and 5 family members, respectively). Therefore, to further elucidate the role of Cys⁵⁶¹ in hCNT3 cation-coupling, hCNT3

mutants C561A, C561V, C561T and C561I were constructed and produced in oocytes. Substitution of hCNT3 Cys⁵⁶¹ with glycine, the amino acid with the smallest side chain, was also included in the series (mutant C561G). Functional activity and cation selectivity were compared to wild-type hCNT3 and mutant C561S by measuring 10 μ M radiolabeled uridine influx in both Na⁺- and H⁺-containing transport medium (100 mM NaCl, pH 7.5 and 100 mM ChCl, pH 5.5, respectively) (Fig. 8-13). Similar to these transporters, C561G and C561A exhibited both Na⁺- and H⁺-coupled influx of radiolabeled uridine. However, relative to transport in the presence of Na⁺ and in contrast to C561A, C561G exhibited reduced influx of uridine in H⁺-containing medium. Extending this trend, substitution of Cys⁵⁶¹ with larger neutral amino acids (mutants C561V, C561T and C561I) led to almost total abolition of uridine influx in H⁺-containing medium, a finding that was confirmed for C561I by corresponding measurements of 100 μ M uridine-induced steady-state currents (Fig. 8-14).

Kinetic parameters for Na⁺-activation of C561G, C561A, C561S, C561T, C561V and C561I, measured as described in Fig. 8-6B, are given in Table 8-2. Replacement of Cys⁵⁶¹ with residues of a similar size (C561A and C561V) allowed full (C561A) or partial (C561V) recovery of Na⁺ apparent affinity (K_{50} values of 10.7 ± 0.7 and 31.3 ± 1.9 mM, respectively). In contrast, C561G, C561T and C561I exhibited reduced affinities for Na⁺ similar to that of hCNT3C- (apparent K_{50} values > 40 mM). The ability of alanine to mimic cysteine at residue position 561 extended to the reciprocal hCNT3C- mutant S561A(C-), which exhibited a partially restored apparent K_{50} value of 20.5 ± 0.9 mM (Na⁺-activation curve not shown; Table 8-2).

Discussion

hCNT3, the most recently discovered and functionally versatile of three human members of the SLC28 (CNT) protein family, is 691 amino acids in length, has a 13 (or possibly 15) TM membrane architecture, and utilizes electrochemical gradients of both Na⁺ and H⁺ to accumulate a broad range of pyrimidine and purine nucleosides and nucleoside drugs within cells (14, 15, 17, 18). Although paralogs hCNT1 and hCNT2

have a similar predicted membrane topology, they function predominantly as Na⁺-coupled transporters, and are pyrimidine nucleoside-preferring and purine nucleoside-preferring, respectively (14, 16, 17, Chapter 6). More widely distributed in cells and tissues than hCNT1 or hCNT2 (12) and with a central role in renal transepithelial nucleoside and nucleoside drug transport (13, 18, 19), the multifunctional capability of hCNT3 makes it the protein of choice for systematic in depth molecular characterization by SCAM. A prerequisite of this approach is the availability of a functional cysteine-less version of the transporter.

Cysteine-less hCNT3C-, in which all 14 endogenous cysteine residues of hCNT3 have been converted to serine, is shown here to have a robust functional phenotype when produced in *Xenopus* oocytes. Similar to wild-type hCNT3, and consistent with correct folding of the cysteine-less transporter, hCNT3C- exhibited broad selectivity for both pyrimidine and purine nucleosides in Na⁺-containing medium (Fig. 8-3A), displayed the characteristic narrowing of this permeant selectivity in H⁺-containing medium (Fig. 8-3A), was processed to the cell surface in amounts equivalent to hCNT3 (Fig. 8-4), exhibited apparent binding affinities for uridine in both Na⁺- and H⁺-containing medium similar to those of the wild-type transporter (Fig. 8-5), and retained the wild-type Na⁺:uridine and H⁺:uridine coupling stoichiometries of 2:1 and 1:1, respectively (Fig. 8-9). Recombinant hCNT3C- is also functional in yeast and was used in initial SCAM analyses to screen residues in TMs 11-13 for reactivity to MTS reagents (9). In oocytes, hCNT3C- was previously used in SCAM analysis of TM 12 to test residues for inhibition by PCMBs (Chapter 7). Consistent with correct folding of the nucleoside binding pocket of hCNT3C-, MTS and PCMBs accessibility to some residues was blocked by exofacial uridine (9, Chapter 7). Taken together, these analyses validate use of hCNT3C- as a template for SCAM analyses of CNT structure and function.

Characterization of hCNT3C- revealed an altered apparent affinity for Na⁺; hCNT3C- and wild-type hCNT3 exhibited apparent K_{50} values for Na⁺-activation of 10 μ M radiolabeled uridine influx of > 40 mM and 11 - 12 mM, respectively (Figs. 8-6A and B). Under voltage clamp conditions of -90 mV with a uridine concentration of 100

μM , Na^+ -activation curves for hCNT3 and hCNT3C- were sufficiently shifted to the left to establish that the change in binding affinity for Na^+ between hCNT3 and hCNT3C- was ~ 11 -fold (apparent K_{50} values of 2.2 and 25 mM, respectively) (Fig. 8-7). This difference, which was also apparent in presteady-state current measurements (Fig. 8-8), was specific to Na^+ and did not extend to H^+ (Fig. 8-6C). The change was also specific to one particular cysteine residue, Cys⁵⁶¹ in TM 12. Reintroduction of cysteine at position 561 (hCNT3C- mutant S561C(C-)) restored wild-type Na^+ binding (Fig. 8-10), while the reciprocal single cysteine-to-serine substitution in hCNT3 (mutant C561S) produced an altered Na^+ binding affinity corresponding to that found for hCNT3C- (Fig. 8-11).

Recently, a naturally-occurring hCNT3 variant has been described in the Spanish population in which a T/C transition leads to the substitution of cysteine at position 602 by arginine (20). This single amino acid replacement in TM 13 led to a shift in Hill coefficient consistent with a change in Na^+ :nucleoside stoichiometry from 2:1 to 1:1. In agreement with the findings presented here, the C602R phenotype was a consequence of the insertion of arginine at this position rather than the loss of cysteine.

Fully processed to the cell surface, hCNT3C- exhibited an altered pattern of *N*-linked glycosylation relative to that of the wild-type protein. As shown in Fig. 8-4, two glycosylated forms of hCNT3/hCNT3C- were apparent on SDS-polyacrylamide gels (100 and 86 kDa). Most hCNT3C- immunoreactivity was associated with the 86 kDa band, in contrast to hCNT3 for which most immunoreactivity was found in the higher molecular weight band of 100 kDa. Since no less than six of the 14 endogenous cysteine residues of hCNT3 are located alongside the four potential *N*-terminal glycosylation acceptor sites in the extracellular *N*-terminal tail of the protein (Fig. 8-1), and since these cysteines likely form intramolecular disulfide bridges within the protein, it is likely that the modified glycosylation status of the cysteine-less transporter is secondary to changes in the secondary/tertiary structure of this extramembraneous region of the protein. The demonstration that aglyco-hCNT3 exhibited normal Na^+ -activation kinetics verified that altered glycosylation was not responsible for the shift in hCNT3C- Na^+ affinity.

As well as replacement of hCNT3 Cys⁵⁶¹ with serine, each of the alternative amino acids found at position 561 in other CNT family members (alanine, valine, threonine and isoleucine) were introduced into hCNT3. To provide a more complete spectrum of neutral amino acid side chain structures in the analysis, cysteine was also mutated to glycine. In addition to cysteine, only alanine at this position (hCNT3 mutant C561A) elicited wild-type cation binding (Table 8-2 and Fig. 8-13). The rank order of Na⁺ binding affinities (cysteine, alanine > valine > glycine, serine, threonine, isoleucine) demonstrated that normal hCNT3 Na⁺-activation was critically dependent upon a combination of residue 561 side chain bulk and polarity. Tolerance of alanine at position 561 was confirmed in the hCNT3C- background, in that mutant S561A(C-) exhibited partially recovered Na⁺ binding affinity (Table 8-2), thereby providing an alternative to hCNT3C- as template for future SCAM analyses of hCNT3 structure and function.

Despite retaining Na⁺-coupled transport capability, albeit with reduced Na⁺-binding affinity, substitution of Cys⁵⁶¹ by valine, threonine and isoleucine had the additional and unanticipated consequence of dramatically decreasing H⁺-coupled uridine transport activity (Figs. 8-13 and 8-14). Relative to Na⁺, substitution of cysteine with the smaller amino acid glycine also led to reduced H⁺-dependent uridine transport activity. Therefore, the nature of the amino acid side chain at position Cys⁵⁶¹ in hCNT3 influences both Na⁺- and H⁺-coupled nucleoside transport, but with seemingly dissimilar structure-function profiles. For example, whereas the apparent affinity of mutant C561V for Na⁺ was only moderately decreased (apparent K_{50} of 31 mM compared to 11 mM for wild-type hCNT3; Table 8-2), H⁺-coupled uridine transport was essentially eliminated (Figs. 8-13 and 8-14). In the opposite direction, the apparent affinity of mutant C561G for Na⁺ was not measurable (Table 8-2), whereas H⁺-coupled uridine transport activity was only slightly decreased compared to that for wild-type hCNT3 (Figs. 8-13 and 8-14). The structural requirements for Na⁺ and H⁺ binding and/or translocation at this single residue position are not, therefore, the same. At the level of the whole protein, other indications that Na⁺ and H⁺ binding and/or translocation have different structural requirements include the demonstration that hCNT3 exhibits different Na⁺ and H⁺ binding stoichiometries (Chapters 5 and 6). Na⁺- and H⁺-coupled hCNT3 also have

markedly different nucleoside and nucleoside drug selectivities, a finding that provides evidence for two distinct cation-dependent conformational states of the protein (Chapter 5).

In a separate study, Cys⁵⁶¹ was independently identified as the cysteine residue responsible for inhibition of wild-type hCNT3 by PCMBS (Chapter 7). Access of this membrane-impermeant probe to Cys⁵⁶¹ required H⁺, but not Na⁺, and was blocked by micromolar concentrations of extracellular uridine. Although this cysteine residue is conserved in Na⁺-specific hCNT1 and hCNT2, neither transporter is affected by PCMBS. When converted to cysteine, two other residues in hCNT3 adjacent to Cys⁵⁶¹ (Ile⁵⁵⁴ and Tyr⁵⁵⁸) also led to H⁺-activated inhibition by PCMBS (Chapter 7). These findings suggest that Cys⁵⁶¹ is located in the translocation pore in a mobile region within or closely adjacent to the nucleoside binding pocket and that accessibility of PCMBS to this residue reports a specific H⁺-induced conformational state of the protein (Chapter 7). Positioned in the middle of TM 12 (Fig. 8-1), this residue position is now also revealed to be capable of modifying the functionality of the protein, with marked influences on both Na⁺:nucleoside and H⁺:nucleoside cotransport. Within the plane of the membrane, Cys⁵⁶¹ is located at the interface between those residues sensitive to inhibition by PCMBS in H⁺-containing medium only and those where inhibition occurs in the presence of both Na⁺ and H⁺ (Chapter 7). Matching the previous observation that H⁺-induced inhibition by PCMBS is specific to hCNT3 and not found in hCNT1/2 (Chapter 7), mutation of hCNT1 Cys⁵⁴⁰ to serine (the cysteine substitution corresponding to hCNT3 C561S) had no influence on Na⁺-binding affinity (Fig. 8-12). hCNT3 has two Na⁺-binding sites, one of which may be Na⁺-specific and the other of which may be shared functionally with H⁺ (Chapters 5 and 7). hCNT3 Cys⁵⁶¹ seems to be primarily associated with the site interacting with both cations.

In conclusion, two independent lines of investigation have converged to identify Cys⁵⁶¹ as a key residue that resides in a conformationally mobile region of hCNT3 and is intimately involved in both Na⁺/nucleoside and H⁺/nucleoside cotransport. With actions seemingly specific to one of two hCNT3 cation binding sites, future investigations of Cys⁵⁶¹ and adjacent residues will be central to understanding the

molecular intricacies of CNT cation/nucleoside cotransport and, in particular, to functionally separating and structurally identifying the two cation binding domains of hCNT3. Without access to a CNT crystal structure, SCAM-based approaches employing hCNT3C- as a template will be essential to these endeavours.

Table 8-1. Uridine kinetic parameters for hCNT3 and hCNT3C-.

		Apparent K_m value (μM)	V_{max} ($\text{pmol/oocyte}\cdot\text{min}^{-1}$)	$V_{max}:K_m$ ratio
hCNT3	NaCl, pH 7.5 ^a	14.7 ± 1.7	22.7 ± 0.7	1.54 ± 0.12
	ChCl, pH 5.5 ^b	62.4 ± 5.4	53.1 ± 1.1	0.85 ± 0.11
hCNT3C-	NaCl, pH 7.5 ^a	18.4 ± 1.5	12.4 ± 0.2	0.67 ± 0.11
	ChCl, pH 5.5 ^b	63.4 ± 5.1	23.2 ± 0.4	0.37 ± 0.11

^a, from Fig. 8-5A-B (100 mM NaCl, pH 7.5); ^b, from Fig. 8-5C-D (100 mM ChCl, pH 5.5).

Table 8-2. Na⁺-activation kinetic parameters for hCNT3, hCNT3C- and mutants.

		Apparent K_{50} value (mM)	V_{max} (pmol/oocyte.min ⁻¹)	Hill Coefficient
hCNT3 ^a	pH 7.5	12.0 ± 0.8	11.9 ± 0.5	1.4 ± 0.1
	pH 8.5	10.7 ± 1.0	12.0 ± 0.7	1.4 ± 0.1
hCNT3C- ^a	pH 7.5	> 40	nd ^e	-
	pH 8.5	> 40	nd ^e	-
S486C(C-) ^b	pH 8.5	> 40	nd ^e	-
S561C(C-) ^b	pH 8.5	7.2 ± 0.6	6.0 ± 0.3	1.4 ± 0.1
S602C(C-) ^b	pH 8.5	> 40	nd ^e	-
S607C(C-) ^b	pH 8.5	> 40	nd ^e	-
C561S ^c	pH 8.5	> 40	nd ^e	-
C561G ^d	pH 8.5	> 40	nd ^e	-
C561A ^d	pH 8.5	10.7 ± 0.6	6.9 ± 0.2	1.5 ± 0.1
C561V ^d	pH 8.5	31.3 ± 1.9	9.1 ± 0.4	1.4 ± 0.1
C561T ^d	pH 8.5	> 40	nd ^e	-
C561I ^d	pH 8.5	> 40	nd ^e	-
S561A(C-) ^d	pH 8.5	20.5 ± 0.9	6.0 ± 0.2	1.4 ± 0.1

^a, from Fig. 8-6A-B; ^b, from Fig. 8-10A-D; ^c, from Fig. 8-11A; ^d, data not shown; ^e, nd, could not be determined; in 100 mM transport media with 0 - 100 mM NaCl (pH 7.5 or 8.5, as indicated, isosmolarity maintained by ChCl).

Table 8-3. H⁺-activation kinetic parameters for hCNT3, hCNT3C- and mutants.

	Apparent K_{50} value (nM)	V_{max} (pmol/oocyte.min ⁻¹)	Hill Coefficient
hCNT3 ^a	690 ± 200	7.0 ± 0.4	0.8 ± 0.1
hCNT3C- ^a	550 ± 100	4.4 ± 0.2	0.8 ± 0.1
S561C(C-) ^b	830 ± 150	7.1 ± 0.3	0.8 ± 0.1
C561S ^c	870 ± 80	4.7 ± 0.1	0.7 ± 0.1

^a, from Fig. 8-6C; ^b, data not shown; ^c, from Fig. 8-11B; in 100 mM ChCl transport media with pH values ranging from 4.5 - 8.5.

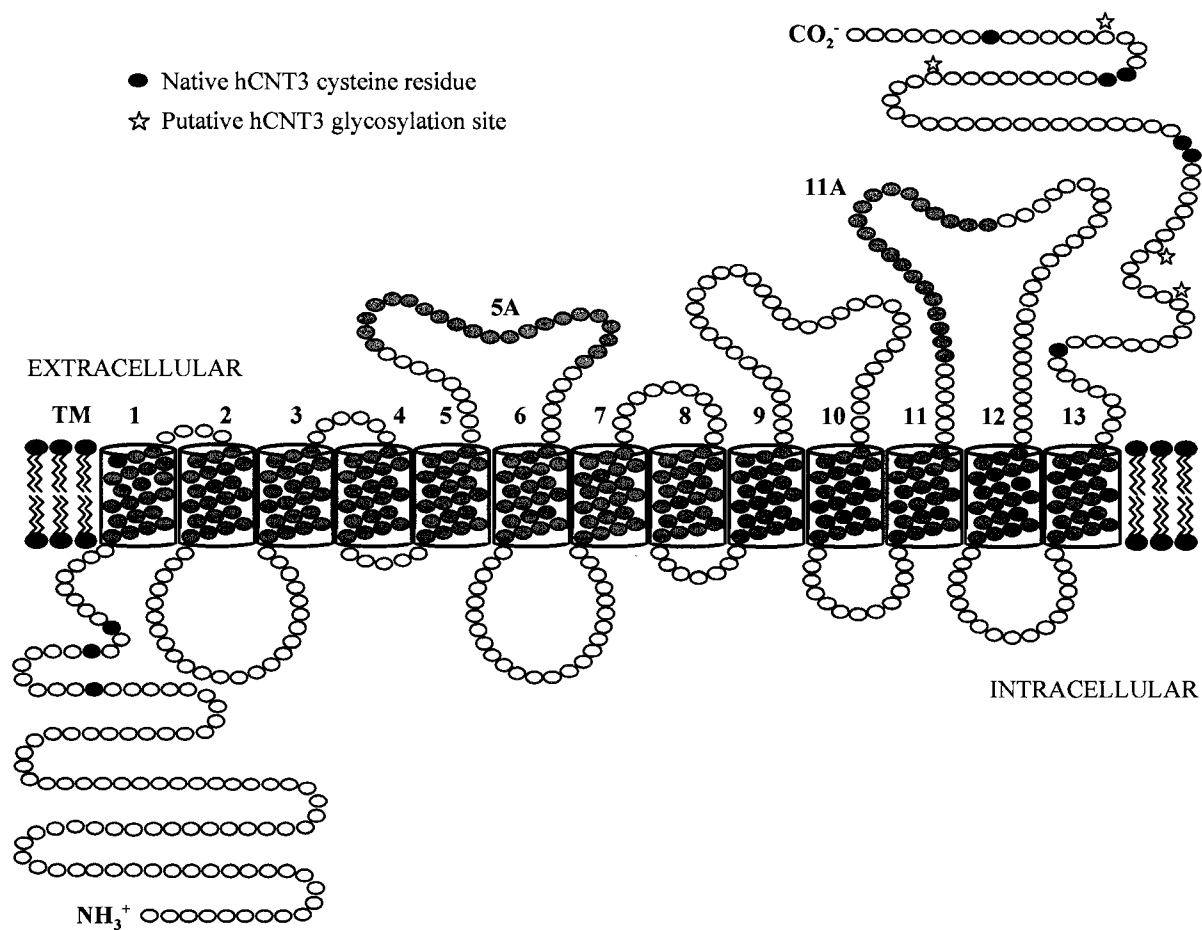


Figure 8-1. Topological model of hCNT3. Membrane-spanning α -helices predicted from bioinformatic analyses of currently identified CNT family members are numbered 1 - 13; 5A and 11A, which are shown as extracellular loops, are weakly predicted to be membrane-spanning α -helices. Cysteine residues and putative glycosylation sites are indicated in *black* and with a *star* symbol, respectively.

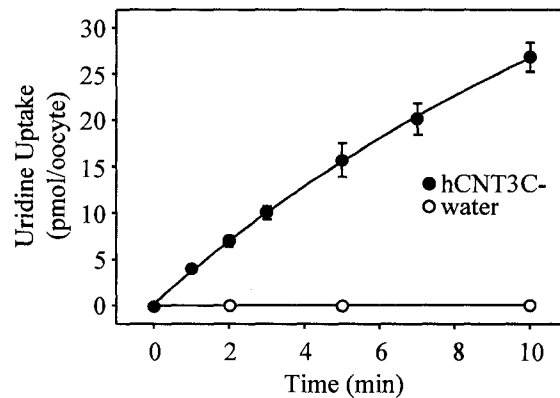


Figure 8-2. Time course of uridine uptake by hCNT3C- in *Xenopus* oocytes. Uptake of 10 μ M radiolabeled uridine by oocytes producing hCNT3C- was measured in 100 mM NaCl transport medium (pH 7.5) for various times up to 10 min (*solid* circles) and compared with that of control water-injected oocytes (*open* circles). Each point is the mean \pm SEM of 10 - 12 oocytes. Error bars are not shown where values were smaller than that represented by the symbols.

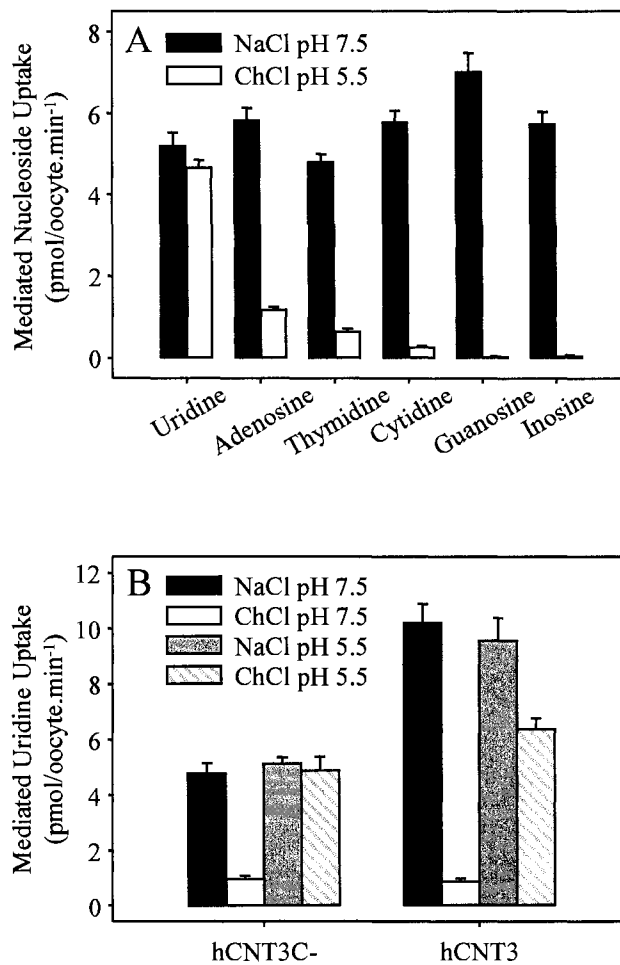


Figure 8-3. Nucleoside and cation selectivity of hCNT3C-. (A) Influx of a panel of physiological radiolabeled nucleosides (10 μ M) by oocytes producing hCNT3C- was measured under initial rate conditions (1 min flux) in transport medium containing 100 mM NaCl pH 7.5 (*black bars*) or ChCl pH 5.5 (*white bars*). (B) Influx (1 min) of 10 μ M radiolabeled uridine by wild-type hCNT3 or hCNT3C- was measured in transport medium containing 100 mM NaCl pH 7.5 (*black bars*), ChCl pH 7.5 (*white bars*), NaCl pH 5.5 (*grey bars*) or ChCl pH 5.5 (*hatched bars*). Values (A and B) were corrected for basal non-mediated uptake in control water-injected oocytes and are means \pm SEM of 10 - 12 oocytes.

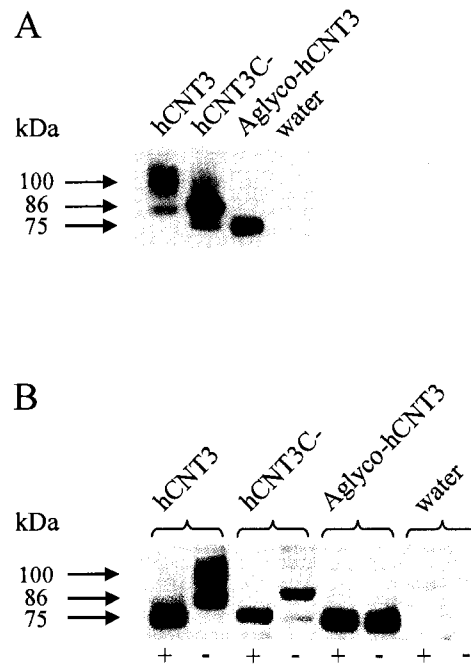


Figure 8-4. Immunoblot analysis of hCNT3, hCNT3C- and aglyco-hCNT3. Labeling of oocytes with sulfo-NHS-LC-biotin was used in conjunction with immobilized streptavidin resin to separate recombinant hCNT3, hCNT3C- and aglyco-hCNT3 cell surface immunoreactivity (A) from that associated with total (plasma + intracellular) membranes (B). Immunoblots of the fractions were probed with anti-hCNT3 antibodies. In (B), (+) and (-) refer to digestion with *N*-glycosidase-F. The positions of molecular weight standards are shown on the left. Water refers to control water-injected oocytes. Blots shown in A and B are from different gels.

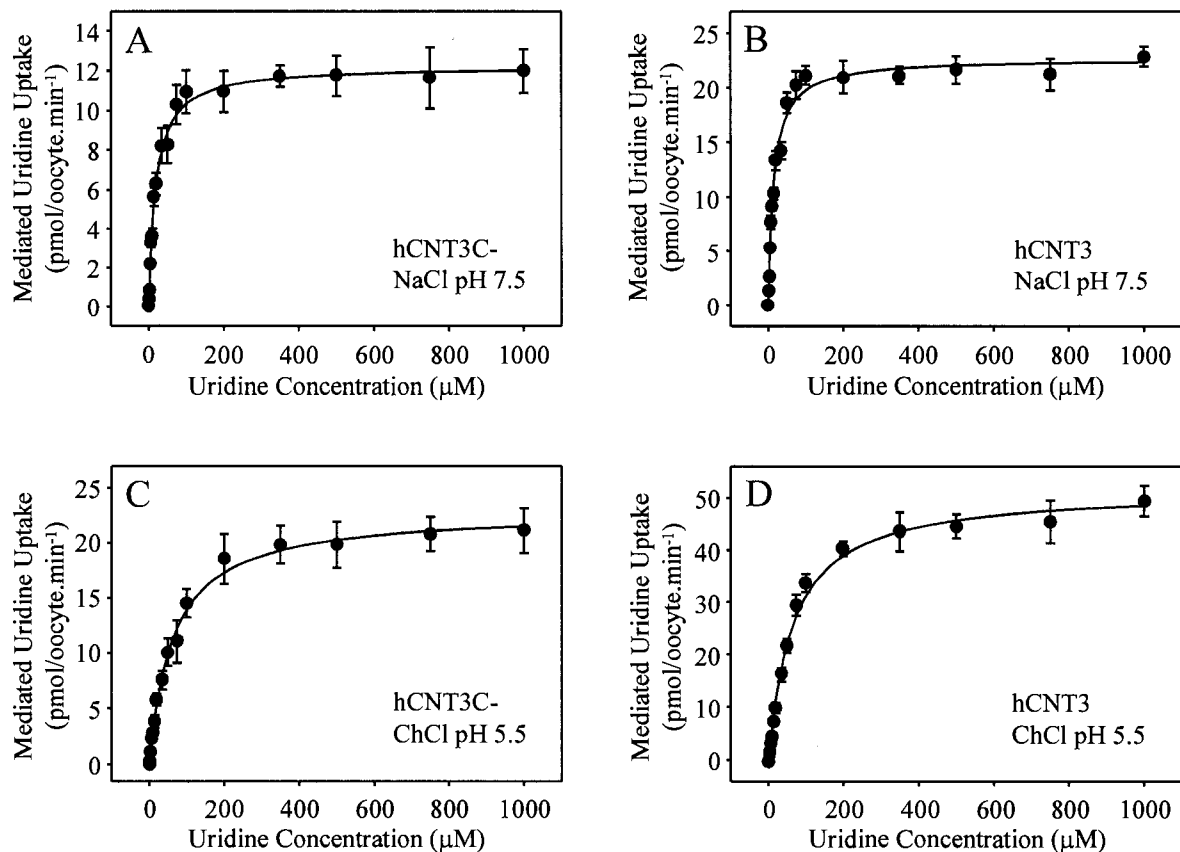


Figure 8-5. Concentration dependence of Na⁺- and H⁺-coupled uridine uptake by oocytes producing hCNT3 and hCNT3C-. Radiolabeled 10 μM uridine influx was measured in 100 mM NaCl transport medium, pH 7.5 (*A* and *B*) and 100 mM ChCl transport medium, pH 5.5 (*C* and *D*) under initial rate conditions (1 min) in oocytes producing hCNT3 (*B* and *D*) and hCNT3C- (*A* and *C*). Corrected for basal (non-mediated) uptake in control water-injected oocytes, each value is the mean ± SEM of 10 - 12 oocytes. Error bars are not shown where values were smaller than that represented by the symbols. Kinetic parameters calculated from the data are presented in Table 8-1.

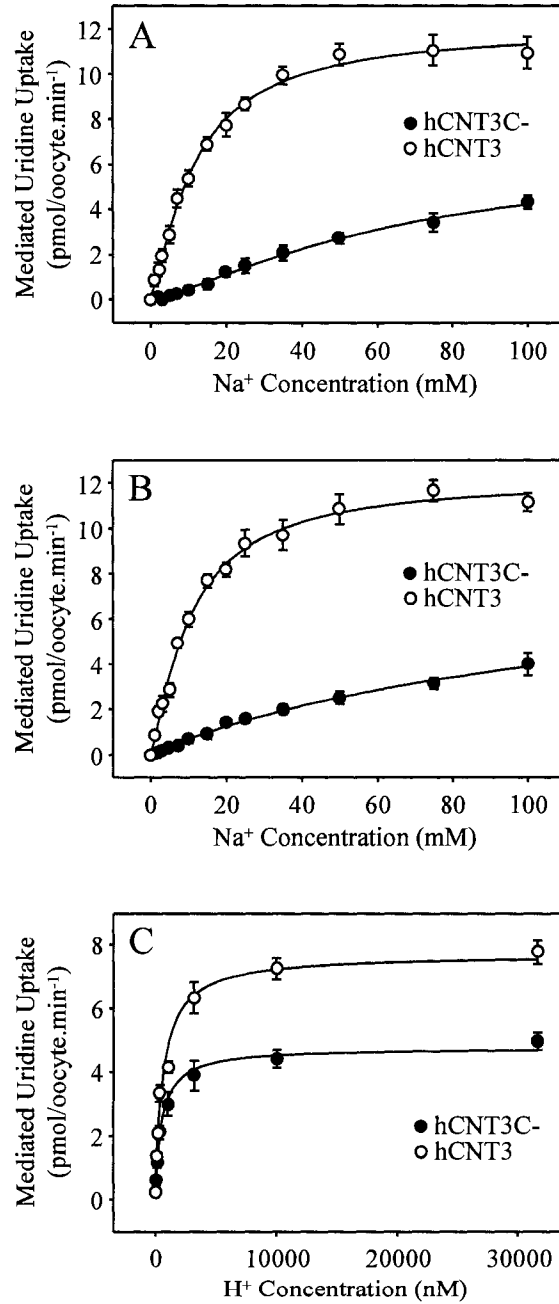


Figure 8-6.

Figure 8-6. Na⁺- and H⁺-activation kinetics of oocytes producing hCNT3 and hCNT3C-. Na⁺-activation curves for oocytes producing hCNT3 (*open circles*) and hCNT3C- (*solid circles*) were measured in transport medium containing 0 - 100 mM NaCl at pH 7.5 (*A*) and pH 8.5 (*B*), with isosmolarity maintained by addition of ChCl. Corresponding H⁺-activation curves were determined in 100 mM ChCl transport medium at pH values ranging from 4.5 to 8.5 (*C*). The radiolabeled uridine concentration was 10 μM (1 min flux). Corrected for basal (non-mediated) uptake in control water-injected oocytes, each value is the mean ± SEM of 10 - 12 oocytes. Error bars are not shown where values were smaller than that represented by the symbols. Kinetic parameters calculated from the data are presented in Tables 8-2 and 8-3.

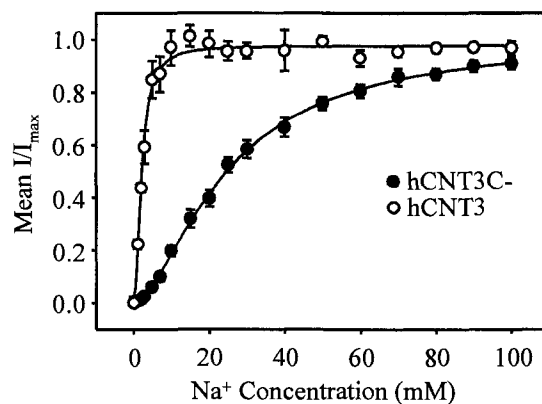


Figure 8-7. Na⁺-activation kinetics of hCNT3 and hCNT3C- determined by electrophysiology. Na⁺-activation curves for hCNT3 (*open circles*) and hCNT3C- (*solid circles*) were determined at a holding potential of -90 mV in transport media of the same composition used in radioisotope flux studies (Fig. 8-6B). The uridine concentration was 100 μ M. Uridine-evoked currents at each Na⁺ concentration were normalized to the respective fitted I_{\max} value and are presented as the mean \pm SEM of 6-8 oocytes. Error bars are not shown where values were smaller than that represented by the symbols. No currents were detected in control water-injected oocytes (data not shown).

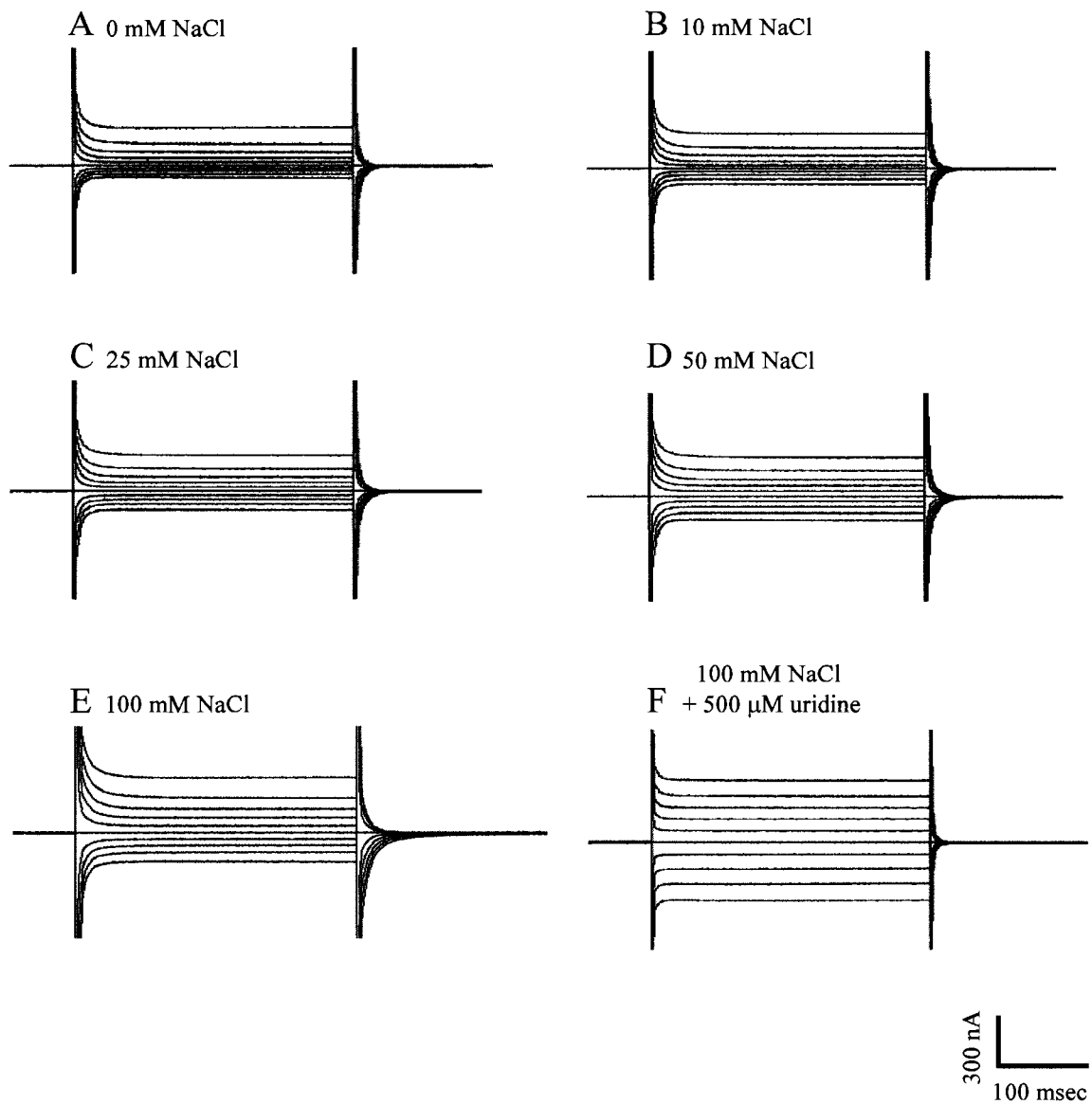


Figure 8-8. Presteady-state currents of hCNT3C-. Oocytes expressing hCNT3C- were held at a holding potential (V_h) of -50 mV and stepped to a range of test potentials (V_t) from -150 to +75 mV in 25 mV increments. Representative traces from a single oocyte are shown in transport medium containing 0 mM NaCl, pH 8.5 (100 mM ChCl, pH 8.5; *A*), 10, 25, 50 and 100 mM NaCl, pH 8.5 (*B-E*, respectively) and 100 mM NaCl, pH 8.5 + 500 μ M uridine (*F*).

A NaCl pH 8.5

100 μ M uridine
(nonradioactive + radioactive)

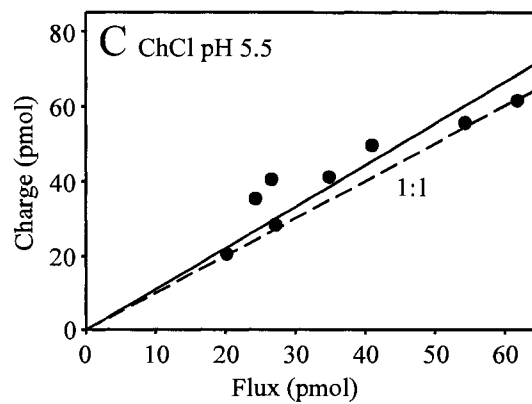
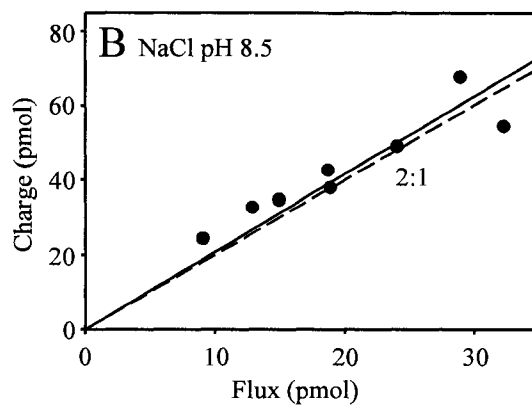
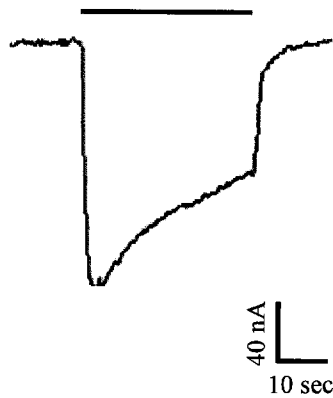


Figure 8-9.

Figure 8-9. Na⁺:uridine and H⁺:uridine stoichiometry of hCNT3C⁻. (A) A representative current trace for an oocyte expressing hCNT3C⁻ clamped at a membrane potential of -90 mV and exposed to 100 μM radiolabeled uridine in 100 mM NaCl, pH 8.5. Integration of the uridine-evoked current over the uptake period yielded the charge moved; this charge, representing net cation influx, was correlated to the net uptake (flux) of radiolabeled uridine by the oocyte during the same time interval. Following the same protocol (V_h of -90 mV; 100 μM uridine), (B) and (C) show charge to flux ratio plots generated for oocytes producing hCNT3C⁻ in either 100 mM NaCl transport medium at pH 8.5 (B) or ChCl transport medium at pH 5.5 (C). Each point represents a single oocyte. Linear regression fits of both data sets passed through the origin and are indicated by *solid* lines. The *dashed* lines represents theoretical 2:1 (B) and 1:1 (C) charge:uptake ratios.

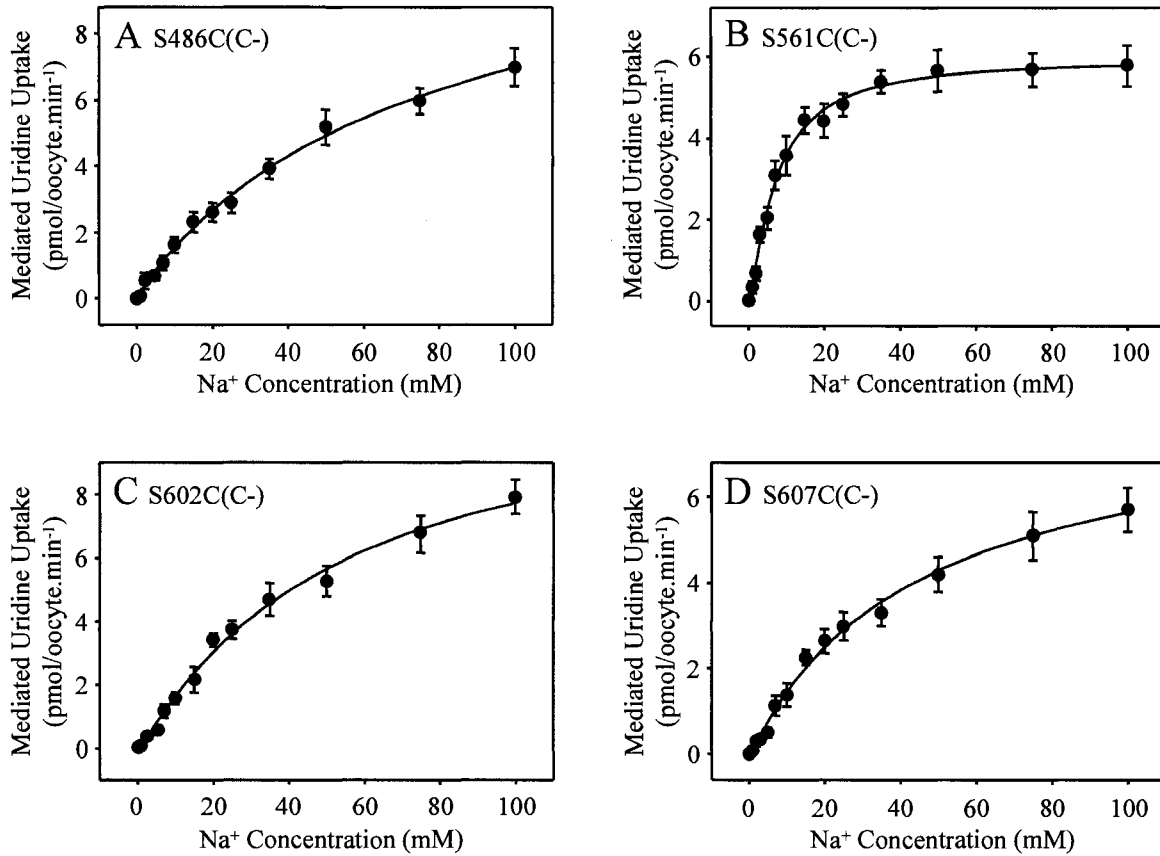


Figure 8-10. Na⁺-activation kinetics of oocytes producing hCNT3C- mutants S486C(C-), S561C(C-), S602C(C-) and S607C(C-). Na⁺-activation curves were determined as described in Fig. 8-6B. The radiolabeled uridine concentration was 10 μ M (1 min flux). Corrected for basal (non-mediated) uptake in control water-injected oocytes, each value is the mean \pm SEM of 10 - 12 oocytes. Error bars are not shown where values were smaller than that represented by the symbols. Kinetic parameters calculated from the data are presented in Table 8-2.

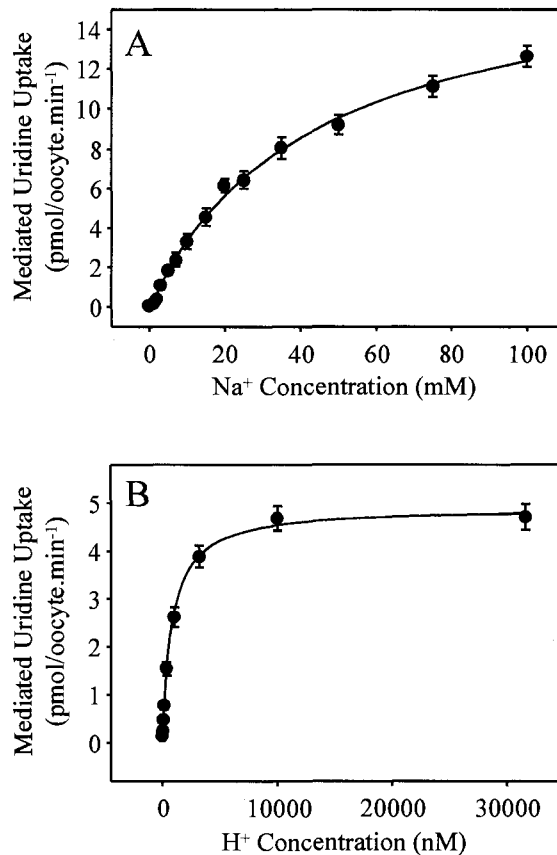


Figure 8-11. Na⁺- and H⁺-activation kinetics of oocytes producing hCNT3 mutant C561S. Na⁺- (A) and H⁺- (B) activation curves were determined as described in Figs. 8-6B and C, respectively. The radiolabeled uridine concentration was 10 μM (1 min flux). Corrected for basal (non-mediated) uptake in control water-injected oocytes, each value is the mean ± SEM of 10 - 12 oocytes. Error bars are not shown where values were smaller than that represented by the symbols. Kinetic parameters calculated from the data are presented in Tables 8-2 and 8-3.

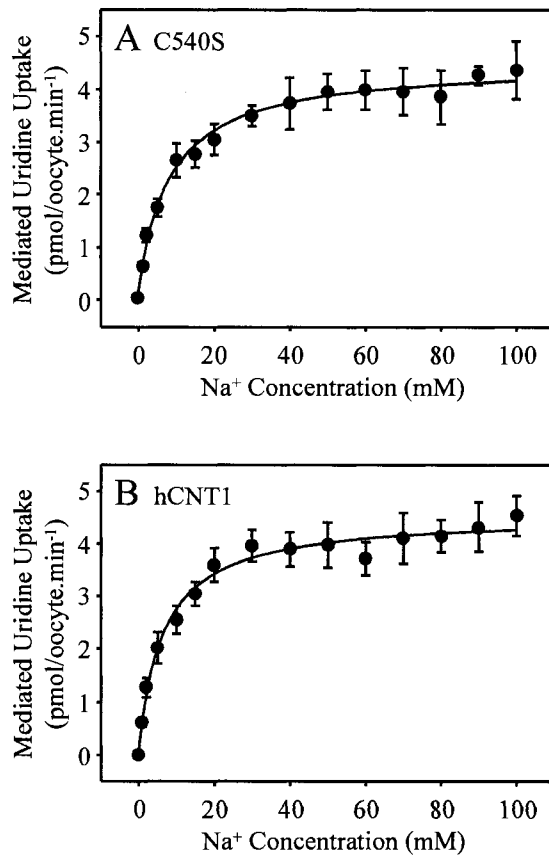


Figure 8-12. Na⁺-activation kinetics of oocytes producing hCNT1 and hCNT1 mutant C540S. Na⁺-activation curves were determined for oocytes expressing hCNT1 mutant C540S (*A*) and wild-type hCNT1 (*B*) as described in Fig. 8-6*B*. The radiolabeled uridine concentration was 10 μ M (1 min flux). Corrected for basal (non-mediated) uptake in control water-injected oocytes, each value is the mean \pm SEM of 10 - 12 oocytes. Error bars are not shown where values were smaller than that represented by the symbols.

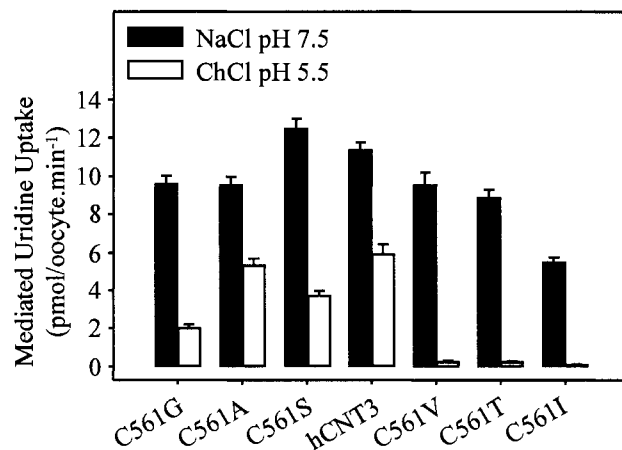


Figure 8-13. Cation selectivity of hCNT3 mutants. Influx of 10 μM radiolabeled uridine by hCNT3 mutants C561G, C561A, C561S, hCNT3, C561V, C561T and C561I was measured under initial rate conditions (1 min flux) in both Na^+ -containing (100 mM NaCl, pH 7.5) and H^+ -containing (100 mM ChCl, pH 5.5) transport medium (*black* and *white* bars, respectively). Values were corrected for basal non-mediated uptake in control water-injected oocytes and are means \pm SEM of 10 - 12 oocytes. Error bars are not shown where values were smaller than that represented by the symbols.

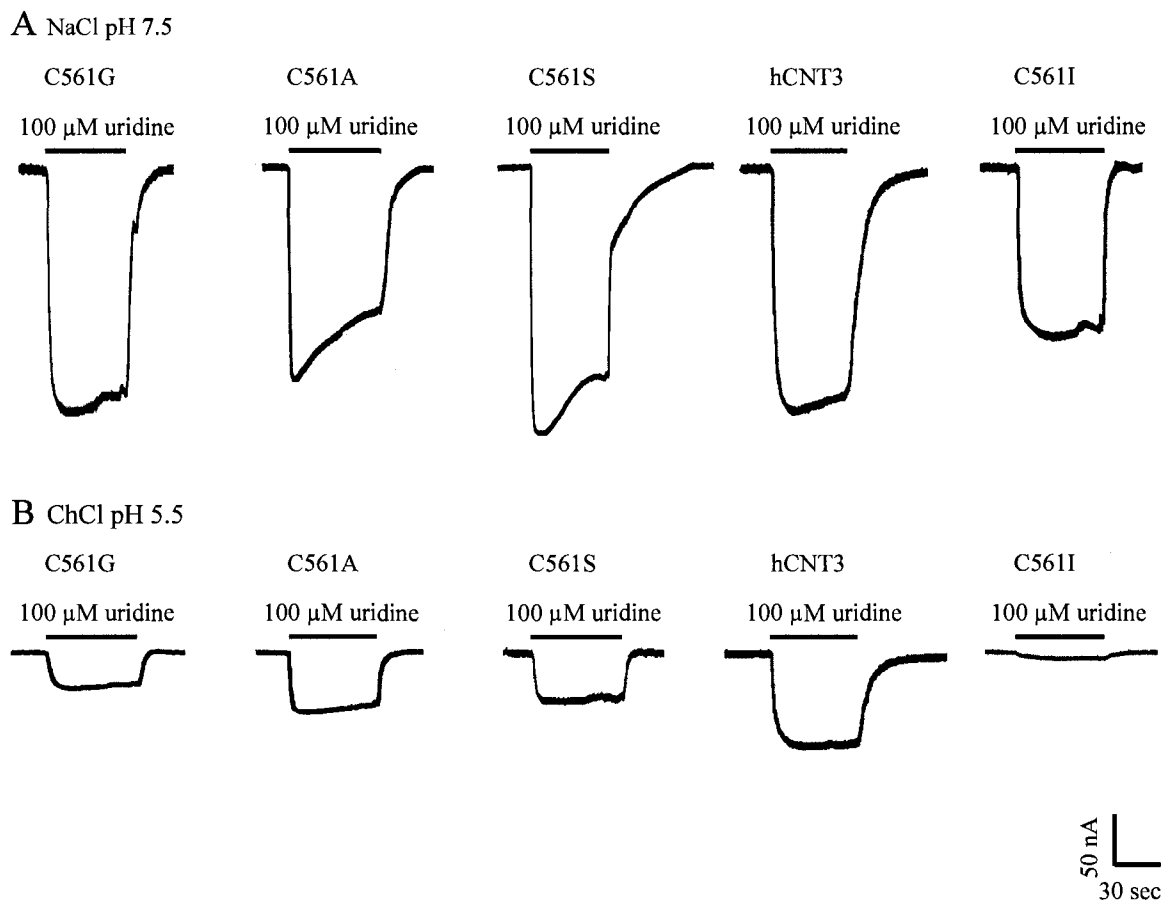


Figure 8-14. Steady-state currents of hCNT3 mutants. Steady-state currents were recorded for wild-type hCNT3 and mutants C561G, C561A, C561S and C561I in oocytes that were voltage-clamped at -90 mV and exposed to 100 μ M uridine in transport medium containing 100 mM NaCl, pH 7.5 (*A*) or 100 mM ChCl, pH 5.5 (*B*). No uridine-induced currents were evident in control water-injected oocytes (data not shown).

Endnotes

¹ Unpublished observation.

Bibliography

1. Zhu, Q., and Casey, J. R. (2007) Topology of transmembrane proteins by scanning cysteine accessibility mutagenesis methodology. *Methods* **41**: 439-450.
2. Kaback, H. R. (2005) Structure and mechanism of the lactose permease. *C. R. Biol.* **328**: 557-567.
3. Heinze, M., Monden, I., and Keller, K. (2004) Cysteine-scanning mutagenesis of transmembrane segment 1 of glucose transporter GLUT1: extracellular accessibility of helix positions. *Biochemistry* **43**: 931-936.
4. Mueckler, M., and Makepeace, C. (2004) Analysis of transmembrane segment 8 of the GLUT1 glucose transporter by cysteine-scanning mutagenesis and substituted cysteine accessibility. *J. Biol. Chem.* **279**: 10494-10499.
5. Fujinaga, J., Tang, X. B., and Casey, J. R. (1999) Topology of the membrane domain of human erythrocyte anion exchange protein, AE1. *J. Biol. Chem.* **274**: 6626-6633.
6. Tang, X. B., Kovacs, M., Sterling, D., and Casey, J. R. (1999) Identification of residues lining the translocation pore of human AE1, plasma membrane anion exchange protein. *J. Biol. Chem.* **274**: 3557-3564.
7. Zhu, Q., Lee, D. W., and Casey, J. R. (2003) Novel topology in C-terminal region of the human plasma membrane anion exchanger, AE1. *J. Biol. Chem.* **278**: 3112-3120.
8. Slepko, E. R., Rainey, J. K., Li, X., Liu, Y., Cheng, F. J., Lindhout, D. A., Sykes, B. D., and Fliegel, L. (2005) Structural and functional characterization of transmembrane segment IV of the NHE isoform of the Na⁺/H⁺ exchanger. *J. Biol. Chem.* **280**: 17863-17872.
9. Zhang, J., Tackaberry, T., Ritzel, M. W., Raborn, T., Barron, G., Baldwin, S. A., Young, J. D., and Cass, C. E. (2006) Cysteine-accessibility analysis of transmembrane domains 11-13 of human concentrative nucleoside transporter 3. *Biochem. J.* **394**: 389-398.

10. Kirsch, R. D., and Joly, E. (1998) An improved PCR-mutagenesis strategy for two-site mutagenesis of sequence swapping between related genes. *Nucleic Acid Res.* **26**: 1848-1850.
11. Yao, S. Y. M., Cass, C. E., and Young, J. D. (2000) The *Xenopus* oocyte expression system for the cDNA cloning and characterization of plasma membrane transport proteins. In *Membrane Transport. A Practical Approach*. (Baldwin, S. A., ed.) Oxford: Oxford University Press; 47-78.
12. Ritzel, M. W. L., Ng, A. M. L., Yao, S. Y. M., Graham, K., Loewen, S. K., Smith, K. M., Ritzel, R. G., Mowles, D. A., Carpenter, P., Chen, X.-Z., Karpinski, E., Hyde, R. J., Baldwin, S. A., Cass, C. E., and Young, J. D. (2001) Molecular identification and characterization of novel human and mouse concentrative Na⁺-nucleoside cotransporter proteins (hCNT3 and mCNT3) broadly selective for purine and pyrimidine nucleosides (system *cib*). *J. Biol. Chem.* **276**: 2914-2927.
13. Damaraju, V. L., Elwi, A. N., Hunter, C., Carpenter, P., Santos, C., Barron, G. M., Sun, X., Baldwin, S. A., Young, J. D., Mackey, J. R., Sawyer, M. B., and Cass, C. E. (2007) Localization of broadly selective equilibrative and concentrative nucleoside transporters, hENT1 and hCNT3, in human kidney. *Am. J. Physiol. Renal Physiol.* **293**: F200-F211.
14. Smith, K. M., Ng, A. M., Yao, S. Y. M., Labeledz, K. A., Knauss, E. E., Wiebe, L. I., Cass, C. E., Baldwin, S. A., Chen, X.-Z., Karpinski, E., and Young, J. D. (2004) Electrophysiological characterization of a recombinant human Na⁺-coupled nucleoside transporter (hCNT1) produced in *Xenopus* oocytes. *J. Physiol.* **558**: 807-823.
15. Yao, S. Y., Ng, A. M., Loewen, S. K., Cass, C. E., Baldwin, S. A., and Young, J. D. (2002) An ancient prevertebrate Na⁺-nucleoside cotransporter (hfCNT) from the Pacific hagfish (*Eptatretus stouti*). *Am. J. Phys. Cell Phys.* **283**: C155-C168.
16. Ritzel, M. W. L., Yao, S. Y. M., Huang, M. Y., Elliot, J. F., Cass, C. E., and Young, J. D. (1997) Molecular cloning and functional expression of cDNAs encoding a human Na⁺-nucleoside cotransporter (hCNT1). *Am. J. Physiol.* **272**: C707-C714.
17. Ritzel, M. W. L., Yao, S. Y. M., Ng, A. M. L., Mackey, J. R., Cass, C. E., and Young, J. D. (1998) Molecular cloning, functional expression and chromosomal

localization of a cDNA encoding a human Na⁺/nucleoside cotransporter (hCNT2) selective for purine nucleosides and uridine. *Mol. Membr. Biol.* **15**: 203-211.

18. Elwi, A. N., Damaraju, V. L., Baldwin, S. A., Young, J. D., Sawyer, M. B., and Cass, C. E. (2006) Renal nucleoside transporters: physiological and clinical implications. *Biochem. Cell. Biol.* **84**: 844-858.
19. Pastor-Anglada, M., Errasti-Murugarren, E., Aymerich, I., and Casado, F. J. (2007) Concentrative nucleoside transporters (CNTs) in epithelia: from absorption to cell signaling. *J. Physiol. Biochem.* **63**: 97-110.
20. Errasti-Murugarren, E., Cano-Soldado, P., Pastor-Anglada, M., and Casado, F. J. (2008) Functional characterization of a nucleoside-derived drug transporter variant (hCNT3C602R) showing altered sodium-binding capacity. *Mol. Pharmacol.* **73**: 379-386.

Chapter 9:

Conserved Glutamate Residues Glu³⁴³ and Glu⁵¹⁹ Provide Mechanistic and Structural Insights into Cation/Nucleoside Cotransport by Human Concentrative Nucleoside Transporter 3 (hCNT3)*

* Publication of a version of this chapter is pending.

Slugoski, M. D., Smith, K. M, Ng, A. M. L., Yao, S. Y. M., Karpinski, E., Cass, C. E., Baldwin, S. A., and Young, J. D. (2008) Conserved glutamate residues E343 and E519 provide mechanistic and structural insights into cation:nucleoside cotransport by human concentrative nucleoside transporter 3 (hCNT3). *J. Biol. Chem.* (submission pending).

Acknowledgements

Dr. Kyla M. Smith was involved in completing the electrophysiology experiments in this study. Mrs. Amy M. L. Ng was involved in construction of the mutants and, together with Dr. Sylvia Y. M. Yao, completed the parallel study in hCNT1. Drs. Edward Karpinski, Carol E. Cass and Stephen A. Baldwin are collaborative principal investigators who assisted with research funding and manuscript preparation. This research was funded by the National Cancer Institute of Canada with funds from the Canadian Cancer Society and Alberta Cancer Board.

Introduction

By virtue of their negative charge and consequent ability to interact directly with coupling cations and/or participate in cation-induced and other protein conformational transitions, glutamate and aspartate residues play key functional and structural roles in a broad spectrum of mammalian and bacterial cation-coupled transporters (1-11). Little, however, is known about their role in concentrative nucleoside transporter (CNT) proteins. The present investigation builds upon a mutagenesis study of conserved glutamate and aspartate residues in hCNT1 (Appendix 4) to undertake a parallel in depth investigation of corresponding residues in hCNT3. By employing the multifunctional capability of hCNT3 as a template for these studies, the present report provides new and novel mechanistic and structural insights into the molecular mechanism(s) of CNT-mediated cation/nucleoside cotransport.

Results

Residues identified for mutagenesis – In the present investigation, site-directed mutagenesis and heterologous expression in *Xenopus laevis* oocytes were employed to analyze the roles of acidic amino acid residues in hCNT3-mediated cation/nucleoside cotransport. The locations of the residues selected for study are shown in Fig. 9-1.

hCNT3 contains ten aspartate and glutamate residues which are conserved in other mammalian members of the CNT protein family (Asp¹⁹², Glu³²⁹, Glu³⁴³, Glu³⁵⁹, Glu⁴¹⁰, Glu⁴³⁴, Asp⁵⁰³, Glu⁵¹⁹, Glu⁵⁵³ and Asp⁵⁸⁶) and were included in the present study for comparison with previous mutagenesis studies of the corresponding residues in hCNT1 (Appendix 4). Also included was one additional glutamate residue unique to, and conserved within, the CNT3/hfCNT subfamily (Glu⁴⁸³). All but one of the selected residues (Asp¹⁹²) were located in the C-terminal half of the protein. In initial mutagenesis experiments, the eleven hCNT3 aspartate and glutamate residues were

individually replaced by the corresponding neutral amino acid (asparagine or glutamine, respectively). All mutations were verified by sequencing the entire coding region of the double-stranded plasmid DNA in both directions. Except for the desired base changes, all sequences were identical to wild-type hCNT3.

Transport activity of hCNT3 mutants – Different from hCNT1/2, hCNT3 transports both purine and pyrimidine nucleosides, and couples nucleoside transport to H⁺, as well as Na⁺ electrochemical gradients (12, Chapters 5 and 6). Each of the eleven hCNT3 mutants were therefore produced in *Xenopus* oocytes and screened for both aspects of hCNT3 functional activity. Measured in Na⁺-containing transport medium (100 mM NaCl, pH 7.5), Table 9-1 presents for each mutant initial rates of transport (1 min flux) of 20 μM radiolabeled uridine (a universal mammalian CNT permeant), inosine (a representative purine nucleoside) and thymidine (a representative pyrimidine nucleoside). Fig. 9-2 compares uridine uptake (20 μM; 1 min flux) in the presence of Na⁺ (100 mM NaCl, pH 7.5) and H⁺ (100 mM ChCl, pH 5.5) with that under Na⁺-free, H⁺-reduced conditions (100 mM ChCl, pH 7.5). The flux values shown in Table 9-1 and Fig. 9-2 (and all subsequent experiments) depict mediated transport activity, defined as the difference in uptake between RNA transcript-injected and control water-injected oocytes. Under all conditions tested, nucleoside uptake by control water-injected oocytes was ≤ 0.1 pmol/oocyte.min⁻¹ (data not shown).

Of the eleven hCNT3 mutants investigated, nine displayed robust levels of broadly selective nucleoside uptake (> 10 pmol/oocyte.min⁻¹) similar to that of wild-type hCNT3 (Table 9-1) and were capable of both Na⁺- and H⁺-dependent uridine uptake (Fig. 9-2). Mutant E343Q, in contrast, exhibited ~ 10% of wild-type hCNT3 uridine transport activity in the presence of Na⁺ and even lower rates of transport in the absence of Na⁺ under acidified or H⁺-reduced conditions. In Na⁺-containing medium, fluxes of inosine and thymidine were reduced to similar extents as uridine. Mutant E519Q was non-functional under all conditions tested. Subsequent studies therefore focused on Glu³⁴³ and Glu⁵¹⁹. Other residues whose mutation produced wild-type functional characteristics were not investigated further.

Additional hCNT3 mutants – To provide additional investigative tools for subsequent experiments, hCNT3 residues Glu³⁴³ and Glu⁵¹⁹ were also mutated to aspartate (to restore the negative charge) and to cysteine (to test for inhibition by thiol-reactive reagents). Table 9-1 and Fig. 9-2 show their properties. Compared to E343Q, reintroduction of the negative charge (mutant E343D) increased both Na⁺- and H⁺-dependent nucleoside influx to ~ 25% of wild-type levels. E343C, in contrast, showed a selective increase in Na⁺-dependent uridine transport activity relative to H⁺-dependent activity. For residue 519, although charge restoration (mutant E519D) returned Na⁺-dependent uridine uptake to wild-type levels, H⁺-dependent uridine uptake in the absence of Na⁺ remained very low. Relative to E519Q, E519C exhibited a small increase in Na⁺-dependent uridine transport activity, with no detectable H⁺-dependent transport. E343D and E519D exhibited wild-type nucleoside selectivity, whereas E343C and E519C preferentially transported uridine relative to inosine and thymidine.

Cell-surface expression of hCNT3 Glu³⁴³ and Glu⁵¹⁹ mutants – To verify that decreased transport activity was not secondary to altered cell-surface expression, oocytes expressing Glu³⁴³ and Glu⁵¹⁹ mutants were subjected to cell-surface labeling with sulfo-NHS-LC-biotin using immobilized streptavidin resin to separate cell-surface protein from that associated with total (plasma + intracellular) membranes. Immunoblots were probed with hCNT3 polyclonal antibodies (13) directed against amino acid residues 45 - 69 of the extramembraneous N-terminal region of the protein. Similar to previous findings (Chapter 8) and consistent with the presence of multiple C-terminal sites of *N*-linked glycosylation, cell surface hCNT3 exhibited discreet immunobands at 100 and 86 kDa (Fig. 9-3). Both these immunobands correspond to glycosylated forms of the transporter, as aglyco-hCNT3 has a lower electrophoretic mobility of 75 kDa (Chapter 8). Antibody specificity was confirmed by lack of immunoreactivity in control, water-injected oocyte membranes.

Patterns of immunoreactivity and staining intensity similar to that of wild-type protein were apparent for E343Q, E343D and E343C (Fig. 9-3A), as well as for E519Q and E519C (Fig. 9-3B). Also present in the plasma membrane, the majority of E519D

immunoreactivity was however associated with the more extensively glycosylated (100 kDa) form of the transporter (Fig. 9-3B). The robust transport activity exhibited by E519D in Table 9-1 and Fig. 9-2 indicates that the mutant's altered glycosylation status had no effect on function. Since all Glu³⁴³ and Glu⁵¹⁹ mutants were present in the plasma membrane similar to wild-type hCNT3, the impaired functional activities of E343Q, E343D, E343C, E519C and E519D resulted from loss of intrinsic transport capability, rather than reduced quantities in plasma membranes.

Nucleoside selectivity of hCNT3 Glu³⁴³ and Glu⁵¹⁹ mutants – There are indications from Table 9-1 that some Glu³⁴³ and Glu⁵¹⁹ mutants may have altered permeant selectivity. To further investigate the role of hCNT3 residues Glu³⁴³ and Glu⁵¹⁹ in nucleoside binding and/or translocation, subsequent experiments investigated the uptake of a full panel of physiological radiolabeled purine and pyrimidine nucleosides (20 μ M) measured in both Na⁺- and H⁺-containing transport medium (100 mM NaCl, pH 7.5 and 100 mM ChCl, pH 5.5, respectively) (Fig. 9-4).

Whereas Na⁺-coupled hCNT3 exhibits broad selectivity for both pyrimidine and purine nucleosides, H⁺-coupled hCNT3 preferentially transports uridine > thymidine, adenosine > cytidine, inosine > guanosine (Chapter 5). These contrasting patterns of nucleoside selectivity were confirmed for wild-type hCNT3 in the present analysis (Fig. 9-4F). Extending the results presented in Table 9-1, a role for hCNT3 residue Glu³⁴³ in nucleoside selectivity was apparent from the nucleoside uptake patterns of both E343Q and E343C. In Na⁺-containing medium, mutant E343Q exhibited a selective 2.6-fold decrease in guanosine influx compared to that for uridine (Fig. 9-4A). Guanosine transport was further decreased (13.6-fold, compared to uridine) in the case of E343C, which also showed an \sim 2-fold reduction in thymidine and inosine transport (Fig. 9-4C). Relative to the pattern of nucleoside transport exhibited by wild-type hCNT3 in H⁺-containing medium (Fig. 9-4F), E343Q and E343C showed increased influx of adenosine, thymidine and cytidine (E343Q), and adenosine and thymidine (E343C). In contrast, restoration of the negative charge (mutant E343D) resulted in wild-type Na⁺- and H⁺-coupled nucleoside selectivity (Fig. 9-4B).

A role in nucleoside selectivity was also apparent for residue Glu⁵¹⁹. In Na⁺-containing medium, mutant E519C exhibited reduced influx of all three purine nucleosides (adenosine, guanosine and inosine) (Fig. 9-4E), while charge replacement (mutant E519D) restored wild-type transport selectivity (Fig. 9-4D). With the exception of very small fluxes of uridine evident for E519D (Fig. 9-4D) (see also Fig. 9-2), neither Glu⁵¹⁹ mutant transported nucleosides in H⁺-containing medium. Mutant E519Q could not be included in this (and subsequent) analyses because of a total lack of Na⁺- and H⁺-coupled transport activity (Table 9-1 and Fig. 9-2).

Uridine transport kinetics of hCNT3 Glu³⁴³ and Glu⁵¹⁹ mutants – Fig. 9-5 presents representative concentration dependence curves for radiolabeled uridine influx in Na⁺-containing medium (100 mM NaCl, pH 7.5) in oocytes producing E343Q, E343D, E343C, E519D, E519C or wild-type hCNT3. Kinetic parameters derived from these curves are summarized in Table 9-2. In good agreement with previous studies (12, Chapter 5), the apparent affinity (K_m) of hCNT3 for uridine influx was $10.9 \pm 0.7 \mu\text{M}$, with a V_{max} value of $23.4 \pm 0.4 \text{ pmol/oocyte}\cdot\text{min}^{-1}$ and a $V_{\text{max}}:K_m$ ratio of 2.1. In comparison to hCNT3, the Glu³⁴³ series of mutants exhibited markedly lower V_{max} values (rank order E343Q > E343D > E343C), with apparent K_m values that were either higher (E343C) or lower (E343Q and E343D) than that of wild-type hCNT3. The $V_{\text{max}}:K_m$ ratio, a measure of transport efficiency, was lowest for E343Q and E343C (both 0.4), and intermediate for the charge-restored mutant E343D (1.3).

In contrast to the Glu³⁴³ series, mutants E519D and E519C exhibited V_{max} values higher than that of wild-type hCNT3. For E519D, this was offset by an ~ 3-fold increase in the apparent K_m value, resulting in an intermediate $V_{\text{max}}:K_m$ ratio (1.1) similar to that of E343D. In contrast, mutant E519C showed a dramatic ~ 80-fold increase in the apparent K_m value, resulting in the lowest $V_{\text{max}}:K_m$ ratio (< 0.1) of all the mutants studied.

Guanosine inhibition kinetics of hCNT3 Glu³⁴³ and Glu⁵¹⁹ mutants – To determine if the decreased uptake of guanosine evident in Na⁺-containing medium for

mutants E343Q, E343C and E519C (Fig. 9-4) reflected altered nucleoside binding, competition experiments were undertaken (Fig. 9-6). Influx of 20 μM radiolabeled uridine by the Glu³⁴³ and Glu⁵¹⁹ series mutants and wild-type hCNT3 was measured in Na⁺-containing medium (100 mM NaCl, pH 7.5) in the presence of increasing concentrations (0 - 1000 μM) of non-labeled guanosine. Because of low solubility, guanosine concentrations greater than 1 mM could not be achieved. In good agreement with the previously reported apparent K_m value of 43 μM for guanosine transport by hCNT3 (12), and consistent with the robust level of guanosine uptake shown by the wild-type transporter in Fig. 9-4F, the IC_{50} value for guanosine inhibition of uridine transport by hCNT3 was $53.7 \pm 8.6 \mu\text{M}$. Corresponding IC_{50} values for guanosine transport-impaired mutants E343Q, E343C and E519C were too high to determine, whereas values of 248 ± 78 and $73.1 \pm 11.3 \mu\text{M}$ were obtained for E343D and E519D, respectively. Therefore, at least in part, decreased guanosine transport reflects alterations to the nucleoside binding pocket.

Na⁺-activation kinetics of hCNT3 Glu³⁴³ and Glu⁵¹⁹ mutants – Na⁺-activation of hCNT3 Glu³⁴³ and Glu⁵¹⁹ mutants was investigated by measuring 20 μM radiolabeled uridine influx as a function of Na⁺ concentration (0 - 100 mM NaCl, pH 8.5) (Fig. 9-7). Kinetic parameters derived from the curves are summarized in Table 9-3. Na⁺-containing medium at pH 8.5 was used to avoid the small, but significant, amount of hCNT3 H⁺-activation that occurs at pH 7.5 (Chapters 5 and 6). Na⁺-coupled uridine transport by hCNT3 at pH 8.5 is kinetically indistinguishable from that at pH 7.5 (Chapters 5 and 8).

In good agreement with previous studies (Chapters 5, 6 and 8), Na⁺-activation of uridine uptake by wild-type hCNT3 occurred with an apparent K_{50} value of 10.5 ± 0.7 mM and a V_{max} value of 10.3 ± 0.4 pmol/oocyte.min⁻¹ (Fig. 9-7F). In marked contrast, E343Q exhibited very low apparent affinity for Na⁺, such that the curve appeared linear with concentration, although uridine uptake at 100 mM Na⁺ was marginally greater than that in the absence of Na⁺ (Fig. 9-7A) (see also Fig. 9-2). Relative to the wild-type transporter, E343D showed a modest increase in apparent affinity for Na⁺ and a marked decrease in V_{max} (Fig. 9-7B). In contrast, E343C

exhibited a dramatic reduction in Na^+ affinity, such that influx approached saturation only at the highest Na^+ concentration used (100 mM) (Fig. 9-7C). E519C showed a similar marked decrease in the apparent binding affinity for Na^+ and the V_{\max} value was also greatly decreased (Fig. 9-7E). Consistent, however, with the robust transport activity shown in Fig. 9-2, E519D exhibited a small increase in apparent affinity for Na^+ with no change in V_{\max} (Fig. 9-7D). All curves were sigmoidal, with calculated Hill coefficients ≥ 1.4 .

H⁺-activation kinetics of hCNT3 Glu³⁴³ and Glu⁵¹⁹ mutants – H^+ -activation of hCNT3 Glu³⁴³ and Glu⁵¹⁹ mutants was investigated by measuring 20 μM radiolabeled uridine influx in 100 mM ChCl transport medium at pH values ranging from 4.5 to 8.5 (Fig. 9-8). Kinetic parameters derived from the curves are summarized alongside those for Na^+ in Table 9-3. In good agreement with previous studies, H^+ -coupled uridine uptake by wild-type hCNT3 occurred with an apparent K_{50} value of 495 ± 106 nM and a corresponding V_{\max} value of 8.7 ± 0.4 pmol/oocyte.min⁻¹ (Chapters 5, 7 and 8) (Fig. 9-8E). Consistent with Fig. 9-2, the H^+ -activation curve for E343Q was linear and independent of H^+ concentration (Fig. 9-8A). The corresponding H^+ -activation curves for E343D (Fig. 9-8B), E343C (Fig. 9-8C) and E519D (Fig. 9-8D) exhibited decreases in both apparent K_{50} and V_{\max} values compared to wild-type hCNT3. Of these, E343D and E519D exhibited the most pronounced shift in H^+ apparent affinity, while E343C and E519D had the lowest V_{\max} values. Similar to hCNT3, Hill coefficients were between 0.7 and 0.8. H^+ -activation kinetics were not determined for mutant E519C which lacked transport activity in H^+ -containing transport medium (Fig. 9-2).

Steady-state currents of hCNT3 Glu³⁴³ and Glu⁵¹⁹ mutants – Complementary to the uridine flux studies of cation dependence shown in Fig. 9-2, steady-state electrophysiological experiments were undertaken to measure uridine-induced Na^+ and H^+ inward currents in oocytes producing E343Q, E343D, E343C, E519D, E519C or, as a control, hCNT3. Representative recordings comparing currents evoked by uridine (200 μM) in the presence of Na^+ (100 mM NaCl, pH 8.5) and H^+ (100 mM ChCl, pH 5.5), as well as in 100 mM ChCl at pH 7.5 and pH 8.5 are shown in Figs. 9-

9A and B. Fig. 9-9C depicts mean currents for ≥ 4 oocytes normalized to that obtained in 100 mM NaCl, pH 8.5.

As demonstrated in previous studies (Chapter 5), wild-type hCNT3 exhibited large inward currents for both Na^+ and H^+ , the latter decreasing as a function of pH (5.5 > 7.5 > 8.5) (Figs. 9-9B and C). No currents were observed in control water-injected oocytes (data not shown). Smaller uridine-induced Na^+ currents were also apparent for all three Glu³⁴³ mutants (Figs. 9-9A and C). Uridine-induced H^+ currents were also evident for E343D and, to a much lesser extent, E343C (Figs. 9-9A and C). Consistent, however, with a lack of H^+ -dependence in radioisotope flux studies (Figs. 9-2 and 9-8A), mutant E343Q exhibited small uridine-induced currents in the absence of Na^+ that were of similar magnitude irrespective of the H^+ concentration in the medium (Figs. 9-9A and C). Increasing the uridine concentration to 1 mM did not influence the magnitude of these currents, either at pH 5.5 or pH 8.5 (Fig. 9-9C). Uridine-induced Na^+ currents were also apparent for E519D and E519C, while H^+ currents were very small (E519D) or not detectable (E519C) (Figs. 9-9B and C).

Cation:nucleoside coupling ratios of hCNT3 Glu³⁴³ and Glu⁵¹⁹ mutants – Na^+ :nucleoside and H^+ :nucleoside stoichiometries of E343C, E343Q, E343D, E519C, E519D and, as a control, wild-type hCNT3 were determined by simultaneously measuring cation currents and radiolabeled uridine uptake under voltage-clamp conditions, as described previously (14, Chapters 5 and 6). Na^+ and H^+ currents were determined in transport media containing 100 mM NaCl at pH 8.5 and 100 mM ChCl at pH 5.5, respectively. The uridine concentration was 200 μM . Charge *versus* flux plots for groups of individual oocytes producing each of the recombinant transporters are shown for Na^+ in Fig. 9-10. Na^+ :uridine stoichiometries, derived from linear regression analyses of the data, together with corresponding H^+ :uridine stoichiometries (data plots not shown) are presented in Table 9-4.

Consistent with mutant E343Q functioning as a partially uncoupled uridine-gated Na^+ channel, there was no correlation between Na^+ current and radiolabeled uridine uptake, and the charge:flux ratios for individual E343Q-producing oocytes

ranged from 0.8 to 39 (Fig. 9-10A and Table 9-4). A similar lack of correlation between Na^+ current and radiolabeled uridine uptake, but with lower overall Na^+ -currents, was also observed for mutant E343C; in this case, charge:flux ratios for individual E343C-producing oocytes ranged from 0.6 to 2.2 (Fig. 9-10C and Table 9-4). Channel-like activity for mutant E343Q also extended to currents measured in 100 mM ChCl, pH 5.5. H^+ :uridine coupling ratios could not, however, be determined for E343C because of low levels of H^+ -coupled activity (Figs. 9-2 and 9-9A). In marked contrast, restoration of the negative charge at this position (mutant E343D) gave 2:1 and 1:1 Na^+ :uridine and H^+ :uridine stoichiometries, respectively, thus restoring wild-type characteristics (Fig. 9-10B and Table 9-4).

Similar to wild-type hCNT3, E519D also exhibited a Na^+ :uridine coupling ratio of 2:1 (Fig. 9-10D and Table 9-4). Different from this, however, mutant E519C gave a calculated Na^+ :uridine stoichiometry of 0.84 ± 0.04 , suggesting cotransport of only one Na^+ per uridine molecule (Fig. 9-10E and Table 9-4). A H^+ :uridine coupling ratio for mutant E519C could not be determined due to a total lack of transport activity in the absence of Na^+ (Fig. 9-2 and Fig. 9-9B) and that for E519D was 0.61 ± 0.09 (Table 9-4).

Current-voltage (I-V) relationships of E343Q – As a further test of the channel-like behavior of mutant E343Q, Fig. 9-11A shows current-voltage (I-V) curves for E343Q-producing oocytes generated as the difference between steady-state currents recorded in the presence and absence of uridine. Measured in Na^+ -containing (100 mM NaCl, pH 8.5), H^+ -containing (100 mM ChCl, pH 5.5) and Na^+ -free, H^+ -reduced (100 mM ChCl, pH 8.5) transport media, E343Q-mediated currents evoked by uridine (100 μM) at potentials between -110 and +60 mV were voltage-dependent and, in contrast to those of wild-type hCNT3 (Chapter 5), reversed polarity at membrane potentials of $\sim +50$ and -50 mV in the presence and absence of Na^+ , respectively. Consistent with the current data in Figs. 9-9A and C, curves in H^+ -containing (100 mM ChCl, pH 5.5) and Na^+ -free, H^+ -reduced (100 mM ChCl, pH 8.5) transport media overlapped. No uridine-induced currents were observed in control water-injected oocytes (data not shown).

Uridine-evoked H^+ currents (100 mM ChCl, pH 5.5) were measured in E343Q-producing oocytes voltage-clamped at representative holding potentials (V_h) of -90, -50, -30, -10 and +10 mV. As shown in Fig. 9-11B, the current induced by 100 μ M uridine at V_h -90 mV was inward, close to zero at -50 mV and outward at -30, -10 and +10 mV. In marked contrast, the same experiment revealed no such outward current for wild-type hCNT3 under equivalent conditions (data not shown). A corresponding direct demonstration of outward Na^+ currents mediated by mutant E343Q was precluded by unstable baseline currents in Na^+ -containing transport medium at $V_h \geq +10$ mV.

Na⁺-activation kinetics of hCNT3 mutant E519C determined by electrophysiology – The Na^+ -activation kinetics of E519C were also investigated by electrophysiology. Fig. 9-12A depicts the relationship between Na^+ concentration and 200 μ M uridine-evoked current for oocytes expressing E519C clamped at a membrane holding potential of -90 mV. For comparison, the corresponding Na^+ -activation curve for wild-type hCNT3 was also determined (Fig. 9-12B). Currents from individual oocytes were normalized to their predicted I_{max} values and subsequently averaged to produce mean kinetic parameters. Similar to the radioisotope flux data in Fig. 9-7E, E519C exhibited an apparent K_{50} value for Na^+ -coupled uridine uptake of 59.5 ± 4.0 mM and a corresponding Hill coefficient of 2.1 ± 0.4 . In agreement with previous studies (Chapters 5, 6 and 8), the apparent K_{50} value for Na^+ -coupled uridine uptake by wild-type hCNT3 under these conditions was 1.6 ± 0.1 mM, and the corresponding Hill coefficient was 1.7 ± 0.6 . As previously determined, the difference in apparent K_{50} value for hCNT3 when determined by electrophysiology (1.6 mM, Fig. 9-12B) compared to radioisotope flux analysis (10.3 mM, Fig. 9-7F and Table 9-3) reflects the difference in membrane potential under the two experimental conditions (-90 *versus* \sim -40 mV, respectively) (Chapters 5 and 8). In contrast, the similar low apparent affinity of E519C for Na^+ in Figs. 9-7E and 9-12A suggests a loss of voltage-dependence of Na^+ K_{50} for this mutant.

p-Chloromercuribenzenesulfonate (PCMBS) inhibition of hCNT3 E343C and E519C – Residues lining the translocation pore can be identified through the use of

hydrophilic thiol-reactive reagents such as PCMBS. In a final series of experiments, uptake of 20 μM radiolabeled uridine was measured in oocytes producing E343C, E519C or hCNT3 incubated in the presence and absence of 200 μM PCMBS and in the presence and absence of 20 mM extracellular uridine. Exposure to PCMBS and uridine was performed on ice to minimize passage across the oocyte plasma membrane. Since wild-type hCNT3 contains a conformationally mobile cysteine residue (Cys⁵⁶¹) that becomes exposed to PCMBS in the H⁺-bound state of the transporter (Chapter 7), reactivity to PCMBS was investigated in Na⁺-containing transport medium (100 mM NaCl) at pH 8.5 (Fig. 9-13). Both E343C and E519C showed marked inhibition by PCMBS consistent with pore-lining status. In the case of E343C, this inhibition was prevented by uridine, suggesting a location close to or within the nucleoside binding pocket. A small amount of uridine protection was also seen for E519C. Under the same conditions, and in agreement with previous results (Chapter 7), there was no inhibition of the wild-type transporter.

Discussion

hCNT3 is the most recently discovered and functionally versatile of three human members of the SLC28 (CNT) protein family. It is 691 amino acids in length, has a 13 (or possibly 15) transmembrane domain (TM) architecture, and utilizes electrochemical gradients of both Na⁺ and H⁺ to accumulate a broad range of pyrimidine and purine nucleosides and nucleoside drugs within cells (12, Chapters 5 and 6). Paralogs hCNT1 and hCNT2, in contrast, have a similar predicted membrane topology, but function predominantly as Na⁺-coupled transporters, and are pyrimidine nucleoside-selective and purine nucleoside-selective, respectively (15, 16). More widely distributed in cells and tissues than hCNT1 or hCNT2 (12), and with a central role in renal transepithelial nucleoside and nucleoside drug transport (13, 17), the multifunctional capability of hCNT3 and robust expression of the recombinant transporter in *Xenopus* oocytes makes it the protein of choice for systematic in depth molecular characterization by site-directed mutagenesis and substituted cysteine accessibility method (SCAM) analysis.

Additionally, hCNT3 mutants are less likely to be retained in intracellular membranes than corresponding mutants of hCNT1/2; since expression at the *Xenopus* oocyte cell surface is a prerequisite for functional analysis, this characteristic is a further advantage of using hCNT3 as a template for mutagenesis studies.

Eleven highly-conserved negatively charged residues are present in hCNT3. Ten of these are also present in hCNT1/2, while one is unique to CNT3/hfCNT subfamily members. In a previous study of hCNT1, five aspartate and glutamate residues (Glu³⁰⁸, Glu³²², Asp⁴⁸², Glu⁴⁹⁸ and Glu⁵³²) were identified as having actual or potential roles in hCNT1 Na⁺/nucleoside cotransport (Appendix 4). The hCNT1 mutants E308D/Q, E322D/Q and E498D exhibited diminished V_{\max} values and increased values for Na⁺ K_{50} and/or uridine K_m . E322Q additionally exhibited variable Na⁺:nucleoside coupling ratios consistent with possible uridine-gated channel-like transport activity (Appendix 4). hCNT1 mutants D482N, E498Q and E532Q/D were retained in intracellular membranes and, therefore, not amenable to functional analysis (Appendix 4). The present study presents a parallel analysis of conserved aspartate and glutamate residues in hCNT3. To facilitate comparison between the present study and the previous investigation of acidic amino acids in hCNT1 (Appendix 4), Table 9-5 provides a side-by-side comparison of hCNT3 and corresponding hCNT1 residue positions. The five hCNT3 residues equivalent to those previously identified in hCNT1 are Glu³²⁹, Glu³⁴³, Asp⁵⁰³, Glu⁵¹⁹ and Glu⁵⁵³.

As summarized in Table 9-5, substitution of nine of the eleven acidic amino acid residues in hCNT3 with the corresponding neutral amino acid was without effect. These included Glu³²⁹ (mutant E329Q), Asp⁵⁰³ (mutant D503N) and Glu⁵⁵³ (mutant E553Q). The latter two equivalent mutants in hCNT1 were retained in intracellular membranes and thus, both of these residues can now be excluded from having roles in CNT structure and function. In contrast, the hCNT1 mutant E308Q (equivalent to hCNT3 E329Q) was processed normally to the cell surface, but exhibited markedly impaired transport activity (Appendix 4). Since hCNT3 E329Q exhibited wild-type transport function (Fig. 9-2 and Table 9-1), it is possible that this residue has roles specific to hCNT1 or, perhaps, to the CNT1/CNT2 subfamily.

Subsequent studies of hCNT3 acidic amino acid residues therefore focused exclusively on the remaining two residue positions (Glu³⁴³ and Glu⁵¹⁹) whose mutation to glutamine led to compromised functional activity. In addition to insertion of the corresponding neutral amino acid at these positions, hCNT3 Glu³⁴³ and Glu⁵¹⁹ were also mutated to aspartate and cysteine. All constructs were targeted to the oocyte plasma membrane in amounts similar to wild-type hCNT3 (Fig. 9-3), enabling their detailed characterization by both radioisotope flux and electrophysiological techniques.

Located in TM 7 (Fig. 9-1), mutation of Glu³⁴³ to glutamine (E343Q), aspartate (E343D) and cysteine (E343C) influenced both nucleoside and cation interactions. E343Q retained the ability to bind and transport uridine, although the V_{\max} value for uridine transport was decreased 14-fold compared to wild-type hCNT3 (Fig. 9-4A and Table 9-2). E343Q also retained the ability to bind and transport Na⁺, but with low apparent affinity. Thus, uridine influx (Fig. 9-2) and uridine-induced currents (Fig. 9-9A) were higher in Na⁺-containing than in Na⁺-free media, while cation-activation analysis revealed a weak linear relationship between Na⁺ concentration and uridine influx (Fig. 9-7A). However, no H⁺-dependence of transport was evident (Figs. 9-2 and 9-8A) and, while small uridine-induced currents were observed in Na⁺-free media, the magnitudes of these currents did not respond to changes in external pH (Figs. 9-9A and C). Extending previous findings for Na⁺ in the case of the corresponding mutant in hCNT1 (Appendix 4), charge:flux experiments revealed uncoupled uridine-induced cation movement through the transporter in both Na⁺- and H⁺-containing transport media, with maximum apparent cation:nucleoside coupling ratios of ~ 40:1 (Fig. 9-10A and Table 9-4). Since the range of apparent coupling ratios encountered in these experiments was similar in both Na⁺- and H⁺-containing transport media (Fig. 9-10A and Table 9-4) and since H⁺ movement did not seem to account for the small pH-independent currents seen under the latter condition (Figs. 9-9A and C), the small local Na⁺ concentrations in the immediate vicinity of the oocyte cell surface, in conjunction with the Na⁺ channel-like properties of the mutant, may have been responsible for the minor E343Q currents seen under otherwise Na⁺-free conditions. The broad nucleoside selectivity shown by E343Q in Na⁺- and H⁺-

containing transport media and the similarly impaired transport of guanosine under both conditions supports this possibility (Fig. 9-4A). Providing important additional evidence of uridine-gated Na^+ channel-like transport activity, hCNT3 mutant E343Q exhibited an ohmic relationship between uridine-induced current and membrane potential (Fig. 9-11). Residues of other transporters for which mutation causes channel-like behavior include Asp²⁰⁴ of the human Na^+ -dependent glucose transporter SGLT1 and Asn¹⁷⁷ of the rat 5-hydroxytryptamine transporter (18, 19).

Restoring the negative charge at hCNT3 residue position Glu³⁴³ by mutation to aspartate (E343D) recovered the wild-type phenotype with respect to both nucleoside and cation selectivity and apparent affinity, although V_{max} values for uridine transport and cation-activation were 4- to 7-fold lower than those for hCNT3 (Tables 9-2 and 9-3). Thus, both the presence and positioning of the negative charge at residue position Glu³⁴³ are critical for normal functional activity.

Further support for the importance of hCNT3 residue Glu³⁴³ arose from mutation to cysteine (E343C). Compromised kinetically with respect to both uridine transport (Fig. 9-5C) and Na^+/H^+ -activation (Figs. 9-7C and 9-8C), E343C exhibited characteristics similar to E343Q, including very low uridine evoked H^+ current activity relative to Na^+ (Figs. 9-9A and C) and variable Na^+ -coupling (Fig. 9-10C and Table 9-4). Although partially uncoupled in a manner similar to E343Q, E343C nevertheless retained sigmoid Na^+ -activation kinetics, indicating retention of both Na^+ -binding sites. Similar to E343Q, E343C showed decreased transport of guanosine, although to a greater extent (Figs. 9-4A and C). There was also diminished transport of other nucleosides (Fig. 9-4C). Therefore, E343C provides additional evidence for functions of this residue position in both cation coupling and nucleoside specificity.

Mutations of hCNT3 Glu⁵¹⁹ revealed a second glutamate residue with key roles in CNT cation/nucleoside cotransport. This residue resides in putative TM 11A (Fig. 9-1) and is centrally positioned in the highly conserved (G/A)XKX₃NEFVA(Y/M/F) motif common to all eukaryote and prokaryote CNTs. Previous indications for a role of this residue in CNT function comes from studies of

the corresponding residue in hCNT1, for which mutant E498D exhibited a modest 50% reduction in V_{\max} value for Na^+ and ~ 2 -fold increase in apparent K_m value for uridine (Appendix 4). Anticipated to show more pronounced phenotypic changes, hCNT1 mutant E498Q was not processed to the cell surface in oocytes (Appendix 4). hCNT1 E498C was also non-functional, presumably for the same reason (Appendix 4). In the case of hCNT3, however, all three hCNT3 Glu⁵¹⁹ mutants (E519Q, E519D and E519C) were processed to the oocyte cell surface similar to wild-type hCNT3 (Fig. 9-3B).

Despite its confirmed presence in the oocyte plasma membrane, hCNT3 mutant E519Q showed no measurable transport activity (Fig. 9-2 and Table 9-1) and is the first reported example of a mutation in hCNT3 rendering the protein totally non-functional. Mutation of Glu⁵¹⁹ to aspartate (E519D), which restored a negative charge at this position, also fully restored Na^+ -coupled functional activity and only small kinetic differences in uridine K_m and V_{\max} and Na^+ K_{50} and V_{\max} values distinguish E519D from the wild-type transporter (Figs. 9-5D and 9-7D, and Tables 9-2 and 9-3). Remarkably however, this protein showed severely reduced H^+ -dependent uridine uptake (~ 10 -fold decrease in V_{\max} compared to hCNT3) (Figs. 9-2 and 9-8D and Table 9-3) and barely detectable uridine-evoked H^+ currents (Figs. 9-9B and C). Altered interaction with H^+ was also evident for E519C and, illustrating this, Figs. 9-9B and C demonstrate total abolition of uridine-evoked H^+ current activity. With respect to other characteristics, E519C showed an altered preference for pyrimidine nucleosides compared to purine nucleosides (uridine > cytidine, thymidine > adenosine, inosine > guanosine) (Fig. 9-4E) and, kinetically, exhibited a > 80-fold decrease in the apparent binding affinity for uridine (Fig. 9-5E and Table 9-2) and an ~ 5 -fold decrease in both Na^+ binding affinity and V_{\max} value (Fig. 9-7E and Table 9-3). In contrast to wild-type hCNT3 (Chapter 5), E519C also exhibited an apparent absence of voltage-dependence of Na^+ K_{50} (Fig. 9-12A). Of even greater significance, flux/charge experiments demonstrated a change in Na^+ :nucleoside stoichiometry from 2:1 to 1:1 (Fig. 9-10E).

Recently, a naturally-occurring hCNT3 variant has been described in the Spanish population in which a T/C transition leads to the substitution of Cys⁶⁰² by arginine (20). This single amino acid replacement in TM 13 leads to a shift in Hill coefficient consistent with a possible change in Na⁺:nucleoside stoichiometry from 2:1 to 1:1. In contrast, hCNT3 mutant E519C retained a sigmoidal Na⁺-activation curve (Fig. 9-7E). With a calculated Hill coefficient of 1.9 (Table 9-3), it is possible that E519C still binds two Na⁺, but that only one is translocated.

In studies of wild-type hCNT1 and hCNT3, it has been established that Na⁺ binds to the transporter first, increasing the affinity for nucleoside, which then binds second (14, Chapter 5). To minimize the potential effects of altered Na⁺ apparent affinity on uridine kinetic parameters, experiments to investigate uridine transport kinetics were undertaken at the maximum possible Na⁺ concentration of 100 mM. It is nevertheless possible that the very large reduction in uridine apparent affinity observed for E519C is, at least in part, secondary to the low apparent binding affinity for Na⁺ and the change in Na⁺:nucleoside coupling ratio from 2:1 to 1:1.

CNTs are currently defined by 13 putative TMs (Fig. 9-1), with two additional TMs (5A and 11A) weakly predicted by computer algorithms (21). Experimental studies using site-specific antibodies and introduced glycosylation sites have confirmed the intracellular location of the N-terminus, the cytoplasmic exposure of the loop linking TMs 4 and 5, and the extracellular location of the C-terminus (21). Both a 13 and 15 TM membrane architecture are consistent with these landmarks. SCAM analysis of TMs 11, 12 and 13 of a functional cysteine-less version of hCNT3 (hCNT3C-) using methanethiosulfonate (MTS) reagents (22) and of TM 12 using PCMBs (Chapter 7), as well as other structure/function studies (*e.g.* 23, Chapter 4) are also consistent with both models.

In the present investigation, the introduced cysteine residues in mutants E343C and E519C were accessible to the membrane-impermeant reagent PCMBs, resulting in marked inhibition of uridine transport activity and suggesting that both residues are pore-lining (Fig. 9-13). In the case of E343C (and to a lesser extent for

E519C), this inhibition was prevented by externally applied uridine, implying a location within, or close to, the nucleoside binding pocket. Similarly, the equivalent TM 7 mutant of hCNT1, E322C, showed uridine-protectable inhibition by both PCMBS and the MTS reagent 2-aminoethyl methanethiosulfonate hydrobromide (MTSEA), confirming that there are topological similarities between the two transporters (Appendix 4). Supporting the pore-lining location of hCNT3 E343, the corresponding residue in hCNT3C-, when converted to cysteine, also results in PCMBS inhibition of uridine uptake (24). Based upon the pattern of PCMBS inhibition and uridine protection observed in SCAM analysis of hCNT3 TM 12 (Chapter 7), it is likely that the uridine binding pocket is centrally positioned approximately half-way across the membrane. With this expectation, the location of Glu³³² close to one end of TM 7 becomes diagnostic with respect to the orientation of the helix and favors a 15 TM rather than 13 TM membrane architecture. This is because insertion of region 5A into the membrane reverses the orientation of subsequent TMs, including TM 7, placing Glu³⁴³ deep within the translocation pore immediately distal to the proposed location of the uridine binding site (Fig. 9-1, *inset*).

From a mechanistic standpoint, this places Glu³⁴³ in a position consistent with this residue forming part of the internal gate of the transporter vestibule. Such a function is strongly suggested by the kinetic characteristics of Glu³⁴³ mutants, where large reductions in V_{\max} relative to wild-type hCNT3 were a consistent feature (Tables 9-2 and 9-3) and, diagnostically, by the partially uncoupled channel-like activity of mutant hCNT3 E343Q and, to a lesser extent, E343C (Figs. 9-10A, 9-10C and 9-11, and Table 9-4). Supported by parallel findings of altered Na⁺-coupling for hCNT1 mutant E322Q (Appendix 4), it was established that both Na⁺- and H⁺-coupling modes of hCNT3 function were compromised and, additionally, that the mutant transporters manifested atypical steady-state currents not seen in the wild-type protein.

A paradigm for the role proposed here for hCNT3 Glu³⁴³ can be found in the potential gating function of negatively charged residues within the common

cation/solute translocation pore of the recently solved three-dimensional crystal structure of the *Aquifex aeolicus* LeuT_{Aa} Na⁺/Cl⁻-dependent leucine transporter (25). In this protein, negatively-charged residues stabilize the transporter in a closed conformation that occludes closely-associated Na⁺ and leucine binding sites halfway across the membrane lipid bilayer. Similar to the mammalian GAT1 Na⁺/Cl⁻-dependent GABA transporter (26, 27), a member of the same protein family as LeuT_{Aa}, hCNT3 (and hCNT1) presteady-state currents largely reflect binding and potential occlusion of extracellular Na⁺. Consistent with a potential gating function for hCNT1 E322, its mutation markedly decreased hCNT1 presteady-state currents (Appendix 4). Examples of other transporters where glutamate and aspartate residues are proposed to stabilize conformational transitions within the transport cycle include the *E. coli* PutP Na⁺/proline transporter (5) and LacY H⁺-coupled lactose permease (2, 3, 28). Introduction of cysteine at position Glu³⁴³ in place of glutamine led to a marginally less severe transport phenotype, possibly because the slight electronegative character of the sulphur atom in part is mitigated against loss of the glutamate negative charge.

As illustrated in Fig. 9-1, hCNT3 Glu⁵¹⁹ and the conserved motif of which it is a part are located in a region of the protein that is potentially exofacial (in the loop linking TMs 11 and 12) or membrane-associated (TM 11A). The functional significance of Glu⁵¹⁹ revealed by the present study strongly favors the latter possibility. In the 15 TM model of hCNT3 topology, region 11A is predicted to be transmembrane (as opposed to a re-entrant loop) in order to preserve the exofacial orientation of the glycosylated C-terminus of the protein. With regions 5A and 11A both transmembrane, the whole of the central TM 6 - 11 region of the protein, not just TM 7, would be in an opposite orientation (Fig. 9-1, *inset*).

hCNT3 and the other CNT3 subfamily member hfCNT each have two cation binding sites (29, Chapters 5 and 6). One hCNT3 site is Na⁺-specific, whereas the second site may functionally interact with both H⁺ and Na⁺ (Chapters 5 and 6). In the case of hfCNT, both sites are specific for Na⁺ (28). hCNT1 and hCNT2, in contrast, have single Na⁺-specific sites (14, Chapter 6). *C. albicans* CaCNT (30) also has a

single cation binding site, in this case H⁺-specific. Other CNT family members that are exclusively H⁺-coupled, and presumed also to have single H⁺-specific binding sites, include *E. coli* NupC (Appendix 2) and *C. elegans* CeCNT3 (31). A central question in CNT energetics is the structural, functional and evolutionary relationship between these various cation binding sites in different CNT family members. In the case of human and other mammalian CNTs, for example, which of the two cation-binding sites of hCNT3 corresponds to the single Na⁺-specific site of hCNT1/2? Another key question in CNT biology is the role of the (G/A)XKX₃NEFVA(Y/M/F) motif. The present findings with respect to hCNT3 Glu⁵¹⁹ provide insights into both these issues. Since mutation of Glu⁵¹⁹ led to (i) complete abolition of transport function (mutant E519Q), (ii) selective reduction of H⁺-dependence (mutant E519D), and (iii) loss of H⁺-dependence in conjunction with a change in Na⁺:uridine stoichiometry from 2:1 to 1:1 (mutant E519C), this residue is shown to be of crucial importance to cation-coupling perhaps, as suggested by the very low Na⁺-binding affinity of E519C, through direct electrostatic interaction with the coupling cation. Alternatively, Glu⁵¹⁹ may facilitate cation-induced conformational transitions. Furthermore, Glu⁵¹⁹ appears to be specifically linked to the hCNT3 cation binding site common to Na⁺ and H⁺. This being the case, and given that Glu⁵¹⁹ and the motif to which it belongs are present in all CNTs, the shared Na⁺/H⁺ binding site of hCNT3 is likely to be the equivalent of the Na⁺-specific site of hCNT1/2 and the H⁺-specific site of NupC, CeCNT3 and CaCNT. As further evidence that changes in CNT cation specificity can be achieved through only minor structural alterations to the translocation pore, substitution of hCNT3 TM 12 residue Cys⁵⁶¹ with larger neutral amino acids also leads to selective loss of H⁺-coupling (Chapter 8).

Finally, and similar to GAT1 (27), electrophysiological studies of presteady-state currents predict that an occlusion step occurs between the binding of successive Na⁺ ions to hCNT3 prior to transport (32). Thus, Na⁺ (or H⁺) binding to the initial (primary) site in hCNT3 may result in a conformational change (occlusion step) thereby resulting in the second (auxiliary) Na⁺-site becoming available. If substitution of Glu⁵¹⁹ with glutamine totally abolishes cation binding to the first of these sites, then complete loss of transport function, as occurs for E519Q, would be

anticipated. By analogy to the effect of introducing cysteine at position Glu⁵¹⁹, it is possible that the slight electronegative character of the sulphur atom in mutant E519C is sufficient to allow low-affinity binding of Na⁺ to the first site, enabling the observed low-efficiency (and sigmoidal) Na⁺-coupled nucleoside transport to occur.

In conclusion, therefore, the present investigation builds upon a parallel study of glutamate and aspartate residues in hCNT1 (Appendix 4) to reveal important new and novel insights into the mechanism(s) of cation-coupling of hCNT3 and other CNT family members. In addition to primary effects on cation coupling, mutation of both Glu³⁴³ and Glu⁵¹⁹ produced changes in nucleoside selectivity, confirming close-proximity integration of cation and nucleoside binding and transport within a common translocation pore, an emerging theme common to other recent investigations of hCNT structure/function relationships (Chapters 4, 5 and 7, Appendix 4). Structurally, the results presented here provide valuable support for a revised 15 TM model of CNT membrane architecture.

Table 9-1. Mediated uptake of radiolabeled nucleosides by hCNT3 and mutants. Uptake of 20 μ M radiolabeled uridine, inosine and thymidine in 100 mM NaCl, pH 7.5 was measured in oocytes expressing hCNT3 mutants or wild-type hCNT3. Values were corrected for basal non-mediated uptake in control water-injected oocytes and are the means \pm SEM of 10 - 12 oocytes.

	Mediated Nucleoside Uptake (pmol/oocyte.min ⁻¹)		
	Uridine	Inosine	Thymidine
D192N	12.2 \pm 0.7	15.3 \pm 0.6	12.5 \pm 0.4
E329Q	16.5 \pm 0.4	19.4 \pm 0.9	13.2 \pm 0.6
E343Q	1.7 \pm 0.1	1.3 \pm 0.1	1.9 \pm 0.1
E343D	4.5 \pm 0.6	3.3 \pm 0.3	4.4 \pm 0.6
E343C	4.0 \pm 0.2	1.1 \pm 0.1	1.9 \pm 0.3
E359Q	14.8 \pm 0.7	18.8 \pm 0.9	13.7 \pm 0.7
E410Q	16.9 \pm 1.1	17.4 \pm 0.9	13.4 \pm 0.6
E434Q	14.3 \pm 0.6	18.5 \pm 1.0	13.8 \pm 0.5
E483Q	15.6 \pm 0.9	18.8 \pm 0.6	11.6 \pm 0.4
D503N	11.7 \pm 0.8	14.6 \pm 0.9	10.4 \pm 0.8
E519Q	< 0.1	< 0.1	< 0.1
E519D	20.7 \pm 0.7	13.5 \pm 0.9	9.6 \pm 0.6
E519C	0.6 \pm 0.1	0.1 \pm 0.1	0.2 \pm 0.1
E553Q	20.8 \pm 1.1	24.4 \pm 0.7	14.2 \pm 0.6
D586N	19.7 \pm 1.0	21.0 \pm 0.8	13.4 \pm 0.5
hCNT3	17.4 \pm 1.1	18.7 \pm 1.0	15.6 \pm 0.7

Table 9-2. Kinetic parameters for uridine uptake mediated by hCNT3 and mutants.

	Apparent K_m^a (μM)	V_{max}^a ($\text{pmol/oocytes}\cdot\text{min}^{-1}$)	$V_{\text{max}}:K_m$ ratio
E343Q	3.9 ± 0.7	1.7 ± 0.1	0.4
E343D	2.4 ± 0.3	3.2 ± 0.1	1.3
E343C	18.9 ± 0.9	7.2 ± 0.1	0.4
E519D	35.0 ± 1.6	40.1 ± 0.5	1.1
E519C	876 ± 57	39.0 ± 0.9	< 0.1
hCNT3	10.9 ± 0.7	23.4 ± 0.4	2.1

^a, from Fig. 9-5.

Table 9-3. Na⁺- and H⁺-activation kinetic parameters for hCNT3 and mutants.

	Na ⁺ -Activation Kinetic Parameters			H ⁺ -Activation Kinetic Parameters		
	Apparent <i>K</i> ₅₀ (mM)	<i>V</i> _{max} (pmol/oocyte. min ⁻¹)	Hill Coefficient	Apparent <i>K</i> ₅₀ (nM)	<i>V</i> _{max} (pmol/oocyte. min ⁻¹)	Hill Coefficient
E343Q	nd	nd	-	nd	nd	-
E343D	6.3 ± 0.4	1.5 ± 0.1	1.8 ± 0.1	46 ± 12	1.9 ± 0.1	0.8 ± 0.1
E343C	40 ± 3	4.8 ± 0.3	1.4 ± 0.1	231 ± 54	0.5 ± 0.1	0.7 ± 0.1
E519D	5.5 ± 0.3	13.0 ± 0.4	1.4 ± 0.1	42 ± 13	0.7 ± 0.1	0.7 ± 0.1
E519C	58 ± 3	2.1 ± 0.1	1.9 ± 0.1	-	-	-
hCNT3	10.5 ± 0.7	10.3 ± 0.4	1.5 ± 0.1	495 ± 106	8.7 ± 0.4	0.7 ± 0.1

^a, from Fig. 9-7 (Na⁺) or Fig. 9-8 (H⁺); nd; not determined.

Table 9-4. Na⁺:uridine and H⁺:uridine stoichiometry for hCNT3 and mutants.

	Na ⁺ :uridine Stoichiometry ^a	H ⁺ :uridine Stoichiometry ^b
E343Q	~ 7.52	~ 7.41
E343D	1.70 ± 0.06	1.15 ± 0.04
E343C	≤ 2.2	nd
E519D	2.13 ± 0.14	0.61 ± 0.09
E519C	0.84 ± 0.04	nd
hCNT3	1.93 ± 0.07	1.02 ± 0.04

^a, from Fig. 9-10; ^b, in transport medium containing 100 mM ChCl, pH 5.5; nd, not determined.

Table 9-5. Comparison of hCNT1 and hCNT3 mutations.

Mutation		Plasma Membrane Expression		Change in Phenotype	
hCNT1 ^a	hCNT3	hCNT1	hCNT3 ^b	hCNT1	hCNT3 ^c
D172N	D192N	nd	nd	wt	wt
E308Q	E329Q	√	nd	Na ⁺ /uridine kinetics	wt
E308D	-	√	-	uridine kinetics	-
E308C	-	√	-	nd	-
E322Q	E343Q	√	√	Na ⁺ /uridine kinetics, uncoupled transport	Na ⁺ /uridine kinetics, no H ⁺ -dependence, uncoupled transport
E322D	E343D	√	√	Na ⁺ /uridine kinetics	Na ⁺ /H ⁺ /uridine kinetics
E322C	E343C	√	√	nd	Na ⁺ /H ⁺ /uridine kinetics, uncoupled transport
E338Q	E359Q	nd	nd	wt	wt
E389Q	E410Q	nd	nd	wt	wt
E413Q	E434Q	nd	nd	wt	wt
-	E483Q	-	nd	-	wt
D482N	D503N	X	nd	? (no activity)	wt
D482E	-	√	-	wt	-
D482C	-	nd	-	? (no activity)	-
E498Q	E519Q	X	√	? (no activity)	non-functional H ⁺ kinetics
E498D	E519D	√	√	wt	Na ⁺ /uridine kinetics, no H ⁺ -dependence, 1:1 Na ⁺ :uridine stoichiometry
E498C	E519C	nd	√	? (no activity)	

Table 9-5 (continued).

Mutation		Plasma Membrane Expression		Change in Phenotype	
hCNT1 ^a	hCNT3	hCNT1	hCNT3 ^b	hCNT1	hCNT3 ^c
E532Q	E553Q	X	nd	-	wt
E532D	-	X	-	-	-
E532C	-	nd	-	? (no activity)	-
D565N	D586N	nd	nd	wt	wt

^a; from Appendix 4; ^b, from Fig. 9-3; ^c, from Fig. 9-2 and Tables 9-1, 9-2, 9-3 and 9-4; nd, not determined; wt, wild-type-like cation-dependent nucleoside transport.

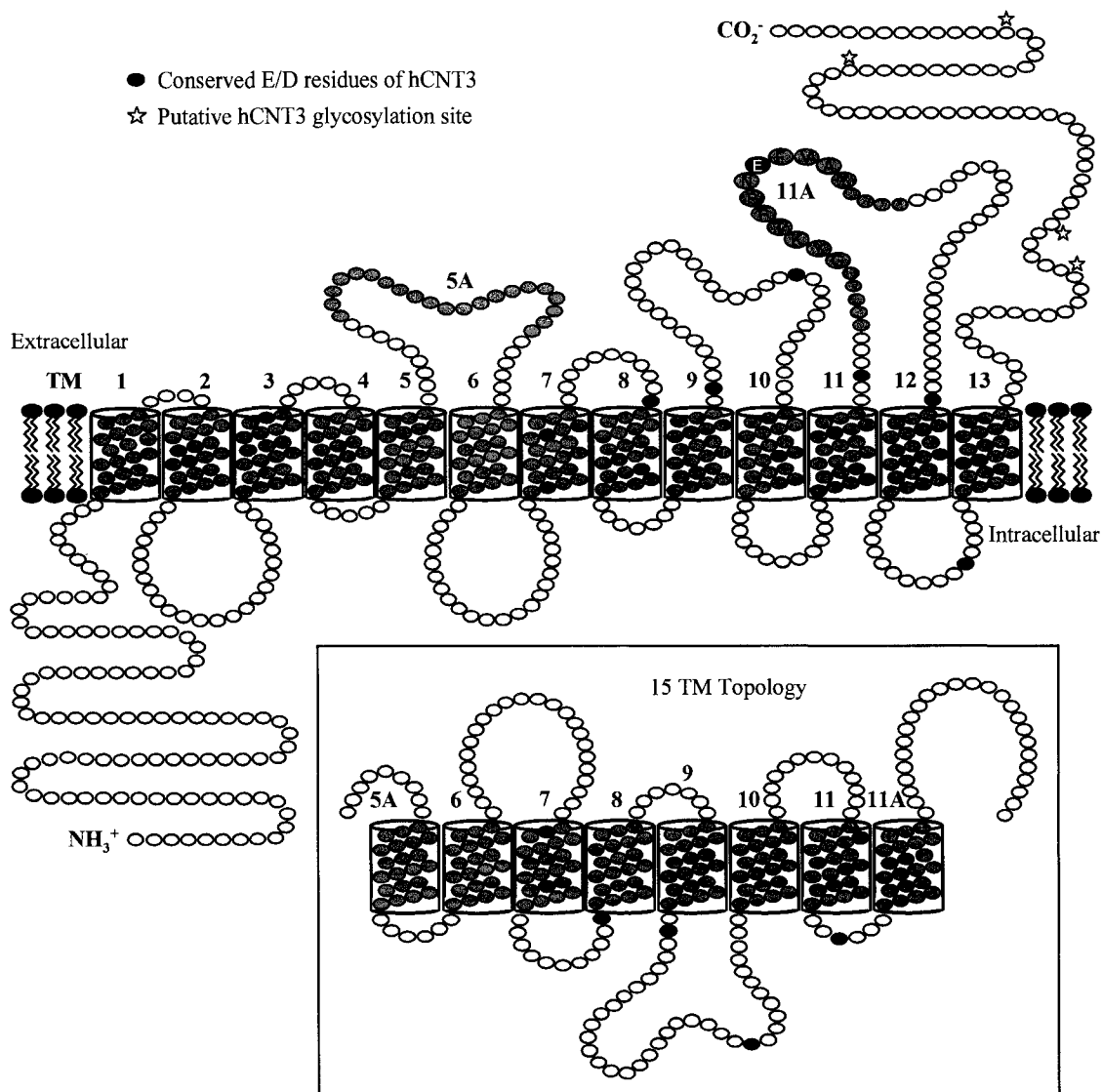


Figure 9-1. Putative hCNT3 topology model. Schematic of proposed hCNT3 (GenBank™ accession number AF305210) membrane architecture with 13 ± 2 TMs, as predicted by bioinformatic analyses of currently identified CNT family members. The location of a conserved (G/A)XKX₃NEFVA(Y/M/F) motif in TM 11A is indicated. Insertion of TMs 5A and 11A into the membrane, resulting in a 15 TM topology and opposite orientations of TMs 6 - 11, is depicted in the *inset*. The positions of highly conserved negatively charged aspartate and glutamate residues are indicated in *black*.

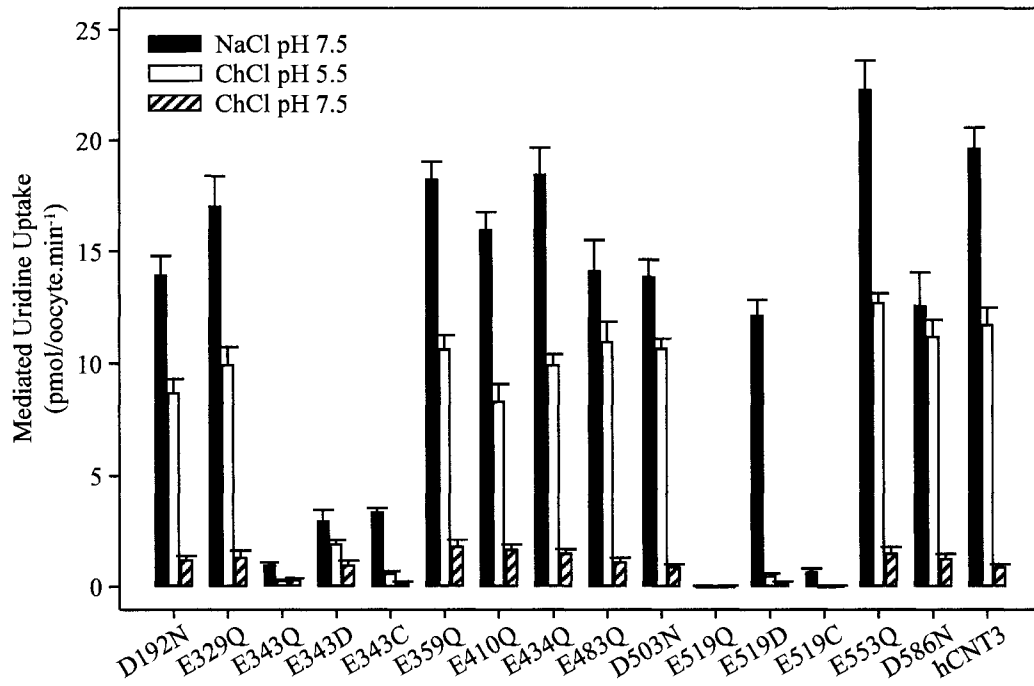


Figure 9-2. Cation selectivity of hCNT3 mutants. Mediated uptake of 20 μ M radiolabeled uridine in transport medium containing 100 mM NaCl pH 7.5 (*black bars*), ChCl pH 5.5 (*open bars*) or ChCl pH 7.5 (*hatched bars*) for oocytes expressing hCNT3 mutants (as indicated) or wild-type hCNT3. Values were corrected for basal non-mediated uptake in control water-injected oocytes and are means \pm SEM of 10 - 12 oocytes.

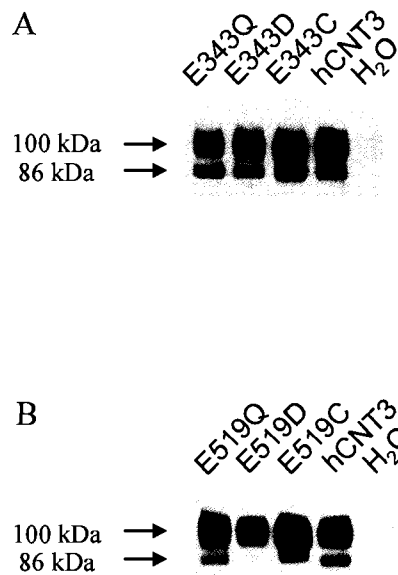


Figure 9-3. Cell-surface expression levels of hCNT3 and mutants. Oocytes injected with RNA transcripts encoding E343Q, E343C or E343D (*A*) or E519Q, E519C or E519D (*B*) or hCNT3 (*A* and *B*) and control water-injected oocytes (*A* and *B*) were assayed for the presence of plasma membrane recombinant protein expression by immunoblotting.

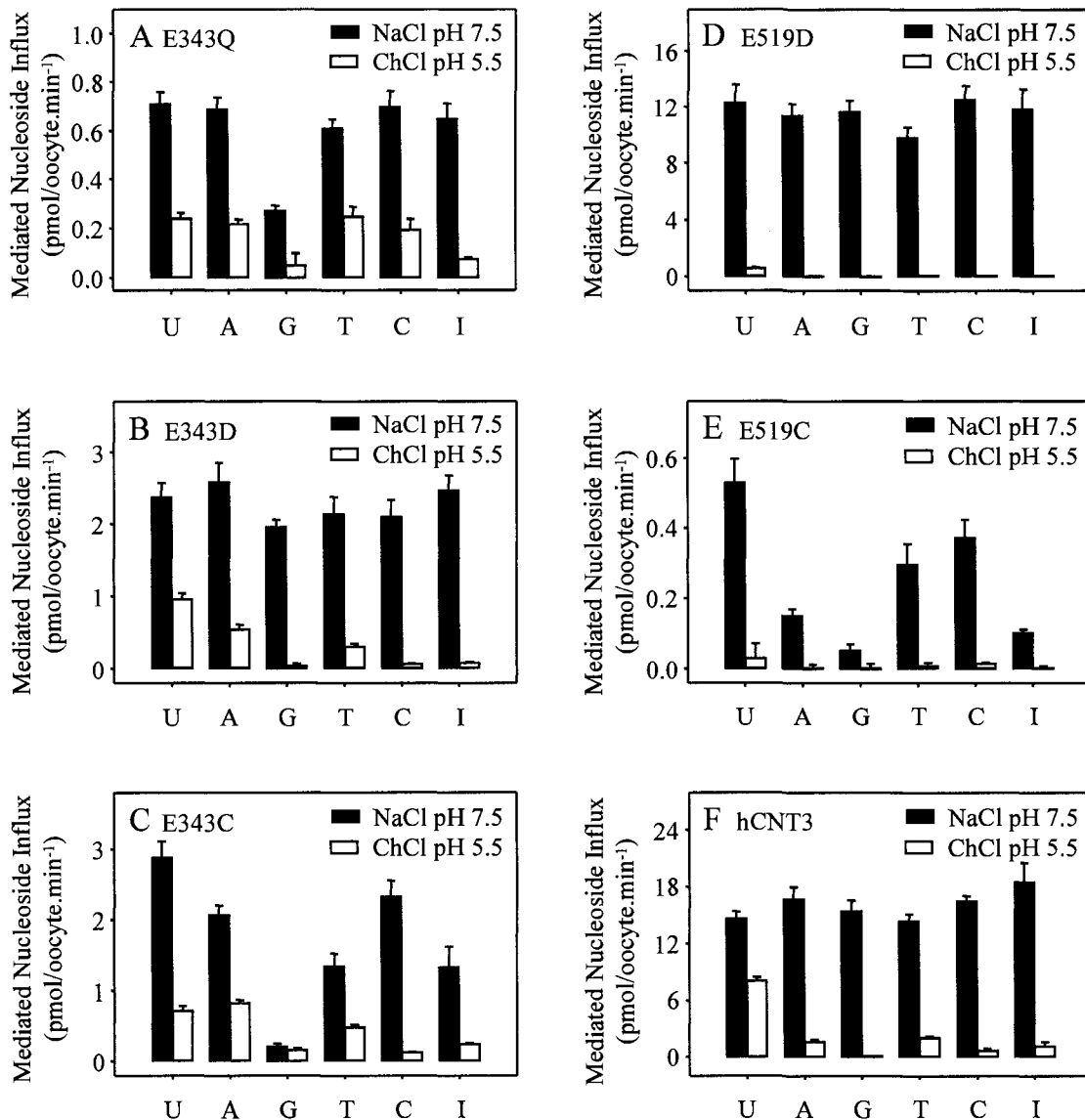


Figure 9-4. Nucleoside selectivity of hCNT3 and mutants. Uptake of 20 μ M radiolabeled uridine (U), adenosine (A), guanosine (G), thymidine (T), cytidine (C) and inosine (I) was measured in oocytes expressing E343Q (A), E343D (B), E343C (C), E519D (D), E519Q (E) or hCNT3 (F) in 100 mM NaCl, pH 7.5 (black bars) and 100 mM ChCl, pH 5.5 (open bars). Values were corrected for basal non-mediated uptake in control water-injected oocytes and are means \pm SEM of 10 - 12 oocytes.

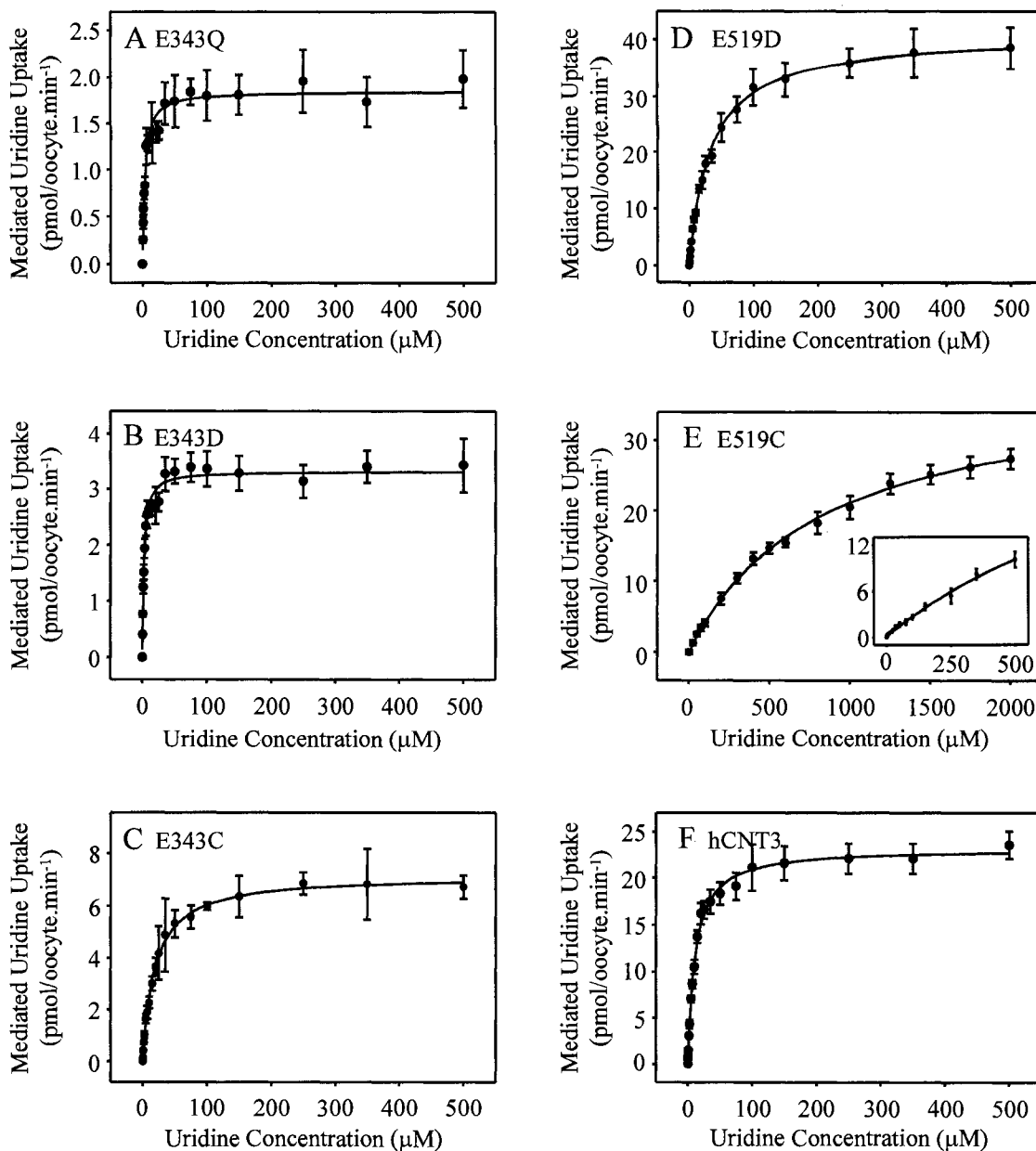


Figure 9-5. Uridine kinetics of hCNT3 and mutants. Radiolabeled uridine uptake was measured under initial rate conditions in 100 mM NaCl transport medium (pH 7.5) in oocytes expressing E343Q (A), E343D (B), E343C (C), E519D (D), E519C (E) or hCNT3 (F) for uridine concentrations ranging from 0 - 500 μM (A - D, E inset only, F) and 0 - 2 mM (E). Data points represent the mean ± SEM of 10 - 12 oocytes. Kinetic parameters calculated from the mediated component of transport (uptake in RNA-injected oocytes *minus* uptake in water-injected oocytes) are presented in Table 9-2.

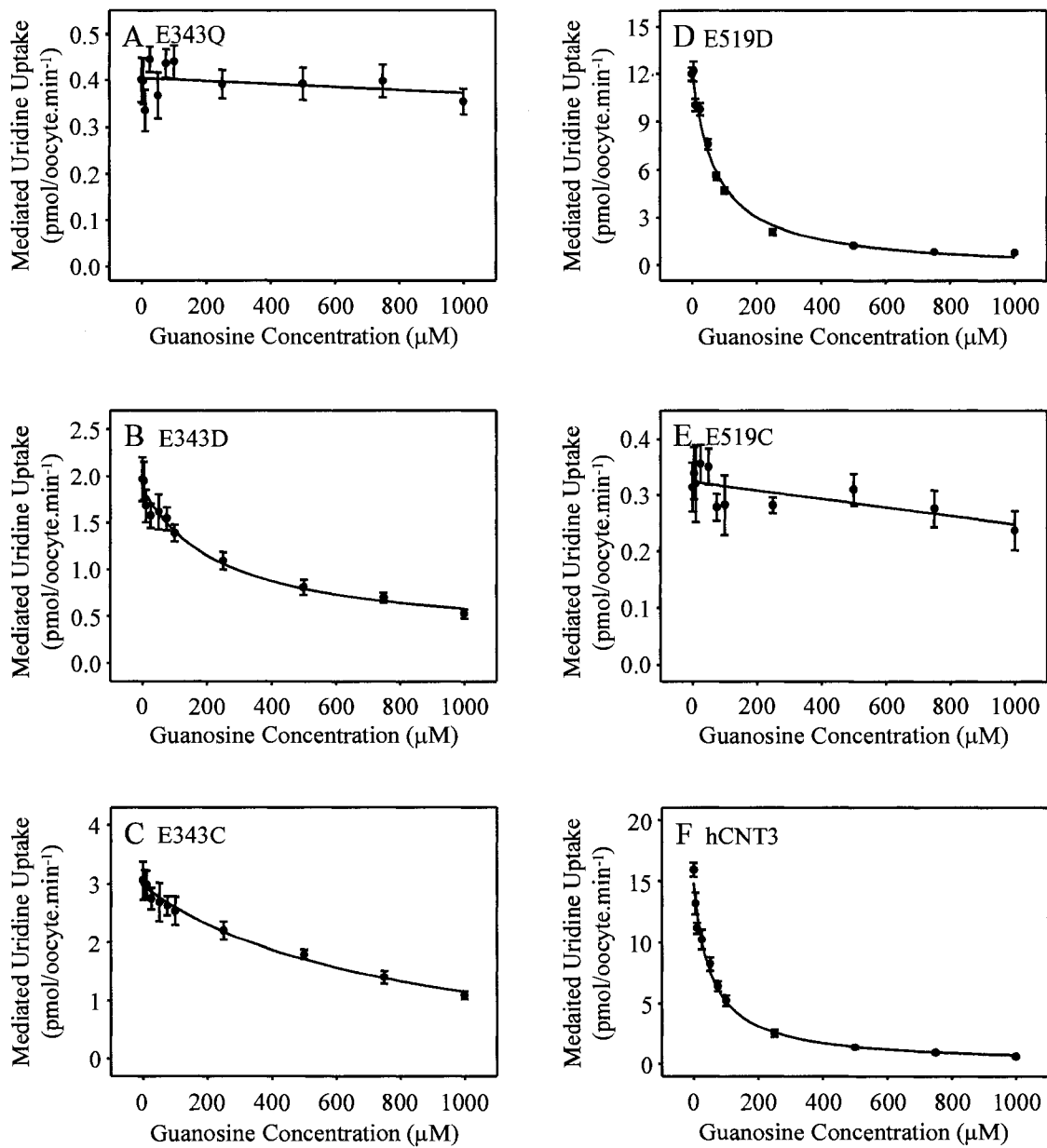


Figure 9-6. Guanosine inhibition of hCNT3 and mutants. Uptake of 20 μM radiolabeled uridine was measured in the presence of 0 - 1000 μM non-labeled guanosine in 100 mM NaCl transport medium (pH 7.5) in oocytes expressing E343Q (A), E343D (B), E343C (C), E519D (D), E519C (E) or hCNT3 (F). Data points represent the mean ± SEM of 10 - 12 oocytes. Kinetic parameters are calculated from the mediated component of transport (uptake in RNA-injected oocytes *minus* uptake in water-injected oocytes).

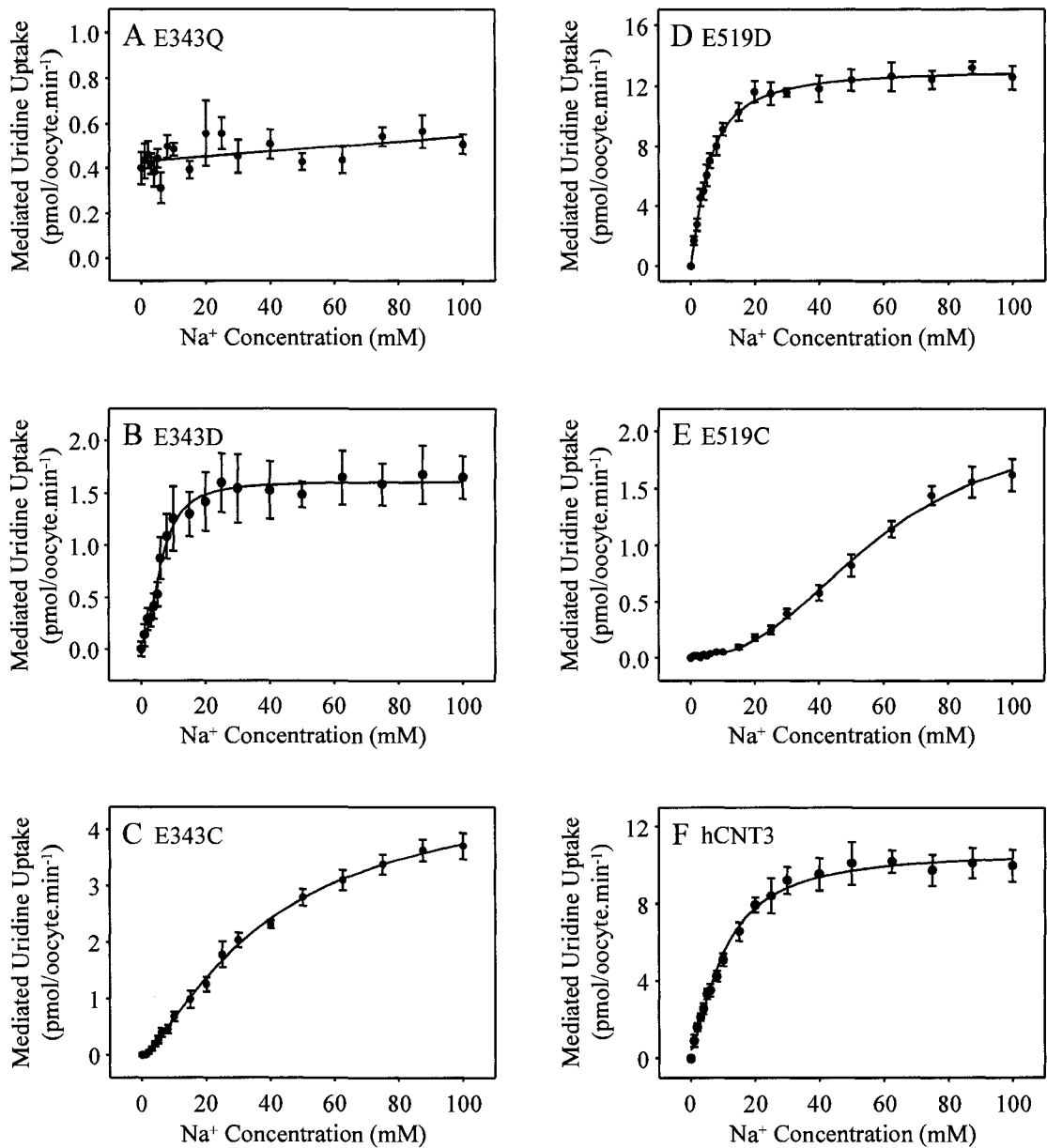


Figure 9-7. Na⁺-activation kinetics of hCNT3 and mutants. Na⁺-activation curves for oocytes expressing E343Q (A), E343D (B), E343C (C), E519D (D), E519C (E) or wild-type hCNT3 (F) were measured in transport medium containing 0 - 100 mM NaCl at pH 8.5 with isomolality maintained by addition of ChCl. A radiolabeled uridine concentration of 20 μM was used. Data points represent the mean ± SEM of 10 - 12 oocytes. Kinetic parameters calculated from the mediated component of transport (uptake in RNA-injected oocytes *minus* uptake in water-injected oocytes) are presented in Table 9-3.

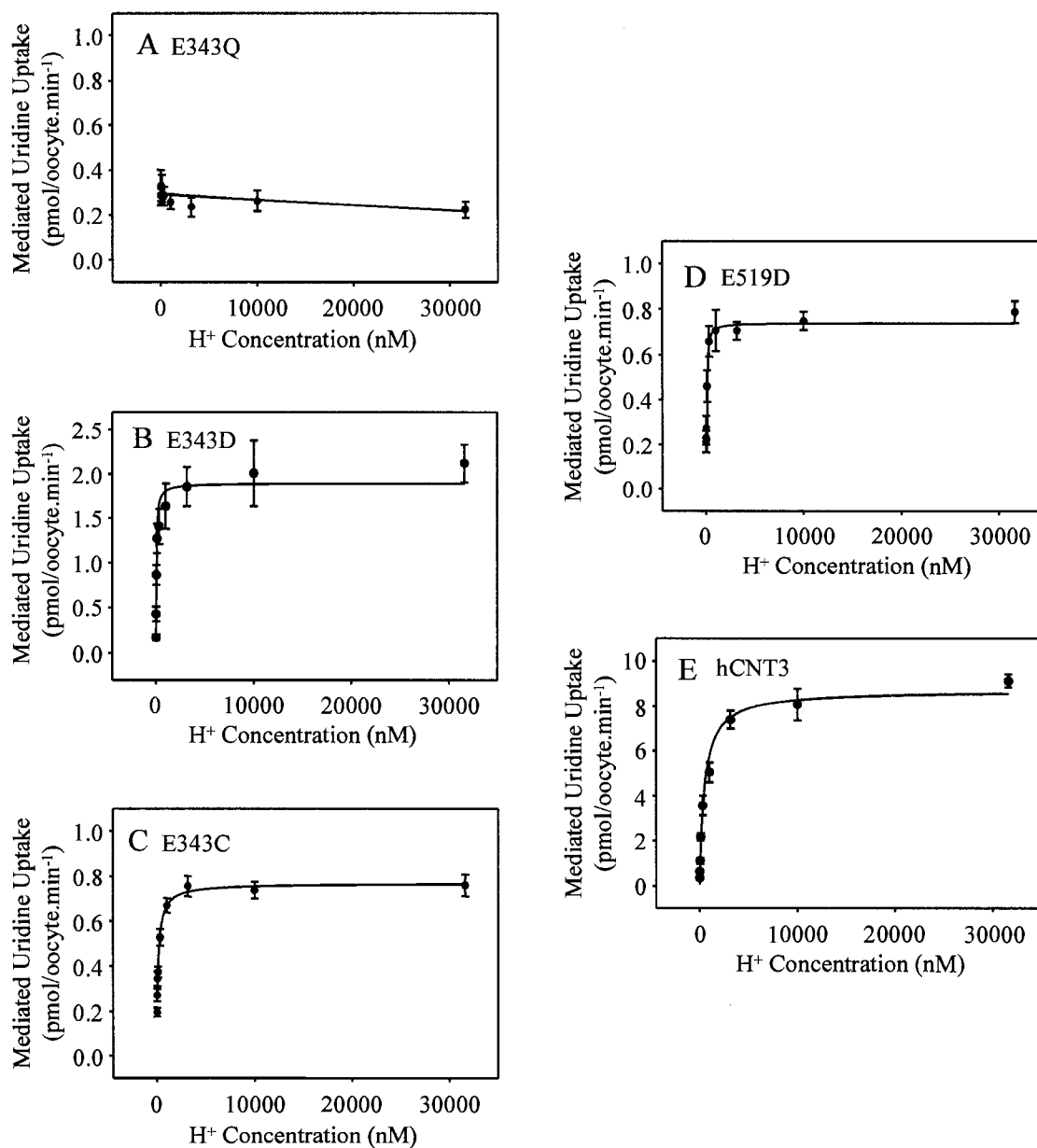


Figure 9-8. H⁺-activation kinetics of hCNT3 and mutants. H⁺-activation curves for oocytes expressing E343Q (A), E343D (B), E343C (C), E519D (D) or hCNT3 (E) were measured in transport medium containing 100 mM ChCl transport medium with pH values ranging from 4.5 to 8.5. A radiolabeled uridine concentration of 20 μ M was used. Data points represent the mean \pm SEM of 10 - 12 oocytes. Kinetic parameters calculated from the mediated component of transport (uptake in RNA-injected oocytes minus uptake in water-injected oocytes) are presented in Table 9-3.

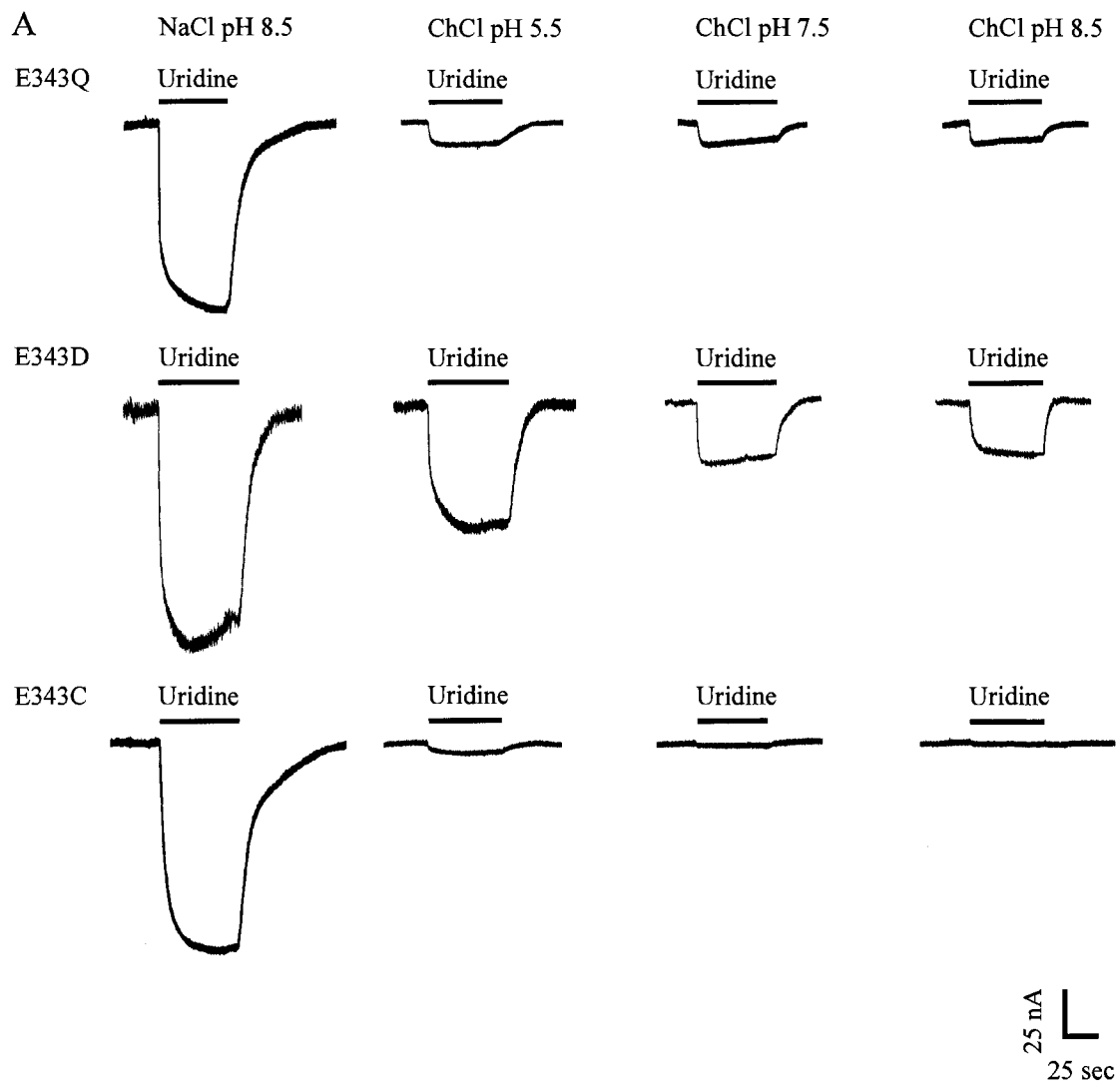


Figure 9-9.

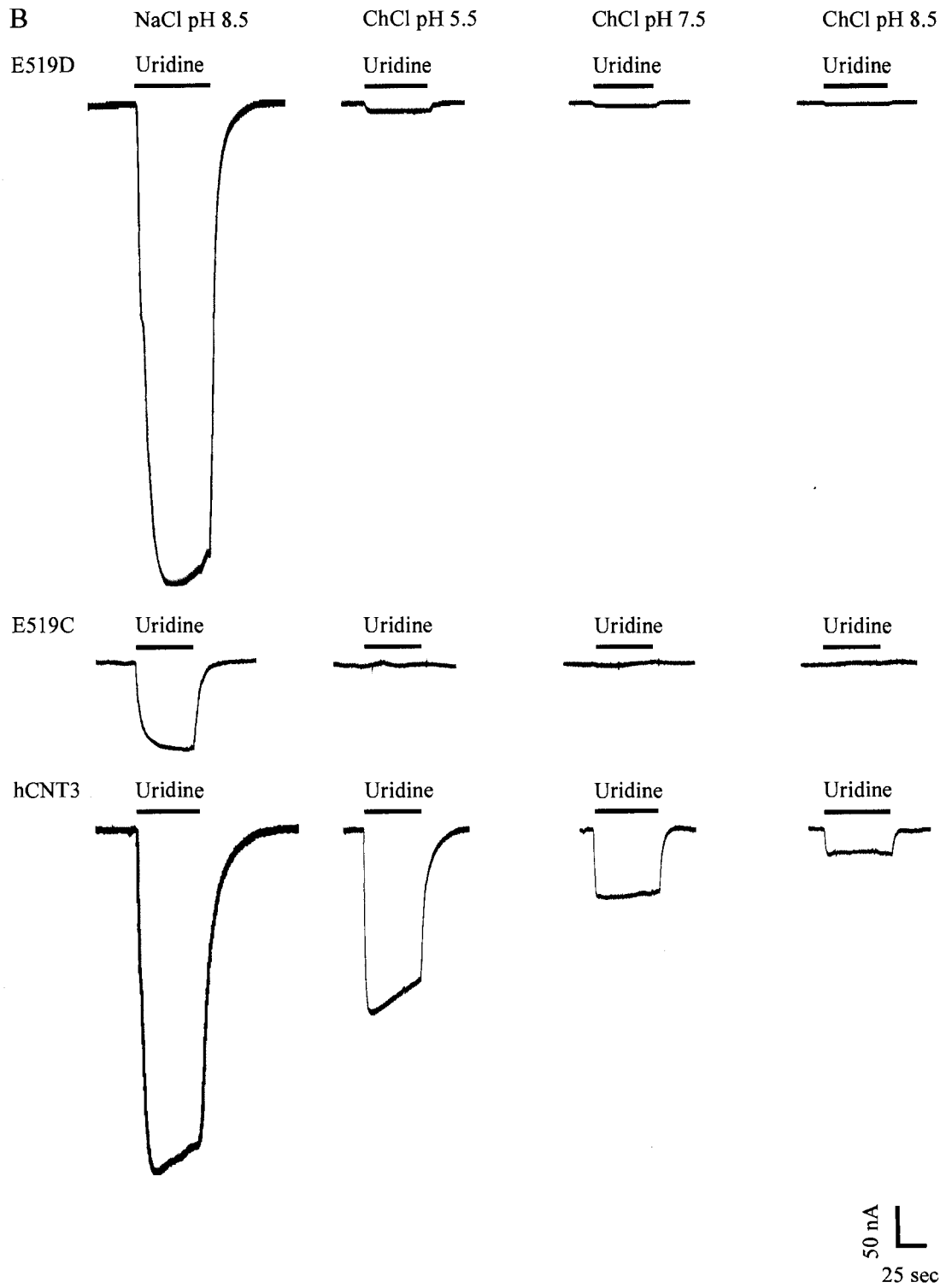


Figure 9-9.

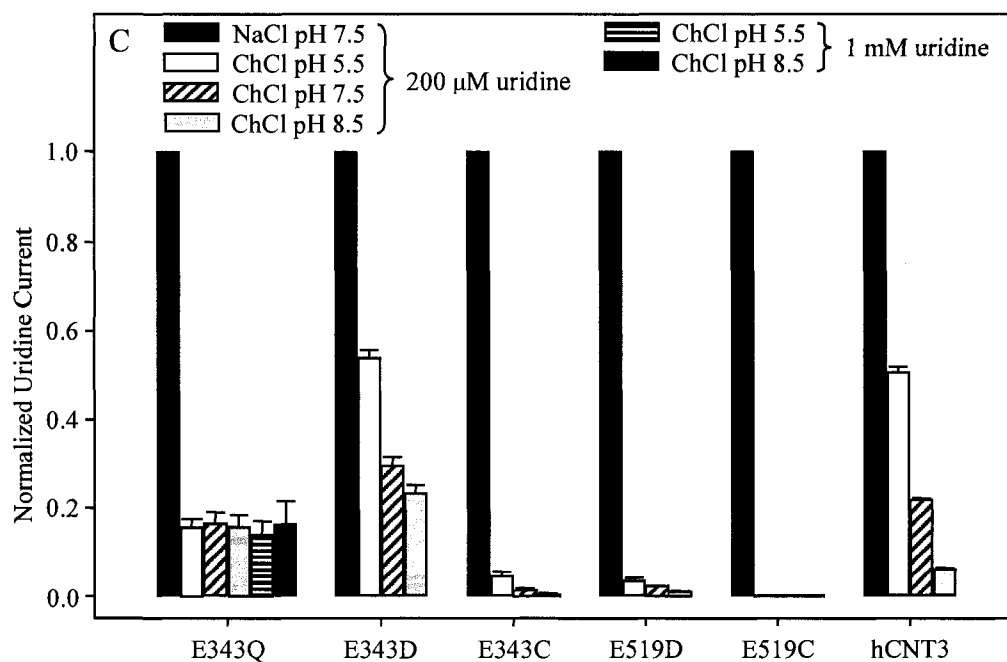


Figure 9-9. Uridine-evoked steady-state currents of hCNT3 and mutants. Uridine-evoked currents in 100 mM NaCl pH 8.5 or 100 mM ChCl pH 5.5, pH 7.5 or pH 8.5 transport media (*right to left* columns, respectively) are shown for representative oocytes producing E343Q, E343D or E343C (*A*) or E519D, E519C or hCNT3 (*B*). No current was detected in control water-injected oocytes (data not shown). Bars indicate the duration of exposure to 200 μ M uridine. The bar graph of (*C*) shows the same uridine-evoked steady-state currents from ≥ 4 oocytes each normalized to current in 100 mM NaCl pH 8.5. Error bars are not shown where values were smaller than that represented by the symbols.

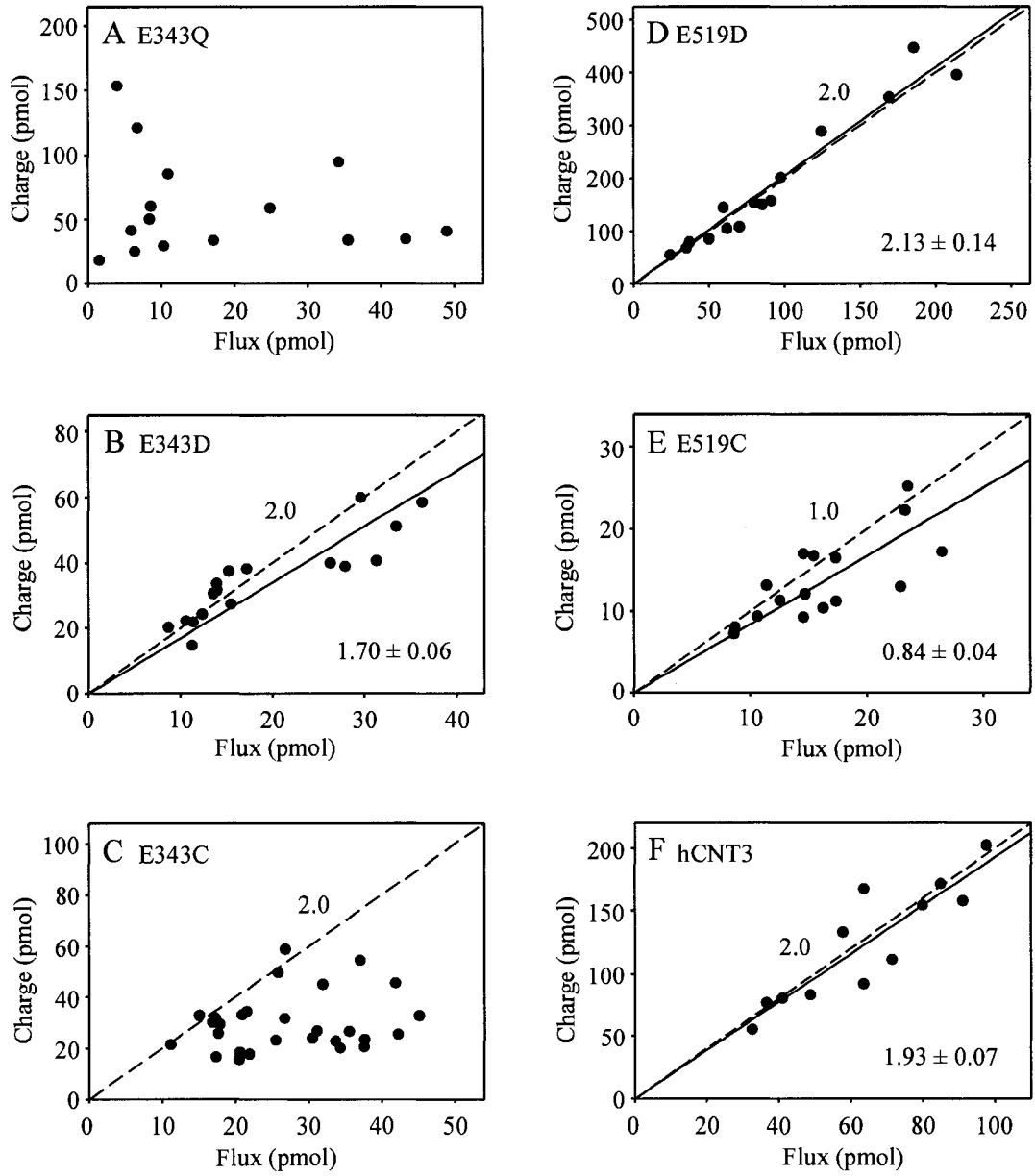


Figure 9-10.

Figure 9-10. Na⁺:uridine stoichiometry of hCNT3 and mutants. Charge to radiolabeled uridine uptake ratio plots were generated with oocytes expressing E343Q (A), E343D (B), E343C (C), E519D (D), E519C (E) or hCNT3 (F) in 100 mM NaCl transport medium at pH 8.5. A uridine concentration of 200 μM was used and the oocytes were clamped at a holding potential of -90 mV. Integration of the uridine-evoked current was used to calculate the net cation influx (charge) and was correlated to the net ³H-uridine influx (flux). Linear fits passed through the origin and linear regression analysis of the data for each plot is indicated by the *solid* line. The *dashed* line represents a theoretical 2:1 (B, C, D and F) and 1:1 (E) charge:uptake ratio. Calculated Na⁺:uridine coupling ratios from these data are presented in Table 9-4.

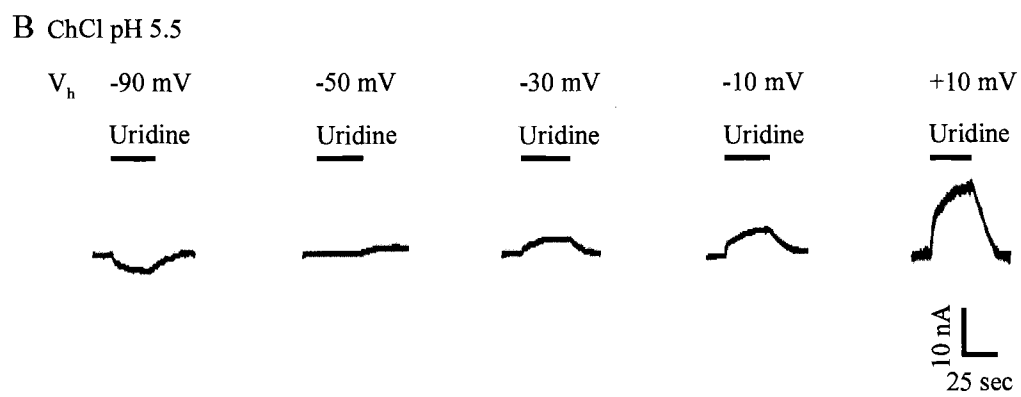
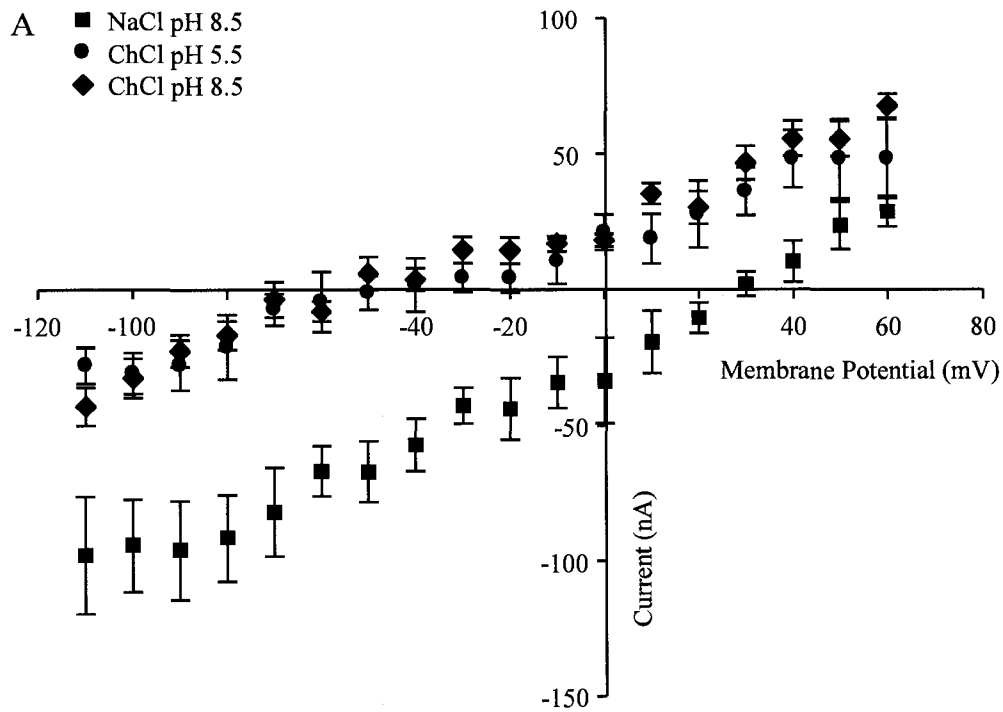


Figure 9-11.

Figure 9-11. Current-voltage relationships of E343Q-mediated uridine transport. (A) Current-voltage (I-V) curves for representative E343Q-producing oocytes in 100 mM NaCl pH 8.5 (*squares*), 100 mM ChCl pH 5.5 (*circles*) and 100 mM ChCl pH 8.5 (*diamonds*) transport media were generated from the difference between steady-state currents recorded in the presence and absence of 100 μ M uridine. Oocytes were clamped at a holding potential (V_h) of -50 mV and pulsed to test (V_t) ranging from -110 to +60 mV in 10 mV increments. Data points represent the mean \pm SEM from 6 - 8 oocytes. No uridine-induced currents were observed in control water-injected oocytes. Error bars are not shown where values were smaller than that represented by the symbols. (B) Representative traces of uridine-evoked currents in 100 mM ChCl pH 5.5 are depicted for a representative oocyte expressing E343Q and clamped at holding potentials (V_h) of -90, -50, -30, -10 and +10 mV, as indicated. No currents were detected in control water-injected oocytes (data not shown). Bars indicate the duration of exposure to 100 μ M uridine.

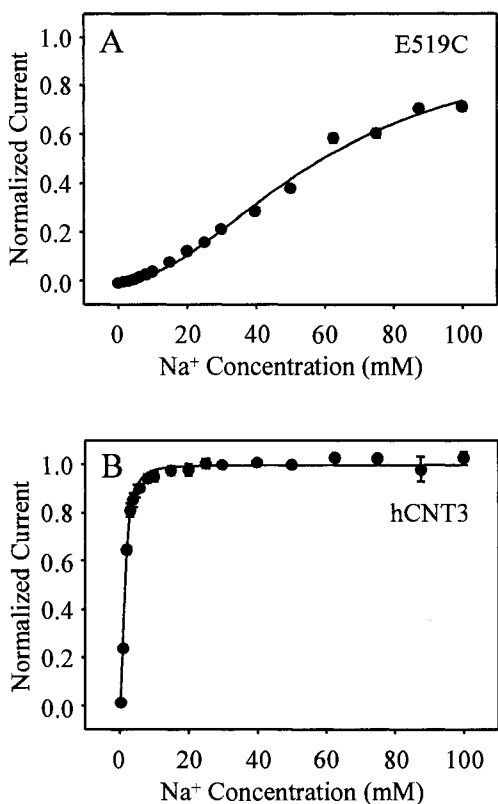


Figure 9-12. Na⁺-activation kinetics of hCNT3 and E519C determined by electrophysiology. The Na⁺-activation curves for E519C (A) and wild-type hCNT3 (B) were determined at a holding potential of -90 mV in 100 mM NaCl pH 8.5 transport medium. The uridine concentrations used were 200 and 20 μ M for E519C and hCNT3, respectively. Uridine-evoked currents at each Na⁺ concentration were normalized to the respective fitted I_{\max} value and are presented as the mean \pm SEM of 8 (E519C) or 5 (hCNT3) oocytes. Error bars are not shown where values were smaller than that represented by the symbols. No currents were detected in control water-injected oocytes (data not shown).

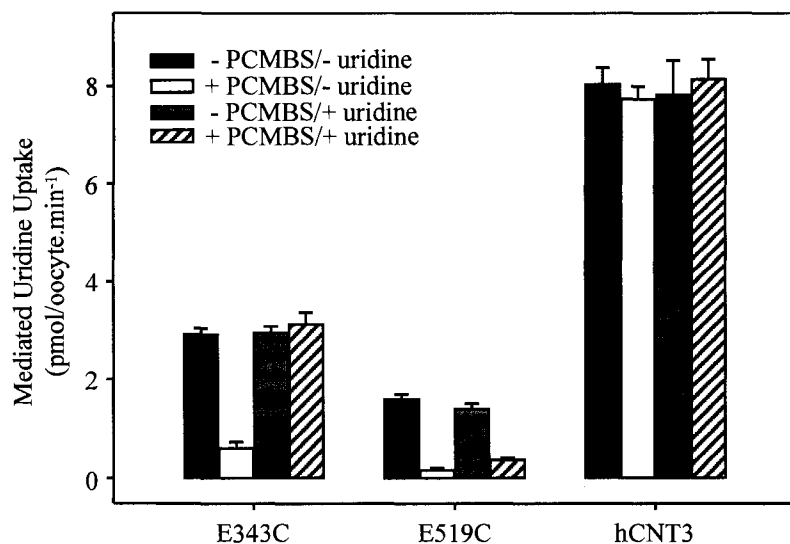


Figure 9-13. PCMBS inhibition of hCNT3-, E343C- and E519C-mediated uridine transport. Radiolabeled uridine uptake (20 μ M) was measured in oocytes producing E343C, E519C or hCNT3 following incubation in the absence (*solid and grey bars*) or presence (*open and hatched bars*) of 500 μ M PCMBS, and in the absence (*solid and open bars*) or presence (*grey and hatched bars*) of 20 mM uridine. The medium for exposure to PCMBS and subsequent assay of transport activity was 100 mM NaCl pH 8.5. Data are presented as mediated transport, calculated as uptake in RNA-injected oocytes *minus* uptake in water-injected oocytes. Each value represents the mean \pm SEM of 10 - 12 oocytes. Error bars are not shown where values were smaller than that represented by the symbols.

Bibliography

1. Pourcher, T., Zani, M. L., and Leblanc, G. (1993) Mutagenesis of acidic residues in putative membrane-spanning segments of the melibiose permease of *Escherichia coli*. I. Effect on Na⁺-dependent transport and binding properties. *J. Biol. Chem.* **268**: 3209-3215.
2. Franco, P. J., and Brooker, R. J. (1994) Functional roles of Glu-269 and Glu-325 within the lactose permease of *Escherichia coli*. *J. Biol. Chem.* **269**: 7379-7386.
3. Kaback, H. R. (1997) A molecular mechanism for energy coupling in a membrane transport protein, the lactose permease of *Escherichia coli*. *Proc. Natl. Acad. Sci. U.S.A.* **94**: 5508-5543.
4. Quick, M., and Jung, H. (1997) Aspartate 55 in the Na⁺/proline permease of *Escherichia coli* is essential for Na⁺-coupled proline uptake. *Biochemistry* **36**: 4631-4636.
5. Quick, M., and Jung, H. (1998) A conserved aspartate residue, Asp187, is important for Na⁺-dependent proline binding and transport by the Na⁺/proline transporter of *Escherichia coli*. *Biochemistry* **37**: 13800-13806.
6. Griffith, D. A., and Pajor, A. M. (1999) Acidic residues involved in cation and substrate interactions in the Na⁺/dicarboxylate cotransporter, NaDC-1. *Biochemistry* **38**: 7524-7531.
7. Pirch, T., Quick, M., Nietschke, M., Langkamp, M., and Jung, H. (2002) Sites important for Na⁺ and substrate binding in the Na⁺/proline transporter of *Escherichia coli*, a member of the Na⁺/solute symporter family. *J. Biol. Chem.* **277**: 8790-8796.
8. Abramson, J., Smirnova, I., Kasho, V., Verner, G., Kaback, H.R., and Iwata, S. (2003) Structure and mechanism of the lactose permease of *Escherichia coli*. *Science* **301**: 610-615.
9. Grewer, C., Watzke, N., Rauen, T., and Bicho, A. (2003) Is the glutamate residue Glu-373 the proton acceptor of the excitatory amino acid carrier 1? *J. Biol. Chem.* **278**: 2585-2592.

10. Noel, J., Germain, D., and Vadnais, J. (2003) Glutamate 346 of human Na⁺-H⁺ exchanger NHE1 is crucial for modulating both the affinity for Na⁺ and the interaction with amiloride derivatives. *Biochemistry* **42**: 15361-15368.

11. Chen, N., Rickey, J., Berfield, J. L., and Reith, M. E. (2004) Aspartate 345 of the dopamine transporter is critical for conformational changes in substrate translocation and cocaine binding. *J. Biol. Chem.* **279**: 5508-5519.

12. Ritzel, M. W. L., Ng, A. M. L., Yao, S. Y. M., Graham, K., Loewen, S. K., Smith, K. M., Ritzel, R. G., Mowles, D. A., Carpenter, P., Chen, X.-Z., Karpinski, E., Hyde, R. J., Baldwin, S. A., Cass, C. E., and Young, J. D. (2001) Molecular identification and characterization of novel human and mouse concentrative Na⁺-nucleoside cotransporter proteins (hCNT3 and mCNT3) broadly selective for purine and pyrimidine nucleosides (system *cib*). *J. Biol. Chem.* **276**: 2914-2927.

13. Damaraju, V. L., Elwi, A. N., Hunter, C., Carpenter, P., Santos, C., Barron, G. M., Sun, X., Baldwin, S. A., Young, J. D., Mackey, J. R., Sawyer, M. B., and Cass, C. E. (2007) Localization of broadly selective equilibrative and concentrative nucleoside transporters, hENT1 and hCNT3, in human kidney. *Am. J. Physiol. Renal Physiol.* **293**: F200-F211.

14. Smith, K. M., Ng, A. M., Yao, S. Y. M., Labedz, K. A., Knauss, E. E., Wiebe, L. I., Cass, C. E., Baldwin, S. A., Chen, X.-Z., Karpinski, E., and Young, J. D. (2004) Electrophysiological characterization of a recombinant human Na⁺-coupled nucleoside transporter (hCNT1) produced in *Xenopus* oocytes. *J. Physiol.* **558**: 807-823.

15. Ritzel, M. W. L., Yao, S. Y. M., Huang, M. Y., Elliot, J. F., Cass, C. E., and Young, J. D. (1997) Molecular cloning and functional expression of cDNAs encoding a human Na⁺-nucleoside cotransporter (hCNT1). *Am. J. Physiol.* **272**: C707-C714.

16. Ritzel, M. W. L., Yao, S. Y. M., Ng, A. M. L., Mackey, J. R., Cass, C. E., and Young, J. D. (1998) Molecular cloning, functional expression and chromosomal localization of a cDNA encoding a human Na⁺/nucleoside cotransporter (hCNT2) selective for purine nucleosides and uridine. *Mol. Membr. Biol.* **15**: 203-211.

17. Pastor-Anglada, M., Errasti-Murugarren, E., Aymerich, I., and Casado, F. J. (2007) Concentrative nucleoside transporters (CNTs) in epithelia: from absorption to cell signaling. *J. Physiol. Biochem.* **63**: 97-110.
18. Quick, M., Loo, D. D. F., and Wright, E. M. (2001) Neutralization of a conserved amino acid residue in the human Na⁺/glucose transporter (hSGLT1) generates a glucose-gated H⁺ channel. *J. Biol. Chem.* **276**: 1728-1734.
19. Lin, F., Lester, H. A., and Marger, S. (1996) Single-channel currents produced by the serotonin transporter and analysis of a mutation affecting ion permeation. *Biophys. J.* **71**: 3126-3135.
20. Errasti-Murugarren, E., Cano-Soldado, P., Pastor-Anglada, M., and Casado, F. J. (2008) Functional characterization of a nucleoside-derived drug transporter variant (hCNT3C602R) showing altered sodium-binding capacity. *Mol. Pharmacol.* **73**: 379-386.
21. Hamilton S. R., Yao, S. Y., Ingram, J. C., Hadden, D. A., Ritzel, M. W., Gallagher, M. P., Henderson, P. J., Cass, C. E., Young, J. D., and Baldwin, S. A. (2001) Subcellular distribution and membrane topology of the mammalian concentrative Na⁺-nucleoside cotransporter, rCNT1. *J. Biol. Chem.* **276**: 27981-27988.
22. Zhang, J., Tackaberry, T., Ritzel, M. W., Raborn, T., Barron, G., Baldwin, S. A., Young, J. D., and Cass, C. E. (2006) Cysteine-accessibility analysis of transmembrane domains 11-13 of human concentrative nucleoside transporter 3. *Biochem. J.* **394**: 389-398.
23. Loewen, S. K., Ng, A. M. L., Yao, S. Y. M., Cass, C. E., Baldwin, S. A., and Young, J. D. (1999) Identification of amino acid residues responsible for the pyrimidine and purine nucleoside specificities of human concentrative Na⁺ nucleoside cotransporters hCNT1 and hCNT2. *J. Biol. Chem.* **274**: 24475-24484.
24. Mulinta, R., Ng, A. M. L., Yao, S. Y. M., Slugoski, M. D., Smith, K. M., Cass, C. E., Baldwin, S. A., and Young, J. D. (2008) Substituted cysteine accessibility method analysis of transmembrane domains 7 and 8 of human concentrative nucleoside transporter 3 (hCNT3) reveal novel discontinuous regions within helices. *J. Biol. Chem.* (submission pending).

25. Yamashita, A., Singh, S. K., Kawate, T., Jin, Y., and Gouaux, E. (2005) Crystal structure of a bacterial homologue of Na⁺/Cl⁻-dependent neurotransmitter transporters. *Nature* **437**: 215-223.
26. Lu, C.-C., and Hilgemann, D. W. (1999) GAT1 (GABA:Na⁺:Cl⁻) cotransport function. Kinetic studies in giant *Xenopus* oocyte membrane patches. *J. Gen. Physiol.* **114**: 445-457.
27. Hilgemann, D. W., and Lu, C.-C. (1999) GAT1 (GABA:Na⁺:Cl⁻) cotransport function. Database reconstruction with an alternating access model. *J. Gen. Physiol.* **114**: 459-475.
28. Kaback, H. R. (2005) Structure and mechanism of the lactose permease. *C. R. Biologies* **328**: 557-567.
29. Yao, S. Y. M., Ng, A. M. L., Loewen, S. K., Cass, C. E., Baldwin, S. A., and Young, J. D. (2002) An ancient prevertebrate Na⁺-nucleoside cotransporter (hfCNT) from the Pacific hagfish (*Eptatretus stouti*). *Am. J. Physiol. Cell Physiol.* **283**: C155-C168.
30. Loewen, S. K., Ng, A. M. L., Mohabir, N. N., Baldwin, S. A., Cass, C. E., and Young, J. D. (2003) Functional characterization of a H⁺/nucleoside cotransporter (CaCNT) from *Candida albicans*, a fungal member of the concentrative nucleoside transporter (CNT) family of membrane proteins. *Yeast* **20**: 661-675.
31. Xiao, G., Wang, J., Tangen, T., and Giacomini, K. M. (2001) A novel proton-dependent nucleoside transporter, CeCNT3, from *Caenorhabditis elegans*. *Mol. Pharmacol.* **59**: 339-348.
32. Smith, K. M., Cass, C. E., Baldwin, S. A., Karpinski, E., and Young, J. D. (2008) Presteady-state currents of human concentrative nucleoside transporter 3 (hCNT3). *J. Physiol.* (submission pending).

Chapter 10:

Novel Topology of the TM 11A Region of Human Concentrative Nucleoside Transporter hCNT3 Revealed by Substituted Cysteine Accessibility Method (SCAM) Analysis*

* Some results presented in this chapter have been published and are presented in Chapter 7. Publication of a version of the remainder of the chapter is pending.

Slugoski, M. D., Ng, A. M. L., Yao, S. Y. M., Smith, K. M., Lin, C. C., Zhang, J., Karpinski, E., Cass, C. E., Baldwin, S. A., and Young, J. D. (2008) A proton-mediated conformational shift identifies a mobile pore-lining cysteine residue (Cys-561) in human concentrative nucleoside transporter 3. *J. Biol. Chem.* **283**: 8496-8507.

Slugoski, M. D., Ng, A. M. L., Yao, S. Y. M., Lin, C. C., Mulinta, R., Cass, C. E., Baldwin, S. A., and Young, J. D. (2008) Novel topology of the TM 11A region of human concentrative nucleoside transporter hCNT3 revealed by substituted cysteine accessibility method (SCAM) analysis. *J. Biol. Chem.* (submission pending).

Acknowledgements

Mrs. Amy M. L. Ng was involved in construction of the single cysteine mutants and, together with Dr. Sylvia Y. M. Yao, completed the SCAM analysis of TMs 11, 12 and 13. Mr. Colin C. Lin assisted with this project by confirming the pattern of uridine protection. Ms. Ras Mulinta was involved in design of the project and completed a parallel SCAM analysis of hCNT3 TMs 7 - 8. Drs. Carol E. Cass and Stephen A. Baldwin are collaborative principal investigators who assisted with research funding and manuscript preparation. This research was funded by the National Cancer Institute of Canada with funds from the Canadian Cancer Society and Alberta Cancer Board.

Introduction

Current models of concentrative nucleoside transporter (CNT) topology have 13 putative transmembrane domains (TMs) (1-4). Two additional TMs (designated 5A and 11A) are weakly predicted by computer algorithms and immunocytochemical experiments with site-specific antibodies, and studies of native and introduced glycosylation sites have confirmed an intracellular N-terminus and an extracellular C-terminus (3). Chimeric studies involving human (h) CNTs and hagfish (hf) CNT, a CNT from the ancient marine prevertebrate the Pacific hagfish *Eptatretus stouti*, have revealed that the functional domains responsible for CNT nucleoside selectivity and cation coupling reside within the C-terminal TM 7 - 13 half of the protein (5, Chapter 5). In contrast to mammalian and other eukaryotic CNTs, NupC, a H⁺-coupled CNT family member from *Escherichia coli*, lacks TMs 1 - 3, but otherwise shares a similar membrane topology (6, Appendix 2).

A functional cysteine-less version of hCNT3 has been generated by mutagenesis of endogenous cysteine residues to serine, resulting in the cysteine-less construct hCNT3C- employed originally in a yeast expression system for substituted cysteine accessibility method (SCAM) analysis of TMs 11, 12 and 13 using methanethiosulfonate (MTS) reagents (7). Subsequently, hCNT3C- was characterized in the *Xenopus laevis* oocyte expression system (Chapter 8), and SCAM analysis projects were initiated with the alternative thiol-specific reagent *p*-chloromercuribenzenesulfonate (PCMBS) (Chapter 7) that will eventually encompass the entire C-terminal half of the protein. Both membrane-impermeant and hydrophilic, PCMBS reactivity with introduced cysteine residues, as measured by transport inhibition, indicates pore-lining status and access from the extracellular medium; the ability of permeant to protect against this inhibition indicates location within, or closely adjacent to, the nucleoside binding pocket (8, 9). Continuing the investigation of hCNT3 C-terminal membrane topology and function, the present study reports results for the TM 11 - 13 part of the protein, including loop regions linking the putative TMs not previously studied using MTS reagents.

In previous structure/function studies of hCNT3, a cluster of conformationally mobile residue positions in TM 12 (Ile⁵⁵⁴, Tyr⁵⁵⁸ and Cys⁵⁶¹) were identified which exhibit H⁺-activated inhibition by PCMBS, with uridine protection evident for Tyr⁵⁵⁸ and Cys⁵⁶¹ (Chapter 7). Located deeper within the plane of the membrane, other uridine-protectable residue positions in TM 12 are PCMBS-sensitive in both H⁺- and Na⁺-containing medium (Chapter 7). Also in previous studies, hCNT3 Glu⁵¹⁹ and the corresponding residue in hCNT1 (Glu⁴⁹⁸) in region TM 11A were identified as having key roles in permeant and cation binding and translocation (Chapter 9, Appendix 4); additionally, hCNT3 E519C showed inhibition of uridine uptake by PCMBS (Chapter 9). Mechanistically, this residue is proposed to be a direct participant in cation coupling via the common hCNT3 Na⁺/H⁺-binding site that, in other CNTs, is either Na⁺-specific (e.g. hCNT1) or H⁺-specific (e.g. NupC) (Chapter 9). The present results identify other residues of functional importance in this region of the protein, confirm the predicted α -helical structures of TMs 11, 12 and 13, and provide evidence for a novel membrane-associated conformation for the TM 11A region. These findings strongly support a revised 15 TM topology model for CNTs. A version of these results for TM 12 is also presented in Chapter 7.

Results

All 14 endogenous cysteine residues of hCNT3 were replaced with serine to produce hCNT3C-, a cysteine-less hCNT3 construct (7, Chapter 8). hCNT3C- retained wild-type hCNT3 functional activity (Chapter 8). In parallel with previous studies (7, Chapter 7), hCNT3C- was used as a template for the construction of single cysteine mutants prior to scanning for functional activity and inhibition by PCMBS. The 133 residues spanning a region between and including TMs 11 - 13 that were investigated in the present study are highlighted in Fig. 10-1.

Functional activity of single cysteine mutants – hCNT3 transports nucleosides using both Na⁺ and H⁺ electrochemical gradients (Chapters 5 and 6). Therefore, to examine the functional activity of single cysteine mutants, uptake of 10 μ M radiolabeled

uridine was determined in both Na⁺-containing, H⁺-reduced and Na⁺-free, acidified medium (100 mM NaCl, pH 8.5 and 100 mM ChCl, pH 5.5, respectively). Na⁺-containing medium was buffered at a pH of 8.5 to avoid the small, but significant, amount of hCNT3 H⁺-activation that occurs at pH 7.5 (Chapters 5 and 6). Previously, Na⁺-coupled uridine transport by hCNT3 at pH 8.5 was verified to be kinetically indistinguishable from that at pH 7.5 (Chapter 8). Initial rates of transport (\pm SEM) for each mutant, in units of pmol/oocyte.min⁻¹, are given in Table 10-1. The uptake of 10 μ M radiolabeled uridine (100 mM NaCl, pH 8.5) by oocytes expressing hCNT3C- showed expected variation between experiments and ranged from 2 and 4 pmol/oocyte.min⁻¹ (data not shown). The flux values reported in Table 10-1, and in subsequent Tables and Figures, depict mediated transport activity, defined as the difference in uptake between RNA transcript-injected and control water-injected oocytes, and are from representative experiments. In all of the studies reported here, uridine uptake in water-injected oocytes was < 0.02 pmol/oocyte.min⁻¹ under all conditions tested (data not shown).

Mutants exhibiting uridine uptake values < 0.1 pmol/oocyte.min⁻¹ were excluded from further analysis (Table 10-1). Only nine out of the 133 residues investigated fell into this category (6.8%) and in every case, the mutation to cysteine resulted in a protein with low functional activity both in Na⁺- and H⁺-containing media (100 mM NaCl, pH 8.5 and 100 mM ChCl, pH 5.5, respectively). The nine amino acids were: Met⁴⁹⁶ and Gly⁴⁹⁸ in TM 11, Glu⁵¹⁹ in TM 11A, Phe⁵⁶³ and Ser⁵⁶⁸ in TM 12, and Arg⁵⁹³, Ala⁵⁹⁴, Ala⁶⁰⁶ and Gly⁶¹⁰ in TM 13.

To facilitate comparisons between the remaining 124 mutants, the uridine transport activity of each construct is also presented as a Na⁺:H⁺ uptake ratio (Table 10-1). Corresponding Na⁺:H⁺ ratios of uridine uptake (10 μ M) for wild-type hCNT3 and cysteine-less hCNT3C- were \sim 1.7 and 1.0, respectively (averaged results from multiple experiments; data not shown) and are in good agreement with previous studies (Chapters 5, 6 and 8). Residue mutations which resulted in Na⁺:H⁺ ratios of uridine uptake < 0.5 and > 2.5 (Table 10-1) are highlighted in the hCNT3 topology schematic shown in Fig. 10-2.

All mutants in TM 11, TM 13 and in the loop between TMs 12 and 13 exhibited $\text{Na}^+:\text{H}^+$ uptake ratios similar to hCNT3/hCNT3C-. In contrast, mutant Y558C(C-) in TM 12 presented a $\text{Na}^+:\text{H}^+$ ratio of 0.2 and three other TM 12 mutants exhibited $\text{Na}^+:\text{H}^+$ ratios > 2.5 (A564C(C-), N565C(C-) and I566C(C-) with ratios equal to 5.0, 3.3 and 2.6, respectively).

A cluster of residues with altered cation-coupling characteristics was also evident in the loop between TMs 11 and 12. Mutation of residue Tyr⁵¹³ to cysteine resulted in a $\text{Na}^+:\text{H}^+$ uptake ratio of 0.4 and the more numerous residues whose mutation to cysteine resulted in $\text{Na}^+:\text{H}^+$ ratios > 2.5 were Gly⁵¹² (3.9), Lys⁵¹⁴ (7.9), Phe⁵¹⁶ (3.1), Ala⁵²² (7.0), Glu⁵²⁴ (2.6) and His⁵²⁵ (2.7). All seven of these residues lie within the predicted TM 11A and, more specifically, five are located within the conserved CNT family (G/A)XKX₃NEFVA(Y/M/F) motif. This motif in hCNT3 corresponds to residues GYKTFFNEFVAY which span the region from Gly⁵¹² to Tyr⁵²³. Although the transport activity of E519C(C-) was < 0.1 pmol/oocyte.min⁻¹ and therefore not analyzed in the present study, the transport activity of two Glu⁵¹⁹ mutants in a wild-type hCNT3 background (E519D and E519C) was previously characterized (Chapter 9). Both of these mutants displayed robust transport of uridine in the presence of Na^+ , but only low (E519D) or not detectable levels of transport activity in the presence of H^+ (E519C) (Chapter 9).

PCMBS inhibition of single cysteine mutants – Wild-type hCNT3 and three TM 12 residues (Ile⁵⁵⁴, Tyr⁵⁵⁸ and Cys⁵⁶¹) were previously reported to be sensitive to inhibition by PCMBS under acidic conditions only (*ie.* in the presence of H^+) (Chapter 7). Previous control experiments have also established lack of inhibition by PCMBS for transport mediated by hCNT3C- in both Na^+ - and H^+ -containing medium (Chapter 7). Therefore, single cysteine mutants of hCNT3C- were tested for inhibition by PCMBS both in Na^+ -containing, H^+ -reduced medium (100 mM NaCl, pH 8.5) and in Na^+ -free, acidified medium (100 mM ChCl, pH 5.5). After 10 min exposure to 200 μM PCMBS, uptake of 10 μM radiolabeled uridine was assayed in medium of the same composition (10, Chapter 7). Results for each individual mutant calculated as a percentage of mediated uridine uptake in the absence of PCMBS are presented in Fig. 10-3 (TM

regions) and Fig. 10-4 (loop regions). For screening purposes, a residue was considered PCMBS-inhibitable upon exhibiting $\leq 60\%$ of uridine uptake (*ie.* $\geq 40\%$ inhibition of uridine uptake) following incubation with PCMBS. Residues that were PCMBS-inhibitable are highlighted in Figs. 10-3 and 10-4, and the corresponding numerical values are presented in Table 10-2. A schematic of the locations of these PCMBS-inhibitable residues is presented in Fig. 10-5.

In TM 11, three residues, Phe⁴⁸², Ser⁴⁸⁷ and Met⁴⁹¹, were PCMBS-inhibitable in both Na⁺- and H⁺-containing medium upon mutation to cysteine. Flanking Phe⁴⁸², mutants E483C(C-) and L484C(C-) were PCMBS-inhibitable in Na⁺-containing medium only and, in the opposite direction, L480C(C-) was PCMBS-inhibitable only in H⁺-containing medium. As described previously (Chapter 7), and as also shown here, TM 12 contains four residues which, upon mutation to cysteine, are PCMBS-inhibitable in the presence of both Na⁺ and H⁺ (Thr⁵⁵⁷, Asn⁵⁶⁵, Gly⁵⁶⁷ and Ile⁵⁷¹) and three which are only PCMBS-inhibitable in the presence of H⁺ (Ile⁵⁵⁴, Tyr⁵⁵⁸ and Ser⁵⁶¹). In TM 13, three mutants were PCMBS-sensitive (A601C(C-), A609C(C-) and L612C(C-)) and were inhibitable in both Na⁺- and H⁺-containing media.

Inhibition of an introduced cysteine residue by PCMBS was previously described for Glu⁵¹⁹ in hCNT3 TM 11A (Chapter 9). Scanning of the loop between TMs 11 and 12, the region which includes TM 11A, revealed additional residues which were also PCMBS-inhibitable. Upon conversion to cysteine in hCNT3C-, residues Met⁵⁰⁶, Tyr⁵¹³, Phe⁵¹⁶, Phe⁵¹⁷, Asn⁵¹⁸, Phe⁵²⁰, Val⁵²¹, Tyr⁵²³ and Leu⁵²⁶ were PCMBS-inhibitable in both Na⁺- and H⁺-containing media. Additionally, Ala⁵²² in Na⁺-containing medium only and Ala⁵⁰⁸, Gly⁵¹² and Gln⁵⁴⁵ in H⁺-containing medium only were also PCMBS-inhibitable. Of these 13 residues, 11 lie within the TM 11A region, and nine are located within the CNT family (G/A)XKX₃NEFVA(Y/M/F) motif. In contrast to this region, none of the residues in the TM 12 - 13 loop, when converted to cysteine in hCNT3C-, demonstrated inhibition by PCMBS under either cation condition.

Uridine protection of PCMBS inhibition – Subsequent experiments investigated the ability of extracellular uridine (20 mM) to protect against inhibition by PCMBS for

residues which were PCMBS-inhibitable in either or both Na⁺- and H⁺-containing media. Results for each individual mutant are presented in Table 10-2 as a percentage of mediated uridine uptake in the absence of PCMBS, and uridine-protectable residues are highlighted in the hCNT3 topology schematic of Fig. 10-5.

In TM 11, three residues exhibited uridine protection from PCMBS inhibition. L480C(C-), which was PCMBS-inhibitable in H⁺-containing medium only, demonstrated full protection against that inhibition and F482C(C-), which was PCMBS-inhibitable in both Na⁺- and H⁺-containing medium, was also fully protectable under both cation conditions. In contrast, M491C(C-), which was also PCMBS-inhibitable under both cation conditions, was partially protectable only in Na⁺-containing medium. As previously described (Chapter 7), five of the seven PCMBS-inhibitable mutants in TM 12 exhibited uridine protection. These were N565C(C-), G567C(C-) and I571C(C-) which were PCMBS-inhibitable in both Na⁺- and H⁺-containing medium, and Y558C(C-) and S561C(C-) which were PCMBS-inhibitable only in the presence of H⁺. Except for Y558C(C-), the four other TM 12 mutants exhibited full protection against PCMBS inhibition. Of the three mutants in TM 13 which were PCMBS-inhibitable in both Na⁺- and H⁺-containing medium, L612C(C-) and A609C(C-) were fully and partially protectable, respectively, by extracellular uridine under both cation conditions.

In the TM 11 - 12 loop, only one mutant inhibitable by PCMBS in both Na⁺ and H⁺-containing media, F516C(C-), exhibited uridine protection under both cation conditions. Y523C(C-) and L526C(C-), which were also PCMBS-inhibitable in the presence of both Na⁺ and H⁺, were only protectable in Na⁺-containing medium. A508C(C-) and G512C(C-), which were PCMBS-inhibitable in H⁺-containing medium only, and A522C(C-), which was PCMBS-inhibitable in Na⁺-containing medium only, also showed uridine protection under their respective cation conditions. All six of the uridine-protectable residues in the TM 11 - 12 loop are located in TM 11A and three of these reside within the CNT family (G/A)XKX₃NEFVA(Y/M/F) motif.

Discussion

Previous studies have used PCMBs to investigate the membrane topology and functions of key regions in hCNT3, including TMs 8, 11A and 12 (Chapters 4, 7 and 9). Incorporating results from TM 12 (Chapter 7), the present investigation reports a SCAM analysis of the entire C-terminal one-third of the protein (hCNT3C- TMs 11 - 13, inclusive) (Fig. 10-1). The functional importance of this region of hCNTs has been highlighted previously by a number of studies. For example, TM 11A residues Glu⁴⁹⁸ and Glu⁵¹⁹ of hCNT1 and hCNT3, respectively, have been identified as playing important roles in nucleoside and cation binding and translocation events (Chapter 9, Appendix 4). In the wild-type hCNT3 background, mutants E519Q and E519C exhibited no and low functional activity, respectively, despite wild-type hCNT3-like abundance at the cell surface (Chapter 9). hCNT3 E519C exhibited decreased apparent affinities for both uridine and Na⁺, a change in Na⁺:nucleoside coupling ratio from 2:1 to 1:1 and loss of H⁺-dependence (Chapter 9). Additionally, the mutant showed inhibition by PCMBs and was partially protectable by the addition of extracellular uridine (Chapter 9). Studies investigating the PCMBs sensitivity of wild-type hCNT3 and the decrease in apparent affinity for Na⁺ exhibited by hCNT3C- identified Cys⁵⁶¹ (TM 12) as a conformationally mobile residue that becomes exposed to PCMBs in the H⁺-bound state of hCNT3 and which has importance for interactions with both Na⁺ and H⁺ (Chapters 7 and 8). A mutation of TM 13 residue, Cys⁶⁰², has also been shown to influence Na⁺ binding and/or translocation events (11). Using a yeast expression system, SCAM analysis of hCNT3C- single cysteine mutants of TMs 11, 12 and 13 identified two residues in TM 11 (Leu⁴⁸⁰ and Ser⁴⁸⁷) and four in TM 12 (Thr⁵⁵⁷, Asn⁵⁶⁵, Gly⁵⁶⁷ and Ile⁵⁷¹) that exhibited uridine-protectable inhibition by MTS reagents (7). These findings are consistent with both TMs 11 and 12 facing the water-accessible uridine permeation pathway. In contrast to the present study, the SCAM analysis of hCNT3 with MTS reagents in yeast focused exclusively on predicted membrane-spanning residues in TMs 11, 12 and 13, and did not include TM 11A and surrounding amino acids.

Initial characterization of the hCNT3C- single cysteine mutants investigated in the present study measured uridine uptake in both Na⁺- and H⁺-containing transport medium (Table 10-1). Of the 133 mutants examined, nine exhibited uridine uptake values < 0.1 pmol/oocyte.min⁻¹ under both conditions (Table 10-1). Two of these mutants were in TM 11 (M496C(C-) and G498C(C-)), one in TM 11A (E519C(C-)), two in TM 12 (F563C(C-) and S568C(C-)) and four in TM 13 (R593C(C-), A594C(C-), A606C(C-) and G610C(C-)). These mutants were excluded from further functional analysis.

Interestingly, the corresponding MTS study examining TMs 11, 12 and 13 in yeast also identified the majority of these same residues, upon mutation to cysteine, to be non-functional (Met⁴⁹⁶, Gly⁴⁹⁸, Phe⁵⁶³, Ala⁵⁹⁴ and Ala⁶⁰⁶) or exhibit low transport activity (Ser⁵⁶⁸, Arg⁵⁹³ and Gly⁶¹⁰) (7). In addition, G598C(C-) was non-functional and I485C(C-), L595C(C-) and F603C(C-) exhibited low transport capacity in yeast (7). Cell surface processing experiments found all of these mutants, except G498C(C-) and L595C(C-), to be present at the yeast cell surface in similar abundance to the wild-type protein (7). Common to both studies, therefore, the following amino acids have potentially important roles in hCNT3 structure and/or function: Met⁴⁹⁶ in TM 11, Phe⁵⁶³ and Ser⁵⁶⁸ in TM 12, and Arg⁵⁹³, Ala⁵⁹⁴, Ala⁶⁰⁶ and Gly⁶¹⁰ in TM 13. In the yeast expression system, mutants M496C(C-) and G598C(C-) were rescued by conversion to alanine (M496A(C-) and G598A(C-), respectively), whereas G498C(C-) and F563C(C-) were not (7). Although broadly similar in overall profile, the observed differences in the functional activity of some mutants indicates the existence of variations in processing, expression and/or conformation of the mature proteins at the cell surface in the *Xenopus* oocyte and yeast expression systems.

hCNT3 couples nucleoside transport to both Na⁺ and H⁺ electrochemical gradients and exhibits a Na⁺:H⁺ ratio of uridine uptake (10 μM) of ~ 1.7 (Chapters 5 and 6). Similarly, hCNT3C- also mediates both Na⁺- and H⁺-coupled uridine transport, although the apparent K₅₀ for Na⁺ is increased ~ 11-fold, decreasing the Na⁺:H⁺ ratio of uridine uptake (10 μM) to ~ 1.0 (Chapter 8). Table 10-1 and Fig. 10-2 highlight those

residues whose mutation to cysteine in hCNT3C- resulted in $\text{Na}^+:\text{H}^+$ uridine uptake ratios either < 0.5 (*ie.* H^+ -preferring) or > 2.5 (*ie.* Na^+ -preferring). Such mutants identify residues likely to be involved directly or indirectly in interactions with the coupling cation. Furthermore, the locations of these residues correspond well with regions of the protein previously identified to be important for hCNT cation interactions.

In a previous study, mutation of hCNT3 Cys⁵⁶¹, a conformationally mobile TM 12 residue located at the Na^+/H^+ boundary of extracellularly-accessible residues, influenced interactions with coupling cation in a manner which was different for Na^+ compared to H^+ (Chapter 7). In good agreement with a role for TM 12 in cation interactions, mutation to cysteine in hCNT3C- resulted in $\text{Na}^+:\text{H}^+$ ratios of uridine uptake < 0.5 for residue Tyr⁵⁵⁸ (*ie.* H^+ -preferring) and > 2.5 for residues Ala⁵⁶⁴, Asn⁵⁶⁵ and Ile⁵⁶⁶ (*ie.* Na^+ -preferring). Also in a previous study, the hCNT3 TM 11A residue Glu⁵¹⁹ was demonstrated to be an important determinant of Na^+/H^+ coupling to the conserved CNT cation binding site that in other family members interacts exclusively with either Na^+ or H^+ (Chapter 9). In the present investigation, mutation to cysteine in hCNT3C- resulted in $\text{Na}^+:\text{H}^+$ ratios of uridine uptake < 0.5 for residue Tyr⁵¹³ and > 2.5 for residues Gly⁵¹², Lys⁵¹⁴, Phe⁵¹⁶, Ala⁵²², Glu⁵²⁴ and His⁵²⁵ in the TM 11 - 12 loop, all of which also reside within TM 11A. Thus, the present results expand this role(s) of hCNT3 Glu⁵¹⁹ (TM 11A) and Cys⁵⁶¹ (TM 12) in cation binding and/or translocation to other adjacent residues in the same regions of the protein.

To summarize the data presented in Table 10-2 and Figs. 10-3 and 10-4, the schematic in Fig. 10-5 highlights those residues identified in hCNT3C- as PCMBs-sensitive and uridine-protectable. In agreement with previous predictions (3, 7), the pattern of PCMBs inhibition evident within TMs 11, 12 and 13 supports a conventional membrane-spanning α -helical architecture for these regions because affected residues, in general, cluster on one face of each of the helices. To more clearly demonstrate this, α -helical wheel projections for each of the TMs are presented in Fig. 10-6, although it is appreciated that the true structures of these regions of the protein may differ appreciably from the perfect α -helices illustrated.

In TM 11, PCMBS inhibition is evident for residues Gly⁴⁸³ and Leu⁴⁸⁴ in Na⁺-containing medium only, Leu⁴⁸⁰ in H⁺-containing medium only and Phe⁴⁸², Ser⁴⁸⁷ and Met⁴⁹¹ in both media. Of these, Leu⁴⁸⁰ (H⁺ only), Phe⁴⁸² (Na⁺ and H⁺) and Met⁴⁹¹ (Na⁺ only) show uridine protection. In the previous study investigating the effects of MTS reagents on these residue positions in yeast, inhibition by MTS reagents in the presence of Na⁺ at neutral pH, and partial protection against that inhibition by uridine, was evident for Leu⁴⁸⁰ and Ser⁴⁸⁷ (7). In the current 13 TM model of hCNT3 topology, the six PCMBS-inhibitable residues in TM 11 span a central to deep region within the helix, including the last putative residue (Leu⁴⁸⁰) of the helix (Fig. 10-5). Uridine protection is evident for residues located at both ends of this region (Met⁴⁹¹ and Leu⁴⁸⁰) (Fig. 10-5). This pattern of inhibition provides strong support for the reversed orientation of this helix. As such, the majority of PCMBS-inhibitable residues would lie exofacially within the helix in a position more likely to be accessible to the extracellular medium and available for PCMBS binding. Five of the six PCMBS-inhibitable residues cluster to one face of the helix (Fig. 10-6) and provide good evidence for an α -helical structure. Residue Phe⁴⁸² however resides on a separate face of the helix. A reversed orientation of TM 11, as predicted by the 15 TM model of hCNT3 membrane topology (Fig. 10-1 *inset*), would place residue Phe⁴⁸² at the exofacial boundary of the TM in a position potentially in contact with the external medium and accessible to PCMBS despite its location in a different face within the helix relative to the other PCMBS-inhibitable residues.

As previously reported (Chapter 7), three residues in TM 12 (Ile⁵⁵⁴, Tyr⁵⁵⁸ and Ser⁵⁶¹) show PCMBS inhibition in H⁺-containing medium only and four additional residues (Thr⁵⁵⁷, Asn⁵⁶⁵, Gly⁵⁶⁷ and Ile⁵⁷¹) show PCMBS inhibition in both Na⁺- and H⁺-containing medium (Fig. 10-5). Of the seven PCMBS-sensitive residues identified in TM 12, five (Tyr⁵⁵⁸, Ser⁵⁶¹, Asn⁵⁶⁵, Gly⁵⁶⁷ and Ile⁵⁷¹) showed uridine protection. In good agreement with these results, the yeast study also identified Thr⁵⁵⁷, Asn⁵⁶⁵, Gly⁵⁶⁷ and Ile⁵⁷¹ as MTS-sensitive in Na⁺-containing medium and these four residues exhibited varying degrees of uridine protection (7). In addition to residing in the extracellular-facing exofacial half of the helix, the H⁺-only PCMBS-inhibitable residues cluster to one face of the helix, whereas those reactive in the presence of both Na⁺ and H⁺ span a

region which is deeper within the helix and extend over a wider aspect of the helix face (Figs. 10-5 and 10-6). Consistent with a conventional α -helical structure for this TM, all of the PCMBS-accessible residues nevertheless reside within one-half of the helix surface. TM 12 Cys⁵⁶¹ is the residue responsible for PCMBS inhibition of wild-type hCNT3 (Chapter 7). This occurs under acidified conditions only, and therefore reports a specific conformational change associated with H⁺ binding (Chapter 7). Adjacent residues Ile⁵⁵⁴ and Tyr⁵⁵⁸ report the same H⁺-mediated conformational transition. Unlike TM 11, the longitudinal dispersal of PCMBS-sensitive residues shown in Fig. 10-5 for TM 12 suggests that the helix is presented in its correct transmembrane orientation. Nevertheless, the finding that residue Ile⁵⁷¹ showed clear evidence of PCMBS inhibition and uridine protection (Table 10-2) indicates that the hCNT3 translocation pore penetrates deep within the membrane.

Although no TM 13 residues were reported as MTS-sensitive (7), the present study identified Ala⁶⁰¹, Ala⁶⁰⁹ and Leu⁶¹² as PCMBS-sensitive in the presence of both Na⁺ and H⁺. Uridine protection from PCMBS inhibition was evident for the two most exofacially located residues, Ala⁶⁰⁹ and Leu⁶¹² (Fig. 10-5). Supporting an α -helical structure for TM 13, these three residues cluster to one face of the helix (Fig. 10-6). Similar to TM 12, but unlike TM 11, the predicted location of Ala⁶⁰¹, Ala⁶⁰⁹ and Leu⁶¹² within the extracellular half of the membrane field (Fig. 10-5) provides evidence that TM 13 is correctly oriented in both the 13 and 15 TM topology models of hCNT3 membrane architecture (Fig. 10-1). Consistent with previous findings for rat (r) CNT1 (3) and the demonstration that all hCNT3 glycosylation sites are confined to the end C-terminal tail region of the transporter affords additional supporting evidence in this regard (Chapter 8).

The TM 11 - 12 loop, encompassing TM 11A, revealed an unexpected and novel pattern of reactivity to PCMBS (Table 10-2 and Figs. 10-4 and 10-5). Fourteen of the 52 residues in this region showed inhibition by PCMBS upon conversion to cysteine in hCNT3C-, including residue Ala⁵²² in Na⁺-containing medium only, Ala⁵⁰⁸, Gly⁵¹² and Gln⁵⁴⁵ in H⁺-containing medium only and Met⁵⁰⁶, Tyr⁵¹³, Phe⁵¹⁶, Phe⁵¹⁷, Asn⁵¹⁸, Phe⁵²⁰, Val⁵²¹, Tyr⁵²³ and Leu⁵²⁶ in both Na⁺- and H⁺-containing medium. Uridine protection

from PCMBS inhibition was evident for six of the residues: Ala⁵²² and Tyr⁵²³ in the presence of Na⁺ only, Ala⁵⁰⁸ and Gly⁵¹² in the presence of H⁺ only and Phe⁵¹⁶ and Leu⁵²⁶ with both Na⁺ and H⁺ present. Together, the results suggest that this region is critically involved in the transport mechanism of hCNT3 and predict at least a portion of it to be membrane-associated. This could be either in the form of a re-entrant loop or as part of a transmembrane domain. The majority of the PCMBS-sensitive residues reside within the previously predicted membrane domain TM 11A. One exception was Met⁵⁰⁶, for which the corresponding hCNT3C- mutant showed PCMBS inhibition in both Na⁺- and H⁺-containing medium, and is positioned immediately adjacent to the TM 11A region. It is possible that the putative boundary of TM 11A is extended to include Met⁵⁰⁶ within the membrane-associated region. The other exception was Gln⁵⁴⁵, which is separated from putative TMs 11A and 12 by 17 and eight residues, respectively (Fig. 10-5). Q545C(C-) showed robust PCMBS inhibition in H⁺-containing medium only and was not uridine-protected. Centrally positioned in the putative exofacial loop region linking TMs 11A and 12 (Fig. 10-1 *inset* and Fig. 10-5), residue Gln⁵⁴⁵ is unlikely to be membrane-associated, but may nevertheless reside in sufficiently close proximity to the exofacial aspect of translocation pore such that the binding of PCMBS interferes with hCNT3 cotransport activity. Since Q545C(C-) was inhibited by PCMBS in H⁺-containing medium only, it may be similar to Cys⁵⁶¹ (Chapter 7) and be reporting a specific H⁺-induced conformation of the transporter.

The overall pattern of PCMBS reactivity in putative TM 11A suggests that this region, or at least part of it, differs from the traditional α -helical structure of membrane-associated TMs. Within the conserved CNT family (G/A)XKX₃NEFVA(Y/M/F) motif of TM 11A, a sequence of eight consecutive residues, extending from Phe⁵¹⁶ to Tyr⁵²³, were PCMBS-sensitive upon conversion to cysteine in both Na⁺- and H⁺-containing media; the only exceptions being Glu⁵¹⁹, which showed low levels of uridine transport activity, and Ala⁵²², which showed PCMBS inhibition in Na⁺-containing medium only. In the wild-type hCNT3 background, mutant E519C exhibited Na⁺-specific nucleoside transport activity and was PCMBS-sensitive in the presence of Na⁺ (Chapter 9). Within this region of eight PCMBS-inhibitable residues, three (Phe⁵¹⁶, Ala⁵²² and Tyr⁵²³) were uridine-protectable. Flanking either end of this block of PCMBS-sensitive residues, and

especially noticeable in the first part of the TM adjacent to Met⁵⁰⁶, the pattern of PCMBS inhibition showed evidence of periodicity consistent with small segments of α -helical content. TM 11A therefore has characteristics of a pore-lining discontinuous helix in which the majority of the residues comprising central conserved (G/A)XKX₃NEFVA(Y/M/F) motif, and including the key glutamate residue Glu⁵¹⁹, adopt a relaxed, extended and possibly mobile conformation within the translocation pore which allows PCMBS binding to most of the residues within the motif. Similar block patterns of PCMBS reactivity also occur in TMs 7 and 8 (12).

As such, the pattern of PCMBS inhibition reported here for TM 11A (and apparent also in TMs 7 and 8 (12)) provides the first functional evidence of extended structures or discontinuous membrane helices evident in crystal structures of recently solved bacterial membrane transport proteins, such as the *A. aeolicus* Na⁺/Cl⁻-dependent LeuT_{Aa} transporter (13). In LeuT_{Aa}, non-traditional transmembrane α -helices are disrupted by the insertion of extended regions of polypeptide which comprise the Na⁺ binding sites of the protein and, upon Na⁺ binding, are stabilized to then favour high-affinity binding of the permeant amino acid leucine (13). Reviewed recently by Screpanti and Hunte (14), such discontinuous membrane helices are proposed to play important mechanistic roles in ion recognition, binding and translocation in secondary active transporters. In the case of TM 11A in hCNT3, the centrally positioned glutamate residue Glu⁵¹⁹, which resides in the conserved (G/A)XKX₃NEFVA(Y/M/F) motif, plays a critical role in cation coupling that is likely manifest in all CNT family members (Chapter 9). Separated only by 26 amino acids, a membrane-associated TM 11A is likely to lie within the translocation pore in close proximity to TM 12, which was previously shown to be mobile and undergo cation-dependent conformational changes (Chapter 7).

The pattern of PCMBS-inhibitable and uridine-protectable residues in TMs 12 and 13 support the current α -helical orientation of these regions, whereas in TM 11, a reversed orientation is more plausible. As such, the membrane-associated TM 11A would be membrane-spanning rather than, for example, a re-entrant loop. A schematic outlining this change in topological architecture is depicted in Fig. 10-7. This is in good

agreement with earlier predictions for TMs 5A and 11A as potentially membrane-spanning (3) as shown in the *inset* of Fig. 10-1. Previously, SCAM analysis of TMs 11, 12 and 13 revealed MTS-sensitive residues buried deep within the TM 11 helix, but the overall patterning was largely inclusive (7). Thus, the present study expands upon these earlier findings and provides solid experimental evidence to support the original hypothesis of an additional TM 11A. As shown in Fig. 10-1 (*inset*), insertion of both TMs 5A and 11A through the membrane bilayer would result in opposite orientation for TMs 6 to 11. In agreement with this, a recent structure-function study of negatively charged residues in hCNT1 has provided evidence for an opposite orientation for TM 7 (Appendix 4). Full PCMBS SCAM analysis of hCNT3C- TMs 7 and 8 is in progress and confirms their opposite orientation (12). Therefore, current evidence favors a 15 TM rather than 13 TM model of hCNT3 membrane architecture (Fig. 10-1).

PCMBS-inhibitable and uridine-protectable residues were identified in TMs 11, 11A, 12 and 13, thereby placing aspects of all four regions within, or in close proximity to, the permeant translocation pathway of hCNT3. At the very least, all of the residues inhibited by PCMBS must be solvent-accessible from the extracellular medium and in a location where PCMBS binding compromises transport activity. Serving as a positive control for the present experiments, the putative intracellular loop between TMs 12 - 13 showed no inhibition by PCMBS despite robust functional activity of all of the mutants. Quantitatively, the residues showing the most severe inhibition by PCMBS were located in TMs 11A and 12, and not TMs 11 and 13 (Table 10-2). For example, TMs 11 and 13 contained no residues where uptake was inhibited by PCMBS by > 80%, whereas TM 11A contained six (Phe⁵¹⁶, Phe⁵¹⁷, Asn⁵¹⁸, Phe⁵²⁰, Tyr⁵²³ and Leu⁵²⁶) and TM 12 contained three (Thr⁵⁵⁷, Tyr⁵⁵⁸ and Gly⁵⁶⁷). Furthermore, the five of these residues that were uridine-protectable (Phe⁵¹⁶, Tyr⁵²³, Leu⁵²⁶, Tyr⁵⁵⁸ and Gly⁵⁶⁷) were fully protected by extracellular uridine (*ie.* uptake restored to 100%) (Table 10-2). This strongly implicates these two TMs in formation of key functional regions of the translocation pore and supports the previous studies implicating residues in TMs 11A (Chapter 9, Appendix 4) and 12 (Chapter 7) to be involved in permeant and cation binding and/or translocation. Additionally, residues which altered the Na⁺:H⁺ ratio of uridine uptake were also located in TM 11A and 12 (Fig. 10-7). In contrast, residues in TMs 11 and 13

were inhibited by PCMBs to a lesser extent and of the five residues that were uridine-protectable, two (Met⁴⁹¹ in TM 11 and Ala⁶⁰⁹ in TM 13) were only partially protected by extracellular uridine (Table 10-2). Similarly, only two hCNT3C- residues in TM 11 (Leu⁴⁸⁰ and Ser⁴⁸⁷) and no residues in TM 13 were identified as inhibitable by MTS reagents in the yeast study and those mutants also displayed only partial inhibition and protection (7). In combination with the fact that PCMBs-accessible residues were more exofacially located in TMs 11 and 13 than in TMs 11A and 12 (Fig. 10-7), these findings suggest that TMs 11 and 13 may be less directly involved in formation of the translocation pore than TMs 11A and 12. Some cases of PCMBs-inhibition and/or uridine-protection may, for example, be secondary indirect effects of cation- or permeant-induced conformational changes, rather than indicators of close-proximity interaction with cation or nucleoside binding domains.

The present study also contributes to two further insights into hCNT3 structure and function. The first relates to cation-dependent conformations adopted by the exofacially-facing form of the protein. In contrast to Na⁺-specific hCNT1 and hCNT2, hCNT3 mediates both Na⁺- and H⁺-coupled nucleoside cotransport (1, 2, 4, 15, Chapters 5 and 6). The cation:nucleoside stoichiometry for hCNT3 H⁺-coupled transport is 1:1 compared to 2:1 for Na⁺ and, when both cations are present, charge/uptake experiments suggest that hCNT3 binds one Na⁺ and one H⁺ (Chapters 5 and 6). The nucleoside and nucleoside drug selectivity pattern of hCNT3 in the presence of H⁺ also differs from that in the presence of Na⁺ (4, Chapter 5). Previously, mutation of hCNT3 Cys⁵⁶¹ in TM 12 was reported to alter Na⁺ and H⁺ kinetics and, together with Tyr⁵⁵⁸ and Ile⁵⁵⁴, forms a face of the helix which becomes extracellularly accessible to PCMBs only in the presence of H⁺ (Fig. 10-6), thus reporting a H⁺-dependent conformation of the protein (Chapters 7 and 8). Building upon these observations, the different patterns of residues exhibiting PCMBs inhibition and uridine protection in Na⁺-containing medium only *versus* H⁺-containing medium only *versus* both transport media provides strong additional support for the existence of multiple Na⁺- and/or H⁺-induced conformational states of hCNT3 (Table 10-2 and Fig. 10-5), some of which, like the H⁺-specific TM 12 Ile⁵⁵⁴/Tyr⁵⁵⁸/Cys⁵⁶¹ cluster, involve subdomains within TMs. Other potential conformational differences are even more subtle. The arrows in Figs. 10-5 and 10-7, for

example, identify residues in TMs 11 and 11A which are PCMBBS-sensitive in both Na⁺- and H⁺-containing media, but uridine-protected only in the presence of Na⁺.

Second, the present studies support the concept of central closely adjacent cation-nucleoside binding domains within a common cation/nucleoside translocation pore. Similar to TM 12, TM 11A contains residues deep within the membrane that are PCMBBS-inhibitable and uridine-protectable. Met⁴⁹¹, a centrally positioned residue in TM 11, also shares this phenotype. In good agreement with this, other cation transporters for which high resolution molecular structures have been solved, including LeuT_{Aa} (13) and Glt_{Ph} (16), also exhibit central cation and permeant binding domains.

In conclusion, this SCAM analyses of the C-terminal one-third of hCNT3 supports a revised topology model for hCNTs, with the insertion of TM 11A as a membrane-spanning discontinuous helix. Confirmation of this new membrane architecture will come from on-going studies of TMs 7 and 8, as well as other remaining portions of the C-terminal half of hCNT3 and by extension of the analysis to TMs in the N-terminal half of the transporter, including TM 5A. Additionally, this study highlights the functional importance of residues in TMs 11A and 12 in key cation and nucleoside binding and/or translocation events.

Table 10-1. Na⁺- and H⁺-mediated uptake of uridine in *Xenopus* oocytes expressing hCNT3C- single cysteine mutants. Influx of 10 μM ³H-uridine was measured in both Na⁺-containing and H⁺-containing medium (100 mM NaCl, pH 8.5 or 100 mM ChCl, pH 5.5, respectively). Na⁺:H⁺ uptake ratios which are < 0.5 or > 2.5 are highlighted with an asterisk (*). Values are corrected for basal non-mediated uptake in control water-injected oocytes. Each value is the mean ± SEM of 10 - 12 oocytes.

TM 11	Mediated Uridine Uptake (pmol/oocyte.min ⁻¹)		Na ⁺ :H ⁺ Ratio
	Na ⁺ (100 mM NaCl, pH 8.5)	H ⁺ (100 mM ChCl, pH 5.5)	
L480C(C-)	0.9 ± 0.1	1.1 ± 0.2	0.8
S481C(C-)	1.2 ± 0.1	0.7 ± 0.1	1.7
F482C(C-)	0.8 ± 0.1	0.7 ± 0.1	1.1
E483C(C-)	0.6 ± 0.1	0.2 ± 0.1	2.5
L484C(C-)	2.6 ± 0.5	2.7 ± 0.3	1.0
I485C(C-) ^b	2.0 ± 0.3	1.4 ± 0.1	1.4
S486C(C-)	3.9 ± 0.4	2.6 ± 0.2	1.5
S487C(C-)	1.4 ± 0.2	1.7 ± 0.2	0.8
Y488C(C-)	2.3 ± 0.2	1.1 ± 0.1	2.2
I489C(C-)	2.3 ± 0.2	2.5 ± 0.3	0.9
F490C(C-)	0.9 ± 0.2	0.4 ± 0.1	2.4
M491C(C-)	2.5 ± 0.3	2.7 ± 0.3	0.9
P492C(C-)	1.0 ± 0.1	0.8 ± 0.1	1.3
F493C(C-)	3.6 ± 0.4	2.3 ± 0.2	1.6
S494C(C-)	0.7 ± 0.1	1.0 ± 0.1	0.8
F495C(C-)	1.6 ± 0.3	1.7 ± 0.2	0.9
M496C(C-) ^a	< 0.1	< 0.1	-
M497C(C-)	2.0 ± 0.2	3.0 ± 0.2	0.7
G498C(C-) ^a	< 0.1	< 0.1	-
V499C(C-)	1.8 ± 0.3	3.0 ± 0.3	0.7
E500C(C-)	4.8 ± 0.3	4.3 ± 0.3	1.1

Table 10-1 (continued).

TM 11 - 12 loop	Mediated Uridine Uptake (pmol/oocyte.min ⁻¹)		Na ⁺ :H ⁺ Ratio
	Na ⁺ (100 mM NaCl, pH 8.5)	H ⁺ (100 mM ChCl, pH 5.5)	
W501C(C-)	3.1 ± 0.6	1.3 ± 0.3	2.4
Q502C(C-)	4.1 ± 0.5	3.5 ± 0.2	1.2
D503C(C-)	2.2 ± 0.2	1.3 ± 0.1	1.7
S504C(C-)	1.7 ± 0.3	1.8 ± 0.2	1.0
F505C(C-)	3.9 ± 0.4	2.9 ± 0.3	1.4
M506C(C-)	2.0 ± 0.2	2.2 ± 0.2	0.9
V507C(C-)	5.0 ± 0.3	5.8 ± 0.4	0.9
A508C(C-)	2.0 ± 0.3	1.3 ± 0.2	1.5
R509C(C-)	6.8 ± 0.3	4.2 ± 0.3	1.6
L510C(C-)	5.4 ± 0.3	5.9 ± 0.4	0.9
I511C(C-)	3.4 ± 0.3	3.7 ± 0.3	0.9
G512C(C-)	1.4 ± 0.2	0.4 ± 0.1	3.9*
Y513C(C-)	1.4 ± 0.1	3.2 ± 0.4	0.4*
K514C(C-)	1.1 ± 0.2	0.1 ± 0.1	7.9*
T515C(C-)	1.9 ± 0.3	2.1 ± 0.2	0.9
F516C(C-)	4.8 ± 0.4	1.5 ± 0.1	3.1*
F517C(C-)	0.3 ± 0.1	0.4 ± 0.1	0.6
N518C(C-)	3.8 ± 0.4	1.6 ± 0.2	2.3
E519C(C-)	< 0.1	< 0.1	-
F520C(C-)	1.2 ± 0.1	1.7 ± 0.1	0.7
V521C(C-)	2.1 ± 0.2	1.0 ± 0.1	2.1
A522C(C-)	1.8 ± 0.1	0.3 ± 0.1	7.0*
Y523C(C-)	1.2 ± 0.2	0.5 ± 0.1	2.5
E524C(C-)	2.7 ± 0.2	1.0 ± 0.1	2.6*
H525C(C-)	4.2 ± 0.4	1.6 ± 0.2	2.7*
L526C(C-)	4.0 ± 0.4	5.5 ± 0.6	0.7
S527C(C-)	2.3 ± 0.2	2.5 ± 0.2	0.9
K528C(C-)	4.0 ± 0.4	4.0 ± 0.2	1.0
W529C(C-)	3.2 ± 0.2	4.5 ± 0.3	0.7
I530C(C-)	3.5 ± 0.4	2.5 ± 0.2	1.4
H531C(C-)	4.5 ± 0.4	3.8 ± 0.2	1.2
L532C(C-)	3.2 ± 0.3	3.6 ± 0.4	0.9
R533C(C-)	4.2 ± 0.4	3.5 ± 0.3	1.2

Table 10-1 (continued).

TM 11 - 12 loop	Mediated Uridine Uptake (pmol/oocyte.min ⁻¹)		Na ⁺ :H ⁺ Ratio
	Na ⁺ (100 mM NaCl, pH 8.5)	H ⁺ (100 mM ChCl, pH 5.5)	
K534C(C-)	3.8 ± 0.2	4.3 ± 0.2	0.9
E535C(C-)	2.5 ± 0.3	1.6 ± 0.1	1.6
G536C(C-)	4.0 ± 0.4	4.1 ± 0.3	1.0
G537C(C-)	3.9 ± 0.3	4.5 ± 0.4	0.9
P538C(C-)	4.3 ± 0.3	3.9 ± 0.3	1.1
K539C(C-)	4.1 ± 0.2	4.6 ± 0.5	0.9
F540C(C-)	3.8 ± 0.3	4.7 ± 0.5	0.8
V541C(C-)	4.1 ± 0.4	4.4 ± 0.4	0.9
N542C(C-)	5.0 ± 0.3	4.8 ± 0.5	1.0
G543C(C-)	5.0 ± 0.2	5.6 ± 0.4	0.9
V544C(C-)	4.3 ± 0.4	5.3 ± 0.3	0.8
Q545C(C-)	3.3 ± 0.1	5.1 ± 0.3	0.7
Q546C(C-)	3.3 ± 0.3	4.7 ± 0.3	0.7
Y547C(C-)	3.5 ± 0.2	4.2 ± 0.4	0.8
I548C(C-)	3.3 ± 0.2	4.4 ± 0.1	0.8
S549C(C-)	3.6 ± 0.2	5.0 ± 0.3	0.7
I550C(C-)	3.6 ± 0.2	4.7 ± 0.4	0.8
R551C(C-)	1.4 ± 0.1	1.4 ± 0.2	1.0
S552C(C-)	3.7 ± 0.2	5.2 ± 0.4	0.7
E553C(C-)	3.7 ± 0.3	5.2 ± 0.6	0.7

Table 10-1 (continued).

TM 12	Mediated Uridine Uptake (pmol/oocyte.min ⁻¹)		Na ⁺ :H ⁺ Ratio
	Na ⁺ (100 mM NaCl, pH 8.5)	H ⁺ (100 mM ChCl, pH 5.5)	
I554C(C-)	2.0 ± 0.3	1.5 ± 0.2	1.3
I555C(C-)	1.9 ± 0.2	2.1 ± 0.2	0.9
A556C(C-)	1.5 ± 0.3	1.5 ± 0.1	1.0
T557C(C-)	2.7 ± 0.3	1.9 ± 0.1	1.4
Y558C(C-)	0.1 ± 0.1 ^c	0.5 ± 0.1	0.2*
A559C(C-)	0.8 ± 0.1	1.0 ± 0.1	0.8
L560C(C-)	2.1 ± 0.3	2.1 ± 0.3	1.0
S561C(C-)	2.4 ± 0.4	3.6 ± 0.2	0.7
G562C(C-)	0.8 ± 0.2	0.5 ± 0.1	1.5
F563C(C-) ^a	< 0.1	< 0.1	-
A564C(C-)	0.5 ± 0.1	0.1 ± 0.1 ^d	5.0*
N565C(C-)	2.6 ± 0.4	0.8 ± 0.1	3.3*
I566C(C-)	0.9 ± 0.2	0.4 ± 0.1	2.6*
G567C(C-)	1.4 ± 0.3	0.9 ± 0.1	1.6
S568C(C-) ^b	< 0.1	< 0.1	-
L569C(C-)	1.8 ± 0.3	1.5 ± 0.2	1.1
G570C(C-)	1.1 ± 0.2	0.7 ± 0.1	1.6
I571C(C-)	3.2 ± 0.4	1.4 ± 0.1	2.3
V572C(C-)	3.3 ± 0.3	2.0 ± 0.2	1.7
I573C(C-)	3.8 ± 0.5	1.8 ± 0.2	2.1
G574C(C-)	0.2 ± 0.1	0.1 ± 0.1	1.4

Table 10-1 (continued).

TM 12 - 13 Loop	Mediated Uridine Uptake (pmol/oocyte.min ⁻¹)		Na ⁺ :H ⁺ Ratio
	Na ⁺ (100 mM NaCl, pH 8.5)	H ⁺ (100 mM ChCl, pH 5.5)	
G575C(C-)	4.6 ± 0.6	3.5 ± 0.3	1.3
L576C(C-)	2.9 ± 0.3	1.7 ± 0.2	1.8
T577C(C-)	3.9 ± 0.5	3.1 ± 0.3	1.2
S578C(C-)	3.7 ± 0.3	3.5 ± 0.2	1.1
M579C(C-)	4.2 ± 0.3	2.9 ± 0.3	1.5
A580C(C-)	4.1 ± 0.3	3.5 ± 0.3	1.2
P581C(C-)	0.6 ± 0.1	0.2 ± 0.1	2.5
S582C(C-)	4.4 ± 0.5	5.7 ± 0.3	0.8
R583C(C-)	1.6 ± 0.3	1.0 ± 0.1	1.7
K584C(C-)	2.3 ± 0.4	1.7 ± 0.2	1.3
R585C(C-)	3.7 ± 0.5	2.2 ± 0.2	1.7
D586C(C-)	4.9 ± 0.4	3.0 ± 0.4	1.6
I587C(C-)	1.2 ± 0.2	1.2 ± 0.1	1.0
A588C(C-)	2.1 ± 0.2	2.7 ± 0.2	0.8
S589C(C-)	3.4 ± 0.4	3.9 ± 0.4	0.9
G590C(C-)	3.5 ± 0.5	3.3 ± 0.2	1.1
A591C(C-)	1.9 ± 0.3	1.9 ± 0.2	1.0

Table 10-1 (continued).

TM 13	Mediated Uridine Uptake (pmol/oocyte.min ⁻¹)		Na ⁺ :H ⁺ Ratio
	Na ⁺ (100 mM NaCl, pH 8.5)	H ⁺ (100 mM ChCl, pH 5.5)	
V592C(C-)	2.0 ± 0.3	1.9 ± 0.2	1.1
R593C(C-) ^b	< 0.1	< 0.1	-
A594C(C-) ^a	< 0.1	< 0.1	-
L595C(C-) ^b	1.4 ± 0.2	1.3 ± 0.1	1.0
I596C(C-)	0.8 ± 0.1	1.1 ± 0.3	0.7
A597C(C-)	2.4 ± 0.3	3.6 ± 0.3	0.7
G598C(C-) ^a	0.8 ± 0.1	1.6 ± 0.3	0.5
T599C(C-)	2.6 ± 0.3	3.0 ± 0.3	0.9
V600C(C-)	2.2 ± 0.2	2.3 ± 0.2	1.0
A601C(C-)	0.4 ± 0.1	0.6 ± 0.1	0.6
S602C(C-)	4.2 ± 0.4	2.1 ± 0.2	2.0
F603C(C-) ^b	3.0 ± 0.4	2.4 ± 0.3	1.3
M604C(C-)	0.7 ± 0.2	0.6 ± 0.1	1.1
T605C(C-)	1.0 ± 0.2	1.7 ± 0.3	0.6
A606C(C-) ^a	< 0.1	< 0.1	-
S607C(C-)	1.8 ± 0.1	1.5 ± 0.2	1.2
I608C(C-)	1.3 ± 0.2	1.8 ± 0.2	0.7
A609C(C-)	0.8 ± 0.1	0.5 ± 0.1	1.6
G610C(C-) ^b	< 0.1	< 0.1	-
I611C(C-)	1.6 ± 0.3	1.7 ± 0.2	1.0
L612C(C-)	2.2 ± 0.2	2.0 ± 0.3	1.1

^a, previously identified as non-functional (7); ^b, previously identified as low-functioning (7); ^c, ^d, quoted to two decimal places in Table 7-1 of Chapter 7, the actual values are 0.11 ± 0.01 (^c) and 0.10 ± 0.01 (^d) pmol/oocyte.min⁻¹.

Table 10-2. Effect of PCMBs on uridine uptake in *Xenopus* oocytes expressing hCNT3C- single cysteine mutants. Influx of 10 μM ^3H -uridine was measured in both Na^+ -containing and H^+ -containing medium (100 mM NaCl, pH 8.5 or 100 mM ChCl, pH 5.5, respectively) following 10 min incubation on ice in the absence or presence of 200 μM PCMBs or 200 μM PCMBs + 20 mM uridine in media of the same composition used to determine uptake (*ie.* containing Na^+ or H^+ , as indicated). Values are corrected for basal non-mediated uptake in control water-injected oocytes and are presented as a percentage of mediated uridine influx in the absence of inhibitor for each individual mutant. Each value is the mean \pm SEM of 10 - 12 oocytes.

TM		Na^+		H^+	
		(100 mM NaCl, pH 8.5)		(100 mM ChCl, pH 5.5)	
		+ PCMBs ^a	+ PCMBs + uridine	+ PCMBs ^a	+ PCMBs + uridine
		(%)	(%)	(%)	(%)
11	L480C(C-) ^b	110 \pm 20	90 \pm 20	53 \pm 8	91 \pm 10
	F482C(C-)	39 \pm 7	91 \pm 20	59 \pm 8	98 \pm 10
	E483C(C-)	52 \pm 6	42 \pm 10	94 \pm 20	85 \pm 10
	L484C(C-)	48 \pm 5	57 \pm 8	95 \pm 10	86 \pm 7
	S487C(C-) ^b	47 \pm 7	45 \pm 5	48 \pm 10	68 \pm 5
	M491C(C-)	38 \pm 4	70 \pm 7	60 \pm 3	65 \pm 7
11 - 12 loop	M506C(C-)	21 \pm 5	21 \pm 5	37 \pm 3	37 \pm 3
	A508C(C-)	86 \pm 10	78 \pm 10	37 \pm 6	94 \pm 20
	G512C(C-)	70 \pm 10	92 \pm 20	54 \pm 10	83 \pm 10
	Y513C(C-)	45 \pm 4	44 \pm 6	60 \pm 9	62 \pm 6
	F516C(C-)	9 \pm 1	100 \pm 10	11 \pm 2	73 \pm 7
	F517C(C-)	12 \pm 3	10 \pm 3	16 \pm 3	20 \pm 3
	N518C(C-)	6 \pm 1	9 \pm 1	5 \pm 1	7 \pm 1
	F520C(C-)	26 \pm 3	17 \pm 3	5 \pm 1	12 \pm 2
	V521C(C-)	26 \pm 3	18 \pm 2	35 \pm 6	27 \pm 3
	A522C(C-)	30 \pm 5	100 \pm 10	90 \pm 9	110 \pm 10
	Y523C(C-)	10 \pm 1	77 \pm 20	3 \pm 2	3 \pm 1
	L526C(C-)	26 \pm 4	120 \pm 10	10 \pm 2	35 \pm 6
	Q545C(C-)	83 \pm 8	81 \pm 7	47 \pm 3	40 \pm 3

Table 10-2 (continued).

TM		Na ⁺		H ⁺	
		(100 mM NaCl, pH 8.5)		(100 mM ChCl, pH 5.5)	
		+ PCMBS ^a	+ PCMBS + uridine	+ PCMBS ^a	+ PCMBS + uridine
		(%)	(%)	(%)	(%)
12	I554C(C-)	98 ± 20	93 ± 8	52 ± 6	67 ± 9
	T557C(C-) ^b	7 ± 1	16 ± 2	22 ± 2	33 ± 2
	Y558C(C-)	92 ± 20	100 ± 20	19 ± 3	71 ± 10
	S561C(C-)	100 ± 20	99 ± 9	54 ± 5	94 ± 8
	N565C(C-) ^b	37 ± 5	110 ± 10	46 ± 9	110 ± 20
	G567C(C-) ^b	17 ± 4	97 ± 20	14 ± 5	94 ± 20
	I571C(C-) ^b	44 ± 8	85 ± 9	30 ± 3	90 ± 8
13	A601C(C-)	57 ± 7	43 ± 8	29 ± 5	29 ± 3
	A609C(C-)	55 ± 5	69 ± 9	60 ± 6	76 ± 10
	L612C(C-)	48 ± 5	100 ± 9	59 ± 3	86 ± 5

^a, mediated uridine influx in the absence of inhibitor is given in pmol/oocytes.min⁻¹ in Table 10-1 for each of the individual mutants; ^b, previously identified as MTS-sensitive residues (7).

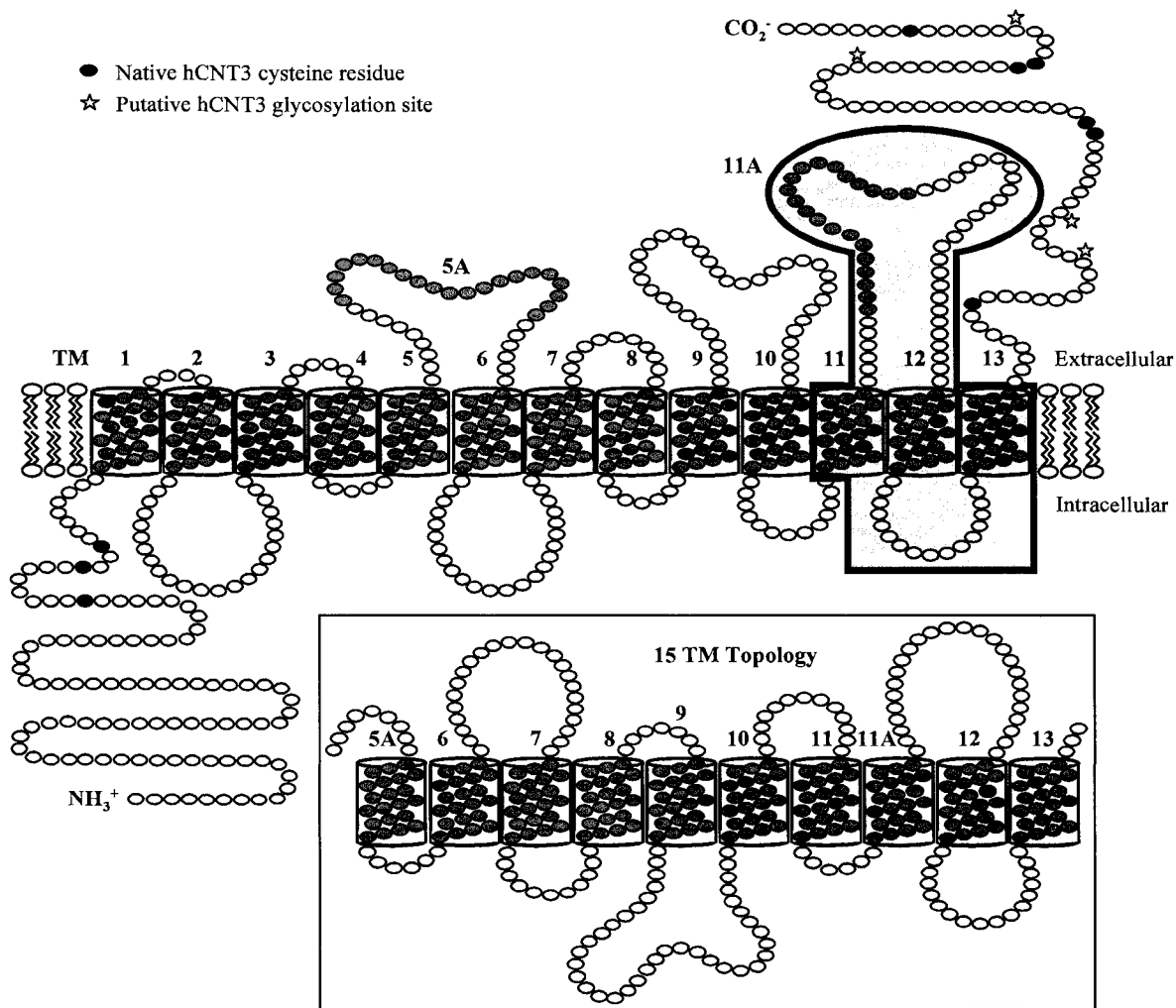


Figure 10-1. Alternative models of hCNT3 topology. Schematic of proposed hCNT3 (GenBank™ accession number AF305210) topology with either 13 or 15 TMs. Insertion of TMs 5A and 11A into the membrane, resulting in a 15 TM membrane architecture and opposite orientations of TMs 6 - 11, is depicted in the *inset*. The position of endogenous cysteine residues are indicated as *black* residues, and putative glycosylation sites are highlighted with a *star* symbol. Residues studied by SCAM analysis are highlighted with a *grey* box.

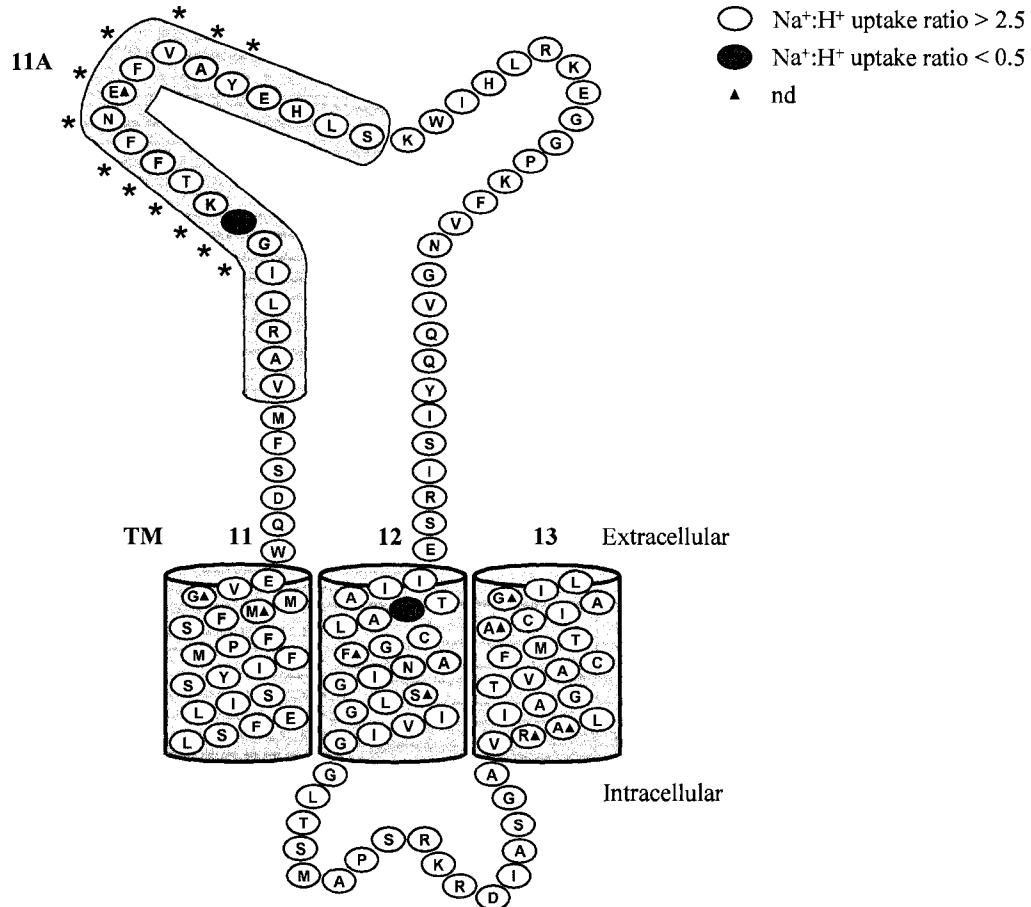


Figure 10-2. hCNT3 TMs 11 - 13 depicting residues with altered $\text{Na}^+:\text{H}^+$ uridine uptake ratios. hCNT3C- mutants exhibiting $\text{Na}^+:\text{H}^+$ uridine uptake ratios > 2.5 are indicated in *yellow*, and those with uptake ratios < 0.5 are shown in *orange* (Table 10-1). The * symbol represents residues which form the conserved CNT family (G/A)XKX₃NEFVA(Y/M/F) motif. Low activity mutants with uridine transport rates < 0.1 pmol/oocyte.min⁻¹ in both Na⁺- and H⁺-containing transport media (100 mM NaCl, pH 8.5 and ChCl, pH 5.5, respectively) are indicated by the ▲ symbol. Corresponding numerical values are given in Table 10-1.

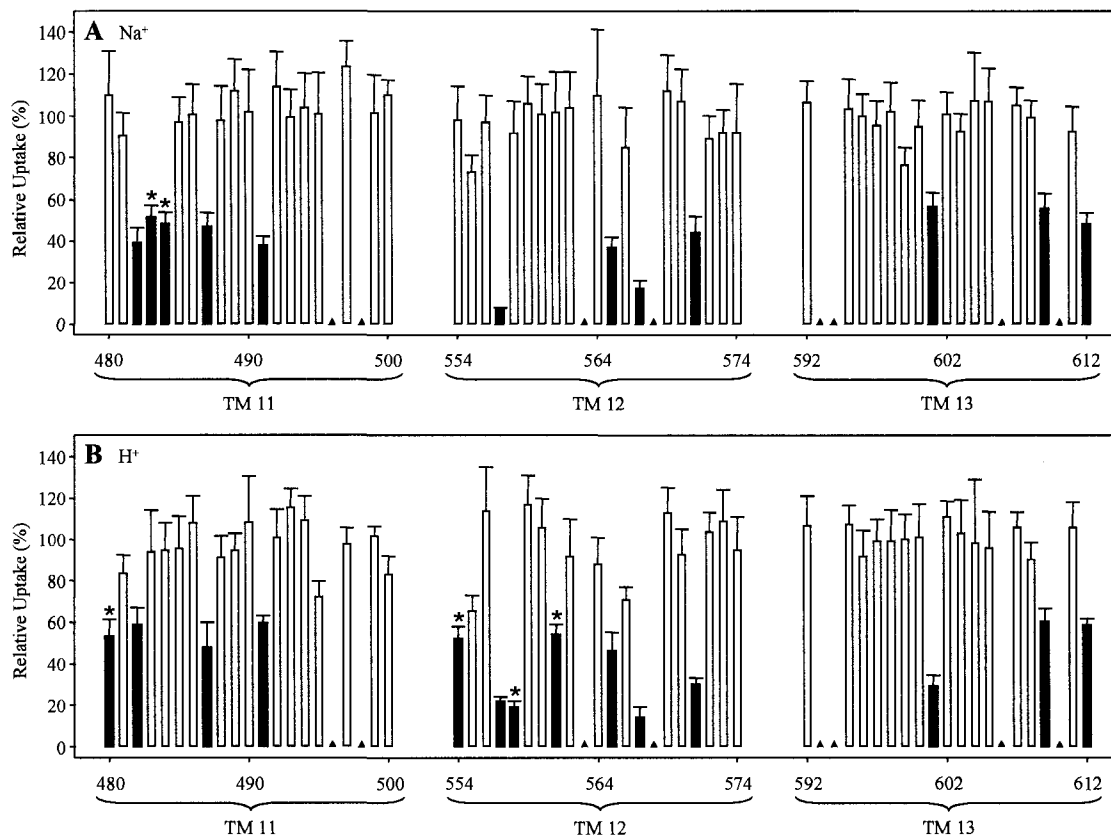


Figure 10-3. PCMBs inhibition of residues in hCNT3C- TMs 11, 12 and 13. Mediated influx of 10 μ M radiolabeled uridine in Na⁺-containing (A) or H⁺-containing (B) medium (100 mM NaCl, pH 8.5 or 100 mM ChCl, pH 5.5, respectively) was measured following 10 min incubation on ice in Na⁺- or H⁺-containing medium (A or B, respectively) in the presence of 200 μ M PCMBs. *Solid* columns indicate residue positions inhibited by PCMBs; the * symbol identifies those residues which exhibit differential inhibition by PCMBs in the two media. Low activity mutants where inhibition was not determined are indicated by the \blacktriangle symbol. Data are presented as mediated transport, calculated as uptake in RNA-injected oocytes *minus* uptake in water-injected oocytes, and are normalized to the respective influx of uridine in the absence of inhibitor. Each value is the mean \pm SEM of 10 - 12 oocytes.

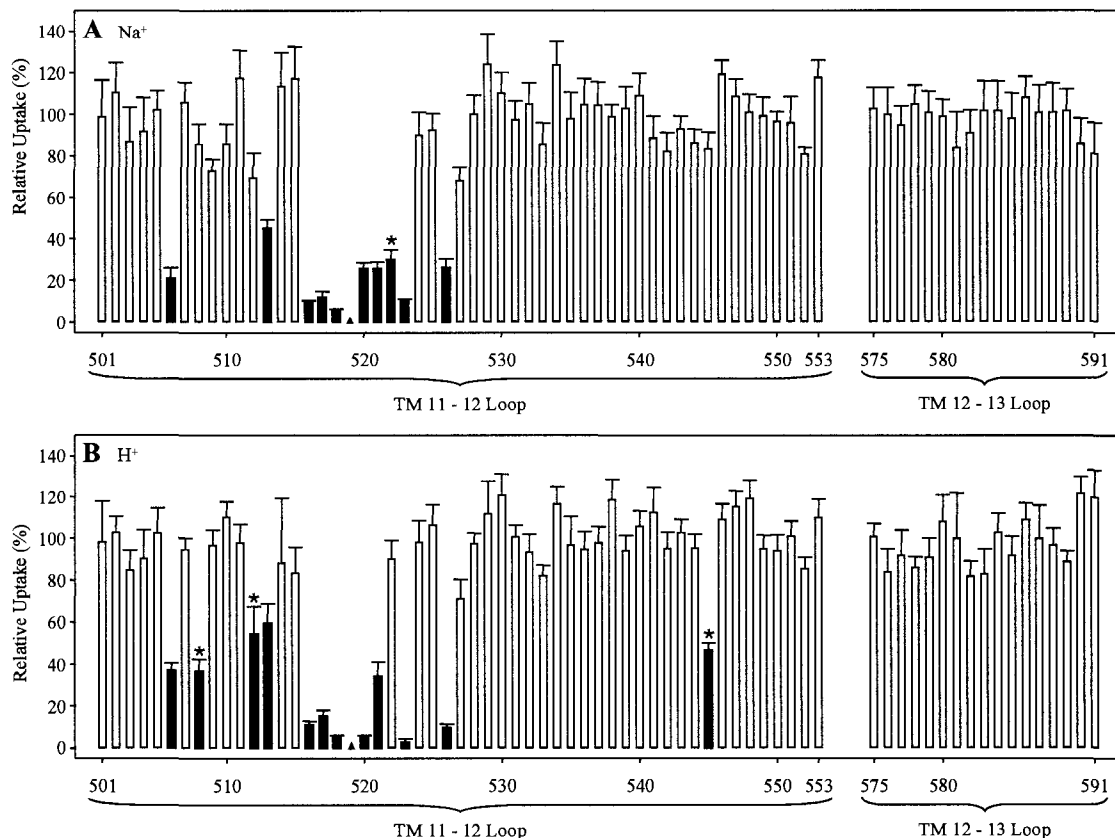


Figure 10-4. PCMBS inhibition of residues in hCNT3C- loop regions between TMs 11 and 12, and TMs 12 and 13. Mediated influx of 10 μ M radiolabeled uridine in Na⁺-containing (A) or H⁺-containing (B) medium (100 mM NaCl, pH 8.5 or 100 mM ChCl, pH 5.5, respectively) was measured following 10 min incubation on ice in Na⁺- or H⁺-containing medium (A or B, respectively) in the presence of 200 μ M PCMBS. *Solid* columns indicate residue positions inhibited by PCMBS; the * symbol identifies those residues which exhibit differential inhibition to PCMBS in the two media. Low activity mutants where inhibition was not determined are indicated by the ▲ symbol. Data are presented as mediated transport, calculated as uptake in RNA-injected oocytes *minus* uptake in water-injected oocytes, and are normalized to the respective influx of uridine in the absence of inhibitor. Each value is the mean \pm SEM of 10 - 12 oocytes.

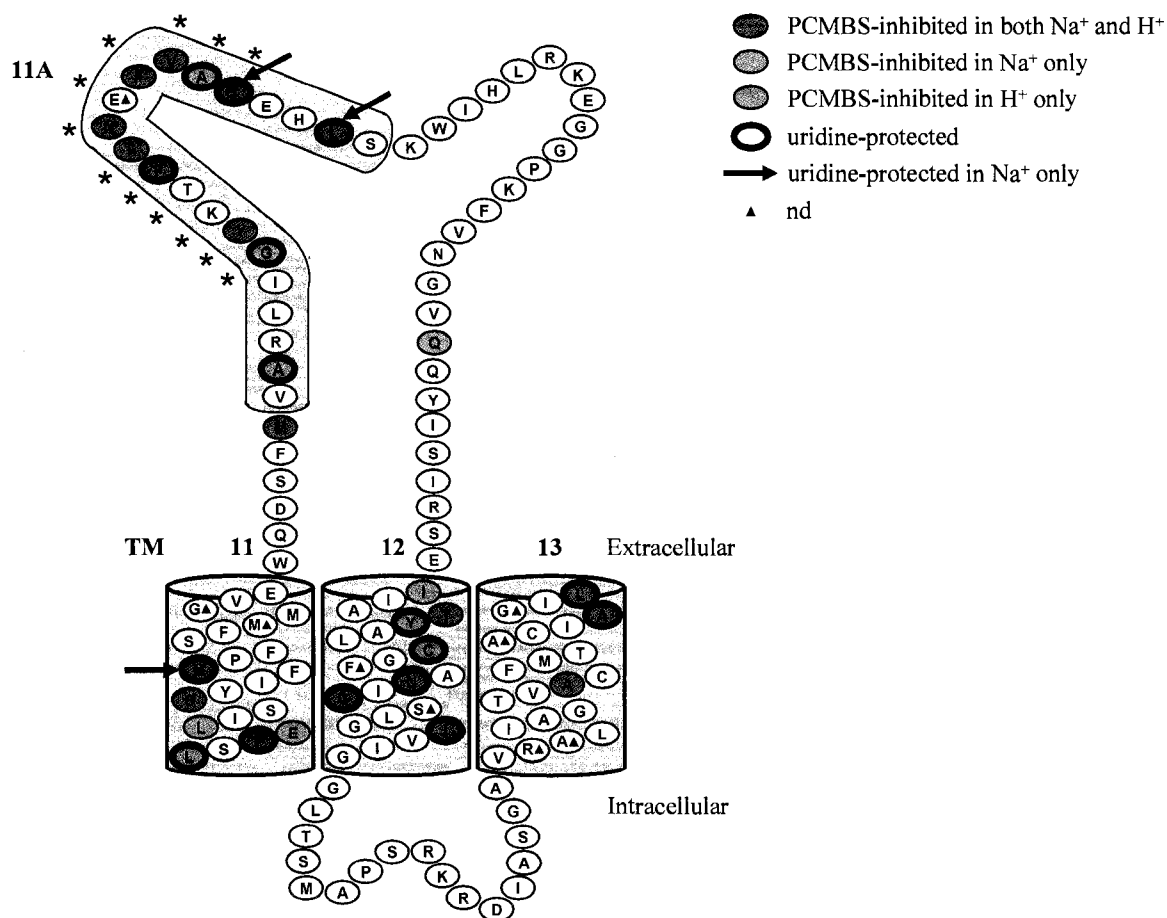


Figure 10-5. hCNT3 TMs 11 - 13 depicting PCMBS-inhibited and uridine-protected residues. hCNT3C- mutants exhibiting inhibition of uridine uptake following incubation with PCMBS in both Na⁺- and H⁺-containing transport medium are indicated in *blue*, those inhibited in Na⁺-containing transport medium only are indicated in *green* and those inhibited in H⁺-containing transport medium only are indicated in *pink*. Residues protected from PCMBS inhibition by excess unlabeled uridine are outlined in *black*. The three residues, Met⁴⁹¹ in TM 11, Tyr⁵²³ and Leu⁵²⁶ in TM 11A, which were inhibited by PCMBS in both Na⁺- and H⁺-containing medium, but protected from that inhibition only in the presence of Na⁺ are indicated by a *black arrow*. The * symbol represents residues which form the conserved CNT family (G/A)XKX₃NEFVA(Y/M/F) motif. Low activity mutants are indicated by the ▲ symbol. Corresponding numerical values are given in Table 10-2.

- PCMBs-inhibited in both Na⁺ and H⁺
- ▒ PCMBs-inhibited in Na⁺ only
- ▓ PCMBs-inhibited in H⁺ only
- † uridine-protected in both Na⁺ and H⁺
- § uridine-protected in Na⁺ only
- * uridine-protected in H⁺ only

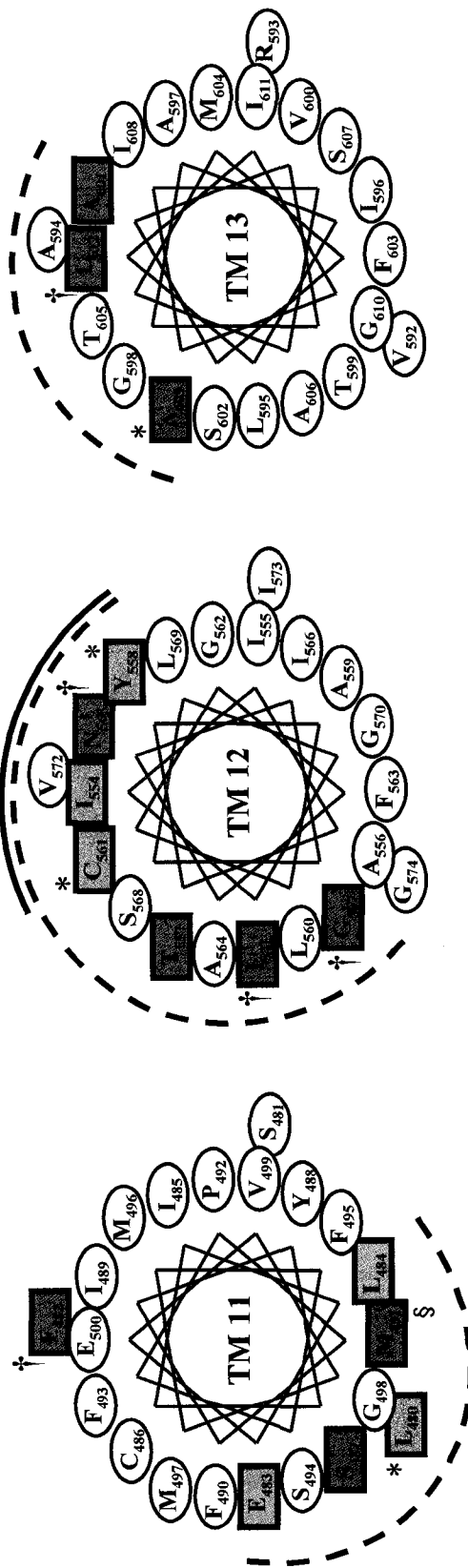


Figure 10-6.

Figure 10-6. Helical wheel projections of hCNT3 TMs 11, 12 and 13. The helical wheel projections, as viewed from the extracellular side of the membrane, highlight in *blue* the locations of hCNT3 residues which are inhibited by PCMBs in both Na⁺- and H⁺-containing media, in *green* those residues inhibited in Na⁺-containing medium only and in *pink* those inhibited in H⁺-containing medium only. Those residues for which uridine-protection was evident in both Na⁺- and H⁺-containing transport medium or in the presence of Na⁺ or H⁺ alone are indicated by the symbols †, § and *, respectively. Corresponding numerical values are given in Table 10-2.

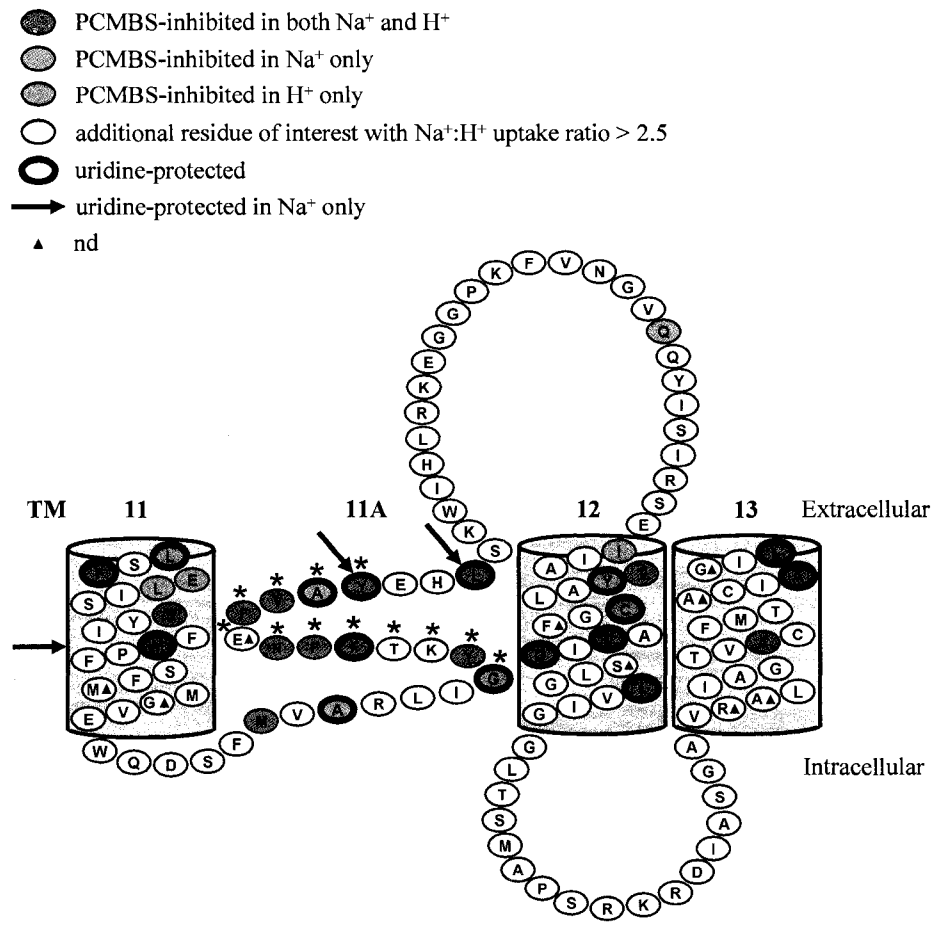


Figure 10-7.

Figure 10-7. Revised hCNT3 TM 11 - 13 topology depicting TM 11A as membrane-spanning. This schematic depicts insertion of TM 11A as membrane-spanning, thus reversing the orientation of TM 11. For illustrative purposes, the endofacial boundary of helix 11A, as illustrated in Figs. 10-1, 10-2 and 10-5, has been shifted by one residue to include the residue Met⁵⁰⁶. PCMBS-inhibited and uridine-protected residues as well as additional residues of interest with Na⁺:H⁺ uridine uptake ratios > 2.5, but not inhibited by PCMBS are highlighted according to Figs. 10-5 and 10-2, respectively. Two residues, Tyr⁵¹³ in TM 11A and Tyr⁵⁵⁸ in TM 12, which exhibited Na⁺:H⁺ uridine uptake ratios < 0.5 were also PCMBS-inhibited and are only indicated as such. The three residues, Met⁴⁹¹ in TM 11, and Tyr⁵²³ and Leu⁵²⁶ in TM 11A, which were inhibited by PCMBS in both Na⁺- and H⁺-containing medium, but protected from that inhibition only in the presence of Na⁺ are indicated by a *black arrow*. The * symbol represents residues which form the conserved CNT family (G/A)XKX₃NEFVA(Y/M/F) motif. Low activity mutants are indicated by the ▲ symbol. Corresponding numerical values are given in Tables 10-1 and 10-2.

Bibliography

1. Ritzel, M. W. L., Yao, S. Y. M., Huang, M. Y., Elliott, J. F., Cass, C. E., and Young, J. D. (1997) Molecular cloning and functional expression of cDNAs encoding a human Na⁺-nucleoside cotransporter (hCNT1). *Am. J. Physiol.* **272**: C707-C714.
2. Ritzel, M. W. L., Yao, S. Y. M., Ng, A. M. L., Mackey, J. R., Cass, C. E., and Young, J. D. (1998) Molecular cloning, functional expression and chromosomal localization of a cDNA encoding a human Na⁺/nucleoside cotransporter (hCNT2) selective for purine nucleosides and uridine. *Mol. Membr. Biol.* **15**: 203-211.
3. Hamilton, S. R., Yao, S. Y. M., Ingram, J. C., Hadden, D. A., Ritzel, M. W. L., Gallagher, M. P., Henderson, P. J. F., Cass, C. E., Young, J. D., and Baldwin, S. A. (2001) Subcellular distribution and membrane topology of the mammalian concentrative nucleoside transporter rCNT1. *J. Biol. Chem.* **276**: 27981-27988.
4. Ritzel, M. W. L., Ng, A. M. L., Yao, S. Y. M., Graham, K., Loewen, S. K., Smith, K. M., Ritzel, R. G., Mowles, D. A., Carpenter, P., Chen, X.-Z., Karpinski, E., Hyde, R. J., Baldwin, S. A., Cass, C. E., and Young, J. D. (2001) Molecular identification and characterization of novel human and mouse concentrative Na⁺-nucleoside cotransporter proteins (hCNT3 and mCNT3) broadly selective for purine and pyrimidine nucleosides (system *cib*). *J. Biol. Chem.* **276**: 2914-2927.
5. Yao, S. Y. M., Ng, A. M. L., Loewen, S. K., Cass, C. E., Baldwin, S. A., and Young, J. D. (2002) An ancient prevertebrate Na⁺-nucleoside cotransporter (hfCNT) from the Pacific hagfish (*Eptatretus stouti*). *Am. J. Physiol. Cell Physiol.* **283**: C155-C168.
6. Craig, J. E., Zhang, Y., and Gallagher, M. P. (1994) Cloning of the nupC gene of *Escherichia coli* encoding a nucleoside transport system, and identification of an adjacent insertion element, IS 186. *Mol. Microbiol.* **11**: 1159-1168.
7. Zhang, J., Tackaberry, T., Ritzel, M. W., Raborn, T., Barron, G., Baldwin, S. A., Young, J. D., and Cass, C. E. (2006) Cysteine-accessibility analysis of transmembrane domains 11-13 of human concentrative nucleoside transporter 3. *Biochem. J.* **394**: 389-398.

8. Yan, R. T., and Maloney, P. C. (1993) Identification of a residue in the translocation pathway of a membrane carrier. *Cell* **75**: 37-44.
9. Yan, R. T., and Maloney, P. C. (1995) Residues in the pathway through a membrane transporter. *Proc. Natl. Acad. Sci. U.S.A.* **92**: 5973-5976.
10. Yao, S. Y. M., Sundaram, M., Chomey, E. G., Cass, C. E., Baldwin, S. A., and Young, J. D. (2001) Identification of Cys₁₄₀ in helix 4 as an exofacial cysteine residue within the substrate-translocation channel of rat equilibrative nitrobenzylthioninosine (NBMPR)-insensitive (ENT2) nucleoside transporter rENT2. *Biochem. J.* **353**: 387-393.
11. Errasti-Murugarren, E., Cano-Soldado, P., Pastor-Anglada, M., and Casado, F. J. (2007) Functional characterization of a nucleoside-derived drug transporter variant (hCNT3C602R) showing altered sodium-binding capacity. *Mol. Pharmacol.* **73**: 379-386.
12. Mulinta, R., Ng, A. M. L., Yao, S. Y. M., Slugoski, M. D., Smith, K. M., Cass, C. E., Baldwin, S. A., and Young, D. (2008) Substituted cysteine accessibility method analysis of transmembrane domains 7 and 8 of human concentrative nucleoside transporter 3 (hCNT3) reveal novel discontinuous regions within helices. *J. Biol. Chem.* (submission pending).
13. Yamashita, A., Singh, S. K., Kawate, T., Jin, Y., and Gouaux, E. (2005) Crystal structure of a bacterial homologue of Na⁺/Cl⁻-dependent neurotransmitter transporter. *Nature* **437**: 215-223.
14. Screpanti, E., and Hunte, C. (2007) Discontinuous membrane helices in transport proteins and their correlation with function. *J. Struct. Biol.* **159**: 261-267.
15. Smith, K. M., Ng, A. M. L., Yao, S. Y. M., Labedz, K. A., Knaus, E. E., Wiebe, L. I., Cass, C. E., Baldwin, S. A., Chen, X.-Z., Karpinski, E., and Young, J. D. (2004) Electrophysiological characterization of a recombinant human Na⁺-coupled nucleoside transporter (hCNT1) produced in *Xenopus* oocytes. *J. Physiol.* **558**: 807-823.
16. Boudker, O., Ryan, R. M., Yernool, D., Shimamoto, K., and Gouaux, E. (2007) Coupling substrate and ion binding to extracellular gate of a sodium-dependent aspartate transporter. *Nature* **445**: 387-393.

Chapter 11:
General Discussion

Synopsis

The major nucleoside transport processes of mammalian cells are mediated by members of two structurally unrelated protein families: the equilibrative nucleoside transporters (ENTs) with four family members (ENT1-4) (1) and the concentrative nucleoside transporters (CNTs) with three family members (CNT1-3) (2, 3). Although the first nucleoside transport protein to be identified at the molecular level was that of CNT1 (4), characterization and structure-function studies of CNT transport mechanisms lag behind those of ENTs. Found predominantly in specialized cells such as intestine, kidney and liver epithelia, CNTs play important physiological and pharmacological roles in the absorption, secretion, distribution and elimination of nucleosides and nucleoside drugs (5-7). The intracellular localization of CNT3 in some cells also hints at possible roles in intracellular nucleoside trafficking (7, 8). In addition to serving as key participants in nucleoside biology and therapeutics, CNTs and the functional diversity that they exhibit offer unique opportunities to study the molecular mechanisms of cation-permeant membrane cotransport.

CNTs mediate nucleoside transport using the electrochemical gradient of the coupling cation. The molecular mechanisms underlying interactions with both the nucleoside permeant and the coupling cation were investigated by heterologous expression of recombinant CNT family members in *Xenopus laevis* oocytes using a combination of both radioisotope flux assays and electrophysiology studies. Detailed kinetic characterization of wild-type CNTs established a basic understanding of the natural phenotypes. This analysis of naturally-occurring protein isoforms in association with multiple sequence alignments between CNT family members and the application of molecular biology techniques to enable chimeric, site-directed mutagenesis and substituted cysteine accessibility method (SCAM) analyses of wild-type and mutant proteins has been successful in uncovering regions and residues of structural and functional importance. Combined, the different characterization and structure-function studies described in this thesis provide insights into the molecular mechanisms involved in both permeant and cation binding and translocation in CNTs.

The first example of a single residue substitution altering the overall apparent affinity of a CNT protein for nucleosides was that of CaCNT/19-20196, an allelic isoform of the H⁺-coupled *Candida albicans* nucleoside transport protein CaCNT (Chapter 3). Sequence alignments of contigs 19-10196 and 19-20196 of the Stanford *C. albicans* genome sequence databank with CaCNT led to the identification of a single residue difference between CaCNT/19-20196 and CaCNT (serine and glycine, respectively) that occurred at position 328 in putative transmembrane domain (TM) 7. This residue position corresponds to a serine/glycine substitution previously shown to contribute to the contrasting pyrimidine and purine nucleoside selectivities of human and rat Na⁺-dependent CNT1 and CNT2 (9, 10). CaCNT/19-10196 differs from CaCNT by four amino acids, but has glycine at position 328. Both CaCNT/19-10196 and -20196 were recreated by site-directed mutagenesis of CaCNT and characterized functionally by heterologous expression in *Xenopus* oocytes. In marked contrast to human and rat CNT1/2, both CaCNT/19-10196 and CaCNT/19-20196 exhibited permeant selectivities for purine nucleosides (adenosine, guanosine and inosine) and uridine similar to that of CaCNT. However, although shown to be H⁺-coupled, CaCNT/19-20196 exhibited an ~ 10-fold higher apparent K_m for uridine than either CaCNT or CaCNT/19-10196. CaCNT/19-20196 also exhibited a low apparent affinity for inosine. Thus, the three proteins correspond to high-affinity (CaCNT, CaCNT/19-10196) and low-affinity (CaCNT/19-20196) allelic isoforms of the *C. albicans* CNT nucleoside transporter.

The influence of specific residues on molecular interactions with permeant was also investigated in the human protein hCNT1 expressed in *Xenopus* oocytes (Chapter 4). Previously, two pairs of adjacent residues in TMs 7 and 8 of hCNT1 (Ser³¹⁹/Gln³²⁰ and Ser³⁵³/Leu³⁵⁴) were identified that, when converted to the corresponding residues in hCNT2 (glycine/methionine and threonine/valine), changed the permeant selectivity of the transporter from pyrimidine nucleoside-selective to purine nucleoside-selective (9). Investigation of the effects of the corresponding mutations in TM 8 alone demonstrated unique S353T- and L354V-induced changes in nucleoside specificity and cation-coupling, respectively. hCNT1 mutation S353T produced a profound decrease in cytidine transport efficiency ($V_{max}:K_m$ ratio) and, in

combination with L354V (S353T/L354V), resulted in a novel uridine-preferring transport phenotype. In addition, the L354V mutation markedly increased the apparent affinity of hCNT1 for Na⁺ and Li⁺. Both hCNT1 TM 8 residues exhibited uridine-protectable inhibition by *p*-chloromercuribenzenesulfonate (PCMBS) when converted to cysteine, suggesting that they occupy positions within or closely adjacent to a common cation/nucleoside translocation pore.

In contrast to pyrimidine nucleoside-preferring hCNT1, hCNT3 transports a broad range of physiologic purine and pyrimidine nucleosides and anticancer and antiviral nucleoside drugs. hCNT3 is a Na⁺/nucleoside symporter, but preliminary studies also suggested that this protein was capable of coupling nucleoside transport with the H⁺ electrochemical gradient (11). H⁺-dependent *Escherichia coli* NupC (Appendix 2) and *C. albicans* CaCNT (12, Chapter 3) are also CNT family members. Chapter 5 used heterologous expression in *Xenopus* oocytes to investigate the specificity, mechanism, energetics and structural basis of hCNT3 cation-coupling. hCNT3 exhibited uniquely broad cation interactions with Na⁺, H⁺ and Li⁺ not shared with hCNT1/2 or NupC/CaCNT, which are exclusively Na⁺- and H⁺-coupled, respectively. Na⁺ and H⁺ activated hCNT3 through a common mechanism to increase nucleoside apparent binding affinity. Direct and indirect methods demonstrated cation:nucleoside coupling stoichiometries of 2:1 in the presence of Na⁺ and both Na⁺ and H⁺, but only 1:1 in the presence of H⁺ alone, suggesting that hCNT3 possesses two Na⁺-binding sites, only one of which is shared by H⁺; the corresponding Na⁺:nucleoside and H⁺:nucleoside coupling stoichiometries of hCNT1 (11) and CaCNT (12) are both 1:1. H⁺-coupled hCNT3 did not transport guanosine, 3'-azido-3'-deoxythymidine (zidovudine; AZT) or 2', 3'-dideoxycytidine (zalcitabine; ddC), demonstrating that Na⁺- and H⁺-bound versions of hCNT3 have significantly different conformations of the nucleoside binding pocket and/or translocation channel. Chimeric studies between hCNT1 and hCNT3 located hCNT3-specific cation interactions to the C-terminal half of hCNT3, setting the stage for site-directed mutagenesis experiments to identify the residues involved.

The CNT family of proteins in mammalian cells contains members of two distinct phylogenetic subfamilies. In humans, hCNT1 and hCNT2 belong to one subfamily, and hCNT3 to the other. All three CNTs mediate inwardly-directed Na^+ /nucleoside cotransport, and are either pyrimidine nucleoside-selective (hCNT1), purine nucleoside-selective (hCNT2), or broadly selective for both pyrimidine and purine nucleosides (hCNT3). While previous studies have characterized cation interactions with both hCNT1 (11) and hCNT3 (Chapter 5), little was known about the corresponding properties of hCNT2. Chapter 6 presented a side-by-side comparison of the cation coupling properties of hCNT2 with other hCNT family members expressed in *Xenopus* oocytes and investigated by both radioisotope flux assays and electrophysiological techniques. Apparent K_{50} values for Na^+ -activation were voltage-dependent and similar in magnitude for all three transporters. Only hCNT3 was also able to couple transport of uridine to uptake of H^+ . The Na^+ :nucleoside stoichiometry of hCNT2, as determined from both Hill coefficients and direct charge:flux measurements, was 1:1. This result was the same as for hCNT1, but different from that of hCNT3 (2:1). The charge-to- $^{22}\text{Na}^+$ uptake stoichiometry was 1:1 for all three hCNTs. Therefore, in parallel with their division into two separate CNT subfamilies, hCNT2 shares common cation specificity and coupling characteristics with hCNT1, which differ markedly from those of hCNT3.

As a member of a separate CNT subfamily, and in contrast to exclusively Na^+ -coupled hCNT1/2, hCNT3 exhibits both Na^+ - and H^+ -mediated nucleoside cotransport and thus exists in at least two different cation-bound states. Using site-directed mutagenesis in combination with heterologous expression in *Xenopus oocytes*, Chapter 7 presented the identification of a C-terminal intramembraneous cysteine residue of hCNT3 (Cys⁵⁶¹) which reversibly binds the hydrophilic thiol-reactive reagent PCMBs. Access of this membrane-impermeant probe to Cys⁵⁶¹, as determined by inhibition of hCNT3 transport activity, required H^+ , but not Na^+ , and was blocked by extracellular uridine. Although this cysteine residue is also present in hCNT1 and hCNT2, these transporters were not affected by PCMBs. Thus, Cys⁵⁶¹ is located in the translocation pore in a mobile region within or closely adjacent to the

nucleoside binding pocket and access of PCMBs to this residue reports a specific H⁺-induced conformational state of the protein.

As a prerequisite to using substituted cysteine accessibility method (SCAM) analysis for further investigation of alternate cation-bound conformations of hCNT3, radioisotope flux and electrophysiological kinetic studies were used to characterize a cysteine-less version of hCNT3 (hCNT3C-) expressed in *Xenopus* oocytes (Chapter 8). All 14 endogenous cysteine residues of hCNT3 were converted to serine in the hCNT3C- construct. Indicative of proper folding, hCNT3C- was processed to the cell surface in amounts similar to wild-type hCNT3. hCNT3C- exhibited hCNT3-like functional properties, but with a specific decrease in apparent affinity for Na⁺ that was not apparent for H⁺. hCNT3-like 2:1 Na⁺:uridine and 1:1 H⁺:uridine coupling ratios were maintained. Site-directed mutagenesis experiments undertaken in both wild-type and hCNT3C- backgrounds identified intramembraneous Cys⁵⁶¹ as the residue responsible for this altered Na⁺-binding phenotype. Substitution of Cys⁵⁶¹ with the larger neutral amino acids threonine, valine and isoleucine largely eliminated H⁺-dependent hCNT3 nucleoside transport activity. This residue, Cys⁵⁶¹, was previously identified to be located in a mobile region of the CNT translocation pore in a position within, or closely adjacent to, the nucleoside binding pocket, such that access of PCMBs to this residue reports a specific H⁺-induced conformational state of the protein (Chapter 7). The investigations presented in Chapter 8 provided additional evidence to place Cys⁵⁶¹ in a location pivotal for cation binding and/or translocation, and validate hCNT3C- as a template for substituted cysteine mutagenesis studies of hCNT3.

Differences among CNT family and subfamily members provide a unique opportunity for investigating the mechanisms of cation coupling. In parallel to a study on hCNT1 (Appendix 4), radioisotope flux and electrophysiological techniques were used in combination with site-directed mutagenesis and heterologous expression in *Xenopus* oocytes to identify two highly conserved pore-lining glutamate residues in hCNT3 (Glu³⁴³ and Glu⁵¹⁹) with essential, but contrasting roles in cation/nucleoside cotransport (Chapter 9). Mutation of Glu³⁴³ resulted in a novel partially-uncoupled

transport phenotype akin to that of a nucleoside-gated Na⁺ channel. Located deep within the translocation pore, Glu³⁴³ may form part of the inward gate of the transporter vestibule. Centrally positioned within the highly conserved CNT family motif (G/A)XKX₃NEFVA(Y/M/F) of TM 11A, Glu⁵¹⁹ was revealed to be vital for cation-coupling through an apparently direct interaction with a shared hCNT3 Na⁺/H⁺-binding site. Similar to the corresponding hCNT1 mutants (Appendix 4), and consistent with close-proximity integration of cation/solute binding within a common cation/permeant translocation pore, mutation of hCNT3 Glu³⁴³ and Glu⁵¹⁹ additionally led to marked alterations in hCNT3 nucleoside transport selectivity.

Although all human (and other eukaryote) CNTs are currently defined by a putative 13 TM topology model with intracellular and extracellular N- and C-termini, respectively, the studies of Chapter 9 and Appendix 4 provided strong evidence instead for an alternate 15 TM membrane architecture. In the absence of crystal structure, valuable topological and other structural information can be gained about residue localization from SCAM analysis with thiol reactive reagents such as PCMBS. In a cysteine-less hCNT3 protein background (hCNT3C-), site-directed mutagenesis was used to individually mutate residues to cysteine prior to heterologous expression in *Xenopus* oocytes to probe for reactivity to PCMBS. In continuation of a previous study using PCMBS to investigate residues in TM 12 (Chapter 7), Chapter 10 expands this analysis to the entire TM 11 to 13 region, including bridging extramembranous loops. In preceding Chapters, residues in TM 11A (Chapter 9, Appendix 4) and in TM 12 (Chapters 7 and 8) have been shown to play important roles in permeant and cation binding and/or translocation in hCNTs. The SCAM study confirmed the functional importance of these key regions (TM 11 - 12 loop and TM 12), supported the currently defined designation of TMs 11, 12 and 13 as membrane-spanning α -helices and identified a novel membrane-associated topology for TM 11A and the highly conserved CNT family motif (G/A)XKX₃NEFVA(Y/M/F) that it contains.

Supporting studies that also investigated mechanisms of concentrative nucleoside transport are presented in Appendices 1 - 4. The identification and

characterization of three single nucleotide polymorphisms (SNPs) of hCNT3 in both *Saccharomyces cerevisiae* and *Xenopus* oocytes is presented in Appendix 1. All three SNPs (S5N, L131F and Y513F) were found to exhibit hCNT3-like phenotypes, including nucleoside kinetic parameters and Na⁺/H⁺-dependence, suggesting that hCNT3 exhibits a high degree of functional conservation. The characterization of a bacterial CNT family member from *E. coli*, NupC, is presented as Appendix 2. Also expressed in *Xenopus* oocytes, H⁺-dependent NupC was primarily selective for pyrimidine nucleosides and adenosine, but was also capable of low levels of inosine uptake. Similar to hCNT3 (Chapter 5), an ordered mechanism of transport in which H⁺ binds prior to nucleoside was proposed based on the kinetics of uridine transport determined as a function of external pH. Appendix 3 presents the characterization of Fui1p, a uridine permease of *Saccharomyces cerevisiae* and a member of the uracil/allantoin permease family. Similar to CNT family members, CaCNT (12, Chapter 3), NupC (Appendix 2) and human and mouse CNT3 (Chapters 5 and 6), transport mediated by Fui1p was H⁺-dependent and, upon expression in *Xenopus* oocytes, exhibited a H⁺:uridine stoichiometry of 1:1. A study investigating the role of highly-conserved negatively charged residues in hCNT1 which corresponds to that for hCNT3 described in Chapter 9 is presented in Appendix 4. Also expressed in *Xenopus* oocytes, residues in TM 7 (Glu³⁰⁸ and Glu³²²) and TM 11A (Glu⁴⁹⁸) were found to play key roles in the Na⁺/nucleoside cotransport of hCNT1.

Together, these studies characterizing nucleoside transport in both wild-type and mutant concentrative nucleoside transport proteins provide valuable information about the molecular mechanisms of cation-dependent nucleoside cotransport. Multiple residues involved in both permeant and cation binding and translocation in CNTs were identified and, although some residues influenced interactions with permeant independent of cation, and vice versa, others influenced both simultaneously. Identification of key individual amino acid residues and the domains and TMs within which they reside contributes valuable information to putative mechanisms of CNT transport and topology. Insights gained from these in depth studies, which focused largely on hCNT3, can be applied to other CNTs and, more globally, to other membrane cotransport proteins.

Molecular Mechanisms of CNT Cation/Nucleoside Cotransport

TMs Involved in Interactions with Nucleosides

The permeant binding and translocation profiles with respect to both nucleosides and nucleoside analogs vary among CNT family members, although the physiological nucleoside uridine is a common permeant for all CNTs characterized thus far. Mammalian CNT1 and CNT2 family members are primarily pyrimidine nucleoside- and purine nucleoside-selective, respectively, although both mediate the transport of uridine and adenosine (2, 3, Chapter 4, Appendix 4). In contrast, CNT3 subfamily members are broadly selective for both pyrimidine and purine nucleosides (13, Chapter 5). Non-mammalian CNT family members also exhibit varied nucleoside selectivities. For example, *C. albicans* CaCNT is purine nucleoside-selective and also transports uridine (12, Chapter 3), whereas the CNT family member from *E. coli*, NupC, is pyrimidine nucleoside-selective, but also transports adenosine and, to a lesser extent, inosine (Appendix 2).

CNT structure-function studies using site-directed mutagenesis identified key TMs and residues involved in permeant binding and translocation. Characterization of a hCNT1/3 chimera implicated the C-terminal half of the protein as the functional domain responsible for determining nucleoside permeant selectivity (Chapter 5). Similar to a study in hCNT1 which implicated key residues in TMs 7 and 8 (Ser³¹⁹/Gln³²⁰ and Ser³⁵³/Leu³⁵⁴, respectively) in nucleoside selectivity (9), the corresponding TM 7 residue in CaCNT (Ser³²⁸), as revealed by a naturally occurring allelic variant, also influenced interactions with permeant (Chapter 3). As a continuation of these studies, individual residues in TM 8 (Ser³⁵³ and Leu³⁵⁴) also proved to be important determinants of hCNT1 nucleoside selectivity and kinetics independent of those contributed by TM 7 (Chapter 4). Studies investigating the highly conserved negatively charged residues of hCNT1 identified two additional TM 7 residues (Glu³⁰⁸ and Glu³²²), as well as a residue in TM 11A (Glu⁴⁹⁸) which, when mutated to corresponding residues lacking the negative charge, also altered nucleoside kinetics (Appendix 4). The parallel study in hCNT3 similarly found the

corresponding TM 7 (Glu³⁴³) and 11A (Glu⁵¹⁹) residues to be important contributors to permeant binding (Chapter 9). Uridine protection from PCMBS inhibition in SCAM analysis experiments identified residues residing in hCNT3 TM 12 (Chapter 7) and in TMs 11, 11A and 13 (Chapter 10) that were located within, or closely adjacent to, the nucleoside binding pocket. Together, and with the caveat that some of the influences may be indirect, these studies present evidence for involvement of TMs 7, 8, 11, 11A, 12 and 13 in forming the translocation pore and associated nucleoside binding domain of CNTs.

TMs Involved in Interactions with Cations

Cation coupling differs among CNT family and subfamily members. CNT1 and CNT2 are both largely Na⁺-specific and share a 1:1 Na⁺:nucleoside coupling stoichiometry (Chapter 6). In contrast, hCNT3 mediates nucleoside transport by coupling to Na⁺, H⁺ and Li⁺ electrochemical gradients with cation:nucleoside coupling stoichiometries of 2:1 for Na⁺ and 1:1 for H⁺ (Chapters 5 and 6). Also belonging to the CNT3 subfamily, hfCNT resembles hCNT1/2 and exhibits only Na⁺-dependent nucleoside transport activity, but shares the 2:1 Na⁺:nucleoside stoichiometry of CNT3 (13). Other CNT family members that are exclusively H⁺-dependent include *C. albicans* CaCNT (12, Chapter 3) and *E. coli* NupC (Appendix 2). Similar to CNT3, CaCNT has a 1:1 H⁺:nucleoside stoichiometry (12, Chapter 3).

Site-directed mutagenesis studies of CNTs have implicated key TMs and residues in cation coupling. A hCNT1/3 chimera implicated the C-terminal half of the protein as the functional domain responsible for cation coupling (Chapter 5). In hCNT1, the TM 8 mutation L354V increased the transporter's apparent affinity for Li⁺, resulting in a phenotype with hCNT3-like characteristics (Chapter 4). Mutating negatively charged residues in hCNT1 identified key residues in TM 7 (Glu³⁰⁸ and Glu³²²) and TM 11A (Glu⁴⁹⁸) with influences on cation kinetic parameters (Appendix 4). These two key regions were also strongly implicated in interactions with cations in the parallel study of the role of negatively charged residues in hCNT3 (Chapter 9).

Also in hCNT3, a residue in TM 12 (Cys⁵⁶¹) was shown to report H⁺-dependent conformational changes that resulted in binding of PCMBs to this residue only under acidic conditions (Chapter 7). SCAM analysis of this particular TM revealed adjacent residues also sensitive to PCMBs only in the presence of H⁺ and residues more deeply embedded in the helix that reacted with PCMBs in the presence of both H⁺ and Na⁺ (Chapter 7). A direct role for hCNT3 TM 12 Cys⁵⁶¹ in interactions with cations was revealed by the decreased apparent affinity for Na⁺ of the cysteine-less hCNT3 construct hCNT3C- and by the decreased rates of H⁺-mediated transport evident for mutants C561T, C561V and C561I (Chapter 8). Likewise, mutation of Glu³⁴³ in TM 7 of hCNT3 influenced both Na⁺- and H⁺-dependent transport functions of the protein (Chapter 8). In addition to TM 12, SCAM analysis of the region from TM 10 to 13 also identified multiple residues in TM 11A which exhibited relative levels of Na⁺- and H⁺-dependent uridine uptake different from that of wild-type hCNT3, and in TMs 11 and 11A exhibited cation-specific inhibition by PCMBs (Chapter 10). Together, and with the caveat that some of the influences may be indirect, these studies implicate residues in TMs 7, 8, 11, 11A and 12 in CNT-cation interactions.

Putative Mechanisms of CNT Cation/Nucleoside Cotransport

In depth kinetic characterization of wild-type CNTs, combined with structure-function studies of CNT family members has provided novel insights into the putative mechanisms of cation/nucleoside cotransport mediated by CNTs. In particular, the unique transport phenotype of hCNT3 provided an opportunity to investigate nucleoside and cation interactions at the molecular level. Taken together, the studies described in this thesis can be interpreted by analogy with other membrane transport proteins for which crystal structures have recently been obtained.

Similar to the recently solved high resolution molecular structures of bacterial cation-transporters such as LacY (14), LeuT_{Aa} (15) and Glt_{Ph} (16, 17), the emerging principle of close-proximity integration of cation/solute binding and transport within

a common cation/permeant translocation pore is a theme also present throughout the CNT structure-function studies presented here. For example, mutation of hCNT1 TM 8 Leu³⁵⁴ influenced both nucleoside selectivity and apparent affinity for Na⁺ and Li⁺ (Chapter 4). Similarly, mutation of hCNT1 TM 7 residues Glu³⁰⁸ and Glu³²² individually altered both uridine and Na⁺ kinetic parameters (Appendix 4). The dual effect of altered cation and nucleoside kinetics was mirrored by mutation of the corresponding residue Glu³⁴³, as well as Glu⁵¹⁹, in hCNT3 (Chapter 9). hCNT3 TM 12 residue Cys⁵⁶¹ exhibits uridine-protectable PCMBS inhibition in the H⁺-bound conformation of the transporter, thus revealing a central position of this residue within a mobile region of the cation/nucleoside translocation machinery. Additionally, some of the uridine-protectable, PCMBS-sensitive residues in hCNT3C- also demonstrated altered Na⁺:H⁺ ratios of uridine uptake, including TM 11A residues Gly⁵¹², Phe⁵¹⁶ and Ala⁵²², as well as TM 12 residues Tyr⁵⁵⁸ and Asn⁵⁶⁵ (Chapters 7 and 10). This suggests that mutation of these residues alters cation interactions, while simultaneously being involved in, or located in close proximity to, the nucleoside binding pocket. Thus, it is likely that the translocation pore of CNTs is shared by both the coupling cation and nucleoside permeant in a manner which permits individual residues to influence the binding and/or translocation of both cation and nucleoside.

Kinetic analysis of nucleoside and cation binding affinities in electrophysiology studies of hCNT1 proposed an ordered mechanism of binding whereby cation binds to the transporter first, increasing the apparent affinity for nucleoside, which binds second (11). Likewise, studies in hCNT3 (Chapter 5) and *E. coli* NupC (Appendix 2) also revealed a similar mechanism of ordered binding. Kinetically, this is revealed by the common finding that the apparent binding affinity for nucleoside increases in the absence of changes to maximal rates of transport as the concentration of Na⁺ or H⁺ is increased. All three hCNTs are proposed to share this common mechanism (Chapter 6).

The division of hCNT1 and hCNT2 into a phylogenetic subfamily distinct from that of hCNT3 is in good agreement with differences in both nucleoside

selectivity and cation coupling. hCNT1 and hCNT2 are Na⁺-specific pyrimidine nucleoside- and purine nucleoside-selective transporters, respectively, and couple nucleoside transport with 1:1 Na⁺:nucleoside stoichiometry (Chapter 6). In contrast, nucleoside selectivity and cation coupling are more complex in hCNT3. In agreement with Hill plot predictions, hCNT3 exhibits 2:1 Na⁺:nucleoside and 1:1 Na⁺:charge stoichiometries, implying that hCNT3 binds and translocates two Na⁺ per molecule of nucleoside (Chapters 5 and 6). Na⁺-coupled transport is broadly selective for both pyrimidine and purine nucleosides (Chapter 5). In contrast to Na⁺, the H⁺:nucleoside stoichiometry of hCNT3 is voltage-independent and, in agreement with Hill plot predictions, is 1:1, suggesting that hCNT3 H⁺-dependent nucleoside transport occurs by the coupling of one H⁺ to one nucleoside molecule (Chapters 5 and 6). The binding of H⁺ to hCNT3 induces a conformational change that reveals exofacial residues in TM 12 which are occluded to extracellular PCMBs under H⁺-reduced conditions (Chapter 7). H⁺-coupled transport favors the uptake of pyrimidine nucleosides (Chapter 5). In the presence of both Na⁺ and H⁺, electrophysiological coupling ratio experiments reveal a phenotype intermediate between that in the presence of Na⁺ or H⁺ alone. Thus, the cation:nucleoside stoichiometry is 2:1, similar to that in the presence of Na⁺ alone, but is voltage-independent, similar to that in the presence of H⁺ alone (Chapter 5). H⁺-induced reactivity of TM 12 residue Cys⁵⁶¹ to PCMBs is evident irrespective of whether Na⁺ is also present in the transport medium (Chapter 7). The nucleoside transport profile of hCNT3 in the presence of both Na⁺ and H⁺ is broadly selective for both pyrimidine and purine nucleosides which is similar to that of Na⁺-coupled hCNT3 (Chapter 5). Thus, hCNT3 exhibits two Na⁺ binding sites, one of which is likely shared with H⁺. H⁺ binding to hCNT3, even in the presence of Na⁺, results in a conformation distinct from that in the presence of Na⁺ alone. However, it is the presence of Na⁺ which appears to dictate the conformation of the nucleoside binding site.

Despite these differences in nucleoside selectivity and cation coupling among hCNTs and other family members, their overall similarities provide support for a common cotransport mechanism. As previously discussed, an ordered mechanism of binding and close-proximity integration of cation/solute binding and transport within

a common cation/permeant translocation pore are likely shared by all three hCNTs and are common to other eukaryote, as well as prokaryote CNTs. Within hCNTs, additional evidence for a common nucleoside binding site stems from the ability of hCNT1 to adopt hCNT2-like nucleoside selectivity via a hCNT3-like intermediate state by mutation of only four TM 7/8 residues (9). Differences in hCNT and other CNT cation coupling characteristics, however, make the structural interpretation of cation binding features more challenging. The properties which require rationalization are that: (i) hCNT1/2 are largely Na⁺-specific and have a single cation binding site (Chapter 6), (ii) hCNT1 has a low affinity for Li⁺ that is increased in hCNT1 mutant L454V (Chapter 4), (iii) hCNT3 can utilize Na⁺, Li⁺ or H⁺ (Chapter 5), (iv) hCNT3 has two Na⁺ binding sites, one of which is shared by H⁺ (Chapters 5 and 6), (v) the hCNT3 cation binding site common to Na⁺ and H⁺ is the primary cation-coupling site of the transporter, such that H⁺ binding to that site alone is capable of driving nucleoside transport (Chapters 5 and 6), (vi) hagfish hfCNT3, like hCNT3, has two cation binding sites, but both are specific for Na⁺ (13), (vii) other CNT family members such as *C. albicans* CaCNT (12, Chapter 3) and *E. coli* NupC (Appendix 2) are exclusively H⁺-coupled and (viii) the H⁺:nucleoside coupling ratio for CaCNT1 (and presumably other H⁺-coupled CNTs) is 1:1 (12, Chapter 3).

From the perspective of hCNT3 there are two alternative possibilities. The first is that hCNT3 shares a common Na⁺/(Li⁺)-specific site with hCNT1/2, and that H⁺-coupling in hCNT3 is a feature of a second Na⁺/H⁺ site unique to hCNT3. In this scenario, the latter site in hfCNT would be Na⁺-specific, while a H⁺-specific version of this site would account for cation coupling in CaCNT and NupC. Instead, it is also possible that the Na⁺/(Li⁺)-specific binding site of CNT1/2 subfamily members corresponds to a common Na⁺/Li⁺/H⁺ binding site in CNT3 proteins. This would be the primary cation binding site for all CNTs and would coordinate interactions with all coupling cations, including Na⁺ for those proteins which are exclusively Na⁺-coupled, such as CNT1/2 and hfCNT, H⁺ for those proteins which are exclusively H⁺-coupled, such as NupC and CaCNT, and Na⁺, Li⁺ or H⁺ for CNT3. Coupling of nucleoside transport to cation binding at this site would result in a 1:1 cation:nucleoside stoichiometry, such as is evident for Na⁺-dependent CNT1/2, H⁺-

dependent CaCNT, and the H⁺-dependent mode of CNT3 (Chapters 3, 5 and 6). In this putative mechanism, the second cation binding site unique to CNT3 subfamily members would be Na⁺-specific and would account for the 2:1 Na⁺:nucleoside coupling of both CNT3 proteins and hfCNT (13, Chapter 5). Important evidence favoring the latter of these two scenarios is provided in Chapter 9 by the demonstration that mutation of hCNT3 Glu⁵¹⁹, the residue in the TM 11A motif (G/A)XKX₃NEFVA(Y/M/F) common to all CNT family members, changes the Na⁺:nucleoside coupling ratio of the transporter from 2:1 to 1:1 at the same time as largely eliminating H⁺-coupled transport activity. In other words, mutation of Glu⁵¹⁹ leads to the functional loss of the hCNT3 site common to Na⁺ and H⁺. The highly conserved nature of this glutamate residue, and the motif to which it belongs, suggests strongly that it contributes similarly to cation coupling in other CNTs, including Na⁺-specific hCNT1/2 and H⁺-specific CaCNT and NupC.

Irrespective of the assignment of cation binding sites, CNT kinetics and cation coupling can be interpreted in terms of a conformational equilibrium model of secondary active transport. Developed by Krupka, this modified ordered binding model of secondary active transport alleviates the stringent sequential carrier states of earlier models and instead allows for flexible cation interactions such as those observed for Na⁺- and H⁺-coupling of hCNT3 (18, 19). In the model, binding of cation (Na⁺ and/or H⁺) shifts the equilibrium between two carrier states to “unlock” or open the nucleoside binding site, thereby promoting active transport.

Presteady-state current analysis of hCNT3-mediated cotransport suggests that in the presence of Na⁺ alone, binding of the first Na⁺ is followed by a slow rate-limiting occlusion step which permits binding of the second Na⁺ followed by nucleoside binding (20). This occlusion step is also evident in hCNT1 (11). hCNT1 E322Q (Appendix 4) and hCNT3 E343Q (Chapter 9) mutants both displayed novel partially-uncoupled transport phenotypes akin to that of a nucleoside-gated channel. In hCNT1 and hCNT3, the uncoupled movement of cation was primarily specific to Na⁺ and, in the case of hCNT3, did not extend to H⁺ (Chapter 9). In agreement with a location deep within the translocation pore, this negatively charged TM 7 residue may

form part of the inward gate of the transporter vestibule. A paradigm for this can be found in the potential gating function of negatively charged residues within the common cation/solute translocation pore of the *Aquifex aeolicus* LeuT_{Aa} Na⁺/Cl⁻-dependent leucine transporter (15). In this protein, negatively-charged residues stabilize the transporter in a closed conformation that occludes closely-associated Na⁺ and leucine binding sites halfway across the membrane bilayer. Similar to the mammalian GAT1 Na⁺/Cl⁻-dependent GABA transporter (21, 22), a member of the same protein family as LeuT_{Aa}, hCNT1 (11) and hCNT3 (20) presteady-state currents largely reflect binding and potential occlusion of extracellular Na⁺. Consistent with a potential gating function for hCNT1 E322, its mutation markedly decreased hCNT1 presteady-state currents (Appendix 4).

Although little is known about the mechanism of transport when both Na⁺ and H⁺ are available for coupling to hCNT3, it is likely that this mode of transport will provide valuable mechanistic insights into CNT function. Electrophysiological studies suggest that in the presence of both Na⁺ and H⁺, one Na⁺ and one H⁺ are bound to the transporter (Chapter 5). However, experimental verification of this by direct determination of the charge:²²Na⁺ coupling stoichiometry in acidified, Na⁺-containing transport medium has yet to be established. In the case of one Na⁺ and one H⁺ binding to hCNT3, it is likely that H⁺ bind first, before Na⁺ based upon (i) differences in apparent K_{50} values for the two cations (Chapter 5), (ii) the H⁺-induced conformation which allows for PCMBs binding to TM 12 Cys⁵⁶¹ is similar to that in the presence of both Na⁺ and H⁺ (Chapter 7) and (iii) arguments presented earlier in this Chapter regarding the nature of the primary hCNT3 cation-coupling site. However, hCNT3-mediated transport in the presence of both Na⁺ and H⁺ is broadly selective for both purine and pyrimidine nucleosides, whereas H⁺-mediated transport favors pyrimidine nucleosides (Chapter 5). Thus, the binding of Na⁺ must alter the nucleoside binding pocket and/or translocation pore to allow purine nucleoside transport. Continuation of the SCAM analysis presented in Chapter 10 to investigate PCMBs inhibition in the presence of both Na⁺ and H⁺, as well as in the absence of coupling cation, will be valuable in understanding the various cation-dependent conformations of hCNT3.

Topology

Initial hydropathy analyses of the first mammalian CNTs to be identified at the molecular level suggested the presence of 14 TMs (4, 23, 24). Subsequent analysis incorporating information from antipeptide antibodies and glycosylation mutants revised the putative CNT topology model to include 13 TMs, although two additional membrane spanning regions (TMs 5A and 11A) were also weakly predicted (5). Evidence presented in this thesis now supports a new TM 15 topology model for mammalian and other eukaryote CNTs. In particular, studies of highly conserved negatively charged residues in hCNT1 and hCNT3 identified glutamate residues in TM 7 (Glu³²² and Glu³⁴³, respectively) and TM 11A (Glu⁴⁹⁸ and Glu⁵¹⁹, respectively) with key functional roles in cation coupling (Chapter 9, Appendix 4). In the case of the TM 7 residues, their potential gating role within the cytoplasmic aspect of the transport vestibule favors an orientation of TM 7 in the membrane opposite to that predicted by the 13 TM model of CNT membrane architecture, but consistent with the topology predicted if the TM 5A region of the protein was indeed transmembrane. Support for TM 5A as membrane spanning comes from a series of experiments on the *E. coli* CNT family member NupC (25). Additionally, SCAM analysis of hCNT3 in a region spanning TMs 7 and 8 also revealed this region of the protein to have an orientation opposite to that predicted in the 13 TM model of topology (26). Furthermore, SCAM analysis of hCNT3 TM 11A found nine amino acids, including Glu⁵¹⁹, in a 12 residue block that were reactive to PCMBBS, four of which were nucleoside protectable (Chapter 10). TM 11A contains the previously identified highly conserved CNT family motif (G/A)XKX₃NEFVA(Y/M/F) (5). Given the pivotal role of this motif in cation coupling, it is highly likely to be membrane-associated as part of the CNT translocation pore. This could either be in the form of a re-entrant loop or as part of a transmembrane domain. The latter possibility is more probable, given that two additional transmembrane regions (TMs 5A and 11A) are needed to preserve the exofacial location of the glycosylated C-terminus of the protein. Together, these results provide strong support for a new revised 15 TM model of topology.

SCAM analysis of hCNT3 also revealed evidence of a novel extended region of polypeptide within the TM 11A putative transmembrane α -helix (Chapter 10). Similar block patterns of PCMBMS reactivity also occur in TMs 7 and 8 (26). These regions in hCNT3 TMs 7, 8 and 11A provide the first functional evidence of extended structures or discontinuous membrane helices evident in crystal structures of recently solved bacterial membrane transport proteins. For example, the crystal structure of the *A. aeolicus* Na^+/Cl^- -dependent LeuT_{Aa} transporter demonstrates non-traditional transmembrane α -helices which are disrupted by the insertion of extended regions of polypeptide (15). In LeuT_{Aa} , these extended regions comprise the Na^+ binding sites of the protein and, upon Na^+ binding, this region is stabilized to then favor the high-affinity binding of permeant, which in this case is leucine (15). The proposed mechanism of transport includes a three-state model with extra- and intracellular gates which alternately allow access to the binding sites from either side of the membrane bilayer. In this model, the extended regions serve as the joint or hinge to allow for conformational changes. The extended regions in LeuT_{Aa} are part of transmembrane helices whereas in the glutamate transporter Glt_{Ph} from *Pyrococcus horikoshii*, the extended regions form the joint of a hairpin-like conformation in a reentrant loop or non-transmembrane helix (16, 17). In the case of hCNT3, SCAM analysis predicts TM 11A to be membrane spanning and thus, more similar to LeuT_{Aa} than Glt_{Ph} (Chapter 10).

Reviewed by Screpanti and Hunte (27), such discontinuous membrane helices are proposed to play important mechanistic roles in ion recognition, binding and translocation in secondary active transporters. Additionally, a common theme throughout the recently solved bacterial transport protein crystal structures is that of inverted internal duplication of domains comprising the discontinuous helices which result in internal symmetry within the translocation pore (27). Similar symmetry within CNTs has yet to be revealed. Nevertheless, the functionally identified extended regions of polypeptide revealed by SCAM analysis of hCNT3 in TMs 7 and 8 (26) and 11A (Chapter 10) strongly support a central role of these TMs in formation of the CNT nucleoside/cation binding and translocation pore. Additional support for this arrangement of TMs with the protein stems from site-directed mutagenesis

studies previously discussed in this Chapter. For example, permeant interactions have been found for residues in TMs 7, 8, 11, 11A, 12 and 13 and interactions with cation have been found for residues in TMs 7, 8, 11A and 12, thus implicating these TMs in formation of the permeant translocation pore (Chapters 3 - 5 and 7 - 10). Important evidence for the central location and role of TM 11A, a discontinuous transmembrane helix, in the translocation pore stems from the identification of Glu⁵¹⁹ and the CNT family motif to which it belongs as a critical determinant of the hCNT3 Na⁺/H⁺-binding site (Chapter 9), as well as the proximity of this region to the adjacent and conformationally mobile TM 12 in which binding of PCMBs to Cys⁵⁶¹ reports a specific H⁺-induced state of the protein (Chapter 7). Of similar mechanistic importance is the proposed gating role of a TM 7 residue in both hCNT1 (Glu³²²) and hCNT3 (Glu³⁴³) whereby the negatively-charged residue is proposed to stabilize the transporter in a closed conformation that occludes cation and nucleoside binding sites positioned midway across the membrane lipid bilayer (Chapter 9, Appendix 4). This gating function is similar to mechanisms proposed for both LeuT_{Aa} and the related mammalian Na⁺/Cl⁻-dependent GABA transporter, GAT1 (15, 21, 22). hCNT TM 7 is immediately adjacent to TM 8, which has also been shown to be important for nucleoside/cation interactions (Chapter 4). In the 15 TM model of hCNT membrane architecture, TMs 7/8 and 11A/12 are separated by a 37 amino acid linker region which likely forms a flexible cytoplasmic loop between TMs 9 and 10. It is possible that this loop enables TMs 7/8 and 11A/12 to come together in the translocation pore in a manner that facilitates conformational transitions within the cation/nucleoside translocation cycle.

Future Directions

The functional characterization and structure-function studies of CNT family members presented here have advanced the current understanding of CNT-mediated nucleoside transport. In addition to identifying key regions and residues, these studies have revealed novel insights into the molecular mechanisms of

cation/nucleoside cotransport and the topological organization of CNT family members. There still remains, however, many unexplored areas of research with respect to the CNT family of nucleoside transport proteins.

Kinetic analysis of the mechanism of nucleoside cotransport has been carried out in detail for hCNT1, less extensively for hCNT3 and only in a preliminary way for hCNT2. Similarly, structure-function studies have primarily focused on hCNT1 and hCNT3. In hCNT3, residues only in the C-terminal half of the protein have been investigated and only in TMs 7, 8, 11, 12 and 13. Thus, many opportunities exist for future characterization both of native proteins (*ie.* hCNT2) and TMs (*ie.* hCNT3 TMs 1 - 6 and 9 - 10). Although SCAM studies of hCNT3 with PCMBs have revealed key insights into topology and putative pore-lining residues, additional information gained from as-yet-uncharacterized regions of hCNT3 will be valuable, as will investigations employing other cysteine-specific reagents. To date, for example, only limited use has been made of methanethiosulfonate (MTS) reagents. Topological information can also be gained from experiments using other investigative techniques, including cysteine-crossing linking and fluorescent labels. In addition to hCNTs, extending these structure-function studies to other CNT family members will be important.

Although initially challenging, experimental procedures for acquiring three-dimensional crystal structures of membrane transport proteins are slowly becoming established (14, 15, 16). Obtaining a crystal structure for a CNT would clarify protein architecture and provide a molecular framework for structure-function relationships. Even a relatively low resolution structure, such as those typically obtained by two-dimensional crystallographic approaches, would be of immense value in this regard. Mutagenesis experiments reported in this thesis have identified several residues potentially capable of locking the protein in conformations suitable for crystallization studies. From a pharmacologic perspective, an understanding of CNT mechanism and structure-function relationships will provide opportunities to aid in the development of custom-designed permeants and inhibitors, which will be useful, for example, in development of new chemotherapeutic compounds and applications.

Ultimately, the information gained from CNT studies will be beneficial to the understanding of cation-dependent membrane transport proteins in general.

Bibliography

1. Young, J. D., Yao, S. Y. M., Sun, L., Cass, C. E., and Baldwin, S. A. (2008) The ENT family of nucleoside and nucleobase transporter proteins. *Xenobiotica* (in press).
2. Gray, J. H., Owen, R. P., and Giacomini, K. M. (2004) The concentrative nucleoside transporter family, SLC28. *Pflugers Arch.* **447**: 728-734.
3. Zhang, J., Visser, F., King, K. M., Baldwin, S. A., Young, J. D., and Cass, C. E. (2007) The role of nucleoside transporters in cancer chemotherapy with nucleoside drugs. *Cancer Metastasis Rev.* **26**: 85-110.
4. Huang, Q. Q., Yao, S. Y. M., Ritzel, M. W. L., Paterson, A. R. P., Cass, C. E., and Young, J. D. (1994) Cloning and functional expression of a complementary DNA encoding a mammalian nucleoside transport protein. *J. Biol. Chem.* **269**: 17757-17760.
5. Hamilton, S. R., Yao, S. Y., Ingram, J. C., Hadden, D. A., Ritzel, M. W., Gallagher, M. P., Henderson, P. J., Cass, C. E., Young, J. D., and Baldwin, S. A. (2001) Subcellular distribution and membrane topology of the mammalian concentrative Na⁺-nucleoside cotransporter, rCNT1. *J. Biol. Chem.* **276**: 27981-27988.
6. Elwi, A. N., Damaraju, V. L., Baldwin, S. A., Young, J. D., Sawyer, M. B., and Cass, C. E. (2006) Renal nucleoside transporters: physiological and clinical implications. *Biochem. Cell. Biol.* **84**: 844-858.
7. Damaraju, V. L., Elwi, A. N., Hunter, C., Carpenter, P., Santos, C., Barron, G. M., Sun, X., Baldwin, S. A., Young, J. D., Mackey, J. R., Sawyer, M. B., and Cass, C. E. (2007) Localization of broadly selective equilibrative and concentrative nucleoside transporters, hENT1 and hCNT3, in human kidney. *Am. J. Physiol. Renal Physiol.* **293**: F200-F211.
8. Mackey, J. R., Galmarini, C. M., Graham, K. A., Joy, A. A., Delmer, A., Dabbagh, L., Glubrecht, D., Jewell, L. D., Lai, R., Lang, T., Hanson, J., Young, J. D., Merle-Béral, H., Binet, J. L., Cass, C. E., and Dumontet, C. (2005) Quantitative analysis of nucleoside transporter and metabolism gene expression in chronic lymphocytic leukemia (CLL): identification of fludarabine-sensitive and -insensitive populations. *Blood* **105**: 767-774.

9. Loewen, S. K., Ng, A. M., Yao, S. Y., Cass, C. E., Baldwin, S. A., and Young, J. D. (1999) Identification of amino acid residues responsible for the pyrimidine and purine nucleoside specificities of human concentrative Na⁺ nucleoside cotransporters hCNT1 and hCNT2. *J. Biol. Chem.* **274**: 24475-24484.
10. Wang, J., and Giacomini, K. M. (1999) Serine 318 is essential for the pyrimidine selectivity of the N2 Na⁺-nucleoside transporter. *J. Biol. Chem.* **274**: 2298-2302.
11. Smith, K. M., Ng, A. M., Yao, S. Y. M., Labeledz, K. A., Knauss, E. E., Wiebe, L. I., Cass, C. E., Baldwin, S. A., Chen, X.-Z., Karpinski, E., and Young, J. D. (2004) Electrophysiological characterization of a recombinant human Na⁺-coupled nucleoside transporter (hCNT1) produced in *Xenopus* oocytes. *J. Physiol.* **558**: 807-823.
12. Loewen, S. K., Ng, A. M. L., Mohabir, N. M., Baldwin, S. A., Cass, C. E., and Young, J. D. (2003) Functional characterization of a H⁺/nucleoside co-transporter (CaCNT) from *Candida albicans*, a fungal member of the concentrative nucleoside transporter (CNT) family of membrane proteins. *Yeast* **20**: 661-675.
13. Yao, S. Y., Ng, A. M., Loewen, S. K., Cass, C. E., Baldwin, S. A., and Young, J. D. (2002) An ancient prevertebrate Na⁺-nucleoside cotransporter (hfCNT) from the Pacific hagfish (*Eptatretus stouti*). *Am. J. Phys. Cell Phys.* **283**: C155-C168.
14. Abramson, J., Smirnova, I., Kasho, V., Verner, G., Kaback, H. R., and Iwata, S. (2003) Structure and mechanism of the lactose permease of *Escherichia coli*. *Science* **301**: 610-605.
15. Yamashita, A., Singh, S. K., Kawate, T., Jin, Y., and Gouaux, E. (2005) Crystal structure of a bacterial homologue of Na⁺/Cl⁻-dependent neurotransmitter transporters. *Nature* **437**: 215-223.
16. Yernool, D., Boudker, O., Jin, Y., and Gouaux, E. (2004) Structure of a glutamate transporter homologue from *Pyrococcus horikoshii*. *Nature* **431**: 811-818.
17. Boudker, O., Ryan, R. M., Yernool, D., Shimamoto, K., and Gouaux, E. (2007) Coupling substrate and ion binding to extracellular gate of a sodium-dependent aspartate transporter. *Nature* **445**: 387-393.

18. Krupta, R. M. (1993) Coupling mechanisms in active transport. *Biochim. Biophys. Acta* **1183**: 105-113.
19. Krupta, R. M. (1994) Interpreting the effects of site-directed mutagenesis on active transport systems. *Biochim. Biophys. Acta*. **1193**: 165-178.
20. Smith, K. M., Cass, C. E., Baldwin, S. A., Karpinski, E., and Young, J. D. (2008) Presteady-state currents of human concentrative nucleoside transporter 3 (hCNT3). *J. Physiol.* (submission pending).
21. Hilgemann, D. W., and Lu, C.-C. (1999) GAT1 (GABA:Na⁺:Cl⁻) cotransport function. Database reconstruction with an alternating access model. *J. Gen. Physiol.* **114**: 459-475.
22. Lu, C.-C., and Hilgemann, D. W. (1999) GAT1 (GABA:Na⁺:Cl⁻) cotransport function. Kinetic studies in giant *Xenopus* oocyte membrane patches. *J. Gen. Physiol.* **114**: 445-457.
23. Che, M., Ortiz, D. F., and Arias, I. M. (1995) Primary structure and functional expression of a cDNA encoding the bile canalicular, purine-specific Na⁺-nucleoside cotransporter, *J. Biol. Chem.* **270**, 13596-13599.
24. Wang, J., Su, S. F., Dresser, M. J., Schaner, M. E., Washington, C. B., and Giacomini, K. M. (1997) Na⁺-dependent purine nucleoside transporter from human kidney: cloning and functional characterization, *Am. J. Physiol.* **273**, F1058-F1065.
25. Xie, H., Sun, L., Hadden, D. A., Mulinta, R., Loewen, S. K., Ingram, J. C., Litherland, G. L., Gallagher, M. P., Henderson, P. J. F., Cass, C. E., Young, J. D., and Baldwin, S. A. (2008) Structure/function relationships in the *Escherichia coli* nucleoside transport protein NupC, a paradigm for the concentrative nucleoside transporter (CNT) family. *Mol. Microbiol.* (submission pending).
26. Mulinta, R., Ng, A. M. L., Yao, S. Y. M., Slugoski, M. D., Smith, K. M., Cass, C. E., Baldwin, S. A., and Young, J. D. (2008) Substituted cysteine accessibility method analysis of transmembrane domains 7 and 8 of human concentrative nucleoside transporter 3 (hCNT3) reveal novel discontinuous regions within helices. *J. Biol. Chem.* (submission pending).

27. Screpanti, E., and Hunte, C. (2007) Discontinuous membrane helices in transport proteins and their correlation with function. *J. Struct. Biol.* **159**: 261-267.

Appendix 1:

Identification and Functional Characterization of Variants in Human Concentrative Nucleoside Transporter 3, hCNT3 (SLC28A3), Arising from Single Nucleotide Polymorphisms in Coding Regions of the hCNT3 Gene*

* This appendix has been published.

Damaraju, V. L., Zhang, J., Visser, F., Tackaberry, T., Dufour, J., Smith, K. M., Slugoski, M. D., Ritzel, M. W., Baldwin, S. A., Young, J. D., and Cass, C. E. (2005) Identification and functional characterization of variants in human concentrative nucleoside transporter 3, hCNT3 (SLC28A3), arising from single nucleotide polymorphisms in coding regions of the hCNT3 gene. *Pharmacogenet. Genomics* **15**: 173-182.

Identification and functional characterization of variants in human concentrative nucleoside transporter 3, hCNT3 (SLC28A3), arising from single nucleotide polymorphisms in coding regions of the hCNT3 gene

Sambasivarao Damaraju^{a,b,*}, Jing Zhang^{a,*}, Frank Visser^a, Tracey Tackaberry^a, Jennifer Dufour^b, Kyla M. Smith^d, Melissa Slugoski^d, Mabel W.L. Ritzel^d, Stephen A. Baldwin^c, James D. Young^d and Carol E. Cass^{a,b}

Introduction Human concentrative nucleoside transporter 3, hCNT3 (SLC28A3), which mediates transport of purine and pyrimidine nucleosides and a variety of antiviral and anticancer nucleoside drugs, was investigated to determine if there are single nucleotide polymorphisms in the coding regions of the hCNT3 gene.

Methods and results Ninety-six DNA samples from Caucasians (Coriell Panel) were sequenced and sixteen variants in exons and flanking intronic regions were identified, of which five were coding variants; three of these were non-synonymous (S5N, L131F, Y513F) and were further investigated for functional alterations of the resulting recombinant proteins in *Saccharomyces cerevisiae* and *Xenopus laevis* oocytes. In yeast, immunostaining and fluorescence quantitation of the reference (wild-type) and variant CNT3 proteins showed similar levels of expression. Kinetic studies were undertaken in yeast with a high through-put semi-automated assay process; reference hCNT3 exhibited K_m values of 1.7 ± 0.3 , 3.6 ± 1.3 , 2.2 ± 0.7 , and $2.1 \pm 0.6 \mu\text{M}$ and V_{max} values of 1402 ± 286 , 1310 ± 113 , 1020 ± 44 , and $1740 \pm 114 \text{ pmol/mg/min}$, respectively, for uridine, cytidine, adenosine and inosine. Similar K_m and V_{max} values were obtained for the three variant proteins assayed in yeast

under identical conditions. All of the characterized hCNT3 variants produced in oocytes retained sodium and proton dependence of uridine transport based on measurements of radioisotope flux and two-electrode voltage-clamp studies.

Conclusion These results suggested a high degree of conservation of function for hCNT3 in the Caucasian population. *Pharmacogenetics and Genomics* 15:173–182 © 2005 Lippincott Williams & Wilkins.

Pharmacogenetics and Genomics 2005, 15:173–182

Keywords: nucleoside transporter, kinetics, membrane transport, genomics, polymorphism, nucleoside drugs, integral membrane protein, coding variants, sodium/proton dependence, quantitative CNT3 protein expression

^aDepartment of Oncology, University of Alberta, Edmonton, Alberta, Canada, ^bPolyomX Program, Cross Cancer Institute, Edmonton, Alberta, Canada, ^cSchool of Biochemistry and Microbiology, University of Leeds, Leeds, UK and ^dDepartment of Physiology, University of Alberta, Edmonton, Alberta, Canada.

Correspondence and requests for reprints to Dr Carol E. Cass, Department of Oncology, Cross Cancer Institute, 11560 University Avenue, Edmonton, Alberta T6G 1Z2, Canada.
Tel: 780-432-8320; fax: 780-432-8425;
e-mail: carol.cass@cancerboard.ab.ca

Received 5 August 2004 Accepted 20 December 2004

Introduction

Uptake and release of nucleosides is mediated by integral membrane nucleoside transporter proteins [1–3]. These proteins also mediate the cellular uptake of nucleoside analogs used in anti-cancer and anti-viral chemotherapy [4,5]. Two major structurally and functionally distinct families of nucleoside transporters have been identified: the concentrative nucleoside transporters (CNTs) and the equilibrative nucleoside transporters (ENTs). Three sodium-dependent CNTs have been identified by molecular cloning from human tissues that differ functionally in their substrate selectivities: hCNT1 (SLC28A1) transports pyrimidine nucleosides, hCNT2 (SLC28A2) transports purine nucleosides and uridine and

hCNT3 (SLC28A3) transports both pyrimidine and purine nucleosides [6–9]. Two equilibrative nucleoside transporters, hENT1 (SLC29A1) and hENT2 (SLC29A2), have been cloned from human tissues and are functionally distinguished by their sensitivity or lack thereof, respectively, to nitrobenzylmercaptapurine ribonucleoside (NBMPR) [3]. Detailed functional studies of recombinant human nucleoside transporter proteins (reviewed in [3,4]) have established correspondence between the transporter proteins and their functional activities as follows: hENT1, *es*; hENT2, *ei*; hCNT1, *ai*; hCNT2, *af*; and hCNT3, *ib*.

The role of nucleoside transporters in the cellular uptake and efficacy of anti-cancer nucleoside drugs is an area of intense investigation. The presence of functional

*These authors made equal contributions to the work presented here.

nucleoside transporter proteins has been demonstrated to be critical for the cytotoxic sensitivity of cultured malignant cells to nucleoside analogs such as gemcitabine, 5-fluoruridine and 5'-deoxy-5-fluoruridine [10,11]. Inter-individual differences in hENT1 protein levels have been observed in immunohistochemical analysis of primary breast tumors, which also revealed some instances of apparent hENT1 deficiency [12]. Recently, a retrospective study that assessed hENT1 abundance in pancreatic cancer samples by immunohistochemistry demonstrated that patients treated with gemcitabine in whom all adenocarcinoma cells had detectable hENT1 had longer median survivals than those for whom hENT1 was present in low quantities or absent altogether [13].

With the completion of the human genome project, there is growing interest in the role of genetic variants in drug transporter and metabolism genes in the observed inter-individual differences in drug efficacy and therapeutic outcome in patient populations [14–18]. Sequencing of 24 transporter genes from a collection of multi-ethnic DNA samples identified several non-synonymous amino acid variants in human transporter proteins, including hENT1, hENT2, hCNT1 and hCNT2. Functional characterization of the observed variants for hENT1 (SLC29A1) produced in recombinant form in *Saccharomyces cerevisiae* and/or oocytes from *Xenopus laevis* demonstrated that the non-synonymous variants resulting in the change of amino acids from I126 T and E391 K showed no differences in the kinetics of uptake of nucleosides. Similar results were obtained with hCNT1 variants except for one with a very low allele frequency (0.5%) in the African-American population in which a deletion of G at nucleotide position 1153 resulted in a frame shift that yielded a non-functional truncated protein in *X. laevis* oocytes [19–21]. Several single nucleotide polymorphisms (SNPs) and insertion/deletion polymorphisms were identified and reported for hCNT2 and hENT2 and await functional characterizations [22,23].

The hCNT3 gene, located on chromosome 9, consists of 18 exons and encodes a 691-residue protein with 13 putative transmembrane domains [8]. The hCNT3 gene is widely expressed in many different tissue types and the protein mediates efficient transport of both purine and pyrimidine nucleosides, including a variety of anticancer nucleoside drugs [8]. However, the hCNT3 gene has not been evaluated for putative polymorphisms in the coding region. The present study was undertaken to assess hCNT3 polymorphisms in the Caucasian population. Since this project was initiated, a report on hCNT3 polymorphisms has been presented in which the authors reported 10 non-synonymous variants, of which seven were rare with an allele frequency of < 1%. One of these, G367R in the DNA from the Asian population, exhibited reduced transport of inosine and thymidine [24]. We

report here the identification of 16 SNPs in the coding and intronic regions of the hCNT3 gene by sequencing of genomic DNA from Caucasian individuals (panel of 96 DNAs from Coriell Institute). Functional characterization of the non-synonymous variants was undertaken by production of the recombinant variant proteins in a yeast expression system under conditions that allowed determination of the kinetic parameters (K_m , V_{max}) for four physiologic nucleosides (uridine, cytidine, adenosine, inosine) using a high-throughput assay described in detail elsewhere [25]. In addition to the novel variants of hCNT3 reported in this study, we also confirm some of the variants reported by Badagnani and Giacomini [24] and deposited in the NCBI and PharmGKB databases (<http://www.ncbi.nlm.nih.gov/SNP> and <http://www.pharmgkb.org/views/variant>).

Methods

Materials

Uridine, cytidine, adenosine, inosine and the ^3H -labeled nucleosides were purchased from Sigma-Aldrich (Sigma-Aldrich Canada Ltd., Oakville, ON, Canada) and Moravak Biochemicals (Brea, CA, USA), respectively. The Quick-Change site-directed mutagenesis kit was purchased from Stratagene (La Jolla, CA, USA). All other materials used were of the highest analytical grade available commercially.

DNA sequencing

Polymorphisms in the hCNT3 gene were identified by dideoxy sequencing in 96 DNA samples from Caucasians (Coriell Panel, Coriell Institute of Medicine, CA, USA). Polymorphic DNA Technologies, Inc (www.polymorphicdna.com) services were utilized for sequencing and analysis. We attempted sequencing all 18 exons in the CNT3 gene (with 50-bp flanking intronic regions), as well as 500-bp upstream and downstream sequences relative to ATG and stop codons, respectively. Table 1 lists the primers and the expected size of the polymerase chain reaction (PCR) amplification products (amplicons) that were successfully sequenced and also contained polymorphisms. After an initial sequencing attempt, the identified polymorphisms were re-confirmed by repeat PCR and sequencing steps. Only those polymorphisms that were found to be reproducible in the two sequencing runs are reported in this paper.

Strains and media

Fu1::TRP1 (MAT α , gal, ura3-52, trp1, lys2, ade2, hisd2000, and Δ fu1::TRP1), which contains a disruption in the gene encoding the endogenous Urd permease (FUI1) [2], was the parental yeast strain used to produce the recombinant human nucleoside transporters [25–27]. Other strains were generated by transformation of the yeast-*Escherichia coli* shuttle vector pYPGE15 (containing the constitutive PGK promoter) [28] into Fu1::TRP1 with a standard lithium acetate method [29]. Yeast strains

Table 1 Primer pairs used to amplify regions of the hCNT3 gene

Amplicon	5' Primer	3' Primer	BP, PCR (Read)
Exon 1	GAAGGAAGAGTGGGGAGGAC	GGTTGGGGCTAAAGTTACAGG	393 (147)
Exon 2	CCAGCACTAGATGCTCCAC	AACCCAGAAGAGCCCAAGAA	451 (205)
Exon 3	GGATTTGTCAAGCTTTTGTGA	TACGACTATGCCCCACAC	400 (196)
Exon 4	TGAGATTATAAGCCGGAAAAA	CAATGAGCCGAGATCACATC	431 (186)
Exon 5	TGATCATGGCTGACTCTAGTCTAA	AAACGGGGTAGGGAAACAAT	475 (192)
Exon 6	ACCCATCAAAGAAGCCAGT	TCATTGCCTCATCTAGGCTTT	538 (290)
Exon 8	TCAAAGGGTTCTCTGCTTATGA	GAACAGCAGTAGTGTAAACAAACCA	471 (214)
Exon 10	CACCATAGAAGACAGGGGAAA	TTCCCTCCATGGACACATT	474 (181)
Exon 14	TGATGTCATGGGATTCAGGT	AAGGAGGGGGATAGGAGACA	497 (269)
Exon 15	CCTGATTCCTGATGGGTAA	CACGCACACTCTAATTAACATAA	552 (298)
Exon 18	CCCCAGTGTCTCTGCTCTTA	CAGTCTTGTGGGGGAAGG	494 (268)
3' NC	TTGCAAGGAATGAAGAAAAACA	GGATTACAACCAAGATGGATCA	591 (300)

Listed are the nucleotide sequences of primers for PCR and the expected size of the PCR amplicons for the hCNT3 gene for various regions. The genomic contiguous sequences from the UCSC database (<http://genome.ucsc.edu/>) were used as a source of genomic sequences to derive flanking exonic and intronic sequences. Some amplicons were difficult to sequence or, when sequenced, showed no polymorphisms (exons 7, 9, 11, 12, 13, 16, 17 and 5' non-coding region). The numbers of base pairs (BP) for each PCR amplicon and of the sequence read within each amplicon are given in brackets.

were maintained in complete minimal media (CMM) containing 0.67% yeast nitrogen base (Difco, Detroit, MI, USA), amino acids (as required to maintain auxotrophic selection), and 2% glucose (CMM/GLU). Agar plates contained CMM with various supplements and 2% agar (Difco). Plasmids were propagated in *E. coli* strain DH5 α (Invitrogen, Carlsbad, CA, USA) and maintained in Luria broth with 100 μ g/ml ampicillin.

Plasmid construction and site-directed mutagenesis

The hCNT3 open reading frame (GenBank accession number AF305210) was subcloned into the yeast expression vector pYPGE15 to generate pYPPhCNT3 as previously described [25]. pYPPhCNT3 served as the template to generate plasmids containing cDNAs encoding the three non-synonymous variant transporter proteins hCNT3/S5N, hCNT3/L131F and hCNT3/Y513F using the QuickChange site-directed mutagenesis kit according to the manufacturer's instructions. The sequence of the three hCNT3 variants was confirmed by DNA sequencing using an ABI PRISM 310 sequence detection system (PerkinElmer Life and Analytical Sciences, Boston, MA, USA).

Nucleoside transport assay in *S. cerevisiae*

Yeast cells producing recombinant reference or non-synonymous variant hCNT3 proteins were grown in CMM/GLU media to A_{600} of 0.7–1.2, washed twice in sodium-containing transport buffer (5 mM D-glucose, 20 mM Tris-HCl, 3 mM K₂HPO₄, 1 mM MgCl₂, 2 mM CaCl₂, and 130 mM NaCl, pH 7.4) and resuspended to $A_{600} = 4.0$ in sodium-containing transport buffer, pH 7.4. All transport assays were performed at room temperature and pH 7.4 using a cell-harvester based method as described previously [25,30]. Transport reactions were initiated by rapid mixing of 50 μ l of yeast suspension with 50 μ l of sodium-containing buffer, pH 7.4, containing $2 \times [^3\text{H}]$ nucleoside in each of the individual wells of 96-well microtiter plates. Nucleoside uptake into yeast cells producing recombinant hCNT3 or hCNT3 variants was

linear for up to 10–15 min and kinetic studies were therefore performed using rates obtained from 5-min exposures to ^3H -labeled nucleosides. At the end of 5-min incubations, the yeast cells were collected on glass-fiber filtermats (Skatron Instruments, Lier, Norway) using the semi-automated cell harvester (Micro96 HARVESTER; Skatron Instruments) with continued washing with demineralized water. The individual filter portions that corresponded to each well of the microtiter plates were excised and transferred to scintillation vials for liquid scintillation counting. Uptake rates are presented as pmol/mg of yeast protein. The quantification of yeast protein was determined using a Bio-Rad protein assay kit (Bio-Rad). K_m and V_{max} values for transport of nucleosides by yeast producing wild-type or variant recombinant hCNT3 were calculated through rate vs. concentration plots using PRISM GraphPad version 3.0 software (GraphPad Software Inc., San Diego, CA, USA). Statistical significance of the reported data sets was evaluated using *t*-tests.

Immunofluorescence and confocal microscopy of yeast

Logarithmically growing yeast (10 OD units, $A_{600} = 0.7$ –1.0) were fixed using 3.7% formaldehyde for 30 min with occasional agitation, after which cells were pelleted and washed with 4 ml of double-distilled H₂O. The pellets were resuspended in 1 ml of 700 μ g/ml Zymolyase-100T (MP Biomedicals, Irvine, CA, USA) in solution B (1.2 M sorbitol, 100 mM potassium phosphate, pH 7.5) for 30–40 min at 30°C. The yeast suspensions (300 μ l) were applied onto poly L-lysine coated coverslips, permeabilized using chilled 1:1 acetone/methanol and incubated first with blocking buffer (2% goat serum in phosphate-buffered saline (PBS, pH 7.2)) for 30 min and then with anti-hCNT3 monoclonal antibodies in PBST (PBS with 1% Triton-X-100) for 30 min. After extensive washing with PBST, the yeast were stained with the secondary antibodies (Alexa Fluor 488 goat anti-mouse immunoglobulin G (IgG; 1:250 dilution in PBS, Molecular Probes, Ontario, Canada)) for 30 min, followed by extensive

washing with PBS. The coverslips were mounted and dried overnight. Confocal images were collected using a Zeiss LSM510 confocal laser scanning microscope with a 40 × 1.3 objective (F-Fluar) using a frame size of 1024 × 1024 pixels with a pixel resolution of 0.1 μm and a pixel depth of 12 bits.

Metamorph version 6.1 software (Universal Imaging Corp, Downingtown, PA, USA) was used to measure pixel intensities of stained yeast over the defined regions. The average fluorescence intensity (defined as total intensity divided by defined region) of each yeast cell was digitalized after background subtraction. Only yeast cells without cell walls were included for fluorescence intensity measurements. About 60 to 120 cells per yeast strain were measured and the data were exported to GraphPad Prism version 4.0 for comparison of the relative abundance of reference hCNT3 and hCNT3 variants (Student's *t*-test).

Expression of recombinant hCNT3 and hCNT3 variants in *Xenopus* oocytes

The cDNAs of hCNT3 and hCNT3 variants were subcloned into vector pGEM-HE. Plasmids were linearized with *Nhe*I (pGEM-HE) and transcribed with T7 polymerase mMESSAGE mMACHINE (Ambion). Stage VI oocytes of *Xenopus laevis* were microinjected with 20 nl of water or 20 nl of water containing RNA transcripts (20 ng) and incubated in modified Barth's medium (changed daily) at 18°C for 72 h prior to the assay of transport activity as described previously [31].

Radioisotope flux studies in *Xenopus* oocytes

Transport was traced using ¹⁴C-labeled uridine at a concentration of 20 μM. Flux measurements were performed at room temperature (20°C) as described previously [9,31] on groups of 10–12 oocytes in 200 μl of transport medium containing 100 mM NaCl, 2 mM KCl, 1 mM CaCl₂, 1 mM MgCl₂, and 10 mM HEPES, pH 8.5. At the end of the incubation period, oocytes were washed rapidly six times with ice-cold transport medium, and individual oocytes were dissolved in 1% (w/v) sodium dodecyl sulfate for quantitation of oocyte-associated radioactivity by liquid scintillation counting (LS 6000 IC; Beckman). Initial rates of transport were determined using an incubation period of 1 min. Choline replaced sodium in Na⁺ dependence experiments, and proton-dependent uptake of uridine was measured in choline-containing transport medium acidified to pH 5.5 (buffered with 10 mM minimal essential salts) [31]. The flux values shown are the means ± SE of 10–12 oocytes.

Measurement of hCNT3- and hCNT3 variant-induced sodium and proton currents in *Xenopus* oocytes

Oocyte membrane currents were measured using a GeneClamp 500B oocyte clamp (Axon Instruments, Inc., Foster City, CA, USA) in the two-electrode,

voltage-clamp mode as described previously [31]. All experiments were performed at room temperature (20°C) and oocytes were discarded if the membrane potential was unstable or more positive than –30 mV. The membrane potential was clamped at a holding potential (*V_h*) of –50 mV. Oocytes were perfused with the same media used for radioisotope flux studies, and cation/nucleoside cotransport was initiated by changing the permeant-free solution to one containing 100 μM uridine.

Results

Genetic variations in hCNT3

Primers were designed for all exons and the flanking 5' and 3' regions (Table 1) in an attempt to sequence and identify polymorphisms in hCNT3. Of the 18 exons and the 5' and 3' non-coding sequences that were PCR amplified and sequenced, only 11 exons and the 3' non-coding region (Table 2) gave sequence information in which SNPs were detected that were either unique (i.e., newly reported in this study) or confirmed (i.e., reported previously in the database at <http://www.ncbi.nlm.nih.gov/SNP> or <http://www.pharmgkb.org/views/variant>). Some amplicons were difficult to sequence (the 5' non-coding region) or, when sequenced, showed no polymorphisms (exons 7, 9, 11, 12, 13, 16 and 17). Of the 16 SNPs that were identified in the hCNT3 gene from the coding and flanking intronic sequences, only two intronic and three coding-region SNPs have been previously reported (Table 2). G > A (S5N, rs11568403), C > T (L461L, rs7853758), and A > G (T89T, rs7867504) polymorphisms and intronic SNPs (rs4877836 and rs3812510 in introns 6 and 7, see Table 2 and Fig. 1) were among those that were previously reported. Two non-synonymous coding-region SNPs and nine intronic SNPs were among the 11 new variants of hCNT3 that were identified in the present study. Table 2 lists the SNPs, nucleotide positions, amino acid changes, and the observed genotype and allele frequencies for the various polymorphisms. The genotype distributions for the reported polymorphisms (Table 2) are consistent with the predictions of the Hardy-Weinberg Equilibrium (HWE) except for SNP L131F and the intronic SNP (rs4877836).

Both synonymous and non-synonymous polymorphisms were found in the hCNT3 gene. Among the coding-region SNPs that were identified were Ser 5 to Asn (S5N) in the N-terminal region, Thr 89 to Thr (T89T) in the N-terminal cytoplasmic tail, Leu 131 to Phe (L131F) in the predicted transmembrane domain 2, Leu 461 to Leu (L461L) in predicted transmembrane domain 10 and Tyr 513 to Phe (Y513F) in one of the extracellular loops (Fig. 1, topology model in the bottom panel).

One SNP in non-coding exon 1 and 10 SNPs in the 50-base flanking intronic regions were also identified (Fig. 1

Table 2 Polymorphisms and allele frequencies for the gene encoding hCNT3 (SLC28A3)

SNP #	Amplicon	Position in Ref mRNA or NCBI SNP ID	Observed genotype								
			NT Position	NT Change	AA & Position	N	HZ	HT	VT	Allele 1	Allele 2
1	Exon 1	(Non coding exon)	(-)27,853	C>T		168	166	2	0	0.99	0.01
2	Exon 2	14, rs11568403	(+)14	G>A	5, S>N	186	184	2	0	0.99	0.01
3	Exon 3	(SNP in intron 2)	(+)27,125	C>T		192	186	6	0	0.98	0.02
4	Exon 4	(SNP in intron 4)	(+)31,021	A>G		184	182	2	0	0.99	0.01
5	Exon 5	267, rs7867504	(+)35,312	A>G	89, T>T	188	90	74	24	0.68	0.32
6	Exon 6	1159	(+)38,270	C>T	131, L>F	192	190	0	2	0.99	0.01
7	Exon 6	(SNP in intron 5)	(+)38,194	G>A		192	190	2	0	0.99	0.01
8	Exon 6	rs4877836	(+)38,470	A>G		192	148	34	10	0.86	0.14
		(SNP in intron 6)									
9	Exon 6		(+)38,460	G>T		192	190	2	0	0.99	0.01
		(SNP in intron 6)									
10	Exon 8		(+)42,602	C>T		124	120	4	0	0.98	0.02
		(SNP in intron 7)									
11	Exon 8	rs3812510	(+)42,733	T>C		124	120	4	0	0.98	0.02
		(SNP in intron 7)									
12	Exon 10	(SNP in intron 9)	(+)46,464	T>C		144	106	32	6	0.85	0.15
13	Exon 14	1381, rs7853758	(+)54,622	C>T	461, L>L	188	138	44	6	0.85	0.15
14	Exon 15	1538	(+)55,179	A>T	513, Y>F	192	170	22	0	0.94	0.06
15	Exon 18	(SNP in 3' NC region)	(+)62,477	A>G		186	140	40	6	0.86	0.14
16	3' NC	(SNP in 3' NC region)	(+)62,900	C>T		190	146	42	2	0.88	0.12

The reference hCNT3 mRNA sequence used for these studies was from accession number NM_022127N. The NCBI SNP database IDs are indicated where available. The exon, intron or non-coding (NC) region SNPs are identified. The nucleotide (NT) position is indicated as (+) or (-) corresponding to the upstream or downstream sequence position relative to the ATG (+1) codon as indicated in the SNPPER database (<http://snpper.chip.org/>); The amino acid (AA) changes as a result of the polymorphisms and the positions in the protein sequence are given. The number of samples (chromosomes, N) that were sequenced varied since some PCR products did not yield readable sequence information. The observed genotype and allele frequencies (allele 1 and 2) are indicated. HZ, homozygous wild-type; HT and VT, heterozygous and homozygous variant or mutant, respectively.

and Table 2). All the polymorphisms reported here have been confirmed by a second round of PCR and DNA sequencing. The 5' putative promoter sequences were not amenable for sequencing despite successful PCR amplification of the fragment. There were no deletion or insertion polymorphisms in the apparently healthy 96 Caucasian DNAs used in this study.

A wide variation in the minor allele frequencies was observed for the different classes of SNPs reported here. In coding regions, the synonymous variants T89T and L461L showed higher minor allele frequencies (15–32%) than the non-synonymous variants, S5N, L131F and Y513F (1–6%). The SNP allele frequencies varied from 1–14% for intronic regions and 12–14% for the 3' non-coding region. The low allele frequencies of the non-synonymous SNPs observed in coding regions of the hCNT3 gene suggested nucleotide conservation and constraints on changes in the amino acids of the hCNT3 protein.

Functional analysis of recombinant hCNT3 variants in yeast

Recombinant hCNT3 and three of the non-synonymous variant proteins were produced in yeast and characterized for their ability to transport several naturally occurring nucleosides (uridine, cytidine, adenosine, inosine). Yeast cells producing recombinant reference (i.e., wild-type) or non-synonymous variant hCNT3 proteins were incubated with 0.5, 1, 2, 5, 10, 20, 50 or 100 μM [^3H]nucleoside in the absence or presence of 10 mM of uridine. The mediated component of nucleoside transport was calcu-

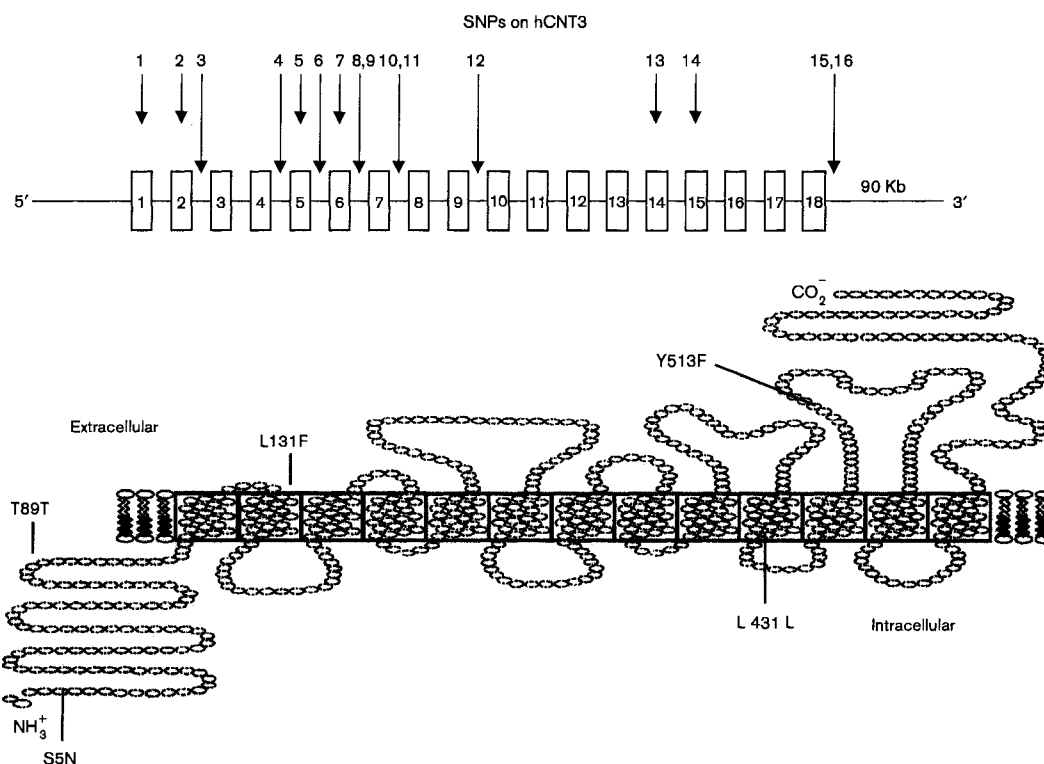
lated as the initial rate of uptake of [^3H]nucleoside at a particular concentration minus the initial rate of uptake at that concentration in the presence of the non-radioactive uridine at 10 mM, and the resulting concentration versus rate data sets were analysed to determine the kinetic parameters for inwardly directed fluxes (Table 3). The four transporters displayed almost identical apparent K_m values (i.e., 2–3 μM) for the various permeants tested and V_{max} values in the range of 1000–2000 pmol/mg protein/min; the differences noted for reference hCNT3 and the hCNT3 variants were not statistically significant according to paired t -test analysis ($P > 0.05$). These results demonstrated that the three non-synonymous variants did not exhibit altered transportability of the naturally occurring pyrimidine and purine nucleosides that were tested.

The apparent K_m values (2–3 μM) for reference and variant hCNT3 produced in yeast were lower than the apparent K_m values previously reported for hCNT3 produced in *Xenopus laevis* oocytes (15–50 μM) [8] and African green monkey kidney (Cos7L) cells (3–11 μM) [32], possibly reflecting differences in post-translational modification in the various expression systems.

Detection and quantitation of hCNT3 and variant hCNT3 produced in yeast

Indirect immunostaining was used to compare the localization and abundance of hCNT3 and hCNT3 variant proteins in yeast. As shown in Fig. 3(a), yeast producing recombinant hCNT3 variants exhibited staining patterns similar to that of reference hCNT3, which

Fig. 1



SNPs on hCNT3. (a), Schematic representation of 18 exons (rectangular bars), introns, and the 5' and 3' sequences for hCNT3 (approximately 90 kb) are shown as a thin line along the axis. Locations of the identified SNPs are numbered from 1–16 (not drawn to scale). The long and short arrows indicate intronic and exonic SNPs, respectively, within the depicted chromosomal structure of the gene for hCNT3. (b) The extracellular and intracellular domains predicted for hCNT3 [8] are indicated in the transmembrane topology model for hCNT3. The variants (S5N, T89T, L131F, L431L, Y513F) are identified in the model. Individual amino acids are omitted for clarity.

Table 3 Kinetic properties of recombinant hCNT3 and variants of hCNT3 produced in *S. cerevisiae*

	Reference hCNT3		hCNT3-S5N		hCNT3-L131F		hCNT3-Y513F	
	K_m (μM)	V_{max} (pmol/mg/min)						
Uridine	1.7 ± 0.3	1402 ± 286	2.3 ± 0.9	1700 ± 198	2.5 ± 0.6	1945 ± 324	2.1 ± 0.6	
Cytidine	3.6 ± 1.3	1310 ± 113	3.5 ± 1.1	1120 ± 147	2.8 ± 0.8	1424 ± 237	2.2 ± 0.5	1577 ± 315
Adenosine	2.2 ± 0.7	1020 ± 44	2.8 ± 0.8	1322 ± 102	2.1 ± 1.1	1230 ± 228	3.0 ± 0.9	1349 ± 245
Inosine	2.1 ± 0.6	1740 ± 114	2.5 ± 0.7	1360 ± 322	2.5 ± 0.8	2038 ± 179	3.2 ± 0.8	1442 ± 130

Initial rates of uptake of [^3H]-labeled uridine, cytidine, adenosine or inosine at graded concentrations were measured in yeast transformed with pYPhCNT3 or pYPhCNT3-S5N, pYPhCNT3-L131F and pYPhCNT3-Y513F as described in Methods. The differences in rates of uptake of [^3H]nucleoside at the indicated concentration alone and in the presence of the same non-radioactive nucleoside were calculated and plotted as a function of extracellular nucleoside concentration, as in Fig. 2. Plots of V versus V/S were constructed for each nucleoside to determine the kinetic parameters, K_m (μM) and V_{max} (pmol/min/mg of protein). Each value represents the mean of three independent experiments.

was predominantly localized to the plasma membrane. No significant fluorescent signal was observed on yeast transformed with the insert-free vector (pYPGE15) or yeast producing recombinant hCNT3 that were treated with either IgG isotype antibodies or secondary antibodies only (data not shown).

To measure the protein abundance of recombinant hCNT3 and its variants, the fluorescence intensities of 60–120 cells per yeast strain were obtained and averaged to calculate mean fluorescence intensities. As presented in Fig. 3(b), yeast producing hCNT3, hCNT3-S5N, hCNT3-L131F or hCNT3-Y513F displayed mean

fluorescence intensities that were not significantly different (Student's *t* test, hCNT3 vs. variant hCNT3, $P > 0.05$), indicating that the non-synonymous SNPs identified in this study had no effect on the production or localization of hCNT3.

Sodium and proton dependence of uridine transport

Compared with hCNT1 and hCNT2, hCNT3 has a greater ability to transport permeant against its concentration gradient because the sodium:nucleoside coupling ratio is 2:1 for hCNT3 and 1:1 for hCNT1 and 2 [8]. Additionally, hCNT3 differs from hCNT1 and hCNT2 in that hCNT3 is also proton dependent [8], indicating that hCNT3 has potential roles in tissues with acidic extracellular environments. To test for possible changes in the sodium and proton dependence of hCNT3 variants, uridine influx and uridine-evoked sodium and proton currents were measured in the *Xenopus* oocyte heterologous expression system. Sodium-dependent uridine influx and uridine-evoked sodium currents were measured at pH 8.5 (to minimize proton-coupled transport) using choline as the sodium substitute. Proton-dependent uridine influx and uridine-evoked proton currents were measured in acidified choline-containing transport medium at pH 5.5.

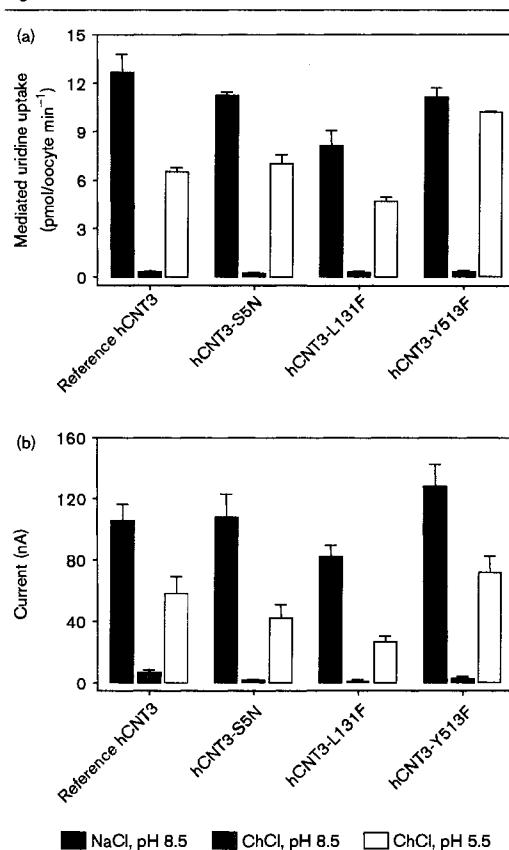
As shown in Fig. 2(a), uridine uptake ($20 \mu\text{M}$) mediated by recombinant hCNT3 and the three non-synonymous variants was sodium-dependent with influx values of 8–12 and 0.2–0.3 pmol/oocyte min^{-1} in sodium-containing and sodium-free media at pH 8.5, respectively. Acidification of the choline-containing transport medium to pH 5.5 induced marked proton-dependent uridine transport by both wild-type and mutant hCNT3 proteins. Uridine uptake in control water-injected oocytes was slow ($< 0.03 \text{ pmol/oocyte min}^{-1}$), and similar in each of the three media tested (data not shown).

In addition to radioisotope flux studies, the two-electrode voltage clamp technique was used to confirm the sodium and proton dependence of hCNT3- and hCNT3 variant-mediated uridine transport. As shown in Fig. 2(b), application of uridine ($100 \mu\text{M}$) to oocytes producing recombinant proteins induced inward sodium and proton currents for all four transporters, demonstrating that hCNT3 and hCNT3 variants function as electrogenic Na^+ /nucleoside and H^+ /nucleoside symporters. Currents returned to baseline upon removal of uridine, and no currents were detected in control water-injected oocytes (data not shown).

Discussion

We have identified 16 hCNT3 SNPs and compared the functional characteristics of the wild-type and non-synonymous variant proteins in yeast and oocyte expression systems to look for changes in transport function.

Fig. 2



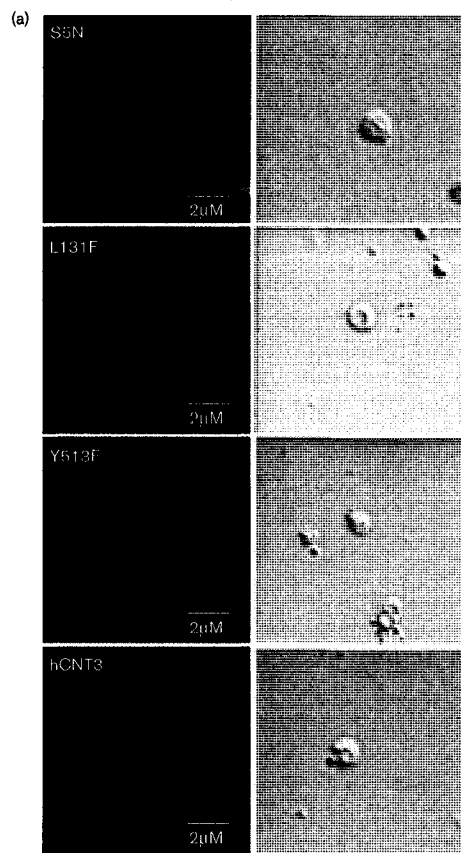
Sodium and proton-dependent transport of uridine. (a) Mediated influx of [¹⁴C]-labeled uridine by recombinant hCNT3 and hCNT3 SNPs expressed in *Xenopus* oocytes. Uptake of uridine ($20 \mu\text{M}$, 20°C , 1-min flux) in oocytes injected with RNA transcripts was measured in transport media containing either 100 mM NaCl (pH 8.5), 100 mM ChCl (pH 8.5) or 100 mM ChCl (pH 5.5). Mediated transport was calculated as uptake in RNA-injected oocytes minus uptake in control water-injected oocytes. Each value represents the mean \pm S.E.M. of 10–12 oocytes. (b) Measurement of sodium and proton currents. Currents were generated by perfusing oocytes producing either hCNT3 or one of the variant hCNT3s with uridine ($100 \mu\text{M}$, 20°C) in the same three media used in (a). Transporter-mediated uridine-evoked currents are expressed as the mean \pm SEM of three different oocytes. No currents were detected in control water-injected oocytes (data not shown).

The observed low allele frequencies for various non-synonymous coding SNPs and the nearly similar abundance of recombinant reference and variant CNT3 proteins in yeast, transport activity in yeast and sodium/proton dependence in oocytes implied high conservation of function in hCNT3 and little genetic diversity of the gene.

A total of 4873 bp were read in each DNA sample and 16 SNPs were identified in 18 exons, flanking introns and the 3' non-coding region of hCNT3 in a Caucasian DNA

panel, yielding a density of one SNP per 304 bp. Coding and non-coding region SNPs typically occur at a frequency of 1 per 346 bp [14]. From a study of 24 transporters, an average frequency of 1 per 141 bp was estimated and for hENT1 the frequency was 1 per 179 bp [22].

Fig. 3



Functional characterization of recombinant hENT1 variants in *S. cerevisiae* [20] also revealed a striking lack of genetic and functional diversity, although various artificial variants with altered functional properties have been produced experimentally. For example, site-directed mutagenesis studies in hENT1 yielded transport-defective mutants in which a conserved Gly 179 in transmembrane domain 5 was changed to either Leu, Cys or Val and point mutations at Gly184 affected both transport function and membrane targeting of hENT1 [33]. There are no reports of naturally occurring polymorphisms at either Gly 179 or 184 in the populations screened for SNPs [20,22]. It is interesting to note that the hENT1 gene [20,22] and the hCNT3 gene (this study) both exhibit low mutability. Both proteins accept a broad range of purine and pyrimidine ribo- and deoxyribo-nucleoside permeants. It is possible that during the course of evolution, mutations affecting function may have been eliminated. Only synonymous SNPs and non-synonymous variants with marginal effects have been conserved, as would be expected from the neutral theory of evolution [22,34].

In the hCNT3 variant L131F, which was a change from an aliphatic to an aromatic amino acid in the predicted transmembrane domain 2, the transport function was not altered, even though the change was potentially deleterious as assessed by the SIFT (Sorting Intolerant from Tolerant) program [35]. Although L131 is highly conserved among hCNT1, hCNT2, rabbit CNT1 (rbCNT1) and rat CNT1 (rCNT1), transmembrane segments 1–3 are believed to be dispensable for function, based on homology to a related bacterial protein (NUPC) that lacks this transmembrane domain [36]. Deletion of transmembrane segments 1–3 in rCNT1 and functional characterization support the dispensable nature of this protein domain [36]. Despite the lack of heterozygotes

Localization and protein abundance of recombinant hCNT3 and its variants produced in yeast. (a) Immunostaining of yeast producing reference or variant hCNT3 proteins. Representative cells producing hCNT3, hCNT3-S5N, hCNT3-L131F or hCNT3-Y513F were treated with anti-hCNT3 IgM as primary antibodies followed by Alexa Fluor 488 goat-anti mouse IgG as secondary antibodies. The images were captured by confocal microscopy as described in Materials and Methods. (b) Average fluorescence intensities of yeast producing reference or variant hCNT3 proteins. After immunostaining, the fluorescence signals of 60–120 yeast cells were quantified using Metamorph version 6.1 software and the mean \pm SE values of average fluorescence intensities were analyzed with GraphPad Prism version 4.0 software.

for L131Y and its apparent deviation from the Hardy–Weinberg equilibrium, we undertook functional characterization of this hCNT3 variant. It remains to be seen if non-Caucasian populations show L131F mutations and heterozygosity. The other hCNT3 variants showed conservative changes (i.e., S5N, polar uncharged substitution; Y513F, aromatic amino acid substitution) and these were non-deleterious and are not conserved in hCNT1 and hCNT2. In contrast, the non-synonymous SNPs of hCNT1, which occur at very low allele frequencies, yielded proteins with altered transport activity in comparison to reference hCNT1 when tested in *Xenopus* oocytes [19,21].

Although the hENT1 and hCNT3 genes did not exhibit insertion or deletion polymorphisms, such polymorphisms were observed in the coding regions of the hENT2 and hCNT1 genes [21]. The intronic SNPs for hCNT3 reported in this study need to be investigated for possible roles in the generation of differentially spliced transcripts. Relatively little is known about the regulation of the human nucleoside transporters and the possible influence of promoter region polymorphisms (regulatory SNPs). There is an increasing body of evidence that regulatory SNPs offer clues to the tissue-specific expression of drug metabolizing enzymes and transporters [4,37]. Immunohistochemical staining using hENT1 antibodies in breast cancer tissues showed considerable variability in transporter abundance [12]. The absence of functional changes observed in recombinant hENT1 variant proteins (based on the naturally occurring variants described for coding regions of hENT1) produced in yeast or oocytes [20] suggests that the variable abundance of hENT1 in breast cancer tissues may be due to variations in regulatory regions. However, variants that might alter mRNA stability or transcription through polymorphisms in 3'-untranslated regions or promoter regions, respectively, of the hENT and hCNT genes have not been described. Interestingly, hCNT3 transcription in human myeloid HL-60 cells is induced by treatment with phorbol ester, and analysis of the hCNT3 5'-genomic sequence in the potential upstream promoter region of the gene has revealed the presence of a eukaryotic phorbol ester response element [9].

Acknowledgements

The authors would like to thank Dr. X. Sun and Ms. G. Barron of the Cell Imaging Facility at the Cross Cancer Institute for their help with confocal image capture and data analysis. CEC is Canada Research Chair of Oncology and JDY is Heritage Scientist of the Alberta Heritage Foundation for Medical Research. Studentship support was from the Canadian Institutes of Health Research (to J.Z.), the Alberta Heritage Foundation for Medical Research (to J.Z. and F.V.) and the Department of Oncology Endowed Studentship (to J.Z. and F.V.). This

work was supported by the Alberta Cancer Board, the Alberta Cancer Foundation and a Canadian Cancer Society operating grant from the National Cancer Institute of Canada.

References

- Cass CE, Young JD, Baldwin SA, Cabrita MA, Graham KA, Griffiths M, *et al.* Nucleoside transporters of mammalian cells. *Pharm Biotechnol* 1999; 12:313–352.
- Vickers MF, Yao SY, Baldwin SA, Young JD, Cass CE. Nucleoside transporter proteins of *Saccharomyces cerevisiae*. Demonstration of a transporter (FUI1) with high uridine selectivity in plasma membranes and a transporter (FUN26) with broad nucleoside selectivity in intracellular membranes. *J Biol Chem* 2000; 275:25931–25938.
- Cabrita MA, Baldwin SA, Young JD, Cass CE. Molecular biology and regulation of nucleoside and nucleobase transporter proteins in eukaryotes and prokaryotes. *Biochem Cell Biol* 2002; 80:623–638.
- Damaraju VL, Damaraju S, Young JD, Baldwin SA, Mackey J, Sawyer MB, *et al.* Nucleoside anticancer drugs: the role of nucleoside transporters in resistance to cancer chemotherapy. *Oncogene* 2003; 22:7524–7536.
- Cass CE. Nucleoside transport. In: Georgopadakou NH (ed.) *Drug Transport in Antimicrobial and Anticancer Chemotherapy*. New York: Marcel Dekker; 1995:403–451.
- Ritzel MW, Yao SY, Huang MY, Elliott JF, Cass CE, Young JD. Molecular cloning and functional expression of cDNAs encoding a human Na⁺-nucleoside cotransporter (hCNT1). *Am J Physiol* 1997; 272:C707–C714.
- Ritzel MW, Yao SY, Ng AM, Mackey JR, Cass CE, Young JD. Molecular cloning, functional expression and chromosomal localization of a cDNA encoding a human Na⁺/nucleoside cotransporter (hCNT2) selective for purine nucleosides and uridine. *Mol Membr Biol* 1998; 15:203–211.
- Ritzel MW, Ng AM, Yao SY, Graham K, Loewen SK, Smith KM, *et al.* Molecular identification and characterization of novel human and mouse concentrative Na⁺-nucleoside cotransporter proteins (hCNT3 and mCNT3) broadly selective for purine and pyrimidine nucleosides (system cib). *J Biol Chem* 2001; 276:2914–2927.
- Ritzel MW, Ng AM, Yao SY, Graham K, Loewen SK, Smith KM, *et al.* Recent molecular advances in studies of the concentrative Na⁺-dependent nucleoside transporter (CNT) family: identification and characterization of novel human and mouse proteins (hCNT3 and mCNT3) broadly selective for purine and pyrimidine nucleosides (system cib). *Mol Membr Biol* 2001; 18:65–72.
- Lang TT, Selner M, Young JD, Cass CE. Acquisition of human concentrative nucleoside transporter 2 (hcnt2) activity by gene transfer confers sensitivity to fluoropyrimidine nucleosides in drug-resistant leukemia cells. *Mol Pharmacol* 2001; 60:1143–1152.
- Mackey JR, Mani RS, Selner M, Mowles D, Young JD, Belt JA, *et al.* Functional nucleoside transporters are required for gemcitabine influx and manifestation of toxicity in cancer cell lines. *Cancer Res* 1998; 58:4349–4357.
- Mackey JR, Jennings LL, Clarke ML, Santos CL, Dabbagh L, Vsianska M, *et al.* Immunohistochemical variation of human equilibrative nucleoside transporter 1 protein in primary breast cancers. *Clin Cancer Res* 2002; 8:110–116.
- Spratlin J, Sangha R, Glubrecht D, Dabbagh L, Young JD, Dumontet C, *et al.* The absence of human equilibrative nucleoside transporter 1 is associated with reduced survival in patients with gemcitabine-treated pancreas adenocarcinoma. *Clin Cancer Res* 2004; 10:6956–6961.
- Cargill M, Altshuler D, Ireland J, Sklar P, Ardlie K, Patil N, *et al.* Characterization of single-nucleotide polymorphisms in coding regions of human genes. *Nat Genet* 1999; 22:231–238.
- Iida A, Saito S, Sekine A, Nakamura Y. [SNP collection, pharmacogenomics, and the future of drug therapy]. *Gan To Kagaku Ryooho* 2002; 29:1665–1673.
- Illmer T, Schuler US, Thiede C, Schwarz UI, Kim RB, Gotthard S, *et al.* MDR1 gene polymorphisms affect therapy outcome in acute myeloid leukemia patients. *Cancer Res* 2002; 62:4955–4962.
- Lu X, Gong S, Monks A, Zaharevitz D, Moscow JA. Correlation of nucleoside and nucleobase transporter gene expression with antimetabolite drug cytotoxicity. *J Exp Ther Oncol* 2002; 2:200–212.
- Sachidanandam R, Weissman D, Schmidt SC, Kakol JM, Stein LD, Marth G, *et al.* A map of human genome sequence variation containing 1.42 million single nucleotide polymorphisms. *Nature* 2001; 409:928–933.

- 19 Gray JH, Owen RP, Urban TJ, Giacomini KM. Functional characterization of genetic variants of the nucleoside transporter, CNT1. *Clin Pharmacol Ther* 2003; **73**:P59.
- 20 Osato DH, Huang CC, Kawamoto M, Johns SJ, Stryke D, Wang J, et al. Functional characterization in yeast of genetic variants in the human equilibrative nucleoside transporter, ENT1. *Pharmacogenetics* 2003; **13**:297-301.
- 21 Gray JH, Mangravite LM, Owen RP, Urban TJ, Chan W, Carlson EJ, et al. Functional and genetic diversity in the concentrative nucleoside transporter, CNT1, in human populations. *Mol Pharmacol* 2004; **65**:512-519.
- 22 Leabman MK, Huang CC, DeYoung J, Carlson EJ, Taylor TR, de la Cruz M, et al. Natural variation in human membrane transporter genes reveals evolutionary and functional constraints. *Proc Natl Acad Sci USA* 2003; **100**:5896-5901.
- 23 Gray JH, Owen RP, Giacomini KM. The concentrative nucleoside transporter family, SLC28. *PLoS Arch* 2004; **447**:728-734.
- 24 Badagnani I, Giacomini KM. Interaction of cladribine and fludarabine with genetic variants in the concentrative nucleoside transporter, CNT3 [abstract]. *Am Soc Clin Pharmacol Ther* 2004; **75**:P18.
- 25 Zhang J, Visser F, Vickers MF, Lang T, Robins MJ, Nielsen LP, et al. Uridine binding motifs of human concentrative nucleoside transporters 1 and 3 produced in *Saccharomyces cerevisiae*. *Mol Pharmacol* 2003; **64**: 1512-1520.
- 26 Vickers MF, Kumar R, Visser F, Zhang J, Charania J, Raborn RT, et al. Comparison of the interaction of uridine, cytidine, and other pyrimidine nucleoside analogues with recombinant human equilibrative nucleoside transporter 2 (hENT2) produced in *Saccharomyces cerevisiae*. *Biochem Cell Biol* 2002; **80**:639-644.
- 27 Visser F, Vickers MF, Ng AM, Baldwin SA, Young JD, Cass CE. Mutation of residue 33 of human equilibrative nucleoside transporters 1 and 2 alters sensitivity to inhibition of transport by diazepam and dipyridamole. *J Biol Chem* 2002; **277**:395-401.
- 28 Brunelli JP, Pall ML. A series of yeast shuttle vectors for expression of cDNAs and other DNA sequences. *Yeast* 1993; **9**:1299-1308.
- 29 Ito H, Fukuda Y, Murata K, Kimura A. Transformation of intact yeast cells treated with alkali cations. *J Bacteriol* 1983; **153**:163-168.
- 30 Vickers MF, Zhang J, Visser F, Tackaberry T, Robins MJ, Nielsen LP, et al. Uridine recognition motifs of human equilibrative nucleoside transporters 1 and 2 produced in *Saccharomyces cerevisiae*. *Nucleosides Nucleotides Nucleic Acids* 2004; **23**:361-373.
- 31 Smith KM, Ng AM, Yao SY, Labedz KA, Knaus EE, Wiebe LI, et al. Electrophysiological characterization of a recombinant human Na⁺-coupled nucleoside transporter (hCNT1) produced in *Xenopus* oocytes. *J Physiol* 2004; **558**:807-823.
- 32 Toan SV, To KK, Leung GP, de Souza MO, Ward JL, Tse CM. Genomic organization and functional characterization of the human concentrative nucleoside transporter-3 isoform (hCNT3) expressed in mammalian cells. *PLoS Arch* 2003; **447**:195-204.
- 33 SenGupta DJ, Lum PY, Lai Y, Shubochkina E, Bakken AH, Schneider G, et al. A single glycine mutation in the equilibrative nucleoside transporter gene, hENT1, alters nucleoside transport activity and sensitivity to nitrobenzylthioinosine. *Biochemistry* 2002; **41**:1512-1519.
- 34 Shu Y, Leabman MK, Feng B, Mangravite LM, Huang CC, Stryke D, et al. Evolutionary conservation predicts function of variants of the human organic cation transporter, OCT1. *Proc Natl Acad Sci USA* 2003; **100**:5902-5907.
- 35 Ng PC, Henikoff S. Accounting for human polymorphisms predicted to affect protein function. *Genome Res* 2002; **12**:436-446.
- 36 Hamilton SR, Yao SY, Ingram JC, Hadden DA, Ritzel MW, Gallagher MP, et al. Subcellular distribution and membrane topology of the mammalian concentrative Na⁺-nucleoside cotransporter rCNT1. *J Biol Chem* 2001; **276**:27981-27988.
- 37 Damaraju S, Sawyer M, Zanke B. Genomic approaches to clinical drug resistance. *Cancer Treat Res* 2002; **112**:347-372.

Appendix 2:

Transport of Physiological Nucleosides and Anti-Viral and Anti-Neoplastic Nucleoside Drugs by Recombinant *Escherischia coli* Nucleoside-H⁺ Cotransporter (NupC) Produced in *Xenopus laevis* Oocytes*

* This appendix has been published.

Loewen, S. K., Yao, S. Y., Slugoski, M. D., Mohabir, N. N., Turner, R. J., Mackey, J. R., Gallagher, M. P., Henderson, P. J., Baldwin, S. A., Cass, C. E., and Young, J. D. (2004) Transport of physiological nucleosides and anti-viral and anti-neoplastic nucleoside drugs by recombinant *Escherischia coli* nucleoside-H⁺ cotransporter (NupC) produced in *Xenopus laevis* oocytes. *Mol. Membr. Biol.* **21**: 1-10.

Transport of physiological nucleosides and anti-viral and anti-neoplastic nucleoside drugs by recombinant *Escherichia coli* nucleoside-H⁺ cotransporter (NupC) produced in *Xenopus laevis* oocytes

Shaun K. Loewent[†], Sylvia Y. M. Yao[†],
Melissa D. Slugoski[†], Nadira N. Mohabir[†],
Raymond J. Turner^{†¶}, John R. Mackey[§],
Joel. H. Weiner[‡], Maurice P. Gallagher[¥],
Peter J. F. Henderson[#], Stephen A. Baldwin[#],
Carol E. Cass[§] and James D. Young^{†*}

Membrane Protein Research Group, Departments of
[†] Physiology; [‡] Biochemistry; and [§] Oncology, University of
Alberta, Edmonton, Alberta T6G 2H7, Canada

[¶] Structural Biology Research Group, Department of
Biological Sciences, University of Calgary, Calgary, Alberta
T2N 1N4, Canada

[¥] Institute of Cell and Molecular Biology, Biology Division,
University of Edinburgh, West Mains Road, Edinburgh EH9
3JR, UK

[#] School of Biochemistry and Molecular Biology, University
of Leeds, Leeds LS2 9JT, UK

Summary

The recently identified human and rodent plasma membrane proteins CNT1, CNT2 and CNT3 belong to a gene family (CNT) that also includes the bacterial nucleoside transport protein NupC. Heterologous expression in *Xenopus* oocytes has established that CNT1-3 correspond functionally to the three major concentrative nucleoside transport processes found in human and other mammalian cells (systems *cit*, *cif* and *cib*, respectively) and mediate Na⁺-linked uptake of both physiological nucleosides and anti-viral and anti-neoplastic nucleoside drugs. Here, one describes a complementary *Xenopus* oocyte transport study of *Escherichia coli* NupC using the plasmid vector pGEM-HE in which the coding region of NupC was flanked by 5'- and 3'-untranslated sequences from a *Xenopus* β -globin gene. Recombinant NupC resembled human (h) and rat (r) CNT1 in nucleoside selectivity, including an ability to transport adenosine and the chemotherapeutic drugs 3'-azido-3'-deoxythymidine (AZT), 2',3'-dideoxycytidine (ddC) and 2'-deoxy-2',2'-difluorocytidine (gemcitabine), but also interacted with inosine and 2',3'-dideoxyinosine (ddI). Apparent affinities were higher than for hCNT1, with apparent K_m values of 1.5–6.3 μ M for adenosine, uridine and gemcitabine, and 112 and 112 μ M, respectively, for AZT and ddC. Unlike the relatively low translocation capacity of hCNT1 and rCNT1 for adenosine, NupC exhibited broadly similar apparent V_{max} values for adenosine, uridine and nucleoside drugs. NupC did not require Na⁺ for activity and was H⁺-dependent. The kinetics of uridine transport measured as a function of external pH were consistent with an ordered transport model in which H⁺ binds to the transporter first followed by the nucleoside. These experiments establish the NupC-pGEM-HE/oocyte system as a useful tool for

characterization of NupC-mediated transport of physiological nucleosides and clinically relevant nucleoside therapeutic drugs.

Keywords: Nucleoside transporters, *Xenopus* oocytes, 3'-deoxy-nucleoside drugs, CNT, NupC.

Abbreviations: AIDS, acquired immunodeficiency syndrome, HIV, human immunodeficiency virus, NT, nucleoside transporter, CNT, concentrative nucleoside transporter, ENT, equilibrative nucleoside transporter, MIP, major intrinsic protein, AZT, 3'-azido-3'-deoxythymidine, ddC, 2',3'-dideoxycytidine, ddI, 2',3'-dideoxyinosine, gemcitabine, 2'-deoxy-2',2'-difluorocytidine, bp, base pair(s), kb, kilobase(s), PCR, polymerase chain reaction, kDa, kilodaltons, TM, transmembrane helix.

Introduction

The capacity for nucleoside uptake mediated by specialized plasma membrane nucleoside transporter (NT) proteins is widespread amongst bacteria (Kubitschek 1968, Kirchman *et al.* 1982) and is required for nucleic acid synthesis and energy metabolism in mammalian cell types that lack *de novo* pathways for nucleotide biosynthesis (Cheeseman *et al.* 2000). NTs also provide the cellular uptake route for many cytotoxic nucleoside derivatives used in the treatment of viral and neoplastic diseases (Baldwin *et al.* 1999). Such drugs may exert more than one therapeutic action. AZT, for example, is used as an anti-viral drug to combat HIV infection in AIDS, but also provides an ancillary benefit by suppressing bacterial infections in immunocompromized individuals (Monno *et al.* 1997). Infectious complications are also common in cancer patients (Sanders *et al.* 1992, Robak 2001). Enteric *Escherichia coli* cells, several variants of which are formidable pathogens, and other disease-causing bacteria compete directly with host transport systems and are proficient scavengers of nucleosides and other nutrients.

In human and other mammalian cells, uptake of nucleosides is brought about by members of the ENT (equilibrative, Na⁺-independent) and CNT (concentrative, Na⁺-dependent) NT families (Baldwin *et al.* 1999). ENTs are widely distributed in eukaryotes, but so far appear to be absent from prokaryotes, while CNTs are present in both. Three CNT isoforms have been identified in humans and rodents (Huang *et al.* 1994, Che *et al.* 1995, Ritzel *et al.* 1997, 1998, 2001, Wang *et al.* 1997). Human (h) and rat (r) CNT1 and CNT2 both transport uridine and adenosine, but are otherwise selective for pyrimidine (hCNT1 and rCNT1) and purine (hCNT2 and rCNT2) nucleosides. hCNT3 and its mouse (m) orthologue mCNT3 transport both pyrimidine and purine nucleosides. The relationships of these proteins to transport processes defined by functional studies are: CNT1 (*cit*), CNT2 (*cif*) and CNT3 (*cib*). Other CNTs that have been

*To whom correspondence should be addressed.
e-mail: james.young@ualberta.ca

characterized functionally include hCNT from an ancient marine pre-vertebrate, the Pacific hagfish (Yao *et al.* 2002), CaCNT from *Candida albicans* (Loewen *et al.* 2003) and CeCNT3 from *Caenorhabditis elegans* (Xiao *et al.* 2001).

At least three NT proteins (NupC, NupG and XapB) have been identified in the *E. coli* inner membrane (Westh-Hansen *et al.* 1987, Craig *et al.* 1994, Seeger *et al.* 1995). All are concentrative, but only one (NupC) shows sequence similarity to mammalian CNTs. *E. coli* also possesses two NupC homologues (YeiJ and YeiM) of undetermined function. In addition, the outer membrane of *E. coli* and other Gram-negative bacteria contains the passive nucleoside-specific channel-forming protein Tsx (Nieweg and Bremer 1997). Tsx has a porin β -barrel membrane topology and is structurally unrelated to the CNT and ENT protein families.

Transport and growth studies with *E. coli* suggest that the NupC and NupG mediated processes accept a broad range of nucleosides as permeants and can be distinguished from each other by the poor ability of NupC to transport guanosine and deoxyguanosine and by different sensitivities to inhibition by showdomycin (Komatsu and Tanaka 1972). XapB, previously considered to be xanthosine-specific, overlaps in permeant selectivity with NupC (Norholm and Dandanell 2001), although the recently established close proximity of the *xapB* and *nupC* genes on the *E. coli* chromosome (54.34' and 54.13', respectively) and their similar inability to transport guanosine raises the possibility that earlier NupC studies may have grouped both activities as a single transport system (Karp *et al.* 2002). Interpretation of *E. coli* NT studies is further complicated by the reported presence of a low affinity, purine nucleoside-selective process of unknown molecular identity (Norholm and Dandanell 2001). This report overcomes these technical limitations by the use of heterologous expression in *Xenopus* oocytes to study nucleoside and nucleoside drug transport by recombinant *E. coli* NupC in an NT-deficient background and in the same membrane environment used previously to study recombinant mammalian CNTs.

Results

Cloning of the NupC gene

When primers designed to encompass the whole open reading frame of *E. coli nupC* (Craig *et al.* 1994) were used for PCR amplification of *E. coli* HB101 chromosomal DNA, a product of the correct size (1203 bp) was obtained. Sub-cloning into the expression vector pGEM-HE yielded a cDNA (plasmid pNupC-HE) whose nucleotide and deduced amino acid sequences were identical to *nupC* GenBank™/EBI Data Bank accession number NC000913. NupC (43.5 kDa) contained 400 amino acid residues in comparison to the > 600 residues of the mammalian CNTs and was 26% identical (37% similar) to hCNT1, 22% identical (33% similar) to hCNT2 and 25% identical (37% similar) to hCNT3 (Figure 1). The smaller NupC protein did not contain the large intracellular amino-terminus and large exofacial carboxyl-terminus characteristic of human and other mammalian CNTs. In mammalian CNTs, the latter domain contains

multiple sites of N-linked glycosylation (Hamilton *et al.* 2001). NupC also lacked the first three transmembrane helices (TMs) of the mammalian proteins and its 10 predicted TMs correspond, therefore, to TMs 4–13 of CNT1–3 (Hamilton *et al.* 2001). Truncated constructs of human and rat CNT1 with TMs 1–3 removed have confirmed the importance of TMs 4–13 as the important core structure of the mammalian transporters (Hamilton *et al.* 2001). NupC showed greatest sequence similarity to the carboxyl-terminal half of hCNT1–3, particularly in TMs 10–12, including the exofacial loop between TMs 11 and 12 (Figure 1). These regions may, therefore, have particular functional and/or structural significance.

Functional production and cation-specificity of NupC in *Xenopus* oocytes

Figure 2(a) (*insert*) presents a representative transport experiment in NaCl medium at pH 5.5 that compares time courses of uptake of 1 μ M [3 H]uridine by NupC-producing and control (water-injected) oocytes. In both, uptake was linear for at least 30 min. After 10 min, the uptake interval selected for subsequent initial rate measurements, influx in NupC-producing oocytes was 49-fold higher than in control oocytes. Consistent with NupC being a H⁺-dependent transporter, influx was pH-dependent. As shown in Figure 2(a), values for NupC-mediated uridine influx (uptake in RNA-injected oocytes minus uptake in water-injected oocytes) increased 6.3-fold between pH 8.5 and 5.5, while basal influx in water-injected oocytes remained unchanged. For comparison, uridine influx (10 μ M) mediated by Na⁺-dependent rCNT1 was independent of external pH (Figure 2(b)). A small (< 5%) slippage component of rCNT1 uridine influx seen when Na⁺ in the transport medium is replaced by equimolar choline⁺ (Huang *et al.* 1994) was also unaffected by changes in external pH (data not shown). In contrast, NupC retained full functional activity in the absence of Na⁺ and, in a representative experiment, NupC-mediated uridine influx (1 μ M) was 0.84 ± 0.19 and 0.97 ± 0.08 pmol/oocyte.10 min⁻¹ in NaCl and choline chloride transport medium, respectively, at pH 5.5 and 0.14 ± 0.03 and 0.16 ± 0.03 pmol/oocyte.10 min⁻¹, respectively, at pH 8.5.

Substrate selectivity of recombinant NupC

Figure 3(a) compares uridine influx (1 μ M, pH 5.5, 10 min flux) with transport of a panel of other radiolabelled nucleosides and nucleobases. Similar to the *cit*-type functional activity of hCNT1 and rCNT1 (Huang *et al.* 1994, Ritzel *et al.* 1997), uridine, cytidine and thymidine gave similar NupC-mediated fluxes, while guanosine was not transported. Unlike rCNT1 and hCNT1, however, there was also modest transport of inosine. This was verified in the insert to Figure 3(a), which shows time courses of inosine uptake by control and NupC-producing oocytes. Discrimination between inosine and guanosine was also observed in competition experiments: inosine inhibited NupC-mediated uridine influx (1 μ M) with an IC₅₀ value of 287 ± 8 μ M, whereas 1 mM guanosine was without effect (data not shown). Figure 3(a) also shows that NupC transported adenosine at a rate similar

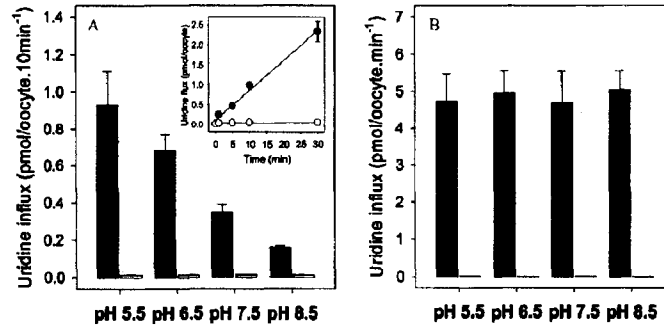


Figure 2. Effect of external pH on NupC- and rCNT1-mediated uridine influx. Uptake of [3 H]uridine in oocytes injected with NupC (a) or rCNT1 (b) RNA transcripts (solid bars) or water alone (open bars) was measured in transport medium containing 100 mM NaCl at pH 5.5, 6.5, 7.5 or 8.5 and uridine concentrations of 1 μ M (20°C, 10 min flux) and 10 μ M (20°C, 1 min flux) for NupC and rCNT1, respectively. *Insert*, time courses of uridine uptake (1 μ M, 20°C) in NaCl transport medium at pH 5.5 by oocytes injected with NupC RNA transcripts (solid circles) or water (open circles) and incubated for 5 days at 18°C in MBM. Each value represents the mean \pm SE of results obtained with 10–12 oocytes.

to uridine. For hCNT1 and rCNT1, in contrast, fluxes of adenosine are 1–2 orders of magnitude lower than for uridine (Yao *et al.* 1996a, Ritzel *et al.* 1997). There was no significant mediated uptake of uracil or hypoxanthine, establishing NupC as a nucleoside-specific transporter.

Nucleoside drug transport by recombinant NupC

Previously, *Xenopus* expression has been used to establish that human and rodent CNTs, in common with the hagfish CNT3 orthologue hCNT, accept anti-viral dideoxynucleosides as permeants (Huang *et al.* 1994, Yao *et al.* 1996b, 2002, Ritzel *et al.* 1997, 1998, 2001). hCNT1 transports AZT and ddC (but not ddl), hCNT2 transports only ddl and hCNT3 transports AZT, ddC and ddl. Similarly, the clinically im-

portant anti-cancer deoxycytidine analogue, gemcitabine, is a permeant of hCNT1 and hCNT3, but not of hCNT2 (Mackey *et al.* 1999). As shown in the radiolabelled drug uptake studies presented in Figure 3(b) (1 μ M, pH 5.5, 10 min flux), NupC also accepted pyrimidine nucleoside analogues as permeants. The magnitudes of the fluxes for 1 μ M AZT and ddC were smaller than that for uridine, but similar to those found previously for human CNTs. NupC-mediated uptake of gemcitabine was intermediate between uridine and AZT/ddC. Consistent with the modest inosine transport by NupC (Figure 3(a)), ddl also showed significantly greater influx in NupC-producing oocytes than in control water-injected oocytes (0.014 ± 0.001 vs 0.004 ± 0.001 pmol/oocyte.10 min $^{-1}$ in Figure 3(b)), suggesting a small amount of NupC-mediated ddl transport.

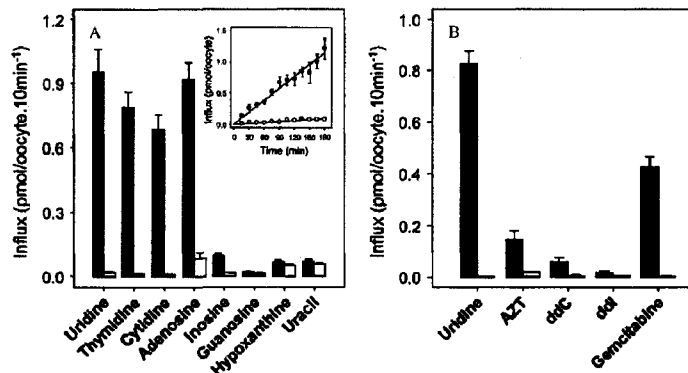


Figure 3. Substrate selectivity and drug transport by NupC. (a) Influx of physiological nucleosides and nucleobases (1 μ M, 20°C, 10 min) was measured in NaCl transport medium at pH 5.5 in oocytes previously injected with NupC RNA transcripts (solid bars) or water alone (open bars). *Insert*, time courses of uridine uptake (1 μ M, 20°C) in NaCl transport medium at pH 5.5 by oocytes injected with NupC RNA transcripts (solid circles) or water (open circles). (b) Fluxes of uridine and nucleoside drugs (AZT, ddC, ddl, gemcitabine) (1 μ M, 20°C, 10 min) were measured in NaCl transport medium at pH 5.5 in oocytes injected with NupC RNA transcripts (solid bars) or water alone (open bars). Each value represents the mean \pm SE of results obtained with 10–12 oocytes.

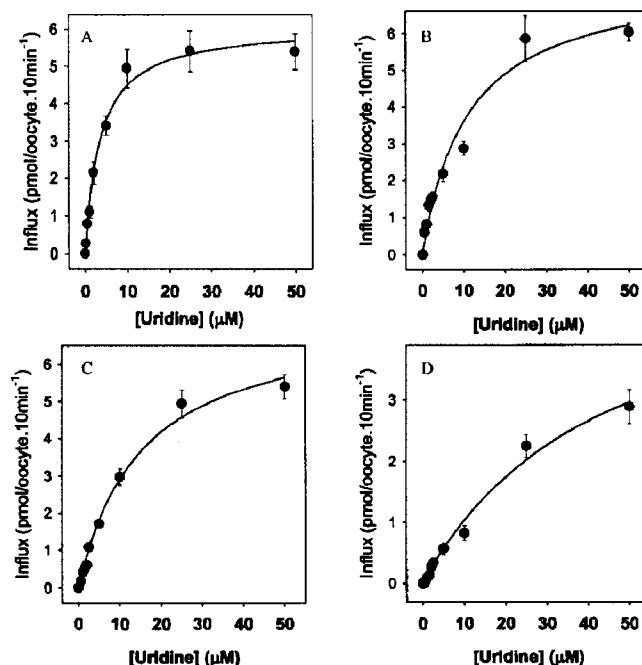


Figure 4. Effect of external pH on the concentration dependence of NupC-mediated uridine influx. Initial rates of nucleoside uptake (10-min fluxes, 20°C) in oocytes injected with NupC RNA transcripts or water alone were measured in transport medium containing 100 mM NaCl at pH 5.5 (a), 6.5 (b), 7.5 (c) and 8.5 (d). Values represent influx of NupC-injected oocytes minus the corresponding influx in water-injected cells. Kinetic parameters from these data are presented in Table 1.

Kinetic properties

Figures 4(a) and 5(a–d) show representative concentration dependence curves for NupC-mediated transport of uridine, adenosine, AZT, ddC and gemcitabine at pH 5.5 (10 min fluxes). Kinetic parameters derived from the data are summarized in Table 1, together with corresponding apparent K_m and V_{max} values for recombinant hCNT1 and rCNT1. To facilitate comparisons between transporters, V_{max} values are presented as pmol/oocyte.min⁻¹. NupC apparent K_m values varied between 1.6–130 μ M (adenosine, uridine, gemcitabine \ll AZT, ddC) and, for physiological nucleosides, were in the same range as values for total uridine and cytidine transport measured in *E. coli* containing multiple NT activities (Mygind and Munch-Petersen 1975, Munch-Petersen and Mygind 1983). In general, NupC apparent K_m values were lower than for hCNT1 and rCNT1, the bacterial and mammalian proteins showing similar relative apparent affinities for the different substrates tested. Apparent V_{max} values for the different NupC permeants differed by a maximum of 3.6-fold, while $V_{max}:K_m$ ratios, a measure of transport efficiency, were greatest for adenosine and uridine, intermediate for gemcitabine, and lowest for AZT and ddC (Table 1). Corresponding $V_{max}:K_m$ ratios for hCNT1 and rCNT1 were uridine > gemcitabine > AZT, ddC > adenosine, reflecting the relatively low V_{max} of adenosine transport by the mammalian proteins. Possible differences in cell surface

expression at the oocyte plasma membrane may contribute to the overall lower transport activity of NupC relative to hCNT1 and rCNT1.

To explore the order of H⁺ and nucleoside binding to the transporter, the concentration dependence of uridine transport (10 min flux) was determined by NupC as a function of external pH (Figure 4(a–d)). Apparent K_m values (μ M) increased 12-fold over the pH range studied (pH 5.5–8.5), while the uridine V_{max} was relatively unchanged (Table 1). These results are consistent with the 1 μ M flux data in Figure 2(a) and suggest a sequential model of transport in which H⁺ binds to the transporter first, increasing the apparent affinity of the protein for nucleoside, which then binds second.

Discussion

Nucleoside drugs are an integral part of chemotherapeutic strategies in the treatment of patients with viral or neoplastic diseases, where infection from bacteria in immunocompromized individuals is a major concern. Published studies of the anti-bacterial actions of anti-viral and anti-cancer nucleoside drugs include the finding that AZT and other anti-HIV nucleoside drugs induce DNA repair responses in *E. coli* (Mamber *et al.* 1990) and the demonstration that AZT has

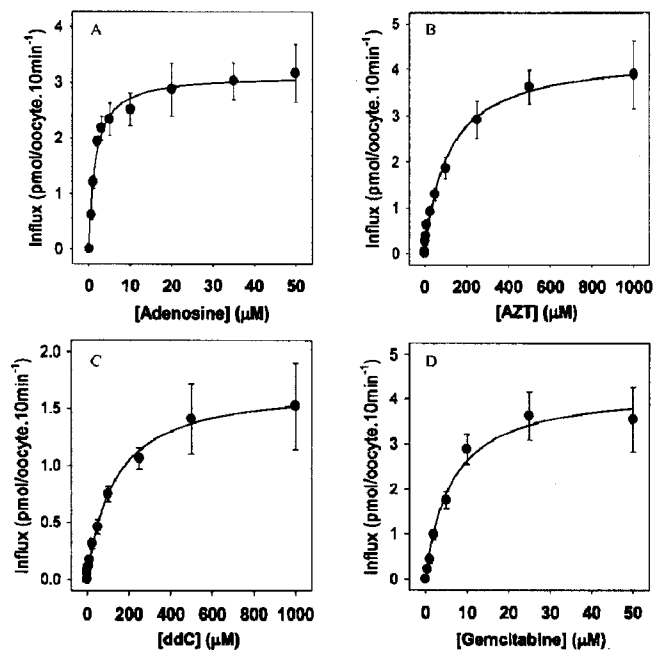


Figure 5. Kinetics of adenosine and nucleoside drug transport by recombinant NupC. (a–d) Initial rates of adenosine and nucleoside drug uptake (10-min fluxes, 20°C) in oocytes injected with NupC RNA transcripts or water alone were measured in transport medium containing 100 mM NaCl at pH 5.5. Values represent influx of NupC-injected oocytes minus the corresponding influx in water-injected cells. Kinetic parameters from these data are presented in Table 1.

anti-bacterial activity against members of the Enterobacteriaceae family (Monno *et al.*, 1997). 5-Azacytidine used in the treatment of myelogenous leukaemia also has antibiotic activity (Friedman 1982). Central to the anti-bacterial efficacy

of such compounds is transportability across the bacterial plasma (inner) membrane.

Previous investigations of nucleoside transport in bacteria have focused primarily on *E. coli*. At least three concen-

Table 1. Kinetic parameters of uridine, adenosine, AZT, ddC and gemcitabine influx mediated by *E. coli* NupC and mammalian CNT1 transport proteins

Nucleoside transporter	Substrate	pH	Apparent K_m (μM)	V_{max} (pmol/oocyte.min ⁻¹)	Ratio V_{max}/K_m	Reference
NupC ^a	Uridine	5.5	3.6±0.5	0.61±0.03 ^c	0.18	
	Uridine	6.5	10±3	0.75±0.08 ^c		
	Uridine	7.5	15±2	0.74±0.04 ^c		
	Uridine	8.5	44±10	0.56±0.08 ^c		
hCNT1	Uridine	7.5	45±16	26±2	0.58	Ritzel <i>et al.</i> (1997)
	Uridine	7.5	37±7	21±1	0.57	Huang <i>et al.</i> (1994)
NupC ^b	Adenosine	5.5	1.6±0.2	0.31±0.01 ^c	0.19	Yao <i>et al.</i> (1996a)
	Adenosine	7.5	26±7	0.07±0.01	0.0027	
rCNT1	AZT	5.5	112±15	0.43±0.02 ^c	0.0038	Yao <i>et al.</i> (1996b)
	AZT	7.5	549±98	26±7	0.048	
NupC ^b	ddC	5.5	130±13	0.17±0.01 ^c	0.0013	Yao <i>et al.</i> (1996b)
	ddC	7.5	503±35	20±5	0.039	
NupC ^b	Gemcitabine	5.5	6.3±1.1	0.43±0.02 ^c	0.068	Mackey <i>et al.</i> (1999)
	Gemcitabine	7.5	24±12	5.8±0.4	0.24	

^aFrom Figure 4.

^bFrom Figure 5.

^cConverted to pmol/oocyte.min⁻¹.

trative nucleoside transport systems have been identified, mediated by the NT proteins NupC, NupG and XapB (Komatsu and Tanaka 1972, Munch-Petersen and Mygind 1983, Norholm and Dandanell 2001). Only NupC has homologues in humans and other mammals. The functional characteristics of these bacterial transport proteins are uncertain and little is known about their transport of anti-viral and anti-neoplastic nucleoside drugs. BLAST searches of bacterial genome databases using *E. coli* NupC sequence as the search template reveal ~40 putative NupC and NupC-related CNT family members in bacteria. Most are found in Gram-negative bacteria, but examples also occur in Gram-positive species (e.g. *Bacillus* spp and *Staphylococcus* spp). This prevalence of CNT gene sequences in bacteria suggests that they fulfil important physiological functions and provides a potential route of cellular uptake for nucleoside drugs in a wide variety of different bacterial organisms. In *E. coli*, micro-array data suggest that NupC and NupG are the predominant NTs expressed under both anaerobic and aerobic conditions (Weiner, J. H., unpublished work).

The goal of the present study was to investigate nucleoside and nucleoside drug transport by *E. coli* NupC. Recombinant NupC was produced in *Xenopus* oocytes to avoid the problems inherent in studying native NupC against a background of other endogenous *E. coli* nucleoside transport activities and to permit functional comparisons with recombinant human and other mammalian CNT proteins produced in the same membrane environment. Using the *Xenopus* plasmid expression vector pGEM-HE incorporating 5'- and 3'-untranslated sequences from a *Xenopus* β -globin gene, the study represents only the second successful production of a functional bacterial membrane transport protein in *Xenopus* oocytes, the other being the *Vibrio parahaemolyticus* Na⁺/galactose cotransporter vSGLT (Leung *et al.* 2002). Bacterial channel proteins that have been expressed in *Xenopus* oocytes include the LctB K⁺ channel from *Bacillus stearothermophilus* (Wolters *et al.* 1999), the Urel H⁺-gated urea channel from *Helicobacter pylori* (Weeks *et al.* 2000) and members of the MIP membrane channel family (Hohmann *et al.* 2000).

E. coli NupC and human and rat CNT1 reportedly differ in their cation preference (H⁺ for NupC, Na⁺ for CNT1). The Na⁺-dependence of recombinant hCNT1 and rCNT1 was established by radioisotope (Huang *et al.* 1994, Ritzel *et al.* 1997) and electrophysiological studies (Mackey *et al.* 1999, Dresser *et al.* 2000, Lostao *et al.* 2000, Yao *et al.* 2000) in *Xenopus* oocytes. The apparent H⁺-dependence of NupC is based upon *E. coli* membrane vesicle studies in Na⁺-free medium using an artificial electron donor (phenazine methosulphate+ascorbate) (Munch-Petersen *et al.* 1979). Although mammalian CNTs function as Na⁺-coupled nucleoside transporters, recent radioisotope and electrophysiological studies in *Xenopus* oocytes have found that H⁺ and Li⁺ can substitute for Na⁺ in CNT3, but not for CNT1, CNT2 or hagfish hCNT (Yao *et al.* 2002).¹ In contrast, Na⁺ replacement and pH dependence radioisotope flux experiments suggest that *C. albicans* CaCNT (Loewen *et al.* 2003)

and *C. elegans* CeCNT3 (Xiao *et al.* 2001) are exclusively H⁺-dependent. In the case of CaCNT, this has been confirmed by electrophysiology (Loewen *et al.* 2003). The experiments reported here suggest that NupC is also exclusively H⁺-dependent, with H⁺ binding to the transporter first, followed by nucleoside. A corresponding ordered binding mechanism has been found for recombinant hCNT1 (Smith, K. M., Ng, A. M. L., Yao, S. Y. M., Labedz, K., Cass, C. E., Baldwin, S. A., Karpinski, E. and Young, J. D., unpublished work) and for CNT1- and CNT2-type functional activity in bovine renal brush-border membrane vesicles (Williams and Jarvis 1991).

By producing recombinant NupC in *Xenopus* oocytes, one was also able to investigate NupC permeant specificity and demonstrate that NupC transports clinically important antiviral and anti-cancer nucleoside drugs. Previously, one has identified two adjacent pairs of residues (Ser³¹⁹/Gln³²⁰ and Ser³⁵³/Leu³⁵⁴) in the TM 7-9 region of hCNT1 that, when mutated together to the corresponding residues in hCNT2 (Gly³¹³/Met³¹⁴ and Thr³⁴⁷/Val³⁴⁸), converted hCNT1 (*cif*-type) into a transporter with *cif*-type functional characteristics (Loewen *et al.* 1999). An intermediate broad specificity *cib*-like transport activity was produced by mutation of the two TM 7 residues alone. The amino acid residues of NupC at these four positions are Gly¹⁴⁶/Gln¹⁴⁷ in TM 4 and Ser¹⁸⁰/Ile¹⁸¹ in TM 5 (equivalent to TMs 7 and 8 of mammalian CNTs) and predict a substrate specificity intermediate between hCNT1 and hCNT2. While NupC is largely pyrimidine nucleoside-selective, the experiments demonstrate that NupC efficiently transports adenosine. Also, NupC transported inosine at a rate ~ 10% that of uridine, an interaction not observed with hCNT1 or rCNT1 (Huang *et al.* 1994, Ritzel *et al.* 1997). The finding that inosine is a modest NupC permeant is supported by experiments showing that *E. coli* transformed with multiple copies of *nupC*-containing plasmid grow on restricted media containing inosine, whereas control cells, which carry only a single copy of *nupC*, do not (Norholm and Dandanell 2001). Relative to CNT1, therefore, NupC has an enhanced capability to transport adenosine and inosine. However, the weak amino acid sequence conservation between TMs 4 and 5 of NupC and TMs 7 and 8 of hCNT1/2 (19% average sequence identity between NupC and hCNT1/2 vs 76% average sequence identity between hCNT1 and hCNT2) suggests that additional, as yet unidentified pore-lining residues are likely to contribute to NupC nucleoside translocation and/or permeant recognition and binding.

In parallel with the selectivity of NupC for physiological pyrimidine nucleosides, adenosine and inosine, recombinant NupC effectively transported gemcitabine, a pyrimidine nucleoside drug widely used in the therapy of solid tumours. NupC also exhibited the capacity to transport anti-viral dideoxynucleoside drugs (AZT, ddC > ddI). Like mammalian CNTs, therefore, NupC is relatively tolerant of substitutions at the 2' and 3' positions of the nucleoside sugar moiety. For both physiological nucleosides and nucleoside drugs, NupC exhibited greater apparent substrate affinities than human or rat CNT1. This kinetic difference also applies to other mammalian CNT (and ENT) proteins, providing the bacterial protein with a potential physiological advantage, but phar-

¹Unpublished data.

macological disadvantage, when competing for nutrients and drugs with host nucleoside transport processes. In the intestinal tract, where enteric bacteria such as *E. coli* normally reside, competition for nucleosides and nucleoside drugs will occur with CNTs present in the intestinal epithelium brush border membrane (Cheeseman *et al.* 2000, Valdés *et al.* 2000, Hamilton *et al.* 2001, Ngo *et al.* 2001). Anti-viral dideoxynucleoside drugs are administered orally and will achieve luminal concentrations in excess of the apparent K_m values reported here for NupC-mediated transport of AZT and ddC. This would imply that enteric micro-organisms are likely to influence the effectiveness of nucleoside drug therapy of host cells, especially intestinal targets, via sequestration of the available drug, but also that nucleoside analogues are likely to have a disruptive influence on the native intestinal microflora of the host. The lower V_{max} values for NupC in Table 1 relative to human and rat CNT1 may reflect differences in oocyte plasma membrane abundance rather than intrinsic differences in transporter catalytic activity.

In summary, this report establishes the utility of the NupC-pGEM-HE/oocyte system as a tool to further understanding of the physiological and pharmacological roles of concentrative NTs in bacteria. The results also demonstrated NupC-mediated transport of anti-viral and anti-neoplastic nucleoside drugs. By facilitating the intracellular accumulation of cytotoxic nucleoside drugs, NupC may contribute to the anti-bacterial actions of these compounds.

Experimental procedures

Molecular cloning of NupC DNA

PCR was performed on *E. coli* HB101 chromosomal DNA using Q1 (5'-ATATTCTAGAAAGGAGAAATAATATGGACCGCGTCTTC-3') as the sense primer and Q2 (5'-ATATAAGCTTTTACAGCACAGTGCTG-3') as the anti-sense primer. Q1 and Q2 corresponded to positions (underlined) 267-282 (Q1) and 1453-1469 (Q2) of the *nupC* gene (Craig *et al.* 1994) and incorporated 5' *Xba*I (Q1) and *Hind*III (Q2) restriction sites (double-underlined). The reaction mixture (100 μ l) contained 10 mM Tris-HCl (pH 8.0), 50 mM KCl, 1.5 mM MgCl₂, 0.01% (w/v) gelatin, 1 μ g HB101 chromosomal DNA, 100 pmol of each primer and 2.5 units of *Taq* polymerase. Amplification was accomplished by incubation at 94°C for 1 min, 47°C for 1.5 min and 72°C for 1.5 min (RoboCycler™40 temperature cycler, Stratagene, La Jolla, CA). After 25 cycles, the reaction mixture was separated on a 1% (w/v) non-denaturing agarose gel (Gibco/BRL, Gaithersburg, MD) containing 0.25 μ g/ml ethidium bromide. The resulting 1203 bp product was ligated into pGEM-3Z (Promega, Madison, WI) and sub-cloned into the enhanced *Xenopus* expression vector pGEM-HE (pNUPC-HE) (Liman *et al.* 1992). By providing additional 5'- and 3'-untranslated regions from a *Xenopus* β -globin gene, the pGEM-HE construct gave ~ 20-fold greater functional activity than pGEM-3Z and was used in subsequent transport characterization of NupC. The 1203 bp insert of pNUPC-HE was sequenced in both directions by *Taq* dideoxy-terminator cycle sequencing using an automated model 373A DNA sequencer (Applied Biosystems, Foster City, CA).

Functional production of recombinant NupC in *Xenopus* oocytes

NupC plasmid DNA was digested with *Nhe*I and transcribed with the T7 RNA polymerase in the presence of 5' m⁷GpppG cap using the

mMessage mMachine™ (Ambion, Austin, TX) *in vitro* transcription system (Ambion, Austin, TX). Healthy defolliculated stage VI *Xenopus* oocytes were microinjected with 40 nl of NupC RNA transcript (1 ng/ml) or 40 nl of water alone and incubated at 18°C in modified Barth's medium at 18°C for 5 days prior to the assay of nucleoside and nucleoside drug transport activity. A 5-day incubation period was used instead of the usual 3 day period (Huang *et al.* 1994) because preliminary studies had established greater activity at 5 days.

NupC radioisotope flux studies

Transport was traced using the appropriate ³H-labelled nucleoside or nucleoside drug (Moravek Biochemicals, Brea, CA or Amersham Biosciences, Baie d'Urfe, QC) at a concentration of 2 μ Ci/ml. [³H]Gemcitabine (2'-deoxy-2',2'-difluorocytidine) was a gift from Eli Lilly Inc. (Indianapolis, IN). Flux measurements were performed at room temperature (20°C) as described previously (Huang *et al.* 1994, Ritzel *et al.* 1997) on groups of 12 oocytes in 200 μ l of transport medium containing either 100 mM NaCl or 100 mM choline chloride and 2 mM KCl, 1 mM CaCl₂, 1 mM MgCl₂ and 10 mM HEPES (pH 5.5, 6.5, 7.5 or 8.5). Unless otherwise specified, the permeant concentration was 1 μ M. To maximize potential transmembrane H⁺-gradients, cells were first washed into pH 7.5 NaCl or choline chloride transport buffer and only exposed to either high (pH 8.5) or low pH medium (pH 5.5 or 6.5) immediately prior to the assay of transport activity. In competition experiments, non-radioactive nucleosides (200 μ M) were added to oocytes simultaneously with [³H]Juridine. At the end of the incubation, extracellular radioactivity was removed by six rapid washes in the appropriate ice-cold transport buffer. Individual oocytes were dissolved in 0.5 ml of 5% (w/v) sodium dodecyl sulphate for quantitation of oocyte-associated ³H by liquid scintillation counting (LS 6000IC, Beckman Canada Inc., Mississauga, ONT). The flux values shown are the means \pm S.E. of 10–12 oocytes and each experiment was performed at least twice on different batches of cells. Kinetic (K_m and V_{max}) parameters \pm SE were determined using ENZFITTER software (Elsevier-Biosoft, Cambridge, UK). It has been established previously that oocytes lack endogenous nucleoside transport processes (Huang *et al.* 1994).

Acknowledgements

This research is funded by the National Cancer Institute of Canada, the Natural Sciences and Engineering Research Council of Canada, the Medical Research Council (UK), the Alberta Heritage Foundation for Medical Research (AHFMR) and the Canadian Foundation for AIDS Research. S.K.L., M.D.S. and N.N.M. were funded by graduate (S.K.L., M.D.S.) and summer studentships (N.N.M.) from the AHFMR. J.D.Y. is a Heritage Medical Scientist of the AHFMR. C.E.C. holds a Canada Research Chair in Oncology at the University of Alberta.

References

- Baldwin, S. A., Mackey, J. R., Cass, C. E. and Young, J. D., 1999, Nucleoside transporters: molecular biology and implications for therapeutic development. *Molecular Medicine Today*, **5**, 216–224.
- Che, M., Ortiz, D. F. and Arias, I. M., 1995, Primary structure and functional expression of a cDNA encoding the bile canalicular, purine-specific Na⁺-nucleoside cotransporter. *Journal of Biological Chemistry*, **270**, 13596–13599.
- Cheeseman, C. I., Mackey, J. R., Cass, C. E., Baldwin, S. A. and Young, J. D., 2000, Molecular mechanism of nucleoside and nucleoside drug transport. Gastrointestinal transport. In *Current Topics in Membranes*, Vol 50, K. E. Barrett and M. Donowitz, eds (San Diego: Academic Press), pp. 330–379.
- Craig, J. E., Zhang, Y. and Gallagher, M. P., 1994, Cloning of the *nupC* gene of *Escherichia coli* encoding a nucleoside transport

- system, and identification of an adjacent insertion element, IS 186. *Molecular Microbiology*, **11**, 1159–1168.
- Dresser, M. J., Gerstl, K. M., Gray, A. T., Loo, D. D. and Giacomini, K. M., 2000, Electrophysiological analysis of the substrate selectivity of a sodium-coupled nucleoside transporter (rCNT1) expressed in *Xenopus laevis* oocytes. *Drug Metabolism and Disposition*, **28**, 1135–1140.
- Friedman, S., 1982, Bactericidal effect of 5-azacytidine on *Escherichia coli* carrying *EcoRII* restriction-modification enzymes. *Journal of Bacteriology*, **151**, 262–268.
- Hamilton, S. R., Yao, S. Y. M., Ingram, J. C., Hadden, D. A., Ritzel, M. W., Gallagher, M. P., Henderson, P. J., Cass, C. E., Young, J. D. and Baldwin, S. A., 2001, Subcellular distribution and membrane topology of the mammalian concentrative Na⁺-nucleoside cotransporter rCNT1. *Journal of Biological Chemistry*, **276**, 27981–27988.
- Hohmann, I., Bill, R. M., Kayingo, I. and Prior, B. A., 2000, Microbial MIP channels. *Trends in Microbiology*, **8**, 33–38.
- Huang, Q. Q., Yao, S. Y. M., Ritzel, M. W. L., Paterson, A. R. P., Cass, C. E. and Young, J. D., 1994, Cloning and functional expression of a complementary DNA encoding a mammalian nucleoside transport protein. *Journal of Biological Chemistry*, **269**, 17757–17760.
- Karp, P. D., Riley, M., Saier, M., Paulsen, I. T., Collado-Vides, J., Paley, S. M., Pellegrini-Toole, A., Bonavides, C. and Gama-Castro, S., 2002, The EcoCyc Database. *Nucleic Acids Research*, **30**, 56–58.
- Kirchman, D., Ducklow, H. and Mitchell, R., 1982, Estimates of bacterial growth from changes in uptake rates and biomass. *Applied and Environmental Microbiology*, **44**, 1296–1307.
- Komatsu, Y. and Tanaka, K., 1972, A showdomycin-resistant mutant of *Escherichia coli* K-12 with altered nucleoside transport character. *Biochimica et Biophysica Acta*, **34**, 891–899.
- Kubitschek, H. E., 1968, Constancy of uptake during the cell cycle in *Escherichia coli*. *Biophysical Journal*, **8**, 1401–1412.
- Leung, D. W., Turk, E., Kim, O. and Wright, E. M., 2002, Functional expression of the *Vibrio parahaemolyticus* Na⁺/galactose (vSGLT) cotransporter in *Xenopus laevis* oocytes. *Journal of Membrane Biology*, **187**, 65–70.
- Liman, E. R., Tytgat, J. and Hess, P., 1992, Subunit stoichiometry of a mammalian K⁺ channel determined by construction of multimeric cDNAs. *Neuron*, **9**, 861–871.
- Loewen, S. K., Ng, A. M. L., Mohabir, N. N., Baldwin, S. A., Cass, C. E. and Young, J. D., 2003, Functional characterization of a H⁺/nucleoside cotransporter (CaCNT) from *Candida albicans*, the first fungal homolog of mammalian/bacterial concentrative nucleoside transporters. *Yeast*, **20**, 661–675.
- Loewen, S. K., Ng, A. M. L., Yao, S. Y. M., Cass, C. E., Baldwin, S. A. and Young, J. D., 1999, Identification of amino acid residues responsible for the pyrimidine and purine nucleoside specificities of human concentrative Na⁺ nucleoside cotransporters hCNT1 and hCNT2. *Journal of Biological Chemistry*, **274**, 24475–24484.
- Lostao, M. P., Mata, J. F., Larrayoz, I. M., Inzillo, S. M., Casado, F. J. and Pastor-Anglada, M., 2000, Electrogenic uptake of nucleosides and nucleoside-derived drugs by the human nucleoside transporter 1 (hCNT1) expressed in *Xenopus laevis* oocytes. *FEBS Letter*, **481**, 137–140.
- Mackey, J. R., Yao, S. Y. M., Smith, K. M., Karpinski, E., Cass, C. E. and Young, J. D., 1999, Gemcitabine transport in *Xenopus* oocytes expressing recombinant plasma membrane mammalian nucleoside transporters. *Journal of the National Cancer Institute*, **21**, 1876–1881.
- Mamber, S. W., Brookshire, K. W. and Forenza, S., 1990, Induction of the SOS response in *Escherichia coli* by azidothymidine and dideoxynucleosides. *Antimicrobial Agents and Chemotherapy*, **34**, 1237–1243.
- Monno, R., Marcuccio, L., Valenza, M. A., Leone, E., Bitetto, C., Larocca, A., Maggi, P. and Quarto, M., 1997, In vitro antimicrobial properties of azidothymidine (AZT). *Acta Microbiologia et Immunologia, Hungary*, **44**, 165–171.
- Munch-Petersen, A. and Mygind, B., 1983, Metabolism of nucleotides, nucleosides and nucleobases in microorganisms. In *Transport of nucleic acid precursors*. A. Munch-Petersen, ed. (London: Academic Press), pp 259–305.
- Munch-Petersen, A., Mygind, B., Nicolaisen, A. and Pihl, N. J., 1979, Nucleoside transport in cells and membrane vesicles from *Escherichia coli* K12. *Journal of Biological Chemistry*, **254**, 3730–3737.
- Mygind, B. and Munch-Petersen, A., 1975, Transport of pyrimidine nucleosides in cells of *Escherichia coli* K12. *European Journal of Biochemistry*, **59**, 365–372.
- Ngo, L. Y., Patil, S. D. and Unadkat, J. D., 2001, Ontogenic and longitudinal activity of Na⁺-nucleoside transporters in the human intestine. *American Journal of Physiology—Gastrointestinal and Liver Physiology*, **280**, G475–G481.
- Nieweg, A. and Bremer, E., 1997, The nucleoside-specific Tsx channel from the outer membrane of *Salmonella typhimurium*, *Klebsiella pneumoniae* and *Enterobacter aerogenes*: functional characterization and DNA sequence analysis of the tsx genes. *Microbiology*, **143**, 603–615.
- Norholm, M. H. and Dandanell, G., 2001, Specificity and topology of the *Escherichia coli* xanthosine permease, a representative of the NHS subfamily of the major facilitator superfamily. *Journal of Bacteriology*, **183**, 4900–4904.
- Ritzel, M. W. L., Ng, A. M. L., Yao, S. Y. M., Graham, K., Loewen, S. K., Smith, K. M., Ritzel, R. G., Mowles, D. A., Carpenter, P., Chen, X.-Z., Karpinski, E., Hyde, R. J., Baldwin, S. A., Cass, C. E. and Young, J. D., 2001, Molecular identification and characterization of novel human and mouse concentrative Na⁺-nucleoside cotransporter proteins (hCNT3 and mCNT3) broadly selective for purine and pyrimidine nucleosides. *Journal of Biological Chemistry*, **276**, 2914–2927.
- Ritzel, M. W. L., Yao, S. Y. M., Huang, M. Y., Elliot, J. F., Cass, C. E. and Young, J. D., 1997, Molecular cloning and functional expression of cDNAs encoding a human Na⁺-nucleoside cotransporters hCNT1. *American Journal of Physiology*, **272**, C707–C714.
- Ritzel, M. W. L., Yao, S. Y. M., Ng, A. M. L., Mackey, J. R., Cass, C. E. and Young, J. D., 1998, Molecular cloning, functional expression and chromosomal localization of a cDNA encoding a human Na⁺/nucleoside cotransporter (hCNT2) selective for purine nucleosides and uridine. *Molecular Membrane Biology*, **15**, 203–211.
- Robak, T., 2001, Cladribine in the treatment of chronic lymphocytic leukemia. *Leukemia & Lymphoma*, **40**, 551–564.
- Sanders, C., Perez, E. A. and Lawrence, H. J., 1992, Opportunistic infections in patients with chronic lymphocytic leukemia following treatment with fludarabine. *American Journal of Hematology*, **39**, 314–315.
- Seeger, C., Poulsen, C. and Dandanell, G., 1995, Identification and characterization of genes (*xapA*, *xapB*, and *xapR*) involved in xanthosine catabolism in *Escherichia coli*. *Journal of Bacteriology*, **177**, 5506–5516.
- Valdés, R., Ortega, M. A., Casado, F. J., Felipe, A., Gil, A., Sanchez-Pozo, A. and Pastor-Anglada, M., 2000, Nutritional regulation of nucleoside transporter expression in rat small intestine. *Gastroenterology*, **119**, 1623–1630.
- Wang, J., Su, S. F., Dresser, M. J., Schaner, M. E., Washington, C. B. and Giacomini, K. M., 1997, Na⁺-dependent purine nucleoside transporter from human kidney: cloning and functional characterization. *American Journal of Physiology*, **273**, F1058–F1065.
- Weeks, D. L., Eskandari, S., Scott, D. R. and Sachs, G., 2000, A H⁺-gated urea channel: the link between *Helicobacter pylori* urease and gastric colonization. *Science*, **287**, 482–485.
- Westh-Hansen, S. E., Jensen, N. and Munch-Petersen, A., 1987, Studies on the sequence and structure of the *Escherichia coli* K-12 *nupG* gene, encoding a nucleoside-transport system. *European Journal of Biochemistry*, **168**, 385–391.
- Williams, T. C. and Jarvis, S. M., 1991, Multiple sodium-dependent nucleoside transport systems in bovine renal brush-border membrane vesicles. *Biochemical Journal*, **274**, 27–33.
- Wolters, M., Madeja, M., Farrell, A. M. and Pongs, O., 1999, *Bacillus stearothermophilus* IctB gene gives rise to functional K⁺ channels in *Escherichia coli* and in *Xenopus* oocytes. *Receptors Channels*, **6**, 477–491.

- Xiao, G., Wang, J., Tangen, T. and Giacomini, K. M., 2001, A novel proton-dependent nucleoside transporter, CeCNT3, from *Caenorhabditis elegans*. *Molecular Pharmacology*, **59**, 339–348.
- Yao, S. Y. M., Cass, C. E. and Young, J. D., 1996b, Transport of antiviral nucleoside analogs 3'-azido-3'-deoxythymidine and 2',3'-dideoxycytidine by a recombinant nucleoside transporter (rCNT1) expressed in *Xenopus* oocytes. *Molecular Pharmacology*, **50**, 388–393.
- Yao, S. Y. M., Cass, C. E. and Young, J. D., 2000, The *Xenopus* oocyte expression system for the cDNA cloning and characterization of plasma membrane transport proteins. In *Membrane Transport. A Practical Approach*, S. A. Baldwin, ed. (Oxford: Oxford University Press), pp 47–78.
- Yao, S. Y. M., Ng, A. M. L., Loewen, S. K., Cass, C. E., Baldwin, S. A. and Young, J. D., 2002, An ancient marine pre-vertebrate Na⁺/nucleoside cotransporter (hfCNT) from the Pacific hagfish (*Eptatretus stouti*). *American Journal of Physiology*, **283**, C155–C168.
- Yao, S. Y. M., Ng, A. M. L., Ritzel, M. W. L., Gati, W. P., Cass, C. E. and Young, J. D., 1996a, Transport of adenosine by recombinant purine- and pyrimidine-selective sodium/nucleoside cotransporters from rat jejunum expressed in *Xenopus laevis* oocytes. *Molecular Pharmacology*, **50**, 1529–1535.

Received 12 February 2003; and in revised form 24 April 2003.

Appendix 3:

Characterization of the Transport Mechanism and Permeant Binding Profile of the Uridine Permease Fui1p of *Saccharomyces cerevisiae**

* This appendix has been published.

Zhang, J., Smith, K. M., Tackaberry, T., Sun, X., Carpenter, P., Slugoski, M. D., Robins, M. J., Nielsen, L. P., Nowak, I., Baldwin, S. A., Young, J. D., and Cass, C. E. (2006) Characterization of the transport mechanism and permeant binding profile of the uridine permease Fui1p of *Saccharomyces cerevisiae*. *J. Biol. Chem.* **281**: 28210-28221.

Characterization of the Transport Mechanism and Permeant Binding Profile of the Uridine Permease Fui1p of *Saccharomyces cerevisiae**

Received for publication, May 30, 2006, and in revised form, July 17, 2006. Published, JBC Papers in Press, July 19, 2006, DOI 10.1074/jbc.M605129200

Jing Zhang^{†§¶}, Kyla M. Smith^{†||}, Tracey Tackaberry^{†§¶}, Xuejun Sun^{§¶}, Pat Carpenter^{†§¶}, Melissa D. Slugoski^{†||}, Morris J. Robins^{†¶}, Lars P. C. Nielsen^{¶¶}, Ireneusz Nowak^{¶¶}, Stephen A. Baldwin^{†¶}, James D. Young^{†¶}, and Carol E. Cass^{†§¶}

From the [†]Membrane Protein Research Group and the Departments of [§]Oncology and ^{||}Physiology, University of Alberta, and the [¶]Cross Cancer Institute, Edmonton, Alberta T6H 1Z2, Canada, the ^{¶¶}Department of Chemistry and Biochemistry, Brigham Young University, Provo, Utah 84602-5700, and the ^{††}Astbury Centre for Structural Molecular Biology, Institute for Membrane and Systems Biology, University of Leeds, Leeds LS2 9JT, United Kingdom

The uptake of Urd into the yeast *Saccharomyces cerevisiae* is mediated by Fui1p, a Urd-specific nucleoside transporter encoded by the *FUI1* gene and a member of the yeast Fur permease family, which also includes the uracil, allantoin, and thiamine permeases. When Fui1p was produced in a double-permease knock-out strain (*fur4Δfui1Δ*) of yeast, Urd uptake was stimulated at acidic pH and sensitive to the protonophore carbonyl cyanide *m*-chlorophenylhydrazone. Electrophysiological analysis of recombinant Fui1p produced in *Xenopus* oocytes demonstrated that Fui1p-mediated Urd uptake was dependent on proton cotransport with a 1:1 stoichiometry. Mutagenesis analysis of three charged amino acids (Glu²⁵⁹, Lys²⁸⁸, and Asp⁴⁷⁴ in putative transmembrane segments 3, 4, and 7, respectively) revealed that only Lys²⁸⁸ was required for maintaining high Urd transport efficiency. Analysis of binding energies between Fui1p and different Urd analogs indicated that Fui1p interacted with C(3')-OH, C(2')-OH, C(5)-H, and N(3)-H of Urd. Fui1p-mediated transport of Urd was inhibited by analogs with modifications at C-5', but was not inhibited significantly by analogs with modifications at C-3', C-5, and N-3 or inversions of configuration at C-2' and C-3'. This characterization of Fui1p contributes to the emerging knowledge of the structure and function of the Fur family of permeases, including the Fui1p orthologs of pathogenic fungi.

Nucleoside transporters are integral membrane proteins that mediate the uptake and release of naturally occurring nucleosides and cytotoxic nucleoside analogs (1–4). Mammalian nucleoside transporters are classified into two structurally unrelated protein families, the concentrative (CNTs)⁶ and equilibrative (ENTs) nucleoside transporters (1, 2, 5). Nucleoside permeation into *Saccharomyces cerevisiae* is mediated by Fui1p, a permease with high specificity for Urd and with no sequence similarities to any of the mammalian nucleoside transporters (6, 7). *S. cerevisiae* cells also salvage nucleobases through Fur4p (uracil permease) and Fyc2p (purine-cytosine permease), but they appear to lack the capacity to transport thymidine and purine nucleosides across plasma membranes (8). Although considerable information is available for the Fur4p and Fyc2p nucleobase transporters of *S. cerevisiae* (9–17), relatively little is known about Fui1p.

Fui1p belongs to the uracil/allantoin permease family (Fur family) of yeast, which also includes Fur4p, Thi10p (thiamine permease), and Dal4p (allantoin permease). Fui1p (629 amino acids, 72 kDa) shares high amino acid identity (50–60%) with the other family members. The predicated topology of Fur4p consists of 10 transmembrane (TM) segments with long N- and C-terminal tails, which have been shown to be intracellular (17). It is believed that the two-dimensional Fur4p structural model could be extended to all members of the yeast uracil/allantoin permease family (14). The similarity of amino acid sequences is greatest in the putative TM segments of the four proteins. Based on the high sequence identity of Fur4p and Fui1p, we hypothesized that these two transporters might have similar transport mechanisms and that Fui1p might operate as an electrogenic proton/permeant symporter. Charged amino acid residues in the membrane-spanning regions of transporters are known to play important roles in permeant binding (18, 19), proton coupling (20), transporter stability and activity (21), and plasma membrane targeting (22). Although Fur4p contains three charged amino acid residues in TM regions, only the one located in TM segment 4 (Lys²⁷²), which is highly conserved in

This work was supported in part by Canadian Cancer Society grants from the National Cancer Institute of Canada (to C. E. C. and J. D. Y.), the Canadian Institutes of Health Research (to C. E. C. and J. D. Y.), and pharmaceutical company unrestricted gift funds (to M. J. R.). The costs of publication of this article were defrayed in part by the payment of page charges. This article must therefore be hereby marked "advertisement" in accordance with 18 U.S.C. Section 1734 solely to indicate this fact.

¹ Supported by studentships from the Canadian Institutes of Health Research and the Alberta Heritage Foundation for Medical Research and Department of Oncology Endowed Studentship.

² J. Rex Goates Professor of Chemistry.

³ Supported by a Brigham Young University undergraduate research fellowship.

⁴ Heritage Scientist of the Alberta Heritage Foundation for Medical Research.

⁵ Canada Research Chair in Oncology. To whom correspondence should be addressed: Dept. of Oncology, Cross Cancer Inst., 11540 University Ave., Edmonton, Alberta T6H 1Z2, Canada. Tel: 780-432-8320; Fax: 780-432-8425; E-mail: carol.cass@cancerboard.ab.ca.

⁶ The abbreviations used are: CNTs, concentrative nucleoside transporters; ENTs, equilibrative nucleoside transporters; TM, transmembrane; h, human; ORF, open reading frame; GFP, green fluorescent protein; CMM, complete minimal medium; FUr, 5-fluorouridine; ChCl, choline chloride; MES, 4-morpholineethanesulfonic acid; CCCP, carbonyl cyanide *m*-chlorophenylhydrazone; MeUrd, methyluridine; ddUrd, dideoxyuridine.

Uridine Permease of Yeast

the uracil/allantoin permease family, was identified as a critical residue involved in uracil binding and translocation (14). The functional importance of the corresponding lysine residue of Fui1p (Lys²⁸⁸) in TM segment 4 and of the only two other charged TM residues (in TM segments 3 and 7) was investigated in this study.

In vivo labeling of DNA using nucleosides and nucleoside analogs such as thymidine and 5-bromo-2'-dUrd has long been a cornerstone of replication studies. *S. cerevisiae* has been used extensively as a model organism in defining the genetic elements required for DNA replication. In the absence of the introduction of heterogeneous nucleoside transporters (e.g. human (h) ENT1) (23), Fui1p is the dominant route that allows entry of nucleosides and nucleoside analogs into *S. cerevisiae*. Among the nucleoside transporters identified so far from bacteria to higher eukaryotes, only *S. cerevisiae* Fui1p mediates transport of Urd but not that of other naturally occurring pyrimidine and purine nucleosides, implying a specialized function for Urd in *S. cerevisiae*. The abundance of Fur4p is determined by extracellular uracil availability by regulation of the efficiency of its ubiquitylation (24). Fui1p has also been shown to be sorted for early vacuolar degradation in cells exposed to toxic levels of Urd, indicating that extracellular Urd controls Fui1p trafficking and prevents harmful Urd uptake that results in a decrease in growth rate (24). Knowledge of the transport mechanism and permeant selectivities of Fui1p will contribute to an understanding of its physiological significance in the budding yeast *S. cerevisiae*, one of the most important model organisms for DNA replication and repair studies.

Fui1p orthologs of *Candida albicans* and *Candida glabrata* with high sequence identities to Fui1p of *S. cerevisiae* (>70%) were revealed from contigs (groups of overlapping clones) of the Stanford *C. albicans* genome sequence data bank and the assembled open reading frame (ORF) data bank of the *C. glabrata* genome (GenBankTM G1:50287475) (25), respectively. One of the most commonly encountered human pathogens, *C. albicans* causes a wide variety of infections, ranging from superficial disorders in generally healthy individuals to invasive, rapidly fatal systemic infections in individuals with impaired immunity. *C. glabrata* has emerged as the second causative agent of human candidiasis worldwide and is more resistant to drug therapy than *C. albicans*. Few classes of drugs are effective against these fungal infections, and drug efficacy is limited by toxicity and side effects. Nucleoside antibiotics such as the nikkomycins and neopolyoxins have been considered as candidate inhibitors of opportunistic candidal infections in AIDS and organ transplant patients (26). Efforts to develop more effective nucleoside analogs are under way (27).

We report here the functional characterization of Fui1p in a double-permease knock-out yeast strain (*fur4Δfui1Δ*) that enabled us to analyze Fui1p-mediated Urd uptake in an otherwise nucleoside transport-free background. Fui1p transported Urd into yeast with high affinity and high capacity in a proton-dependent manner. The roles of three charged amino acid residues (Glu²⁵⁹, Lys²⁸⁸, and Asp⁴⁷⁹) in putative TM segments 3, 4, and 7, as well as the cellular location of the mutant transporters, were investigated using site-directed mutagenesis and green fluorescent protein (GFP) and c-Myc tags. Of the three charged

residues, only Lys²⁸⁸ was important for the transport capacity of Fui1p. A quantitative inhibitor sensitivity assay was used to gain an understanding of the structural regions of Urd that interact with Fui1p. Because transportability is a potential determinant of the cytotoxic efficacy of nucleoside analog drugs, knowledge of the Urd binding profile of Fui1p will guide the design of novel antifungal nucleoside analogs that may selectively target Fui1p orthologs in pathogenic fungi.

MATERIALS AND METHODS

Strains and Media—BY4742-YBR021W (*MATα, his3, leu2, lys2, ura3, fur4Δ*), which contains a disruption in *FUR4*, the gene encoding the endogenous uracil permease, was purchased from the American Type Culture Collection (Manassas, VA) and used as the parental yeast strain to generate the double-permease knock-out strain *fur4Δfui1Δ* (previously named *fui1::HIS3*) by deleting *FUI1* using the PCR-mediated one-step gene disruption method as described previously (28). Other strains were generated by transformation of the yeast-*Escherichia coli* shuttle vector pYPGE15 (29) into *fur4Δfui1Δ* using a standard lithium acetate method (30).

Yeast strains were maintained in complete minimal medium (CMM) containing 0.67% yeast nitrogen base (Difco), amino acids (as required to maintain auxotrophic selection), and 2% glucose (CMM/Glc). Agar plates contained CMM with various supplements and 2% agar (Difco). Plasmids were propagated in *E. coli* strain TOP10F⁺ (Invitrogen) and maintained in Luria broth with ampicillin (100 μg/ml).

Plasmid Construction—All oligonucleotide primers were synthesized by Invitrogen. For *S. cerevisiae* expression, the *FUI1* ORFs were amplified from vector pYSE2-FUI1 (6) by PCR methodology using primers 5'-XbaI-FUI1 (5'-CTG TCTAGA ATG CCG GTA TCT GAT TCT GGA TTC-3', with the restriction site underlined) and 3'-XhoI-FUI1 (5'-CGA CTC GAG TTA GAT ATA TCG TAT CTT TTC ATA GC-3'). For construction of c-Myc-tagged Fui1p, the c-Myc tag (CAG ATC CTC TTC TGA GAT GAG TTT TTG TTC) was introduced into primer 3'-XhoI-FUI1. For *Xenopus* oocyte expression, primers 5'-BamHI-FUI1 (5'-GTC GGA TCC ATG CCG GTA TCT GAT TCT GGA TTC-3') and 3'-XbaI-FUI1 (5'-CGA TCT AGA TTA GAT ATA TCG TAT CTT TTC ATA G-3') were used. To construct GFP-tagged Fui1p, the ORF of *FUI1* without a stop codon was first amplified using forward primer 5'-XbaI-FUI1 and a reverse primer containing (3' to 5') 21 bases with homology to *FUI1* and a unique tag sequence complementary to the first 50 nucleotides of the ORF of GFP. C-terminally GFP-tagged Fui1p was obtained by overlapping PCR using the product of the first run PCR and the pGFPuv vector (Promega, Madison, WI) as templates and 5'-XbaI-FUI1 and 3'-KpnI-GFP (5'-CTG GGT ACC CTA TTT GTA GAG CTC ATCCAT GCC) as primers. GFP-ORF was also amplified by PCR using forward primer 5'-XbaI-GFP (5'-CGT TCT AGA ATG GCC AGC AAA GGA GAA CTT-3') and reverse primer 3'-EcoRI-GFP (5'-CGT GAA TTC CTA TTT GTA GAG CTC ATCCAT GCC). The amplified ORFs were inserted into pYPGE15 (a high copy number episomal yeast vector that expresses the inserted DNA constitutively under the transcriptional control of the phosphoglycerate kinase promoter) to generate pYPFUI1, pYP-

Uridine Permease of Yeast

FUI1-GFP, and pYPGFP or into the *Xenopus* expression vector pGEM-HE to generate pGEFUI1, pYPFUI1-K288A, pYPFUI1-K288E, pYPFUI1-K288R, pYPFUI1-E259A, pYPFUI1-D474A, and pYPFUI1-E259A,D474A and the corresponding GFP- and c-Myc-tagged versions were generated using the QuikChange XL site-directed mutagenesis kit (Stratagene, La Jolla, CA). The PCRs were performed using *Pwo* polymerase (Roche Applied Science), and all constructs were verified by DNA sequencing using an ABI PRISM 310 sequence detection system (PerkinElmer Life Sciences).

Nucleoside Transport in *S. cerevisiae*—The uptake of [³H]Urd or 5-[³H]fluorouridine (FUrd; Moravsek Biochemicals Inc., Brea, CA) into logarithmically proliferating yeast cells was measured using a cell harvester as described previously (31, 32). Yeast cells containing pYPFUI1, pYPFUI1-GFP, or individual mutant transporters were grown in CMM/Glc to $A_{600} = 0.7$ – 0.9 , washed twice with fresh medium, and resuspended to $A_{600} = 4.0$. Uptake assays were performed at room temperature at pH 4.5 unless specified otherwise by adding 50- μ l portions of yeast suspensions to 50- μ l portions of twice concentrated ³H-labeled nucleoside in CMM/Glc in 96-well microtiter plates. Yeast cells were collected on filter mats using a Micro96 cell harvester (Skatron Instruments, Lier, Norway) and rapidly washed with deionized water. The individual filter circles corresponding to wells of the microtiter plates were removed from filter mats and transferred to vials for scintillation counting.

The binding of Urd and its analogs to recombinant Fui1p was assessed by measuring their abilities to inhibit inward transport of 1 μ M [³H]Urd in an “inhibitor sensitivity” assay as follows. Yeast cells producing Fui1p were incubated with 1 μ M [³H]Urd for 30 s in the absence or presence of graded concentrations of Urd or Urd analogs. The 30-s exposures to [³H]Urd were shown in time course experiments to be sufficient to provide true initial rates of uptake into yeast cells, thereby providing rates of transport across plasma membranes rather than rates of intracellular metabolism (see Fig. 1, upper panel). Each experiment was repeated at least three times. Nonspecific radioactivity was determined in the presence of 10 mM nonradioactive Urd, and these values were subtracted from total uptake values. Data were subjected to nonlinear regression analysis using GraphPad Prism software (Version 3.0; GraphPad Software, Inc., San Diego, CA) to obtain IC_{50} values (concentrations that inhibited reactions by 50%) for Urd and Urd analogs. K_i (inhibitory constant) values were determined from the Cheng-Prusoff equation (33) and the K_m values for Urd. Gibbs free energy (ΔG°) was calculated from $\Delta G^\circ = -RT \ln(K_i)$, where R is the gas constant and T is the absolute temperature. The thermodynamic stability of transporter-inhibitor complexes was quantitatively estimated from ΔG° as described (34).

Measurements of Fui1p-induced H^+ Currents and H^+ /Urd Coupling Ratios—pGEFUI1 was linearized with NheI and transcribed with T7 polymerase using the mMMESSAGE mMACHINE™ transcription system (Ambion, Inc., Austin, TX). *In vitro* synthesized transcripts were injected into isolated mature stage VI oocytes from *Xenopus laevis* as described previously (35). Mock-injected oocytes were injected with water alone. Electrophysiological studies used transport medium in which choline was substituted for sodium, *i.e.* 100 mM choline chloride

(ChCl), 2 mM KCl, 1 mM CaCl₂, 1 mM MgCl₂, and 10 mM HEPES (for pH values >6.5) or 10 mM MES (for pH values \leq 6.5). Proton dependence was tested in ChCl-containing transport medium at pH 4.5–8.5.

Urd-induced membrane currents were measured in Fui1p-producing oocytes at room temperature (20 °C) using a GeneClamp 500B oocyte clamp (Axon Instruments, Foster City, CA) in the two-electrode voltage-clamp mode as described previously (35) and interfaced to an IBM-compatible PC via a Digidata 1200A/D converter and controlled by pCLAMP software (Version 8.0; Axon Instruments). The microelectrodes were filled with 3 M KCl and had resistances that ranged from 0.5 to 2.5 M Ω megaohms. Oocytes were penetrated with the microelectrodes, and their membrane potentials were monitored for periods of 10–15 min. Oocytes were discarded when membrane potentials were unstable or more positive than -30 mV. The oocyte membrane potential was clamped at a holding potential of -50 mV, and Urd was added in the appropriate transport medium. Current signals were filtered at 20 Hz (four-pole Bessel filter) and sampled at intervals of 20 ms. For data presentation, the signals were further filtered at 0.5 Hz by the pCLAMP program suite.

The H^+ /Urd coupling ratio for Fui1p was determined by simultaneously measuring H^+ currents and uptake of [¹⁴C]Urd (200 μ M, 1 μ Ci/ml; Amersham Biosciences) under voltage-clamp conditions. Individual Fui1p-producing oocytes were placed in a perfusion chamber and voltage-clamped at a holding potential of -50 mV in sodium-free (100 mM ChCl) and nucleoside-free medium (pH 5.5) for a 10-min period to monitor base-line currents. When the base line was stable, the nucleoside-free medium was exchanged with medium of the same composition containing [¹⁴C]Urd. Current was measured for 2 min, and uptake was terminated by washing the oocyte with nucleoside-free medium until the current returned to the base line. The oocyte was then transferred to a scintillation vial and solubilized with 1% (w/v) SDS for quantitation of oocyte-associated radioactivity. Urd-induced current was calculated as the difference between base-line current and total inward current. The total charge translocated into the oocyte during the uptake period was calculated from the current-time integral and correlated with the measured radiolabeled flux for each oocyte to determine the charge/uptake ratio. Basal [¹⁴C]Urd uptake was determined in control water-injected oocytes (from the same donor frog) under equivalent conditions and used to correct for endogenous non-mediated nucleoside uptake over the same incubation period. Coupling ratios (\pm S.E.) were calculated from slopes of least-squares fits of Urd-dependent charge versus Urd accumulation in oocytes.

Confocal Microscopy of Yeast—Logarithmically growing yeast cells transformed with a GFP-tagged vector (10 μ M, $A_{600} = 0.7$ – 0.9) were mixed with 30 μ l of anti-fading mounting medium, smeared on a glass slide, and checked for green fluorescence using an excitation wavelength of 488 nm. Confocal images were collected using a Zeiss LSM510 confocal laser scanning microscope with a 63 \times 1.4 objective (Plan-Apochromat) using a frame size of 512 \times 512 pixels with a pixel resolution of 0.08 μ m and a pixel depth of 8 bits.

Isolation of Plasma Membranes and Immunoblotting—Yeast membranes were fractionated on sucrose gradients as described (36). Briefly, 1 liter of yeast cells at $A_{600} = 1$ was collected, washed with sucrose breaking buffer (0.4 M sucrose, 1 mM EDTA, and 10 mM Tris (pH 7.4)) containing additional protease inhibitors (Complete protease inhibitor mixture, Roche Applied Science), and lysed by vortexing in the presence of glass beads (425–600 μm ; Sigma) for 15 min at 4 °C. Unbroken cells and glass beads were removed from lysates by centrifugation at 500 $\times g$ for 20 min at 4 °C, and membrane fractions were obtained by centrifugation of lysates at 21,000 $\times g$ for 40 min at 4 °C. The resulting crude membrane pellets were resuspended in sucrose breaking buffer containing protease inhibitors. The crude membranes were layered onto a stepwise sucrose gradient (0.4, 1.1, 1.65, and 2.25 M sucrose) containing 10 mM Tris, 1 mM EDTA (pH 7.4), and protein inhibitor mixture. After centrifugation at 80,000 $\times g$ (Beckman SW 41 Ti rotor) for 14 h at 4 °C, fractions of band 3 from the top, which contained enriched plasma membranes, were collected and resuspended with sucrose breaking buffer containing protease inhibitors. After centrifugation at 21,000 $\times g$ for 90 min at 4 °C, the pellets were dissolved with sucrose breaking buffer, and the proteins present in the membranes were separated electrophoretically and analyzed by immunoblotting as described previously (31).

The primary antibodies used in immunoblotting were monoclonal antibodies against the c-Myc epitope tag (9E10; BABCO, Richmond, CA), against Pma1 (plasma membrane marker; Abcam, Cambridge, MA), against Dpm1p (dolichol phosphate mannosyl synthase endoplasmic reticulum membrane marker; Invitrogen), and against the V-ATPase 100-kDa subunit (vacuole membrane marker; Invitrogen). The proteins were visualized by enhanced chemiluminescence (ECL, Amersham Biosciences) and autoradiography on a film. The film was scanned, and the quantities of the proteins were evaluated using ImageQuant software (Version 5.2; GE Healthcare).

Urd Analogs—The structures of Urd and its analogs were given previously (31). The Urd analogs used in this study were either obtained from R.I. Chemical, Inc. (Orange, CA) or synthesized as described previously (31). Stock solutions of test compounds were prepared in water or Me_2SO (Sigma), and the final concentration of Me_2SO in transport reactions was 0.1% when Me_2SO was used as a solvent.

RESULTS

Transport Characteristics of Fui1p

The *fur4 Δ fui1 Δ* yeast strain with or without pYPGE15 has no active uptake of Urd as described previously (28). At pH 4.5, the uptake of 1 μM [^3H]Urd into *fur4 Δ fui1 Δ* yeast containing pYPFUI1 was rapid and linear over 90 s, with a mean rate (\pm S.E.) of 285 \pm 5 pmol/mg of protein/s (Fig. 1, upper panel). This rate was reduced to 0.3 \pm 0.1 pmol/mg of protein/s in the presence of 10 mM nonradioactive Urd, indicating the presence of functional Fui1p in yeast plasma membranes. Urd uptake rates were determined for all subsequent experiments using incubation periods of 30 s for recombinant Fui1p produced in yeast, thereby providing large signal-to-noise ratios while

Uridine Permease of Yeast

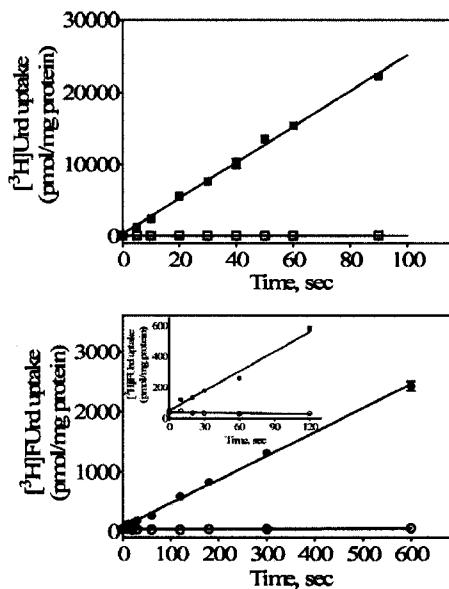


FIGURE 1. Time courses of Urd and FUrD transport into yeast. The uptake of 1 μM [^3H]Urd (upper panel) or [^3H]FUrD (lower panel) by *fur4 Δ fui1 Δ* yeast transformed with pYPFUI1 was measured in CMM/Glc (pH 4.5) either alone (■ and ●) or with 10 mM nonradioactive Urd (□ and ○). The inset in the lower panel shows the time courses for the first 120 s of [^3H]FUrD uptake. Each data point represents the means \pm S.E. of eight determinations; error bars are not shown where they are smaller than the symbol. Each curve represents one of three identical experiments that gave qualitatively similar uptake rates.

maintaining initial rates of uptake. FUrD is cytotoxic to *S. cerevisiae* (6, 7), and the evidence that its transport into yeast is mediated by Fui1p is based on the association of resistance to FUrD with the disruption of the *FUI1* gene (7). The time course for uptake of 1 μM [^3H]FUrD into *fur4 Δ fui1 Δ* containing pYPFUI1 was linear for at least 10 min (Fig. 1, lower panel), and its rate (4.0 \pm 0.2 pmol/mg of protein/s) was the same as that observed during the first 120 s (inset), indicating that uptake intervals of 10 min provided initial rates, evidently because the transport step of the FUrD uptake process was rate-limiting. The uptake rate of FUrD was only 1.5% of that of Urd, indicating that FUrD was a poor permeant for Fui1p. Consistent with the results of a previous study (6), similar experiments with other ^3H -labeled nucleosides demonstrated that adenosine, inosine, guanosine, cytidine, and thymidine were not transported by Fui1p (data not shown).

Fui1p-mediated Urd uptake in yeast was strictly pH-dependent, with an optimum at pH 4–5, and the protonophore carbonyl cyanide *m*-chlorophenylhydrazone (CCCP; 400 μM) strongly inhibited Urd uptake at every pH condition tested (Fig. 2A). Fui1p-mediated Urd uptake (pH 5.0) was sensitive to CCCP in a concentration-dependent manner, with a mean IC_{50}

Uridine Permease of Yeast

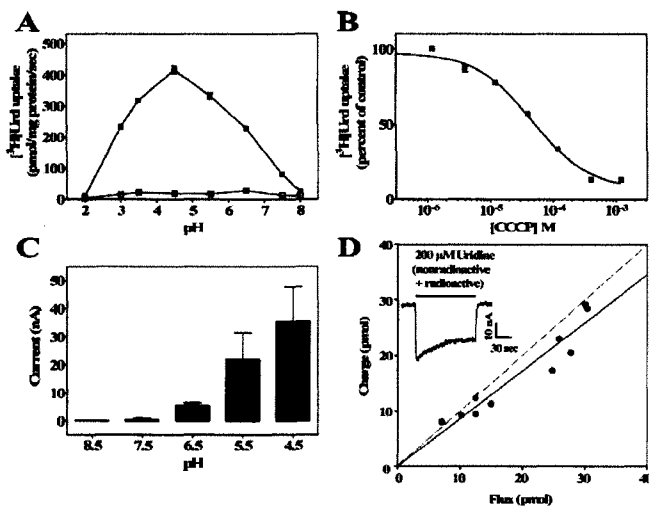


FIGURE 2. pH and proton dependence of Urd uptake mediated by Fui1p. A, effects of pH and CCCP on Urd transport into yeast. The uptake of $1 \mu\text{M}$ [^3H]Urd into *fur4 Δ fui1 Δ* yeast producing Fui1p was measured over 30 s in transport medium at different pH values in the presence (□) and absence (■) of $400 \mu\text{M}$ CCCP. Each data point represents the mean \pm S.E. of eight determinations; error bars are not shown where they are smaller than the symbol. B, inhibitory effects of CCCP on Urd transport mediated in yeast by Fui1p. *fur4 Δ fui1 Δ* yeast cells transformed with pYFUI1 were incubated with CCCP at graded concentrations for 5 min before initiation of the transport assay. The uptake of $1 \mu\text{M}$ [^3H]Urd was measured over a 30-s incubation period in the presence and absence of CCCP. Uptake values in the presence of CCCP are given as the percentage of uptake values in the absence of CCCP. Each data point represents the mean \pm S.E. of quadruplicate determinations; error bars are not shown where they are smaller than the symbol. Three or four independent experiments gave similar results; data from individual representative experiments are shown. C, proton currents induced in oocytes by exposure of recombinant Fui1p to Urd. Shown are averaged inward currents in Fui1p-producing oocytes perfused with $100 \mu\text{M}$ Urd in sodium-free (100 mM ChCl) transport medium at a membrane potential of -50 mV. Currents are the means \pm S.E. of five different oocytes from the same batch of cells used on the same day. No currents were observed in control water-injected oocytes. D, stoichiometry of H^+ /Urd symport by recombinant Fui1p. A plot of charge versus [^3H]Urd uptake was generated with 10 different Fui1p-producing oocytes in transport medium containing 100 mM ChCl and acidified to pH 5.5 at a membrane holding potential of -50 mV. Integration of the Urd-induced current was used to calculate the net cation influx (charge) and was correlated to the net [^3H]Urd influx (flux). Each data point represents a single oocyte. Linear regression analysis of the data is indicated by the solid line. The dashed line indicates a theoretical 1:1 charge/uptake ratio. Linear fits passed through the origin. The inset is a representative example of the current generated during application of [^3H]Urd in a Fui1p-producing oocyte.

value (\pm S.E.) of $50 \pm 4 \mu\text{M}$ (Fig. 2B), indicating that a proton gradient was required for Fui1p function.

The pH dependence of Fui1p was also studied in *Xenopus* oocytes producing recombinant Fui1p. Fig. 2C illustrates the effect of an imposed H^+ gradient on Urd-induced proton currents mediated by Fui1p. Perfusion of Fui1p-producing oocytes with medium containing $100 \mu\text{M}$ Urd induced net inward currents, the magnitude of which increased as the extracellular pH was lowered. Inward currents were not detected at pH 8.5, strongly supporting the conclusion that protons were cotransported with Urd. No currents were observed in control water-injected oocytes under any of the conditions tested.

The H^+ /nucleoside stoichiometry of FUI1 was directly determined by simultaneously measuring Urd-induced currents and [^3H]Urd uptake under voltage-clamp conditions. The H^+ /nucleoside coupling ratio was determined in sodium-

free medium (pH 5.5) at a membrane potential of -50 mV. The inset in Fig. 2D shows a representative Urd-dependent current recording in a Fui1p-producing oocyte. Each data point in Fig. 2D represents a single oocyte, and the H^+ /nucleoside coupling ratio, given by the slope of the linear fit of charge (psec) versus uptake (pmol), was 0.86 ± 0.09 , indicating a proton/Urd stoichiometry of 1:1. Urd is metabolized only slowly by oocytes, mostly by phosphorylation into less permeable forms (37). It is therefore unlikely that the measured H^+ /nucleoside stoichiometry of Fui1p was influenced by flow of acid or base produced by addition of Urd. As evidence of this, the current recording in the inset in Fig. 2D returned to zero as soon as externally applied Urd was removed.

Mutational Analysis of Charged Amino Acid Residues in Putative TM Segments 3, 4, and 7

There are only three charged residues in the 10 TM segments in the topology model of Fui1p (38): glutamate, lysine, and aspartate at positions 259, 288, and 474, respectively. The hydrophobic locations of these charged residues suggested that they could be important in transporter structure and function. To determine the effects of mutations of these amino acids, site-directed mutagenesis was undertaken at Glu²⁵⁹, Lys²⁸⁸, and Asp⁴⁷⁴. All of the resulting mutants (Fui1p-K288A, Fui1p-K288E, Fui1p-K288R, Fui1p-E259A, Fui1p-D474A, and Fui1p-E259A,D474A) and their GFP- and c-Myc-tagged proteins remained functional, although some exhibited substantial changes in kinetic properties. The apparent K_m and V_{max} values for Urd transport by yeast producing wild-type or mutant Fui1p were determined by measuring initial uptake rates at increasing concentrations of [^3H]Urd (Fig. 3). In all cases, Urd uptake conformed to simple Michaelis-Menten kinetics (Fig. 3, upper panel). Wild-type Fui1p showed high apparent affinity and capacity for Urd uptake ($K_m = 10.8 \pm 0.9 \mu\text{M}$ and $V_{max} = 2500 \pm 60$ pmol/mg of protein/s, mean \pm S.E., $n = 3$). The apparent K_m of Fui1p reported here was lower than that reported previously ($20 \mu\text{M}$) (6), probably because the contribution to Urd uptake by the uracil permease Fur4p was eliminated in this study by using the double-permease knock-out strain *fur4 Δ fui1 Δ* .

Replacement of either or both of the acidic glutamate and

Uridine Permease of Yeast

aspartate residues at positions 259 and 474 of Fui1p, respectively, with a neutral alanine residue had relatively small effects on the kinetic parameters of uptake (Fig. 3 and Table 1), indicating that these residues in TM segments 3 and 7, respectively, were not critical for Urd uptake. In contrast, the replacement of lysine at position 288 with alanine produced a mutant (Fui1p-K288A) with a significantly reduced V_{max} value compared with that of wild-type Fui1p, although the apparent K_m values of wild-type and mutant

Fui1p were similar. The resulting transport efficiency (V_{max}/K_m) was only 12% of that of wild-type Fui1p. This result also confirmed that the uptake kinetics represented those of the transport process rather than metabolism because the only difference between the two yeast strains was the alteration of a single amino acid residue in Fui1p. To determine whether replacement of the positive charge of the lysine residue was responsible for the reduced transportability, further site-directed mutagenesis was carried out to analyze the function of Lys²⁸⁸. Replacement of this residue with positively charged arginine or negatively charged aspartate produced Fui1p-K288R and Fui1p-K288E, respectively, both of which displayed kinetic properties similar to those of Fui1p-K288A (Fig. 3 and Table 1). This result suggested that Lys²⁸⁸ was evidently critical for maintaining the high transport efficiency of Fui1p but not for proton binding and/or translocation, a conclusion that was supported by the results obtained when Urd uptake was measured in buffers at different pH values in that none of the Lys²⁸⁸ mutants showed altered pH dependence of uptake (data not shown). Urd uptake by Fui1p-E259A, Fui1p-D474A, or the Fui1p-E259A,D474A double mutant (with the negative charges removed from both residues 259 and 474) also exhibited strong dependence on pH, with optimal uptake into yeast occurring at pH 5.0 (data not shown), indicating that Glu²⁵⁹ and Asp⁴⁷⁴ were also not required for proton binding and/or translocation.

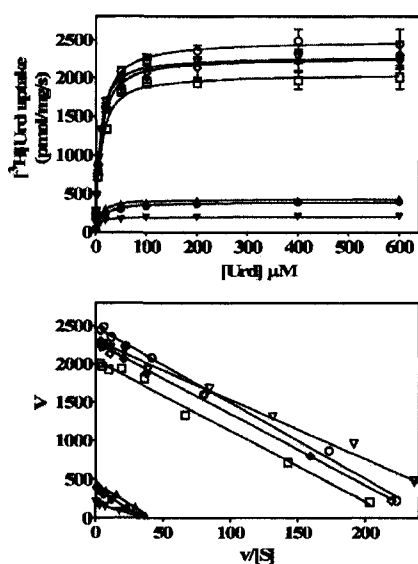


FIGURE 3. Kinetic properties of Fui1p and Fui1p mutants. The mediated component of Urd transport (uptake rates of [³H]Urd at particular Urd concentrations minus uptake rates at those concentrations in the presence of 10 mM nonradioactive Urd) was plotted as a function of concentration (upper panel) and subsequently converted to v versus $v/[S]$ plots (lower panel) to determine the kinetic constants for wild-type Fui1p (○), Fui1p-E259A (□), Fui1p-K288A (▽), Fui1p-K288E (▲), Fui1p-K288R (●), Fui1p-D474A (◇), and Fui1p-E259A,D474A (▽) using GraphPad Prism software. The lower panel is the Eadie-Hofstee plot of the data presented in the upper panel. Each value is the mean \pm S.E. of nine determinations, and error bars are not shown where they were smaller than the data points. Each curve represents one of three identical experiments that gave qualitatively similar results.

TABLE 1

Kinetic properties of Urd transport by wild-type and mutant Fui1p

The K_m and V_{max} values were determined using GraphPad Prism software by nonlinear regression analysis. Representative plots for Urd transport by Fui1p, Fui1p-K288A, Fui1p-K288E, Fui1p-K288R, Fui1p-E259A, Fui1p-D474A, and Fui1p-E259A,D474A are shown in Fig. 3. The K_m and V_{max} values shown are the means \pm S.E. of three separate experiments. The normalized V_{max}/K_m values were obtained by dividing the V_{max}/K_m values by the corresponding relative abundance values as determined by immunoblot analysis as illustrated in Fig. 5 (B and C).

Fui1p	Apparent K_m μM	Apparent V_{max} $\mu mol/mg/s$	V_{max}/K_m	V_{max}/K_m (normalized to protein abundance)
Wild-type	10.8 \pm 0.9	2500 \pm 60	232	232
E259A	9.2 \pm 1.5	2100 \pm 94	228	204
K288A	7.8 \pm 1.1	210 \pm 28	27	9.2
K288R	12.2 \pm 1.5	380 \pm 41	31	22
K288E	13.5 \pm 2.0	390 \pm 37	29	5.0
D474A	9.1 \pm 1.3	2200 \pm 88	241	180
E259A,D474A	7.9 \pm 1.8	2210 \pm 92	280	190

Cellular Resistance to FURd by Yeast Producing Wild-type Fui1p or Its Mutants

Yeast cells are sensitive to FURd, and disruption of the *FUI1* gene results in resistance to FURd cytotoxicity (7). To determine whether any of the *FUI1* mutations altered sensitivity to FURd, *fur4Δfui1Δ* yeast cells producing either wild-type Fui1p or one of the Fui1p mutants were exposed to graded concentrations of FURd. Similar growth patterns were observed for all situations in the absence of FURd (Fig. 4). When *fur4Δfui1Δ* yeast cells that contained the insert-free vector (pYPGE15) were plated on solid medium containing graded concentrations of FURd (Fig. 4), growth was observed at the highest concentration tested (100 μM), whereas growth of *fur4Δfui1Δ* yeast producing wild-type Fui1p, Fui1p-E259A, or Fui1p-D474A was inhibited at the lowest concentration tested (5 μM). No growth was observed in *fur4Δfui1Δ* yeast producing the Fui1p-E259A,D474A double mutant at 5 μM FURd (data not shown). When *fur4Δfui1Δ* yeast cells were transformed with plasmids containing inserts encoding any of the three Lys²⁸⁸ mutants, resistance to FURd was

Downloaded from www.jbc.org at University of Alberta Libraries on February 15, 2008

Uridine Permease of Yeast

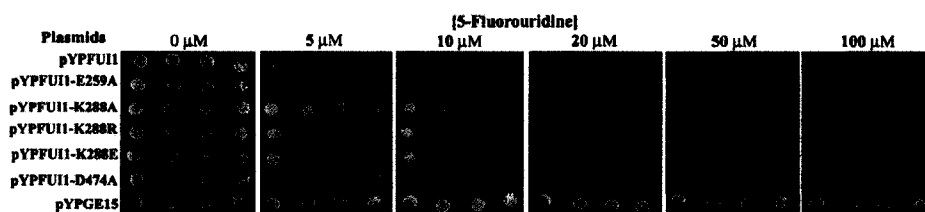


FIGURE 4. Cellular resistance to 5-FUrd. *fur4Δfui1Δ* yeast cells transformed with plasmid pYPFU11, pYPFU11-E259A, pYPFU11-K288A, pYPFU11-K288R, pYPFU11-K288E, pYPFU11-D474A, or pYPGE15 and grown in CMM/Glc under logarithmic conditions were harvested and resuspended in CMM/Glc to A_{600} values of 1.0, 0.1, 0.01, and 0.001. Ten- μ l portions of the diluted cultures were plated on solid medium containing graded concentrations (0–100 μ M) of 5-FUrd, and cell growth on the plates was assessed after 3 days at 30 °C.

observed at 5, 10, and 20 μ M (Fig. 4), suggesting a role of Lys^{288} in 5-FUrd transport.

Detection of GFP- and c-Myc-tagged Fui1p and Fui1p Mutants

Because some of the Fui1p mutants exhibited reduced V_{max} values for Urd in comparison with wild-type Fui1p, the GFP tag was used to determine whether impaired transporter capacity was due to changes in localization. Wild-type and mutant Fui1p-GFP proteins displayed kinetic parameters that were within 98–104% of those obtained for the corresponding untagged versions (data not shown), indicating that addition of the GFP tag to the C-terminal end of the wild-type and mutant Fui1p proteins did not change their transport properties. As shown in Fig. 5A, yeast producing Fui1p mutants exhibited fluorescence patterns similar to those of wild-type Fui1p, which showed plasma membrane localization and intracellular accumulations. The intracellular patterns varied from bright fluorescent areas, which were likely due to retention of overexpressed proteins in vacuoles for degradation (24), to fluorescent circles, which were likely due to the presence of the proteins in intracellular membranes. Diffuse green fluorescence was observed in yeast transformed with pYPGFP, and no fluorescence was observed in yeast transformed with the insert-free vector (pYPGE15) (Fig. 5A, lower panels).

Considering that GFP is relatively large and therefore may itself contribute to the retention of the tagged protein in intracellular compartments, Fui1p and its mutants were also C-terminally tagged with c-Myc and quantified by immunoblotting. c-Myc-tagged Fui1p and its mutants exhibited kinetic properties that were within 96–103% of those obtained for the corresponding untagged versions (data not shown), indicating that the c-Myc tag did not change the transport properties of Fui1p or its mutants and could therefore be used for the quantification studies described below.

Yeast plasma membranes were isolated, fractionated, and analyzed by immunoblotting (Fig. 5, B and C). Four major bands were collected after equilibrium density centrifugation on sucrose gradients and subjected to immunoblotting (Fig. 5B). When the abundance of Pma1 (a plasma membrane marker) was compared with that of Dpm1p and V-ATPase (endoplasmic reticulum and vacuolar membrane markers, respectively), it was evident that band 3 contained enriched fractions of plasma membranes (Fig. 5B) with relatively small quantities of intracellular membranes (Fig. 5C). The band den-

sities of c-Myc-tagged Fui1p and its mutants were digitized by densitometry using ImageQuant software and normalized to the band densities of the corresponding Pma1 (loading controls). The value of the ratio of the density of the c-Myc-tagged transporter to that of the corresponding Pma1 represented the abundance of c-Myc-tagged Fui1p or its mutants. The “relative abundance” of each of the Fui1p mutants was expressed as the ratio of its abundance to that of c-Myc-tagged wild-type Fui1p, which was taken as 1 (Fig. 5D). With the exception of a large increase in Fui1p-K288A, the Fui1p mutants exhibited small differences in abundance relative to that of c-Myc-tagged wild-type Fui1p. When the V_{max}/K_m values of Fui1p and its mutants were normalized to their corresponding relative abundance levels (shown in Fig. 5D), all three Lys^{288} mutants exhibited <10% of the transport efficiency of wild-type Fui1p, whereas the other mutants exhibited transport efficiencies that were similar to that of wild-type Fui1p (Table 1), confirming a critical role of Lys^{288} in Fui1p function.

Interaction of Urd Analogs with Fui1p

To gain an understanding of the structural regions of Urd that interact with Fui1p, inhibitor sensitivity assays using Urd analogs with modifications of the base and/or sugar moieties were used as described previously in studies of recombinant human transporters produced in yeast (28, 31, 39). The inhibition of initial rates of Urd uptake (i.e. the transport step in the uptake process) was assumed to be competitive because (i) the inhibitors tested were close structural analogs of Urd, and (ii) Fui1p was most likely to be the only plasma membrane protein that interacted with the potential inhibitors. Representative concentration-effect curves of some of the analogs for inhibition of Fui1p-mediated Urd transport are shown in Fig. 6. In all cases, the Hill coefficients of the concentration-effect curves were close to -1 (mean \pm S.E. of -0.9 ± 0.2), indicating a single binding site for the inhibitors. The mean K_i values (\pm S.E.) and the corresponding Gibbs free energy values are listed in Table 2.

Base Modifications—There appeared to be strong interactions between Fui1p and C-5 of Urd because addition of a substituent with different sizes at C-5 resulted in K_i values of >3 mM and decreases of >12.9 kJ/mol in ΔG^0 values. Because 2'-dUrd is a low affinity inhibitor of Urd uptake, the inability of 5-fluoro-2'-dUrd, 5-bromo-2'-dUrd, 5-iodo-2'-dUrd, 5-ethyl-2'-dUrd, and thymidine to inhibit Urd uptake was likely due primarily to modifications at C-5. Position 3 of the base moiety

Uridine Permease of Yeast

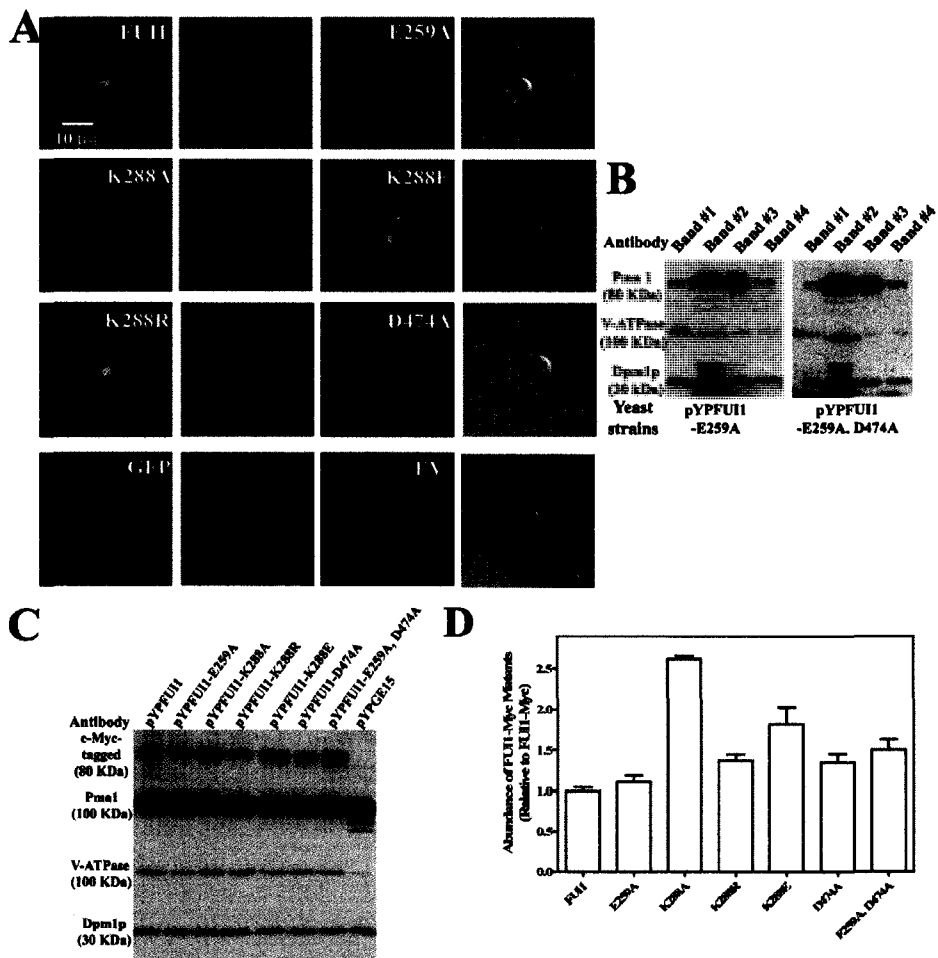


FIGURE 5. Localization and protein abundance of GFP- or c-Myc-tagged wild-type Fui1p and its mutants produced in yeast. *A*, plasma membrane and intracellular locations of GFP-tagged wild-type Fui1p and its mutants. Representative *fur4Δfui1Δ* yeast cells producing GFP alone (control) or GFP-fused Fui1p, Fui1p-E259A, Fui1p-K288A, Fui1p-K288R, Fui1p-K288E, Fui1p-D474A, or Fui1p-E259A, D474A (not shown) were immobilized on glass slides using polylysine and viewed under a confocal microscope. *EV*, empty vector (pYPGE15). *B*, immunoblotting to detect enrichment of plasma membranes. Membranes from *fur4Δfui1Δ* yeast producing c-Myc-fused Fui1p-E259A or Fui1p-E259A, D474A were subjected to fractionation by continuous sucrose gradient centrifugation as described under "Materials and Methods," and four major fractions were isolated and subjected to immunoblotting using monoclonal antibodies against Pma1, Dpm1p, and the V-ATPase 100-kDa subunit. *C*, immunoblotting to detect c-Myc-tagged Fui1p and its mutants in yeast. Plasma membranes were isolated as described under "Materials and Methods" from *fur4Δfui1Δ* yeast producing Fui1p or c-Myc-fused Fui1p, Fui1p-E259A, Fui1p-K288A, Fui1p-K288R, Fui1p-K288E, Fui1p-D474A, or Fui1p-E259A, D474A. Plasma membrane preparations (10 μg of protein/sample) were subjected to SDS-PAGE, after which the proteins were transferred to polyvinylidene fluoride membranes that were subjected to immunoblotting with monoclonal antibodies against c-Myc, Pma1, Dpm1p, and the V-ATPase 100-kDa subunit. Results were similar for three independent experiments, only one of which is shown. The molecular mass of each protein is indicated. *D*, relative abundance of c-Myc-tagged Fui1p and its mutants in isolated yeast plasma membranes. The bands detected by immunoblotting as illustrated in *B* were quantified using ImageQuant software (Version 5.2). The band densities of c-Myc-tagged Fui1p mutants were normalized to those of the corresponding Pma1 proteins, and the resulting values (representing the abundance of each of the c-Myc-tagged mutants) are presented as a ratio relative to the abundance of c-Myc-tagged wild-type Fui1p. The means ± S.E. of average protein abundance (*n* = 3) were determined with GraphPad Prism software.

Downloaded from www.jbc.org at University of Alberta Libraries on February 15, 2008

Uridine Permease of Yeast

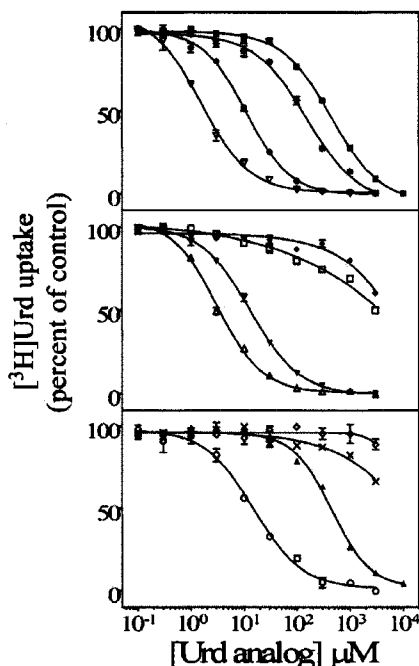


FIGURE 6. Inhibition of recombinant Fui1p-mediated Urd uptake by some Urd analogs. The uptake of 1 μM [³H]Urd into *fur4Δfui1Δ* yeast producing Fui1p was measured over a period of 30 s in the presence of graded concentrations of test compounds. The test compounds were Urd (●), 2'-dUrd (■), 3'-dUrd (▼), 2',5'-ddUrd (♦), 5'-O-MeUrd (▼), 1-(β-D-xylofuranosyl)uracil (◆), 5'-chloro-5'-dUrd (Δ), 5'-azido-5'-dUrd (○), 5-fluoro-5'-dUrd (▲), 3-MeUrd (◇), and Furd (×). Uptake values in the presence of Urd compounds are given as a percentage of uptake values in their absence. Each data point represents the mean ± S.E. of quadruplicate determinations; error bars are not shown where they are smaller than the symbol. Three or four independent experiments gave similar results, and results from representative experiments are shown.

(N(3)-H) also contributed a recognition determinant for Fui1p/Urd interactions because 3-methyluridine (MeUrd) did not inhibit Urd uptake ($K_i > 3$ mM). There was a difference of >12.9 kJ/mol in binding energy relative to the ΔG^0 of Urd, suggesting loss of hydrogen bonding. Hydrogen bonding between Fui1p and position 3 of the base was further supported by the effect of the change of N(3)-H to C(3)-H, which is not a donor for hydrogen bonding; 3-deaza-Urd yielded a K_i of >3 mM.

Sugar Modifications—The C(2')-OH group appeared to be a critical determinant for high affinity binding of Urd by Fui1p because its removal (2'-dUrd) produced a difference of 8.9 kJ/mol in ΔG^0 , with a 51-fold increase in K_i , suggesting that hydrogen bonding could be important. Any further modifications at C-2', e.g. substitution of an azido group for a hydrogen atom at C-2' of 2'-dUrd (2'-azido-2'-dUrd), addition of a

TABLE 2
 K_i and Gibbs free energy values for inhibition of Fui1p-mediated Urd uptake in yeast by Urd analogs

The uptake of 1 μM [³H]Urd into *fur4Δfui1Δ* yeast expressing pYPFUI1 was measured over 30 s in the presence of graded concentrations of nonradioactive Urd or Urd analogs. $K_{0.5}$ values (mean ± S.E., $n = 3-4$) were determined using GraphPad Prism software (Version 3.0) and were converted to K_i values (33) using a K_m (mean ± S.E., $n = 3$) of 10.8 ± 0.9 μM for recombinant Fui1p. Gibbs free energy (ΔG^0) was calculated from $\Delta G^0 = -RT \ln(K_i)$.

Urd compounds	K_i μM	ΔG^0	$\delta(\Delta G^0)$
Urd	10.2 ± 0.4	26.1	0
Base modifications			
5-Bromo-Urd ^a	>3000 ^b		
FUrd ^a	>3000 ^b		
5-Iodo-Urd ^a	>3000 ^b		
5-MeUrd	>3000 ^b		
3-MeUrd	>3000 ^b		
3-Deaza-Urd	>3000 ^b		
Sugar modifications			
2'-dUrd	520 ± 57	17.2	8.9
3'-dUrd	>3000 ^b	<13.2	>12.9
5'-dUrd	2.7 ± 0.7	29.1	-3.0
1-(β-D-Arabinofuranosyl)uracil	>3000 ^b		
1-(β-D-Xylofuranosyl)uracil	>3000 ^b		
2',5'-ddUrd	>3000 ^b		
2',5'-ddUrd	144 ± 36	20.1	6.0
3',5'-ddUrd	>3000 ^b		
2'-O-MeUrd	>3000 ^b	<15.8	>8.0
3'-O-MeUrd	>3000 ^b		
5'-O-MeUrd	13.6 ± 3.5	25.4	0.7
2'-Azido-2'-dUrd	>2000 ^b	<14.1	>12
3'-Azido-3'-dUrd	>2000 ^b		
5'-Azido-5'-dUrd	14.4 ± 1.9	25.3	0.8
5'-Chloro-5'-dUrd	2.3 ± 0.3	29.4	-3.3
2',3'-O-Isopropylidene-Urd	>3000 ^b		
Base and sugar modifications			
3'-Azido-3'-deoxythymidine	>3000 ^b		
5-Bromo-2'-dUrd	>3000 ^b		
5-Ethyl-2'-dUrd	>3000 ^b		
5-Fluoro-2'-dUrd ^a	>3000 ^b		
5-Iodo-2'-dUrd	>3000 ^b		
Thymidine ^a	>3000 ^b		
5-Fluoro-5'-dUrd ^a	438 ± 47	17.6	8.5

^a The inhibitory effects of these Urd analogs were tested at 1 or 10 mM in our previous study (6). In the previous study (6), yeast cells were preincubated with the Urd analog (1 or 10 mM) for 20 min before the addition of [³H]Urd, whereas in this study, the Urd analogs and [³H]Urd were added simultaneously as described under "Materials and Methods." This difference in the experimental conditions explains why greater inhibition of some Urd analogs was observed in the previous study than in this study.

^b Inhibition of <50% was observed.

^c No inhibition was observed.

methyl group (2'-O-MeUrd), or inversion of the orientation of the hydroxyl group (1-(β-D-arabinofuranosyl)uracil), dramatically reduced interactions with Fui1p (apparent affinities for 2'-azido-2'-dUrd, 2'-O-MeUrd, and 1-(β-D-arabinofuranosyl)uracil of $K_i > 3$ mM).

The C(3')-OH group also appeared to interact strongly with Fui1p because its removal (3'-dUrd) yielded K_i values of >3 mM, with losses of >12.9 kJ/mol in ΔG^0 . Although 2'-dUrd inhibited Fui1p-mediated Urd uptake, the additional removal of the C(3')-OH group (2',3'-dideoxyuridine (ddUrd)) abolished the inhibitory effects. The contribution of the C(3')-OH group as a recognition determinant for binding to Fui1p was also apparent from the effects of substitution of an azido or O-methyl group at these positions; Fui1p-mediated Urd uptake remained unchanged in the presence of high concentrations of 3'-azido-3'-dUrd or 3'-O-MeUrd. 3'-Azido-3'-deoxythymidine failed to inhibit Fui1p-mediated Urd uptake. Although Fui1p strongly bound Urd with the C(3')-OH group below the

Uridine Permease of Yeast

sugar ring plane, its affinity for 1-(β -D-xylofuranosyl)uracil, an epimer of Urd with the C(3')-OH group oriented above the plane of the sugar ring, was markedly reduced ($K_i > 3$ mM). The inverted orientation of the hydroxyl group evidently produced an analog that could no longer interact with Fui1p. Similarly, 2',3'-O-isopropylidene-Urd failed to inhibit Urd uptake, as was also observed with 2',3'-ddUrd.

C-5' of Urd was not required for binding to Fui1p because 5'-dUrd and 5'-chloro-5'-dUrd were both potent inhibitors, with somewhat lower K_i values than Urd itself (t test, $p < 0.05$). Fui1p displayed relatively high affinities for 5'-azido-5'-dUrd and 5'-O-MeUrd (Fig. 5), supplying further evidence that the C(5')-OH group was not essential for Fui1p/Urd interactions. Although Fui1p exhibited a low apparent affinity for 2'-dUrd ($K_i = 520 \pm 57 \mu\text{M}$), the additional removal of the C(40)-OH group partially restored the affinity for Fui1p (2',5'-ddUrd, $K_i = 144 \pm 36 \mu\text{M}$). The slightly higher binding energy of 2',5'-ddUrd compared with 2'-dUrd ($\delta(\Delta G^\circ) = -2.9$ kJ/mol relative to the ΔG° of 2'-dUrd) was evidently due to energy gained by removal of the hydroxyl group at C-5', resulting in an analog that has a better fit in the binding pocket of Fui1p. Also, inhibition of Fui1p-mediated Urd transport with FURd was barely detectable, whereas relatively high concentrations of 5-fluoro-5'-dUrd ($K_i = 438 \pm 47 \mu\text{M}$) inhibited Urd uptake.

DISCUSSION

Fui1p is the primary permease involved in the uptake of nucleosides into the yeast *S. cerevisiae* (39). The uracil permease Fur4p exhibits weak transportability for Urd.⁷ Compared with other nucleoside transporters identified so far, Fui1p exhibits highly specific permeant selectivity. As a high affinity, high capacity transporter for Urd, Fui1p has also been suggested to mediate the uptake of the cytotoxic nucleoside analog FURd and was initially discovered because a mutant selected for resistance to FURd had lost the capacity to import Urd as well as FURd (7). We undertook this study to characterize the transport mechanism and to identify structural determinants of Urd that are important for binding to Fui1p.

Results from experiments with both yeast and oocytes producing wild-type Fui1p suggested a simple proton/Urd cotransport mechanism. The optimal Urd transportability under acidic conditions and the sensitivity to proton uncoupling by CCCP suggested that Fui1p functions through a secondary active transport process. Two-electrode voltage-clamp analysis of oocytes producing recombinant Fui1p showed that proton currents induced by Urd were stimulated and inhibited by externally acidic and alkaline pH environments, respectively, and that the H^+ /Urd coupling ratio was 1:1. In yeast and plants, protons are likely to be the preferred coupling ions for nutrient transport, and the proton electrochemical gradient is maintained by plasma membrane H^+ -ATPase (41, 42). Utilization of the transmembrane proton gradient to energize active transport has been demonstrated for other members of the Fur family of transporters (15, 43), as well as for ENTs of parasitic protozoa (3) and CNTs of *C. albicans* and *C. elegans* (44, 45). In contrast, mammalian CNTs function predominantly as Na^+ /nucleoside symporters, although hCNT3 is also able to utilize pro-

tons (46). The H^+ -ATPase from *S. cerevisiae* is known to be essential for intracellular pH regulation, nutrient uptake, and cell growth (42). H^+ -ATPase activity determines cellular H^+ extrusion, which might affect extracellular proton concentrations and thus regulate the rate of Urd uptake mediated by Fui1p. One of the mechanisms of growth control by H^+ -ATPase in yeast may be modulating the uptake of extracellular nutrients, including Urd.

Highly conserved charged residues within TM segments of transporter proteins are likely candidates for involvement in binding and translocation of ions. According to the topology model for the Fur family (17), the predicted TM segments of Fur4p contain three charged amino acid residues (Glu²⁴³, Lys²⁷², and Glu⁵³⁹ in putative TM segments 3, 4, and 9, respectively) that are highly conserved in other family members, of which only the lysine residue was shown to be important for activity (14). In this study, the kinetic properties of the three conserved charged amino acid residues in putative TM segments 3, 4, and 7 of Fui1p were characterized in mutagenesis and transport assays. The two negatively charged residues (Glu²⁵⁹ and Asp⁴⁷⁴ in TM segments 3 and 7, respectively) were not essential for Fui1p function because mutation to alanine had no effect on transport activity. In addition, neither Glu²⁵⁹ nor Asp⁴⁷⁴ appeared to be involved in the sensing or binding of protons because removal of the negative charge separately or in tandem did not change the proton dependence of Urd transport. However, although mutation of the conserved lysine (Lys²⁸⁸) in TM segment 4 of Fui1p to positively charged, negatively charged, or neutral residues resulted in similar affinities for Urd, it resulted in greatly decreased V_{max} values for Urd transport. In contrast, mutation of the corresponding lysine (Lys²⁷²) in TM segment 4 of Fur4p changed both the binding and translocation of uracil (14).

The results of the GFP and c-Myc tagging studies established that the decreases in the transport capacity of the Fui1p Lys²⁸⁸ mutants were not due to decreased abundance of the mutant proteins in yeast plasma membranes relative to wild-type Fui1p. The GFP-tagged mutant proteins also had similar cellular distribution patterns. Thus, Lys²⁸⁸ *per se* was important for Urd transport capacity. K_{cat}/K_m is a measure of catalytic efficiency, and $K_{\text{cat}} = V_{\text{max}}/[E]_T$, where $[E]_T$ is the amount of transporter. $[E]_T$ of the Fui1p Lys²⁸⁸ mutants was not reduced compared with that of wild-type Fui1p. Replacement of lysine at position 288 with arginine, glutamate, or alanine affected Urd transport efficiency similarly, suggesting that this lysine, which lies toward the extracellular aspect of putative TM segment 4 of Fui1p, plays a key role in Urd translocation. The effects of these substitutions were further demonstrated by the FURd cytotoxicity profiles of the Lys²⁸⁸ mutants. Yeast producing the Lys²⁸⁸ mutants survived in medium containing low FURd concentrations, which killed yeast producing either Fui1p or its Glu²⁵⁹ and/or Asp⁴⁷⁴ mutants. In the presence of higher concentrations of FURd (e.g. 100 μM), the Lys²⁸⁸ mutants were also killed, indicating that the Lys²⁸⁸ mutants were functional but had reduced transport capacities.

Structural regions of the Urd molecule involved in binding to Fui1p were probed by analysis of inhibition profiles and binding energies as described previously (31, 47). These regions were identified as C(2')-OH, C(3')-OH, C-5, and N(3)-H. The loss of >12.9 kJ/mol of Gibbs free energy when the C(3')-OH and

⁷ J. Zhang and C. E. Cass, unpublished data.

Uridine Permease of Yeast

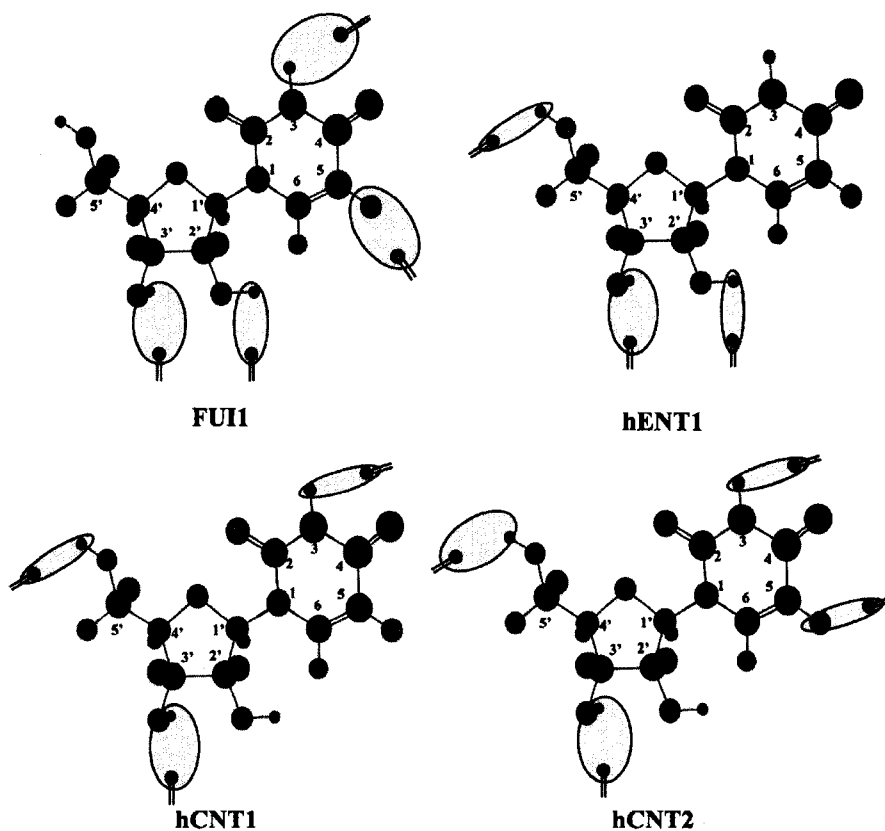


FIGURE 7. Models of interactions between Urd and Fui1p, hENT1, hCNT1, or hCNT2. Structural determinants of Urd that are proposed to interact with amino acid residues in the transporter-binding pocket and their interactions are indicated as ovals, the sizes of which correspond to the values of binding energy. The binding models for human nucleoside transporters were derived from previous studies (28, 31, 39). Functional groups of the transporter are speculative and for presentation purposes only. Numbering for Urd is indicated. The three-dimensional structure of Urd was generated using ChemDraw Chem3D software.

N(3)-H groups were modified suggested that these groups were involved in hydrogen bonding with Fui1p. Fui1p also exhibited low affinities for Urd analogs with C-5 modifications. Removal of the C(2')-OH group resulted in a loss of 8.9 kJ/mol of binding energy. The C-5' region in the sugar moiety did not appear to be required for Urd binding because modifications at this position did not cause substantial losses in binding energy. The unchanged (or even increased with both C-2' and C-5' modifications) affinities for Urd analogs with C-5' substituents indicated that this position could be modified without seriously affecting binding to Fui1p.

The Urd binding profiles of Fui1p have both similarities and distinct differences compared with those of the human members of the ENT and CNT families of nucleoside transporters (Fig. 7). The importance of the 3'-hydroxyl group for

binding interactions with hCNTs and hENTs, which are structurally unrelated proteins, is well established (31, 39, 48, 49). In this work, the 3'-hydroxyl was also identified as a critical functional group for nucleoside binding to Fui1p. Any changes at C-3', including removal of the hydroxyl group or inversion of its configuration, dramatically altered the Fui1p/Urd analog interactions. C-2', which plays a minor or moderate role in Urd interactions with hCNT and hENT proteins, was involved in strong interactions with Fui1p. Interestingly, Fui1p had no major interactions with C(5')-OH, whereas hCNTs and hENTs interact with C(5')-OH to various degrees (28, 31, 39). These results suggest that new Urd analogs might be designed to specifically target fungal nucleoside transporters.

In summary, Fui1p of *S. cerevisiae* was demonstrated to be an

electrogenic transporter with a H^+ /Urd coupling stoichiometry of 1:1. Fui1p mediates the high affinity transport of Urd and the low but significant transport of the cytotoxic nucleoside analog FUrd. Studies of the Urd analog binding profiles of Fui1p revealed substantial differences from those of the human nucleoside transporters (hCNTs and hENTs). This raises possibilities for the design and application of Urd analog drugs with cytotoxic substituent(s) that would be transported differentially by fungal and human nucleoside transporters. Of the three charged residues in the membrane-spanning regions of Fui1p, only the lysine at position 288 was found to be important for transport of Urd. Because all of the Lys²⁸⁸ mutants were found to be targeted to yeast plasma membranes with minimal changes in abundance, the severe impairment of transport capacity likely resulted from defects in the translocation process. Additional studies are needed to fully elucidate the structural features of Fui1p that are critical for permeant binding and translocation.

REFERENCES

- Baldwin, S. A., Mackey, J. R., Cass, C. E., and Young, J. D. (1999) *Mol. Med. Today* **5**, 216–224
- Cass, C. E., Young, J. D., Baldwin, S. A., Cabrita, M. A., Graham, K. A., Griffiths, M., Jennings, L. L., Mackey, J. R., Ng, A. M. L., Ritzel, M. W. L., Vickers, M. F., and Yao, S. Y. M. (1999) in *Membrane Transporters as Drug Targets* (Amidon, G. L., and Sadée, W., eds) 1st Ed. Kluwer Academic/Plenum Publishers, New York
- Landfear, S. M., Ullman, B., Carter, N. S., and Sanchez, M. A. (2004) *Eukaryot. Cell* **3**, 245–254
- Pastor-Anglada, M., Molina-Arcas, M., Casado, F. J., Bellosillo, B., Colomer, D., and Gil, J. (2004) *Leukemia (Basingstoke)* **18**, 385–393
- Vickers, M. F., Young, J. D., Baldwin, S. A., and Cass, C. E. (2000) *Emerg. Ther. Targets* **4**, 515–539
- Vickers, M. F., Yao, S. Y. M., Baldwin, S. A., Young, J. D., and Cass, C. E. (2000) *J. Biol. Chem.* **275**, 25931–25938
- Wagner, R., de Montigny, J., de Wergifosse, P., Souciet, J. L., and Potier, S. (1998) *FEMS Microbiol. Lett.* **159**, 69–75
- Visser, F., Zhang, J., Raborn, R. T., Baldwin, S. A., Young, J. D., and Cass, C. E. (2005) *Mol. Pharmacol.* **67**, 1291–1298
- Volland, C., Garnier, C., and Haguenaer-Tsapis, R. (1992) *J. Biol. Chem.* **267**, 23767–23771
- Seron, K., Blondel, M. O., Haguenaer-Tsapis, R., and Volland, C. (1999) *J. Bacteriol.* **181**, 1793–1800
- Volland, C., Urban-Grimal, D., Geraud, G., and Haguenaer-Tsapis, R. (1994) *J. Biol. Chem.* **269**, 9833–9841
- Pinson, B., Pillois, X., Brethes, D., Chevallier, J., and Napias, C. (1996) *Eur. J. Biochem.* **239**, 439–444
- Pinson, B., Napias, C., Chevallier, J., Van den Broek, P. J., and Brethes, D. (1997) *J. Biol. Chem.* **272**, 28918–28924
- Pinson, B., Chevallier, J., and Urban-Grimal, D. (1999) *Biochem. J.* **339**, 37–42
- Eddy, A. A., and Hopkins, P. (1998) *Biochem. J.* **336**, 125–130
- Marchal, C., Haguenaer-Tsapis, R., and Urban-Grimal, D. (2000) *J. Biol. Chem.* **275**, 23608–23614
- Garnier, C., Blondel, M. O., and Haguenaer-Tsapis, R. (1996) *Mol. Microbiol.* **21**, 1061–1073
- Unkles, S. E., Rouch, D. A., Wang, Y., Siddiqi, M. Y., Glass, A. D., and Kinghorn, J. R. (2004) *Proc. Natl. Acad. Sci. U. S. A.* **101**, 17549–17554
- Muth, T. R., and Schuldiner, S. (2000) *EMBO J.* **19**, 234–240
- Grewer, C., Watzke, N., Rauen, T., and Bicho, A. (2003) *J. Biol. Chem.* **278**, 2585–2592
- Kaback, H. R. (1997) *Proc. Natl. Acad. Sci. U. S. A.* **94**, 5539–5543
- Arastu-Kapur, S., Ford, E., Ullman, B., and Carter, N. S. (2003) *J. Biol. Chem.* **278**, 33327–33333
- Vernis, L., Piskur, J., and Diffley, J. F. (2003) *Nucleic Acids Res.* **31**, e120
- Blondel, M. O., Morvan, J., Dupre, S., Urban-Grimal, D., Haguenaer-Tsapis, R., and Volland, C. (2004) *Mol. Biol. Cell* **15**, 883–895
- Dujon, B., Sherman, D., Fischer, G., Durrens, P., Casaregola, S., Lafontaine, I., de Montigny, J., Marck, C., Neuveglise, C., Talla, E., Goffard, N., Franjeul, L., Aigle, M., Anthouard, V., Babour, A., Barbe, V., Barnay, S., Blanchin, S., Beckerich, J. M., Beyne, E., Bleykasten, C., Boisrame, A., Boyer, J., Cattolico, L., Confanioleri, F., De Daruvar, A., Despons, L., Fabre, E., Fairhead, C., Ferry-Dumazet, H., Groppi, A., Hantraye, F., Hennequin, C., Jauniaux, N., Joyet, P., Kachouri, R., Kerrest, A., Kuszul, R., Lemaire, M., Lesur, I., Ma, L., Muller, H., Nicaud, J. M., Nikolski, M., Ozlas, S., Ozier-Kalogeropoulos, O., Pellenz, S., Potier, S., Richard, G. F., Straub, M. L., Suleau, A., Swennen, D., Tekcia, F., Wesolowski-Louvel, M., Westhof, E., Wirth, B., Zeniou-Meyer, M., Zivanovic, I., Bolutin-Fukuhara, M., Thierry, A., Bouchier, C., Caudron, B., Scarpelli, C., Gaillardin, C., Weissenbach, J., Wincker, P., and Souciet, J. L. (2004) *Nature* **430**, 35–44
- Kimura, K., and Bugg, T. D. (2003) *Nat. Prod. Rep.* **20**, 252–273
- Rapp, R. P. (2004) *Pharmacotherapy* **24**, 45–285; quiz 295–325
- Zhang, J., Smith, K. M., Tackaherry, T., Visser, F., Robins, M. J., Nielsen, L. P., Nowak, I., Karpinski, E., Baldwin, S. A., Young, J. D., and Cass, C. E. (2005) *Mol. Pharmacol.* **68**, 830–839
- Brunelli, J. P., and Pall, M. L. (1993) *Yeast* **9**, 1309–1318
- Ito, H., Fukuda, Y., Murata, K., and Kimura, A. (1983) *J. Bacteriol.* **153**, 163–168
- Zhang, J., Visser, F., Vickers, M. F., Lang, T., Robins, M. J., Nielsen, L. P., Nowak, I., Baldwin, S. A., Young, J. D., and Cass, C. E. (2003) *Mol. Pharmacol.* **64**, 1512–1520
- Visser, F., Baldwin, S. A., Isaac, R. E., Young, J. D., and Cass, C. E. (2005) *J. Biol. Chem.* **280**, 11025–11034
- Cheng, Y., and Prusoff, W. H. (1973) *Biochem. Pharmacol.* **22**, 3099–3108
- De Koning, H. P., and Jarvis, S. M. (2001) *Acta Trop.* **80**, 245–250
- Smith, K. M., Ng, A. M. L., Yao, S. Y. M., Labeledz, K. A., Knaus, E. E., Wiebe, L. I., Cass, C. E., Baldwin, S. A., Chen, X.-Z., Karpinski, E., and Young, J. D. (2004) *J. Physiol.* **558**, 807–823
- Ausuhel, F. M., Brent, R., Kingston, R. E., Moore, D. D., Seidman, J. G., Smith, J. A., and Struhl, K. (eds) (1997) *Current Protocols in Molecular Biology*, John Wiley & Sons, New York
- Huang, Q. Q., Harvey, C. M., Paterson, A. R., Cass, C. E., and Young, J. D. (1993) *J. Biol. Chem.* **268**, 20613–20619
- de Montigny, J., Straub, M. L., Wagner, R., Bach, M. L., and Chevallier, M. R. (1998) *Yeast* **14**, 1051–1059
- Vickers, M. F., Zhang, J., Visser, F., Tackaherry, T., Robins, M. J., Nielsen, L. P., Nowak, I., Baldwin, S. A., Young, J. D., and Cass, C. E. (2004) *Nucleosides Nucleotides Nucleic Acids* **23**, 361–373
- Acton, E. M., Goerner, R. N., Uh, H. S., Ryan, K. J., Henry, D. W., Cass, C. E., and LePage, G. A. (1979) *J. Med. Chem.* **22**, 518–525
- Serrano, R. (1984) *Curr. Top. Cell. Regul.* **23**, 87–126
- Serrano, R., Kiehlbrandt, M. C., and Fink, G. R. (1986) *Nature* **319**, 689–693
- Hopkins, P., Chevallier, C., Jund, R., and Eddy, A. A. (1988) *FEMS Microbiol. Lett.* **49**, 173–177
- Slugoski, M. D., Loewen, S. K., Ng, A. M. L., Baldwin, S. A., Cass, C. E., and Young, J. D. (2004) *Yeast* **21**, 1269–1277
- Xiao, G., Wang, J., Tangen, T., and Giacomini, K. M. (2001) *Mol. Pharmacol.* **59**, 339–348
- Ritzel, M. W. L., Ng, A. M. L., Yao, S. Y. M., Graham, K., Loewen, S. K., Smith, K. M., Hyde, R. J., Karpinski, E., Cass, C. E., Baldwin, S. A., and Young, J. D. (2001) *Mol. Membr. Biol.* **18**, 65–72
- Wallace, L. J., Candlish, D., and De Koning, H. P. (2002) *J. Biol. Chem.* **277**, 26149–26156
- Vickers, M. F., Kumar, R., Visser, F., Zhang, J., Charania, J., Raborn, R. T., Baldwin, S. A., Young, J. D., and Cass, C. E. (2002) *Biochem. Cell Biol.* **80**, 639–644
- Patil, S. D., Ngo, L. Y., and Unadkat, J. D. (2000) *Cancer Chemother. Pharmacol.* **46**, 394–402

Appendix 4:

Conserved Glutamate Residues are Critically Involved in Na⁺/Nucleoside Cotransport by Human Concentrative Nucleoside Transporter 1 (hCNT1)*

* This appendix has been published.

Yao, S. Y. M., Ng, A. M., Slugoski, M. D., Smith, K. M., Mulinta, R., Karpinski, E., Cass, C. E., Baldwin, S. A., and Young, J. D. (2007) Conserved glutamate residues are critically involved in Na⁺/nucleoside cotransport by human concentrative nucleoside transporter 1 (hCNT1). *J. Biol. Chem.* **282**: 30607-30617.

Conserved Glutamate Residues Are Critically Involved in Na⁺/Nucleoside Cotransport by Human Concentrative Nucleoside Transporter 1 (hCNT1)*

Received for publication, April 18, 2007, and in revised form, August 16, 2007. Published, JBC Papers in Press, August 17, 2007, DOI 10.1074/jbc.M703285200

Sylvia Y. M. Yao[‡], Amy M. L. Ng[‡], Melissa D. Slugoski^{‡1}, Kyla M. Smith[‡], Ras Mulinta[‡], Edward Karpinski[‡], Carol E. Cass^{§¶2}, Stephen A. Baldwin[‡], and James D. Young^{‡3}

From the Membrane Protein Research Group, Departments of [‡]Physiology and [§]Oncology, University of Alberta and [¶]Cross Cancer Institute, Edmonton, Alberta T6G 2H7, Canada and the ¹Astbury Centre for Structural Molecular Biology, Institute of Membrane and Systems Biology, University of Leeds, Leeds LS2 9JT, United Kingdom

Human concentrative nucleoside transporter 1 (hCNT1), the first discovered of three human members of the SLC28 (CNT) protein family, is a Na⁺/nucleoside cotransporter with 650 amino acids. The potential functional roles of 10 conserved aspartate and glutamate residues in hCNT1 were investigated by site-directed mutagenesis and heterologous expression in *Xenopus* oocytes. Initially, each of the 10 residues was replaced by the corresponding neutral amino acid (asparagine or glutamine). Five of the resulting mutants showed unchanged Na⁺-dependent uridine transport activity (D172N, E338Q, E389Q, E413Q, and D565N) and were not investigated further. Three were retained in intracellular membranes (D482N, E498Q, and E532Q) and thus could not be assessed functionally. The remaining two (E308Q and E322Q) were present in normal quantities at cell surfaces but exhibited low intrinsic transport activities. Charge replacement with the alternate acidic amino acid enabled correct processing of D482E and E498D, but not of E532D, to cell surfaces and also yielded partially functional E308D and E322D. Relative to wild-type hCNT1, only D482E exhibited normal transport kinetics, whereas E308D, E308Q, E322D, E322Q, and E498D displayed increased $K_{50}^{\text{Na}^+}$ and/or K_m^{uridine} values and diminished $V_{\text{max}}^{\text{Na}^+}$ and $V_{\text{max}}^{\text{uridine}}$ values. E322Q additionally exhibited uridine-gated uncoupled Na⁺ transport. Together, these findings demonstrate roles for Glu-308, Glu-322, and Glu-498 in Na⁺/nucleoside cotransport and suggest locations within a common cation/nucleoside translocation pore. Glu-322, the residue having the greatest influence on hCNT1 transport function, exhibited uridine-protected inhibition by *p*-chloromercuriphenyl sulfonate and 2-aminoethyl methanethiosulfonate when converted to cysteine.

Most nucleosides, including nucleoside analogs with antineoplastic and/or antiviral activity, are hydrophilic molecules that require specialized plasma membrane nucleoside transporter (NT)⁴ proteins for uptake into or release from cells (1–3). NT-mediated transport is a critical determinant of nucleoside and nucleotide metabolism and, for nucleoside drugs, their pharmacologic actions (3–5). By regulating adenosine availability to cell-surface purinoreceptors, NTs also profoundly affect neurotransmission, vascular tone, and other physiological processes (5, 6). Two structurally unrelated families of integral membrane proteins exist in human and other mammalian cells as follows: the SLC28 concentrative nucleoside transporter (CNT) family, and the SLC29 equilibrative nucleoside transporter (ENT) family (3, 6–8). ENTs are normally present in most, possibly all, cell types (8). CNTs, in contrast, are found predominantly in intestinal and renal epithelia and other specialized cells, suggesting important roles in absorption, secretion, distribution, and elimination of nucleosides and nucleoside drugs (1–4, 6, 7).

In humans (h), hCNT1 and hCNT2 are pyrimidine nucleoside-selective and purine nucleoside-selective, respectively, whereas hCNT3 transports both pyrimidine and purine nucleosides (9–11). Together, these proteins and their orthologs account for the three major concentrative nucleoside transport processes of human and other mammalian cells. Nonmammalian members of the CNT protein family that have been characterized include hCNT from the ancient marine prevertebrate the Pacific hagfish *Eptatretus stouti* (12), CaCNT from the pathogenic yeast *Candida albicans* (13), CeCNT3 from the nematode *Caenorhabditis elegans* (14), and NupC from the bacterium *Escherichia coli* (15). hCNT1, hCNT2, and hCNT are predominantly Na⁺-coupled nucleoside transporters, whereas hCNT3 can utilize electrochemical gradients of either Na⁺ or H⁺ to accumulate nucleosides within cells (12, 16–18). CaCNT, CeCNT3, and NupC function exclusively as H⁺/nucleoside cotransporters (13–15). Na⁺/nucleoside coupling sto-

* This work was supported in part by the National Cancer Institute of Canada, the Canadian Cancer Society, and the Alberta Cancer Board. The costs of publication of this article were defrayed in part by the payment of page charges. This article must therefore be hereby marked "advertisement" in accordance with 18 U.S.C. Section 1734 solely to indicate this fact.

¹ Supported by a studentship from the Alberta Heritage Foundation for Medical Research.

² Holds a Canada Research Chair in Oncology at the University of Alberta.

³ Heritage Scientist of the Alberta Heritage Foundation for Medical Research. To whom correspondence and reprint requests should be addressed: Dept. of Physiology, 7-55 Medical Sciences Bldg., University of Alberta, Edmonton, Alberta T6G 2H7, Canada. Tel.: 780-492-5895; Fax: 780-492-7566; E-mail: james.young@ualberta.ca.

⁴ The abbreviations used are: NT, nucleoside transporter; CNT, concentrative nucleoside transporter; ENT, equilibrative nucleoside transporter; MTS, methanethiosulfonate; MTSEA, 2-aminoethyl methanethiosulfonate hydrobromide; MTSES, sodium (2-sulfonatoethyl) methanethiosulfonate; MTSET, [(triethylammonium)ethyl] methanethiosulfonate bromide; PCMBs, sodium *p*-chloromercuriphenyl sulfonate; TM, putative transmembrane helix; h, human.

hCNT1 Glutamate Residues

ichiometries are 1:1 for hCNT1 and hCNT2 and 2:1 for hCNT3 and hfCNT (12, 16–19). H⁺/nucleoside coupling ratios for hCNT3 and CaCNT are both 1:1 (13, 17–19).

Although considerable progress has been made in molecular studies of ENT proteins (6, 8), studies of structurally and functionally important residues within the CNT protein family are still at an early stage. Topological investigations suggest that hCNT1–3 and other eukaryote CNT family members have a 13 (or possibly 15)-transmembrane helix (TM) architecture, and multiple alignments reveal strong sequence similarities within the C-terminal half of the proteins (20). Prokaryote CNTs lack the first three TMs of their eukaryote counterparts, and functional expression of N-terminally truncated human/rat CNT1 in *Xenopus* oocytes has established that the first three TMs are not required for Na⁺-dependent uridine transport activity (20). Consistent with these findings, chimeric studies between hCNT1 and hfCNT (12) and between hCNT1 and hCNT3 (17) have demonstrated that residues involved in Na⁺- and H⁺-coupling reside in the C-terminal half of the protein.

In hCNT1, two sets of adjacent residues in TM 7 and 8 have been identified (Ser-319/Gln-320 and Ser-353/Leu-354) that, when converted to the corresponding residues in hCNT2, change the nucleoside specificity of the transporter from CNT1-type to CNT2-type (21). Mutation of Ser-319 in TM 7 of hCNT1 to glycine was sufficient to enable transport of purine nucleosides, whereas mutation of the adjacent residue Gln-320 to methionine (which had no effect on its own) augmented this transport. The additional mutation of Ser-353 in TM 8 of hCNT1 to threonine converted S319G/Q320M from broadly selective (CNT3-type) to purine nucleoside-selective (CNT2-type) but with relatively low adenosine transport activity. Further mutation of Leu-354 to valine increased the adenosine transport capability of S319G/Q320M/S353T, producing a full CNT2-type phenotype. Residues in both TMs 7 and 8 therefore play key roles in determining hCNT1/2 nucleoside selectivities. Confirming this, the double TM 8 mutant (S353T/L354V) was recently shown to exhibit a unique uridine-preferring transport phenotype (22). Mutation of Leu-354 alone markedly increased the affinity of the transporter for Na⁺ and Li⁺, demonstrating that TM 8 also has a role in cation coupling (22).

Although negatively charged amino acid residues play key functional and structural roles in a broad spectrum of mammalian and bacterial cation-coupled transporters (23–33), essentially nothing is known about their roles in CNTs. Using hCNT1 as the template, we report here the consequences of individually mutating 10 aspartate and glutamate residues that are highly conserved in mammalian CNTs. We identified three residues (Glu-308, Glu-322, and Glu-498) with roles in CNT Na⁺ and nucleoside binding and translocation.

EXPERIMENTAL PROCEDURES

Site-directed Mutagenesis and DNA Sequencing—hCNT1 cDNA (GenBankTM accession number U62968) in the *Xenopus* expression vector pGEM-HE (34) provided the template for construction of hCNT1 mutants by the oligonucleotide-directed technique (35), using reagents from the QuikChange[®] site-directed mutagenesis kit (Stratagene) according to the manufacturer's directions. Constructs were sequenced in both

directions by *Taq* dye deoxy terminator cycle sequencing to ensure that only the correct mutation had been introduced.

Production of Wild-type and Mutant hCNT1 Proteins in *Xenopus* Oocytes—hCNT1 cDNAs were transcribed with T7 polymerase and expressed in oocytes of *Xenopus laevis* by standard procedures (36). Healthy defolliculated stage VI oocytes were microinjected with 10 nl of water or 10 nl of water containing RNA transcript (1 ng/ml) and incubated in modified Barth's medium at 18 °C for 72 h prior to the assay of transport activity.

Flux Assays—Transport was traced using ¹⁴C/³H-labeled nucleosides at 1 μCi/ml. Flux measurements were performed at room temperature (20 °C) as described previously (36, 37). Briefly, groups of 12 oocytes were incubated in 200 μl of transport medium containing either 100 mM NaCl or choline chloride and 2 mM KCl, 1 mM CaCl₂, 1 mM MgCl₂, and 10 mM HEPES, pH 7.5. Unless otherwise indicated, the uridine concentration was 10 μM. At the end of the incubation period, extracellular label was removed by six rapid washes in ice-cold Na⁺-free (choline chloride) transport medium, and individual oocytes were dissolved in 1% (w/v) SDS for quantitation of oocyte-associated radioactivity by liquid scintillation counting (LS 6000 IC; Beckman). Initial rates of transport (influx) were determined using an incubation period of 1 min, except for mutants E322Q and E322D, which had low transport activity and required a longer incubation time (5 min) to achieve cellular uptake comparable with that of wild-type hCNT1 and the other mutants. In PCMBs inhibition studies, oocytes were pretreated with PCMBs (0.1 mM) on ice for 30 min and then washed five times with ice-cold transport medium to remove excess organomercurial before the assay of transport activity. Corresponding pretreatment with the MTS reagents MTSEA, MTSES, and MTSET (2.5, 10, and 1 mM, respectively) was performed at room temperature for 5 min. To demonstrate substrate protection, unlabeled uridine (20 mM) was included along with inhibitor during the preincubation step (38). The flux values shown are means ± S.E. of 10–12 oocytes, and each experiment was performed at least twice on different batches of cells. Kinetic (*K_m*, *K₅₀*, *V_{max}*, and Hill coefficient) parameters (± S.E.) were determined using SigmaPlot software (Jandel Scientific). Statistical significance of the reported data sets was evaluated using *t* tests.

Electrophysiology—Steady-state and presteady-state currents were measured using the two-microelectrode voltage clamp as described previously (16).

Na⁺/Nucleoside Stoichiometry—Coupling ratios were determined by direct charge/flux measurements (16, 17, 19).

Isolation of Membranes and Immunoblotting—Total membranes (plasma + intracellular membranes) and purified plasma membranes were isolated by centrifugation from groups of 100 oocytes at 4 °C in the presence of protease inhibitors as described previously (39, 40). Colloidal silica (Sigma) was used to increase the gravitational density of plasma membranes and enhance their yield and purity (40). Protein was determined by the bicinchoninic acid protein assay (Pierce) using bovine serum albumin as standard.

For immunoblotting, oocyte membranes (1 μg of plasma membrane protein or total membrane protein) were resolved

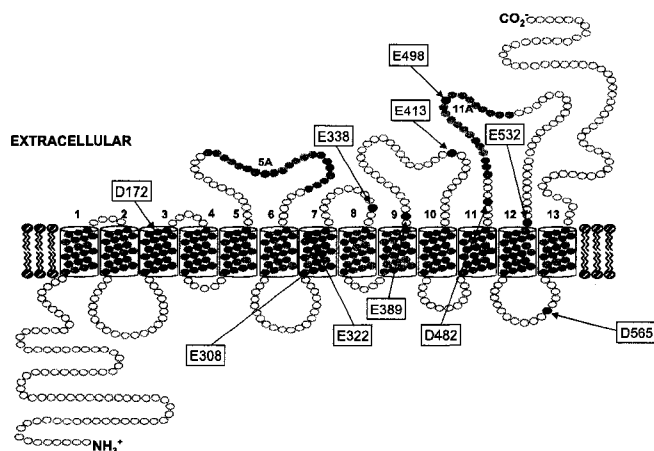


FIGURE 1. Topological model of hCNT1. Membrane-spanning α -helices predicted from bioinformatic analyses of currently identified CNT family members are numbered 1–13 (strongly predicted) and 5A and 11A (weakly predicted). Highly conserved acidic amino acid residues are indicated with filled circles.

TABLE 1
Uridine uptake by wild-type hCNT1 and mutants expressed in *Xenopus* oocytes

Oocytes producing recombinant hCNT1 and hCNT1 mutants were incubated in transport medium with or without Na^+ at 20 °C as described under "Experimental Procedures." Each value is the mean \pm S.E. from 10 to 12 oocytes. For influx in the presence of Na^+ , significant differences in mediated uridine uptake ($p < 0.05$) compared with wild-type hCNT1 are indicated by *.

	Mediated uridine uptake		Protein expression ^a
	Na ⁺ medium	Na ⁺ -free medium	
	<i>pmol/oocyte·min⁻¹</i>		
hCNT1	5.0 \pm 0.7	0.06 \pm 0.01	+
D172N	4.9 \pm 0.4	0.12 \pm 0.02	ND ^b
E308Q	0.7 \pm 0.1*	<0.01	+
E222Q	0.2 \pm 0.1*	<0.01	+
E338Q	4.7 \pm 0.6	0.03 \pm 0.01	ND
E389Q	3.8 \pm 0.3	0.05 \pm 0.01	ND
E413Q	5.4 \pm 0.6	0.07 \pm 0.02	ND
D482N	0.1 \pm 0.1*	<0.01	–
E498Q	<0.01*	<0.01	–
E532Q	<0.01*	<0.01	–
D565N	5.4 \pm 0.5	0.08 \pm 0.02	ND

^a Relative expression in the plasma membrane is from Fig. 3.

^b ND indicates not determined.

on 12% SDS-polyacrylamide gels (41). The electrophoresed proteins were transferred to polyvinylidene difluoride membranes and probed with affinity-purified anti-hCNT1-(31–55) polyclonal antibodies (22). Blots were then incubated with horseradish peroxidase-conjugated anti-rabbit antibodies (Amersham Biosciences) and developed with enhanced chemiluminescence reagents (Amersham Biosciences).

RESULTS

Residues Identified for Mutagenesis—In this study, we employed site-directed mutagenesis and heterologous expression in *Xenopus* oocytes to analyze the roles of hCNT1 acidic amino acid residues. The locations of the residues selected for study are shown in Fig. 1.

hCNT1 Glutamate Residues

hCNT1 contains 51 aspartate and glutamate residues. Of these, 10 are conserved in other mammalian CNT family members and were included in the present analysis (hCNT1 residues Asp-172, Glu-308, Glu-322, Glu-338, Glu-389, Glu-413, Asp-482, Glu-498, Glu-532, and Asp-565). All but one (Asp-172) were located in the C-terminal half of the protein. In initial mutagenesis experiments, each of the 10 hCNT1 aspartate and glutamate residues were individually replaced by the corresponding neutral amino acids (asparagine or glutamine, respectively). All mutations were verified by sequencing the entire coding region of the double-stranded plasmid DNA in both directions. Except for the desired base changes, all sequences were identical to wild-type hCNT1.

Uridine Uptake and Cell-surface Expression of Wild-type hCNT1 and Mutants

The hCNT1 mutant transporters were expressed in *Xenopus* oocytes and assayed for uridine transport activity (10 μM uridine influx, 1 min fluxes) in the presence and absence of Na^+ as described under "Experimental Procedures." Representative values for mediated uridine uptake, corrected for basal nonmediated uptake in control water-injected oocytes, are presented in Table 1. Five of the mutants (D172N, E338Q, E389Q, E413Q, and D565N) exhibited >75% of wild-type Na^+ -dependent transport activity and were not investigated further. In contrast, substitution of Glu-308 reduced transport activity by almost 90%, whereas mutation of E322Q, D482N, E498Q, and E532Q resulted in >99% loss of uridine transport activity. The time course of uridine uptake by wild-type hCNT1 shown in Fig. 2A demonstrates that the measured fluxes corresponded to initial rates of transport. Fig. 2A also demonstrates the absence of uridine uptake in water-injected oocytes.

Cell-surface expression of mutants E308Q, E322Q, D482N, E498Q, and E532Q was investigated by immunoblotting of purified oocyte plasma membranes using polyclonal antibodies (22) directed against amino acid residues 31–55 at the N terminus of the protein (Fig. 3A). Wild-type hCNT1 and transporters with mutations at positions 308 and 322 were present in similar amounts, indicating that these single amino acid substitutions resulted in loss of intrinsic hCNT1 transport activity without altering surface quantities in the oocyte plasma membrane. Antibody specificity was confirmed by lack of immunoreactivity in membranes prepared from control water-injected oocytes. Unlike E308Q and E322Q, very little plasma membrane immunoreactivity was detected for the transporters having mutations at positions 482, 498, and 532, indicating that the lack of transport activity was associated with reduced cell-surface expression.

hCNT1 Glutamate Residues

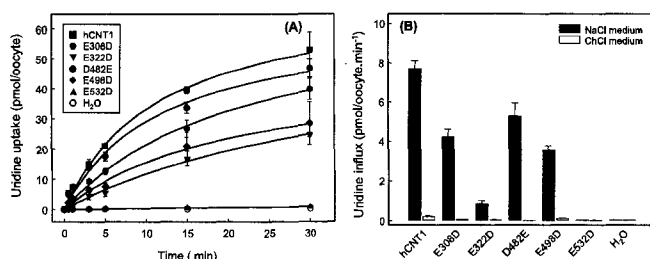


FIGURE 2. Expression of wild-type hCNT1 and mutants in *Xenopus* oocytes. Oocytes were injected with 10 ng of RNA transcripts or water alone and incubated for 3 days. *A*, Time courses of radiolabeled uridine uptake by wild-type hCNT1 and mutants (10 μ M, 20 $^{\circ}$ C). *B*, Initial rates of radiolabeled uridine uptake (10 μ M, 20 $^{\circ}$ C) measured in the presence or absence of Na^+ in the incubation medium. H_2O , control water-injected oocytes. Each value is the mean \pm S.E. from 10 to 12 oocytes.

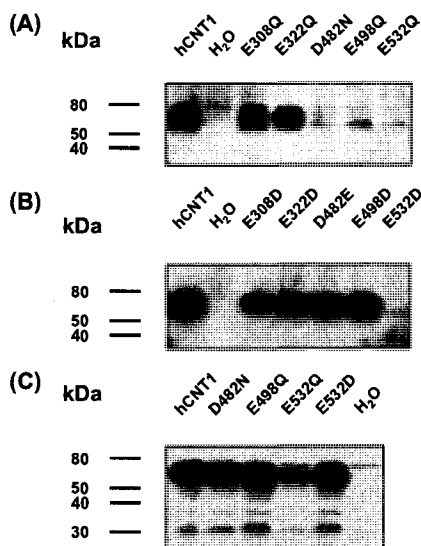


FIGURE 3. Immunoblot analysis of wild-type hCNT1 and mutants. Plasma membranes (1 μ g of protein) (*A* and *B*) and total membranes (1 μ g of protein) (*C*) were obtained from oocytes producing wild-type hCNT1 and hCNT1 mutants. Membranes were subjected to SDS-PAGE and transferred to polyvinylidene difluoride membranes for immunoblotting with anti-hCNT1-(31-55) antibody. The positions of molecular weight standards are shown on the left. H_2O , membranes from control water-injected oocytes. Blots *A-C* are from different gels.

In a second round of mutagenesis experiments, Glu-308, Glu-322, Asp-482, Glu-498, and Glu-532 of hCNT1 were replaced by the alternative negatively charged amino acid (*i.e.* glutamate to aspartate or aspartate to glutamate). Time courses of uridine uptake in the presence and absence of Na^+ and the initial rate of uridine accumulation in the presence and absence of Na^+ by E308D, E322D, D482E, E498D, and E532D produced in *Xenopus* oocytes are shown in Fig. 2*A*. Relative to the corresponding

asparagine and glutamine mutations (Table 1), oocytes expressing E308D, D482E, or E498D exhibited higher uridine transport activities with fluxes that were broadly similar to those of wild-type hCNT1. E322D, in contrast, displayed only partial transport activity. In all cases, uridine uptake was Na^+ -dependent (Fig. 2*B*). Transport was also concentrative because the 15- and 30-min uptake values exceeded the initial extracellular uridine concentration of 10 μ M (Fig. 2*A*), assuming an intracellular water volume of 1 μ l (36, 37). Immunological analysis revealed that low activity

E322D was present in normal quantities at the cell surfaces (Fig. 3*B*), demonstrating that its low transport activity was not because of defective insertion and/or stability of the transporter in oocyte plasma membranes. Unlike the other positions, hCNT1 with Glu-532 substituted by aspartate (E532D) lacked functional activity (Fig. 2, *A* and *B*) and remained undetectable at the cell surface by immunoblotting (Fig. 3*B*). The immunoblots shown in Fig. 3*C* demonstrated that oocyte total membranes (plasma + intracellular membranes) contained mutants D482N, E498Q, E532Q, and E532D, indicating that the "no activity" mutants were present within cells, confirming improper targeting to the plasma membrane.

Kinetic Characterization of Wild-type hCNT1 and Mutants—To further elucidate the effects of individual replacement of amino acids Glu-308, Glu-322, Asp-482, and Glu-498 on hCNT1 transport function, mutants E308D, E308Q, E322D, E322Q, D482E, E498D, and wild-type hCNT1 were characterized for Na^+ activation and uridine concentration dependence kinetics. Na^+ activation was investigated by measuring 10 μ M uridine influx as a function of Na^+ concentration (Fig. 4), whereas the concentration dependence of uridine uptake was determined at a saturating concentration (100 mM) of Na^+ (Fig. 5). Kinetic parameters derived from these data, including measures of apparent Na^+ affinities ($K_{50}^{\text{Na}^+}$), apparent uridine affinities (K_m^{uridine}), and maximal rates of transport ($V_{\text{max}}^{\text{Na}^+}$ and $V_{\text{max}}^{\text{uridine}}$) are summarized in Table 2.

In agreement with previous studies (16, 18), the rate of uridine transport by oocytes expressing wild-type hCNT1 increased markedly as the Na^+ concentration was increased from 0 to 100 mM and was essentially saturated at Na^+ concentrations above 40 mM. In contrast, rates of uridine transport by oocytes producing E308Q, E322D, or E322Q did not reach saturation, even at the highest concentration of Na^+ (100 mM) (Fig. 4). Hill-type analysis of the data yielded an apparent $K_{50}^{\text{Na}^+}$ value of 8.2 mM for wild-type hCNT1 compared with 20 mM for E308D and >40 mM for E308Q, E322D, and E322Q. E308Q, E322D, and E322Q also showed major reductions in $V_{\text{max}}^{\text{Na}^+}$ values (<1 pmol/oocyte \cdot min $^{-1}$, compared with 5.6 pmol/oocyte \cdot min $^{-1}$ for wild-type hCNT1). $V_{\text{max}}^{\text{Na}^+}:K_{50}^{\text{Na}^+}$ ratios (a measure of transport efficiency) were 0.68 for wild-type hCNT1, 0.17 for E308D, and <0.03 for E308Q, E322D, and

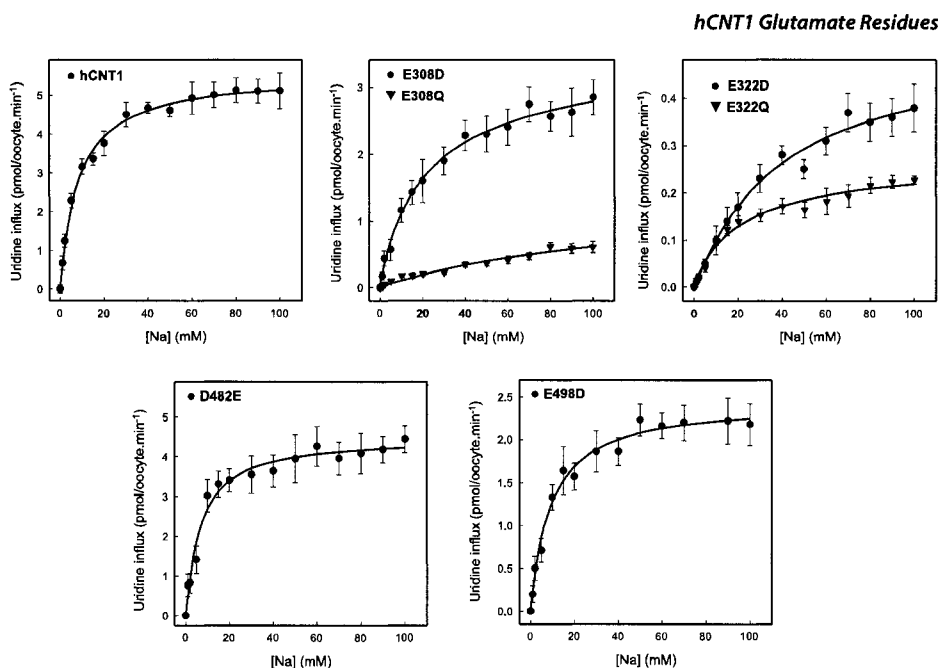


FIGURE 4. Sodium activation kinetics of wild-type hCNT1 and mutants. Initial rates of transporter-mediated radiolabeled uridine uptake (10 μM , 20 $^\circ\text{C}$) were measured in transport media containing 0–100 mM NaCl, using choline chloride to maintain isosmolality. Each value is the mean \pm S.E. from 10 to 12 oocytes. Mediated transport was calculated as uptake in RNA-injected oocytes minus uptake in oocytes injected with water alone. Kinetic parameters derived from the data are presented in Table 2.

E322Q. In the absence of Na^+ , uridine uptake by all mutants was close to zero, indicating an absence of measurable slippage (uncoupled, Na^+ -independent uridine uptake). As also shown in Fig. 4 and summarized in Table 2, D482E and E498D exhibited Na^+ activation kinetics broadly similar to those of wild-type hCNT1. In the case of E498D, however, there was a noticeable reduction in the $V_{\text{max}}^{\text{Na}^+}$ values (2.5 pmol/oocyte \cdot min $^{-1}$), leading to a corresponding decrease in the $V_{\text{max}}^{\text{Na}^+}/K_{\text{m}}^{\text{Na}^+}$ ratio (0.26). Where measurable (hCNT1, E308D, D482E, and E498D), Hill coefficients were consistent with a Na^+ :uridine coupling ratio of 1:1 (16, 18, 19).

To minimize the potential effects of altered Na^+ apparent affinity on uridine kinetic parameters, experiments to investigate uridine transport kinetics were undertaken at the maximum possible Na^+ concentration of 100 mM. As shown in Fig. 5 and summarized in Table 2, only D482E exhibited uridine transport kinetics similar to those of wild-type hCNT1 ($K_{\text{m}}^{\text{uridine}}$ 26 and 29 μM , $V_{\text{max}}^{\text{uridine}}$ 18 and 19 pmol/oocyte \cdot min $^{-1}$, and $V_{\text{max}}^{\text{uridine}}/K_{\text{m}}^{\text{uridine}}$ ratios 0.69 and 0.66, respectively). All other mutants exhibited reduced apparent affinities for uridine and/or decreases in $V_{\text{max}}^{\text{uridine}}$ values. Mutants with increased $K_{\text{m}}^{\text{uridine}}$ values were E308D (108 μM), E308Q (46 μM), E322Q (79 μM), and E498D (64 μM), and dramatic reductions in $V_{\text{max}}^{\text{uridine}}$ values were seen for

E308Q, E322D, and E322Q (3.8, 1.8, and 1.2 pmol/oocyte \cdot min $^{-1}$, respectively). Compared with a value of 0.66 for wild-type hCNT1, $V_{\text{max}}^{\text{uridine}}/K_{\text{m}}^{\text{uridine}}$ ratios ranged from 0.18 and 0.25 for E308D and E498D, respectively, to 0.08, 0.06, and 0.02 for E308Q, E322D, and E322Q, respectively. The nucleoside selectivities of E308D, E322D, D482E, and E498D were identical to wild-type hCNT1 (Table 3).

Electrophysiological Characterization of Wild-type hCNT1 and Mutants—In steady-state electrophysiological experiments (16), all mutants (E308D, E308Q, E322D, E322Q, D482E, and E498D) were confirmed to mediate uridine-induced Na^+ inward currents (Fig. 6A). No currents were detected in the absence of Na^+ or in control water-injected oocytes. Measured in the same batch of oocytes on the same day, there was excellent correlation between the magnitudes of the currents recorded and the corresponding Na^+ -dependent fluxes of radiolabeled uridine (Fig. 6B). The one exception was mutant E322Q, which exhibited an elevated uridine-induced Na^+ current disproportionate to its very low Na^+ -dependent uridine transport activity (compare, for example, E322D and E322Q in Fig. 6, A and B).

In parallel presteady-state electrophysiological experiments performed in the absence of uridine, oocytes producing wild-type hCNT1 and mutants E308D, E308Q, E322D, and E322Q

hCNT1 Glutamate Residues

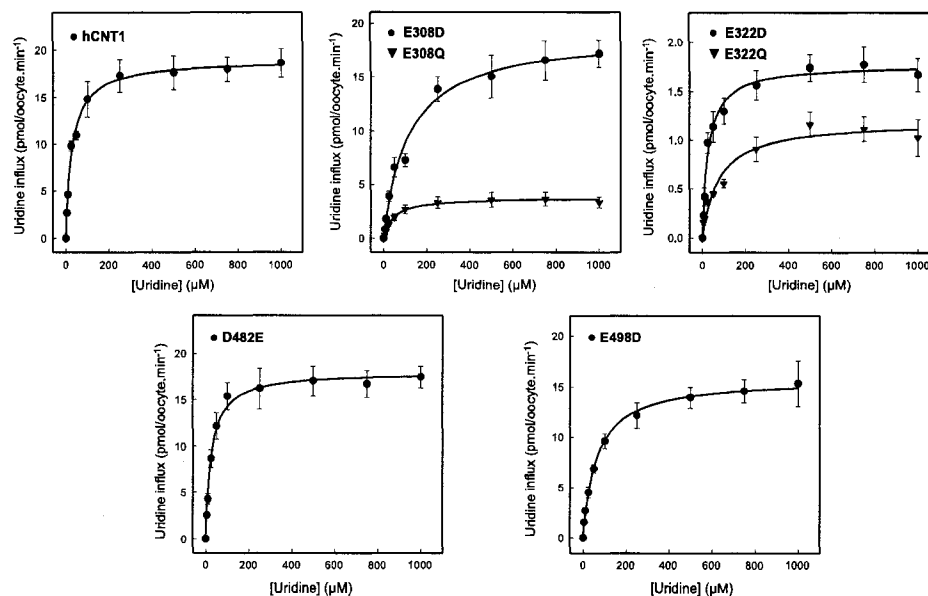


FIGURE 5. Uridine kinetics of wild-type hCNT1 and mutants. Initial rates of transporter-mediated radiolabeled uridine uptake (20 °C) were measured in transport medium containing 100 mM NaCl. Each value is the mean \pm S.E. from 10 to 12 oocytes. Mediated transport was calculated as uptake in RNA-injected oocytes minus uptake in oocytes injected with water alone. Kinetic parameters derived from the data are presented in Table 2.

TABLE 2
Kinetic properties of wild-type hCNT1 and mutants
Significant differences in kinetic parameters ($p < 0.05$) compared with wild-type hCNT1 are indicated by *.

	Na ⁺ activation ^a				Uridine kinetics ^b			
	$K_{50}^{Na^+}$ mM	$V_{max}^{Na^+}$ pmol/oocyte·min ⁻¹	Hill coefficient	$V_{max}^{Na^+} \cdot K_{50}^{Na^+}$ ratio	$K_m^{uridine}$ μ M	$V_{max}^{uridine}$ pmol/oocyte·min ⁻¹	$V_{max}^{uridine} \cdot K_m^{uridine}$ ratio	
hCNT1	8.2 \pm 0.1	5.6 \pm 0.1	0.8 \pm 0.1	0.68	29 \pm 3	19 \pm 1	0.66	
E308D	20 \pm 2*	3.3 \pm 0.1*	1.2 \pm 0.1	0.17	108 \pm 12*	19 \pm 1	0.18	
E308Q	>40*	<1*		<0.03	46 \pm 4*	3.8 \pm 0.1*	0.08	
E322D	>40*	<1*		<0.03	28 \pm 3	1.8 \pm 0.1*	0.06	
E322Q	>40*	<1*		<0.03	79 \pm 18*	1.2 \pm 0.1*	0.02	
D482E	7.2 \pm 1.0	4.6 \pm 0.2	0.8 \pm 0.1	0.64	26 \pm 2	18 \pm 1	0.69	
E498D	9.5 \pm 1.1	2.5 \pm 0.1*	0.9 \pm 0.1	0.26	64 \pm 4*	16 \pm 1	0.25	

^a Data are from Fig. 4.
^b Data are from Fig. 5.

were voltage-clamped at a holding potential (V_h) of -50 mV, and presteady-state currents were activated by voltage steps to a series of test potentials (V_t) (Fig. 7, A and B). In agreement with previous studies (16), current relaxations that were largely eliminated upon removal of external Na⁺ were observed for wild-type hCNT1. Presteady-state currents were greatly reduced in mutant E322D and absent from mutants E308Q, E308D, E322Q, and control water-injected oocytes.

Na⁺:Nucleoside Coupling Ratios of Wild-type hCNT1 and Mutants—The Na⁺/uridine coupling stoichiometries of wild-type hCNT1 and mutants E308Q and E322Q were determined by simultaneously measuring Na⁺ currents and radiolabeled uridine uptake under voltage-clamp conditions. The linear cor-

relations between integrated uridine-dependent charge and radiolabeled uridine accumulation measured in Na⁺-containing transport medium (100 mM) gave calculated Na⁺/nucleoside coupling ratios of 0.88 ± 0.06 and 0.82 ± 0.03 for hCNT1 and E308Q, respectively (Fig. 8, A and B). Consistent with E322Q functioning as a partially uncoupled uridine-gated Na⁺ channel, there was no correlation between Na⁺ current and radiolabeled uridine uptake, charge:flux ratios for individual E322Q-producing oocytes ranging from 5 to 74 (Fig. 8C).

PCMS and MTS Inhibition of Uridine Transport by Wild-type hCNT1 and Mutants—Residues lining the translocation pore can be identified through the use of hydrophilic thiol-reactive reagents such as *p*-chloromercuribenzenesulfonate

hCNT1 Glutamate Residues

TABLE 3
Nucleoside uptake by wild-type hCNT1 and mutants expressed in *Xenopus* oocytes

Oocytes producing recombinant hCNT1 and hCNT1 mutants were incubated with different radiolabeled nucleosides (10 μ M) in NaCl transport medium at 20 °C as described under "Experimental Procedures." Each value is corrected for basal uptake in control water-injected oocytes and is the mean \pm S.E. from 10 to 12 oocytes. Significant differences in mediated nucleoside uptake ($p < 0.05$) compared with wild-type hCNT1 are indicated by *. To permit a side-by-side comparison of pyrimidine and purine nucleoside uptake, all fluxes were determined using a 5-min incubation interval.

	Mediated uptake					
	Uridine	Cytidine	Thymidine	Adenosine	Guanosine	Inosine
	<i>pmol/oocyte\cdot5 min$^{-1}$</i>					
hCNT1	9.6 \pm 0.1	4.0 \pm 0.3	5.6 \pm 0.7	0.14 \pm 0.06	<0.01	<0.01
E308D	6.2 \pm 1.1*	2.1 \pm 0.3*	5.0 \pm 0.5	0.20 \pm 0.13	<0.01	<0.01
E322D	1.2 \pm 0.2*	0.2 \pm 0.02*	1.3 \pm 0.2*	0.13 \pm 0.08	<0.01	<0.01
D482E	12 \pm 1	4.6 \pm 0.9	7.4 \pm 0.8	0.16 \pm 0.03	<0.01	<0.01
E498D	7.6 \pm 0.7	3.1 \pm 0.4	4.1 \pm 0.4	0.05 \pm 0.02	<0.01	<0.01

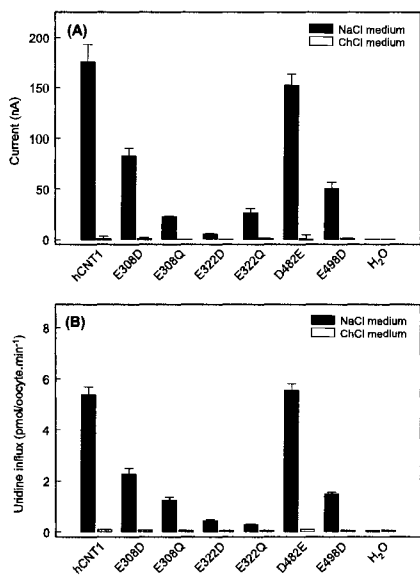


FIGURE 6. Uridine-induced steady-state currents of wild-type hCNT1 and mutants. Oocytes were injected with 10 ng of RNA transcripts or water alone and incubated for 3 days. *A*, averaged inward currents in hCNT1- and mutant-producing oocytes perfused with 1 mM uridine in the presence or absence of 100 mM Na⁺ in the incubation medium. Each value is the mean \pm S.E. from five oocytes. No currents were observed in control water-injected oocytes. *B*, initial rates of radiolabeled uridine uptake (10 μ M, 20 °C) measured in the presence or absence of 100 mM Na⁺ in the incubation medium. H₂O, control water-injected oocytes. Each value is the mean \pm S.E. from 10 to 12 oocytes.

(PCMBs) and methanethiosulfonate (MTS) derivatives (22, 38, 42–45). Thus, a final series of mutagenesis experiments was undertaken in which hCNT1 acidic amino acid residues Glu-308, Glu-322, Asp-482, Glu-498, and Glu-532 were individually replaced by cysteine. Consistent with our other studies of these positions, substitution of Asp-482, Glu-498, and Glu-532 with cysteine yielded transporters that were nonfunctional in oocytes (data not shown) and could not be investigated further. Relative to wild-type hCNT1, however, mutants E308C and E322C showed reduced but measurable influx of uridine (Fig.

9A). Both were present in oocyte plasma membranes in amounts similar to those of wild-type hCNT1 (Fig. 9B). Although wild-type hCNT1 contains 20 endogenous cysteine residues, and consistent with results of previous studies (38), there was no change in hCNT1-mediated uridine uptake following incubation with membrane-impermeant PCMBs at a concentration of 0.1 mM (Fig. 9A). PCMBs exposure also had no measurable effect on E308C transport activity. In contrast, uridine uptake by E322C was strongly inhibited by PCMBs, and the presence of extracellular uridine (20 mM) protected the transporter against this inhibition (Fig. 9A).

Fig. 10 extends this analysis by showing the corresponding inhibitory effects of three MTS reagents with different sizes (MTSEA < MTSES < MTSET), charges (MTSEA and MTSES, negatively charged; MTSET, positively charged), and membrane permeabilities (MTSEA, membrane-permeable; MTSES and MTSET, membrane-impermeable). Reflecting their different reactivities with thiol groups, MTSEA, MTSES, and MTSET were tested on wild-type hCNT1 and mutants E308C and E322C at concentrations of 2.5, 10, and 1 mM, respectively. Only MTSEA gave significant inhibition, and only E322C was affected (Fig. 10A). Like PCMBs, addition of uridine (20 mM) to the extracellular medium protected E322C against MTSEA inhibition (Fig. 10B).

DISCUSSION

As shown in Fig. 1 for hCNT1, current models of hCNT topology have 13 putative TMs (9–11, 20). Computer algorithms also weakly predict two additional potential transmembrane regions, designated in Fig. 1 as TMs 5A and 11A (20). Location of the N and C termini as intracellular and extracellular, respectively, derives from immunocytochemical experiments with site-specific antibodies, and from studies of native and introduced glycosylation sites (20). Cytoplasmic exposure of the loop linking TMs 4 and 5 has been similarly confirmed (20). Both a 13 TM and 15 TM membrane architecture are consistent with these landmarks. Initial substituted cysteine accessibility method analyses of TMs 11, 12, and 13 of a functional cysteine-free version of a human CNT3 (hCNT3C⁻) using MTS reagents (46), as well as other published structure/function studies (e.g. 21, 22), are also consistent with both models. TMs 1–3 of human and rat CNT1 are not required for Na⁺-dependent uridine transport activity (20).

The present study identified five conserved acidic amino acid residues of Na⁺/nucleoside cotransporter hCNT1 (Glu-308,

hCNT1 Glutamate Residues

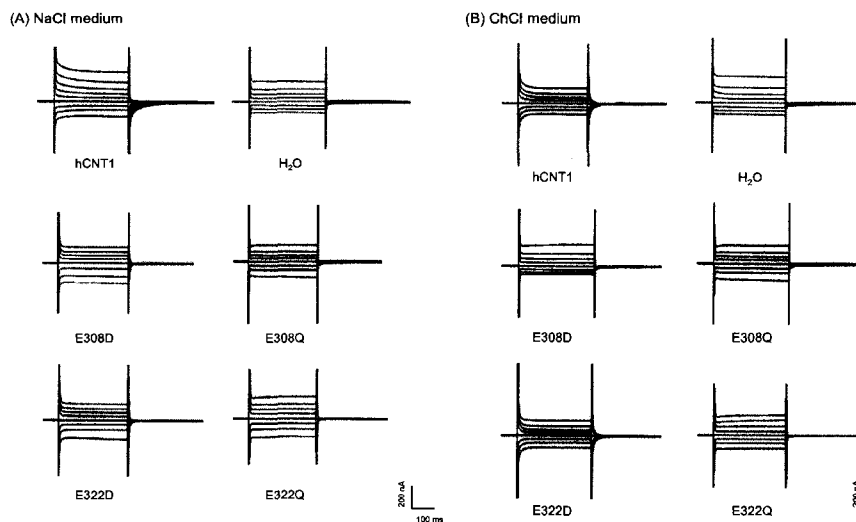


FIGURE 7. Wild-type hCNT1 and mutant presteady-state currents elicited by voltage pulse. The oocyte membrane was held at a holding potential (V_h) of -50 mV and stepped to a range of test potentials (V_t) from -125 to $+50$ mV (25-mV increments). *A*, NaCl transport medium; *B*, choline chloride transport medium.

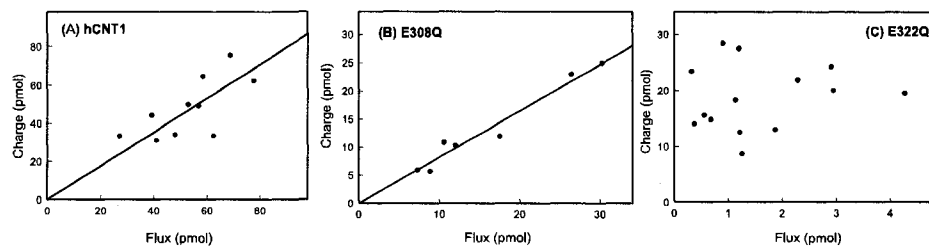


FIGURE 8. Stoichiometry of wild-type hCNT1, E308Q, and E322Q. Oocytes were clamped at V_h of -50 mV and perfused with $200 \mu\text{M}$ [^3H]uridine. Integration of the uridine-evoked current over the uptake period (1 min) yielded the charge moved, which was converted to picomoles and plotted against radiolabeled uridine uptake (pmol) in the same oocyte. The experiment was performed in 10, 7, and 14 individual oocytes for wild-type hCNT1 (*A*), E308Q (*B*), and E322Q (*C*), respectively. Nucleoside-induced current was obtained as the difference between base-line current and the inward nucleoside-induced current. Radiolabeled fluxes were corrected for basal nonmediated uridine uptake in oocytes injected with water alone. The slope (\pm S.E.) of the linear fits (Na^+ /nucleoside coupling ratio) for wild-type hCNT1 and mutant E308Q are indicated by the *straight lines*.

Glu-322, Asp-482, Glu-498, and Glu-532) whose mutation to the corresponding neutral amino acid (glutamine or asparagine) dramatically reduced transport activity of the recombinant protein produced in *Xenopus* oocytes. All are situated in the C-terminal half of the protein, a region previously implicated in both nucleoside and cation translocation (12, 17, 21). Glu-308 and Glu-322 are located in predicted TM 7; Asp-482 is adjacent to the extracellular face of TM 11; Glu-498 is located in the middle of TM11A; and Glu-532 is on the extracellular boundary of TM 12 (Fig. 1). Although TM 7 mutants E308Q and E322Q targeted normally to cell surfaces, their impaired intrinsic transport activities suggested key roles for both glutamate residues in hCNT1-mediated transport. D482N, E498Q,

and E532Q, in contrast, were retained in intracellular membranes. Mutant E532D, in which the negative charge of Glu-532 was replaced with aspartate, was also retained in intracellular membranes, implying an absolute requirement of this glutamate residue to achieve normal cell-surface levels. The predicted location of Glu-532 on the immediate extramembranous surface of TM 12 (Fig. 1) suggests that it may be necessary for the anchoring and/or correct membrane configuration of this TM. Replacement of Asp-482 with glutamate, and Glu-498 with aspartate, in contrast, yielded normal processing to cell surfaces and resulted in uridine fluxes broadly similar to those of wild-type hCNT1. The functional activities of TM 7 mutants E308Q and E322Q were also partially restored by replacement

Downloaded from www.jbc.org at University of Alberta Libraries on March 20, 2008

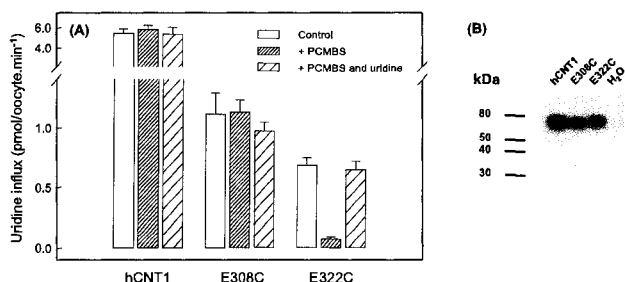


FIGURE 9. PCMB5 inhibition of wild-type hCNT1, E308C, and E322C. *A*, oocytes producing wild-type hCNT1 or mutants E308C or E322C were incubated with or without PCMB5 (0.1 mM) in NaCl transport medium at 1 °C in the absence or presence of unlabeled uridine (20 mM). After 30 min, excess PCMB5 and uridine were removed by washing in ice-cold medium. Initial rates of uridine uptake were then determined (10 μM) at 20 °C. Each value is the mean ± S.E. from 10 to 12 oocytes and was corrected by subtraction of the corresponding basal uptake value in control water-injected oocytes. *B*, immunoblot analysis of plasma membranes (1 μg of protein) from oocytes producing wild-type hCNT1, E308C, or E322C. Plasma membranes were subjected to SDS-PAGE and transferred to polyvinylidene difluoride membranes for immunoblotting with anti-hCNT1-(31–55) antibodies. The positions of molecular weight standards are shown on the left. H₂O, membranes from control water-injected oocytes.

hCNT1 Glutamate Residues

respectively). A consequence of this is that the central TM 6–11 region of the protein may be in an orientation opposite to that shown in Fig. 1 (please see below).

Residues Glu-308 and Glu-322—Effects on hCNT1 transport kinetics were also apparent by mutation of Glu-308 and Glu-322. In the presence of a saturating concentration of Na⁺, substitution of Glu-308 by aspartate (mutant E308D) resulted in an almost 4-fold increase in $K_m^{uridine}$ with no change in $V_{max}^{uridine}$. A 3-fold increase in $K_{50}^{Na^+}$ combined with a modest reduction in $V_{max}^{Na^+}$ was also observed. Therefore, both $V_{max}^{Na^+}$, $K_{50}^{Na^+}$ and $V_{max}^{uridine}:K_m^{uridine}$ ratios of the transporter were affected. More pronounced kinetic effects were apparent for E308Q

and E322D/E322Q, a consistent feature of these mutants being a dramatic reduction in apparent affinities for Na⁺ (increase in $K_{50}^{Na^+}$) as well as $V_{max}^{Na^+}$ and $V_{max}^{uridine}$ values. Two of the mutants (E308Q and E322Q) also exhibited reductions in apparent affinities for uridine (increase in $K_m^{uridine}$). As a result, $V_{max}^{Na^+}:K_{50}^{Na^+}$ and $V_{max}^{uridine}:K_m^{uridine}$ ratios were severely compromised, indicating critical roles for Glu-308 and Glu-322 in cation and nucleoside binding and/or translocation. Because removal of the carboxylate groups at these positions (mutants E308Q and E322Q) still allowed residual Na⁺-dependent uridine transport activity, albeit with very low kinetic efficiency, electrostatic interactions involving Glu-308 and Glu-322 must not in themselves be obligatory for function.

Residues Asp-482 and Glu-498—Relative to wild-type hCNT1, replacement of Asp-482 with glutamate (mutant D482E) resulted in no change in $V_{max}^{Na^+}$, $V_{max}^{uridine}$, $K_{50}^{Na^+}$, or $K_m^{uridine}$, indicating that this residue is unlikely to have a mechanistic role in hCNT1 Na⁺/nucleoside cotransport. Mutation of Glu-498 to aspartate (mutant E498D), however, led to a >50% reduction in $V_{max}^{Na^+}$ and an almost 2-fold increase in the $K_m^{uridine}$ value such that both the $V_{max}^{Na^+}:K_{50}^{Na^+}$ and $V_{max}^{uridine}:K_m^{uridine}$ ratios were reduced relative to those of wild-type hCNT1. Although substitution of Glu-498 with glutamine would be predicted to exhibit more marked changes in transport function, mutant E498Q was not processed to cell surfaces and thus could not be characterized. Consistent with a key role for Glu-498, it is centrally positioned in the most highly conserved sequence motif in the entire CNT family (G/A)XKX₃NEFVA(Y/M/F). Mutation of Glu-519, the residue in hCNT3 that corresponds to hCNT1 Glu-498, impaired both the Na⁺/nucleoside and H⁺/nucleoside transport activities of the transporter.⁵

As illustrated in Fig. 1, Glu-498 and the conserved motif of which it is a part are located in a region of the protein that is potentially exofacial (in the loop linking TMs 11 and 12) or membrane-associated (TM 11A). The functional significance of Glu-498 revealed by this study favors the latter possibility. If TM 11A is transmembrane (as opposed to a re-entrant loop), there is the likelihood that the TM 5A region is also transmembrane (to preserve the experimentally determined endofacial and exofacial locations of the N and C termini of the protein,

Similar to the proposed roles of Asp-187 in the *E. coli* PutP Na⁺/proline transporter (27), Glu-269 and Glu-325 of *E. coli* LacY H⁺-coupled lactose permease (24, 25, 47), and Asp-369 and Asp-404 of the *Aquifex aeolicus* LeuT_{aa} Na⁺/Cl⁻-dependent leucine transporter (48), the profound and complementary effects of hCNT1 Glu-308 and Glu-322 mutations on both $V_{max}^{Na^+}$ and $V_{max}^{uridine}$ values suggest that these residues may facilitate conformational transitions within the Na⁺/nucleoside transport cycle. As indicated by the observed effects of Glu-308 and Glu-322 mutations on binding affinities for Na⁺ and uridine, secondary roles in cation and nucleoside binding are also possible. Examples where this occurs in other transporters include Asp-55 of PutP (26), and glutamate and aspartate residues in the *E. coli* MelB Na⁺/melibiose and GlpT glycerol 3-phosphate transporters (23, 49), the mammalian NaDC-1 Na⁺/dicarboxylate transporter (28), the Na⁺/H⁺-coupled EAAC1 glutamate transporter (30), the NHE1 Na⁺/H⁺ exchanger (31), and the Na⁺/Cl⁻-dependent dopamine transporter (32). As hypothesized for Glu-325 of LacY (33), individual acidic amino residues can accommodate inter-related functions in both conformational transitions and cation/solute binding. The functional consequence of removal of the carboxyl group of LacY Glu-325 is a reduction in the lactose

⁵ S. Y. M. Yao, A. M. L. Ng, M. D. Slugoski, K. M. Smith, R. Mulinta, E. Karpinski, C. E. Cass, S. A. Baldwin, and J. D. Young, unpublished observations.

Downloaded from www.jbc.org at University of Alberta Libraries on March 20, 2008

hCNT1 Glutamate Residues

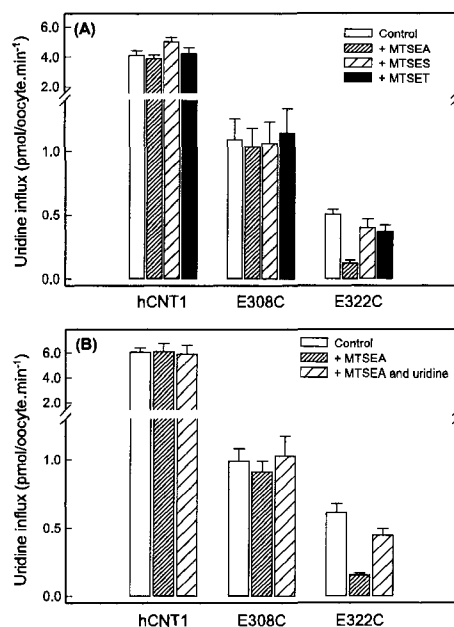


FIGURE 10. MTS reagent inhibition of wild-type hCNT1, E308C, and E322C. *A*, oocytes producing wild-type hCNT1 or mutants E308C or E322C were incubated with or without MTSEA (2.5 mM), MTSES (10 mM), or MTSET (1 mM) in NaCl transport medium at 20 °C. After 5 min, excess MTS reagents were removed by washing in ice-cold medium. Initial rates of uridine uptake were then determined (10 μM) at 20 °C. *B*, protection from MTSEA inhibition by uridine. Oocytes producing wild-type hCNT1 or mutants E308C or E322C were incubated with or without MTSEA (2.5 mM) in NaCl transport medium at 20 °C in the absence or presence of unlabeled uridine (20 mM). After 5 min, excess MTSEA and uridine were removed by washing in ice-cold medium. Initial rates of uridine uptake were then determined (10 μM) at 20 °C. Each value is the mean ± S.E. from 10 to 12 oocytes and was corrected by subtraction of the corresponding basal uptake value in control water-injected oocytes.

transport $V_{max}:K_m$ ratio with the major effect on V_{max} (50), a kinetic outcome similar to that seen here for mutation of hCNT1 residues Glu-308 and Glu-322.

Mutant E308Q retained the wild-type Na^+ /nucleoside coupling ratio of 1:1. In addition to possessing low level Na^+ -dependent uridine transport activity, however, and different from E308Q, mutant E322Q also exhibited features consistent with uncoupled Na^+ transport. This was manifested by disproportionately high uridine-induced Na^+ currents causing variable Na^+ /nucleoside charge:flux ratios in excess of the expected wild-type value of 1:1. Residues of other transporters where mutation causes channel-like behavior include Asp-204 of the human SGLT1 and Asn-177 of the rat 5-hydroxytryptamine transporter (51–52).

Glu-308 and Glu-322 are both located on the putative hydrophilic surface of TM 7 (21). This surface also includes the residues Asn-315 and Ser-319 (previously shown to determine

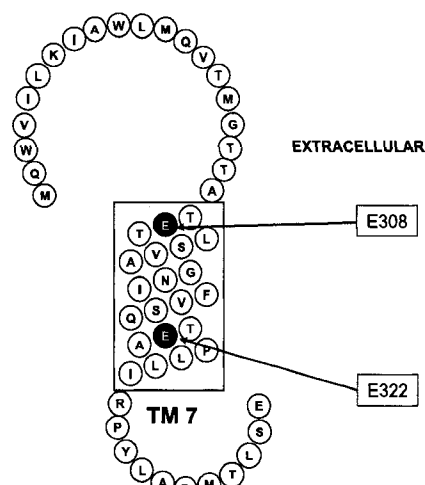


FIGURE 11. Topological model of TM7 of hCNT1. Residues Glu-308 and Glu-322 are indicated with filled circles. Helix orientation is that predicted by a 15-TM membrane architecture.

hCNT1/2 nucleoside selectivities) (21). The present results further strengthen the functional importance of TM 7 and suggest that the helix face containing these four residues lines a common Na^+ /nucleoside translocation pore. TM 8 is also likely to be pore-lining (22). In TM 7, Glu-322 is located close to its extracellular aspect according to the putative 13-TM topology model shown in Fig. 1, but it would be close to its intracellular aspect if TMs 6–11 were in the opposite orientation as predicted by the alternate 15-TM models of hCNT3 topology. When converted to cysteine (mutant E322C), this residue was accessible to membrane-impermeant PCMBs added to the extracellular medium, which resulted in marked transport inhibition that was prevented by externally applied uridine. Supporting the pore-lining location of Glu-322, the corresponding residue in a cysteine-free version of hCNT3 (hCNT3C⁻) (46), when converted to cysteine, also resulted in PCMBs inhibition of uridine uptake.⁵ The smallest of the MTS reagents tested (MTSEA) was also inhibitory against hCNT1 E322C. As with PCMBs, externally applied uridine protected the transporter against MTSEA inhibition. Therefore, Glu-322 evidently lies within the permeant translocation channel in a position with restricted access that is occluded by uridine. Potentially located deep inside the translocation channel in a position within or in close proximity below the uridine binding pocket, this is more consistent with the TM 7 orientation shown in Fig. 11 (15-TM model) than with that in Fig. 1 (13-TM model). Lack of a corresponding effect of PCMBs and MTS reagents on uridine transport by E308C may reflect the more external location of this residue within the translocation vestibule (Fig. 11). Possibly, therefore, Glu-308 and Glu-322 may include parts of the extracellular and internal gates of the transporter, respectively,

a function supported by the channel-like behavior of mutant E322Q revealed by steady-state currents, and by the potential gating function of negatively charged residues within the common cation/solute translocation pore of the recently solved three-dimensional crystal structure of *A. aeolicus* LeuT_{AA} (48). In the latter protein, negatively charged residues stabilize the transporter in a closed conformation that occludes closely associated Na⁺ and leucine-binding sites halfway across the membrane bilayer. Similar to the mammalian GAT1 Na⁺/Cl⁻-dependent γ -aminobutyric acid transporter (53, 54), a member of the same protein family as LeuT_{AA}, hCNT1 (and hCNT3) presteady-state currents largely reflect binding and potential occlusion of extracellular Na⁺. Consistent with a gating function for residues Glu-308 and Glu-322, their mutation markedly impaired hCNT1 presteady-state currents.

Conclusions—The present results for hCNT1 suggest close proximity integration of cation/solute binding and transport within a common cation/permeant translocation pore, and reveal important roles for three postulated intramembranous glutamate residues (Glu-308, Glu-322, and Glu-498) in cation/nucleoside translocation. Setting the stage for additional future substituted cysteine accessibility method and other analyses of hCNT structure and function, the findings favor a revised 15-TM model of hCNT1 membrane architecture.

REFERENCES

- Cass, C. E. (1995) in *Drug Transport in Antimicrobial and Anticancer Chemotherapy* (Gengopadakou, N. H., ed) pp. 403–451, Marcel Dekker, Inc., New York
- Griffith, D. A., and Jarvis, S. M. (1996) *Biochim. Biophys. Acta* **1286**, 153–181
- Young, J. D., Cheeseman, C. I., Mackey, J. R., Cass, C. E., and Baldwin, S. A. (2000) *Curr. Top. Membr.* **50**, 329–378
- Damaraju, V. L., Damaraju, S., Young, J. D., Baldwin, S. A., Mackey, J., Sawyer, M. B., and Cass, C. E. (2003) *Oncogene* **22**, 7524–7536
- Latini, S., and Pedata, F. (2001) *J. Neurochem.* **79**, 463–494
- King, A. E., Ackley, M. A., Cass, C. E., Young, J. D., and Baldwin, S. A. (2006) *Trends Pharmacol. Sci.* **27**, 416–425
- Gray, J. H., Owen, R. P., and Giacomini, K. M. (2004) *Pfluegers Arch.* **447**, 728–734
- Baldwin, S. A., Beal, P. R., Yao, S. Y. M., King, A. E., Cass, C. E., and Young, J. D. (2004) *Pfluegers Arch.* **447**, 735–743
- Ritzel, M. W. L., Yao, S. Y. M., Huang, M. Y., Elliott, J. F., Cass, C. E., and Young, J. D. (1997) *Am. J. Physiol.* **272**, C707–C714
- Ritzel, M. W. L., Yao, S. Y. M., Ng, A. M. L., Mackey, J. R., Cass, C. E., and Young, J. D. (1998) *Mol. Membr. Biol.* **15**, 203–211
- Ritzel, M. W. L., Ng, A. M. L., Yao, S. Y. M., Graham, K., Loewen, S. K., Smith, K. M., Ritzel, R. G., Mowles, D. A., Carpenter, P., Chen, X. Z., Karpinski, E., Hyde, R. J., Baldwin, S. A., Cass, C. E., and Young, J. D. (2001) *J. Biol. Chem.* **276**, 2914–2927
- Yao, S. Y. M., Ng, A. M. L., Loewen, S. K., Cass, C. E., Baldwin, S. A., and Young, J. D. (2002) *Am. J. Physiol.* **283**, C155–C168
- Loewen, S. K., Ng, A. M. L., Mohabir, N. N., Baldwin, S. A., Cass, C. E., Young, J. D. (2003) *Yeast* **20**, 661–675
- Xiao, G., Wang, J., Tangen, T., and Giacomini, K. M. (2001) *Mol. Pharmacol.* **59**, 339–348
- Loewen, S. K., Yao, S. Y. M., Slugoski, M. D., Mohabir, N. N., Turner, R. J., Mackey, J. R., Weiner, J. H., Gallagher, M. P., Henderson, P. J., Baldwin, S. A., Cass, C. E., and Young, J. D. (2004) *Mol. Membr. Biol.* **21**, 1–10
- Smith, K. M., Ng, A. M. L., Yao, S. Y. M., Labeledz, K. A., Knaus, E. E., Wiebe, L. I., Cass, C. E., Baldwin, S. A., Chen, X. Z., Karpinski, E., and Young, J. D. (2004) *J. Physiol. (Lond.)* **558**, 807–823
- Smith, K. M., Slugoski, M. D., Loewen, S. K., Ng, A. M. L., Yao, S. Y. M., Chen, X.-Z., Karpinski, E., Cass, C. E., Baldwin, S. A., and Young, J. D. (2005) *J. Biol. Chem.* **280**, 25436–25449
- Ritzel, M. W. L., Ng, A. M. L., Yao, S. Y. M., Graham, K., Loewen, S. K., Smith, K. M., Hyde, R. J., Karpinski, E., Cass, C. E., Baldwin, S. A., and Young, J. D. (2001) *Mol. Membr. Biol.* **18**, 65–72
- Smith, K. M., Slugoski, M. D., Cass, C. E., Baldwin, S. A., Karpinski, E., and Young, J. D. (2007) *Mol. Membr. Biol.* **24**, 53–64
- Hamilton, S. R., Yao, S. Y. M., Ingram, J. C., Hadden, D. A., Ritzel, M. W. L., Gallagher, M. P., Henderson, P. J., F., Cass, C. E., Young, J. D., and Baldwin, S. A. (2001) *J. Biol. Chem.* **276**, 27981–27988
- Loewen, S. K., Ng, A. M. L., Yao, S. Y. M., Cass, C. E., Baldwin, S. A., and Young, J. D. (1999) *J. Biol. Chem.* **274**, 24475–24484
- Slugoski, M. D., Loewen, S. K., Ng, A. M. L., Smith, K. M., Yao, S. Y. M., Karpinski, E., Cass, C. E., Baldwin, S. A., and Young, J. D. (2007) *Biochemistry* **46**, 1684–1693
- Pourcher, T., Zani, M. L., and Leblanc, G. (1993) *J. Biol. Chem.* **268**, 3209–3215
- Franco, P. J., and Brooker, R. J. (1994) *J. Biol. Chem.* **269**, 7379–7386
- Kaback, H. R. (1997) *Proc. Natl. Acad. Sci. U. S. A.* **94**, 5508–5543
- Quick, M., and Jung, H. (1997) *Biochemistry* **36**, 4631–4636
- Quick, M., and Jung, H. (1998) *Biochemistry* **37**, 13800–13806
- Griffith, D. A., and Pajor, A. M. (1999) *Biochemistry* **38**, 7524–7531
- Pirch, T., Quick, M., Nietschke, M., Langkamp, M., and Jung, H. (2002) *J. Biol. Chem.* **277**, 8790–8796
- Grewer, C., Watzke, N., Rauen, T., and Bicho, A. (2003) *J. Biol. Chem.* **278**, 2585–2592
- Noel, J., Germain, D., and Vadnais, J. (2003) *Biochemistry* **42**, 15361–15368
- Chen, N., Rickey, J., Berfield, J. L., and Reith, M. E. (2004) *J. Biol. Chem.* **279**, 5508–5519
- Abramson, J., Smirnova, I., Kasho, V., Verner, G., Kaback, H. R., and Iwata, S. (2003) *Science* **301**, 610–615
- Linan, E. R., Tytgat, J., and Hess, P. (1992) *Neuron* **9**, 861–871
- Kirsch, R. D., and Joly, E. (1998) *Nucleic Acids Res.* **26**, 1848–1850
- Yao, S. Y. M., Cass, C. E., and Young, J. D. (2000) in *Membrane Transport: A Practical Approach* (Baldwin, S. A., ed) pp. 47–78, Oxford University Press, Oxford
- Huang, Q. Q., Yao, S. Y. M., Ritzel, M. W., Paterson, A. R., Cass, C. E., and Young, J. D. (1994) *J. Biol. Chem.* **269**, 17757–17760
- Yao, S. Y. M., Sundaram, M., Chomey, E. G., Cass, C. E., Baldwin, S. A., and Young, J. D. (2001) *Biochem. J.* **353**, 387–393
- Sundaram, M., Yao, S. Y. M., Ingram, J. C., Berry, Z. A., Abidi, F., Cass, C. E., Baldwin, S. A., and Young, J. D. (2001) *J. Biol. Chem.* **276**, 45270–45272
- Kamsteeg, E. J., and Deen, P. M. T. (2001) *Biochim. Biophys. Res. Commun.* **282**, 683–690
- Laemmli, U. K. (1970) *Nature* **227**, 680–685
- Rothstein, A. (1970) *Curr. Top. Membr. Transp.* **1**, 135–176
- Yan, R. T., and Maloney, P. C. (1993) *Cell* **75**, 37–44
- Yan, R. T., and Maloney, P. C. (1995) *Proc. Natl. Acad. Sci. U. S. A.* **92**, 5973–5976
- Zhu, Q., and Casey, J. R. (2007) *Methods (San Diego)* **41**, 439–450
- Zhang, J., Tackaberry, B., Ritzel, M. W., Raborn, T., Baldwin, S. A., Young, J. D., and Carol, C. E. (2006) *Biochem. J.* **394**, 389–398
- Kaback, H. R. (2005) *C. R. Biologies* **328**, 557–567
- Yamashita, A., Singh, S. K., Kawate, T., Jin, Y., and Gouaux, E. (2005) *Nature* **437**, 215–223
- Huang, Y., Lemieux, M. J., Song, J., Auer, M., and Wang, D. N. (2003) *Science* **301**, 616–620
- Weinglass, A. B., Smirnova, I. N., and Kaback, H. R. (2001) *Biochemistry* **40**, 769–776
- Quick, M., Loo, D. D. F., and Wright, E. M. (2001) *J. Biol. Chem.* **276**, 1728–1734
- Lin, F., Lester, H. A., and Marger, S. (1996) *Biophys. J.* **71**, 3126–3135
- Lu, C.-C., and Hilgemann, D. W. (1999) *J. Gen. Physiol.* **114**, 445–457
- Hilgemann, D. W., and Lu, C.-C. (1999) *J. Gen. Physiol.* **114**, 459–475